http://researchcommons.waikato.ac.nz/

Research Commons at the University of Waikato

Copyright Statement:

The digital copy of this thesis is protected by the Copyright Act 1994 (New Zealand).

The thesis may be consulted by you, provided you comply with the provisions of the Act and the following conditions of use:

- Any use you make of these documents or images must be for research or private study purposes only, and you may not make them available to any other person.
- Authors control the copyright of their thesis. You will recognise the author's right to be identified as the author of the thesis, and due acknowledgement will be made to the author where appropriate.
- You will obtain the author's permission before publishing any material from the thesis.

# Volcanic geology, geochemistry and geochronology of the Kapowai Caldera Complex, Coromandel Volcanic Zone, New Zealand.

A thesis
submitted in fulfillment of the requirements
for the degree of Ph.D. in Earth Sciences
at the University of Waikato
by

**Stephen J. P. Krippner**

The University of Waikato
*Te Whare Wānanga o Waikato*

February 2000

**S.J.P. Krippner**

Volcanic geology, geochemistry and geochronology of the Kapowai Caldera Complex, Coromandel Volcanic Zone, New Zealand.

Ph.D

February 2000

# Abstract

Kapowai Caldera Complex (KCC) is a late Miocene (ca. 8.5-4.9 Ma) caldera volcano situated in the central Coromandel Volcanic Zone (CVZ), North Island, New Zealand. It is the largest (10 x 11 km diameter) onland caldera known within the CVZ, and is the source of the most widespread rhyolitic pyroclastic sequence (Wharepapa Eruptive Sequence; WES) within this zone. This study investigates the structural and petrological evolution of the KCC based upon detailed geological mapping, mineralogical, petrological and geochemical analysis, and K/Ar dating.

KCC is defined by a combination of remote sensing imagery (Landsat-MSS and SAR), geophysical anomalies (magnetic and gravity) and geological facies. Intracaldera KCC structures identified include structural boundaries, faults and intrusives. Observed structural boundaries are high-angle normal faults with minimum displacements varying from 40 - 100m. Faults have NW, N and NE orientations, and extend laterally for ca. 1-8 km. Displacements are highly variable, but are typically concealed by thick pyroclastics and lava flows. The intracaldera succession overlies pre-caldera andesitic-dacitic formations (lava, tuff and breccia) and consists of a sequence of thick andesitic-rhyolitic pyroclastic deposits (ignimbrite and tuff), numerous rhyolitic lava domes, flows and dikes, and andesitic-dacitic lavas and dikes. Interbedded within this sequence are volcaniclastic to carbonaceous siltstones and sandstones. Several episodes of epithermal alteration and associated mineralisation are recorded at the KCC and there is significant control on the location of alteration zones by both caldera-related structures (structural boundaries, faults) and regional NE-trending faults.

Two distinctive, genetically unrelated calc-alkaline magma suites of basaltic andesite to low silica andesite (56 - 64 wt.% $SiO_2$), and low to high silica rhyolite (71 - 78 wt.% $SiO_2$) were erupted. Both suites are characterised by enriched LILE relative to HFSE, and negative Nb anomalies consistent with a continental-arc subduction-related origin. REE abundances are similar in both pre-caldera and caldera-related andesitic-dacitic lavas, although between rhyolite lavas there are significant differences in HREE abundances relative to LREE. Andesitic-dacitic source magmas were generated within the mantle wedge and modified during migration to the base of the crust. Subsequent differentiation occurred by crystal fractionation, crustal assimilation, and hybridisation during migration to high-level magma reservoirs. Rhyolitic source magmas are suggested to be generated by partial melting of continental crust. Differentiation of parental magmas then occurred by crystal fractionation and crustal assimilation, during ascent and storage in high-level silicic magma chambers.

An intracaldera facies association defined at the KCC includes thick infilling proximal and medial pyroclastic facies, effusive facies, and minor lacustrine, hydrothermal alteration and mass wasting facies. Facies vary in geometry, distribution, thickness and lithology, but are all linked to active and passive caldera processes. Exocaldera facies association includes caldera rim and distal pyroclastic subfacies.

Compared with most Taupo Volcanic Zone (TVZ) calderas, the KCC shows some similarities, but has smaller dimensions and erupted smaller magmatic volumes (ca. < 30 $km^3$) over a longer time interval (ca. 3.6 Ma). These features imply differences in magma volumes, crustal thickness, and lower rates of subduction and extension within the late Miocene CVZ arc system compared to the modern TVZ system.

# Acknowledgements

Many people have assisted or helped me during my Ph.D. Firstly, thanks to my chief supervisor, Assoc. Professor Roger Briggs for suggesting a topic of broad scope and many challenges. Thanks Roger for your guidance, advice and encouragement during this study. Thanks to my second supervisor, Dr Richard Smith for your helpful and constructive suggestions during the study. Also I am grateful to both supervisors for your valuable comments on thesis chapters and for their prompt return.

I am grateful to John Gumbley (Department of Conservation) who gained permission for me to work in the Coromandel State Forest, and Fletcher Forests and later Northland Forest Managers Ltd for giving me permission to access the Coroglen Forestry block. Many thanks to Derek Boyd for permission to access the Paul Rd block, and private landowners in the Rangihau and Kapowai valleys for access across their private land.

Thanks to Stephen Brown (University of Canterbury) for prompt analysis of XRF data, and Louise Frick (Monash University) for analysis of REE by ICP-MS. Dr John Patterson (Victoria University, Wellington) kindly assisted me with the electron microprobe. I am also grateful to Dr Tetsu Itaya (Hiruzen Research Institute, Japan) and Dr Raymond Soong (IGNS, Lower Hutt) for $K^{40}$ and $Ar^{40}$ analyses and determination of radiometric ages.

Many people supplied various technical data or reports relating to the study for which I am grateful. Unpublished technical reports and aeromagnetic surveys were supplied by Murray Stevens (Heritage Mining Co. Ltd). Professor Cam Nelson (University of Waikato) and Dr Phil Shane (University of Auckland) both supplied unpublished glass chemistry of distal Neogene tephras and provided constructive suggestions on tephra correlations.

Grant and scholarship monies awarded to me during this study were received from the New Zealand Lottery Grants Board and the Education Endowment Trust, AusIMM New Zealand Branch. I am grateful to these two organisations for their financial contributions.

Renat Radosinsky and Annette Rodgers made valuable contributions in helping with sample preparation, XRD analysis, and other technical matters arising during this study. Thanks also to Mike Vennard, Stephen Bergin, Elaine Norton, and Sydney Wright for various administrative issues.

Jason Laurent, Rodney Milner, Andrew Rumsby, and Brent Hawthorn kindly assisted me at various stages during my fieldwork, and I am grateful to them for their support.

Finally, the biggest thankyou goes to my wife, Michelle. Thanks for your unending love, support, and much needed encouragement throughout my Ph.D years.

# TABLE OF CONTENTS


Abstract ii
Acknowledgements iii
Table of contents iv
List of figures vii
List of tables xiv

**Chapter One Introduction**
1.1 Introduction 1
1.2 Geological Setting 2
1.3 Tectonic Setting 4
1.4 Physiography 6
1.5 Landuse and access 11
1.6 Research objectives and thesis outline 11
1.7 Previous work 14

**Chapter Two Caldera Recognition and Intracaldera Structures**
2.1 Introduction 17
2.2 Recognition of the Kapowai Caldera Complex 17
Remote sensing 18
Geophysical surveys 20
Geological mapping 24
2.3 Intracaldera structures 26
Topographical boundary 28
Caldera floor 30
2.4 Adjacent regional faults 37
2.5 Timing of structural elements 40
2.6 Relationship to regional structure 42
2.7 Comparison with TVZ caldera structures 45

**Chapter 3 Kapowai Caldera Complex Stratigraphy**
3.1 Introduction 48
3.2 New K/Ar dates 48
3.3 Kapowai Caldera Complex stratigraphy 50
3.4 Pre-caldera stratigraphy 51
3.5 Caldera complex stratigraphy 54
Pre-WES caldera stratigraphy 56
WES stratigraphy 81
Post-WES caldera stratigraphy 83

**Chapter 4 Lithic Fragments in Kapowai Caldera Complex Pyroclastic Deposits**
4.1 Introduction 91
4.2 Lithic occurrence and abundance 91
4.3 Lithic lithology 93
Lava lithics 93
Pyroclastic lithics 98
Volcanic breccia lithics 102
Plutonic lithics 104
Sedimentary lithics 104
Hydrothermally altered lithics 104
4.4. Provenance of KCC lithic fragments 108

**Chapter 5 Wharepapa Eruptive Sequence**

5.1 Introduction 111
5.2 Intracaldera WES 111
Lithology 113
Stratigraphic variation 116
Componentry 119
Post-depositional modification 125
Source vent location 131
Distribution 134
Ignimbrite emplacement and facies 136
Eruptive evolution 138
Collapse mechanism 138
5.3 Exocaldera WES 139
Central CVZ ignimbrites 141
Ignimbrites outside the CVZ 145
Co-ignimbrite tephra correlation 145
5.4 WES volume 153

**Chapter 6 Petrography and Mineralogy of KCC Volcanic Rocks**

6.1 Introduction 157
6.2 Petrography 157
Andesite lavas 157
Rhyolite lavas 161
Ignimbrites 165
6.3 Mineralogy 170
Feldspar 170
Pyroxene 172
Amphibole 172
Biotite 174
Fe-Ti oxides 174
6.4 Petrological Processes 177

**Chapter 7 Geochemistry and Petrogenesis**

7.1 Introduction 180
7.2 Methodology 180
XRF 180
ICP-MS 181
7.3 Geochemical classification 181
7.4 Major and trace element variation 184
7.5 Recognition of magma groups 188
Andesitic-dacitic magmas 188
Rhyolitic magmas 191
7.6 Comparison with central CVZ volcanic rocks 197
Andesite-dacite lavas 198
Rhyolite lavas 199
7.7 Petrogenesis of KCC magmas 199
Source characteristics 201
Crystal fractionation 202
Magma mixing 204
Crustal contamination 205
Summary of petrogenesis 207
Pre-caldera and caldera-related andesitic-dacitic magmas 207
Rhyolitic magmas 207

**Chapter 8 Epithermal Alteration**

8.1 Introduction 213
8.2 Historical Au-Ag mining 214
8.3 Epithermal alteration 215
Alteration types 216

Mineral transformation 217
Alteration mineralogy 219
Textural changes 226
8.4 Distribution of alteration 226
Central KCC 226
Upper Kapowai valley 228
Upper Kauaeranga valley 229
Altered lithic fragments 231
8.5 Structural control 232
Caldera structures 232
Regional structural influence 233
8.6 Timing of alteration 234
8.7 Characteristics of KCC epithermal system(s) 234
8.8 Comparison with other calderas 236
TVZ calderas 236
Mineralised calderas/caldera complexes 237

**Chapter 9 Caldera Facies and Evolution of the Kapowai Caldera Complex**

9.1 Introduction 240
9.2 Caldera facies 240
Intracaldera facies association 241
Exocaldera facies association 247
9.3 Evolution of the Kapowai Caldera Complex 250
Period I 254
Period II 255
Period III 256
Period IV 257
Compositional evolution 257
9.4 Comparison with TVZ calderas 260
Dimension and morphology 261
Longevity 262
Evolution 262

**Chapter 10 Summary and Implications**

10.1 Introduction 266
10.2 Summary 266
10.3 Implications 269
10.4 Future studies 273

**References** 276

**Appendices**

I Sample catalogue 293
II Pyroclastic parameters 306
III K/Ar dating: sample preparation and K/Ar analysis 309
IV Componentry data 312
V Electron microprobe data 321
VI XRF data 332
VII ICP-MS data 339
VIII XRD traces 343

# LIST OF FIGURES

## Chapter One

Figure 1.1 Location of the Kapowai Caldera Complex (KCC) in central Coromandel Peninsula, North Island, New Zealand. 1

Figure 1.2 Regional geology of the central Coromandel Volcanic Zone (CVZ). 3

Figure 1.3 Distribution and age of Miocene - Present volcanic arcs in the North Island, New Zealand. 5

Figure 1.4 Models for the evolution of continental volcanic arcs in the North Island, New Zealand. 7

Figure 1.5 Physiography of the Kapowai Caldera Complex. Inset, location of study area in Coromandel Peninsula. 9

Figure 1.6 Rhyolite lava domes and dome complexes in the upper Oteao valley. 10

Figure 1.7 Volcanic landforms in the Slip Stream - Rangihau Stream area. 10

Figure 1.8 Landuse and access with the Kapowai Caldera Complex. 12

## Chapter Two

Figure 2.1 Landsat-3 MSS image of the Kapowai Caldera Complex and structural interpretation. 19

Figure 2.2 JERS-1 SAR image of the Kapowai Caldera Complex and structural interpretation. 21

Figure 2.3 Magnetic anomaly map of the Kapowai Caldera Complex. 23

Figure 2.4 Bouguer gravity anomaly map of the Kapowai Caldera Complex. 25

Figure 2.5 Definition of key structures associated with caldera development. 26

Figure 2.6 Location of intracaldera structures at the Kapowai Caldera Complex. 27

Figure 2.7 Eastern margin of the Kapowai Caldera Complex topographic boundary. 29

Figure 2.8 Western margin of the Kapowai Caldera Complex topographic boundary. 29

Figure 2.9 Geological map of collapse zone in the Rangihau Stream - Slip Stream area. 31

Figure 2.10 Structural boundary exposed in the Rangihau Stream - Slip Stream area. 33

Figure 2.11 Intrusive rhyolite lava in the Kapowai valley floor. 35

Figure 2.12 Shear zone 200 m west of the Haukawakawa Fault. 37

Figure 2.13 Major faults adjacent to the Kapowai Caldera Complex. 39

Figure 2.14 Temporal relationships between intracaldera structures of the Kapowai Caldera Complex. 41

Figure 2.15 Onland regional structures of the CVZ. 44

## Chapter Three

Figure 3.1 Taurahuehue Andesite lava outcrop in the floor of the Kauaeranga valley. 53

Figure 3.2 Composite sections of Taurahuehue Andesite showing internal lithologic variation. 55

Figure 3.3 Webb Creek Ignimbrite outcrops in a tributary stream of the Kauaeranga River. 57

Figure 3.4 Webb Creek Ignimbrite sections in the Kauaeranga valley. 58

Figure 3.5 Welcome Jack Rhyolite dome outcrops in the central Kapowai Caldera Complex. 59

Figure 3.6 Inclined volcaniclastic siltstone (Tarawaere Member) in the floor of the Kauaeranga valley. 61

Figure 3.7 Composite sections of Tarawaere Member (Wainora Formation) in tributaries of the Kauaeranga River. 62

Figure 3.8 Composite sections of Colorado Pyroclastics in the Kauaeranga valley. 64

Figure 3.9 Bulls Run Rhyolite exposed in the Rangihau Stream. 65

Figure 3.10 SE margin of Table Mountain, formed of thick (up to 150 m) columnar jointed Taurauikau Andesite. 66

Figure 3.11 Trig Q Ignimbrite outcrop at Trig Q. 67

Figure 3.12 Internal vertical stratigraphy of Trig Q Ignimbrite at Trig Q. 68

Figure 3.13 Geological map of the Haukawakawa Member (Wainora Formation) in the Haukawakawa Stream valley. 70

Figure 3.14 Geological map of the Haukawakawa Member (Wainora Formation) in the Slip Stream valley. 71

Figure 3.15 A, Rangihau Rhyolite dome in the central Kapowai Caldera Complex. B, Platy jointed lava of Rangihau Rhyolite in the Rangihau Stream. 73

Figure 3.16 Waiwhatawhata Rhyolite domes in the Oteao valley. 73

Figure 3.17 Sketch of outcrop exposed on western bank in the Kapowai valley floor. 75

Figure 3.18 Kokonga Rhyolite dome between Kapowai and Awahau valleys. 76

Figure 3.19 Wharepapa Rhyolite lava plug (ca. 25 m high) near Oteao Rd. 77

Figure 3.20 A, Ruahine Rhyolite forming the 4.5 km Tanehua-Ruahine ridge. B, Ruahine Rhyolite outcrop on the northern margin of the Tanehua-Ruahine ridge. 79

Figure 3.21 Juvenile components of the Oteao Ignimbrite. 80

Figure 3.22 Basal contacts of intracaldera WES-1 Ignimbrite with volcaniclastic lacustrine siltstones (Haukawakawa Member and Tarawaere Member) in the Kapowai Caldera Complex. 82

Figure 3.23 Acadia Rhyolite dome in the central Kapowai Caldera Complex. 83

Figure 3.24 Big Beetle Rhyolite dome in the central Kapowai Caldera Complex. 84

Figure 3.25 Pinnacles Rhyolite dome in the upper Kauaeranga valley. 85

Figure 3.26 Sketch of Precipice Rhyolite dike section on the western bank of the Kapowai valley floor. 87

Figure 3.27 Tauranikau Rhyolite lava outcrops, upper Kauaeranga valley. 88

Figure 3.28 A, Kauaeranga Rhyolite forming steep sided lava dome in the upper Kauaeranga valley. B, Intrusive contact between Kauaeranga Rhyolite and WES-1 Ignimbrite at the same location. 89

## Chapter Four

Figure 4.1 Occurrence of lithic fragments in Kapowai Caldera Complex ignimbrites. 92

Figure 4.2 Photomicrographs of lava lithics sampled from Kapowai Caldera Complex ignimbrites. 95

Figure 4.3 Photomicrographs of pyroclastic lithic fragments sampled from Kapowai Caldera Complex ignimbrites. 101

## Chapter Five

Figure 5.1 Intracaldera WES outcrops. 112

Figure 5.2 Proximal WES section exposed on the eastern escarpment of the Slip Stream valley. 117

Figure 5.3 Stratigraphic variation in intracaldera WES. 118

Figure 5.4 Interbedded WES-1a vitric tuffs in the Haukawakawa Stream valley and upper Kauaeranga River valley. 120

Figure 5.5 $K_2O$ vs $SiO_2$ plot of electron microprobe WES glass shard and XRF juvenile and whole rock analyses. 122

Figure 5.6 Variation in feldspar composition of pumice phenocrysts and matrix crystals in WES ignimbrites. 122

Figure 5.7 Photomicrographs of pumice rich WES-1 Ignimbrite with well defined vitroclastic texture. 124

Figure 5.8 Vapour phase altered WES-1 Ignimbrite with relict vitroclastic texture consisting of very fine cristobalite and K-feldspar. 126

Figure 5.9 Map of clastic dikes within WES-1 Ignimbrite, lower Kapowai valley. 127

Figure 5.10 Clastic dikes deforming WES-1 Ignimbrite in the lower Kapowai valley. 128

Figure 5.11 Rose diagram of clastic dike structures within WES-1 Ignimbrite in the lower Kapowai valley. 129

Figure 5.12 Detail of two major clastic dikes. 130

Figure 5.13 Maximum lithic size (ML) data (mm) for intracaldera WES ignimbrites. 132

Figure 5.14 Variation in ML(mm) and MJ(mm) vs distance for WES ignimbrites. 133

Figure 5.15 Thick (up to 400 m) WES in the upper Kapowai valley. 134

Figure 5.16 Intracaldera distribution and thickness(m) of WES-1 and WES-4 Ignimbrites. 135

Figure 5.17 Lithic concentration zones (LCZ) in WES-1 Ignimbrite. 137

Figure 5.18 Geological map of upper Rangihau valley illustrating structural boundary and possible subsidence zone associated with the WES eruption. 140

Figure 5.19 Map of exocaldera correlative WES ignimbrite and other major central CVZ ignimbrites. 144

Figure 5.20 Tukemokihi Stream, Mangapoike River section. 147

Figure 5.21 Comparison of WES glass chemistry to Tukemokihi Stream tephras. 148

Figure 5.22 Stratigraphic column of the Mahia Peninsula tephra-bearing Neogene sequence, showing the position and relative thickness of macroscopic tephra beds. 149

Figure 5.23 Mahia Peninsula tephras compared with WES ignimbrite glass shards. 150

Figure 5.24 Megascopic tephras in DSDP Leg 90 cores. 151

Figure 5.25 Comparison of WES glass shard major element chemistry with silicic Miocene-Pliocene tephras observed in DSDP Leg 90 cores. 152

Figure 5.26 CaO-FeO plot of the closest matching tephra compositions compared to WES glass shard compositions. 152

Figure 5.27 Isopach map of exocaldera correlative WES. 154

## Chapter Six

Figure 6.1 Photomicrographs of pre-caldera and caldera-related andesite lavas of the Kapowai Caldera Complex. 159

Figure 6.2 Photomicrographs of examples of the four KCC rhyolite lava groups. 165

Figure 6.3 Photomicrograph of Webb Creek Ignimbrite. 167

Figure 6.4 Photomicrograph of Trig Q Ignimbrite. 167

Figure 6.5 Photomicrograph of Manuka Ignimbrite. 168

Figure 6.6 Photomicrograph of Oteao Ignimbrite. 169

Figure 6.7 Plagioclase feldspar phenocryst and crystal compositions in volcanic units of the Kapowai Caldera Complex. 171

Figure 6.8 Pyroxene phenocryst and crystal compositions in volcanic units of the Kapowai Caldera Complex. 173

Figure 6.9 Biotite phenocryst compositions in volcanic units of the Kapowai Caldera Complex. 174

Figure 6.10 Variation in composition between titanomagnetite and ilmenite phenocrysts in Kapowai Caldera Complex andesite and rhyolite lavas. 175

Figure 6.11 Partitioning of titanomagnetite and ilmenite pairs in the system MgO-MnO-Al203 for selected rhyolite lavas of the Kapowai Caldera Complex. 176

Figure 6.12 Calculated temperatures of selected rhyolite lavas of the Kapowai Caldera Complex based upon co-existing titanomagnetite and ilmenite phenocrysts. 176

**Chapter Seven**

Figure 7.1 TAS classification of selected volcanic rocks (normalised to 100%, volatile free) from the Kapowai Caldera Complex. 182

Figure 7.2 Subdivision of Kapowai Caldera Complex volcanic rocks into low-K, medium-K and high-K types (data normalised to 100% volatile free). 183

Figure 7.3 Major element variation diagrams for selected Kapowai Caldera Complex lavas, ignimbrites and lava lithic fragments. 185

Figure 7.4 Trace element variation diagrams for selected Kapowai Caldera Complex lavas, ignimbrites and lava lithic fragments. 186

Figure 7.5 Bivariate plots of pre-caldera and caldera-related andesite lavas of the Kapowai Caldera Complex. 189

Figure 7.6 Multi-element diagram of pre-caldera and caldera-related andesite lavas of the Kapowai Caldera Complex. 190

Figure 7.7 REE variations in pre-caldera and caldera andesite lavas of the Kapowai Caldera Complex. 190

Figure 7.8 Bivariate plots of Kapowai Caldera Complex rhyolite lavas. 192

Figure 7.9 Multi-element diagram of rhyolite lavas of the Kapowai Caldera Complex. 194

Figure 7.10 Chondrite normalised REE abundances for selected rhyolite lavas of the Kapowai Caldera Complex. 195

Figure 7.11 Zr-$SiO_2$ plot of Kapowai Caldera Complex rhyolite lavas, illustrating low Zr abundances in lavas which contain the highest abundance of accessory zircon, and the most depleted MREE and HREE abundances. 197

Figure 7.12 Bivariate diagrams comparing pre-caldera and caldera-related andesitic-dacitic lavas at the Kapowai Caldera Complex with other central CVZ andesitic-dacitic lavas. 198

Figure 7.13 Comparison of group I - IV Kapowai Caldera Complex rhyolite lavas of this study with other central CVZ rhyolite lavas. 200

Figure 7.14 Highly incompatible element ratios and element bivariate diagrams for Kapowai Caldera Complex volcanic rocks. 202

Figure 7.15 Chondrite normalised REE diagram of pre-caldera and caldera-related andesite lavas compared to the range of REE abundances in Kapowai Caldera Complex rhyolite lavas. 203

Figure 7.16 Bivariate incompatible element ratio - incompatible element plots illustrating no crystal fractionation relationship between Kapowai Caldera Complex volcanic rocks. 204

Figure 7.17 Incompatible element - element ratio diagrams of Kapowai Caldera Complex volcanic rocks as a test for magma mixing. 206

Figure 7.18 MORB normalised multi-element diagram comparing average pre-caldera and caldera-related Kapowai Caldera Complex andesite compositions with Mercury Basalt from Opito Bay, Kuaotunu Peninsula 208

Figure 7.19 Multi-element diagram comparing possible basaltic parental composition (Opito Bay basalt) with average rhyolitic composition at the Kapowai Caldera Complex. 209

Figure 7.20 Plot of $K_2O$ vs Rb for Kapowai Caldera Complex andesitic and rhyolitic lavas. 209

Figure 7.21 Simplified petrogenetic model (not to scale) for the generation of intermediate and silicic magmas erupted at the Kapowai Caldera Complex. 211

## Chapter Eight

Figure 8.1 A, Welcome Jack Rhyolite dome host to the majority of epithermal Au-Ag deposits in central KCC, Slip Stream valley. B, Tailings of the Welcome Jack Mine, central Kapowai Caldera Complex 214

Figure 8.2 Hydrothermal system associated with silicic volcanism. 216

Figure 8.3 General stability fields for primary phenocrysts/crystals and alteration minerals in hydrothermally altered rocks of the Kapowai Caldera Complex. 218

Figure 8.4 Secondary mineral replacements and associated chemical changes observed for altered rocks in the Kapowai Caldera Complex. 220

Figure 8.5 Chlorite present in propylitic altered rhyolite and ignimbrite. 221

Figure 8.6 Bulk XRD trace of sericitic altered Welcome Jack Rhyolite lava. 222

Figure 8.7 XRD traces of clay minerals from hydrothermally altered rocks from the Kapowai Caldera Complex. 223

Figure 8.8 Photomicrographs of selected hydrothermally altered lava, pyroclastic and lithic fragments from the Kapowai Caldera Complex. 225

Figure 8.9 Distribution of epithermal alteration types and associated Au-Ag ore structures at the Welcome Jack Rhyolite dome, central Kapowai Caldera Complex. 227

Figure 8.10 Zones of propylitic altered welded ignimbrite in the Kapowai valley. 229

Figure 8.11 Location of propylitic alteration and jasper-infilling veinlets, upper Kauaeranga valley. 230

Figure 8.12 Outcrops of hydrothermally altered Kapowai Caldera Complex lavas and ignimbrite. 231

Figure 8.13 Summary of structural elements and epithermal alteration zones at the Kapowai Caldera Complex. 233

Figure 8.14 Calculated stability relations among common alteration minerals at the Kapowai Caldera Complex. 235

Figure 8.15 Location of active geothermal systems in the TVZ compared to the regional structural pattern and caldera structures. 236

Figure 8.16 Structural map of the Toquima caldera complex highlighting control of alteration and mineralisation by major faults, and volcanic structures. 237

Figure 8.17 Variable distribution of alteration and mineralisation at Tavua caldera, Fiji. 238

## Chapter Nine

Figure 9.1 Distribution of intracaldera facies at the Kapowai Caldera Complex. 242

**Figure 9.2** Distribution of exocaldera facies derived from the Kapowai Caldera Complex, and location of topographic highs. 249

**Figure 9.3** Simplified schematic reconstruction of the major phases in the evolution of the Kapowai Caldera Complex. 258

**Figure 9.4** Temporal variation of compositions erupted at the Kapowai Caldera Complex. 260

**Figure 9.5** Comparison of the dimension and morphology of the Kapowai Caldera Complex with known calderas of the TVZ. 261

# LIST OF TABLES


## Chapter Three

Table 3.1. Previously determined total rock K/Ar and fission track ages for Kapowai Caldera Complex units. 49

Table 3.2 New K/Ar dates for Kapowai Caldera Complex volcanic rocks determined in this study. 49

Table 3.3 Stratigraphic nomenclature for units of the Kapowai Caldera Complex. 50

Table 3.4 Summary stratigraphy of the Kapowai Caldera Complex. 51

## Chapter Four

Table 4.1 Summary of typical abundances and sizes of lithic fragments in major Kapowai Caldera Complex ignimbrites. 93

Table 4.2 Definition of lava lithic types and occurrence in Kapowai Caldera Complex ignimbrites. 96

Table 4.3 Modal mineralogy for selected rhyolite lava lithics sampled from Kapowai Caldera Complex ignimbrites. 97

Table 4.4 Modal mineralogy for selected dacite lava lithics sampled from Kapowai Caldera Complex ignimbrites. 99

Table 4.5 Modal mineralogy for selected andesite lava lithics sampled from Kapowai Caldera Complex ignimbrites. 99

Table 4.6 Correlation of lava lithic fragments in Kapowai Caldera Complex ignimbrites with exposed lavas. 100

Table 4.7 Definition of welded ignimbrite lithic types and occurrence in Kapowai Caldera Complex ignimbrites. 103

Table 4.8 Modal componentry for selected welded ignimbrite lithics sampled from Kapowai Caldera Complex ignimbrites. 103

Table 4.9 Definition of welded tuff lithic types and occurrence in Kapowai Caldera Complex ignimbrites. 105

Table 4.10 Definition of hydrothermally altered lava lithic types and occurrence in Kapowai Caldera Complex ignimbrites. 107

Table 4.11 Definition of hydrothermally altered pyroclastic lithic types and occurrence in Kapowai Caldera Complex ignimbrites. 107

## Chapter Five

Table 5.1 Lithological summary of intracaldera WES units. 115

Table 5.2 Whole rock and individual pumice clast major element (normalised to 100 %, volatile free) and trace element XRF analyses of WES-1 and WES-4 Ignimbrites. 121

Table 5.3 Feldspar phenocryst and crystal compositions in WES-1 and WES-4 Ignimbrites. 123

Table 5.4 Orthopyroxene phenocryst and crystal compositions in WES-1 Ignimbrite. 123

Table 5.5 Ilmenite compositions in WES-1 Ignimbrite. 123

Table 5.6 Modal componentry of selected WES units. 125

Table 5.7 Summary of key marker ignimbrites in the central CVZ and potential correlation to intracaldera WES defined in this study. 142

Table 5.8 Microprobe analyses of WES glass in pumice and glass shards normalised to 100% volatile free. 146

Table 5.9 Minimum intracaldera volume calculation for WES-1 and WES-4 Ignimbrites. 155

**Chapter Six**

Table 6.1 Modal mineralogy for selected pre-caldera and caldera-related andesite-dacite lavas. 160

Table 6.2 Modal mineralogy for selected Group I rhyolite lavas of the Kapowai Caldera Complex. 163

Table 6.3 Modal mineralogy for selected Group II-IV rhyolite lavas of the Kapowai Caldera Complex. 164

Table 6.4 Modal componentry for selected Kapowai Caldera Complex ignimbrites. 166

**Chapter Seven**

Table 7.1 Summary phenocryst mineralogy and geochemistry of pre-caldera and caldera-related andesitic-dacitic magma types at the Kapowai Caldera Complex. 191

Table 7.2 Summary phenocryst mineralogy and geochemistry of rhyolitic magma types at the Kapowai Caldera Complex. 197

**Chapter Eight**

Table 8.1 Production summary of Kapowai Caldera Complex gold-siliver mines. 215

**Chapter Nine**

Table 9.1 Summary of the lithology, composition, and mineralogy for intracaldera ignimbrites at the Kapowai Caldera Complex. 252

Table 9.2 Summary of the lithology, composition, volume, and age of rhyolite lavas and dikes at the Kapowai Caldera Complex. 253

**Chapter Ten**

Table 10.1 Comparison of the nature of the subduction systems and calderas within the CVZ and onland TVZ. 270

Table 10.1 Comparison of the Kapowai Caldera Complex with North American calderas/ caldera complexes. 272

**Appendix II**

Table II.1 Definition of welding terms applied to Kapowai Caldera Complex ignimbrites. 306

Table II.2 Vesicularity of juvenile clasts in Kapowai Caldera Complex pyroclastic deposits. 306

Table II.3 Definition of juvenile clast fibrousity for Kapowai Caldera Complex pyroclastic deposits. 307

Table II.4 Definition of juvenile clast lenticularity for Kapowai Caldera Complex pyroclastic deposits. 307

Table II.5 Abundance terms used to qualify relative proportions of pyroclastic components in Kapowai Caldera Complex pyroclastic deposits 307

Table II.6 Pyroclastic grain size limits 308

**Appendix III**

Table III.1. Sample numbers, location (+ grid reference) and lithology of Kapowai Caldera Complex volcanic rocks dated by the K/Ar method at the Hiruzen Research Institute, Japan, and at the Institute of Geological and Nuclear Sciences (IGNS), Lower Hutt, Wellington. 310

**Appendix IV**

Table IV.1 Component (juvenile, lithic, and crystal) size and abundance for intracaldera Kapowai Caldera Complex ignimbrites. 314

**Appendix V**

Table V.1 Electron microprobe analyses and calculated end member compositions of feldspar phenocrysts and crystals in Kapowai Caldera Complex volcanic units. 322

Table V.2 Electron microprobe analyses and calculated end member compositions of pyroxene phenocrysts and crystals in Kapowai Caldera Complex volcanic units. 325

Table V.3 Electron microprobe analyses and calculated Mg# composition of amphibole phenocrysts in Slip Rhyolite lava. 329

Table V.4 Electron microprobe analyses and calculated Mg# composition of biotite phenocrysts in Kapowai Caldera Complex volcanic units. 329

Table V.5 Electron microprobe analyses of Fe-Ti oxide phenocrysts in Kapowai Caldera Complex volcanic units. 330

**Appendix VI**

Table VI.1 Whole rock major element (normalised to 100%, volatile free) and trace element XRF analyses of pre-caldera and caldera andesite lavas of the Kapowai Caldera Complex. 333

Table VI.2 Whole rock major element (normalised to 100%, volatile free) and trace element XRF analyses of Kapowai Caldera Complex rhyolite lavas. 334

Table VI.3 Whole rock major element (normalised to 100%, volatile free) and trace element XRF analyses of lava lithic fragments sampled from Kapowai Caldera Complex ignimbrites. 336

Table VI. 4 Whole rock and juvenile major element (normalised to 100%, volatile free) and trace element XRF analyses of Kapowai Caldera Complex ignimbrites. 337

**Appendix VII**

Table VII.1 Whole rock trace element and REE analyses of group I rhyolite lavas of the Kapowai Caldera Complex determined by ICP-MS. 340

Table VII.2 Whole rock trace element and REE analyses of group II-IV rhyolite lavas of the Kapowai Caldera Complex determined by ICP-MS. 341

Table VII.3 Trace element and REE analyses of andesite lavas and ignimbrites of the Kapowai Caldera Complex determined by ICP-MS. 342

# Chapter One

# INTRODUCTION

## 1.1 Introduction

Kapowai Caldera Complex (KCC) is the largest onshore caldera volcano yet defined within the Coromandel Volcanic Zone (CVZ), in northern New Zealand. KCC is located 10 km west of Tairua, in the central Coromandel Peninsula (Figure 1.1). KCC is a 10 x 11 km, composite collapse caldera, formed during eruption of several small to large volume andesitic-rhyolitic ignimbrites. The intracaldera volcanic succession includes thick pyroclastics (ignimbrite and tuff), rhyolitic lava domes, and andesitic-dacitic lava flows and dikes. Volcanic activity spanned the period from ca. 8.5 - 4.9 Ma with quiescent periods indicated by thick (up to 50m) volcaniclastic lacustrine siltstones. Several episodes of intracaldera epithermal alteration and mineralisation are also recognised at the KCC.

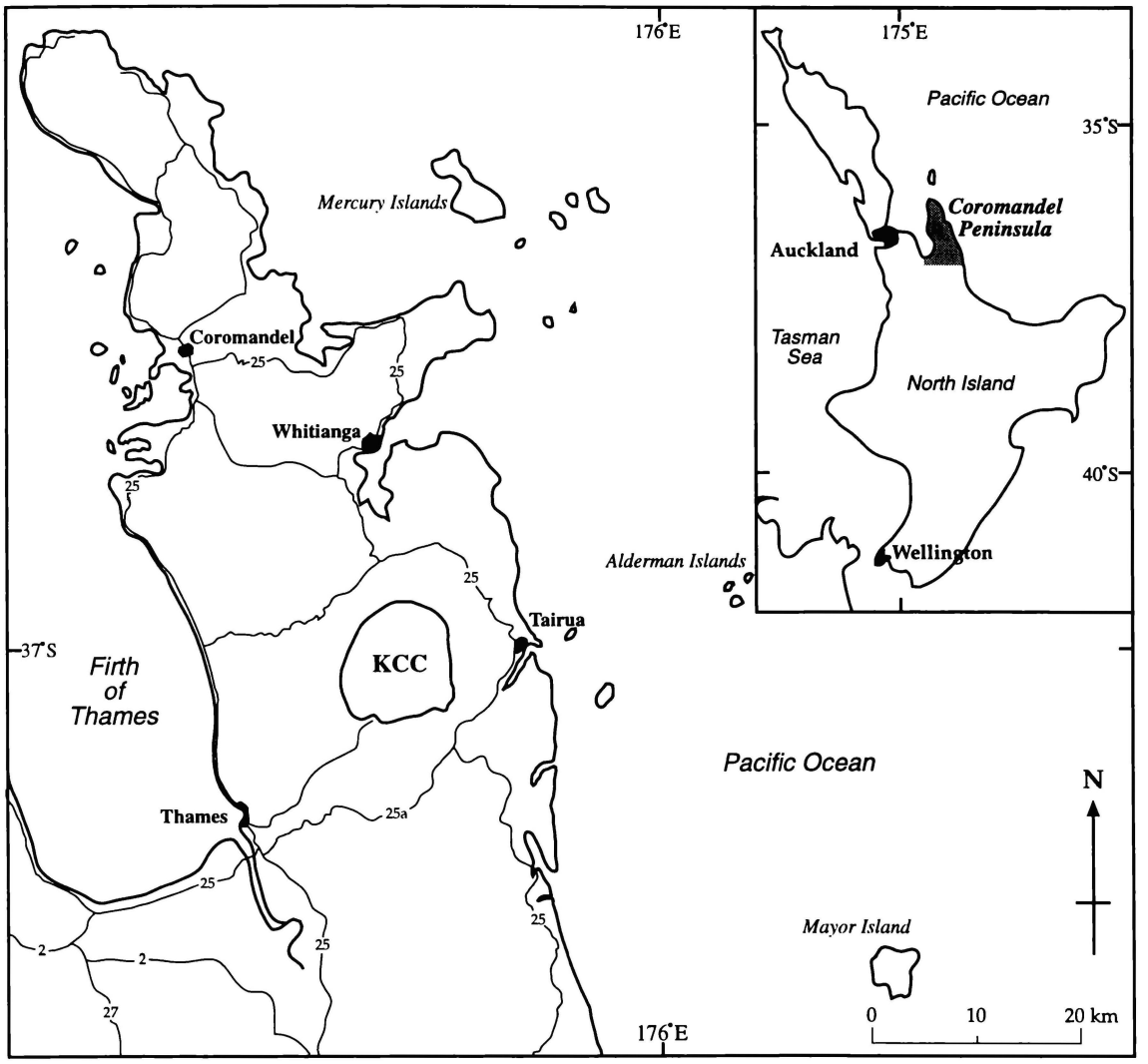


Figure 1.1 Location of the Kapowai Caldera Complex (KCC) in central Coromandel Peninsula, North Island, New Zealand.

KCC is one of several extinct Miocene-Pliocene calderas within the CVZ. CVZ calderas are significant to New Zealand volcanology, as they exhibit deeply eroded intracaldera structures and successions seldom exposed in the well studied Quaternary caldera volcanoes of the Taupo Volcanic Zone (TVZ). Aside from their volcanological significance, they are important elements in (i) the late Miocene geological development of northern New Zealand; (ii) New Zealand Neogene tephrostratigraphy; and (iii) modelling epithermal systems associated with New Zealand silicic calderas. Detailed studies of CVZ caldera volcanoes however, are limited (Briggs and Fulton, 1990).

The fundamental aim of this research is to elucidate the structural and petrological evolution of the KCC. To achieve this, geological mapping and sampling was undertaken within and on the margins of the caldera. Samples collected were analysed for petrographic, geochemical, mineral and radiometric age data, which are presented and discussed in this thesis.

## 1.2 Geological setting

KCC occurs in the central CVZ, which is a major volcanic province in north-eastern North Island, New Zealand. The CVZ extends from Great Barrier Island 12 km north of Coromandel Peninsula to Te Puke in the south, and was active from the mid Miocene until late Pliocene (Skinner, 1986). The zone is characterised by calc-alkaline (andesite-dacite-rhyolite) and mixed tholeiitic-high alumina/calc-alkaline (basalt) effusive and explosive volcanism (Adams et al., 1994).

Although dominated by Neogene volcanic rocks, the geological succession in the CVZ, also includes Mesozoic basement rocks, late Tertiary-early Neogene marine sedimentary rocks and Quaternary sediments (Figure 1.2). The oldest rocks in the CVZ are late Jurassic conglomerates, greywackes and argillites (Manaia Hill Group) which have been strongly folded and faulted during the Rangitata Orogeny (Kear, 1955; Skinner, 1972). Unconformably overlying these basement rocks are Oligocene limestones, calcareous siltstones, carbonaceous sandstones, and coal seams of the Torehina Formation, and early Miocene conglomerates, sandstones, and siltstones of the Colville Formation (Kear, 1955; Skinner, 1969). These units only outcrop in small areas of northern CVZ (Skinner, 1976).

Volcanism began in the early Miocene (ca. 18 Ma) in northern CVZ and continued until the late Pliocene (ca.2.2 Ma) in southern CVZ (Adams et al., 1994; Takagi, 1995; Briggs et al., 1996). Compositions of erupted rocks have varied with time, and there are three general trends:
(1) Western CVZ is dominated by andesite-dacite lavas and breccias (Coromandel Group) erupted from ca. 18-9 Ma (Skinner, 1976; Adams, et al., 1994).

(2) More evolved dacite-rhyolite magmas (Whitianga Group) were erupted in eastern CVZ from ca. 10-2.5 Ma (Adams et al., 1994; Takagi, 1995).

(3) Mafic magmas were erupted from ca. 9-5 Ma (Mercury Basalts Subgroup) and are also restricted to eastern CVZ (Skinner, 1976, Adams et al., 1994).

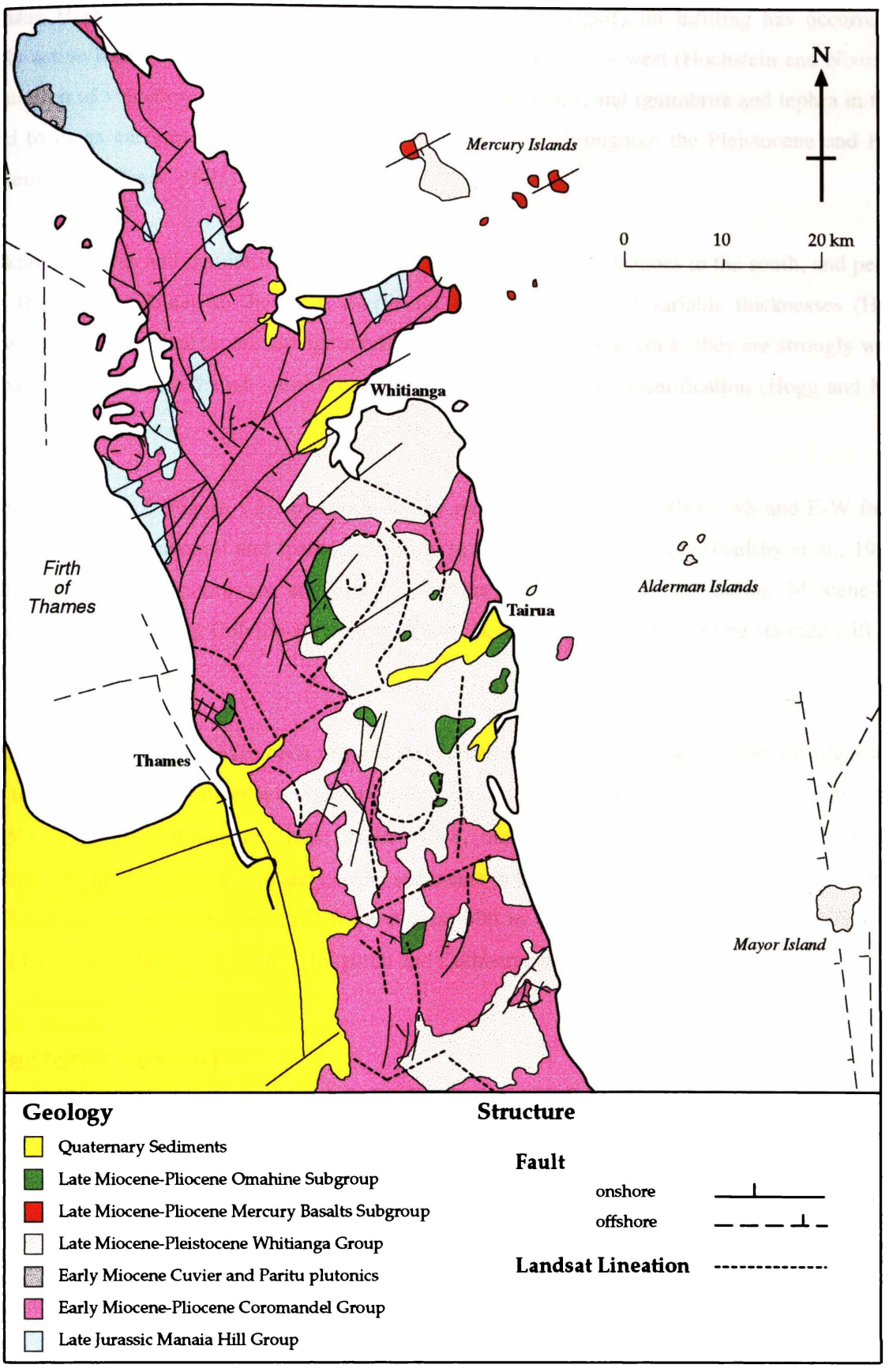


Figure 1.2 Regional geology of the central Coromandel Volcanic Zone (CVZ). Modified from Skinner (1995).

Overlying the Mesozoic-Tertiary succession are Quaternary sediments, and thin distal tephras and ignimbrites. Accumulation of alluvium and/or coastal dune sands has occurred in most low-lying coastal areas in eastern Coromandel Peninsula, with significant areas associated with the Whitianga, Whangapoua, and Tairua Harbours (Abrahamson, 1987). However, the most significant infilling has occurred in the presently active Hauraki Rift (see below) which borders the CVZ to the west (Hochstein and Nixon, 1979). Accumulation of volcanogenic alluvium, marine and estuarine muds, and ignimbrite and tephra in the rift is believed to be as early as 7 Ma, and has occurred periodically throughout the Pleistocene and Holocene (Hochstein and Ballance, 1993).

Calc-alkaline tephras and ignimbrites derived from Quaternary TVZ volcanoes to the south, and peralkaline tephras from Mayor Island to the west, overlie the CVZ succession at variable thicknesses (Hogg and McCraw, 1983). Individual tephra and ignimbrites are difficult to distinguish as they are strongly weathered and mixed within soils, although some are distinctive enough to allow identification (Hogg and McCraw, 1983).

Structures in the CVZ (Figure 1.2) are dominated by major NE faults, but NNW, NS and E-W faults also occur, implying both temporal and spatial variability in the regional stress field (Gadsby et al., 1990). The controls on this fault pattern are suggested to be the plate motion vector during Miocene-Pliocene subduction, the NE trending Colville-Havre trough system, and the active NS trending Hauraki Rift (Gadsby et al., 1990).

Numerous arcuate structures have been mapped throughout the CVZ, and some of these are suggested to be related to extinct caldera volcanoes (Skinner, 1986; Belliss and Christie, 1994). Post-Neogene NE tilting (ca. 3-5°) is common throughout most of the CVZ, but is exemplified best by the Plio-Pleistocene succession of ignimbrites, alluvium and coastal sediments in the southern sector (Kamp, 1988; Briggs et al., 1996). Most of this tilting has resulted from at least 400 m of eastward uplift along the NNW-trending Hauraki Fault since the late Miocene (Houghton and Cuthbertson, 1989).

## 1.3 Tectonic setting

Ballance (1976) defined two volcanic arcs in the Coromandel Peninsula; Coromandel Arc to the west consisting solely of andesite/dacite volcanism; and Whitianga Arc to the east, where volcanism is segregated between a central, silicic-dominated region, and northern and southern regions, where mafic volcanism dominates. Skinner (1986) defined the CVZ as the combination of these two arcs and the whole CVZ as the central sub-aerial sector of the larger Hauraki Volcanic Region (HVR). The HVR includes the Hauraki Rift, a young, active continental rift adjacent to the western CVZ (Hochstein and Nixon, 1979), and the Kiwitahi Volcanic Zone (KVZ), a belt of Miocene-Pliocene low-K andesite volcanoes further to the west (Cole, 1978; Black et al., 1992).

A continental arc setting for the CVZ was inferred from the calc-alkaline basaltic/low-K andesitic/dacitic/rhyolitic magma association and the linear extent of the eruptives (Ballance, 1976). CVZ is one of three continental volcanic arcs in northern North Island, active from the Miocene to Pliocene (Figure 1.3). The two northern arcs, Waitakere Arc (western Northland Peninsula) and Northland Arc (eastern Northland Peninsula) have a similar linear extent and age (22 - 16 Ma) (Hayward, 1979; Hayward, 1993; Black et al., 1995). Hayward (1993) and Black et al. (1995) suggest that CVZ volcanism is an extension of the Northland Arc.

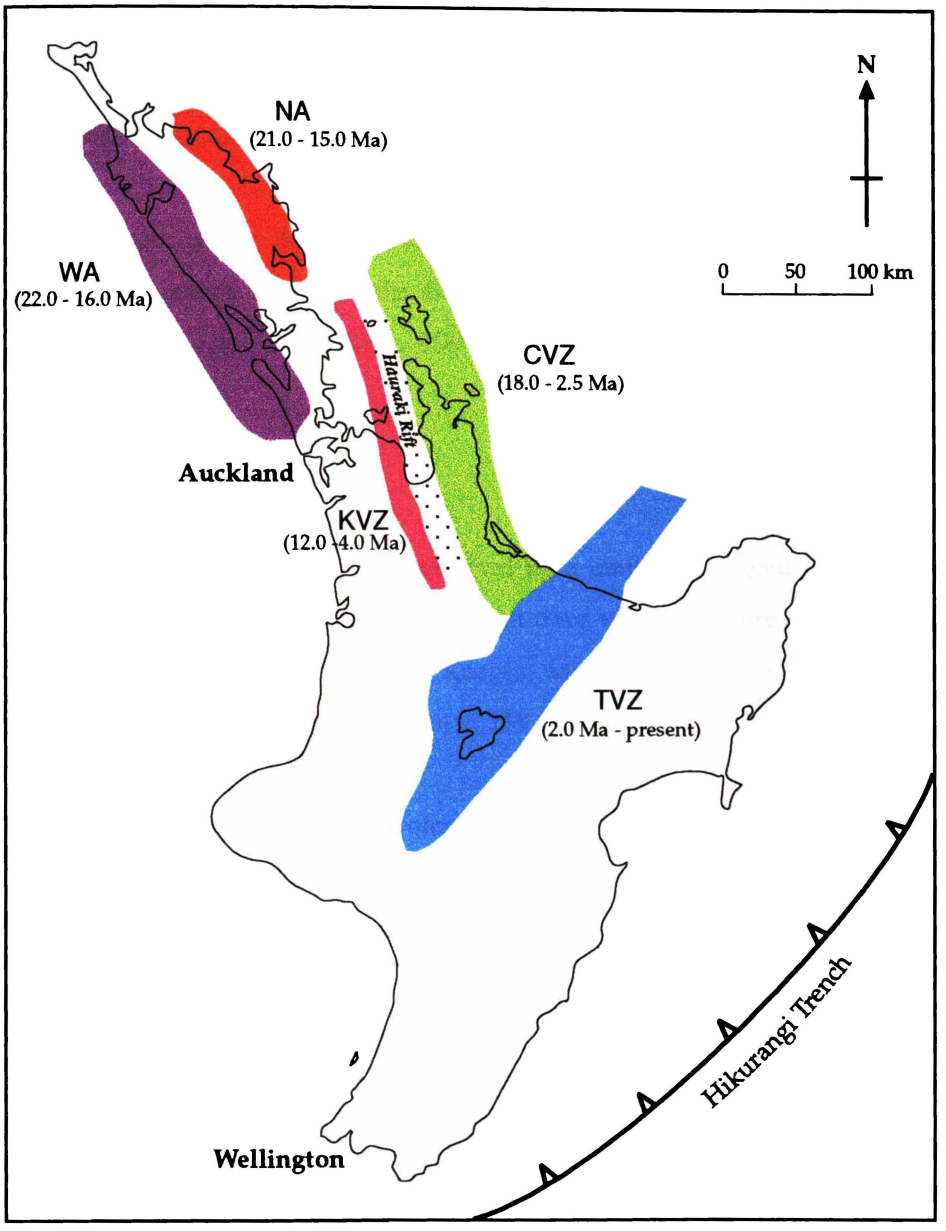


Figure 1.3 Distribution and age of Miocene-Present volcanic arcs in the North Island, New Zealand. Modified from Skinner (1986) and Adams, et al. (1994). WA (Waitakere Arc); NA (Northland Arc); KVZ (Kiwitahi Volcanic Zone); CVZ (Coromandel Volcanic Zone); TVZ (Taupo Volcanic Zone).

Two models (Figure 1.4) describing the initiation and evolution of the North Island volcanic arcs have been developed. Ballance (1976), Cole (1979), Hayward (1979), and Cole and Lewis (1981) regarded the Waitakere Arc, Northland Arc and CVZ orientations to be NW and related the volcanism to a southwest-

plunging subduction system. The change to the present-day NE orientation seen in the TVZ is considered to be partly due to a change in the position of the shift pole (Walcott, 1984) and partly to dextral movement along the North Island Shear Belt and Vening Meinesz Fracture Zone, together with sea-floor spreading in the South Fiji Basin (36 - 26 Ma) and Havre Trough (4 Ma - present) (Cole, 1986).

A second model was suggested by Brothers (1984) and further developed by Kamp (1984) who proposed that before the Miocene, underplating of the North Island by the Pacific plate involved rapid shallow subduction (not accompanied by volcanism) for a distance of 600 km from the NNE orientated subduction zone to the Northland Peninsula. Progressive steepening of the subduction zone (from 10 to 50°) created "time-lines" of volcanoes that become progressively younger to the SE as the critical depth (80 - 100 km) for production of andesitic magma moved trenchwards.

These two models have been widely debated, with neither fully accepted (Ballance, 1988). New radiometric and biostratigraphic data appears to favour the Ballance (and others) model (Hayward, 1993). Recently, additional theories have been proposed (Kear, 1994; Herzer, 1995), based in part upon the two earlier models.

## 1.4 Physiography

KCC covers an area of ca. 120 km$^2$. It is characterised by a complex, rugged bushclad terrain including numerous escarpments, ridges, steep and rolling hills and river valleys (Figure 1.5). The western sector of the KCC lies within the N-S trending Coromandel Ranges, where elevations range up to 846 m. The eastern sector has maximum elevations ranging from 227 m to 759 m.

Most of the landforms within the KCC have a volcanic origin. Silicic lavas have produced several landform types including: (i) steeply sloped (50-75° slope), domical lava domes. Examples occur in the Rangihau (e.g. Rangihau dome, Acadia dome, Big Beetle dome), Kauaeranga (e.g. Kauaeranga dome), and Oteao (Waiwhatawhata dome) valleys (Figure 1.6); (ii) near vertically sloped, vent plugs, which occur near Oteao Road (Wharepapa plug) and in the upper Kauaeranga valley (Tauranikau plug); (iii) rhyolite lava dome complexes, consisting of several individual lava domes. Examples of these occur in the Rangihau (e.g. Bulls Run dome complex) and Kauaeranga (e.g. Camp dome complex) valleys; and (iv) linear silicic lava dome complexes. Examples include the ca. 4 km long, Tanehua-Ruahine ridge forming the eastern ridge of the Kapowai valley, and the ca. 1.5 km Pinnacles ridge in the upper Kauaeranga valley.

Significant landforms produced by intermediate lavas are not common. Two exceptions are: (i) the ca. 7 km$^2$ Waiwawa plateau (which includes Table Mountain) formed by the eruption of sheet lava flows and intrusions within a major depression, and (ii) the ca. 2.5 km Haukawakawa ridge formed by at least two andesitic volcanoes, erupted along a N-S structural trend.

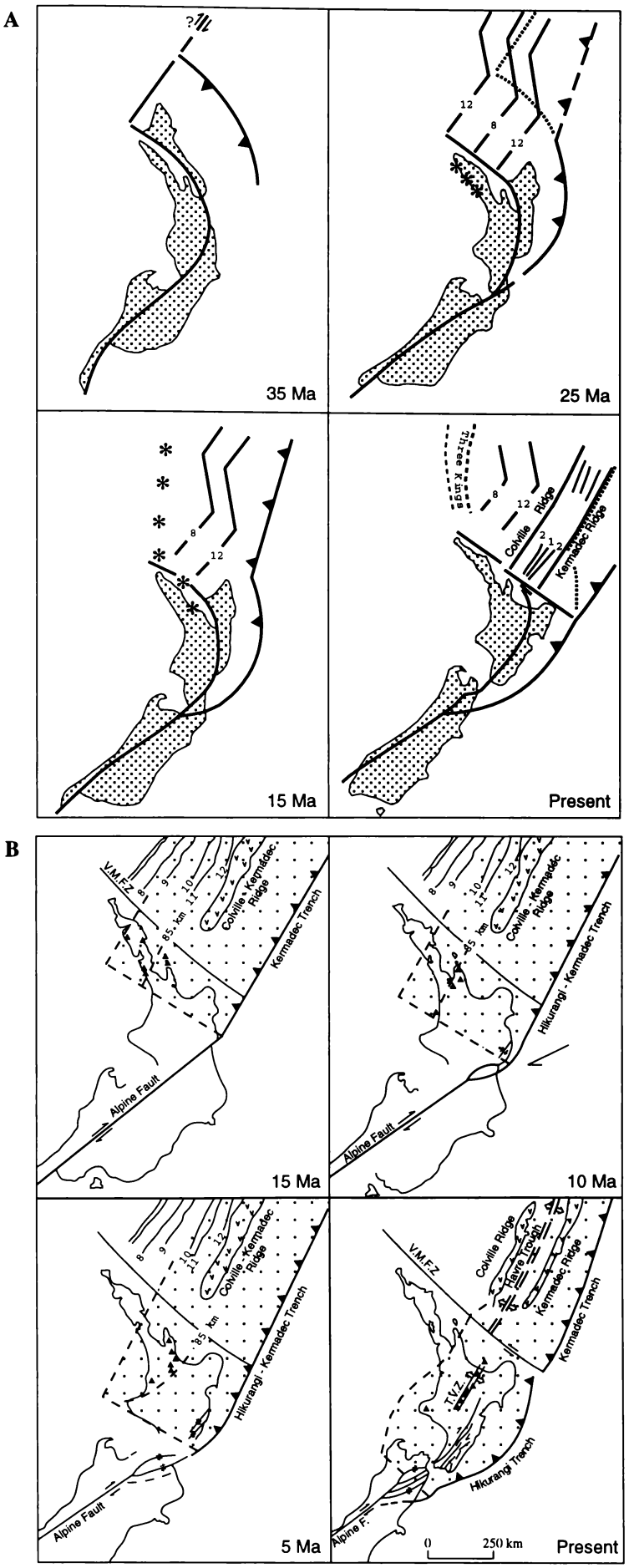


Figure 1.4 Models for the evolution of continental volcanic arcs in the North Island, New Zealand. A - Ballance (1976); B - Kamp (1984).

Explosive volcanism had a major influence on the KCC landscape. Thick, intracaldera ignimbrites form several near-horizontal plateaux. Examples occur between Oteao and Slip Streams (inclined ca. 10° NNE), between Oteao and Rangihau valleys, on the southern margin of the Haukawakawa ridge, and on the western margin of the Tanehua-Ruahine ridge. Plateaux presently cover small areas (< 1.5 $km^2$), but are likely to have been more extensive and continuous. Most are dissected by fluvial systems.

Aside from ignimbrite plateaux, explosive volcanism may be associated with several locally depressed areas. A subcircular depression covering ca. 3 $km^2$ occurs in the Rangihau valley (Figure 1.7), and in the lower Kapowai valley a ca. 2 $km^2$ depression occurs. These two areas may relate to structural collapse zones, and as such will be further discussed in relation to caldera structures (Chapter Two).

Climate is a significant control on landscape modification. High annual rainfalls (3663 mm mean annual rainfall: recorded at the Pinnacles (T12/511586)) and warm temperatures (14.9°C mean annual temperature, recorded at Thames), in the Coromandel Peninsula can lead to locally high erosion rates (Sources: Environment Waikato; National Institute of Water and Atmospheric Research). Significantly, the warm, wet climate has also resulted in a deep weathering profile across most of the Coromandel Peninsula.

Drainage patterns developed in the KCC are considered to be generally mature, given that volcanism ceased at ca. 5 Ma. The four major fluvial systems developed within the Kapowai, Rangihau, Waiwawa, and Kauaeranga catchments, each reflect mechanical differences in the geological substrate. Hard, unaltered andesite and rhyolite lavas are not easily eroded and so only minor tributaries are developed where these lithologies form the bedrock. Conversely major valley and tributary systems (e.g. Kapowai valley) are formed where the bedrock consists of weakly welded pyroclastics (ignimbrite and tuff).

Aside from lithological influences, fluvial systems also reflect other more localised controls. These include structural features such as faults (i.e. Oteao Stream, Kapowai River and Waiwawa River), zones of hydrothermal alteration of the bedrock (i.e. Kapowai and Waiwawa Rivers) and landslides.

Slope failures are common in hydrothermally altered rocks, and occur on a variety of scales from shallow soil slips to translational slides (e.g. The Big Slip, Slip Stream valley), and large scale rotational slides. Rock falls and slopes failures occurring in unaltered rocks are mostly attributable to high slope angles (e.g. Table Mountain, upper Kauaeranga valley). These features are common not only within the KCC, but throughout the Coromandel Peninsula (Skinner, 1995; Bassett, 1998; Simpson, 1999).

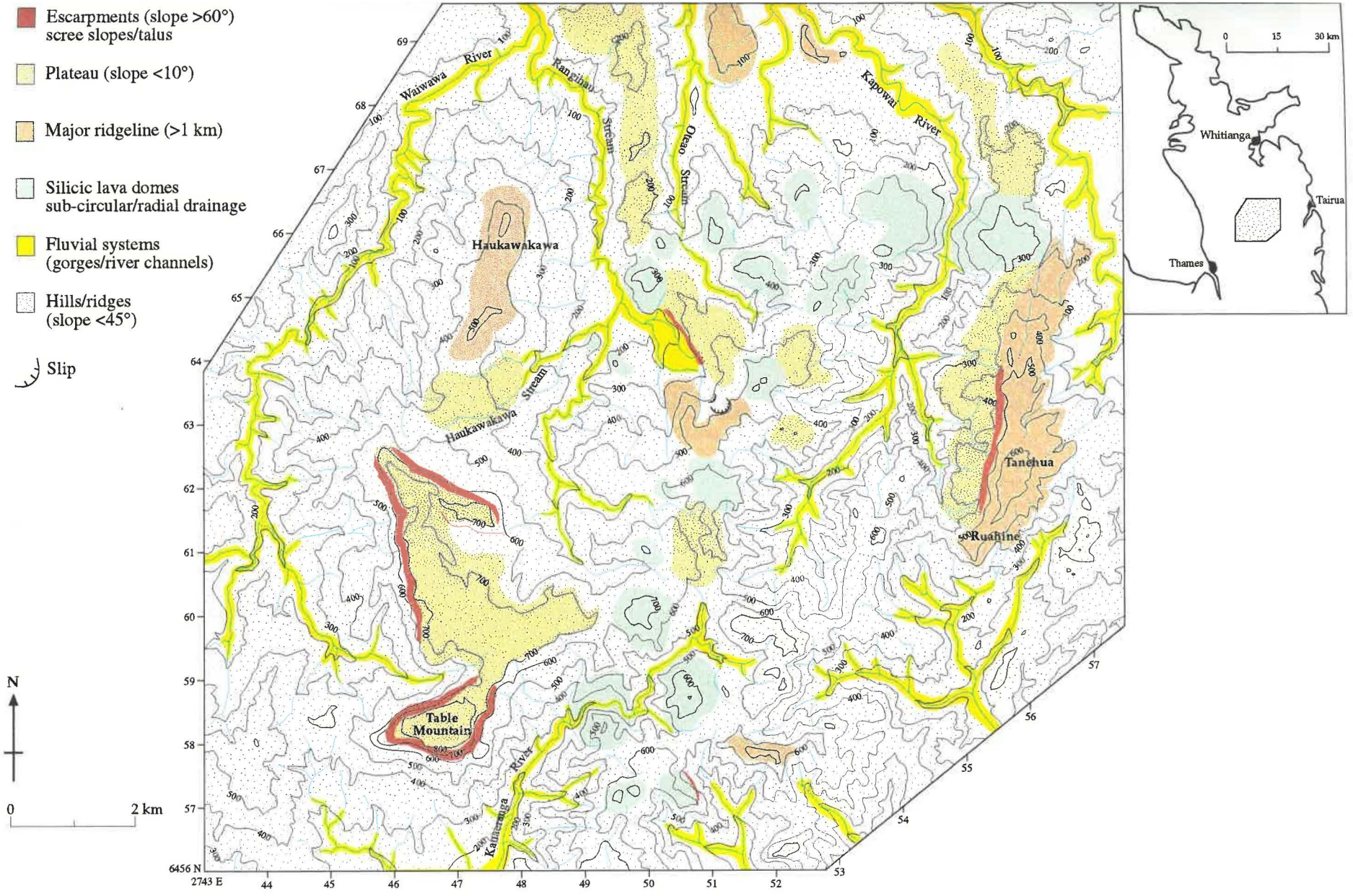


Figure 1.5 Physiography of the Kapowai Caldera Complex. Inset, location of study area in the Coromandel Peninsula.

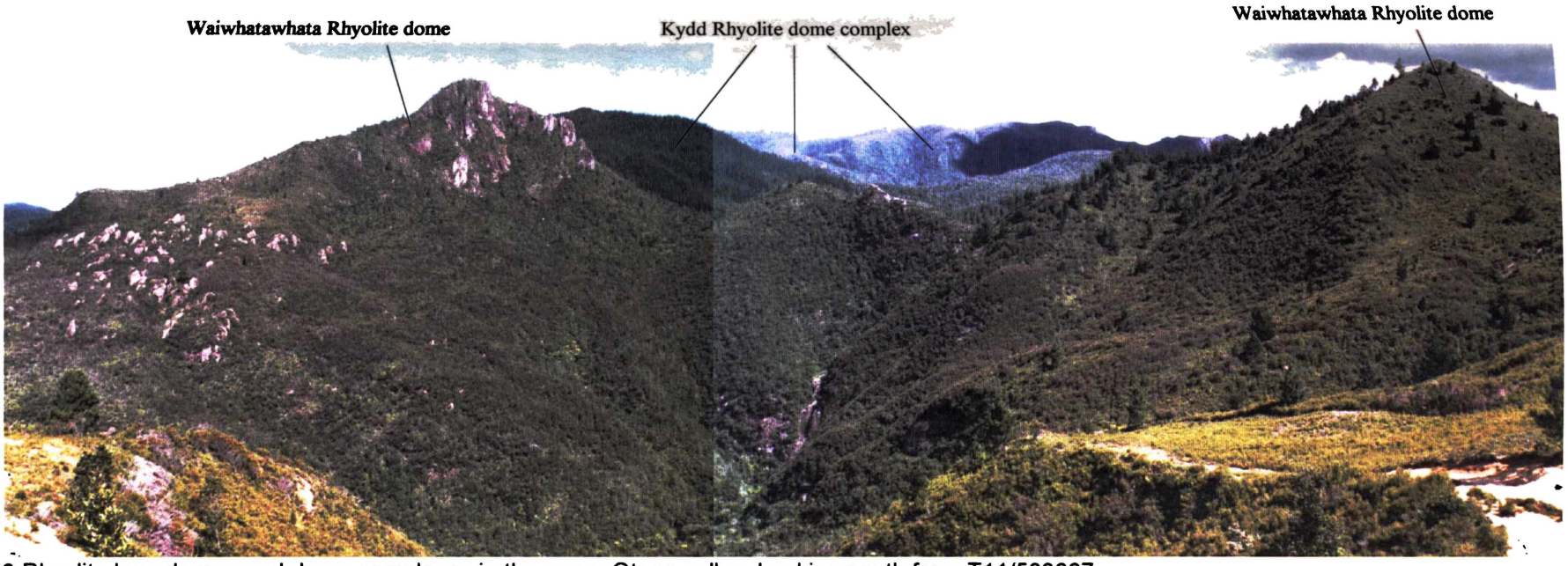


Figure 1.6 Rhyolite lava domes and dome complexes in the upper Oteao valley. Looking south from T11/503667.

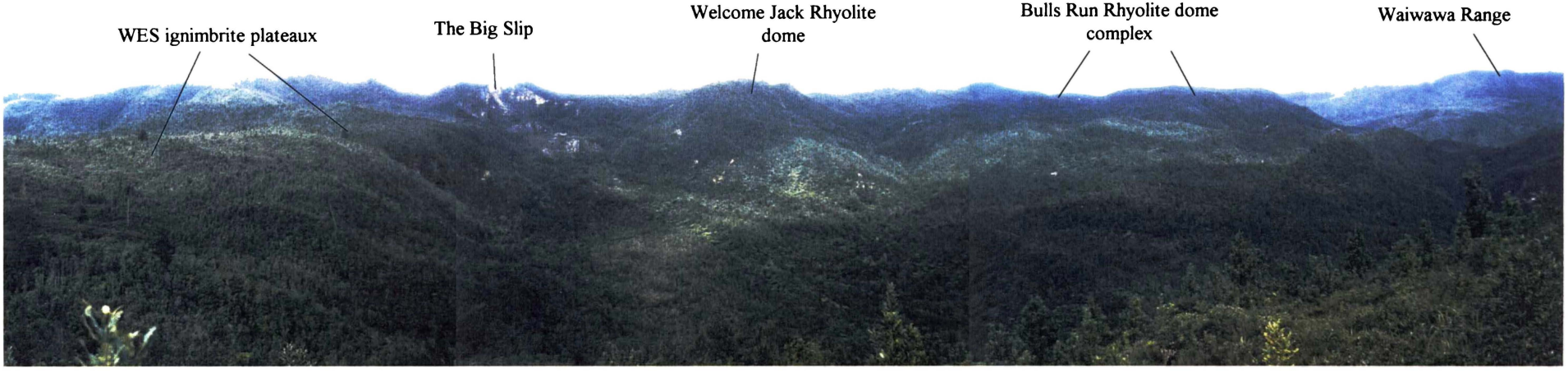


Figure 1.7 Volcanic landforms in the Slip Stream - Rangihau Stream area. View south from Rangihau Rhyolite dome (T11/503653). Note depression in centre foreground bounded by escarpment on its western margin.

## 1.5 Landuse and access

Coromandel Forest Park (CFP) consisting of native species, dominates the present landuse of the KCC (Figure 1.8). Within the KCC, the forest is regenerating, following extensive logging of podocarp species (primarily *Agathis australis*) during the late 19th to early 20th centuries (Reid, 1953; Hayward, 1978). CFP in the KCC area is significant in that it supports several rare fauna (*Apteryx australis, Callaeas cinerea, Calcites lucidus, Nestor meridionalis, Leiopelma hochstetteri*), and rare, mature podocarp populations (*Nothofagus truncata, Agathis australis, Podocarpus totara*). Two ecological areas in the Waiwawa and Kapowai River headwaters have been established to preserve and enhance the survivability of these rare species (Burns, 1984; Burns, 1985).

Private pastoral land, lifestyle blocks, and a private exotic forestry block occur in the northern sector of the KCC and together total less then 1/4 of the total area.

Access into the KCC area is via Kauaeranga Valley Road in the south, and Rangihau Road and Kapowai Road in the north. Marked tramping tracks, private forestry roads, former mine and kauri packtracks, and other unmarked tracks were used to gain further access (Figure 1.8).

## 1.6 Research objectives and thesis outline

The main aim of this research is to elucidate the structural and volcanological evolution of the KCC. To achieve this, several objectives have been established. These are to:

(i) define the caldera structure and describe intracaldera structural elements,

(ii) detail the intracaldera stratigraphy,

(ii) document the physical characteristics of the final caldera collapse event; Wharepapa Eruptive Sequence (WES),

(iii) establish geochemical characteristics for KCC derived volcanic rocks,

(iv) describe intracaldera epithermal alteration patterns, and

(v) develop a caldera facies model for the KCC combining structural, stratigraphic and geochemical data.

From 1996 to 1999, field sampling and mapping was undertaken within and adjacent to the KCC. Geochemical and mineralogical analysis of selected samples was then completed using facilities in the Department of Earth Sciences, University of Waikato; Department of Geological Sciences, University of Canterbury; Analytical Facility, Victoria University of Wellington; and Monash University, Australia. Synthesis and interpretation of the data obtained is presented in this thesis, which is written in a chapter format.

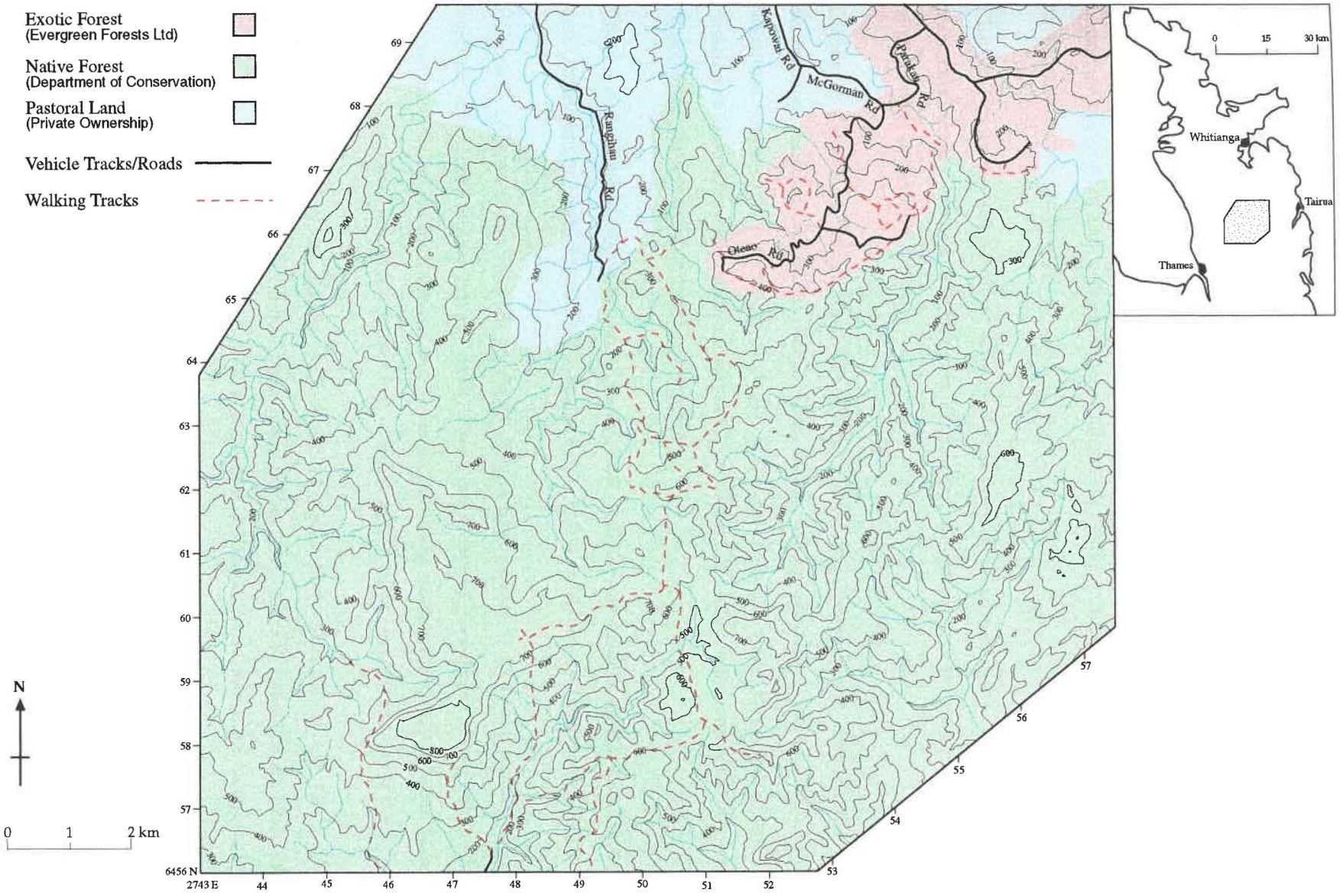


Figure 1.8. Landuse and access within the Kapowai Caldera Complex.

Chapter 2 describes evidence for the existence of the KCC, which includes remote sensing, geophysical and geological analysis. Definition of intracaldera structures, including structural collapse zones and intrusives is also presented here. The influence of the regional structural pattern on the development of the KCC is also discussed.

Chapters 3 presents the pre-caldera and caldera stratigraphy of the KCC. Stratigraphy presented here revises previous work in light of 16 new K/Ar ages, coupled with a more detailed field stratigraphy. There is also an important recognition that several caldera collapse cycles have occurred at the KCC, rather than a single event as previously inferred.

Chapter 4 describes the lithology and correlation of lithic fragments in KCC pyroclastic deposits. Lithic fragments are used to assist in defining the intracaldera stratigraphy and to constrain the physical parameters of pyroclastic deposits.

Chapter 5 focuses on the physical volcanology of the largest pyroclastic eruption from the KCC, the Wharepapa Eruptive Sequence (WES). Description of the eruptive sequence, lithology, and spatial variations are given here. Constraints are placed on source vent locations and emplacement mechanisms of constituent ignimbrites. Exocaldera correlations to central CVZ ignimbrites, and distal co-ignimbrite tephras (based upon glass shard chemistry) is attempted.

Chapter 6 presents petrographic and mineralogical data for pre-caldera and caldera units. Petrographic descriptions are provided for all KCC volcanic rocks, and mineral chemistry is presented for selected units.

Chapter 7 documents the volcanic geochemistry and petrogenesis of KCC magmas. 72 XRF and 26 REE analyses of selected pre-caldera and caldera units are presented. Geochemical data are used to (i) classify the volcanic rocks; (ii) illustrate variation in major and trace element chemistry between erupted rocks; and (iii) place constraints on the petrogenesis of andesitic and rhyolitic magmas erupted at the KCC.

Chapter 8 documents the pattern and nature of epithermal alteration at the KCC. Descriptions of mineralogical changes in silicic host rocks using petrographic and XRD analysis are presented. The timing of alteration, and the influence of caldera and regional structures in controlling epithermal systems at the KCC are discussed.

Chapter 9 presents a facies model for the KCC. This model integrates structural, stratigraphic, and petrological data presented in earlier chapters into a caldera facies framework. The geological and geochemical evolution of the KCC is also discussed.

Chapter 10 presents the conclusions of this study. Key advancements and implications of this research, and suggestions for future studies are discussed.

## 1.7 Previous work

Early geological studies of the Coromandel Peninsula were motivated by the discovery of precious metal deposits during the mid-late 19th Century. These studies documented ore occurrences and suggested possible origins. Early in the 20th Century, non-economic research was undertaken which included petrographic studies of the rocks, including several from the KCC area (Sollas and McKay, 1905).

It was not until geological surveys began in the early 1900's, incorporating broad stratigraphic subdivisions and geological mapping, that a general understanding of the regional geology emerged. Surveys by Fraser (1910) and Bell and Fraser (1912) covered the Whitianga-Tairua-Thames area which includes the KCC. These surveys described the geology and included observations of the actively mined ores in the central KCC.

Following closure of mines throughout the peninsula, geological studies diminished. Regional geological mapping began again with publication of the 1:250 000 Auckland geology map (Schofield, 1967), although for most of the Coromandel region, the geology was based on earlier geological surveys. A revision of regional CVZ geology was initiated by Skinner (1976) mapping in northern Coromandel. This was extended south with two geological maps covering the Coromandel Harbour (Skinner, 1993) and Mercury Bay (Skinner, 1995) areas at 1: 50 000. These two maps combined, cover two thirds of the KCC area. The geology of the Waihi area has also recently been updated (Brathwaite and Christie, 1996). Further mapping at this scale is in progress for the Whangamata-Thames area (R. Brathwaite pers comm., 1998).

Localised geological research has been undertaken by University of Auckland and University of Waikato graduate students. University of Auckland students have generally focused on epithermal and porphyry type ore deposits, and geophysical studies in western and northern Coromandel Peninsula. University of Waikato students have mapped areas of silicic volcanic geology, and local hydrothermal alteration centres in eastern parts of the peninsula. Student theses relevant to the KCC are Hayward (1971), who mapped the geology of the Table Mountain area, and Moore (1976), Adams (1992), McGunnigle (1995), Karl (1996), and Guay (1999) who mapped areas adjacent to the northern, eastern, and southeastern topographic boundary.

Recent precious metal prospecting in the Coromandel region by exploration companies, has focused on re-examining known ore bodies using new technologies, and exploration for new ores. As a result, open file exploration reports are available for various ore deposits in the CVZ. The central KCC has been actively explored by numerous companies, and several mining reports documenting the nature of the ore and host rock are available (e.g. Couper, 1982; Robson, et al. 1994). Regional aeromagnetic surveys of the CVZ have also been completed (Rabone, 1991).

Detailed studies of CVZ caldera volcanoes are limited. Briggs and Fulton (1990) described a complexly faulted, volcanic - lacustrine section exposed along the Whiritoa coastline (eastern Coromandel Peninsula).

Applying a caldera facies approach, they suggested that this represented a section through the intracaldera component of a caldera (Tunaiti caldera). Briggs et al. (1998) presented geophysical and structural evidence for the existence of a caldera in the Whitianga area, and described the petrology of ignimbrites and lavas erupted from the caldera. Bromley and Brathwaite (1991) presented a detailed geophysical survey of the Waihi Basin and concluded that its subsurface structure resembled that of a caldera-derived depression. Rabone (1991) used aeromagnetic data to infer the presence of several caldera structures throughout the CVZ.

# Chapter Two

# CALDERA RECOGNITION AND INTRACALDERA STRUCTURES

## 2.1 Introduction

Caldera volcanoes significantly modify the geological and geophysical character of the local upper crust. Modification includes the development of large diameter (up to 60 km) sub-circular collapse structures, and deposition of large volumes (up to > 3000 $km^3$) of pyroclastic material (ignimbrite and tephra) onto the adjacent landscape (Lipman, 1984). Recognition of extinct caldera volcanoes relies upon identifying these and other features using a combination of geological, geophysical and remote sensing parameters (Briggs and Fulton, 1990; Nairn et al., 1994; Campos-Enriquiz and Garduno-Monroy, 1995). The first part of this chapter provides evidence for the existence of the KCC using this integrated approach.

Structures associated with caldera volcanoes are varied and unique for each volcano. Common to all, is the topographic boundary or caldera rim. Intracaldera structures formed within the margins of this boundary (i.e. caldera floor) can include structural collapse zones, pre- and post-collapse volcanism, and intrusive and resurgent structures (Lipman, 1984). The topographic boundary and intracaldera structures of the KCC are defined and discussed in the second part of this chapter.

## 2.2 Recognition of the Kapowai Caldera Complex

Skinner (1983) first suggested that a caldera volcano existed within an area centred on the Rangihau and Kapowai Rivers, in central Coromandel Peninsula. This was based upon a sub-circular lineation visible on a Landsat image (Pel-328), and the presence of lithologies (rhyolitic ignimbrites and lava domes) typically associated with caldera volcanoes (see below). Skinner (1983) defined the margins of the caldera as extending west to the Waiwawa and Ounora Rivers, north to Whitianga estuary and south to Hikuai-Pauanui for a total diameter of 25 km. Skinner (1993, 1995) reaffirmed these dimensions, but also defined an inner rhyolite dome ring which had a diameter of 10 km.

This section re-evaluates and provides additional evidence for the presence of a caldera in the Rangihau-Kapowai-Kauaeranga area using a combination of remote sensing, geophysical and geological data. Evidence is given to indicate that the caldera has had several collapse episodes, and hence the term caldera complex is used (Lipman, 1975; Cole et al., 1998).

## Remote Sensing

Two remote sensing images covering the KCC were obtained from the Image Processing Group, Landcare Research NZ Ltd. These images are used to define the caldera boundary and indicate possible intracaldera structures. Structures adjacent to the KCC are also defined by these images.

### *MSS Image*

Multi-Spectral Scanner (MSS) images are useful for delineating major structures over regional areas (Cochrane and Tianfeng, 1983). The MSS records only the surficial electromagnetic radiation so that any structures indicated must have some surface manifestation (Christie et al., 1994). A MSS image covering the Coromandel region was taken by the Landsat-3 satellite on the 21 June 1981. This image has been used extensively to map structures throughout the CVZ (Skinner, 1993; Skinner, 1995; Christie et al., 1994).

The most significant feature on the entire image is a 10 km x 12 km (oriented N-S), subcircular feature located 10 km west of Tairua, in the central Coromandel Peninsula (Figure 2.1). The feature is continuous and clearly indicated, except for the NW margin, where it is slightly obscured. Aside from a marked bulge in the SE margin and a distorted southern margin, the lineation is well curved. This feature is interpreted as the caldera rim or topographic boundary of the KCC (see below).

Within this subcircular feature, are several linear, curvilinear and circular features. These vary in strike and length, but are all interpreted as faults. A major lineation striking NNE, extends for ca. 8.25 km through the Kapowai valley and crosses the southern topographic boundary. This lineation parallels the regional structural trend, so it most likely relates to the regional pattern, rather than to the caldera. Two continuous, curvilinear features extending up to 9.5 km, strike NW-SE and cross the centre of the caldera. As these trend independently of the regional pattern, and do not extend outside the caldera, they are most likely related to caldera collapse events.

A ca. 4.5 km diameter circular feature occurs in the NE sector. This is discontinuous and ends at the NNE striking linear feature (described above) and the northern topographic boundary. A second arcuate feature with ca. 4.2 km diameter, occurs in the W sector, centred on the NE margin of the Waiwawa Range. This may form the southern margin of a larger oblong feature trending N-S. These circular features are interpreted as defining the structural boundary of caldera collapse zones, and are relatively old, as the collapse zones have been infilled by younger pyroclastics and/or lavas.

Several NNE and NE-trending lineations occur east of the eastern topographic boundary. These lineations are interpreted as faults associated with the dominant regional structural trend and are not related to caldera development (Skinner, 1995).

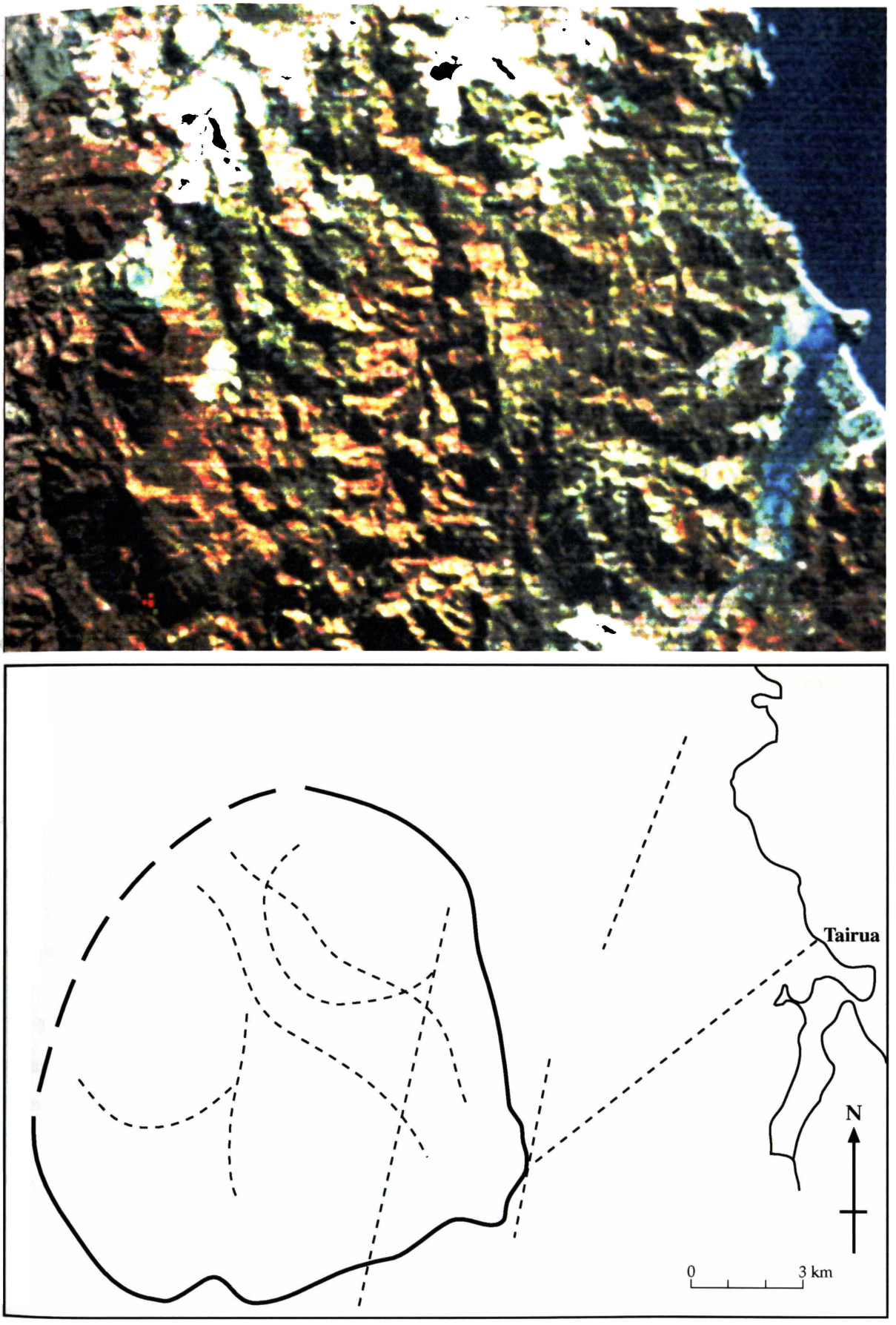


Figure 2.1 Landsat MSS image of the Kapowai Caldera Complex and structural interpretation. Topographic boundary is bolded. Lineations (faults, collapse boundaries) are dashed. Image courtesy of Landcare Research Ltd.

*SAR Image*

Radar generated remote sensing images have benefits over MSS, in that it penetrates a proportion of the vegetation canopy, and has a monochromatic appearance, which is useful for highlighting linear features. Hence, it is well suited to the bush-clad, rugged terrain of the CVZ (Belliss and Christie, 1994). A Synthetic Aperture Radar (SAR) image of the Coromandel region was taken by the JERS-1(Japan Earth Resources-1) satellite on the 5 November 1993. This image has been used to re-interpret structures mapped using earlier imagery and to reveal additional features.

The SAR image is characterised by numerous circular and linear features (Belliss and Christie, 1994). A major circular feature is present at the same location (i.e. 10 km west of Tairua) as in the MSS image (Figure 2.2). Compared to the MSS image, it has a similar diameter but is not as clearly defined and has a more circular form. As with the MSS image, this is interpreted as the topographic boundary of the KCC.

Within the topographic boundary, several lineations (interpreted as faults) are visible. The most continuous of these crosses the KCC with similar strikes (NW-SE) and extents as in the MSS image. A lineation located within the Kapowai valley has a greater extent (ca. 10 km), but is less continuous compared to that seen in the MSS image. Two lineations striking almost perpendicular to each other, in the western sector equate to the subcircular (structural boundary) feature seen in the MSS image.

Outside the topographic boundary, several features are evident. A curvilinear feature occurs ca. 1.5 km east of the eastern margin of the topographic boundary, and may represent a fault or the margin of an older topographic boundary. A smaller, but continuously circular feature occurs ca. 1.8 km NE of the eastern topographic boundary. This feature may indicate a collapse structure which is independent of the KCC. Several linear features are also visible trending NE towards the northern Tairua coast. These are interpreted as faults related to the regional structural trend.

The MSS and SAR images together provide evidence for the existence of a major (10 x 12 km) composite collapse structure located 10 km west of Tairua. Within this structure are several subcircular features in the northeastern and western sectors and several linear or curvilinear features striking NW-SE and NNE-SSW. Subcircular features are interpreted as the margins of collapse zones. Linear and curvilinear features indicate faulting associated with caldera activity or to the regional tectonic pattern. External linear and curvilinear features do not show any relation to the KCC, but are related to the regional structural pattern.

## Geophysical Surveys

Geophysical surveys may provide an indication of the upper crustal modification caused by caldera collapse and associated infill sequences. They can also provide a basis for the existence of extinct calderas and reveal magma bodies at depth beneath active calderas (e.g. Wilson et al., 1984).

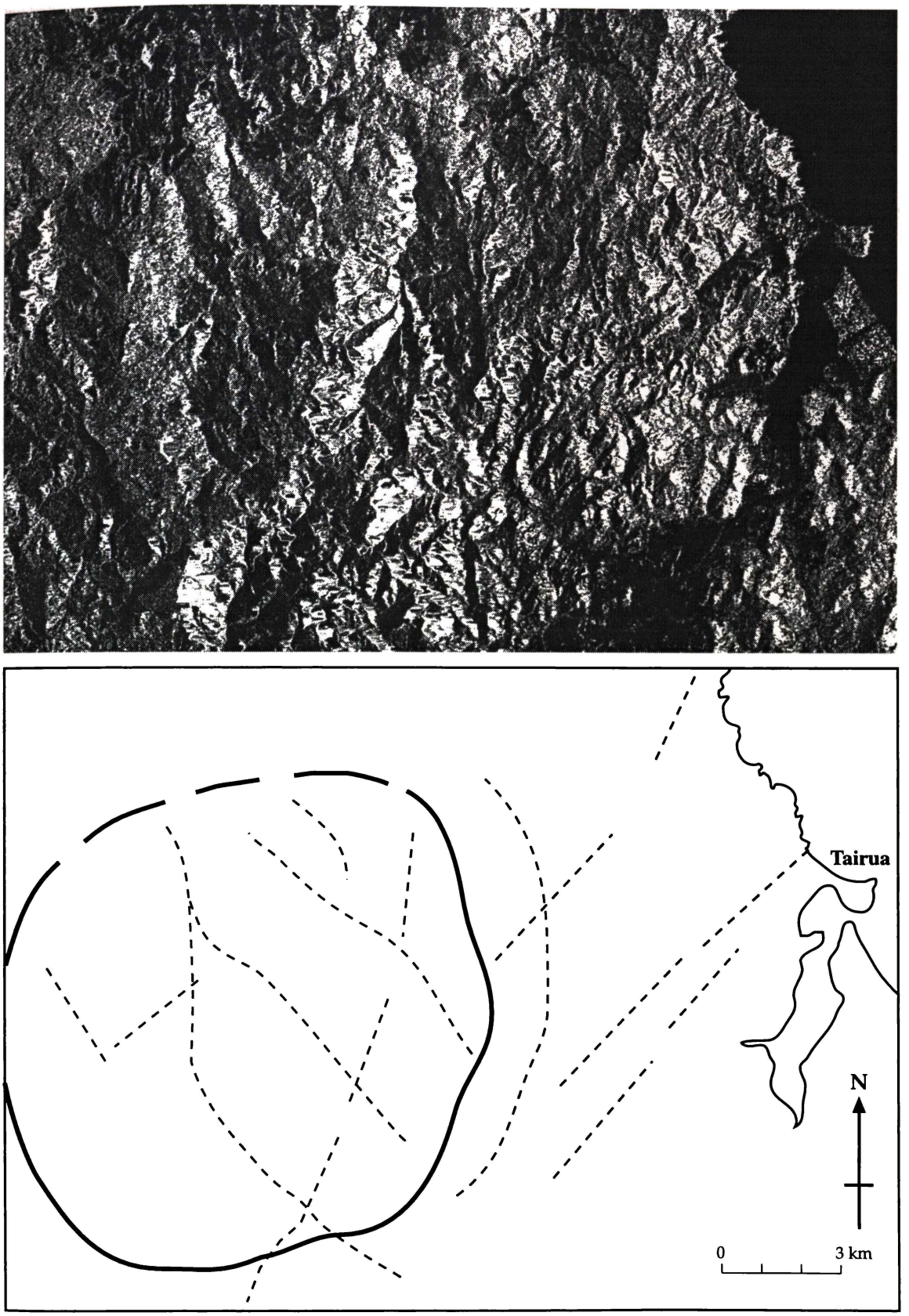


Figure 2.2 SAR image of the Kapowai Caldera Complex and structural interpretation. Topographic boundary is bolded. Lineations (faults, collapse boundaries) are dashed. Image courtesy of Landcare Research Ltd.

Several magnetic and gravity surveys cover the KCC at various resolutions. Other geophysical techniques such as resistivity have not been applied, but have been used at other locations within the CVZ (e.g. Bromley and Brathwaite, 1991).

***Magnetic Anomaly Pattern***

Magnetic anomalies associated with caldera volcanoes generally exhibit a sub-circular, low-intensity negative anomaly pattern bound by higher intensity, positive anomalies (Davy and Caldwell, 1998). This reflects the geometry of caldera collapse and the magnetic susceptibility contrast between caldera infill deposits (e.g. lacustrine sediments, ignimbrites, and hydrothermal alteration zones) and pre-caldera units.

Low resolution magnetic surveys of the CVZ have provided a basis for interpreting structures (Hunt and Symes, 1977). However, a higher resolution, low-level aeromagnetic survey compilation (Rabone, 1991) has enhanced the delineation of structures and allowed for improved interpretation (Figure 2.3). This compilation is used as the basis for describing the magnetic anomaly pattern at the KCC.

The magnetic anomaly pattern indicates a sub-circular area centred 10 km west of Coroglen, corresponding to the features observed in the MSS and SAR images. This pattern is characterised by relatively low magnetic intensities and subdued lateral gradients surrounded by an area of otherwise relatively high-amplitude, disturbed magnetic relief (Rabone, 1991).

There are several areas of moderate to steep magnetic gradients that coincide with the remote sensing defined topographic boundary. A large positive anomaly (+900nT) striking NNE, on the eastern Kapowai valley, corresponds with the eastern topographic boundary defined in the MSS and SAR images. This anomaly is elongate, and is most likely associated with the Ruahine Rhyolite dome complex which forms the N-trending Tanehua-Ruahine Ridge. On the southern margin of the boundary, several positive and negative magnetic anomalies occur. Most of the moderate positive anomalies (> 400nT) correspond with unaltered rhyolite lava domes, and the negative anomalies probably relate to deeply weathered zones. A similar pattern is present along the northern margin, although there is no clear correlation between the anomalies and exposed lithologies.

On the western topographic boundary, there is a sharp gradation from negative anomalies (< 0nT) west of the boundary to positive anomalies (> 200nT) east of the boundary. This corresponds with hydrothermally altered pre-caldera andesite to the west and unaltered, caldera-related andesite-dacite lavas and pyroclastics to the east of the topographic boundary. Several factors may be influencing this pattern which include: (i) a contrast between hydrothermally altered pre-caldera rocks which have weaker magnetic susceptibility compared to unaltered caldera-related rocks; and (ii) a possible difference in the magnetic polarity of the older pre-caldera rocks compared to the younger caldera-related rocks (Soengkono et al., 1992).

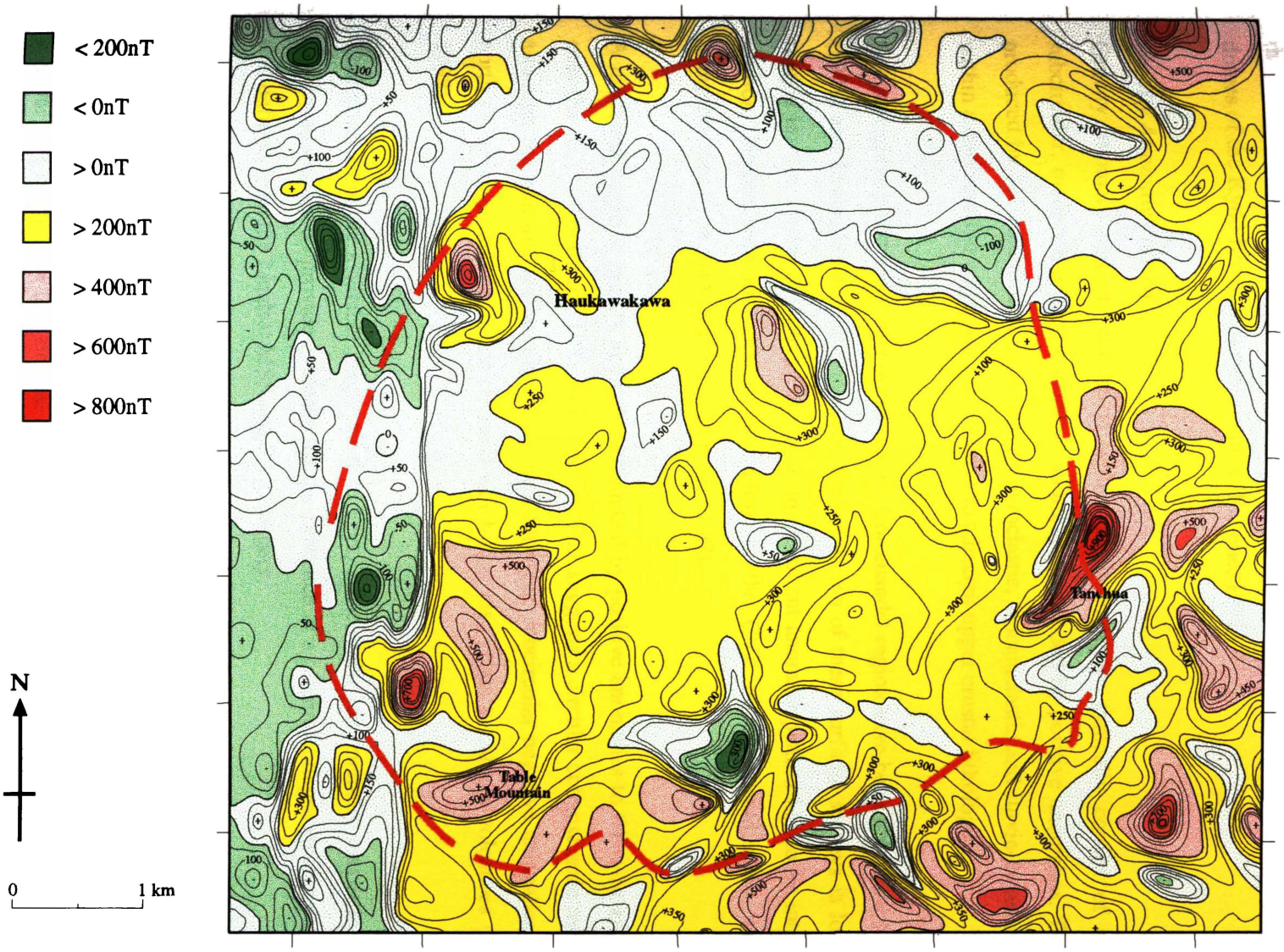


Figure 2.3 Magnetic anomaly map of the Kapowai Caldera Complex. Adapted from Rabone (1991). Dashed red line is the topographic boundary defined from the Landsat MSS image.

Within the Landsat MSS-defined topographic boundary, several features are present. Negative or flat magnetic anomalies typically correspond to either areas of hydrothermal alteration, mineralisation (Robson et al., 1994), or deep weathering. Significantly, an oblong negative anomaly (-200nT) is associated with the 3 $km^2$, locally depressed area and volcaniclastic lacustrine sediments present in the Rangihau Stream-Slip Stream area. A centrally situated bipolar anomaly is attributable to rhyolite domes of the Kydd Rhyolite dome complex (Rabone, 1991).

***Gravity Anomaly Pattern***

Gravity anomaly patterns associated with caldera volcanoes typically consist of a circular to subcircular, moderate to strong negative anomaly surrounded by positive anomalies. This pattern is produced by accumulations of low density pyroclastic, volcaniclastic and fluvio-lacustrine sediments within a depressed or collapsed zone relative to adjacent upper crustal lithologies.

Bouguer gravity anomaly maps of the onland Coromandel region have been published by Woodward (1971) and Fenaughty (1986). However, the resolution of these surficial surveys is low due to the rugged terrain. Hence the interpretation of any resultant anomaly pattern has to be interpreted with caution. Higher resolution gravity surveying in the CVZ region should allow more detailed interpretations to be made (Malengreau et al., 1997).

A moderate negative gravity anomaly surrounded by positive anomalies to the west and east occurs over the KCC (Woodward, 1971) (Figure 2.4). This suggests a circular collapse zone may be present, although the margins are not clearly defined. Stronger, subcircular negative anomalies occur to the north (Whitianga) and southeast (Hikuai) which may also relate to caldera volcanoes (Briggs et al., 1998).

Therefore, from the available geophysical surveys, sub-circular low-intensity magnetic and negative gravity anomalies do provide evidence for the existence of a caldera collapse structure comparable to that defined from the Landsat MSS and SAR imagery.

## Geological Mapping

A revision of central CVZ geology provided initial geological evidence for the existence of a caldera volcano (Skinner, 1983). This included the presence of thick pyroclastics (ignimbrite and tephra), a circular ring of rhyolite lava domes, and central lacustrine siltstones. Further mapping differentiated several ignimbrite units, two main rhyolite lava types, and documented the general petrology of erupted units (Skinner, 1993; 1995). A number of linear structures, including shear zones, faults and volcanic centres were mapped or inferred, but no collapse structures were identified.

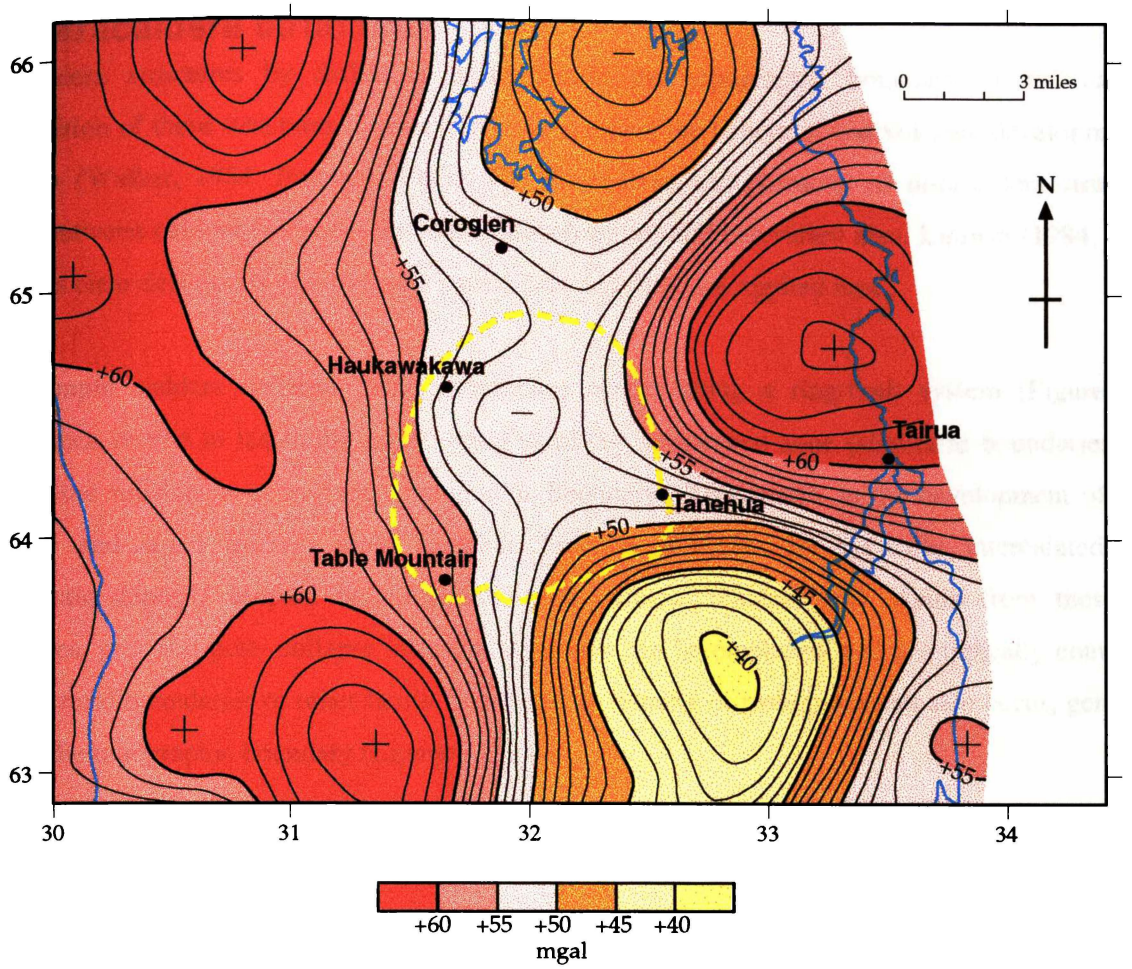


Figure 2.4 Bouguer gravity anomaly map of the Kapowai Caldera Complex. Adapted from Woodward (1971). Yellow dashed line is the topographic boundary defined from the Landsat MSS image.

Geological mapping in this study has confirmed several of the features described by Skinner (1993, 1995). However, the stratigraphy and structure is revised by detailed mapping, petrological analysis and new radiometric dates on selected units (see Chapters 3 to 6). This revision provides evidence for multiple collapse events at the KCC.

Several thick ignimbrites dominate the intracaldera succession, and these are locally interbedded with lacustrine siltstones and intruded by rhyolitic and andesitic lavas and dikes. Field evidence and lithic fragment populations also suggests multiple episodes of hydrothermal activity within the caldera. Exocaldera ignimbrites occur adjacent to the KCC and some are correlatable with intracaldera ignimbrites (see Chapter 5).

Most structures mapped by Skinner (1993, 1995) are interpretive and not readily observed in the field. This research only defines structures actually observed in the field or visible on remote sensing imagery or aerial photos.

## 2.3 Intracaldera structures

Intracaldera structures by definition occur within the topographic boundary of the caldera. Recognition of these structures is central to understanding the structural and volcanic development of calderas (Walker, 1984; Branney, 1995). The dimensions and character of intracaldera structures varies between caldera volcanoes and the terminology applied has varied also. Lipman (1984, 1997) provides clear definitions of intracaldera structures and these are applied here.

In a simple, caldera collapse cycle, subsidence occurs along a ring-fault system (Figure 2.5). Subsidence results in instability of the margins of the subsidence zone (structural boundaries) and outside the subsidence zone (inner topographic boundary). This results in the development of large (mega-) and small (meso-) scale landslide breccias. Breccias are typically intercalated with pyroclastic deposits erupted in association with collapse (caldera fill). Aside from these key structures, pre- and post- collapse intrusive structures can be emplaced, and are typically controlled by structural boundaries or other faults. Structural up-doming or resurgence can also occur, generally within the topographic boundary (Lipman, 1984).

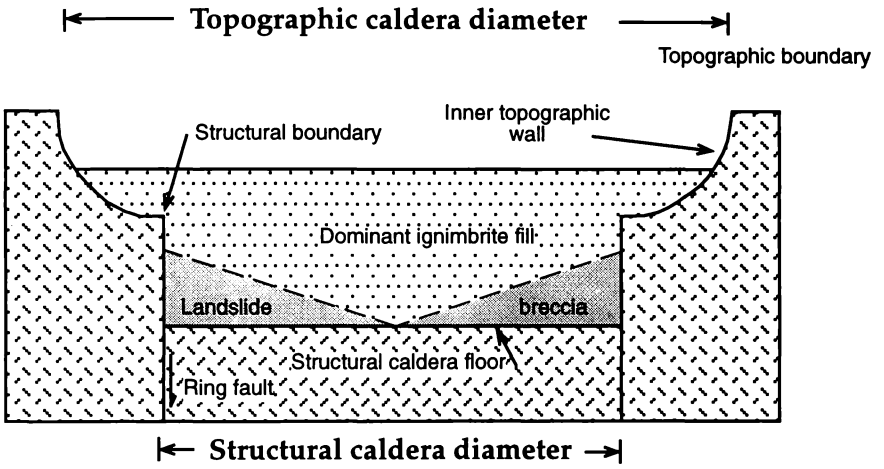


Figure 2.5 Definition of key structures associated with caldera development. Adapted from Lipman (1997).

Figure 2.6 presents a summary of intracaldera structures defined at the KCC. These structures are revealed using a combination of satellite imagery, aerial photos, and geological mapping.

For most of the structures defined at the KCC, the exact nature of their deformation, extent and age is difficult to establish. This is mainly due to their burial by successive, widespread, thick infilling pyroclastic sequences associated with multiple caldera collapse cycles. Associated localised mass wasting and hydrothermal alteration may also conceal intracaldera structures. Thus the definition and discussion of the structures that follow, is in some cases speculative. Initially the topographic boundary is described and then structures associated with the caldera floor are discussed.

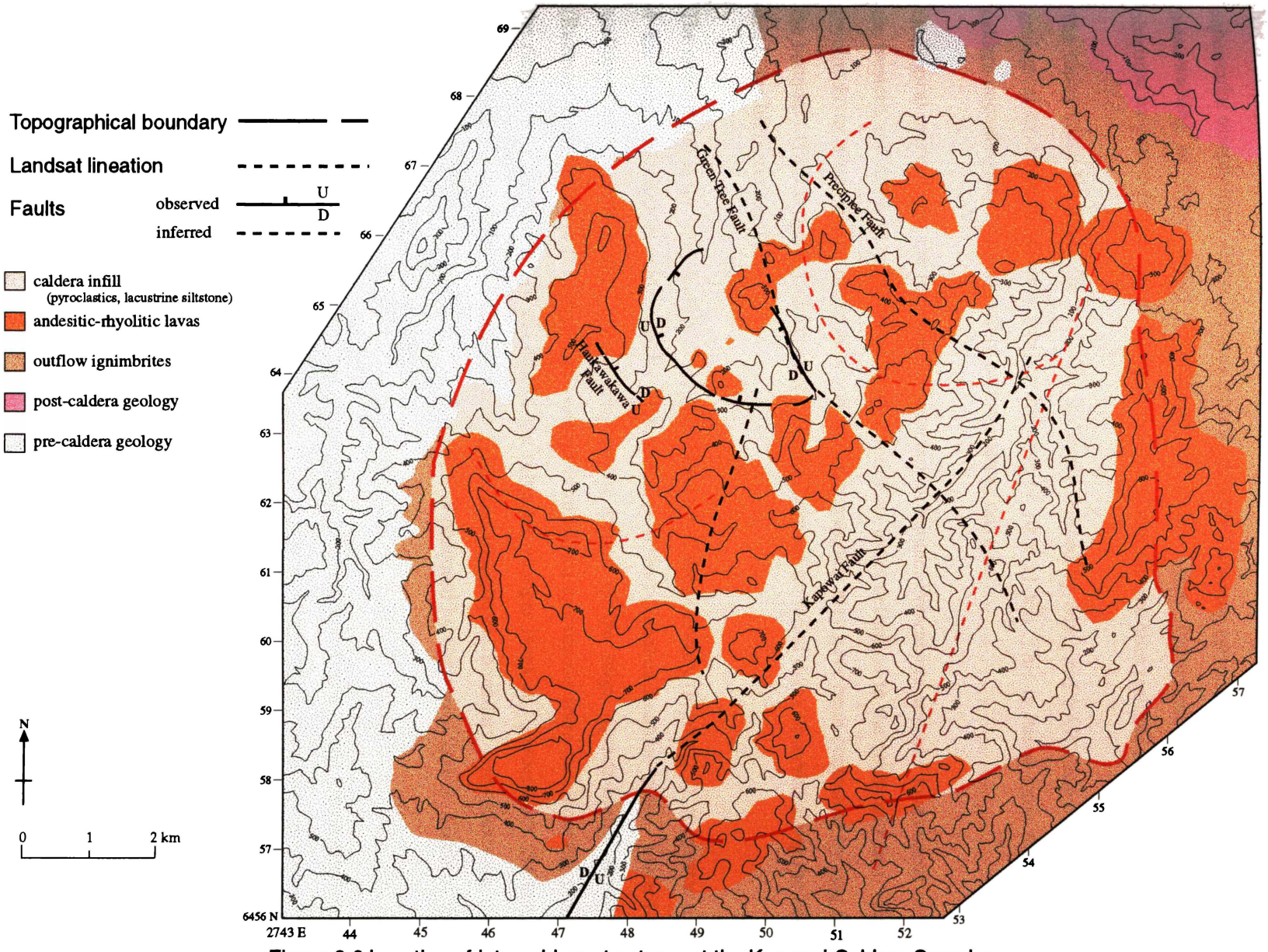


Figure 2.6 Location of intracaldera structures at the Kapowai Caldera Complex

## Topographic Boundary

The topographical boundary is defined as the unconformity between pre-caldera rocks outside the central collapse zone and post-collapse caldera fill deposits (Lipman, 1984). When clearly exposed, this boundary has a distinctive topographical expression, scalloped inward-sloping escarpments, and has a circular to subcircular morphology. These features initially develop following subsidence and are further modified by mass-wasting as slopes revert towards an equilibrium state. Topographic boundaries are typically obscured by post-collapse volcanism, hydrothermal alteration, and later tectonic activity.

The topographic boundary for the KCC is clearly defined by MSS and SAR imagery (see above), but geological evidence indicates a smaller diameter of 10 x 11 km. This is based upon the pre-caldera - caldera unconformity exposed mainly on the western margin.

Geological evidence for the topographic boundary is limited. Pre-caldera andesite lavas occur only along the western and northern margins, severely limiting its exact definition in the south and east. However, rhyolite lavas which define the eastern and southern margins, may have been controlled by ring faults of the boundary (Elston, 1984; Colucci et al., 1991). There are no radial dikes observed along the boundary, due to the high erosional level.

The eastern rim is the most readily distinguished sector of the boundary (Figure 2.7). It equates to the ca. 4 km long, 400-500 m wide, locally elevated (514-659m) Tanehua-Ruahine ridge. Inward-sloping, scalloped escarpments occur only on the western margin of the ridge. Quartz-biotite rhyolite lavas (Ruahine Rhyolite) form the ridge, and younger intracaldera ignimbrites form an onlapping plateaux on the ridge's western margin. To the east of the ridge are younger lavas and pyroclastics (Skinner, 1995; Karl, 1996). North of the Tanehua-Ruahine ridge, the topographic boundary coincides with a rhyolite dome (Kokonga Rhyolite Dome), and further north is obscured by thick pyroclastics. South of the ridge, the boundary is also obscured by pyroclastics.

There is no direct physiographic evidence to define the southern margin of the topographic boundary, although the topography is locally elevated (682-773m) and several rhyolite lava domes (Pinnacles Rhyolite; Camp Rhyolite) occur along the remote sensing defined boundary. Continuing to the southwestern margin, the boundary is delineated by the unconformity between pre-caldera andesite lavas/breccias (Taurahuehue Andesite) and overlying KCC pyroclastics (Webb Creek Ignimbrite), but the boundary has no physiographic expression.

The western margin is the most obscured portion of the topographic boundary on the MSS and SAR images. In the field, the boundary is defined by pre-caldera andesite lavas and caldera-related andesite lavas and the arcuate Waiwawa valley (Figure 2.8), but it is obscured by thick ignimbrites. The NNE-trending Waiwawa Fault (Skinner, 1993) which displaces only pre-caldera andesites may relate to caldera activity, but does not define the topographic boundary.

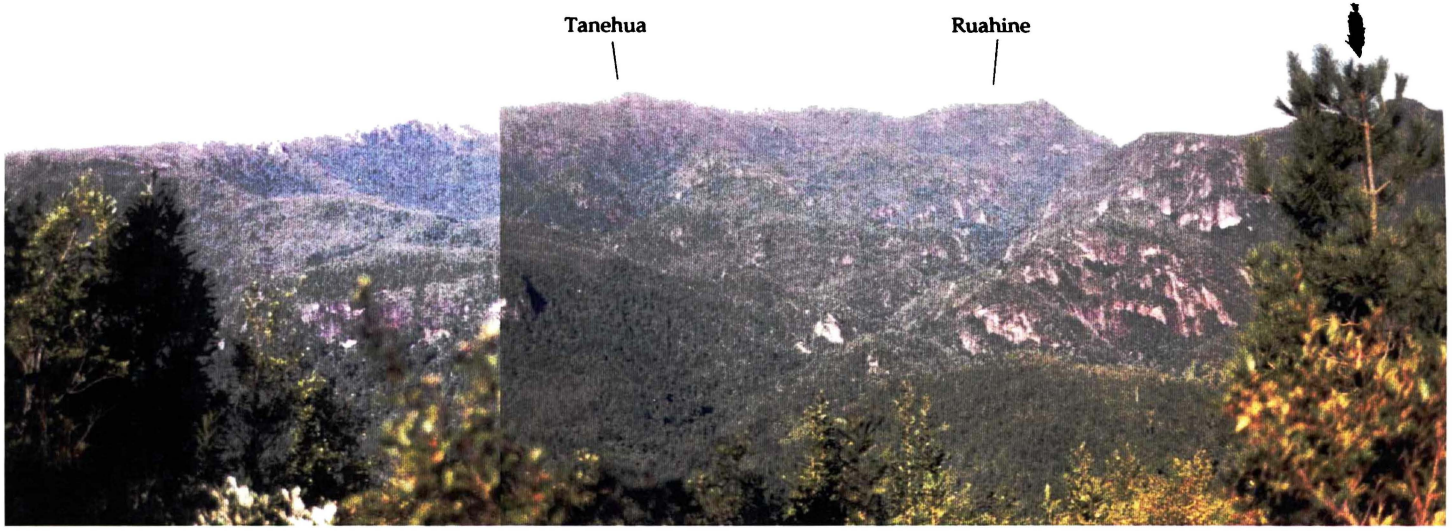


Figure 2.7 Eastern margin of the Kapowai Caldera Complex topographic boundary. Boundary defined by the Tanehua-Ruahine ridge (Ruahine Rhyolite). Intracaldera ignimbrite (WES) infills the Kapowai valley in the foreground and onlaps to the Tanehua-Ruahine ridge. View east from T11/536657.

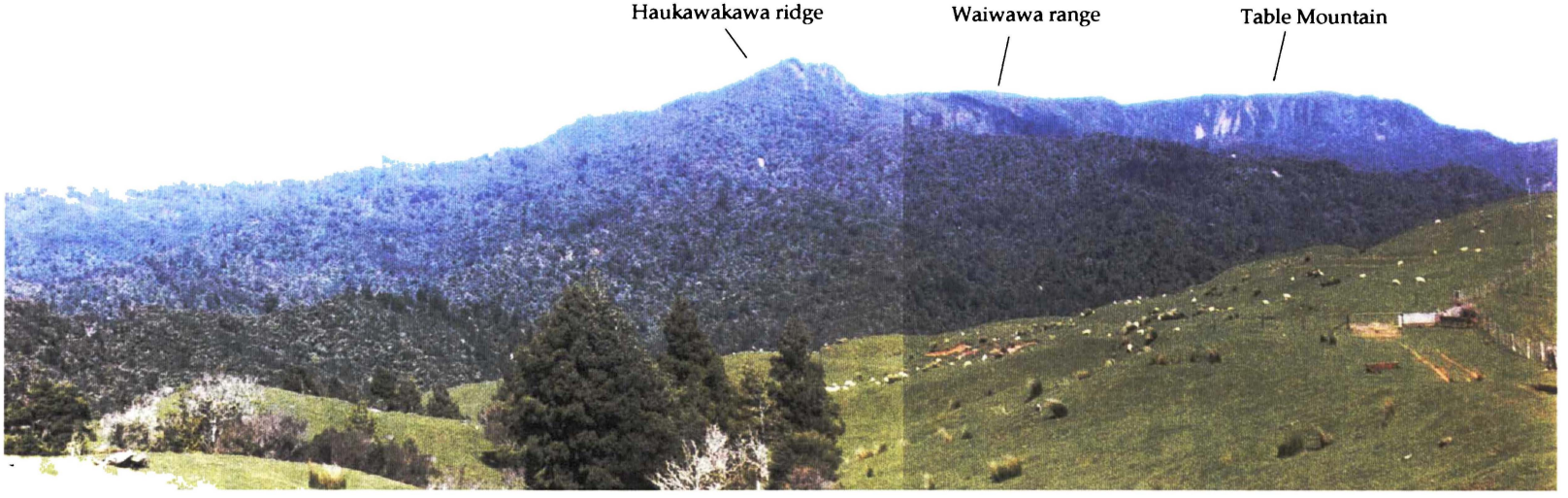


Figure 2.8 Western margin of the Kapowai Caldera Complex topographic boundary. Pre-caldera (Maumaupaki Formation) lavas form the ridge in centre. Caldera-related lavas (Taurauikau Andesite) form the Haukawakawa ridge, Waiwawa range and Table Mountain. View east from T11/436657.

The northern margin is obscured in the MSS and SAR images but is defined by localised pre-caldera andesites which outcrop between thick ignimbrites (WES-1 and WES-4 Ignimbrite; Trig Q Ignimbrite).

## Caldera Floor

Caldera floors are defined as the caldera derived material deposited within the topographic boundary (Lipman, 1984). Caldera floors are typically lithologically and structurally complex, and for caldera complexes, consist of several structural collapse zones and associated multiple caldera collapse facies (Christiansen, 1984; Lipman et al., 1996).

The KCC caldera floor is characterised by the presence of exposed and concealed structural collapse zones and numerous intrusive bodies. Infilling the caldera floor is a sequence of thick (100-500 m) pyroclastics (dominantly ignimbrite with minor tuff), pre- and post- collapse rhyolite lava domes, andesite lavas and dikes, and localised volcaniclastic lacustrine sequences.

### *Structural Boundaries*

Structural or collapse boundaries define zones of major subsidence attributable to a single caldera collapse event (Heiken and McCoy, 1984; Lipman, 1984; Marti et al., 1994). Structural boundaries were originally considered to be defined by inward-dipping ring faults (Lipman, 1984), although recently it has been suggested that the boundaries may be defined in some cases as the outer limit of subsidence, and not necessarily associated with ring faults (Branney, 1995)

Single structural boundaries are typically present in young, active calderas (e.g. Rotorua and Reporoa calderas) (Wilson et al., 1995). However at older, longer lived calderas, multiple, nested structural boundaries are common (Christiansen, 1984; Skilling, 1993). Several collapse zones with or without exposed structural boundaries are defined within the caldera floor of the KCC.

### Rangihau Stream-Slip Stream

In the Rangihau Stream-Slip Stream area, a ca. 3 $km^2$ NW-SE trending, locally subsided, oblong area occurs (Figure 2.9). On the eastern margin of this area, a NNW-striking, 80-100 m high, high-angle normal fault scarp occurs (Figure 2.10a). The footwall on this fault plane consists solely of WES pyroclastics, which significantly contain interbedded proximal lithic lag breccia and thick (3-3.5 m) tephra (Chapter 5). The northern limit of this scarp ends at the Rangihau Rhyolite dome, and to the south, it passes into Kydd Rhyolite lava domes.

A high-angle, arcuate normal fault scarp defines the southwestern margin of the depressed area (Figure 2.10b). This scarp extends for 2 km and is obscured by the Welcome Jack Rhyolite dome to the east and WES pyroclastics to the north. As with the eastern scarp, WES pyroclastics are exposed on the footwall, although no lithic lag breccia or thick tephra has been observed. A minimum displacement of 80 m has occurred along this scarp.

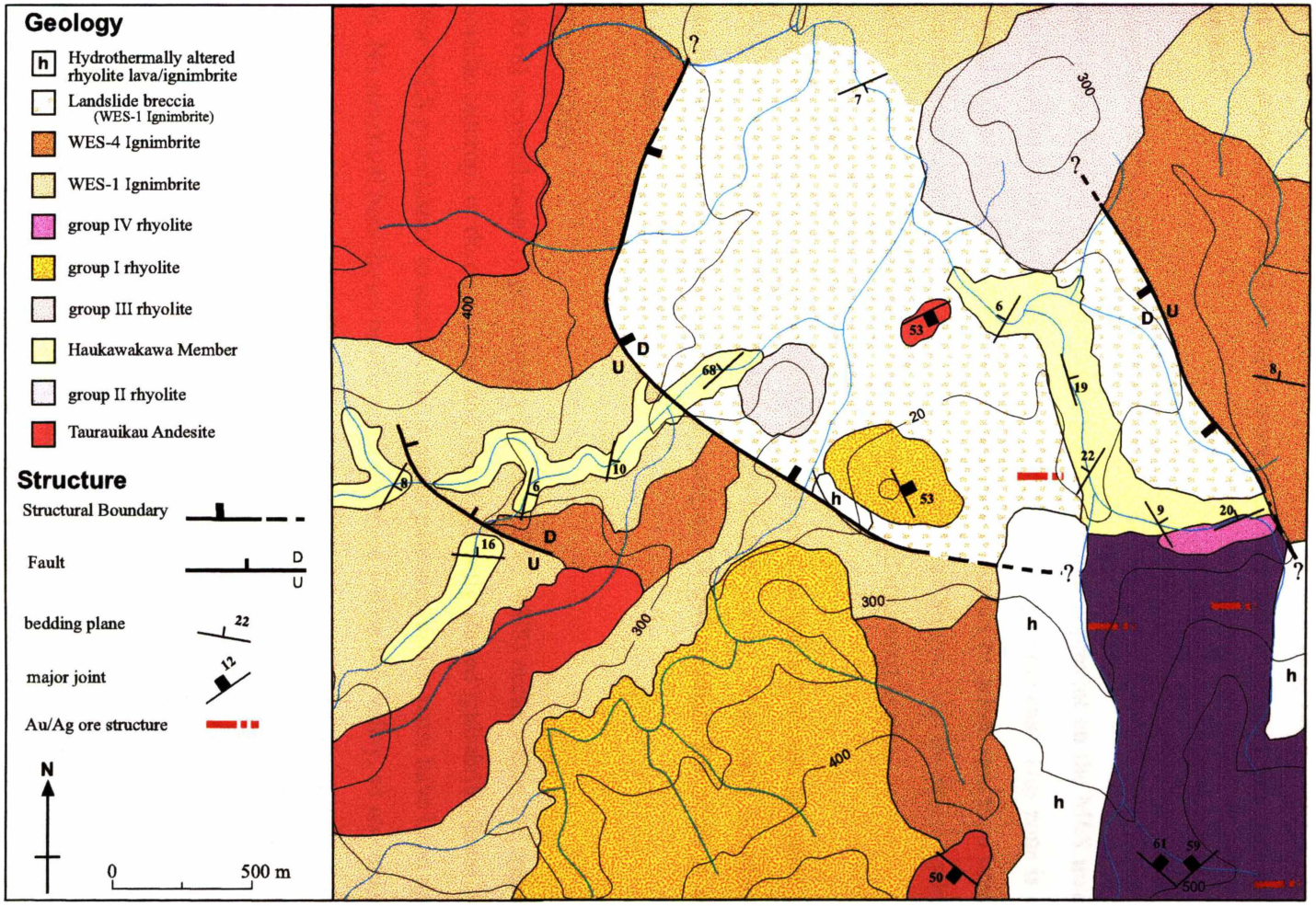


Figure 2.9 Geological map of collapse zone in the Rangihau Stream-Slip Stream area.

The floor of this depressed area consists of chaotically striking, gently to moderately tilted (9-20°) volcaniclastic lacustrine siltstones, overlain by WES landslide breccias derived from the walls of the collapse boundaries.

The presence of an almost continuous arcuate fault scarp bounding a locally depressed area, and the presence of proximal pyroclastic facies implies that this is an area of caldera collapse. Indeed, it is suggested that this represents caldera collapse associated with the WES, and this will be discussed further in Chapter 5.

### Oteao valley-lower Kapowai valley

In the NE sector of the KCC, a 4.5 km diameter circular lineation is present on the MSS image. This is confined by the Rangihau valley to the west and the Kapowai valley to the east. This zone is elevated to the south, but locally depressed to the north. There is no field evidence to define structural boundaries for this area, although the circular lineation coincides with the Oteao Stream, and intersects hydrothermally altered ignimbrite in the Kapowai valley suggesting some buried structural feature.

If this is a collapse zone, it is a relatively old structure as it is infilled by the youngest pyroclastic sequence (WES). It also contains several rhyolite domes located within (Wharepapa Rhyolite; Kapowai Rhyolite; Kydd Rhyolite dome complex) or on the margins (Waiwhatawhata Rhyolite) of the feature, although their relationship to the structure is not clear.

### Upper Kapowai valley

Thick (400-500 m) accumulations of pyroclastics (dominated by WES) occur within the upper Kapowai valley, and sporadic outcrops of rhyolite lavas, and hydrothermally altered ignimbrites/lavas occur in the valley floor. For WES pyroclastics to accumulate, a major paleodepression must have been present prior to the eruption. No structural boundaries or scarps are observed within this valley, so no caldera collapse zone can be clearly defined. However, the valley is bounded by a series of rhyolite lava domes (e.g. Ruahine Rhyolite; Kydd Rhyolite dome complex) which may relate to a buried collapse structure.

***Pre- and post-collapse effusive volcanism***

Multiple intracaldera effusive structures are typically seen in eroded calderas. Intrusives can be emplaced before, after or independent of caldera collapse and their distribution is typically controlled by caldera faults, or pyroclastic vents (Lipman, 1984). Pre-caldera silicic lavas occur at many caldera volcanoes and are typically truncated following caldera collapse (Elston, 1984; Christiansen, 1984; Metz and Mahood, 1985).

Several effusive rhyolite lavas (Ruahine Rhyolite; Pinnacles Rhyolite; Camp Rhyolite) coincide with the KCC topographic boundary, and are elevated above the intracaldera sequence. Ruahine Rhyolite lava forms the 4.5 km Tanehua-Ruahine ridge. This ridge defines the eastern

topographic boundary and its emplacement is likely to have been controlled by concealed caldera ring faults. WES pyroclastics onlap and form narrow plateaux on the western side of the ridge, suggesting that the ridge pre-dates the WES. Several silicic lavas (Camp Rhyolite; Pinnacles Rhyolite) coinciding with the southeastern margin of the topographic boundary appear to intrude WES pyroclastics suggesting a post-WES age for these domes.

A

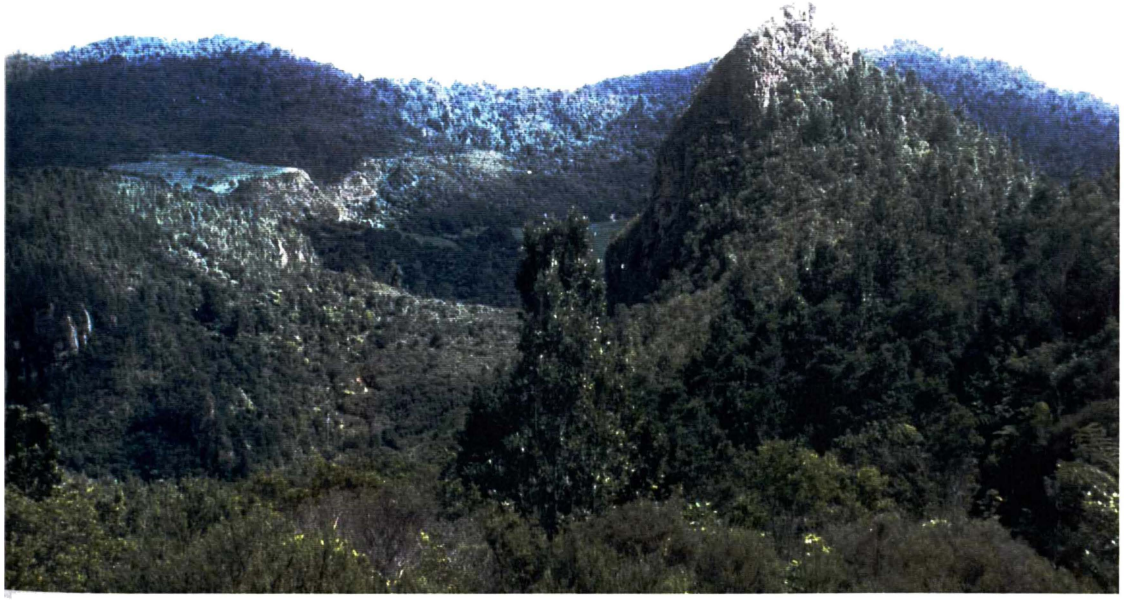

B

Figure 2.10 Structural boundary exposed in the Rangihau Stream-Slip Stream area. A, 80 - 100 m high-angle, normal fault scarp which defines the eastern boundary. WES pyroclastics outcrop on the scarp and lacustrine siltstones (Haukawakawa Member) are exposed in centre foreground. View east from T11/500641. B, High-angle, normal fault scarp with WES pyroclastics exposed on the footwall, which defines the western boundary. Big Beetle Rhyolite dome in centre right. Taurauikau Andesite forms ridge in background. View NW from T11/499638.

Numerous intrusive structures occur within the KCC. Several examples of rhyolites intruding ignimbrite are observed within the KCC. In the Kapowai valley, several rhyolite lava dikes (Precipice Rhyolite) intrude ignimbrite (Colorado Pyroclastics, CP-2 Ignimbrite) and other rhyolite lavas (Kapowai Rhyolite) (Figure 2.11). The margins of the intrusive rhyolite are glassy, but where the rhyolite intrudes ignimbrite, the contact is also brecciated. In the Kauaeranga valley, rhyolite lava (Kauaeranga Rhyolite) intrudes ignimbrite (WES-1 Ignimbrite). Within the rhyolite, the glass content increases towards the contact (Hayward, 1974b) implying a thermal gradient from cooler at the contact to hotter towards the intrusive.

Intrusive rhyolite lavas are also observed to locally deform overlying units. In the Slip Stream valley, Slip Rhyolite lava intrudes older volcaniclastic siltstone (Haukawakawa Member). Near the contact, the lava has generated up to 20° of tilting which decreases away from the contact. At the contact between Kauaeranga Rhyolite and overlying WES-1 ignimbrite in the upper Kauaeranga valley, the ignimbrite is tilted up to ca. 10° by the intruding rhyolite dome.

Intrusive structures also host or control epithermal mineralisation. The Welcome Jack Rhyolite Dome controls the occurrence of major Au-Ag bearing epithermal quartz veins/reefs and breccia pipes. Veins strike E-W and are hosted within the hydrothermally altered Welcome Jack Rhyolite lava and peripheral hydrothermally altered intracaldera pyroclastics.

Aside from silicic lavas, andesitic lava dikes have also intruded through the intracaldera pyroclastic pile. Andesite lavas (Taurauikau Andesite) form large plateau lava fields and localised dikes in the western sector of the caldera (Hayward, 1974), and several small (1-5 m) dikes in the central KCC (see Figure 2.9).

## Faults

Numerous faults have been defined within and adjacent to the KCC during this study and by previous workers (Skinner, 1993, 1995). These have been grouped into intracaldera (which occur completely within the KCC), and exocaldera faults, which mostly occur outside, but can extend into the KCC. Recognition of faults is hampered by the thick vegetation cover and paucity of continuous outcrop. Several faults have been observed in the field, or are inferred on the basis of Landsat MSS, SAR imagery or aerial photos.

### *Intracaldera faults*

Several intracaldera faults have been defined in this study. Most of these are likely to be related to caldera collapse cycles and/or associated deformation, but relationships for most faults are poorly constrained because of limited exposure.

A

B

**Figure 2.11** Intrusive rhyolite lava in the Kapowai valley floor (T11/552660). A, Precipice Rhyolite lava dike intruding Colorado Pyroclastics (CP-2 ignimbrite). B, Brecciated, glassy margin of the rhyolite-ignimbrite contact. Lens diameter is 55 mm.

## Haukawakawa Fault

Haukawakawa Fault occurs in the Haukawakawa valley, central KCC. It has a NW-SE trend, and has an observable extent of ca. 700 m, but this is inferred to extend at least a further 100 m either side. It displaces Haukawakawa Member siltstones and overlying WES-1 Ignimbrite by a minimum of 20 m. It is a high-angle (ca. 70°) normal fault, and is related to subsidence associated with the WES eruption.

200 m west of the Haukawakawa Fault is a shear zone which strikes obliquely to the fault (Figure 2.12). The shear zone is characterised by two parallel high-angle faults which downthrust WES-1 ignimbrite. Faults are bounded by gently inclined Haukawakawa Member to the north and undeformed crystal tuff and WES-1 ignimbrite to the south. Within the shear zone, ignimbrite (presumably WES-1 ignimbrite) is intensely sheared to mylonite. The relationship of this shear zone to the Haukawakawa Fault is not directly known, although it may represent a minor splay fault.

### Precipice Fault

Precipice Fault extends from the northern margin of the KCC along a NW-SE strike to the Kapowai valley. It parallels the Precipice Stream and extends through to the eastern margin of the Tanehua-Ruahine Ridge. Precipice Fault is defined from remote sensing imagery, and although no displacement has been observed, it is considered a concealed fault because it coincides with the location of several rhyolite lava domes (Kydd Rhyolite dome complex), and a zone of hydrothermal alteration. The timing and deformation history of this fault is unclear, although no displacement of WES is observed along the fault, implying that it has been inactive since before the WES.

### Green Tree Fault

Sub-parallel and south of the Precipice Fault, is the Green Tree Fault. This extends from the northern KCC along a SW strike through the Green Tree valley, and into the upper Kapowai valley. Significantly, it coincides with the eastern structural boundary of the WES collapse zone implying a genetic relationship with this boundary. A zone of hydrothermal alteration also occurs near its SE limit.

No displacement has been observed along the fault. However, because it coincides with the eastern structural boundary of the WES, it is most likely related to that eruptive event or was present shortly before. As this fault generally parallels the Precipice Fault and has a similar extent, there may also be some upper crustal structural relationship between these two faults.

### Starvation Fault

Like most other intracaldera faults, Starvation Fault is defined initially by remote sensing imagery. It extends ca. 4 km north from the upper Kauaeranga valley to the southern margin of the WES structural boundary. Although displacement has not been observed along its strike, it is considered a concealed fault mainly because andesitic lava dikes (Taurauikau Andesite), and zones of hydrothermal alteration occur along its strike.

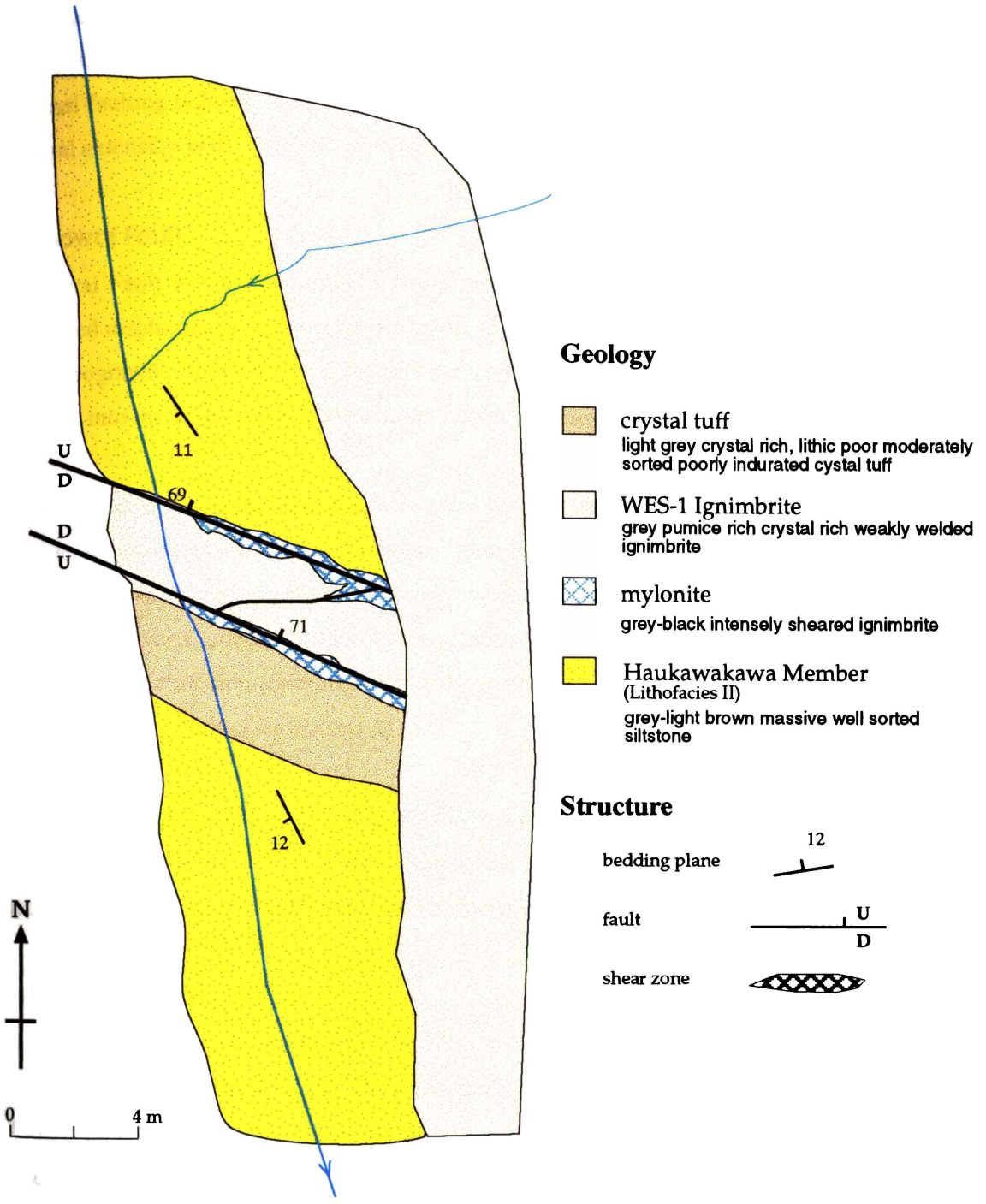


Figure 2.12 Shear zone 200 m west of the Haukawakawa Fault. Tributary stream of the Haukawakawa Stream (T11/478644).

The displacement history and timing of the Starvation Fault is obscured by lack of an observable fault plane and displaced units. However, it is likely that the fault pre-dates emplacement of the Taurauikau Andesite lava dikes, and the hydrothermal alteration zones.

## 2.4 Adjacent regional faults

Several faults occur adjacent to or near the KCC topographic boundary (Figure 2.13) and some of these extend into the caldera. All of these faults have N to NE trends and so are considered to be related to the

regional fault pattern in the central CVZ (Clarke et al., 1990). It is difficult to establish the exact character of these faults because of concealment, although displacements observed typically imply extensional or normal faulting (Clarke et al., 1990). This is consistent with most silicic volcanic provinces where upper crustal extension is the dominant tectonic feature (Jackson and White, 1989; Cole, 1990).

### Kapowai Fault

Kapowai Fault was defined initially from Landsat MSS and SAR imagery, and was later confirmed by observed displacement in the upper Kauaeranga valley. It extends NE from outside the southern margin of the topographic boundary, and follows the upper Kauaeranga valley almost to its headwaters. It then crosses into the western headwaters of the Kapowai valley, and extends for most of this valley's length.

Along most of its strike it is concealed and displacement is seldom observed. However, in the upper Kauaeranga valley, it displaces Tarawaere Member siltstones by ca. 80 m. The fault also coincides with the location of several rhyolite lava domes (Kauaeranga Rhyolite dome, Tauranikau Rhyolite dome) and intersects several zones of hydrothermal alteration in the Kauaeranga and Kapowai valleys. The occurrence of alteration zones along its strike suggests that it acted as a structural control for the migration of hydrothermal fluids (see chapter 8).

Displacement of Tarawaere Member implies that this fault was active after the deposition of this unit (i.e. early KCC activity). As it is difficult to establish whether units overlying Tarawaere Member (e.g. WES) have been displaced, no constraints can be placed on the exact age of the fault.

### Waiwawa Fault

Waiwawa Fault follows the trend of the Waiwawa valley, to the west of the KCC. It strikes NNE for ca. 6 km from the headwaters of the Waiwawa River to its confluence with the Five Mile Stream (Skinner, 1993). Its southern limit corresponds with a major zone of hydrothermally altered pre-caldera andesitic-dacitic lavas and breccias (Maumaupaki Formation; Taurahuehue Andesite).

Skinner (1993) used the Waiwawa Fault to define the western boundary of the KCC. However, the fault only displaces pre-caldera andesitic-dacitic units and therefore does not represent the unconformity between pre-caldera and caldera-related rocks which is typically used to define topographic or caldera boundaries (Lipman, 1984). As Waiwawa Fault has a similar orientation to other faults within the central CVZ, it is considered to be a regional fault and is not directly related to the KCC. As only pre-caldera units have been displaced by the fault, a pre-caldera age is implied.

### Coroglen Fault

Coroglen Fault is defined as extending ENE from the Toranoho valley to the Whitianga estuary Skinner (1993). Only pre-caldera units have been displaced implying a pre-caldera age (cf. Skinner, 1993), and as it has a similar strike to other regional faults, it is not considered to be related to the KCC.

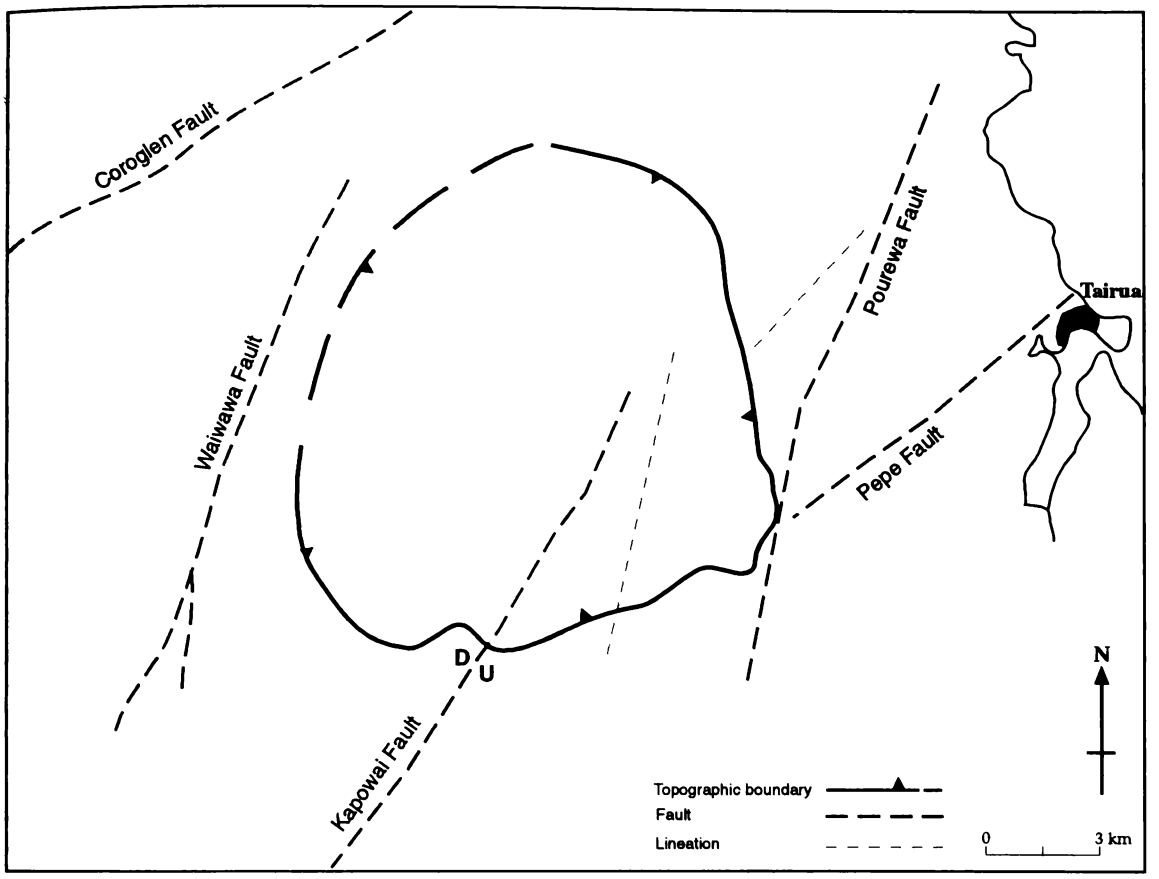


Figure 2.13. Major faults adjacent to the Kapowai Caldera Complex. Modified from Skinner (1993, 1995). Faults and lineations have a general NE-SW strike comparable with the central and southern CVZ regional trend.

### Pourewa Fault

Pourewa Fault is suggested on the basis of a lineation observed on both Landsat MSS and SAR imagery, and observed displacement (Skinner, 1995). It extends NNE for ca. 16 km from near the SE margin of the KCC to southwest of Tapuaetahi Bay on the east coast. Displacement of pre- and post-caldera units has been reported (e.g. Skinner, 1995) implying that this fault has been active during or after activity at the KCC. As the Pourewa Fault has a similar orientation to the regional fault pattern, it is considered to be related to this pattern and not the KCC.

### Pepe Fault

Pepe Fault is defined by a lineation observable from remote sensing images and geological mapping (Skinner, 1995), that extends from near the eastern topographic boundary of the KCC to just north of Tairua, on the east coast. For most of its extent it is concealed, although some local displacement of pre-

caldera and caldera-related units has been observed (Skinner, 1995), which implies that it was active during or after KCC activity.

### Other lineations

Two additional lineations occur near the topographic boundary of the KCC. A lineation observed on both Landsat MSS and SAR imagery occurs to the east of the Kapowai Fault. It strikes NNE and extends for ca. 8 km from outside the southern topographic boundary through to the eastern Kapowai valley. There is no surface displacement observed with this lineation and so it may represent an older, buried structure. As it extends outside the topographic boundary and has a similar orientation to the regional fault pattern, it is likely to be a regional fault, and is not related to the KCC.

NE of the Tanehua-Ruahine ridge is a NE-trending lineation that extends for ca. 4.5 km. No displacement is observed with this lineation. As it has a similar orientation to other regional faults in this area, it may also be related to the regional fault pattern.

## 2.5 Timing of structural elements

Structural elements at the KCC vary in their type, extent, and orientation. The characteristics of KCC structures have been described above, and this section discusses the timing and age relationships of them. For the majority of structures it is difficult to constrain their age or deformation history mainly because they are concealed by successive thick pyroclastic deposits, andesitic or rhyolitic lavas, or are buried by younger structures. However, a general sequence is suggested (Figure 2.14) and this can be subdivided into structures that are pre-, syn-, and post-WES (Wharepapa Eruptive Sequence).

### Pre-WES

The topographic boundary is the oldest structural feature at the KCC. It is likely that it initially had a different morphology and dimension compared to its present form. Successive caldera collapse cycles have modified its form, although it is difficult to establish these changes as the boundary is consistently obscured by pyroclastics or lavas.

Structural collapse boundaries, faults, and intrusives associated with successive eruptive sequences have also been present prior to the WES. Collapse zones have been tentatively identified in the lower Oteao valley-lower Kapowai valley, and in the upper Kapowai valley based upon sub-circular remote sensing lineations, and significant thickness of intracaldera ignimbrites.

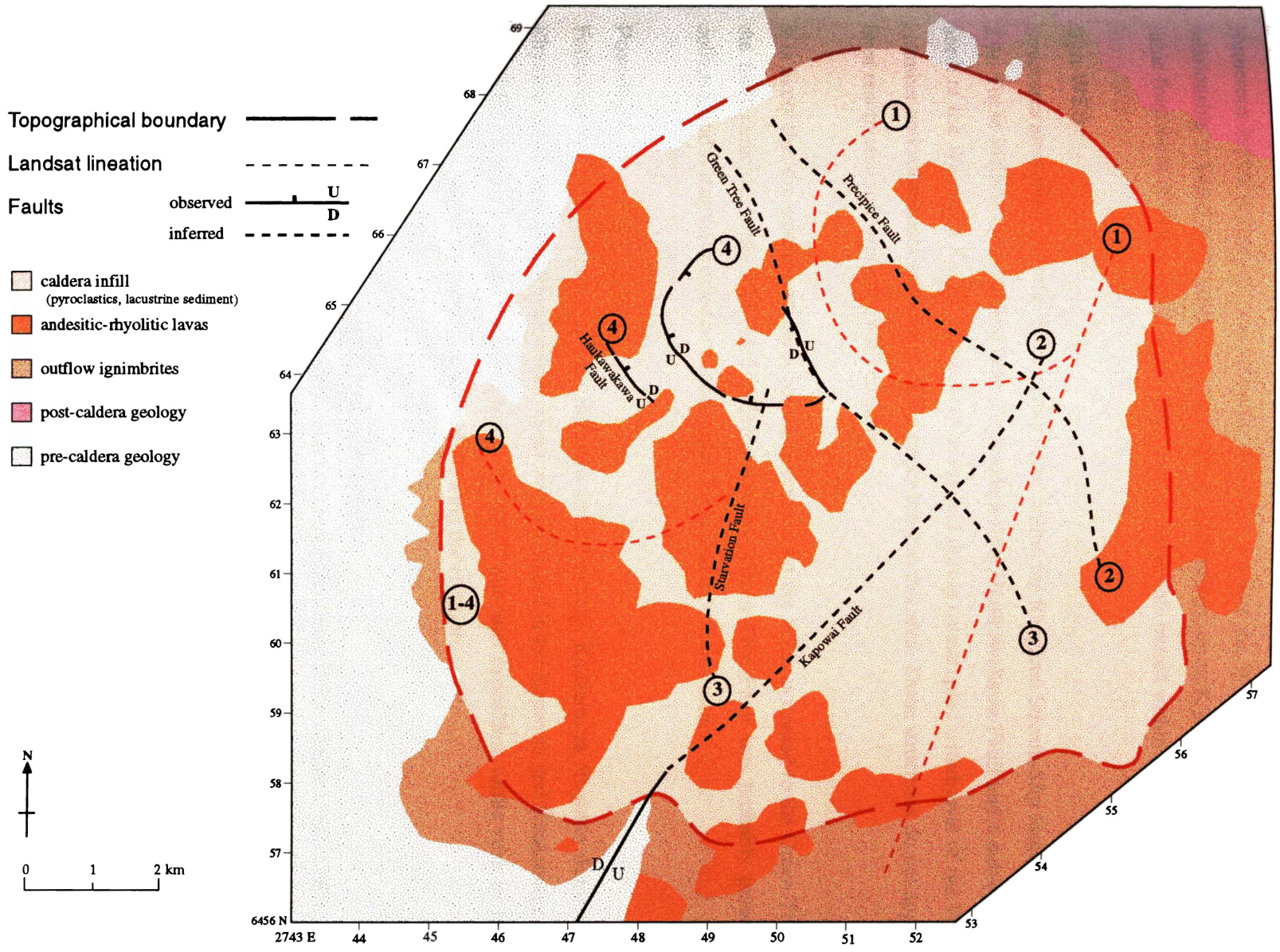


Figure 2.14. Temporal relationships between intracaldera structures of the Kapowai Caldera Complex. Numbers provide a suggested sequence from (1) the oldest to (4), the youngest structure.

Kapowai Fault, Precipice Fault and Green Tree Fault are inferred to have developed prior to the WES. For these, deformation histories are likely to be independent, although there may be some link between the Precipice Fault and Green Tree Fault because of similar orientations and extent.

Numerous intrusive rhyolitic and andesitic structures pre-date the WES. For exposed structures, the age relationship is based upon contact or geomorphic relationships, or on K/Ar ages. It is inferred based upon lithic fragments in welded ignimbrites, that other intrusives are buried within the volcanic pile.

### Syn-WES

Structures associated with the WES locally occur within the Rangihau Stream-Slip Stream valleys (Figure 2.9). These include the structural boundary/caldera floor, Haukawakawa Fault and a sub-circular feature north of the Waiwawa Range. These were developed during catastrophic withdrawal of the WES magma chamber and subsequent subsidence of the upper crust in this area. These structures do not appear to have been reactivated following the WES eruption.

It is likely that the eastern structural boundary defined for the WES, is related to the Green Tree Fault, as the fault coincides with it in the Slip Stream valley. Green Tree Fault was probably present prior to collapse, and it may have acted as a mechanism for subsidence in this area.

### Post-WES

Following the WES eruption, several intrusive structures (e.g. Kauaeranga Rhyolite dome; Tauranikau Rhyolite dome; Precipice Rhyolite lava dikes) were emplaced in the Kapowai and Kauaeranga valleys. No post-WES faulting has been observed within the KCC, although exocaldera faults such as the Pourewa Fault and Pepe Fault may have been active following the eruption.

## 2.6 Relationship to regional structure

KCC lies within a weakly active, extensional fault zone (Brothers, 1986; Clarke et al., 1990). The zone is weakly active with minor earthquakes occasionally recorded. Historic earthquake activity is punctuated by an earthquake swarm which occurred near the northern margin of the KCC topographic boundary (New Zealand Seismological Observatory, 1970; Backshall, 1982). This swarm occurred from August-September 1970 and consisted of many small magnitude earthquakes interspersed with larger (max. magnitude 4.4) events. Interpretation of this event is inhibited by the limited seismic recorder stations in the Coromandel region, but the epicentres were confined to a small area implying a limited zone of deformation (New Zealand Seismological Observatory, 1970). The relationship of this seismic sequence to the KCC is unknown.

Extension within the CVZ developed from the Miocene and was active through to the Pleistocene. The resulting fault pattern reflects the imprint of this major extensional period (Kaikoura Orogeny) on pre-existing late Mesozoic (Rangitata Orogeny) structures. Faults active during the Rangitata Orogeny were reactivated during the Kaikoura Orogeny, but with a different displacement character (Skinner, 1986).

Several major regional structures have been defined within the central CVZ (Figure 2.15). To the south of the KCC, the 10-12 km wide, NNE-trending Waiorongomai-Tairua Fault Zone (WTFZ) extends for ca. 40 km and ends near the southeastern sector of the KCC (Skinner, 1983). This incorporates the prevalent NNE-NE fault trend within the central CVZ, although occasional cross-cutting faults are also present. Overlapping the WTFZ east of Whangamata, is the Karangahake-Ohui Structural Trend (KOST) which extends NE from Karangahake in the south to Ohui on the east coast of the peninsula (Rabone, 1991; Merchant et al., 1988). These regional structures together represent a major extensional tectonic corridor extending from southern to central CVZ (Merchant et al., 1988).

The KCC itself lies within a 9-11 km wide, N-S striking graben interpreted from a series of gravity surveys (O'Leary, 1978). Normal faults which define the eastern and western boundaries are concealed, but suggested to be translated by NE to E-trending faults (O'Leary, 1978). Because of its similar orientation and extensional character, Whitianga Graben may be considered to be a northern continuation of the tectonic corridor defined by the WTFZ and KOST.

The only direct imprint of these regional CVZ structures on the KCC, is the NE-trending Kapowai Fault which passes through the Kapowai and Kauaeranga valleys. It has a similar NE strike to the regional fault pattern and appears to be independent of any intracaldera KCC structures. The relationship of other intracaldera KCC faults and lineations to the regional pattern is difficult to assess, but as they have significantly different orientations (i.e. NW or N) to the pattern, they are inferred to be related to caldera collapse rather than regional extension.

Parallel to the CVZ is the Hauraki Rift, a major Pliocene-Recent extensional structure. Initially, it was developed behind the eastern CVZ volcanic arc, but it now occupies an oblique position to the present plate boundary (Hochstein and Nixon, 1979; Cole, 1990). The influence of the Hauraki Rift on the KCC is not directly observed, but it is implied to influence the regional fault pattern especially to the west and north of the KCC (Skinner, 1993).

Apart from faults and graben structures, caldera structures have also been suggested to the north and south of the KCC. A caldera has been postulated for the Whitianga Volcanic Centre, 12 km north of the KCC, based upon thick ignimbrites, numerous rhyolite lava domes and a sub-circular gravity anomaly (Skinner, 1986; Briggs et al., 1998). However, no topographic boundary or structural boundaries have been observed to confirm a caldera origin for these features.

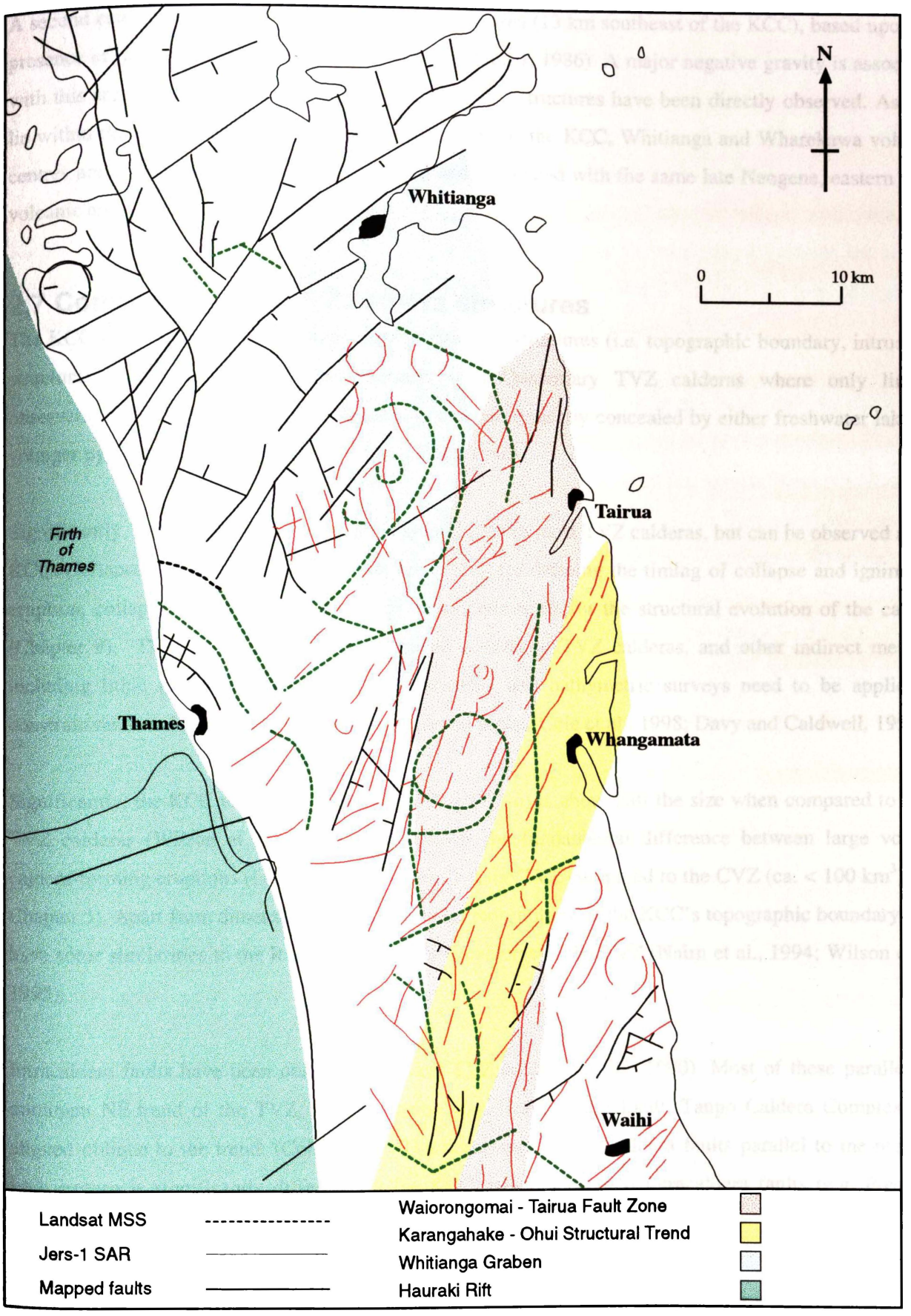


Figure 2.15 Onland regional structures of the central CVZ. Landsat MSS and mapped faults from Skinner (1995). Jers-1 SAR lineations from Belliss and Christie (1994), Whitianga graben from O'Leary (1978), WTFZ from Skinner (1983), KOST from Merchant et al. (1988), and Hauraki Rift from Hochstein and Nixon (1979).

A second caldera has been inferred in the Wharekawa area (13 km southeast of the KCC), based upon the presence of thick ignimbrites, and rhyolite domes (Skinner, 1986). A major negative gravity is associated with this area (Woodward, 1971), but no caldera-related structures have been directly observed. As they lie within the same N to NE trending tectonic corridor as the KCC, Whitianga and Wharekawa volcanic centres are considered to be structurally related and associated with the same late Neogene, eastern CVZ volcanic arc system.

## 2.7 Comparison with TVZ caldera structures

The KCC allows direct observation of most intracaldera structures (i.e. topographic boundary, intrusives, structural boundaries, faults). This contrasts with Quaternary TVZ calderas where only limited observations of these structures are available as they are typically concealed by either freshwater lakes or younger pyroclastic deposits (cf. Nairn, 1981; Cole, 1990).

Significantly, structural collapse boundaries are not seen in most TVZ calderas, but can be observed at the KCC. Collapse zones and their boundaries are crucial for defining the timing of collapse and ignimbrite eruption, collapse mechanisms, and provide direct constraints for the structural evolution of the caldera (Chapter 9). This information cannot be gained directly at TVZ calderas, and other indirect methods including lithic fragment analysis, gravity, magnetic, and bathymetric surveys need to be applied to constrain the location and extent of these subsidence zones (Cole et al., 1998; Davy and Caldwell, 1998).

Significantly, the KCC topographic diameter (10 x 11 km) is about half the size when compared to most TVZ calderas (Wilson et al., 1995). This reflects the fundamental difference between large volume caldera-forming eruptions (i.e. typically >100 $km^3$) at the TVZ compared to the CVZ (ca. < 100 $km^3$) (see Chapter 5). Apart from dimensions, the sub-circular morphology of the KCC's topographic boundary does have some similarities to the Reporoa and Rotorua calderas of the TVZ (Nairn et al., 1994; Wilson et al., 1995).

Intracaldera faults have been observed for most TVZ calderas (Cole, 1990). Most of these parallel the dominant NE-trend of the TVZ, however some (e.g. Horomatangi Fault, Taupo Caldera Complex) are aligned oblique to the trend. (Cole, 1990). The dominance of intracaldera faults parallel to the regional fault pattern is significantly different for the KCC, where identified intracaldera faults (e.g. Precipice Fault, Green Tree Fault) are oblique to the regional fault trend.

Rhyolite lava domes are a common structural feature of many TVZ calderas. Some of these have been erupted parallel to the regional fault pattern and form major lineaments (e.g. Tarawera Rhyolite dome complex; Cole, 1990). Others have been erupted along lineaments oblique to the regional faults (e.g. NS trending Whakaahu rhyolite lava dome complex) (Wilson et al., 1986). Dikes of andesitic composition

have not been reported within TVZ calderas, however basaltic dikes are common. Most of these parallel the regional fault trend (e.g. basalt dikes in the Tarawera Rift; Nairn and Cole, 1981) while others (e.g. Rotokawau Basalt) are oblique to it (Cole, 1990).

Therefore the influence of regional structures on the location of TVZ calderas and intracaldera structures is variable. Some young TVZ calderas (e.g. Taupo, Kapenga, Okataina) have developed within the main axis of regional extension (i.e. Taupo Fault Belt), and some structures within these calderas are aligned along this trend (Cole, 1990; Wilson et al., 1995). However, for other TVZ calderas (e.g. Mangakino, Rotorua) their is no clear relationship with the current regional fault pattern.

In comparison, there is some evidence at the KCC that regional structures have only had a limited influence on the development of intracaldera structures, apart from the major N to NE-trending tectonic corridor which has influenced the location of the KCC. Only one NE-trending regional fault (i.e. Kapowai Fault) passes through the KCC. Kapowai Fault displaces intracaldera units (i.e. Tarawaere Member) and appears to have controlled the distribution of intracaldera rhyolite domes (i.e. Kauaeranga Rhyolite dome, Tauranikau Rhyolite dome) and hydrothermal alteration zones. All other intracaldera faults are not aligned parallel to the regional trend, and in some instances (e.g. Green Tree Fault) are directly related to caldera collapse structures.

# Chapter Three

# KAPOWAI CALDERA COMPLEX STRATIGRAPHY

## 3.1 Introduction

Recently published geological maps covering the KCC use broad, composite lithostratigraphic units to map the geology (Skinner, 1993; 1995). These units are separated by regional unconformities, and defined in part by biostratigraphic and sporadic radiometric (K/Ar and Fission Track) dating. This has produced a general stratigraphic record for the CVZ region, but a detailed stratigraphy for individual volcanic centres, including the KCC, has not been established.

In this research, the stratigraphy of the KCC is mapped using the regional stratigraphy as a framework, but individual units are mapped in relation to the caldera, not to regional units. 16 new K/Ar dates have been obtained for selected mapping units within the KCC, and these enhance the field stratigraphy. A new 1: 25 000 geological map is presented for the KCC (see map pocket) based mainly upon revisions in stratigraphy and structure.

Differentiation of pyroclastic units is a cornerstone of this revision. Previously, ignimbrites were grouped as members of the Wharepapa Ignimbrite, together with basal lacustrine siltstones and interbedded tuffs (Skinner, 1993; 1995). This research defines several new ignimbrites and recognises that they represent individual eruptions and may be related to caldera collapse events.

Stratigraphic study of pyroclastic deposits depends upon describing components, documenting their lateral and vertical variation and correlation. Parameters used to describe pyroclastic lithologies, need to be carefully established and consistently applied. Most of these have been defined by previous workers (e.g. Fisher and Schmincke, 1984), although some key parameters, including component abundance and juvenile morphologic description are not defined in the literature. In this research, parameters have been established to describe the major characteristics of pyroclastic lithologies. Definitions for these can be found in Appendix II.

## 3.2 New K/Ar dates

Geochronological studies of extinct caldera volcanoes is fundamental because the succession is typically complex and field stratigraphic relations are difficult to establish (e.g. Lipman et al., 1996). Field relationships between caldera-related lavas, especially rhyolite lavas, and pyroclastics are generally the most difficult to ascertain, so radiometric dating in this research has focused on rhyolite lavas. Other ages have been determined for the major ignimbrite units and pre- and caldera-related andesite lavas. Samples selected were chosen on the basis of field stratigraphic control and sample freshness.

Limited radiometric ages have been determined for some intracaldera KCC units (Table 3.1) (Adams et al., 1994; Takagi, 1995). Additional K/Ar ages determined in this study are summarised in Table 3.2.

Table 3.1. Previously determined total rock K/Ar and fission track ages for Kapowai Caldera Complex units. See Takagi (1995) and Adams et al. (1994) for analytical method and additional details.

| Dating No. | Formation | Lithology | Grid Ref. | K wt.% | rad. 40Ar | Age |
|---|---|---|---|---|---|---|
| **Takagi, 1995** | | | | | | **(K/Ar)** |
| 45366 | Whitianga Group | rhyolite lava | T11/494686 | 1.971 ± 0.039 | 70.39 ± 8.31 | 9.18 ± 1.10 |
| 45368 | Bessons Island | andesite lava | T11/492687 | 1.334 ± 0.027 | 51.40 ± 0.69 | 9.90 ± 0.24 |
| 45369 | Whitianga Group | Trig Q Ignimbrite | T11/520722 | 2.148 ± 0.043 | 66.82 ± 2.73 | 8.00 ± 0.36 |
| **Adams et al., 1994** | | | | | | |
| 12769 | Taurahuehue Andesite | basaltic andesite lava | T11/490688 | 1.043 | 0.374 | 9.2 ± 0.9 |
| 12414 | Tapuaetahi Andesite | andesite lava | T12/489584 | 1.353 | 0.476 | 9.0 ± 0.4 |
| 12387 | Taurauikau Andesite | andesite lava | T11/478665 | 1.258 | 0.379 | 7.6 ± 0.4 |
| 12413 | Taurauikau Andesite | andesite lava | T12/485594 | 1.103 | 0.346 | 8.1 ± 0.2 |
| | | | | $\rho_s \times 10^4 cm^{-2}$ | $\rho_i \times 10^4 cm^{-2}$ | **(F-track)** |
| 10566 | Wharepapa Ignimbrite | ignimbrite | T11/604781 | 70.5 | 481 | 8.2 ± 0.7 |
| 10567 | Wharepapa Ignimbrite | ignimbrite | T11/600766 | 73.0 | 412 | 9.2 ±1.9 |

Radiometric K/Ar dating of mineral separates was the chosen dating method in this research. This was chosen because it is a well established technique, and is routinely used to date Neogene volcanic rocks in New Zealand (Black et al., 1992; Adams et al., 1994). 16 K/Ar dates were determined for selected units by analysing plagioclase or biotite mineral separates extracted from whole rock samples. Results are presented in Table 3.2. Sample preparation methods and analytical measurements are presented in Appendix III.

Table 3.2. New K/Ar dates for Kapowai Caldera Complex volcanic rocks determined in this study. Samples KC1 - KC10 analysed at the Hiruzen Research Institute, Japan. Samples KC11 - KC16 analysed at the Institute of Geological and Nuclear Sciences, Lower Hutt.

| Dating No. | Sample | Unit | Min | Grid Ref. | Lab No. | K wt.% | rad. 40Ar | Age |
|---|---|---|---|---|---|---|---|---|
| KC1 | W99614 | WES-1 Ignimbrite | plag | T11/511643 | S36-151 | 0.262 ± 0.013 | 5.48 ± 0.12 | 5.38 ± 0.29 |
| KC2 | W99886 | WES-1 Ignimbrite | plag | T11/551679 | S36-153 | 0.345 ± 0.017 | 8.29 ± 0.18 | 6.18 ± 0.34 |
| KC3 | W99612 | Oteao Ignimbrite | plag | T11/534670 | S36-156 | 0.240 ± 0.012 | 5.30 ± 0.14 | 5.68 ± 0.32 |
| KC4 | W99693 | Webb Creek Ignimbrite | plag | T12/486572 | S36-154 | 0.294 ± 0.015 | 6.16 ± 0.20 | 5.39 ± 0.32 |
| KC5 | W99600 | Rangihau Rhyolite | plag | T11/499654 | S36-155 | 0.281 ± 0.014 | 7.52 ± 0.15 | 6.89 ± 0.37 |
| KC6 | W99912 | Precipice Rhyolite | plag | T11/522660 | S36-152 | 0.211 ± 0.011 | 4.20 ± 0.08 | 5.12 ± 0.28 |
| KC7 | W99908 | Precipice Rhyolite | plag | T11/522660 | S36-149 | 0.254 ± 0.013 | 5.12 ± 0.33 | 5.19 ± 0.42 |
| KC8 | W991002 | Kokonga Rhyolite | plag | T11/556654 | S36-150 | 0.221 ± 0.011 | 5.60 ± 0.14 | 6.51 ± 0.36 |
| KC9 | W991005 | Ruahine Rhyolite | plag | T11/565648 | S36-148 | 0.400 ± 0.020 | 9.09 ± 0.15 | 5.86 ± 0.31 |
| KC10 | W99835 | Welcome Jack Rhyolite | biot | T11/511623 | S36-157 | 6.128 ± 0.123 | 200.8 ± 3.4 | 8.42 ± 0.22 |
| KC11 | W99876 | Kauaeranga Rhyolite | plag | T12/489583 | 22254 | 0.22 ± 0.002 | 0.042 ± 0.003 | 4.9 ± 0.6 |
| KC12 | W99994 | Camp Rhyolite | plag | T12/504578 | 22255 | 0.29 ± 0.003 | 0.060 ± 0.004 | 5.3 ± 0.3 |
| KC13 | W99706 | Taurauikau Andesite | plag | T12/484596 | 22256 | 0.29 ± 0.003 | 0.096 ± 0.012 | 8.5 ± 0.6 |
| KC14 | W99816 | Taurauikau Andesite | plag | T11/484647 | 22257 | 0.31 ± 0.003 | 0.092 ± 0.017 | 7.6 ± 0.5 |
| KC15 | W99691 | Taurahuehue Andesite | plag | T12/482572 | 22258 | 0.28 ± 0.003 | 0.072 ± 0.014 | 6.6 ± 0.3 |
| KC16 | W99733 | Taurauikau Andesite | plag | T11/484636 | 22259 | 0.29 ± 0.003 | 0.072 ± 0.010 | 6.4 ± 0.4 |

## 3.3 Kapowai Caldera Complex stratigraphy

The stratigraphy of the KCC has previously been mapped as part of the Whitianga Group (silicic volcanics) and Coromandel Group (andesitic-dacitic volcanics) (Schofield, 1967). Schofield (1967) subdivided Whitianga Group into Coroglen Subgroup which included all pyroclastics and associated epiclastics, and Minden Rhyolite Subgroup for all rhyolite lavas. In the Whitianga area, Skinner (1993, 1995) further divided Coroglen Subgroup into three formations, with the Wharepapa Ignimbrite Formation including all KCC derived pyroclastics (four members). Skinner (1993, 1995) also divided Minden Rhyolite into Rangihau Rhyolite Formation and Ruahine Rhyolite Formation respectively (Table 3.3).

Table 3.3. Stratigraphic nomenclature for units of the Kapowai Caldera Complex. After Skinner (1993, 1995).

| Group | Subgroup | Formations | Members |
|---|---|---|---|
| Whitianga | Coroglen | Wharepapa Ignimbrite | Wainora Member |
| | | | Pepe Ignimbrite Member |
| | | | Hot Water Beach Ignimbrite Flow Member |
| | | | Trig Q Lenticulite Member |
| | Minden Rhyolite | Rangihau Rhyolite | |
| | | Ruahine Rhyolite | |
| Coromandel | Waiwawa | Maumaupaki Formation | |
| | | Taurahuehue Andesite | |
| | | Tapuaetahi Andesite | |
| | Omahine | Taurauikau Andesite | |

This research utilises Skinner's (1993, 1995) stratigraphic framework as a basis for revision of the KCC geology. A more detailed stratigraphic approach is applied which recognises volcanic units as representing individual eruptive events. The stratigraphy of the KCC is divided into two successions, pre-caldera and intracaldera. Intracaldera stratigraphy is further subdivided by the Wharepapa Eruptive Sequence (WES), so that there is a pre-WES, WES, and post-WES succession (Table 3.4).

The pre-caldera sequence consists of several andesitic-dacitic lava, breccia, epiclastic and tuff units. These are distinguished on the basis of lithology and field relationships. Pre-WES stratigraphy consists of a thick pyroclastic succession of andesitic-rhyolitic ignimbrites and tuffs, andesite intrusives and lavas, rhyolite lava domes and volcaniclastic lacustrine sequences. WES consists of a thick ignimbrite, tuff and lithic lag breccia sequence. The post-WES succession consists of rhyolite lava domes and dikes.

Revised field stratigraphy together with new K/Ar age results have significant implications for the eruptive history of the KCC. Key features are the large variation in age for the Taurauikau Andesite (previously considered a post-caldera unit), eruptive ages determined for the oldest (8.42 Ma) and youngest (4.9 Ma) caldera related unit, and recognition that the WES is the youngest KCC derived explosive eruptive event (mean age of 5.8 Ma).

Table 3.4 Summary stratigraphy of the Kapowai Caldera Complex. Biostratigraphic and K/Ar dates are from Hayward (1974a, b), Skinner (1993; 1995), Adams et al. (1994), Takagi (1995) and this study. * Age of unit within or near the KCC.

| Succession | Age (Ma) | Lava | Pyroclastic | Sedimentary |
|---|---|---|---|---|
| Post-WES | 4.9 | Kauaeranga Rhyolite | | |
| | | Tauranikau Rhyolite | | |
| | 5.12 - 5.19 | Precipice Rhyolite | | |
| | 5.3 | Camp Rhyolite | | |
| | | Pinnacles Rhyolite | | |
| | | Big Beetle Rhyolite | | |
| | | Acadia Rhyolite | | |
| WES | 6.2 - 5.4 | | Wharepapa Eruptive Sequence | |
| Pre-WES | 5.68 | | Oteao Ignimbrite | |
| | 5.86 | Ruahine Rhyolite | | |
| | | Kydd Rhyolite | | |
| | | Wharepapa Rhyolite | | |
| | | Slip Rhyolite | | |
| | | Kapowai Rhyolite | | |
| | 6.51 | Kokonga Rhyolite | | |
| | | Miller Flat Rhyolite | Manuka Ignimbrite | |
| | | Starvation Rhyolite | | |
| | | Waiwhatawhata Rhyolite | | |
| | 6.89 | Rangihau Rhyolite | | |
| | Taranaki series | | | Haukawakawa |
| | 8.00* | | Trig Q Ignimbrite | |
| | 8.5 - 6.4 | Taurauikau Andesite | | |
| | | Bulls Run Rhyolite | | |
| | | Scots Rhyolite | | |
| | | Moss Creek Rhyolite | Colorado Pyroclastics | |
| | Taranaki series | | | Tarawaere Member |
| | | Atuatumoe Rhyolite | | |
| | | Moyles Rhyolite | | |
| | 8.42 | Welcome Jack Rhyolite | | |
| | | | Webb Creek Ignimbrite | Walwawa Member |
| Pre-Caldera | 9.0* | Tapuaetahi Andesite | | |
| | 9.5* | Taurahuehue Andesite | | |
| | 11.2* | Maumaupaki Formation | | |

## 3.4 Pre-Caldera Stratigraphy

The oldest pre-caldera rocks outcropping near or on the KCC topographic boundary are andesitic-dacite lavas and breccias of the Coromandel Group (Skinner, 1976). Coromandel Group is defined by Skinner (1976) to include all CVZ volcanic rocks of low $SiO_2$ and low $K_2O$ tholeiitic andesite to calc-alkaline andesite/dacite composition. Three main lithostratigraphic units are recognised and follow a similar definition of Skinner (1993, 1995).

### Maumaupaki Formation (cn)

Plagioclase-quartz-hornblende-orthopyroxene-biotite phyric andesitic-dacitic lavas/breccias are the oldest rocks outcropping near the KCC topographic boundary. These lavas/breccias correlate to the Maumaupaki Formation, a composite group of andesite-dacite lavas and breccias within Kuaotunu Subgroup of the Coromandel Group (Skinner, 1993).

Lavas and breccias are the main lithotypes. Lavas are dark grey, coarse grained, and porphyritic. Phenocrysts (35-40%) consist of plagioclase, hornblende, orthopyroxene, minor corroded quartz, and rare biotite. Lavas are well jointed (10-15 cm joint spacing). Breccias are monolithologic and contain angular

to subangular, block to coarse lapilli lava clasts within a coarse grained matrix. Hydrothermal alteration of Maumaupaki Formation occurs, but is restricted to outcrops in the Waiwawa valley (Skinner, 1993).

Major outcrops of Maumaupaki Formation occur in the Waiwawa valley and extend west to the Te Mata and Te Kaka valleys (Skinner, 1993). Minor outcrops are present in the lower Kapowai valley (T11/529693) and headwaters of Parakau Stream (T11/576663). Maximum exposed thickness ranges from ca. 120m (lower Kapowai valley) to ca. 200m in the Waiwawa valley. Outcrops in the lower Kapowai valley are locally elevated relative to adjacent younger volcaniclastics (Haukawakawa Member), pyroclastics (WES-1 Ignimbrite) and rhyolite lavas (Pukekotare Rhyolite) (Guay, 1999). This suggests that these were exposed at the time of caldera activity, perhaps uplifted along KCC rim faults.

A basal contact for Maumaupaki Formation is not observed within the KCC. Furthermore, no overlying contacts are observed, although several units are inferred to unconformably overlie Maumaupaki Formation. These include Taurahuehue Andesite in the Waiwawa valley, and WES in the lower Kapowai valley. Maumaupaki Formation is inferred to underlie the northern sector of the caldera fill sequence. Evidence for this is the presence of Maumaupaki Formation-correlative lavas occurring as lithic fragments within some ignimbrites (chapter four), and the occurrence of lavas/breccias to the west and north of the main outcrop distribution.

On the basis of field stratigraphy and distribution, together with correlative lithic fragments in younger pyroclastic units, Maumaupaki Formation is considered to predate caldera activity. K/Ar dating of Maumaupaki Formation to the west and NW of the KCC yields an age of 11.2 ± 0.3 Ma (Skinner, 1993).

### Taurahuehue Andesite (at)

Unconformably overlying Maumaupaki Formation are andesite lavas with subordinate breccias and tuffs. Regionally, these are mapped as Taurahuehue Andesite, a unit within the Waiwawa Subgroup (Skinner, 1986; 1993).

Outcrops of Taurahuehue Andesite form north-trending ridgelines between the Waiwawa and Oteao valleys and between the Oteao and Kapowai valleys. In the Kauaeranga valley, Taurahuehue Andesite outcrops along the upper valley floor (Figure 3.1), and continues southwest towards Thames. Sporadic outcrops are also present in the upper Waiwawa valley.

Taurahuehue Andesite consists predominantly of two-pyroxene andesite lavas with minor autoclastic breccias, and rare tuffs. Lavas are typically dark grey, medium grained, porphyritic, and platy jointed (5-10 cm joint spacing). Phenocrysts (25-30 %) consist of plagioclase, orthopyroxene, clinopyroxene and Fe-Ti oxides. Hayward (1974) also reported hornblende as a phenocryst in some lavas, although it has not

been observed in this research. Autoclastic breccias are monolithologic, clast supported, and clast size varies from < 10 mm to 120 mm. Andesitic tuffs are moderately sorted and typically vitric dominated.

Figure 3.1 Taurahuehue Andesite lava outcrop in the floor of the Kauaeranga valley (T11/478566).

Hayward (1974b) described lithological variations within the Taurahuehue Andesite, and correlated some units within the Kauaeranga valley. Additional sections within the Kauaeranga valley are described in Figure 3.2. Lava is the dominant lithology and typically several lava flows are recognised at most sections. Lavas are thin (minimum thickness up to 18 m) and generally grade into thick autoclastic breccias (up to 12 m). Andesitic vitric tuffs are rare, but typically form thick beds (up to 1.5 m).

Local incipient hydrothermal alteration occurs within some outcrops in the Kauaeranga valley. Jasper veinlets are observed near the Kauaeranga River-Webb Creek confluence. Propylitic and sericitic alteration of Taurahuehue Andesite was mapped in the Waiwawa valley by Skinner (1993).

Taurahuehue Andesite unconformably overlies Maumaupaki Formation in the Waiwawa valley, and is unconformably overlain by Webb Creek Ignimbrite in the Kauaeranga valley (T12/486572), and by Waiwawa Member in Waiwawa valley (T12/457594). These latter contacts define the unconformity between pre-caldera and caldera units. In the northern sector of the KCC, Taurahuehue Andesite is unconformably overlain by Colorado Pyroclastics, Trig Q Ignimbrite and WES-1 Ignimbrite, although the contact is seldom seen. K/Ar dating of Taurahuehue Andesite to the west of the KCC yielded a weighted mean age of 9.5 ± 0.6 Ma (Adams et al., 1994). A single $K/Ar_{(plagioclase)}$ age of 6.6 ± 0.3 Ma was obtained in this research for Taurahuehue Andesite in the Kauaeranga valley. This age is significantly younger

compared to other published K/Ar dates from the western KCC margin. The unit sampled for dating may represent a younger valley-infilling lava flow, not previously recognised.

### Tapuaetahi Andesite (ap)

Tapuaetahi Andesite forms two minor dikes in the lower Kapowai valley (T11/543688; T11/527702), and extensive outcrops of lava and breccia to the east of the KCC (Adams, 1992).

Tapuaetahi Andesite consists of a grey, medium grained, porphyritic andesitic-dacitic lava. Phenocrysts (30-35 %) consist of plagioclase, quartz, orthopyroxene, clinopyroxene and Fe-Ti oxides. Lavas are typically moderately jointed (10-15 cm joint spacing).

Tapuaetahi Andesite intrudes Maumaupaki Formation, and is overlain by WES pyroclastics. K/Ar ages of correlative exocaldera Tapuaetahi Andesite in the Boat Harbour-Tairua area yield a mean age of 8.75 ± 0.5 Ma (Skinner, 1995). No age has been determined for Tapuaetahi Andesite outcropping on the margins of the KCC.

## 3.5 Caldera complex stratigraphy

A quiescent period followed andesitic-dacitic volcanism in the Kauaeranga-Tairua-Coroglen area, and this is recorded by a thick sequence of volcaniclastic lacustrine siltstones and sandstones (Waiwawa Member). Thin, interbedded silicic tephras and reworked volcanic detritus are recorded within this sequence, implying some contemporaneous, small scale explosive silicic volcanism within the area or from other centres in the CVZ. Quiescence ended with the first large scale explosive silicic eruptions (Webb Creek Ignimbrite), and this was followed by numerous explosive episodes and associated effusive volcanism.

Explosive and effusive silicic volcanism in the CVZ, including the KCC has been mapped as the Coroglen Subgroup, and Minden Rhyolite Subgroup, respectively, of the Whitianga Group (Skinner, 1986; Skinner, 1995). However, as the succession at the KCC records a complex, intercalated succession of explosive and effusive volcanism (including both silicic and andesitic compositions), all explosive and effusive units are assigned in this study as members of the Rangihau Subgroup. Rangihau Subgroup in effect records the volcanic stratigraphy for the KCC, which now differs significantly from earlier work (i.e. Skinner, 1993; 1995) by differentiating the pyroclastic, effusive and lacustrine stratigraphy.

KCC ignimbrites defined by Skinner (1993, 1995) were grouped together and mapped as flow members of one single eruptive event, the Wharepapa Ignimbrite. This research recognises that individual ignimbrites represent separate large volume pyroclastic eruptions, with or without associated caldera collapse, and so there are many more ignimbrite units recognised at the KCC than previously thought. Since intracaldera ignimbrites typically have a limited outcrop distribution, they are identified and defined on the basis of a unique component lithology and/or mineralogy.

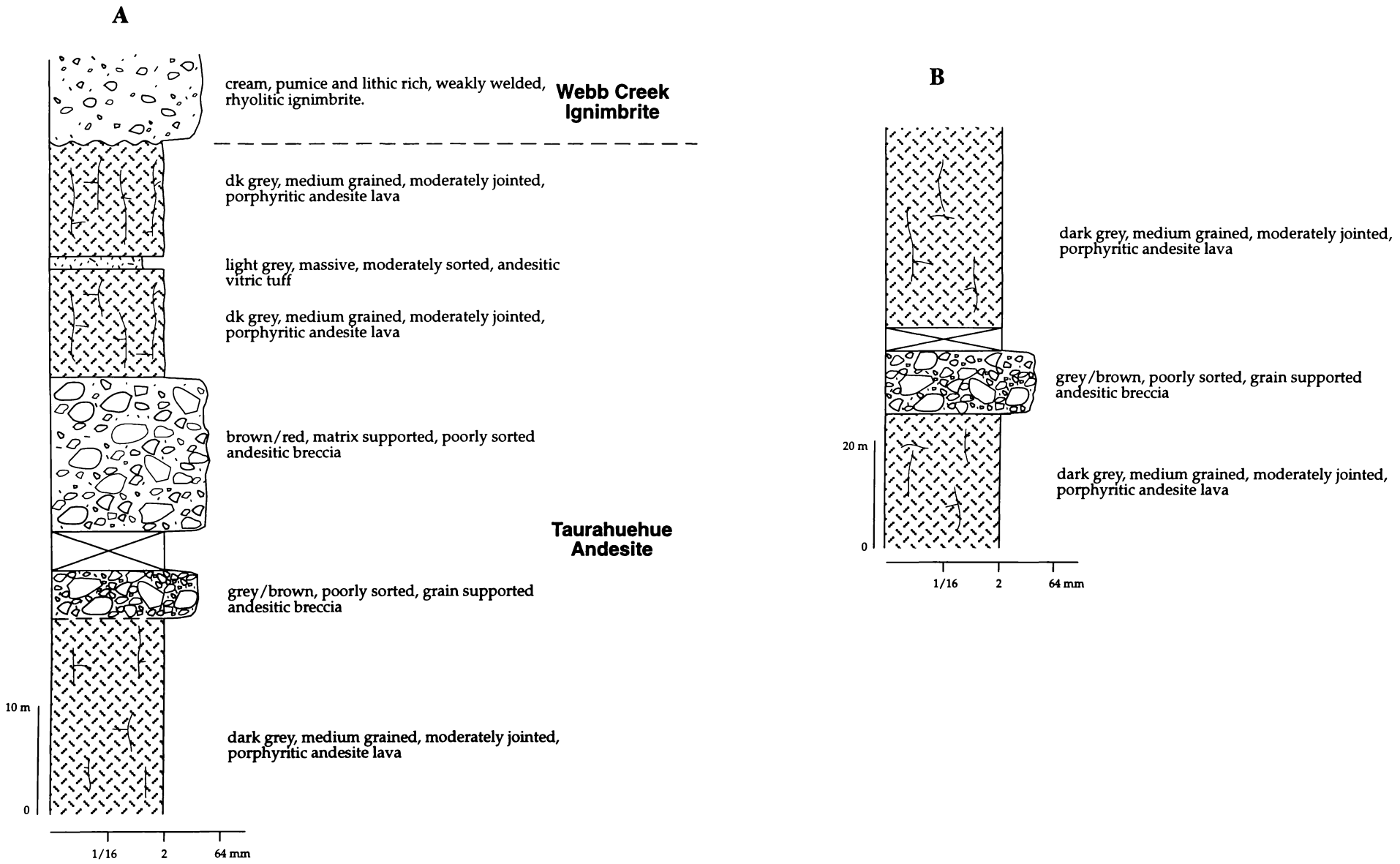


Figure 3.2 Composite sections of Taurahuehue Andesite showing internal lithologic variation. A, Webb Creek Section (T12/482572-T12/486572). B, Kid Stream Section (T12/481578-T12/479582).

Four rhyolite lava groups are defined at the KCC on the basis of phenocryst mineralogy. These are plagioclase-pyroxene phyric rhyolites (group I; K), quartz-plagioclase-biotite phyric (group II; U), plagioclase phyric (group III; R), and plagioclase-amphibole phyric (group IV; S). No stratigraphic relationships are inferred or suggested by these groupings.

Volcaniclastic lacustrine stratigraphy revises the work of Hayward (1974a) and Skinner (1993; 1995). Three areas of intracaldera lacustrine sequences occur in the Waiwawa-Wainora, Kauaeranga, and Rangihau areas. Wainora Formation (Hayward, 1974a) is re-erected to include all volcaniclastic lacustrine sequences outcropping adjacent to, or within the KCC, and three members are defined. Waiwawa Member is erected for lacustrine sequences in the Waiwawa and Wainora valleys that overlie Taurahuehue Andesite and pre-date lacustrine sequences in the Kauaeranga and Rangihau valleys. Tarawaere Member is erected to include all Kauaeranga valley lacustrine sequences that overly Webb Creek Ignimbrite. Haukawakawa Member includes all lacustrine sequences outcropping in the Rangihau valley, which pre-date the WES. The age relationship between Tarawaere and Haukawakawa Members is difficult to determine, but as Haukawakawa Member directly underlies WES pyroclastics, it is defined as the youngest unit.

### *Pre-WES caldera stratigraphy*

#### Waiwawa Member (new) (ww)

Unconformably overlying Taurahuehue Andesite in the Waiwawa and Wainora valleys is a thick volcaniclastic lacustrine sequence. Previously defined as the Wainora Formation (Hayward, 1974a) and Wainora Member (Skinner, 1995), it is defined in this study as the Waiwawa Member of the Wainora Formation.

Waiwawa Member consists of basal carbonaceous gravels and conformable highly carbonaceous, volcaniclastic sandstones and siltstones (Hayward, 1974a). Beds are typically brown-black, massive or mm-laminated. Freshwater mussels (*Hyridella* s.s.), and several plant fossils (*Fagus novaezelandiae*, *Melicytus* aff. *ramiflorus*, *Neopanax* aff. *simplex*) occur within the sequence (Hayward, 1973, 1974a). The sequence has a maximum thickness of 35 m, and is gently tilted to the NE (Hayward, 1974a).

Waiwawa Member unconformably overlies Taurahuehue Andesite and itself is overlain by Colorado Pyroclastics. A Pliocene age on the basis of palynological studies was suggested, although a Taranakian (late Miocene) age could not be discounted (Hayward, 1974a).

#### Webb Creek Ignimbrite (new) (wi)

Webb Creek Ignimbrite outcrops within the Kauaeranga valley floor and along its tributaries (Figure 3.3). It generally forms the bed of streams, and has poor topographic expression. Thickness ranges from ca. 30 m to 75 m in the Kauaeranga valley. Webb Creek Ignimbrite is the oldest ignimbrite outcropping within

KCC, and represents one of the earliest large scale silicic pyroclastic eruptions in the Kauaeranga-Rangihau-Kapowai area.

Webb Creek Ignimbrite is light grey, pumice-rich, lithic-rich, weakly welded and sporadically incipiently hydrothermally altered. There is a single juvenile type (25-35 %) present which is a cream, non-lenticular, non-fibrous, subrounded pumice. Pumice phenocrysts (< 3 %) include plagioclase and Fe-Ti oxides. The matrix is fine ash-sized, and contains plagioclase, quartz, orthopyroxene, clinopyroxene, amphibole, and Fe-Ti oxide crystals. Lithic fragments are abundant (25-75 %), angular to subangular, lapilli to block size, and include rhyolite, dacite and andesite lavas, and rare welded ignimbrite. Significantly, no volcaniclastic siltstone lithics are present.

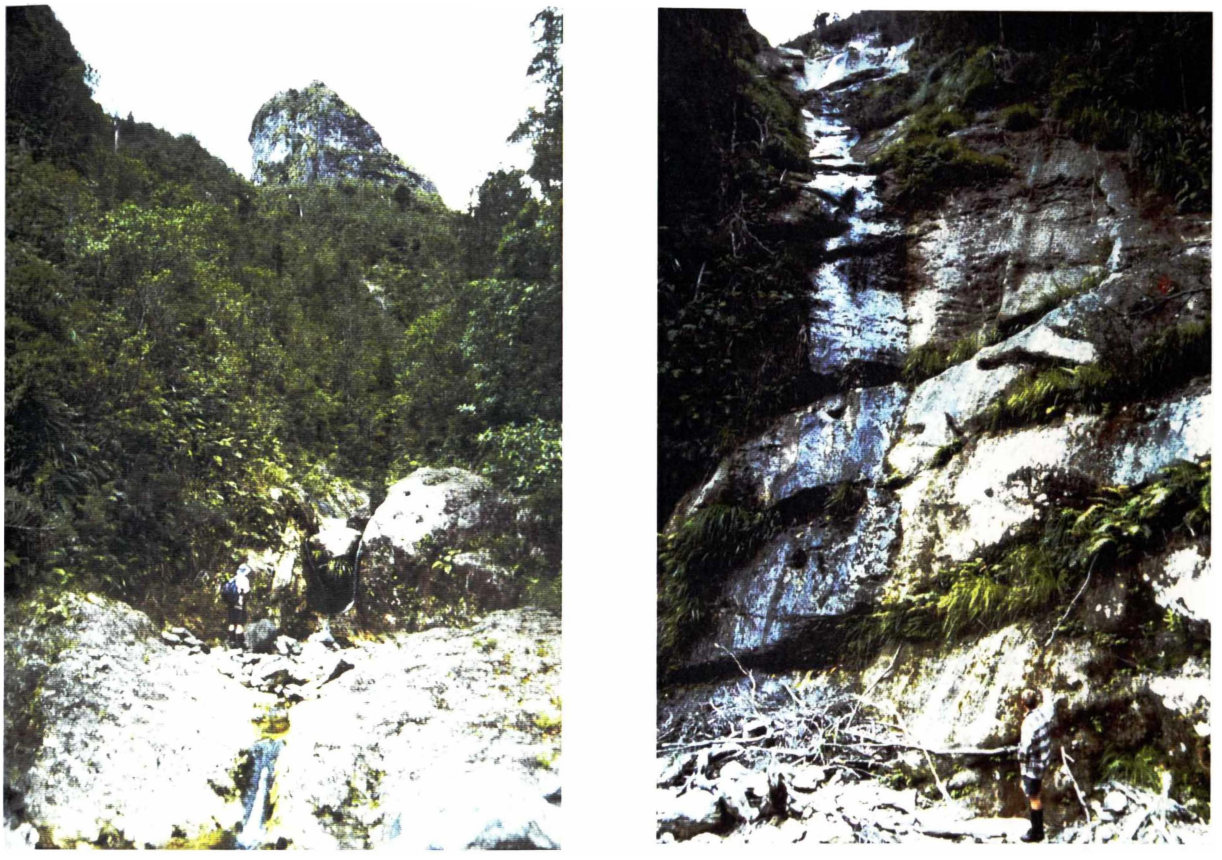

A B

Figure 3.3 Webb Creek Ignimbrite outcrops in a tributary stream of the Kauaeranga River. A, Webb Creek Ignimbrite (foreground) intruded by Tauranikau Rhyolite lava (background). B, ca. 30 m section of Webb Creek Ignimbrite (T12/505583).

Vertical variations are observed in lithic size and abundance, but the nature of the juvenile component and matrix remain consistent (Figure 3.4a, b). Two lithic concentration zones are observed at heights of ca. 22 m and 36 m in the Webb Creek section, suggesting a composite depositional sequence. Lateral changes are difficult to assess because of limited outcrop.

Local incipient to strong propylitic alteration of Webb Creek Ignimbrite occurs in the Kauaeranga valley. From T12/485578 to T12/486580, Webb Creek Ignimbrite is strongly propylitic altered and sporadic veinlets of quartz and chalcedony occur (see Chapter 8).

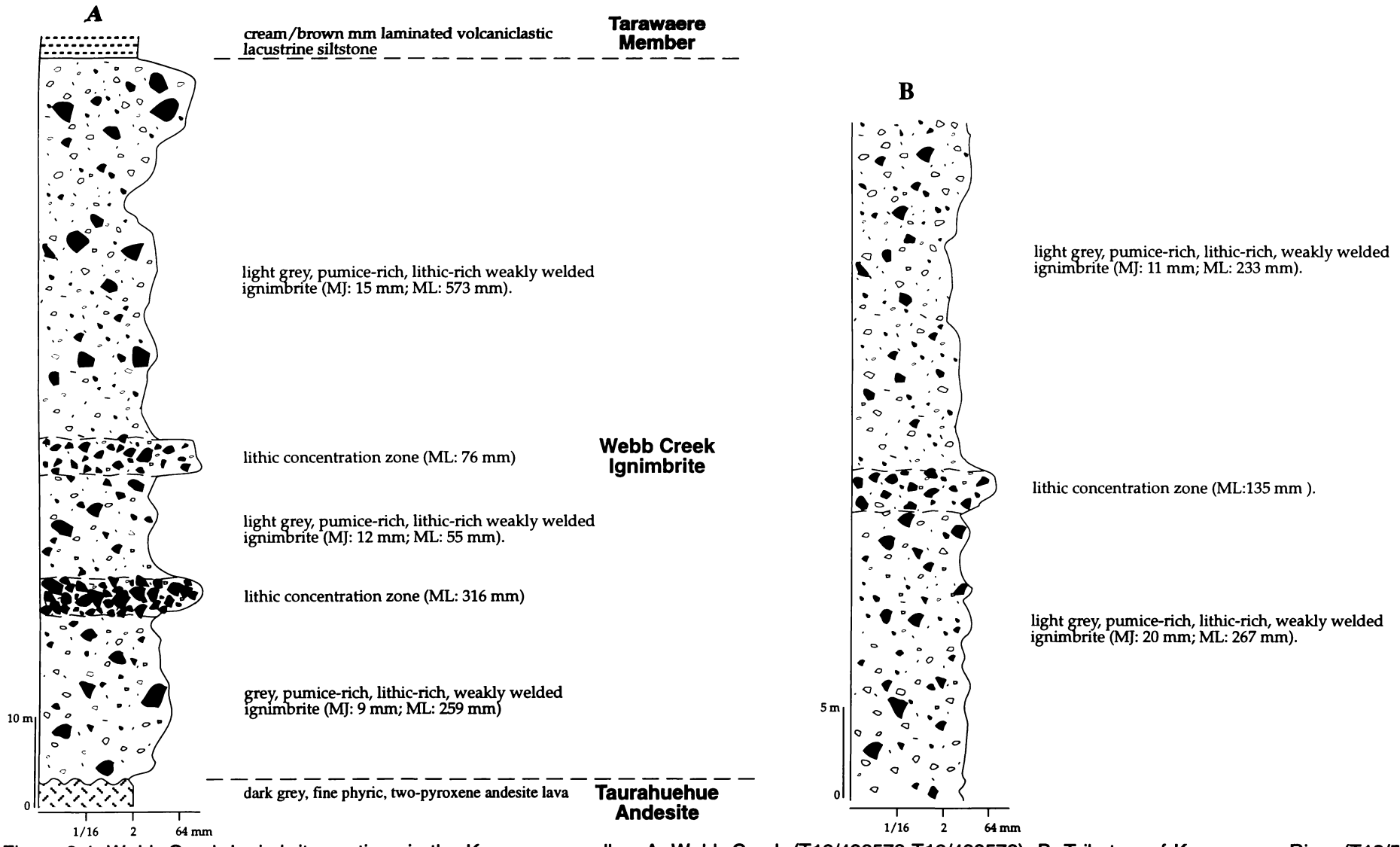


Figure 3.4. Webb Creek Ignimbrite sections in the Kauaeranga valley. A, Webb Creek (T12/486572-T12/488572). B, Tributary of Kauaeranga River (T12/501586-T12/506582).

Webb Creek Ignimbrite unconformably overlies Taurahuehue Andesite and is overlain by volcaniclastic siltstones and breccias (T12/488573) of the Tarawaere Member (Wainora Formation). This implies an age younger than ca. 9.5 Ma but no older than Taranakian. A $K/Ar_{(plagioclase)}$ age of 5.39 ± 0.32 Ma was determined, but this is considered too young based on the mean age of 5.8 Ma obtained for overlying WES-1 Ignimbrite. The dated sample may have been affected by incipient weathering or hydrothermal alteration, resulting in a younger K/Ar age.

### Welcome Jack Rhyolite (new) (uj)

Welcome Jack Rhyolite forms a ca. 1 km ridge (Figure 3.5) and dome between Slip Stream and Mine Creek in the central KCC. It covers an area of ca. 2 $km^2$ with a minimum estimated volume of 0.8 $km^3$.

Welcome Jack Rhyolite is a light grey, fine grained, porphyritic rhyolite lava. Phenocrysts (10 %) consist of quartz, biotite, plagioclase and Fe-Ti oxides. Amygdules occur in some lavas and mm-flow banding is common. Propylitic and sericitic alteration and associated Au-Ag mineralisation occurs sporadically within and on the margins of the lava dome (see Chapter 8).

**Figure 3.5** Western margin of the Welcome Jack Rhyolite dome in the central Kapowai Caldera Complex. View NE from T11/504627.

WES ignimbrite overlies Welcome Jack Rhyolite in the saddle (T11/509621) between the 641m spot height and the Welcome Jack Dome. Slip Rhyolite dike intrudes Welcome Jack Rhyolite on its northern margin, associated with the E-W striking structural boundary fault. Propylitic and sericitic alteration of Welcome Jack Rhyolite post-dates the emplacement of the rhyolite and intrusion of the Slip Rhyolite. These field relations imply that Welcome Jack Rhyolite was erupted early in the evolution of the KCC. A single $K/Ar_{(biotite)}$ age of 8.42 ± 0.02 Ma obtained in this study supports this inference.

### Moyles Rhyolite (new) (ko)

Moyles Rhyolite forms weathered outcrops in Colorado Stream, Kauaeranga valley. Outcrops are minor (< 2 m) and sporadic (T12/467572).

Moyles Rhyolite is a light grey, fine grained porphyritic rhyolite lava. Phenocrysts (5 %) consist of plagioclase, orthopyroxene and Fe-Ti oxides. Phenocrysts are weathered and typically altered to clay minerals.

No direct contacts are observed, but in the Colorado Stream section, Moyles Rhyolite appears to overlie Taurahuehue Andesite, and itself is overlain by Tarawaere Member. Previously mapped forming the Moyles Dome (Hayward, 1974b), these outcrops are instead weathered Taurahuehue Andesite.

### Atuatumoe Rhyolite (ka)

Atuatumoe Rhyolite forms a dome in the Kauaeranga valley, near the southern topographic boundary. The dome covers ca. 1 $km^2$ and has an estimated minimum volume of 0.4 $km^3$.

Atuatumoe Rhyolite is a light grey/blue, fine grained, porphyritic rhyolite lava. Phenocrysts (5 %) consist of plagioclase, orthopyroxene, and Fe-Ti oxides. Rhyolite lava is the major lithology although rhyolitic breccia outcrops at the base of the dome, in Atuatumoe Stream (T12/484562).

Atuatumoe Rhyolite intrudes Taurahuehue Andesite and Webb Creek Ignimbrite. It appears to be overlain by WES pyroclastics, although no direct contact has been observed. A younger (i.e. post-WES) age cannot be discounted, as adjacent rhyolite lava domes have a post-WES age.

### Tarawaere Member (new) (wt)

Hayward (1974a) described volcaniclastic lacustrine siltstones, sandstones and breccias outcropping in the Kauaeranga valley and included them in the Wainora Formation. However, outcrops in the Kauaeranga valley, are now recognised to predate deposits in the Waiwawa area (Waiwawa Member). They also lack a similar fossil population and abundance, and are typically massive and finer grained than Waiwawa Member deposits. To recognise these differences, Tarawaere Member is erected for lacustrine sequences in the upper Kauaeranga valley.

Tarawaere Member occurs sporadically along the Kauaeranga valley floor (up to 5 m thick) and forms more significant outcrops in tributary valleys (up to 20 m). Syndepositional (e.g. intrasequence faulting) and post-induration deformation (e.g. tilting) of the sequence is observed at several localities (Figure 3.6), but analysis of the overall deformation pattern is hampered by discontinuity of outcrop.

Five lithotypes are recognised within the sequence. Type (I) is a brown, massive, well sorted siltstone. Type (II) is a brown-grey, mm-laminated moderately sorted volcaniclastic siltstone. Interbedded crystal, vitric and lithic rich beds are common. Type (III) is a grey, well sorted massive to mm-laminated siltstone with occasional interbedded crystal and vitric tuffs. Type (IV) is a dark grey-black, poorly sorted carbonaceous sandstone or siltstone. Type (V) is a grey-brown, poorly sorted volcaniclastic sandstone which may include interbedded crystal and/or vitric tuff beds. Lithotypes vary in thickness and occurrence within exposed sequences (Figure 3.7).

Tarawaere Member unconformably overlies Webb Creek Ignimbrite and is overlain by Colorado Pyroclastics (T12/468574) and WES (T12/491574). No biostratigraphic age has been determined, as no fossils have been observed in Tarawaere Member.

**Figure 3.6** Inclined volcaniclastic lacustrine siltstone (Tarawaere Member) in the floor of the Kauaeranga valley (T11/488583). Hammer is 30 cm long.

### Colorado Pyroclastics (new) (cp)

Colorado Pyroclastics is an informal formation of intracaldera undifferentiated ignimbrites, tuffs and minor interbedded volcaniclastic lacustrine siltstones that post-date Webb Creek Ignimbrite and Waiwawa and Tarawaere Members, but pre-date Taurauikau Andesite. Colorado Pyroclastics occur in the NW Kauaeranga valley, eastern margin of the upper Waiwawa valley and sporadically in northern and eastern sectors of the KCC.

In the NW Kauaeranga valley, a series of ignimbrites and tuffs (CP-1) with occasional interbedded lacustrine siltstones outcrop (Figure 3.8). Ignimbrites are typically cream-light grey, pumice-rich, lithic-poor and weakly welded. Juvenile types vary but are generally cream, incipiently to poorly vesicular, poorly fibrous, non lenticular pumice (although moderately lenticular types occur). Matrix crystals consist of plagioclase, orthopyroxene, clinopyroxene, minor amphibole, rare biotite and Fe-Ti oxides. Lithics consist of andesite, rhyolite and rare welded ignimbrite fragments. Units overlie either Waiwawa Member or Taurahuehue Andesite.

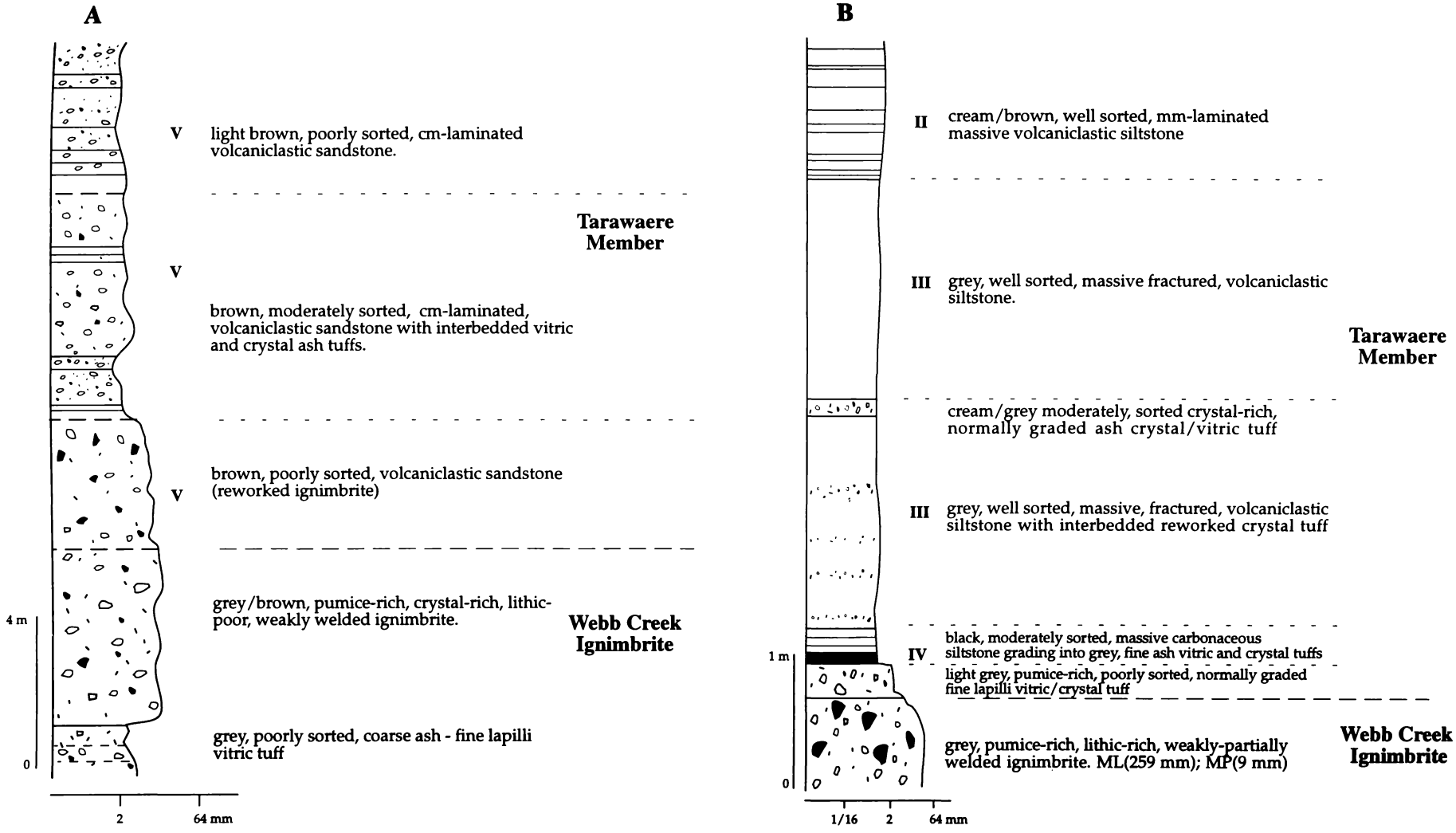


Figure 3.7. Composite sections of Tarawaere Member (Wainora Formation) in tributaries of the Kauaeranga River. A, Derek's Creek Section (T12/484582). B, Webb Creek Section (T12/489572-T12/488573).

A cream, lithic rich weakly welded ignimbrite (CP-2) occurs along ca. 100 m of the Kapowai valley floor (T11/552660-T11/552559). A single juvenile type present is a cream, non-lenticular, incipiently vesicular, non-fibrous vapour phase altered pumice. Matrix crystals consist of plagioclase, amphibole and Fe-Ti oxides. Lithic fragments include andesite, dacite and rhyolite lavas, lacustrine siltstones, vitric and crystals tuffs, and welded ignimbrite fragments. Convolute, and dish and pillar structures are present within the ignimbrite suggesting a subaqueous emplacement environment (cf. Nelson et al., 1989; Bailey and Carr, 1994). The ignimbrite is intruded by Precipice Rhyolite lava dikes, and is overlain by WES pyroclastics.

Strong propylitic alteration of ignimbrite(s) occurs at several localities upstream of CP-2 ignimbrite at T11/541641 and T11/532623. These ignimbrites occur in the Kapowai valley floor, they are considered to pre-date WES. No absolute correlation can be made to other ignimbrites due to the strong alteration, but they are likely to be of a similar age as CP-2. A propylitic altered ignimbrite occurring on the eastern margin (T11/495633) of the Welcome Jack Rhyolite dome is also considered to be of a similar age to ignimbrites of the Colorado Pyroclastics. It overlies Welcome Jack Rhyolite, and is inferred to be overlain by WES-1 Ignimbrite.

An ignimbrite (CP-3) underlying Trig Q Ignimbrite in the northern KCC, is also included in the Colorado Pyroclastics. This ignimbrite is cream, pumice-rich, lithic-poor and weakly welded. It has an upper case-hardened, cream/pink pumice concentration zone. Two juvenile types are present; Type I is a cream, incipiently vesicular, poorly fibrous, non-lenticular pumice, and contains phenocrysts of plagioclase and Fe-Ti oxides. Type II is an orange/pink, poorly vesicular, incipiently fibrous, non-lenticular, plagioclase-pyroxene phyric pumice. Lithics (3 %) consist of dacite and rhyolite lavas, minor welded ignimbrite, and rare siltstone fragments. A correlation with ignimbrites in the Kauaeranga and Kapowai valleys is likely, but as it has a similar pumice morphology and mineralogy to several of these ignimbrites, no precise correlation can be made.

Colorado Pyroclastics record a period of multiple, small volume explosive eruptions from the KCC. Their age is constrained by the underlying Webb Creek Ignimbrite, and Taurauikau Andesite which intrudes ignimbrites in the Kauaeranga and Waiwawa valley. In other areas of the KCC, Colorado Pyroclastics are overlain by Trig Q Ignimbrite or WES deposits. Correlation of individual eruptive units is difficult as outcrops are discontinuous, and compositions are similar within multiple units.

### Moss Creek Rhyolite (new) (um)

Moss Creek Rhyolite consists of an eroded, relict ca. 0.5 $km^2$ dome in the headwaters of the Waiwawa River, in the southwestern sector of the KCC. Outcrops are sporadic and are typically moderately to strongly weathered.

Moss Creek Rhyolite is a grey, fine grained, porphyritic rhyolite lava. Phenocrysts consist of plagioclase, biotite and Fe-Ti oxides.

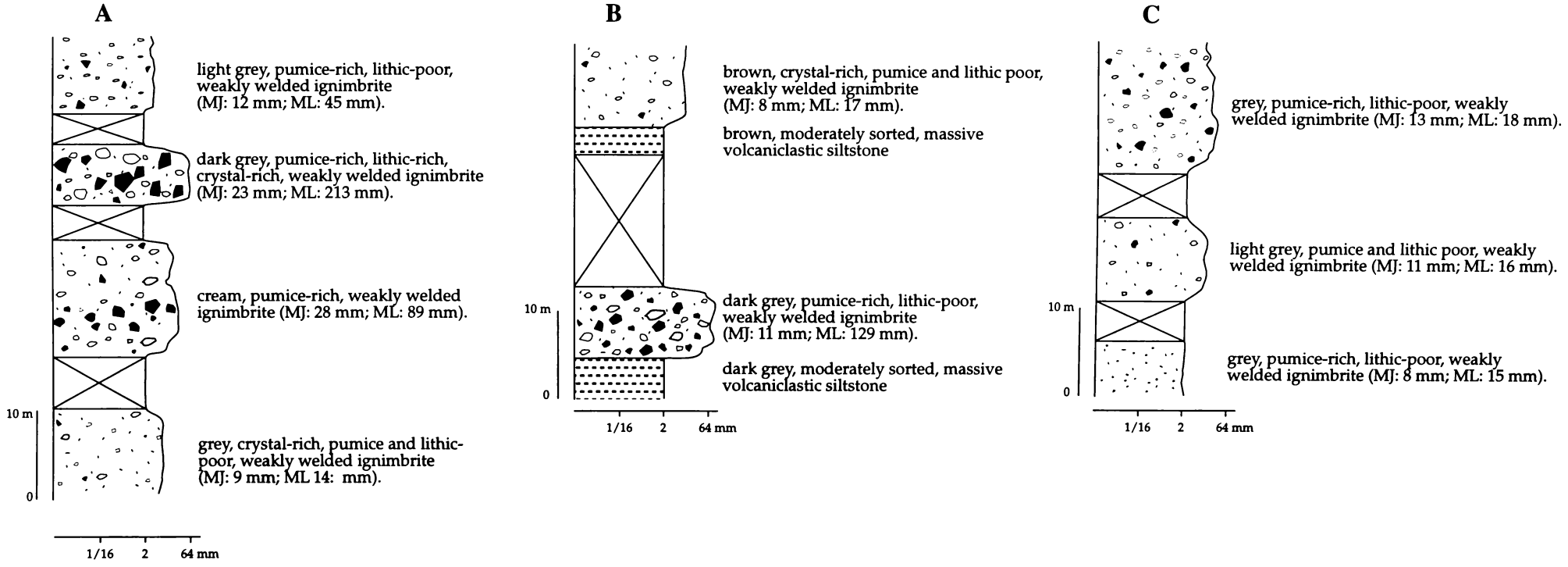


Figure 3.8 Composite sections of Colorado Pyroclastics in the Kauaeranga valley. A, Moyle Ridge Section (T12/472572-T12/472574). B, Colorado Stream Section (T12/468574). C, Rowe Stream Section (T12/482592).

Stratigraphic relations to Moss Creek Rhyolite are limited. It is intruded by Taurauikau Andesite and itself has intruded through Colorado Pyroclastics.

### Scots Rhyolite (new) (us)

Scots Rhyolite consists of an eroded ridge between the Pinnacles Rhyolite and Tauranikau Rhyolite in the southeastern sector of the KCC.

Scots Rhyolite is a light grey, fine grained, porphyritic rhyolite lava. Phenocrysts (5 %) consist of plagioclase, biotite and Fe-Ti oxides. The lava is typically glassy and lacks amygdules.

Scots Rhyolite is overlain by WES-1 Ignimbrite. No contacts are observed with Tauranikau Rhyolite or Pinnacles Rhyolite, but it is inferred to pre-date these lavas as it is more eroded.

### Bulls Run Rhyolite (new) (ku)

Bulls Run Rhyolite forms a major rhyolite dome complex in the central KCC (Figure 3.9). On the basis of physiographic evidence, the complex comprises a minimum of four lava domes. The comples covers ca. 5 $km^2$ and has a minimum estimated volume of 1 $km^3$.

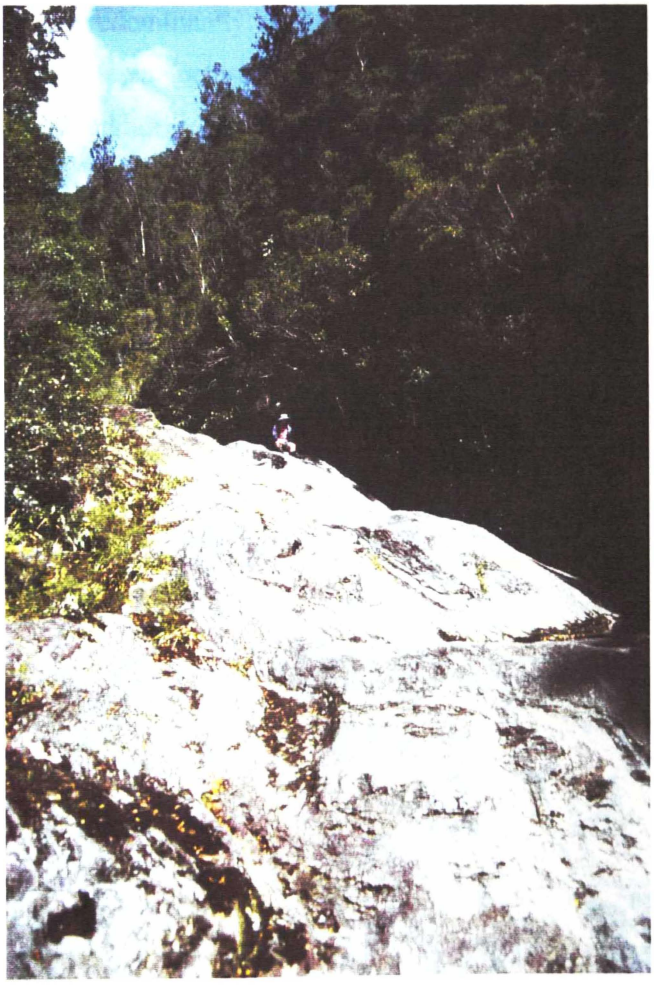

Figure 3.9 Bulls Run Rhyolite lava exposed in the Rangihau Stream (T11/489621).

Bulls Run Rhyolite is a light grey, fine grained, porphyritic rhyolite lava. Phenocrysts (3-5 %) consist of plagioclase, orthopyroxene, clinopyroxene and Fe-Ti oxides. Mm-flow banding and minor, small (< 0.5 cm) amygdules occur. Sericitic alteration occurs in the central complex and on its southeastern margin (Chapter 8).

Contacts with Bulls Run Rhyolite are limited. WES pyroclastics cover the northern flanks of the complex suggesting that it pre-dates WES eruptions. Taurauikau Andesite dikes intrude Bulls Run Rhyolite on its northeastern margin (T11/500626).

### Taurauikau Andesite (ot)

Taurauikau Andesite is a widespread intracaldera formation which includes thick lavas and dikes in the western sector of the KCC (Figure 3.10) and also andesitic dikes in the central KCC. Taurauikau Andesite was defined as a formation within the Omahine Subgroup, which incorporates formations of the Coromandel Group that post-date mid-Taranakian rhyolite and ignimbrite of the Whitianga Group (Skinner, 1995). This definition is not valid for the KCC succession as Taurauikau Andesite occurs within the ignimbrite-tuff-rhyolite lava succession (i.e. Rangihau Subgroup).

Taurauikau Andesite consists predominantly of dark grey, coarse grained, porphyritic, andesite lava. Phenocrysts (40-45 %) consist of plagioclase, orthopyroxene, clinopyroxene and Fe-Ti oxides. Plateau-forming lava flows (with associated but rare autoclastic breccia) are the most common lithotype, with minor sporadic dikes. Lavas which occur in the Table Mountain-Waiwawa range area are characterised by well developed columnar jointing. Dikes vary from ca. 1 to 5m widths, and consist of a similar dark grey, coarse phyric texture, and mineralogy as the lavas.

Figure 3.10 SE margin of Table Mountain, formed of thick (up to 150 m) columnar jointed Taurauikau Andesite. WES pyroclastics outcrop on lower flanks (centre left). Camp Rhyolite dome in foreground left.

Field relationships with Taurauikau Andesite vary significantly throughout the KCC, and several stratigraphic relations are known. Taurauikau Andesite intrudes Colorado Pyroclastics in the Waiwawa and Kauaeranga valleys, and intrudes Bulls Run Rhyolite dome complex on its NE margin. Taurauikau Andesite is overlain by WES pyroclastics in the Kauaeranga and Rangihau valleys, but intrudes the same sequence in the Slip Stream and Oteao valleys. This implies that Taurauikau Andesite erupted sporadically throughout periods of the KCC's development.

These varying field relations are supported by a wide range in K/Ar ages from 8.5 to 6.4 Ma. K/Ar ages of Taurauikau Andesite from Table Mountain yield ages of 8.1 ± 0.2 Ma (Adams et al., 1994) and 8.5 ± 0.6 Ma (this study). Taurauikau Andesite sampled from the Haukawakawa ridge give ages of 7.6 ± 0.4 Ma (Adams et al., 1994) and 7.6 ± 0.5 Ma (this study). A younger age of 6.4 ± 0.4 Ma has also been obtained from outcrops in the Rangihau valley (T11/484636).

### Trig Q Ignimbrite (new) (qi)

Trig Q Ignimbrite outcrops in the northern sector of the KCC where it forms a prominent N-trending ridge (Figure 3.11). In situ outcrops of Trig Q Ignimbrite also occur in the lower Kapowai valley (T11/525698; T11/525715) and a remnant boulder field occurs at the State Highway 25-Kapowai Rd intersection (T11/520723).

Figure 3.11 Trig Q Ignimbrite outcrop at Trig Q (T11/515701). Hammer is 30 cm long.

Trig Q Ignimbrite is a light brown-black, pumice-rich, crystal-rich, weakly to partially welded compositionally zoned (dacitic-rhyolitic) ignimbrite. Three compositional zones are defined on the basis of juvenile composition and degree of welding (Figure 3.12). Zone boundaries are gradational and planar. Zones are only recognised in vertical sections along the ridge outcrop (T11/515700 to T11/515705), and are not clearly defined at other outcrops.

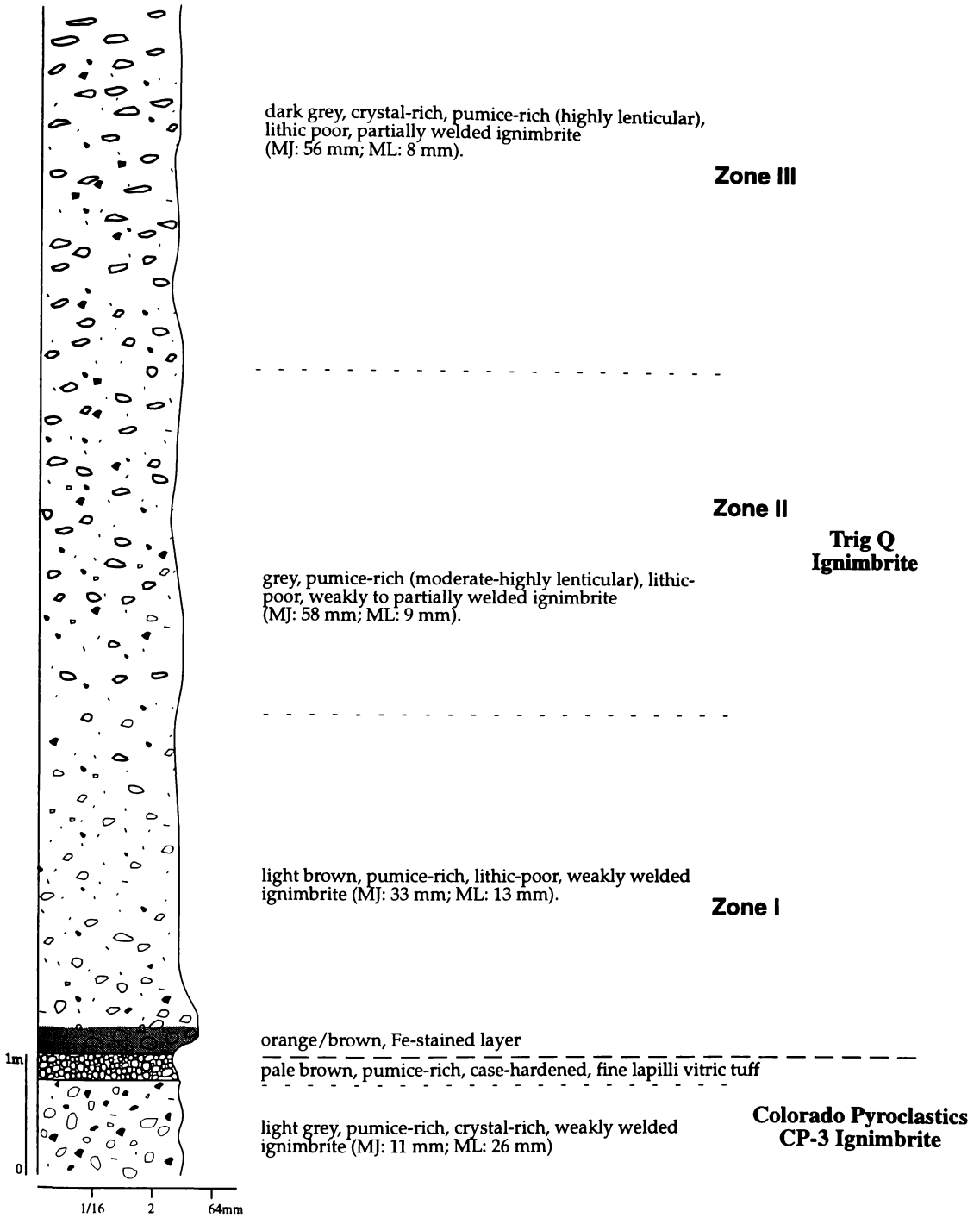


Figure 3.12 Internal vertical stratigraphy of Trig Q Ignimbrite at Trig Q (T11/515701).

Zone I is the basal zone and unconformably overlies CP-3 Ignimbrite (Colorado Pyroclastics). The zone consists of a 1.5-2 m, brown, pumice-rich, lithic-poor, weakly welded ignimbrite. A single juvenile type present is a cream, incipiently vesicular, non-lenticular, incipiently fibrous pumice. Phenocrysts (< 3 %)

consist of plagioclase, orthopyroxene and Fe-Ti oxides. Lithic fragments (3 %) consist of andesite and rhyolite lavas, and minor welded ignimbrite.

Zone II occurs above zone I and consists of a 6-8 m, dark grey, pumice-rich, crystal-rich, weakly to partially welded ignimbrite. Juvenile clast within this zone are dark grey/black glassy, poorly fibrous, moderately lenticular, incipiently vesicular pumice. Phenocrysts (< 3 %) consist of plagioclase, orthopyroxene and Fe-Ti oxides. Lithic fragments (1 %) consist of andesite and rhyolite lavas.

Zone III occurs above zone II and consists of an 8-10 m, black, pumice-rich, crystal-rich, partially welded ignimbrite. Juvenile clasts present are black highly lenticular, poorly fibrous, incipiently vesicular, plagioclase phyric pumice. Phenocrysts (< 1 %) consist of plagioclase, orthopyroxene and Fe-Ti oxides. Lithic fragments (1 %) consist of andesite and rhyolite lavas.

A correlative to Trig Q Ignimbrite may be the moderately to highly lenticular, plagioclase-orthopyroxene bearing, moderately welded Ferry Landing Ignimbrite (Bardebes, 1997), which forms 10-12 m high bluffs north of Ferry Landing, Whitianga. The similar composition and lenticular juvenile clast morphology of Ferry Landing Ignimbrite suggests a correlation to Trig Q Ignimbrite. Other correlatives to Trig Q Ignimbrite may include floats of similar lithology observed in the Wainora Stream, Kauaeranga valley. These possible correlations suggest that Trig Q Ignimbrite had a more widespread distribution than is indicated by its present outcrops within the KCC.

Discontinuous outcrop and paucity of lithics inhibit defining a source for Trig Q Ignimbrite. Sources in the KCC or Whitianga Volcanic Centre are possible, but on a thickness basis alone, KCC is the favoured source caldera.

Trig Q Ignimbrite unconformably overlies a pale brown, pumice-rich, weakly welded ignimbrite (CP-3 Ignimbrite). The contact is sharp and planar implying some basal erosion of this underlying unit. No other contacts are observed, although WES-1 Ignimbrite overlies it at the northern margin of the Trig Q ridge (T11/512720). Lithic fragments of Trig Q Ignimbrite are observed in WES ignimbrites, supporting a pre-WES age. A single K/Ar age of 8.00 ± 0.36 Ma was obtained on Trig Q Ignimbrite near Kapowai Road (T11/520722) (Takagi, 1995).

### Haukawakawa Member (new) (wh)

Volcaniclastic lacustrine siltstones cover ca. 0.6 $km^2$ in the Haukawakawa Stream-Slip Stream area (Figure 3.13, 3.14). These were previously mapped as Wainora Member (Skinner, 1995), but are now recognised as a separate unit (Haukawakawa Member) within the Wainora Formation, as these volcaniclastic siltstones are younger, or have different lithological characteristics (e.g. lack macro-fossils) compared with Waiwawa Member and Tarawaere Member sequences.

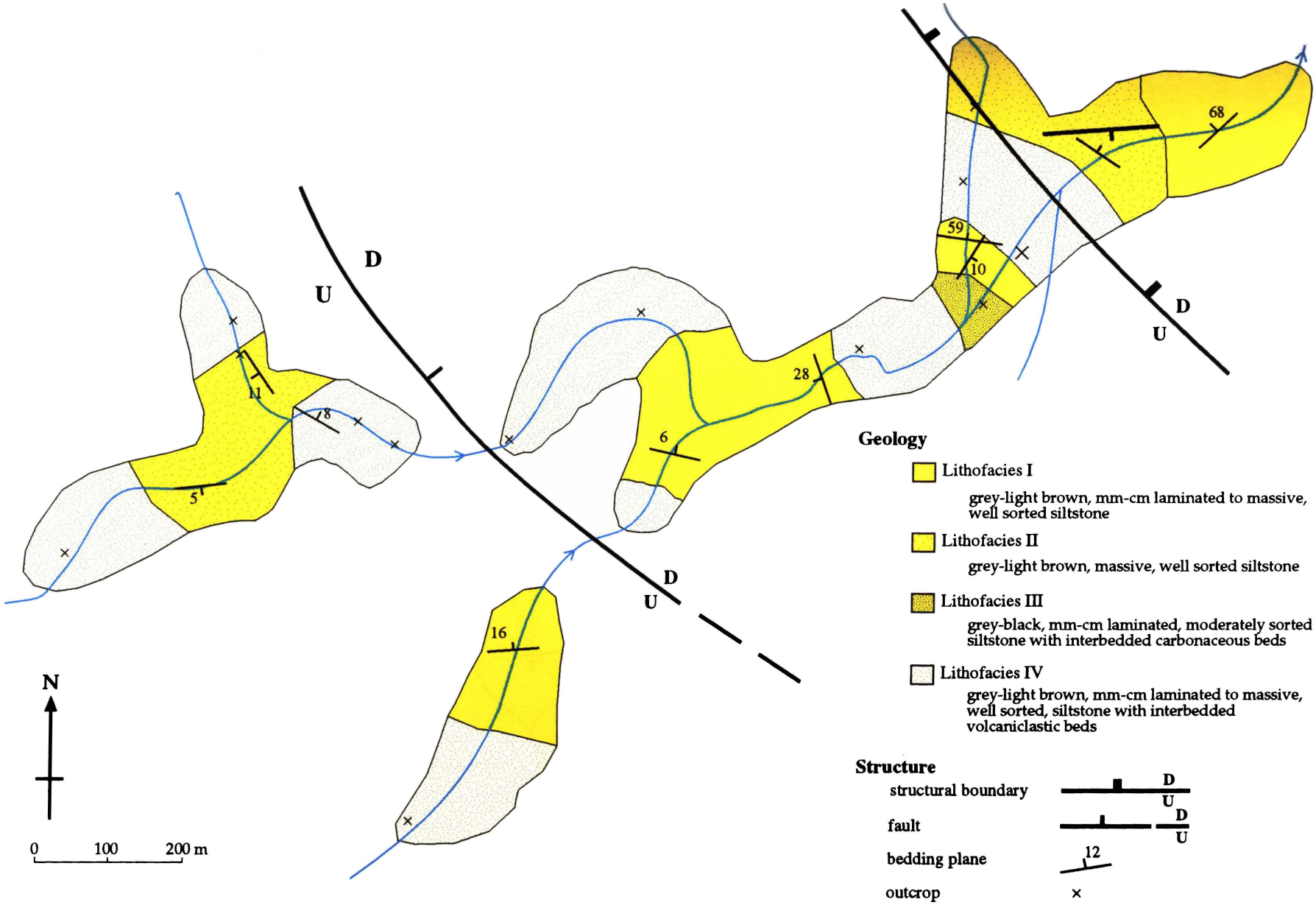


Figure 3.13 Geological map of Haukawakawa Member (Wainora Formation) in the Haukawakawa Stream valley.

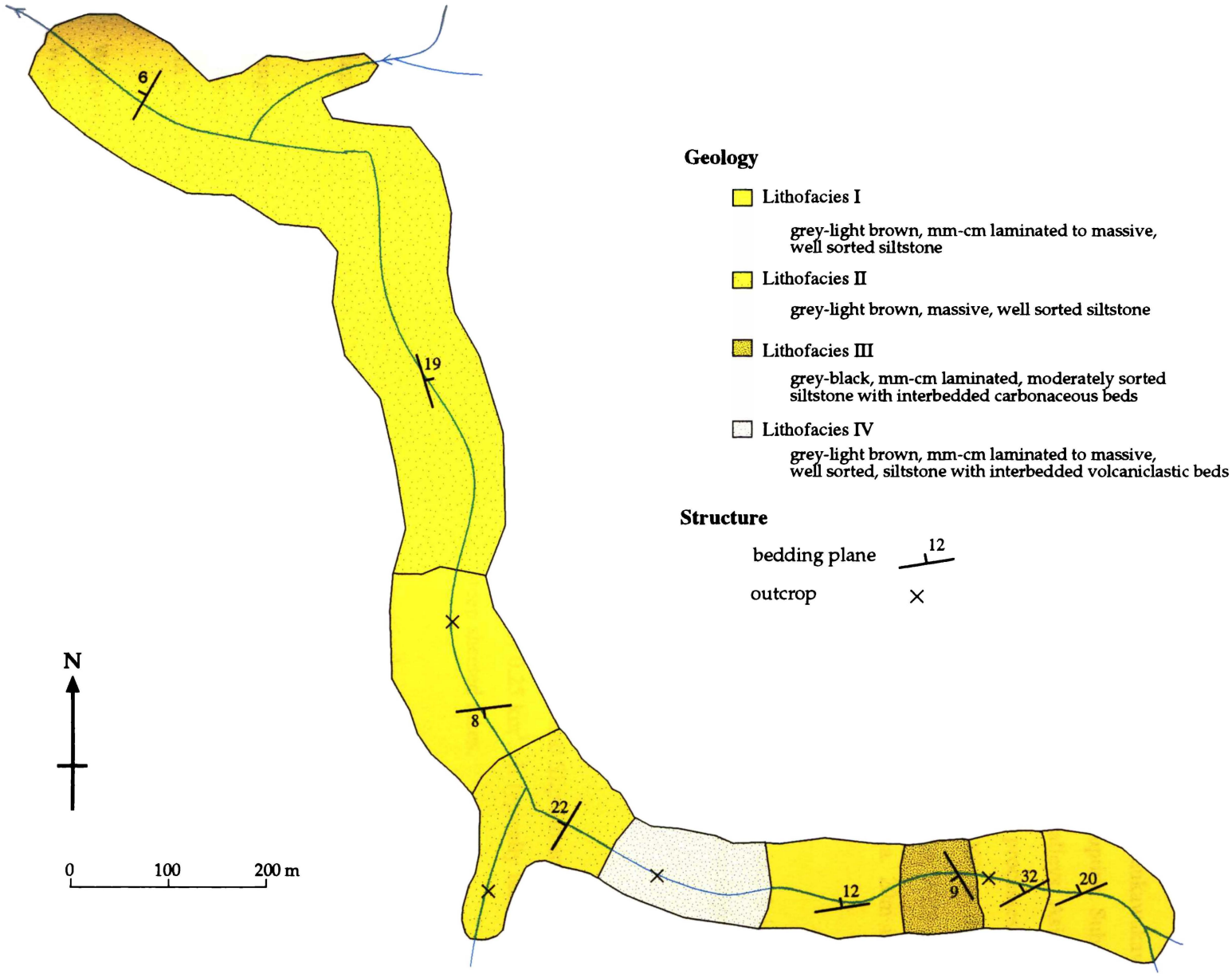


Figure 3.14 Geological map of Haukawakawa Member (Wainora Formation) in the Slip Stream valley.

Four lithotypes are recognised in the Haukawakawa Member and follow those defined for Tarawaere Member. Type (I) is a brown, massive, well sorted siltstone. Type (II) is a brown-grey, mm-laminated moderately sorted volcaniclastic siltstone. Type (III) is a grey, well sorted, massive to mm-laminated siltstone. Type (IV) is a dark grey-black poorly sorted carbonaceous sandstone or siltstone. Lithotypes vary in thickness and occurrence.

Deformation of the Haukawakawa Member is common in both the Slip Stream and Haukawakawa Stream valleys. Major deformation is attributable to subsidence associated with the WES eruption. Subsidence has resulted in a series of rotated, inclined, and uplifted blocks throughout the two valleys. Aside from this widespread area, there are also localised zones of deformation attributable to other processes. Intrusion of the Slip Rhyolite lava has locally tilted Haukawakawa Member siltstones (up to 20°) in the upper Slip Stream valley (T11/504640-T11/509640). High angle normal faulting, associated with WES collapse, has offset Haukawakawa Member siltstones (and overlying WES-1 Ignimbrite) by ca. 20m in the upper Haukawakawa Stream valley.

Haukawakawa Member appears to onlap the northern margin of Welcome Jack Dome. It is overlain by WES-1 Ignimbrite, and is intruded by Slip Rhyolite and Rangihau Rhyolite. No biostratigraphic age has been determined since no fossils have been observed within the sequence.

### Rangihau Rhyolite (rr)

Rangihau Rhyolite forms a lava dome near the confluence of Rangihau and Slip Streams (Figure 3.15a, b). It covers ca. 0.75 $km^2$ and has a minimum estimated volume of 0.25 $km^3$. It typically lacks the columnar jointing associated with plugs or spines, but forms very steep sheeted faces.

Rangihau Rhyolite is a light grey/blue, fine grained, porphyritic rhyolite lava. Phenocrysts (5 %) consist of plagioclase and Fe-Ti oxides. The lava typically lacks flow banding and amygdules.

Rangihau Rhyolite is overlain by WES pyroclastics on its southern and northern margins. No contacts are observed, but it is inferred to intrude Haukawakawa Member. A single $K/Ar_{(plagioclase)}$ age of 6.89 ± 0.37 Ma was obtained in this study.

### Waiwhatawhata Rhyolite (new) (kw)

Waiwhatawhata Rhyolite forms three eroded lava domes in the Oteao valley (Figure 3.16). Domes cover ca. 1.2 $km^2$ and have an estimated minimum volume of 0.25 $km^3$.

Waiwhatawhata Rhyolite is a light grey/blue, fine grained, porphyritic rhyolite lava. Phenocrysts (5 %) consist of plagioclase, orthopyroxene, clinopyroxene and Fe-Ti oxides. Mm-scale flow banding and amygdules (up to 5 mm) occur.

WES-1 Ignimbrite overlies Waiwhatawhata Rhyolite on its northern (T11/511670) and southern (T11/512659) margins, but relationships with other units are not exposed.

A

B

**Figure 3.15.** A, Rangihau Rhyolite dome in the central Kapowai Caldera Complex. View north from T11/501639. B, Platy jointed lava of Rangihau Rhyolite dome, in the Rangihau Stream (T11/499654).

**Figure 3.16** Waiwhatawhata Rhyolite domes in the Oteao valley. Dome in background right is part of the Kydd Rhyolite dome complex.

### Starvation Rhyolite (new) (ks)

Starvation Rhyolite forms a lava dome on the northern ridge of the upper Kauaeranga valley. It covers ca. 0.9 $km^2$ and has an estimated minimum volume of 0.09 $km^3$. Outcrops are sporadic and are typically moderately weathered.

Starvation Rhyolite consists of a light grey/pink, fine grained, porphyritic rhyolite lava. Phenocrysts (5 %) are composed of plagioclase, orthopyroxene, clinopyroxene and Fe-Ti oxides. Mm-scale flow banding is common.

No direct contacts are observed with Starvation Rhyolite, although WES pyroclastics overlie the eastern and northwestern margins of the dome.

### Miller Flat Rhyolite (new) (sm)

Miller Flat Rhyolite forms localised outcrops on the eastern and southwestern margins of the Kapowai Rhyolite dome.

Miller Flat Rhyolite consists of light grey, fine grained, mm-scale flow banded, porphyritic rhyolite lava. Phenocrysts (10 %) consist of plagioclase, amphibole, pyroxene and Fe-Ti oxides.

Stratigraphic relations with Miller Flat Rhyolite are limited. Miller Flat Rhyolite is overlain by Manuka Ignimbrite (T11/554671), and is suggested to be overlain by WES pyroclastics and Kapowai Rhyolite.

### Manuka Ignimbrite (new) (mi)

Manuka Ignimbrite outcrops downstream of the Kapowai Rhyolite dome in the Kapowai valley. Outcrops are generally limited to the valley floor, although outcrops also occur near Oteao Road.

Manuka Ignimbrite is a pink/cream, pumice-rich, lithic-rich, vapour phase altered, weakly welded rhyolitic ignimbrite. A single juvenile type is present which is a cream, poorly vesicular, incipiently lenticular, poorly fibrous, occasionally vapour phase altered pumice. Phenocrysts (< 1 %) consist of plagioclase, orthopyroxene, clinopyroxene, rare amphibole and Fe-Ti oxides. Matrix crystals (3 %) consist of plagioclase, orthopyroxene, clinopyroxene, amphibole and Fe-Ti oxides. The lithic (5-7 %) assemblage consists of andesite, dacite, and rhyolite lavas, and welded ignimbrite fragments. Lithics are typically fine to coarse lapilli size, and angular to subangular.

Manuka Ignimbrite is overlain by Oteao Ignimbrite near Oteao Rd (T11/541679), and by inclined WES-1 Ignimbrite (T11/554671) in the Kapowai valley floor (Figure 3.17).

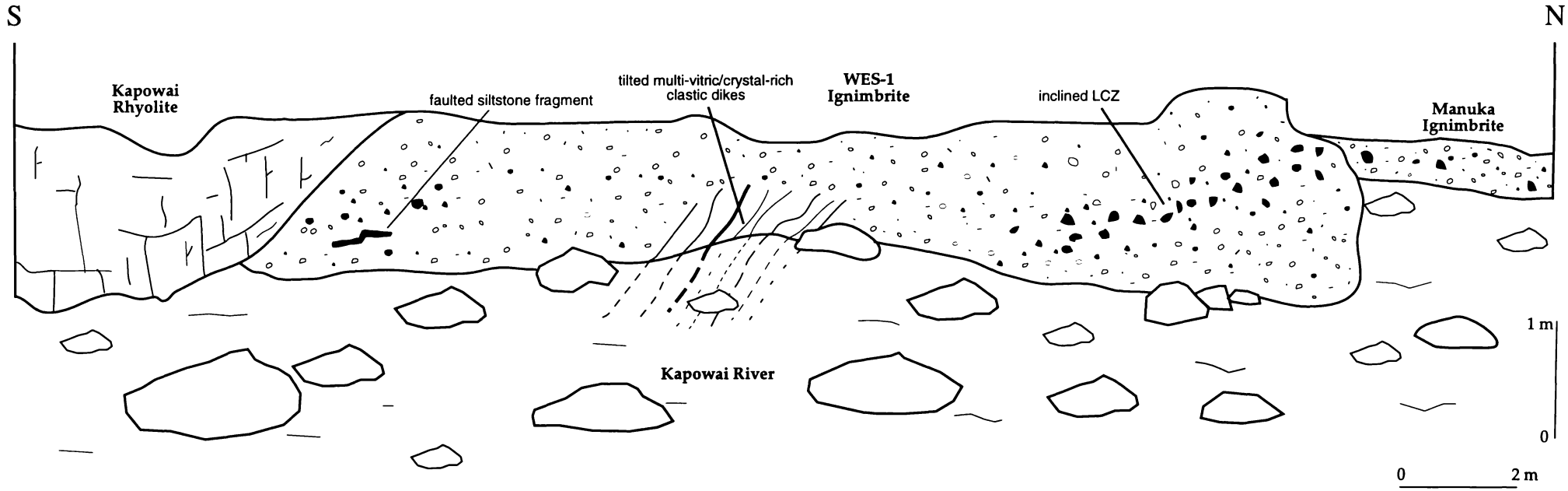


Figure 3.17 Sketch of outcrop exposed on western bank in Kapowai valley floor (T11/554671). Manuka Ignimbrite overlain by inclined WES-1 Ignimbrite.

### Kokonga Rhyolite (new) (kg)

Kokonga Rhyolite forms a single dome in the eastern sector of the KCC between the Kapowai and Awahau valleys (Figure 3.18). It covers ca. 2 $km^2$ and has a minimum estimated volume of 0.6 $km^3$.

Kokonga Rhyolite consists of a light grey/pink, fine grained, porphyritic rhyolite lava. Phenocrysts (7 %) are composed of plagioclase, orthopyroxene, clinopyroxene and Fe-Ti oxides.

Kokonga Rhyolite is overlain by WES pyroclastics and appears to post-date Colorado Pyroclastics. No contact is observed with Kapowai Rhyolite. A single K/Ar date obtained in this research yields an age of 6.51 ± 0.36 Ma.

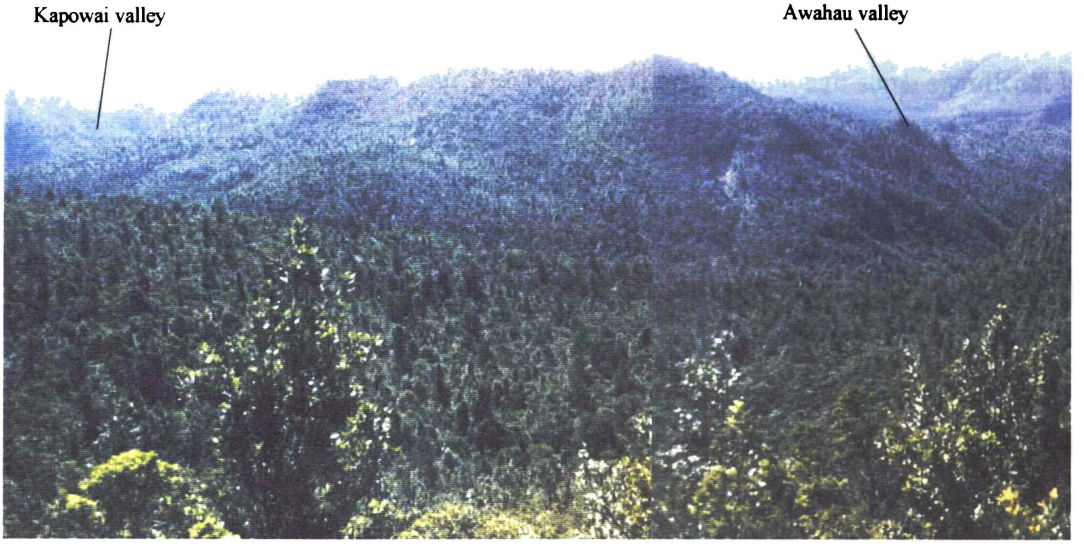


Figure 3.18 Kokonga Rhyolite dome between Kapowai and Awahau valleys. View north from T11/561651.

### Kapowai Rhyolite (new) (kk)

Kapowai Rhyolite forms a lava dome in the western margin of the Kapowai valley. The lava dome covers ca. 1.75 $km^2$ and has a minimum estimated volume of 0.35 $km^3$.

Kapowai Rhyolite consists of light grey/blue, fine grained, porphyritic rhyolite lava. Phenocrysts (20-30 %) consist of plagioclase, orthopyroxene, clinopyroxene and Fe-Ti oxides. Mm-scale flow banding is common, and amygdules (typically < 0.5 cm) are rare.

Kapowai Rhyolite is unconformably overlain by Oteao Ignimbrite and intrudes Manuka Ignimbrite (T11/554671). WES pyroclastics overlie Kapowai Rhyolite on its northern (T11/528679) and southern margins

### Slip Rhyolite (new) (ss)

Slip Rhyolite forms a minor dike (< 3 m wide) on the northern margin of the Welcome Jack Rhyolite.

Slip Rhyolite consists of a grey, fine grained, porphyritic, rhyolite lava. Phenocrysts (10 %) consist of plagioclase, amphibole and Fe-Ti oxides. Mm-scale flow banding occurs in most outcrops.

Slip Rhyolite intrudes volcaniclastic lacustrine siltstone (Haukawakawa Member), and is inferred to intrude Welcome Jack Rhyolite. Haukawakawa Member is deformed and inclined at the contact. As Slip Rhyolite occus along the strike of the southern WES structural boundary, its emplacement may relate to the WES. However, whether it was intruded prior to or after the WES is unclear.

### Wharepapa Rhyolite (new) (kh)

Wharepapa Rhyolite forms a dome complex in the northeastern sector of the KCC. It covers ca. 0.9 $km^2$ and has a minimum estimated volume of 0.1 $km^3$. Outcrops are sporadic, although some significant lava plugs occur (Figure 3.19).

Wharepapa Rhyolite consists of a light grey/blue, fine grained, porphyritic rhyolite lava. Phenocrysts (3 %) consist of plagioclase, orthopyroxene and Fe-Ti oxides. Mm-scale flow banding and amygdules (up to 12 mm) occur in most outcrops.

WES pyroclastics appear to overlie Wharepapa Rhyolite on its northern and western margins. The relationship to other rhyolite lavas is unclear, but with a similar mineralogy, Wharepapa Rhyolite is inferred to have a similar age to adjacent Kydd Rhyolite, Waiwhatawhata Rhyolite and Kapowai Rhyolite.

Figure 3.19 Wharepapa Rhyolite lava plug (ca. 25 m high) near Oteao Road (T11/528664).

### Kydd Rhyolite (new) (ky)

Kydd Rhyolite forms a rhyolite lava dome complex consisting of at least 3 rhyolite domes and sporadic lava plugs between the western Kapowai valley and Oteao valley. The complex covers ca. 3 $km^2$ and has a minimum estimated volume of 1.2 $km^3$.

Two lithologies are present within the Kydd Rhyolite dome complex:
Type I consists of light grey/pink, fine grained, porphyritic, rhyolite lava. Phenocrysts (5 %) consist of plagioclase, orthopyroxene, clinopyroxene and Fe-Ti oxides. Type I lava is typically deeply weathered, except for exposures in Oteao Stream, and is the most abundant lithology, occurring throughout the complex.

Type II consists of black, fine grained, porphyritic glassy obsidian. Phenocrysts are composed of plagioclase, orthopyroxene, clinopyroxene and Fe-Ti oxides. Obsidian is typically fresh and appears to be confined to the upper Oteao valley (T11/519649)

Kydd Rhyolite is overlain by WES pyroclastics on its western, northern and eastern margins, implying a pre-WES age. Contacts with other units (i.e. rhyolite lavas) are not observed.

### Ruahine Rhyolite (ur)

Ruahine Rhyolite forms the prominent N-trending, Tanehua-Ruahine ridge (Figure 3.20a) in the eastern KCC. The ridge consists of at least four rhyolite domes covering a combined area of ca. 4.5 $km^2$ and estimated minimum volume of 1.3 $km^3$. Outcrops of Ruahine Rhyolite lava occur across the ridge, especially on its margins (Figure 3.20b), and also extend up to 1 km east of the ridge.

Ruahine Rhyolite consists of light grey, medium grained, porphyritic rhyolite lava. Phenocrysts (15 %) consist of plagioclase, quartz, biotite and Fe-Ti oxides. Ruahine Rhyolite lava is typically well jointed, and lacks flow banding and amygdules.

WES pyroclastics onlap Ruahine Rhyolite, and this is best observed on the western margin of the Tanehua-Ruahine ridge. Ruahine Rhyolite was emplaced through earlier pyroclastics (Webb Creek Ignimbrite, Colorado Pyroclastics), although no direct contacts are observed. A single $K/Ar_{(plagioclase)}$ age for Ruahine Rhyolite determined in this study, yielded an age of 5.86 ± 0.31 Ma.

### Oteao Ignimbrite (new) (oi)

Sporadic outcrops of Oteao Ignimbrite are restricted to scarps on the eastern and northern flanks of the Kapowai Rhyolite dome in the NE sector of the KCC. Limited, discontinuous exposures reflect burial by younger ignimbrites (i.e. WES), and small eruption volumes typical for andesitic ignimbrites.

A

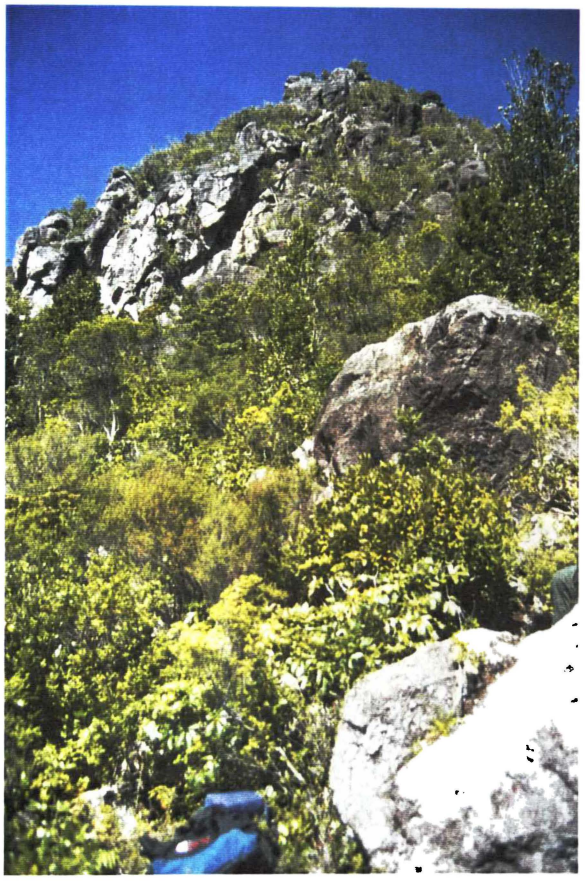

B

Figure 3.20. A, Ruahine Rhyolite forming the 4.5 km Tanehua-Ruahine ridge, which defines the eastern topographic boundary of the Kapowai Caldera Complex. View north from The Pinnacles (T12/521579). B, Ruahine Rhyolite outcrop on the northern margin of the Tanehua-Ruahine ridge (T11/565648).

At its main outcrop on Oteao Road (T11/534670), Oteao Ignimbrite is a dark grey, juvenile-rich (60%), lithic-poor (< 3%), crystal-rich, weakly welded andesitic ignimbrite. The juvenile population consists of four types (scoria, pumice, mingled scoria-pumice and mixed scoria-pumice) (Figure 3.21). Scoria clasts

(65%) are black-dark grey, moderately vesicular, poorly fibrous, incipiently lenticular and moderately phyric (MJ: 71 mm). Pumice (12 %) are cream/white, poorly vesicular, moderately fibrous, incipiently lenticular and poorly phyric (MJ: 29 mm). Mingled scoria-pumice (20 %) are black-white streaked, moderately vesicular, poorly fibrous, moderately lenticular and poorly phyric (MJ: 62 mm). Mixed scoria-pumice (< 3 %) are pale brown, poorly vesicular, non fibrous, non-lenticular and poorly phyric (MJ: 36 mm).

The crystal assemblage consists of plagioclase, clinopyroxene, orthopyroxene, and Fe-Ti oxides. The lithic population (3-5%) consists of pyroxene andesite (Taurahuehue Andesite) and pyroxene dacite (Maumaupaki Formation) lavas, pyroxene rhyolite lavas (Kapowai Rhyolite), welded ignimbrite (Manuka Ignimbrite), and hydrothermally altered lava. Lithics are typically fine lapilli size and subrounded to subangular. The matrix is grey suggesting a mix of black scoria and cream pumice glass shards.

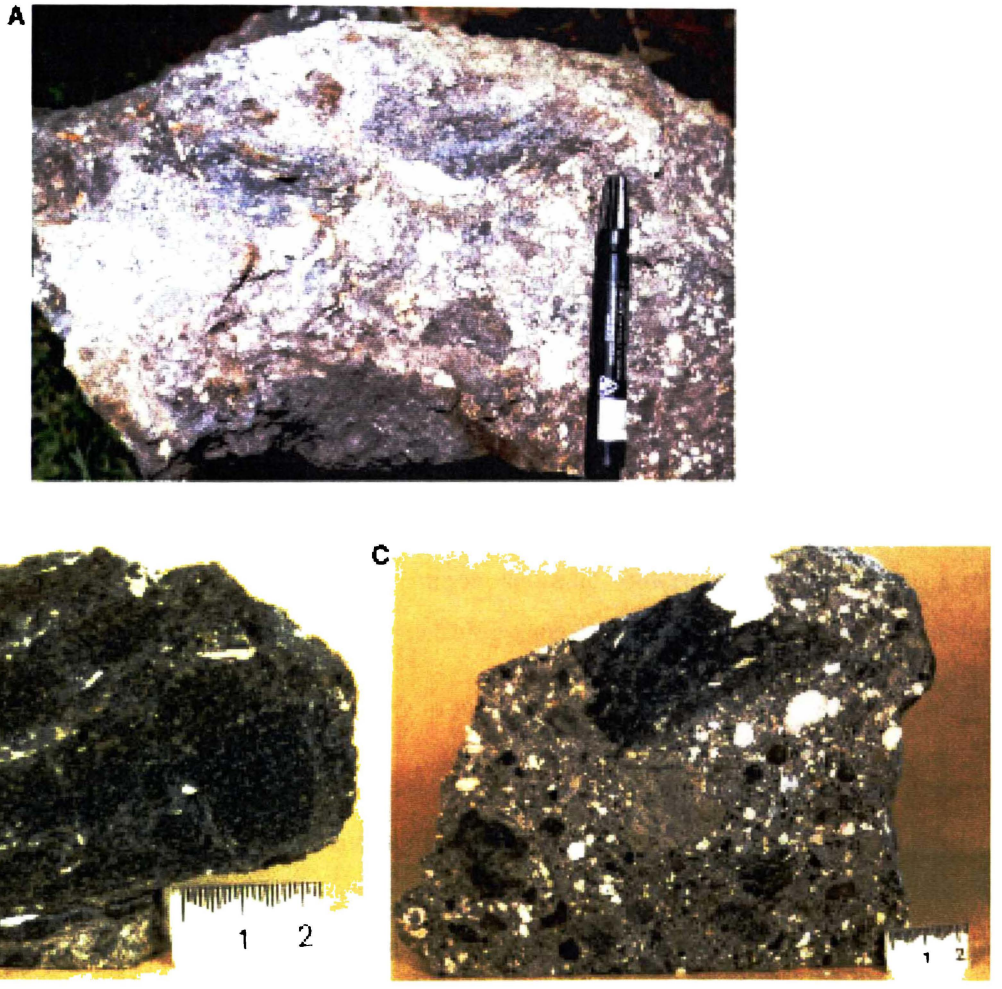


Figure 3.21 Juvenile components of the Oteao Ignimbrite. A, Whole rock with scoria, pumice and scoria with mingled pumice. Black pen is 125 mm in length B. Mingled scoria-pumice clast. Scale in cm. C, Whole rock with pumice, scoria, mingled scoria-pumice and mixed scoria/pumice (centre) present. Scale in cm.

Scoria clasts/glass shards in Oteao Ignimbrite are unaltered and unweathered, although pumice clasts/glass shards are incipiently weathered. Minor vapour phase alteration of Oteao Ignimbrite is restricted to northernmost outcrops near the Oteao Ignimbrite-Manuka Ignimbrite contact. Vapour phase alteration of

the matrix glass results in a change from dark grey/black to pink-grey hue, and black scoria clasts are altered to a grey-yellow hue. Phenocrysts and matrix crystals are not altered, implying only incipient to weak vapour phase alteration of the ignimbrite.

Stratigraphic contacts with Oteao Ignimbrite are very limited. However, three field relationships are evident; (i) vapour phase altered Oteao Ignimbrite unconformably overlies Manuka Ignimbrite to the south of Oteao Road (T11/540680); (ii) Oteao Ignimbrite forms the paleorelief in the Wharepapa Stream valley, over which younger WES was emplaced; and (iii) Oteao Ignimbrite post-dates eruption of the Kapowai Rhyolite dome, as Oteao Ignimbrite outcrops on the upper margins of the dome, and Oteao Ignimbrite contains lithics of Kapowai Rhyolite lava.

Significant lithic fragments found within Oteao Ignimbrite include Manuka Ignimbrite, Taurahuehue Andesite and Maumaupaki Formation lavas and various rhyolite lavas (Kapowai Rhyolite). Significantly, no WES pyroclastics or volcaniclastic siltstone lithics have been observed.

Field evidence, together with the lithic population, constrains eruption of Oteao Ignimbrite to late within the KCC caldera evolution, but prior to the WES. A $K/Ar_{(plagioclase)}$ age of 5.68 ± 0.32 Ma was obtained in this study, which supports the field stratigraphy.

### *WES stratigraphy*

### Wharepapa Eruptive Sequence (WES)

Wharepapa Eruptive Sequence (WES) consists of a sequence of multiple pyroclastic flow and fall deposits. WES deposits are the most widespread intracaldera unit outcropping throughout the KCC, apart from the Waiwawa valley where it forms minor sporadic outcrops. Only general stratigraphic characteristics are described in this section. The petrology, geochemistry, and physical volcanology of the sequence is fully described in Chapter Five.

WES consists of five key lithologies. WES-1 consists of basal light grey-light brown, pumice-rich, lithic-rich weakly welded rhyolitic ignimbrite. Fine lapilli-ash vitric tuffs (WES-1a) occur interbedded near the base of WES-1 Ignimbrite. Fine lapilli-ash vitric and crystal tuffs (WES-2) separate WES-1 and WES-3 or 4 units. Localised lithic lag breccia (WES-3) occurs interbedded between WES-2 and WES-4. The final unit is a light grey, pumice-rich, lithic-rich, weakly welded rhyolitic ignimbrite (WES-4 Ignimbrite).

WES deposits overlie all other KCC pyroclastic units and most effusive lavas. Several basal contacts between WES-1 Ignimbrite and volcaniclastic lacustrine siltstone (Tarawaere Member; Haukawakawa Member) are exposed in the KCC (Figure 3.22). Contacts are typically inclined and sharp. No units overlie the WES, but several rhyolite lavas (i.e. Tauranikau Rhyolite and Kauaeranga Rhyolite) and andesitic dikes (Taurauikau Andesite) intrude the sequence in the southern and central sectors of the KCC.

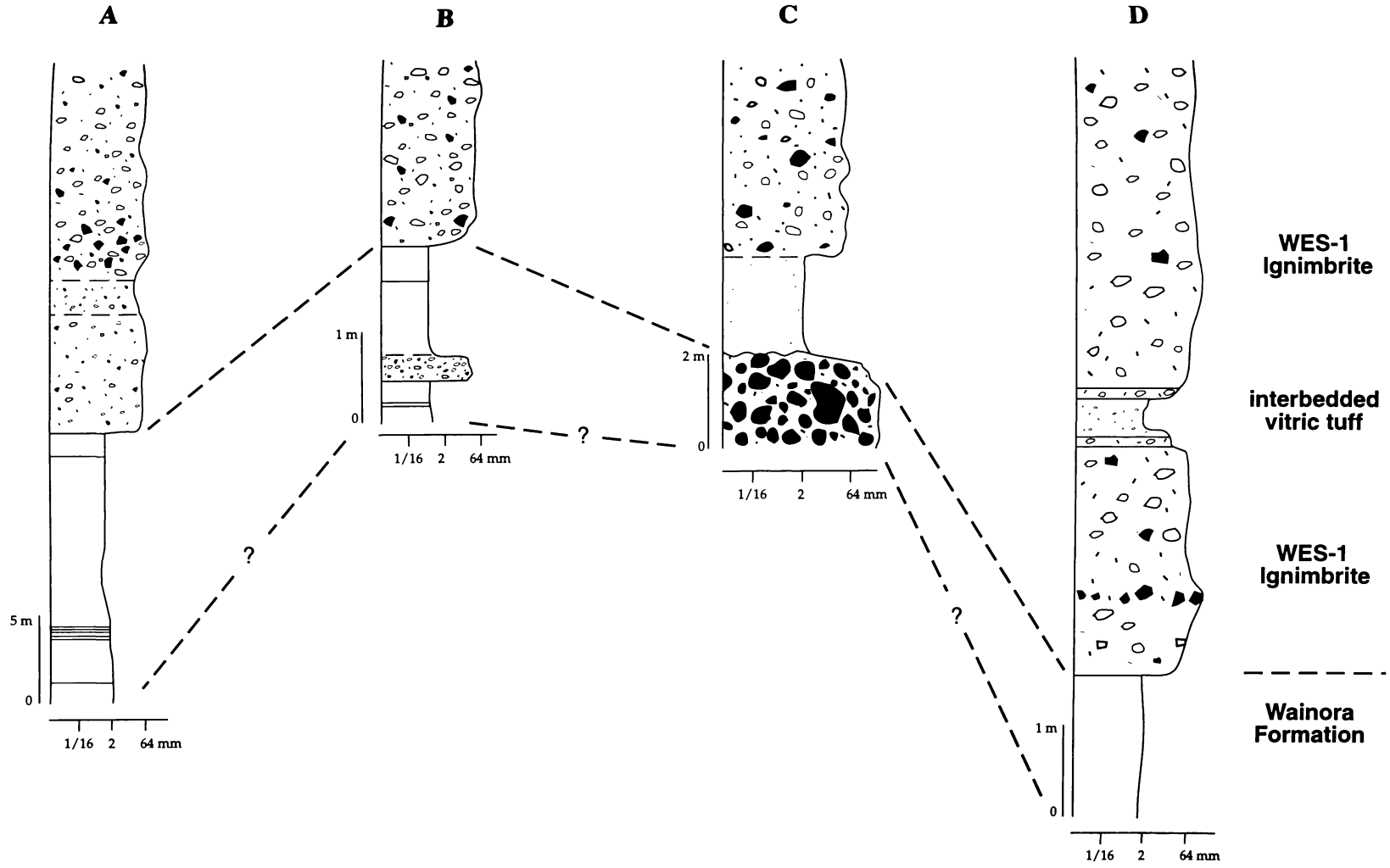


Figure 3.22 Basal contacts of intracaldera WES-1 Ignimbrite with volcaniclastic lacustrine siltstone (Haukawakawa Member and Tarawaere Member) in the Kapowai Caldera Complex. A, Section exposed in tributary of the Haukawakawa Stream (T11/485642). B, Section exposed near farm track (T11/487650). C, Section exposed in northern bank of Kapowai River (T11/543687). D, Composite section exposed along southern bank of Kauaeranga valley floor (T488583). Dashed lines indicate correlation of Wainora Formation between sections.

The lithic assemblage in WES units further constrains its relative age. Welded ignimbrite fragments include Trig Q Ignimbrite, Webb Creek Ignimbrite, and Oteao Ignimbrite. Andesite and dacite lavas include Maumaupaki Formation and Taurahuehue Andesite. A variety of rhyolite lavas have been sampled, and some are correlated to Slip Rhyolite and Rangihau Rhyolite. These lithologies together imply that WES is the final large scale explosive sequence erupted from the KCC.

Two new $K/Ar_{(plagioclase)}$ ages of intracaldera WES ignimbrite determined in this study yield a mean age of 5.78 ± 0.3 Ma. All other radiometric age data reported for WES pyroclastics are from exocaldera correlatives, and have produced older ages. Fission-track ages published by Adams et al. (1994) on the Wharepapa Ignimbrite have a mean age of 8.7 ± 1.3 Ma, however the locations chosen for this fission-track dating are questionable because either the ignimbrite has been hydrothermally altered or the ignimbrite sampled may not be a WES correlative as defined in this study (see chapter 5).

### *Post - WES caldera stratigraphy*

#### Acadia Rhyolite (new) (ra)

Acadia Rhyolite forms a lava dome at the confluence of the Haukawakawa Stream and Rangihau Stream (Figure 3.23). It covers ca. 0.15 $km^2$ and has an estimated minimum volume of 0.015 $km^3$.

Acadia Rhyolite consists of a light grey, medium grained, porphyritic rhyolite lava. Phenocrysts (5 %) consist of plagioclase and Fe-Ti oxides. Amygdules are rare, but mm-scale flow banding is present in some outcrops.

Figure 3.23 Acadia Rhyolite dome in the central Kapowai Caldera Complex. View southwest from T11/496648.

Acadia Rhyolite is inferred to postdate WES as it intrudes WES pyroclastics on its SW margin, and it occurs within the SW collapse boundary associated with the WES.

### Big Beetle Rhyolite (new) (kb)

Big Beetle Rhyolite forms a very steep lava dome between Rangihau Stream and Rangihau Rd track in the central KCC (Figure 3.24). It covers ca. 0.2 $km^2$ and has a minimum estimated volume of 0.02 $km^3$.

Big Beetle Rhyolite consists of a light grey, fine grained, porphyritic rhyolite lava. Phenocrysts (10 %) consist of plagioclase, orthopyroxene, clinopyroxene and Fe-Ti oxides. Flow banding is uncommon, and the lava is typically platy jointed.

No direct contacts are observed with Big Beetle Rhyolite. However, as it appears to have been emplaced through WES pyroclastics, and it occurs within the SW collapse boundary associated with the WES, it is considered to post-date the WES.

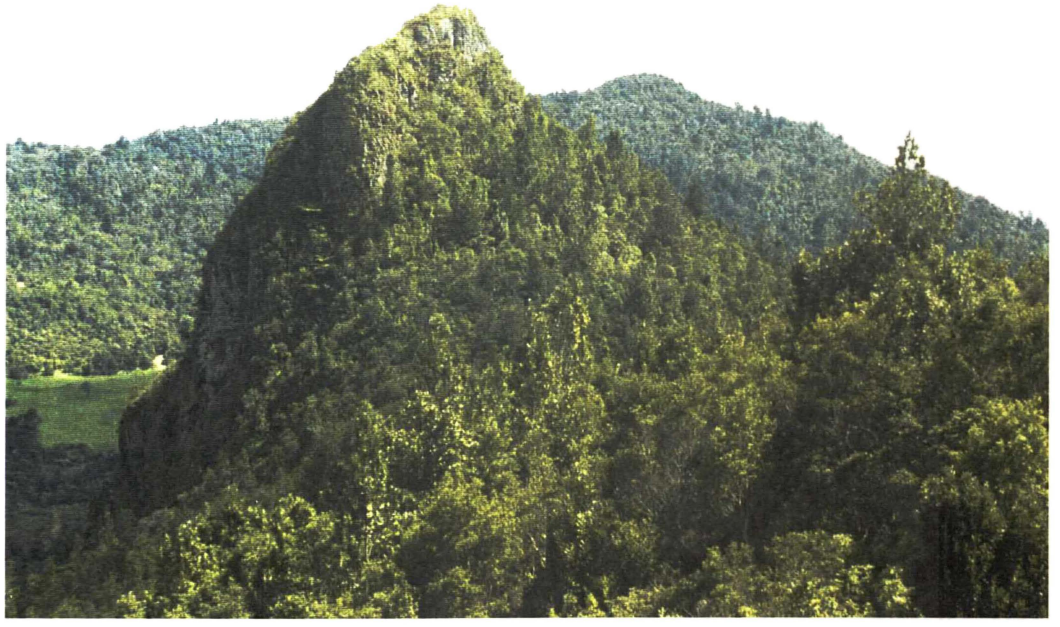

Figure 3.24 Big Beetle Rhyolite dome in the central Kapowai Caldera Complex. Haukawakawa ridge (Taurauikau Andesite) in background. View NW from T11/501639.

### Pinnacles Rhyolite (new) (kp)

Pinnacles Rhyolite lava forms a steep, strongly dissected lava dome in the headwaters of the Hikuai, 1st and 2nd branches of the Tairua, and Kauaeranga Rivers in the southeastern sector of the KCC (Figure 3.25). It covers an area of ca. 1 $km^2$ and has a minimum estimated volume of 0.5 $km^3$.

Pinnacles Rhyolite consists of a light grey, fine grained, porphyritic rhyolite lava. Phenocrysts (7 %) consist of plagioclase, orthopyroxene and Fe-Ti oxides. Mm-scale flow banding occasionally occurs and amygdules are rare.

Pinnacles Rhyolite lava intrudes WES pyroclastics, but other contacts are not exposed. As Pinnacles Rhyolite dome has a similar elevation and composition as Camp Rhyolite, and it also occurs on the southern topographic boundary, it may have a similar age.

Figure 3.25 Pinnacles Rhyolite dome in the upper Kauaeranga valley. Looking east from T12/508580. WES-1 Ignimbrite forms outcrops in foreground and in the Second Branch, Tairua River valley (centre).

### Camp Rhyolite (new) (kc)

Camp Rhyolite forms a lava dome complex consisting of at least 3 rhyolite lava domes in the southern KCC. The dome complex covers ca. 2 $km^2$ and has an estimated minimum volume of 0.2 $km^3$. Camp Rhyolite coincides with and defines the southern margin of the topographic boundary.

Three main lithotypes are present within Camp Rhyolite. Type I is a light grey, fine grained, porphyritic rhyolite lava. Phenocrysts (10 %) consist of plagioclase, orthopyroxene, clinopyroxene and Fe-Ti oxides. Mm-scale flow banding is common, and amygdules are rare, but where present are typically < 0. 3 cm. Type I forms the major lithotype in the Camp Rhyolite dome complex.

Type II consits of a dark grey-black, medium grained, glassy porphyritic rhyolite lava. Phenocrysts (15 %) consist of plagioclase, orthopyroxene, clinopyroxene and Fe-Ti oxides. The lava typically lacks flow banding and amygdules. Type II forms minor, sporadic outcrops within the complex (e.g. T12/504578 and T12/495574).

Type III is a dark grey-black, monolithologic, poorly sorted rhyolitic breccia. Clasts up to 15 mm occur and consist of obsidian and rhyolite lava fragments. Type III forms sporadic outcrops on the margin of domes (e.g. T12/495574) within the complex.

Camp Rhyolite appears to intrude WES pyroclastics, although no contacts are observed. Contacts with other units are also not observed, but it is inferred to have a similar age to Pinnacles Rhyolite (see above). A $K/Ar_{(plagioclase)}$ age of 5.3 ± 0.3 Ma was determined in this study, implying a post-WES age.

### Precipice Rhyolite (new) (kd)

Precipice Rhyolite forms two dikes in the floor of the Kapowai valley (Figure 3.26). Dike A is 5 m wide and intrudes CP-2 Ignimbrite (Colorado Pyroclastics). The dike margin is glassy and brecciated (see Figure 2.10). Dike B is 2 m wide and intrudes along the contact between Kapowai Rhyolite lava and CP-2 Ignimbrite. The right margin of dike B is sharp and glassy where it intrudes lava, and irregular and slightly brecciated where it intrudes ignimbrite (left margin).

Both dikes consist of dark grey-black, fine grained, glassy, porphyritic rhyolite lavas. Phenocrysts (5-7 %) consist of plagioclase, orthopyroxene, clinopyroxene and Fe-Ti oxides.

Precipice Rhyolite intrudes Colorado Pyroclastics and Kapowai Rhyolite. Two $K/Ar_{(plagioclase)}$ ages of Precipice Rhyolite lava dikes determined in this study, yield ages of 5.12 ± 0.28 Ma, and 5.19 ± 0.42 Ma respectively. This implies a post-WES age, although no contacts have been observed with WES to confirm or refute this.

### Tauranikau Rhyolite (new) (kt)

Tauranikau Rhyolite forms a steep sided rhyolite dome and several lava plugs (Figure 3.27a, b) in the upper Kauaeranga valley. It covers an area of ca. 1.3 $km^2$ and has an estimated volume of 0.35 $km^3$.

Tauranikau Rhyolite consists of a light grey, fine grained, porphyritic rhyolite lava. Phenocrysts (7 %) consist of plagioclase, orthopyroxene and Fe-Ti oxides. Mm-scale flow banding is common in most outcrops, and amygdules occasionally occur.

Tauranikau Rhyolite intrudes and deforms WES pyroclastics, implying a post-WES age. No other contacts between Tauranikau Rhyolite and other rhyolite domes or pyroclastics have been observed.

### Kauaeranga Rhyolite (new) (ke)

Kauaeranga Rhyolite outcrops downstream of Tauranikau Rhyolite, in the upper Kauaeranga valley. It forms a steep sided lava dome (Figure 3.28a) which covers ca. 1.2 $km^2$ and has a minimum estimated volume of 0.5 $km^3$.

Kauaeranga Rhyolite consists of a grey/pink, fine grained, porphyritic rhyolite lava. Phenocrysts (7 %) consist of plagioclase, orthopyroxene and Fe-Ti oxides. Amygdules occasionally occur, and mm-scale flow banding is common in most outcrops.

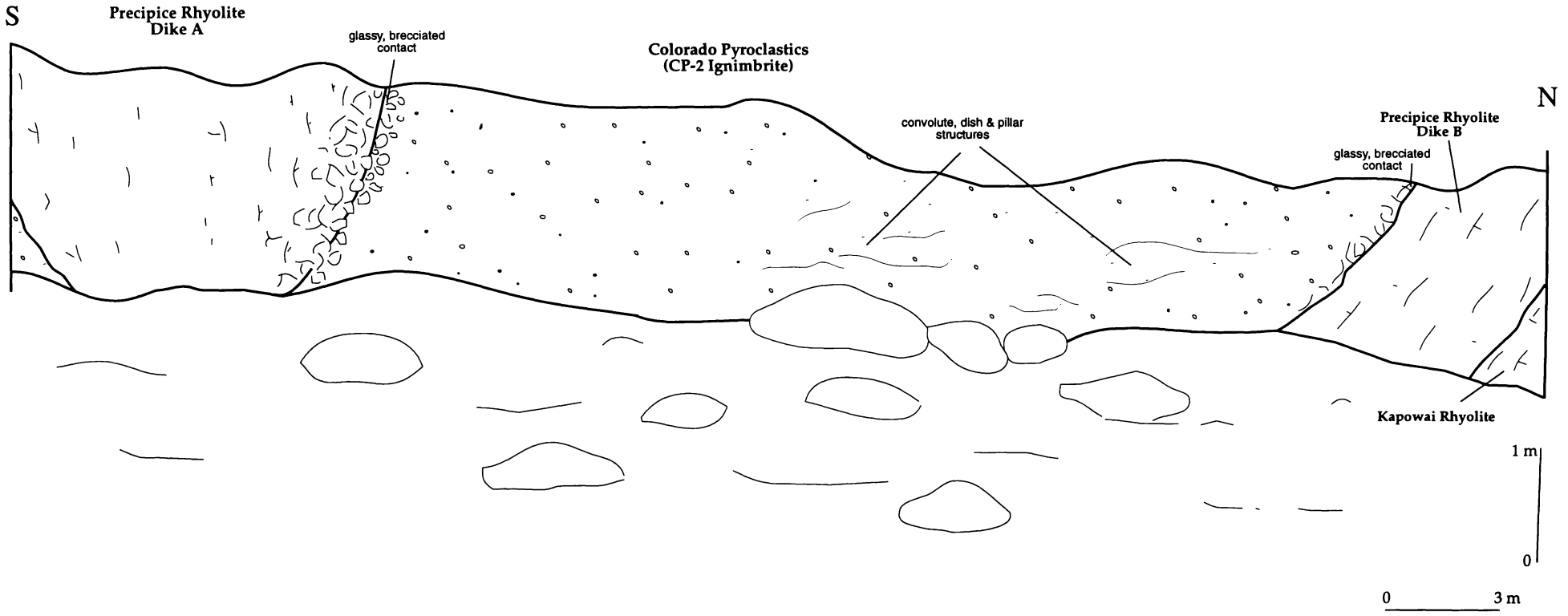


Figure 3.26 Sketch of Precipice Rhyolite lava dike section on the western bank of the Kapowai valley floor (T11/552660). Dike A intrudes CP-2 Ignimbrite (Colorado Pyroclastics) and Dike B intrudes along the contact between CP-2 Ignimbrite and Kapowai Rhyolite.

An intrusive contact between Kauaeranga Rhyolite and WES-1 Ignimbrite (Figure 3.28b) is observed downstream of the Kauaeranga Gorge (T12/489583) implying a post-WES age. A single $K/Ar_{(plagioclase)}$ age determined in this study yields an age of 4.9 ± 0.6 Ma, confirming a late KCC age.

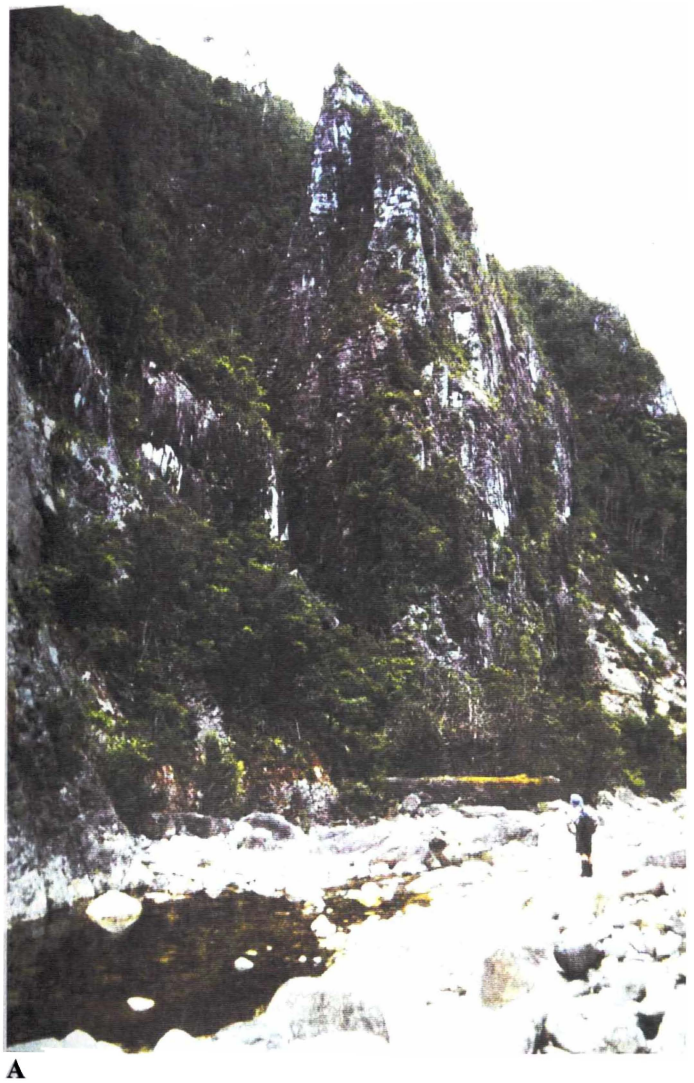

A

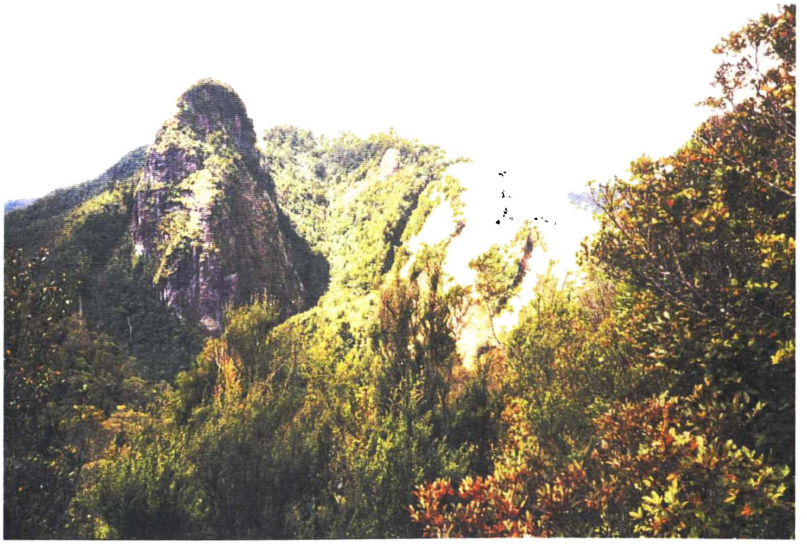

B

Figure 3.27 Tauranikau Rhyolite lava outcrops, upper Kauaeranga valley. A, Tauranikau Rhyolite lava exposed in Kauaeranga valley floor (T12/505593). B, Tauranikau Rhyolite lava spine exposed in tributary of upper Kauaeranga valley. View NE from T12/502581.

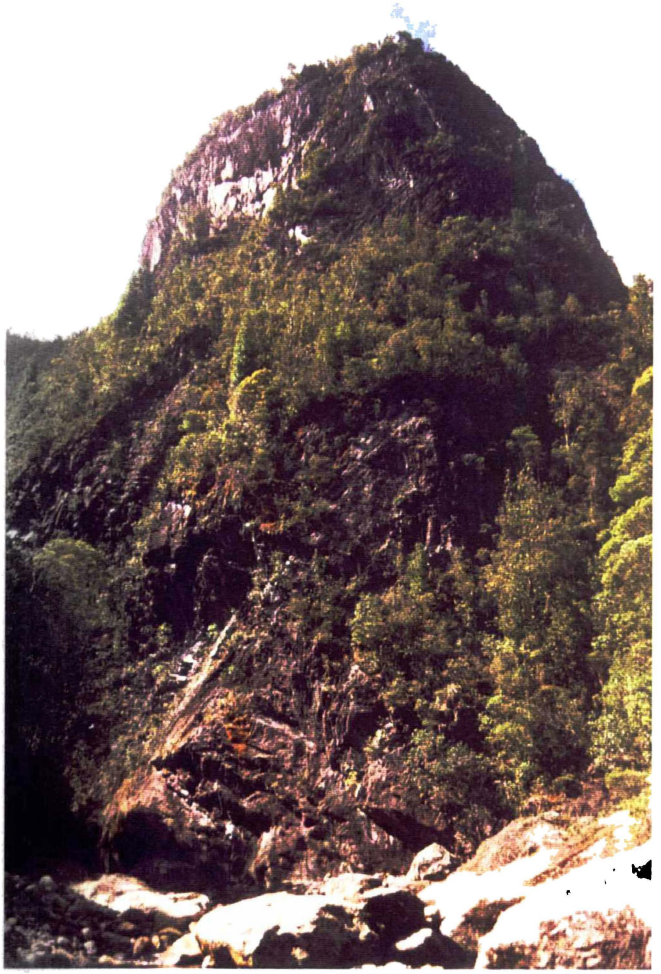

A

B

Figure 3.28 A, Kauaeranga Rhyolite forming steep sided lava dome in the upper Kauaeranga valley (T12/489583). WES-1 Ignimbrite outcrops in foreground right. B, Intrusive contact between Kauaeranga Rhyolite (left) and WES-1 Ignimbrite (right) at the same location.

# Chapter Four

# LITHIC FRAGMENTS IN KCC PYROCLASTIC DEPOSITS

## 4.1 Introduction

Large scale explosive eruptions at caldera volcanoes incorporate a variety of lithic fragments from the volcanic pile and sub-volcanic crust. Analysis of these fragments can constrain physical aspects of host pyroclastic deposits, and constrain the volcanic stratigraphy and petrogenesis of caldera volcanoes. Lithic lithology, morphology and componentry can provide information on eruptive and depositional processes (Suzuki-Kamata, 1988; Buesch, 1992; Bryan et al., 1998), and vent dynamics and evolution (Druitt, 1985; Hildreth and Mahood, 1986; Potter and Oberthal, 1987; Suzuki-Kamata et al., 1993). Distinctive lithic fragments or lithic assemblages can assist in characterising pyroclastic deposits, as well as aiding correlation (Hildreth and Mahood, 1985). As lithic fragments represent upper crustal lithologies, they can constrain the local composition of the sub-volcanic crust (e.g. Cole et al., 1998; Krippner et al., 1998).

Intracaldera lithic fragment analysis can be limited by: (i) poor recognition of the paleotopography and/or vent (Buesch, 1992); and (ii) alteration caused by contact or low grade regional metamorphism, metasomatism, hydrothermal fluids, and load compaction (Eichelberger and Koch, 1979; Hildreth and Mahood, 1985).

In this chapter, the lithology and petrography of lithic fragments in KCC ignimbrites is presented and some correlations to outcropping pre-caldera and caldera units are made. In other chapters, lithic fragments are used to (i) constrain caldera stratigraphy (Chapter Three); (ii) constrain the vent location and eruptive stratigraphy of the Wharepapa Eruptive Sequence (WES) (Chapter Five); (iii) constrain the sub-volcanic crustal composition and petrogenesis of KCC magmas (Chapter Seven); and (iv) provide evidence for buried hydrothermal systems (Chapter Eight).

## 4.2 Lithic occurrence and abundance

Approximately 1000 lithic fragments were sampled from KCC pyroclastic deposits. At sampling localities, lithic lithology, maximum lithic size (ML), and lithic abundance was recorded (Appendix IV). For most sampled lithics, thin sections were prepared for classification and petrographic analysis.

Lithic fragments are found in all KCC ignimbrites, but are rare components in crystal and vitric tuffs. Fragments occur within ignimbrite matrix as non-concentrated and non-sorted single clasts (Figure 4.1), or as discrete concentrated pods or zones. Lithic concentration zones are frequently observed in the WES and Webb Creek Ignimbrites at many intracaldera localities. Lithics also occur as lag breccias, but these are rarely observed and restricted to the WES.

Lithic fragments typically display angular-subangular morphology and vary in size from ash (< 1mm) to block (2.3 m max.). In ignimbrites, lithic fragments vary from 3-20 % abundance in the matrix, but can increase to 75 % in lithic concentration zones and 85 % in lag breccias (Table 4.1). Tuffs typically contain < 1 % lithics and these are generally < 5 mm.

A

B

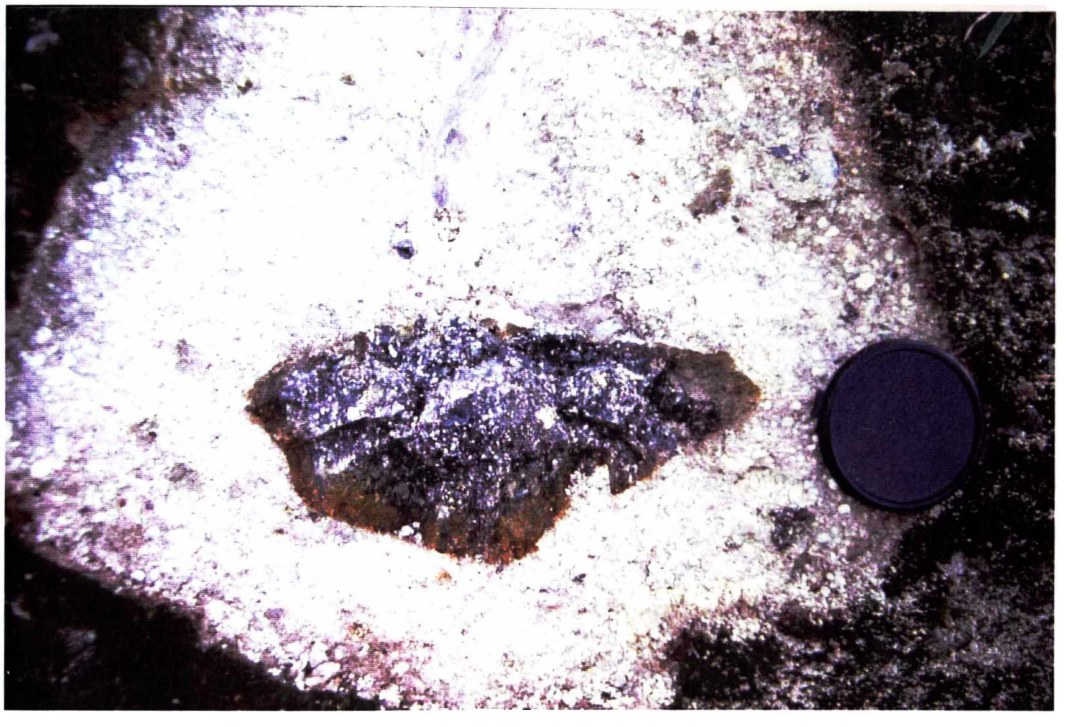

C

Figure 4.1 Occurrence of lithic fragments in Kapowai Caldera Complex ignimbrites. A, Faulted lacustrine siltstone in WES-1 Ignimbrite (T11/554671). Lens cap diameter is 55 mm. B, Pale green, weakly propylitic altered welded ignimbrite lithic in WES-1 Ignimbrite (T11/534677). Coin diameter is 25 mm. C, Black, glassy porphyritic rhyolite lava lithic in basal Trig Q Ignimbrite (T11/515701).

Accessory and minor accidental lithics dominate the lithic populations. Accessory lithics are defined here as pre-existing upper crustal rock incorporated into an explosive eruption by abrasion and erosion of the conduit or vent (Cas and Wright, 1987). At the KCC, these include a variety of pre-caldera andesite and dacite lavas, caldera related rhyolite lavas, welded ignimbrites and hydrothermal altered lithologies (lava and ignimbrite). Accidental lithics are defined as pre-existing surficial country rock included within a pyroclastic flow (Cas and Wright, 1987).

Table 4.1 Summary of typical abundances and sizes of lithic fragments in major Kapowai Caldera Complex ignimbrites.

| | WES-1 | WES-4 | Otaao | Manuka | Trig Q | Webb Creek |
|---|---|---|---|---|---|---|
| Lithic Abundance(%) | 5 - 15 | 5 - 10 | 3 - 5 | 7 - 10 | 3 - 5 | 5 - 20 |
| Max. Lithic (mm): matrix | 440 | 508 | 12 | 68 | 26 | 573 |
| LCZ | 170 | 212 | | | | 316 |

Differentiating between these two lithic provenances is difficult. Angular-subangular lithics are common which suggest they are vent derived. However, as intracaldera ignimbrites have undergone minimal transport distances, accessory lithics may be little modified, so surficial provenance is typically difficult to establish. Large (0.5-2 m) angular-subangular lithics in proximal pyroclastic sections provide the only clear evidence for a vent provenance.

## 4.3 Lithic lithology

Lithic fragment lithologies are dominated by lava (rhyolite, dacite and andesite) and pyroclastic (welded ignimbrite and tuff) fragments. Other lithologies include minor sedimentary (siltstone, sandstone, and breccia), hydrothermally altered (lava, welded ignimbrite, and welded tuff), and rare plutonic (micro-granodiorite) fragments.

The dominance of volcanic lithic lithologies is consistent with other lithic assemblages reported from other CVZ ignimbrites (e.g. McGunnigle, 1995; Bardebes, 1997) and TVZ ignimbrites (Cole et al., 1998; Krippner et al., 1998). Several lithologies which are not present in the KCC, are Tertiary and Mesozoic basement fragments (cf. Krippner et al., 1998), although Skinner (1995) reported the presence of sillimanite hornfels and quartz-orthopyroxene-plagioclase granulite from ignimbrites in the Waiwawa valley.

### Lava lithics

Lava lithics are the most abundant and largest lithic constituent in KCC ignimbrites. Rhyolite, dacite, and andesite lava lithologies are present (Figure 4.2). Within each lithology, subdivision on the basis of phenocryst assemblage enables definition of subgroups (Table 4.2).

#### *Rhyolite lavas*

Rhyolite lava lithics are consistently present in all KCC ignimbrites. Three major groups are defined. Plagioclase-pyroxene phyric (RPP) group have a pyroxene phase as the major ferromagnesian phenocryst. Minor amphibole occurs in some RPP lavas. RPP lava lithics are the most common and diverse rhyolite group. Plagioclase phyric (RP) group has plagioclase as the only phenocryst phase. Plagioclase-amphibole phyric (RPA) group has amphibole as the major ferromagnesian phenocryst. Orthopyroxene phenocrysts occur in some RPA lithics.

Rhyolite phenocrysts consist of plagioclase, orthopyroxene, clinopyroxene, amphibole and Fe-Ti oxides (Table 4.3). Plagioclase phenocrysts (3.1 mm max.) are subhedral, prismatic or tabular and show compositional zonation and polysynthetic twinning. Fe-Ti oxides and glass inclusions are common. Orthopyroxene phenocrysts (1.8 mm max.) are subhedral, prismatic and typically contain Fe-Ti oxide inclusions. Clinopyroxene phenocrysts (1.3 mm max.) are subhedral, stubby prismatic, and occasionally contain Fe-Ti oxides. Amphibole phenocrysts (1.0 mm max.) are subhedral, prismatic and typically occur as discrete phenocrysts or with plagioclase in glomerocrysts. Fe-Ti oxide phenocrysts (0.55 mm max.) are anhedral, equant (titanomagnetite) and subhedral or anhedral, prismatic ilmenite. Embayed margins are common.

Rhyolite lava lithics exhibit a variety of textures. Mm-scale flow banding is common in most lithics. Glomerocrysts occur in some lavas, although single phenocrysts are more common. Groundmass textures include glassy, perlitic, spherulitic, snow-flake and devitrified, and intersertal. Amygdules ranging from < 0.5 mm to > 1cm are common and consist of quartz, tridymite, cristobalite, chalcedony, biotite, zeolite and Fe-Ti oxides.

***Dacite lavas***

Dacite lavas are less abundant than rhyolite lava fragments and are present in most KCC ignimbrites. Three major dacite lava lithic groups are defined. Plagioclase-pyroxene phyric (DPP) group includes all dacite lava lithics with a pyroxene phase as the most abundant ferromagnesian mineral. DPP is the most common dacite lava lithic group. Pyroxene phases include orthopyroxene and clinopyroxene. Minor phases present may include amphibole and/or biotite. Plagioclase-quartz phyric (DPQ) group includes all dacitic lava lithics which contain abundant xenocrystic quartz phenocrysts. Plagioclase-amphibole phyric (DPA) group includes all dacitic lavas which have amphibole as the major ferromagnesian phase. Minor phenocrysts include orthopyroxene, clinopyroxene and biotite.

Dacite phenocrysts consist of plagioclase, orthopyroxene, clinopyroxene, amphibole and Fe-Ti oxides (Table 4.4). Plagioclase phenocrysts (3.8 mm max.) are subhedral, prismatic or tabular. Quartz phenocrysts (2.4 mm max.) are anhedral, equant and typically have embayed or resorbed margins. Orthopyroxene phenocrysts (1.6 mm max.) are subhedral, prismatic and typically contain Fe-Ti oxide inclusions. Clinopyroxene phenocrysts (2.1 mm max.) are subhedral, tabular or stubby prismatic. Amphibole phenocrysts (2.5 mm max.) are euhedral to subhedral prismatic and occasionally have thin, black reaction rims. Fe-Ti oxide phenocrysts (0.5 mm max.) are anhedral, equant (titanomagnetite) or anhedral, prismatic (ilmenite).

Groundmass textures include intergranular, intersertal, pilotaxitic, and glassy or perlitic. Amygdules are common and infilling mineral phases include tridymite, cristobalite, zeolite, quartz, biotite and Fe-Ti oxides.

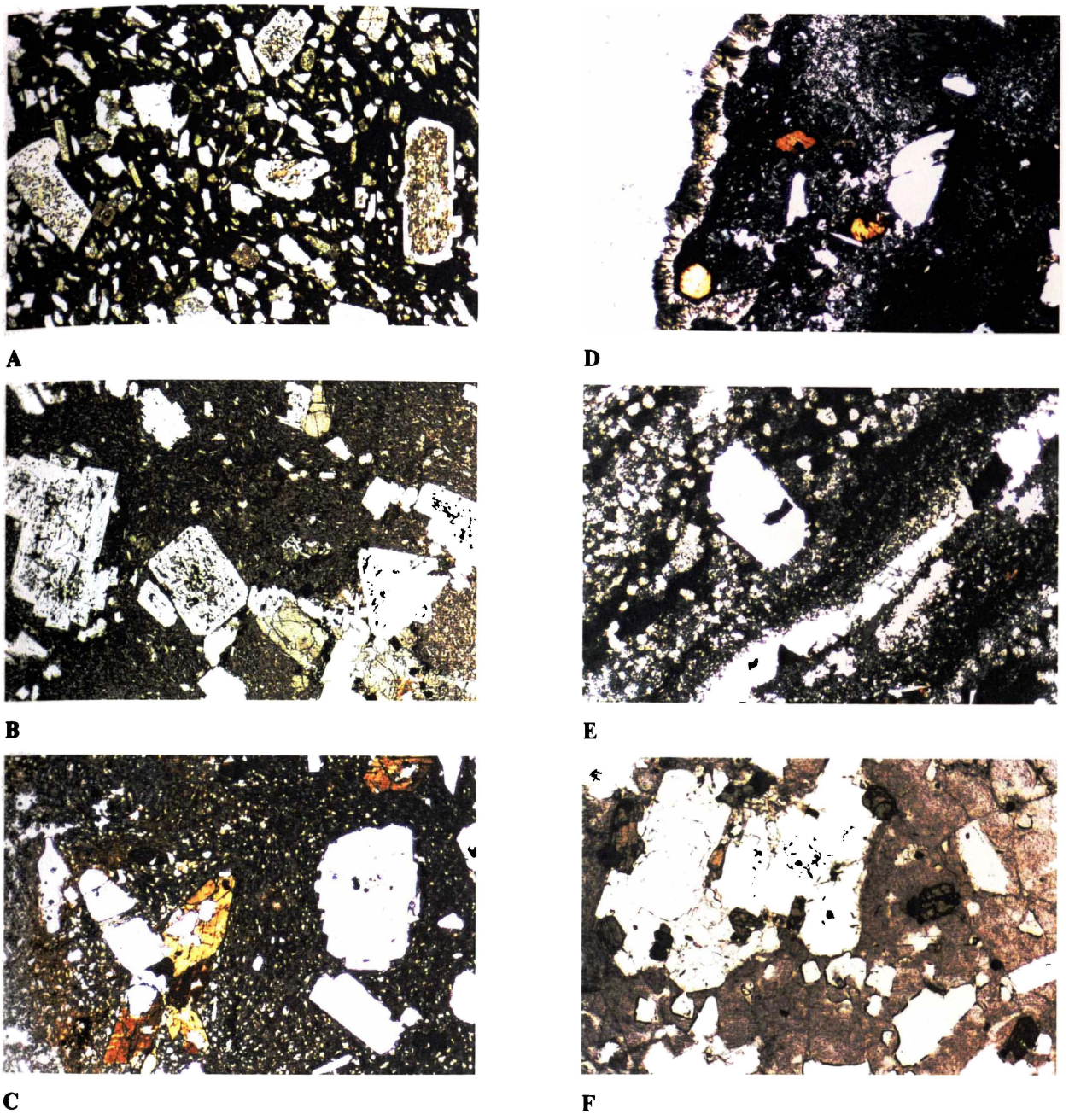

Figure 4.2. Photomicrographs of lava lithics sampled from Kapowai Caldera Complex ignimbrites. A, two-pyroxene andesite (APP; W99674LA). B, two-pyroxene andesite (APP; W99897LD). C, hornblende dacite (DPA; W99913LI). D, plagioclase phyric rhyolite lava with zeolites infilling amygdule rimmed by tridymite and cristobalite (RPP; W99693LA). E, rhyolite lava with granular biotite in groundmass (RPP; W99694LB). F, glassy, perlitic rhyolite lava (RPP; W99897LC). Length of each image is 4 mm.

***Andesite lavas***

Two major groups of andesite lava lithics are defined. Plagioclase-pyroxene phyric (APP) group andesites have a pyroxene phase(s) as the dominant phenocryst. Orthopyroxene and clinopyroxene are present together in most lithics, although either can also occur on its own. Plagioclase-amphibole phyric (APA) group includes all andesite lava lithics that have amphibole as the major ferromagnesian phase. Minor phenocrysts include orthopyroxene and clinopyroxene.

Table 4.2 Definition of lava lithic types and occurrence in Kapowai Caldera Complex ignimbrites. Dashed line indicates occurrence of lithic type in ignimbrite. plag = plagioclase; qtz = quartz; opx = orthopyroxene; cpx = clinopyroxene; biot = biotite; amph = amphibole; devit = devitrified; f band = flow banded; amygda = amygdaloidal; spheru = spherulitic; trid = tridymite; zeol = zeolite; crist = cristobalite; chal = chalcedony.

| Lithology | | Phenocryst Assemblage | Groundmass Assemblage | Groundmass Texture | WES-1 | WES-4 | Oteao | Trig Q | Manuka | Webb Creek |
|---|---|---|---|---|---|---|---|---|---|---|
| Rhyolite | RP | plag Fe-Ti oxides | plag qtz biot Fe-Ti oxides | hyalopilitic perlitic devit f band intersertal pilotaxitic amygda(trid/biot) | - | - | | | - | - |
| | RPP | plag opx Fe-Ti oxides | plag opx Fe-Ti oxides | hyalopilitic perlitic spheru f band amygda(trid/qtz/biot/amph) | - | - | - | - | - | - |
| | | plag cpx Fe-Ti oxides | plag qtz cpx Fe-Ti oxides | devit glassy spheru hyalopilitic amygda(trid) | - | | | | | |
| | | plag opx cpx Fe-Ti oxides | plag opx cpx Fe-Ti oxides | devit glassy hyalopilitic intersertal spheru amygda(chal/trid/zeol/biot/ Fe-Ti oxides) | - | - | | | - | - |
| | | plag opx cpx amph Fe-Ti oxides | plag opx cpx amph | glassy perlitic hyalopilitic | - | | | | | - |
| | | plag opx amph Fe-Ti oxides | plag opx amph Fe-Ti oxides | glassy perlitic hyalopilitic | - | | | | | |
| | RPA | plag amph Fe-Ti oxides | plag amph Fe-Ti oxides | devit amygda(trid/amph/ Fe-Ti oxides)/spheru f band | - | | | | - | |
| | | plag amph opx Fe-Ti oxides | plag Fe-Ti oxides | devit f band spheru amygda(qtz) | | - | | | | |
| | Dacite | plag qtz biot amph opx Fe-Ti oxides | plag opx Fe-Ti oxides | devit intersertal glassy | - | | | | | |
| | DPP | plag cpx Fe-Ti oxides | plag cpx Fe-Ti oxides | intersertal intergranular pilotaxitic perlitic hyalopilitic | - | | | | - | - |
| | | plag opx cpx Fe-Ti oxides | plag opx cpx Fe-Ti oxides | devit glassy perlitic intersertal pilotaxitic amygda(trid/zeol/qtz/biot/ Fe-Ti oxides) | - | - | - | - | - | - |
| | | plag opx amph biot Fe-Ti oxides | plag opx Fe-Ti oxides | devit intersertal | | - | | | - | |
| | DPA | plag amph opx cpx Fe-Ti oxides | plag opx cpx Fe-Ti oxides | intersertal pilotaxitic | - | | | | | |
| Andesite | | plag cpx Fe-Ti oxides | plag Fe-Ti oxides | hyalopilitic perlitic | - | | | | | |
| | | plag opx cpx Fe-Ti oxides | plag opx cpx Fe-Ti oxides | intersertal pilotaxitic intergranular hyalopilitic devit amygda(trid/crist/zeol) | - | | | | - | - |
| | APA | plag amph Fe-Ti oxides | plag amph Fe-Ti oxides | intergranular pilotaxitic | - | - | | | | |
| | | plag amph opx cpx Fe-Ti oxides | plag opx amph Fe-Ti oxides | devit intersertal | - | | | | | - |

Table 4.3 Modal mineralogy for selected rhyolite lava lithics sampled from Kapowai Caldera Complex ignimbrites.

| Sample | W99693LA | W99975LE | W99901LQ | W99831LI | W99967LB | W99780LE | W99898LC | W99938LB | W99975LH | W99891LB | W99694LH |
|---|---|---|---|---|---|---|---|---|---|---|---|
| **Lithic Group** | **RPP** | **RPP** | **RPP** | **RPP** | **RPP** | **RP** | **RP** | **RP** | **RP** | **RPA** | **RPA** |
| **Phenocrysts** | | | | | | | | | | | |
| Plagioclase | 6.3 | 8.3 | 5.6 | 8.0 | 4.6 | 6.3 | 6..8 | 1.5 | 4.3 | 11.6 | 8.0 |
| Quartz | | | | | | | | | | | |
| Orthopyroxene | 0.8 | 0.2 | 0.6 | 0.3 | 0.3 | | | | | | |
| Clinopyroxene | 0.6 | | | | | | | | | | |
| Amphibole | | | | | | | | | | 0.5 | 0.7 |
| Fe-Ti oxides (>0.05mm) | 0.4 | 0.4 | 0.3 | 0.1 | 0.2 | 1.6 | 2.3 | 0.3 | 0.1 | 1.6 | 0.6 |
| **Total Phenocrysts** | **8.1** | **8.9** | **6.5** | **8.4** | **5.1** | **7.9** | **9.1** | **1.8** | **4.3** | **13.7** | **9.3** |
| **Secondary Minerals** | | | | | | | | | | | |
| Tridymite | 3.0 | | 1.9 | | | | | | | | |
| Cristobalite | 9.1 | | 1.4 | | | | | | | | |
| Zeolite | 8.2 | | | | | | | | | | |
| **Groundmass** | | | | | | | | | | | |
| Devitrified glass | 54.3 | 86.1 | 84.7 | 82.3 | 93.3 | 92.0 | 54.6 | 93.6 | 91.0 | 84.0 | 84.1 |
| Plagioclase lath | 15.0 | 5.0 | 4.6 | 9.3 | 1.6 | 0.1 | 3.3 | 4.6 | 2.6 | 0.3 | 3.3 |
| Granular Pyroxenes | | | | | | | | | | | |
| Granular Biotite | 0.8 | | 0.9 | | | | | | | 2.0 | 2.0 |
| Fe-Ti oxides (<0.05mm) | 1.8 | | | | | | | | 2.0 | | |
| Granular quartz | | | | | | | 33.0 | | | | 1.3 |
| Glass Patches | | | | | | | | | | | |
| Vesicles | | | | | | | | | | | |
| **Total Groundmass** | **71.9** | **91.1** | **90.2** | **91.6** | **94.9** | **92.1** | **90.9** | **98.2** | **95.6** | **86.3** | **90.7** |
| **TOTAL** | **100.0** | **100.0** | **100.0** | **100.0** | **100.0** | **100.0** | **100.0** | **100.0** | **100.0** | **100.0** | **100.0** |

Andesite lava lithic phenocrysts consist of plagioclase, orthopyroxene, clinopyroxene, amphibole and Fe-Ti oxides (Table 4.5). Plagioclase phenocrysts (4.2 mm max.) are subhedral, prismatic or tabular and typically contain abundant glass, pyroxene and Fe-Ti oxide inclusions. Orthopyroxene phenocrysts (2.6 mm max.) are subhedral, prismatic and commonly contain Fe-Ti oxide inclusions. Clinopyroxene phenocrysts (2.8 mm max.) are subhedral, tabular or stubby prismatic and occasionally have thin black reaction rims. Amphibole phenocrysts (2.5 mm max.) are subhedral, prismatic, typically have thin black reaction rims, and contain plagioclase, pyroxene and Fe-Ti oxide inclusions. Fe-Ti oxide phenocrysts (0.75 mm max.) are anhedral, equant (titanomagnetite) or anhedral, prismatic (ilmenite).

Groundmass textures vary from hyalopilitic to intersertal to intergranular. Glass is perlitic in some lithics and devitrified in most. Amygdules are rare, and where present are infilled by tridymite, cristobalite and zeolite.

Andesite lava lithics are found in all KCC ignimbrites. Pre-caldera andesites are likely to underlie the volcanic pile, so their presence in most lithic populations should be expected. Caldera-related andesite lavas (Taurauikau Andesite) make up a minor component of the andesite lava lithic population. The restricted distribution of these lavas in the KCC (i.e. only in western sector) is likely to be the major reason for this.

***Correlation***

Correlating lava lithic fragments to known outcropping lavas is based upon phenocryst assemblages. Only a limited number of correlations can be suggested because not all lava lithic compositions sampled have a surface analogue (Table 4.6). Lavas which do not have a surface correlative are inferred to occur in the unexposed volcanic pile.

## Pyroclastic lithics

Welded ignimbrite and tuff lithics are a common constituent in KCC ignimbrites (Figure 4.3). These provide conclusive evidence for multiple explosive eruptions at the KCC and assist in constraining the timing of eruptive events. WES deposits contain the greatest diversity of welded ignimbrite lithics, implying that this was the youngest and largest explosive episode from the KCC.

***Welded ignimbrite***

Numerous welded ignimbrite varieties have been sampled from KCC ignimbrites. Differentiating welded ignimbrite lithic fragments is difficult because of similarity in composition and components, and variable hydrothermal alteration. Four main non-altered groups have been defined (Table 4.7). Groups are defined on the basis of commonality of physical properties which includes lithic & juvenile clast morphology, clast sizes and abundances, and juvenile and matrix crystal assemblages (Table 4.8). Several hydrothermally altered welded ignimbrite groups are defined later in this chapter.

*Table 4.4 Modal mineralogy for selected dacite lava lithics sampled from Kapowai Caldera Complex ignimbrites.*

| **Sample** | **W99862LE** | **W99886LH** | **W99931LG** | **W99867LB** | **W99896LD** | **W99950LJ** | **W99913LI** | **W99632LA** |
|---|---|---|---|---|---|---|---|---|
| **Lithic Group** | **DPP** | **DPP** | **DPP** | **DPP** | **DPP** | **DPQ** | **DPA** | **DPA** |
| **Phenocrysts** | | | | | | | | |
| Plagioclase | 16.6 | 4.0 | 16.0 | 15.3 | 4.0 | 20.6 | 21.6 | 17.3 |
| Quartz | | | | | 0.2 | 6.6 | | |
| Orthopyroxene | 0.9 | 3.0 | 2.6 | 0.3 | 0.6 | 1.3 | | 0.6 |
| Clinopyroxene | 1.0 | | 2.3 | 0.3 | | | | |
| Amphibole | | | | | | 9.3 | 2.6 | 2.5 |
| Biotite | | | | | | 4.6 | | |
| Fe-Ti oxides (>0.05mm) | 2.0 | 1.6 | 0.4 | 2.3 | 0.3 | 2.0 | 1.0 | 0.8 |
| **Total Phenocrysts** | **20.5** | **8.6** | **21.3** | **18.2** | **5.1** | **44.4** | **25.2** | **21.2** |
| **Groundmass** | | | | | | | | |
| Devitrified glass | 79.4 | 82.3 | 78.6 | 74.6 | 73.6 | 40.5 | 66..6 | 6.3 |
| Plagioclase lath | | 9.0 | 0.1 | 3.3 | 19.3 | 14.0 | 8.0 | 67.0 |
| Granular Pyroxenes | | 0.1 | | | | | | |
| Granular Biotite | | | | 3.6 | | | | 4.3 |
| Fe-Ti oxides (<0.05mm) | 0.1 | | | | 2.0 | 0.8 | | 1.2 |
| Glass Patches | | | | | | | | |
| Vesicles | | | | | | | | |
| **Total Groundmass** | **79.5** | **91.4** | **78.7** | **81.5** | **94.9** | **55.3** | **74.6** | **78.8** |
| TOTAL | 100.0 | 100.0 | 100.0 | 100.0 | 100.0 | 100.0 | 100.0 | 100.0 |

Table 4.5 Modal mineralogy for selected andesite lava lithics sampled from Kapowai Caldera Complex ignimbrites.

| **Sample** | **W99694LD** | **W99848LG** | **W99899LB** | **W99943LB** | **W99901LH** | **W99974LC** | **W99972LF** | **W99642LA** | **W99874LD** | **W99950LF** |
|---|---|---|---|---|---|---|---|---|---|---|
| **Lithic Group** | **APP** | **APP** | **APP** | **APP** | **APP** | **APP** | **APP** | **APA** | **APA** | **APA** |
| **Phenocrysts** | | | | | | | | | | |
| Plagioclase | 20.6 | 5.6 | 7.3 | 26.0 | 21.3 | 16.3 | 17.0 | 24.6 | 12.0 | 32.6 |
| Quartz | | | | | | | | | | 4.0 |
| Orthopyroxene | 9.9 | 0.3 | 2.0 | 0.6 | 0.6 | 3.3 | 1.3 | 1.6 | | 1.3 |
| Clinopyroxene | 5.6 | 1.3 | 4.3 | 1.3 | 2.3 | 2.0 | 1.3 | 1.3 | | 1.0 |
| Amphibole | | | | | | | | 2.6 | 3.6 | 7.0 |
| Biotite | | | | | | | | | | 7.3 |
| Fe-Ti oxides (>0.05mm) | 1.0 | | 1.2 | 1.6 | 1.3 | 1.6 | 0.6 | 0.3 | 0.6 | 0.3 |
| **Total Phenocrysts** | **37.1** | **7.2** | **14.8** | **29.5** | **25.5** | **23.2** | **20.2** | **30.4** | **16.2** | **53.5** |
| **Secondary Minerals** | | | | | | | | | | |
| undifferentiated clays | | | | | | | | 5.0 | 11.3 | |
| **Groundmass** | | | | | | | | | | |
| Devitrified glass | 58.6 | 88.5 | 36.3 | 65.6 | 41.6 | 41.6 | 56.3 | 46.3 | 34.6 | 30.2 |
| Plagioclase lath | 4.3 | 4.3 | 36.6 | 3.6 | 25.6 | 31.6 | 19.9 | 11.0 | 27.0 | 13.3 |
| Granular Pyroxenes | | | | | 1.0 | | | | 2.6 | |
| Granular Biotite | | | | 1.0 | | | | | | |
| Fe-Ti oxides (<0.05mm) | | | 12.3 | 0.3 | 6.3 | 3.6 | 3.6 | 7.3 | 8.0 | 3.0 |
| Glass Patches | | | | | | | | | | |
| Vesicles | | | | | | | | | | |
| **Total Groundmass** | **62.9** | **92.8** | **85.2** | **70.5** | **74.5** | **76.8** | **79.8** | **64.6** | **72.2** | **46.5** |
| TOTAL | 100.0 | 100.0 | 100.0 | 100.0 | 100.0 | 100.0 | 100.0 | 100.0 | 100.0 | 100.0 |

Table 4.6. Correlation of lava lithic fragments in Kapowai Caldera Complex ignimbrites with exposed lavas. plag = plagioclase; qtz = quartz; opx = orthopyroxene; cpx = clinopyroxene; amph = amphibole; biot = biotite.

| Lithology | | Phenocryst Assemblage | Correlative Lava Unit |
|---|---|---|---|
| Rhyolite | RP | plag Fe-Ti oxides | group III rhyolite lava |
| | RPP | plag opx Fe-Ti oxides | group I rhyolite lava |
| | | plag cpx Fe-Ti oxides | group I rhyolite lava |
| | | plag opx cpx Fe-Ti oxides | group I rhyolite lava |
| | | plag opx cpx amph Fe-Ti oxides | group IV rhyolite lava |
| | | plag opx amph Fe-Ti oxides | group IV rhyolite lava |
| | RPA | plag amph Fe-Ti oxides | group IV rhyolite lava |
| | | plag amph opx Fe-Ti oxides | |
| Dacite | | plag qtz biot amph opx Fe-Ti oxides | Maumaupaki Formation |
| | DPP | plag cpx Fe-Ti oxides | |
| | | plag opx cpx Fe-Ti oxides | |
| | | plag opx amph biot Fe-Ti oxides | Maumaupaki Formation |
| | DPA | plag amph opx cpx Fe-Ti oxides | Maumaupaki Formation |
| Andesite | | plag cpx Fe-Ti oxides | |
| | | plag opx cpx Fe-Ti oxides | Taurauikau Andesite/Taurahuehue Andesite |
| | APA | plag amph Fe-Ti oxides | Maumaupaki Formation |
| | | plag amph opx cpx Fe-Ti oxides | Maumaupaki Formation |

It is assumed that most welded ignimbrite lithics are proximal and generally represent KCC derived ignimbrites. However, some lithics may represent ignimbrites which infilled the KCC and were erupted from adjacent CVZ calderas. Welded ignimbrite lithics range up to 2 m in lag breccias, but are typically < 10 mm to 60 mm.

Cream-light grey, pumice and crystal-rich welded ignimbrite lithics (WEB) are the most abundant group. A single juvenile variety is present which is a cream, non fibrous, incipiently lenticular, weakly vesicular, plagioclase-orthopyroxene phyric pumice. Matrix crystals consist of plagioclase, orthopyroxene and Fe-Ti oxides. Lithic fragments are common (3-5 %) and consist predominantly of rhyolite (RPP) and andesite (APP, APA) lavas. The matrix is fine grained and poorly vitroclastic. The single, non fibrous, incipiently lenticular pumice variety and plagioclase-orthopyroxene mineralogy is similar to the Webb Creek Ignimbrite.

Grey, pumice-rich and lithic-poor, welded ignimbrite lithics with moderate to highly lenticular pumice clasts form a distinctive lithic group (TRI). A single juvenile variety is present which is a grey-brown, moderate to highly lenticular, non-fibrous, incipiently vesicular, plagioclase phyric pumice. Matrix crystals consist of plagioclase, minor orthopyroxene and Fe-Ti oxides. Lithics are rare and consist of rhyolite lava (RPP). The matrix is fine grained and has a poorly developed vitroclastic texture. Moderate to highly lenticular pumice, rare lithics and plagioclase-orthopyroxene mineralogy resembles the Trig Q Ignimbrite.

Brown-orange/brown, pumice-rich, lithic-poor welded ignimbrite lithics form another distinctive group (KAP). A single juvenile type is present which is an incipiently lenticular, poorly fibrous, poorly vesicular pumice. Matrix crystals include plagioclase, orthopyroxene, clinopyroxene, amphibole and Fe-Ti oxides. Matrix is fine grained and has a poorly to highly developed vitroclastic texture. Single brown/orange pumice and high pumice abundance, coupled with plagioclase-pyroxene-amphibole mineralogy is similar to the Manuka Ignimbrite.

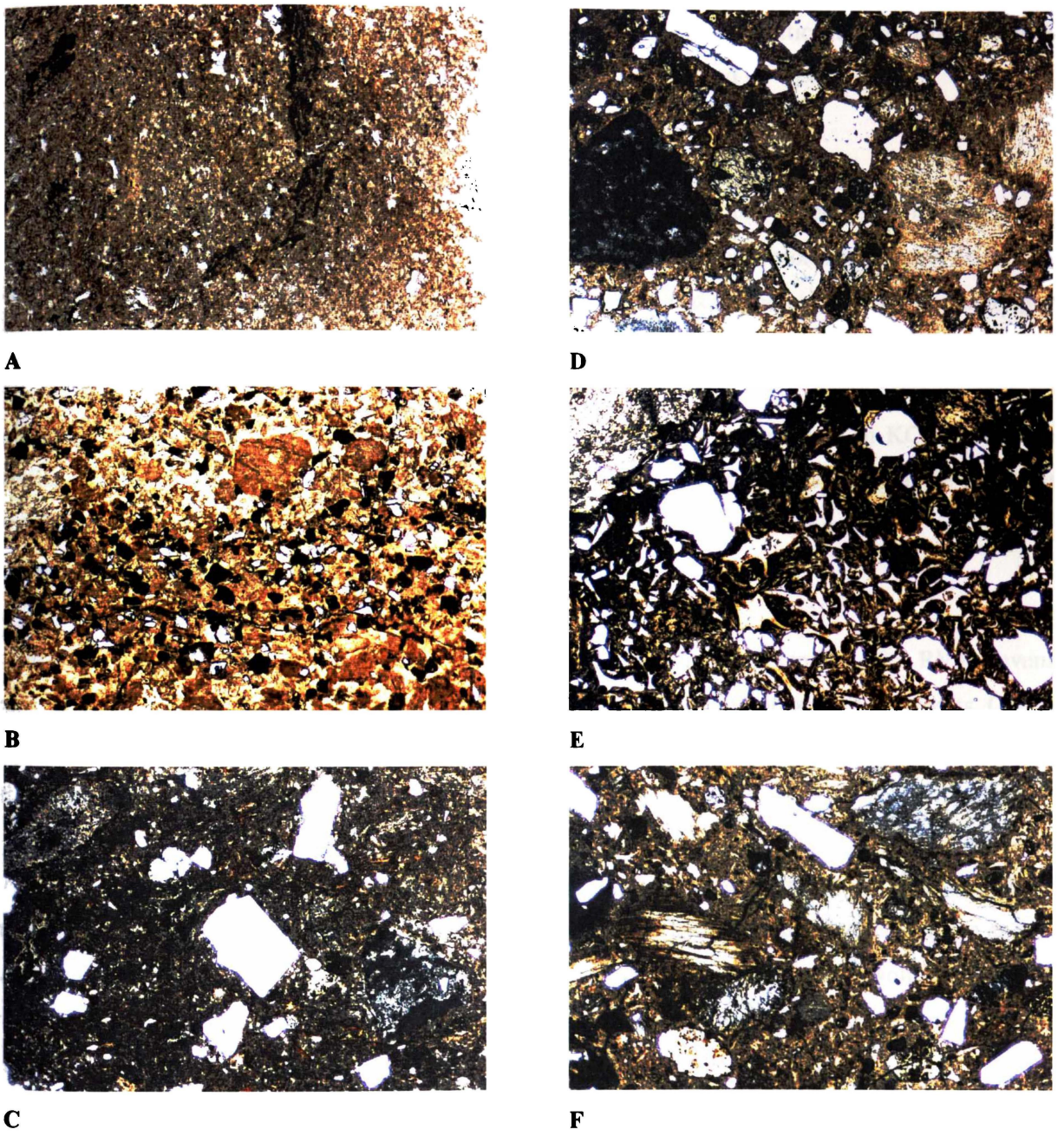


Figure 4.3 Photomicrographs of pyroclastic lithic fragments sampled from Kapowai Caldera Complex ignimbrites. A, vitric ash tuff (RVT; W99896LE). B, weakly silicified vitric ash tuff with interbedded crystal tuff (RVT; W99728LC). C, vapour phase altered welded ignimbrite (VPA; W99606LE). D, crystal-rich silicified welded ignimbrite (WSI; W99762LA). E, coarsely vitroclastic welded ignimbrite (WSI; W99892LG). F, silicified welded ignimbrite (SSI; W99886LO). Length of each image is 4 mm.

Numerous vapour phase altered welded ignimbrite lithics (VAP) have been sampled. Lithics are typically pink, dark pink or orange and have a variety of juvenile types and lithic fragments. Juvenile clasts are

typically of rhyolitic composition, but are commonly altered to clay minerals and/or very fine grained feldspar and quartz polymorph (tridymite, cristobalite) crystals. The matrix crystals include plagioclase, orthopyroxene, clinopyroxene, amphibole, biotite and Fe-Ti oxides. Matrix is fine grained and altered to either clay (kaolinite), feldspar, tridymite or cristobalite.

Numerous other welded ignimbrite lithics have been sampled and these are grouped into an undifferentiated welded ignimbrite lithic group (UND). These display a variety of colours, component morphology, abundance and mineralogy. Juvenile clasts are rhyolitic or dacitic pumice. Matrix crystals include plagioclase, orthopyroxene, clinopyroxene, amphibole, biotite and Fe-Ti oxides.

***Welded tuff***

Welded tuff lithic fragments consist of numerous vitric and crystal ash tuff varieties. Correlating welded tuffs to surface analogues is difficult because of the similar juvenile composition and mineral assemblage of most exposed tuffs and lithics. Three major lithic types are defined on the basis of the dominant grain type and composition (Table 4.9).

Light grey-brown, pumice and lithic-rich rhyolitic vitric tuffs (RVT) are common in KCC ignimbrites. Juvenile grains are abundant (> 50 %) and are typically ash sized glass shards and pumice fragments. Crystals are rare and consist of plagioclase, quartz, orthopyroxene, clinopyroxene and Fe-Ti oxides. Lithic fragments are ash sized and consist predominantly of rhyolite lava.

Cream-brown, crystal-rich rhyolitic crystal tuffs (RCT) are less common compared with RVT. Juvenile grains (< 30 %) are typically ash sized and consist of glass shards and minor pumice fragments. Crystals are common and include plagioclase, quartz, orthopyroxene, clinopyroxene, amphibole and Fe-Ti oxides. Lithic fragments include a variety of rhyolite lavas.

Grey-brown, crystal-poor, lithic-rich rhyolitic lithic tuffs (RLT) are rare fragments in KCC ignimbrites. Lithic fragments within RLT are common and include a variety of rhyolite, minor dacite, and rare andesite lavas of ash to fine lapilli size. Juvenile grains (< 30 %) are ash size and consist of rhyolitic glass shards with minor pumice fragments. Crystals include plagioclase, orthopyroxene, clinopyroxene and Fe-Ti oxides.

### Volcanic breccia lithics

Volcanic breccia (BRE) lithics are rare or absent in most KCC ignimbrite lithic populations. Breccias are typically poorly sorted, monolithologic and contain ash to fine lapilli rhyolite lava clasts. Breccia lithic fragments most likely represent autoclastic breccias formed in conjunction with rhyolite lava domes or flows. Several surface analogues are seen within the KCC in the Webb Creek Rhyolite and Kydd Rhyolite complexes, but correlations to these or other rhyolite lavas are difficult to make.

*Table 4.7 Definition of welded ignimbrite lithic types and occurrence in Kapowai Caldera Complex ignimbrites. Dash indicates occurrence of lithic type in ignimbrite. r = rich; p = poor; i = incipiently; h = highly; plag = plagioclase; qtz = quartz; opx = orthopyroxene; cpx = clinopyroxene; amph = amphibole; biot = biotite.*

| Type | Lithology | Juvenile | Crystal Assemblage | Matrix | WES-1 | WES-4 | Oteao | Manuka | Trig Q | Webb Creek |
|---|---|---|---|---|---|---|---|---|---|---|
| WEB | light grey pum r lith r rhyolitic | brown/yellow p lenticular p fibrous i vesicular | plag qtz opx cpx Fe-Ti oxides | fine ash v.p.a relict vitr | - | - | | | | |
| TRI | dark brown pum r lith p dacitic | black h lenticular i vesicular i fibr plag phyric | plag opx cpx Fe-Ti oxides | fine ash devit relict vitr | - | - | | | | |
| KAP | brown pum r rhyolitic | light brown i vesicular i fibrous i lenticular | plag opx cpx amph Fe-Ti oxides | fine ash devit relict vitr | - | - | - | | | |
| VAP | pink-orange rhyolitic | variable | plag qtz opx cpx amph Fe-Ti oxides | fine ash vitroclastic | - | | | - | | |
| UND | grey-brown rhyolitic | variable | plag qtz opx cpx amph biot Fe-Ti oxides | fine ash vitroclastic | - | - | - | - | - | - |

Table 4.8 Modal componentry for selected welded ignimbrite lithics sampled from Kapowai Caldera Complex ignimbrites.

| Sample | W99849LI | W99867LD | W99773LA | W99923LA | W99950LR | W99849LH | W99846LH | W99886LJ | W99938LA |
|---|---|---|---|---|---|---|---|---|---|
| **Lithic Group** | **WEB** | **WEB** | **WEB** | **TRI** | **TRI** | **MAN** | **MAN** | **VAP** | **VAP** |
| **Juvenile** | **14.3** | **16.1** | **7.0** | **19.6** | **35.3** | **30.0** | **14.5** | **13.6** | **17.4** |
| **Crystal** | | | | | | | | | |
| Plagioclase | 5.6 | 11.3 | 7.0 | 7.3 | 12.3 | 9.6 | 7.4 | 8.6 | 6.5 |
| Orthopyroxene | 0.1 | 0.6 | 0.2 | 1.3 | 1.3 | 1.0 | 0.6 | 0.4 | 0.5 |
| Clinopyroxene | | 1.0 | | | 0.6 | 0.3 | 0.3 | 0.1 | |
| Amphibole | | | | | | | | | |
| Biotite | | | | | | | | | |
| Fe-Ti oxides (>0.05mm) | 1.0 | 1.3 | | 0.6 | 2.6 | 1.2 | 0.3 | 0.6 | 0.3 |
| **Total** | | | | | | | | | |
| **Lithic** | | | | | | | | | |
| Volcanic | 13.0 | 8.3 | 38.6 | 1.0 | 0.3 | 7.6 | 3.3 | 5.8 | 2.6 |
| Sedimentary | | | 9.0 | | | | | 3.2 | |
| **Matrix** | | | | | | | | | |
| Glass Shard | 65.0 | 56.4 | 35.6 | 64..2 | 42.3 | 45.3 | 67.6 | 58.2 | 64.3 |
| Pumice Fragment | 1.0 | 5.0 | 2.6 | 5.0 | 5..3 | 5.0 | 6.0 | 9.5 | 6.4 |
| Fe-Ti oxides (<0.05mm) | | | | 1.0 | | | | | 2.0 |
| **TOTAL** | **100.0** | **100.0** | **100.0** | **100.0** | **100.0** | **100.0** | **100.0** | **100.0** | **100.0** |

### Plutonic lithics

Plutonic (PLU) lithic fragments are rare constituents in KCC ignimbrites, and have only been sampled from WES ignimbrites. Plutonic lithics sampled are leucocratic, plagioclase-orthoclase micro-granodiorites. Granodiorites are grey, fine to medium grained, equigranular and incipiently weathered or altered. Crystals consist of plagioclase, minor orthoclase, rare biotite, and Fe-Ti oxides. Plagioclase crystals (1 mm max.) are subhedral, prismatic or stubby prismatic and show polysynthetic twinning and minor compositional zonation. Orthoclase crystals (0.75 mm max.) are subhedral, prismatic and show occasional twinning. Biotite crystals are fine grained (< 0.5 mm) and are brown-light brown pleochroic. Fe-Ti oxides (< 0.5 mm) consist of anhedral, equant titanomagnetite and ilmenite.

### Sedimentary lithics

Volcaniclastic siltstone (VSI), sandstone (VSA) and breccia (VBR) lithics are rare, but significant constituents of KCC ignimbrite populations. Sedimentary lithics are common especially in WES ignimbrites, but are rare in other ignimbrites.

Sedimentary fragments vary in colour, sorting, and induration, but typically contain volcanic detritus, including felsic and mafic crystals, pumice fragments, glass shards, and volcanic rock fragments (typically rhyolite and dacite lavas).

### Hydrothermally altered lithics

Hydrothermally altered lithic fragments are minor constituents in KCC ignimbrites. Altered lithics are volumetrically dominated by altered lavas and altered welded ignimbrites (Table 4.10). Hydrothermally altered lithics are important as they indicate that buried hydrothermal systems occur within the KCC (see Chapter 8). Most hydrothermally altered lithics are derived from discrete alteration zones and are not altered in situ with the host ignimbrite, although in situ alteration of lithics has occurred in the Slip Stream (T11/511633) and Kapowai River (T11/545643) valleys.

#### *Hydrothermally altered lavas*

Hydrothermally altered rhyolite, dacite and andesite lavas have been sampled from KCC ignimbrites. Altered lava compositions are differentiated by the abundance of relict phenocrysts, alteration mineralogy, and relict textures. Only sericitic and propylitic alteration varieties have been observed. Sericitic alteration is defined by the crystallisation of quartz, sericite, and pyrite. Propylitic alteration is defined by the crystallisation of calcite and chlorite.

Numerous sericitic (SRL) and propylitic (PRL) altered rhyolite lava lithics have been sampled from KCC ignimbrites. These lavas are difficult to correlate due to their alteration, but as with the uncorrelated unaltered rhyolite lavas, they infer the presence of buried rhyolite lavas in the volcanic pile at the KCC.

Table 4.9 Definition of welded tuff lithic types and occurrence in Kapowai Caldera Complex ignimbrites. Dash indicates occurrence of lithic type in ignimbrite. r = rich; p = poor; plag = plagioclase; qtz = quartz; opx = orthopyroxene; cpx = clinopyroxene; vitr = vitroclastic; v.p.a. = vapour phase altered.

| Type | Lithology | Crystal assemblage | Matrix | WES-1 | WES-4 | Oteao | Manuka | Trig Q | Webb Creek |
|---|---|---|---|---|---|---|---|---|---|
| RVT | light grey-brown pum r lith r rhyolitic | plag qtz opx cpx Fe-Ti oxides | fine ash v.p.a relict vitr | - | - | - | - | - | - |
| RCT | cream-brown pum r lith p rhyolitic | plag opx cpx Fe-Ti oxides | fine ash devit relict vitr | - | - | | - | | |
| RLT | grey-brown lith r cry p rhyolitic | plag opx cpx Fe-Ti oxides | fine ash devit relict vitr | - | | | | | |

Within altered rhyolite lavas, plagioclase phenocrysts are partially or totally altered to calcite, sericite or very fine grained quartz. Pyroxene phenocrysts are partially or totally altered to chlorite, quartz or sericite. Original textures are partially or totally destroyed by alteration, although the relative size and abundance of secondary crystals can indicate the likely original texture.

Silicified dacite lavas (SDL) occur in several KCC ignimbrites. In these lavas, plagioclase phenocrysts are partially or completely altered to calcite, sericite or quartz crystals, and pyroxene phenocrysts are partially or totally altered to quartz or sericite. Relict phenocryst assemblages (plagioclase-pyroxene-quartz) in some lithics suggest that some of these may represent Maumaupaki Formation lavas. As with rhyolite lavas, original textures are partially or completely destroyed, but are inferred on the basis of relative crystal size and crystal abundance.

Some andesite lava lithics exhibit silicified (SAL) alteration. Relict phenocryst assemblages (plagioclase-orthopyroxene-clinopyroxene) and fine grained porphyritic texture, suggest that some of these lavas may represent altered Taurahuehue Andesite. Plagioclase phenocrysts are completely or partially altered to calcite. Pyroxene phenocrysts are altered to chlorite or other clay minerals.

***Hydrothermally altered welded ignimbrites***

Silicified and propylitic altered welded ignimbrite lithics are a significant component in the lithic population of Webb Creek, Manuka, Trig Q and WES Ignimbrites (Table 4.11). There is a variation in the extent of alteration in both types, and this is indicated by the abundance of altered minerals and degree of depletion of the original texture.

Silicification is the most common alteration type and ranges from weak (WSI) to strong silicification (SSI). Plagioclase crystals are unaltered, or partially to totally altered to quartz or clay minerals. Pyroxene crystals are partially or totally altered to clay minerals or quartz. The original vitroclastic texture is progressively replaced by a mosaic of fine or very fine grained quartz crystals or sericite.

Propylitic alteration is divided into weak (WPI) and strong (SPI) alteration. Plagioclase crystals are altered to calcite and minor clay minerals (i.e. illite, kaolinite). Pyroxene crystals are altered initially to chlorite and then to clay minerals. Glass shards are typically recrystallised to sericite. Crystallisation of pyrite and pyrrhotite has occurred in some samples.

Table 4.10 Definition of hydrothermally altered lava lithic types and occurrence in Kapowai Caldera Complex ignimbrites. Dash indicates occurrence of lithic type in ignimbrite. plag = plagioclase; qtz = quartz; pyx = pyroxene; amph = amphibole; biot = biotite; calc = calcite; chlor = chlorite; pyr = pyrite; crist = cristobalite; zeol = zeolite; devit = devitrified; spheru = spherulitic; amyg = amygdaloidal.

| Lithology | | Phenocryst Assemblage | Groundmass Assemblage | Groundmass Texture | WES-1 | WES-4 | Oteao | Manuka |
|---|---|---|---|---|---|---|---|---|
| Rhyolite | SRL | plag | plag qtz Fe-Ti oxides | devit qtz mosaic | - | - | | - |
| | | plag relict pyx | plag qtz chlor Fe-Ti oxides | devit stockwork qtz chlor | - | | | |
| | | plag qtz relict pyx | plag qtz biot Fe-Ti oxides | spheru qtz mosaic | | - | | - |
| | | - | qtz Fe-Ti oxides | qtz mosaic | - | | | |
| | PRL | plag calc chlor | plag calc chlor Fe-Ti oxides | devit intersertal pilotaxitic amyg(qtz/crist) | | | | |
| | | plag chlor | plag qtz chlor Fe-Ti oxides | intersertal pilotaxitic devit amyg(qtz/calc) | | | | |
| | | calc | qtz calc Fe-Ti oxides | devit spheru qtz veinlets amyg(qtz/ Fe-Ti oxides) | | | | |
| Dacite | SDL | plag amph(chlor) pyr | plag chlor pyrit Fe-Ti oxides | intersertal | | | | - |
| | | plag opx Fe-Ti oxides | plag qtz biot Fe-Ti oxides | qtz mosaic | | - | | - |
| Andesite | SAL | relict plag | relict plag relict pyx Fe-Ti oxides | relict intersertal amyg(zeol/qtz) | - | - | | |
| | | plag opx relict cpx | plag pyx Fe-Ti oxides | relict intersertal pilotaxitic qtz veinlets | | | | - |
| | | plag opx cpx | plag pyx Fe-Ti oxides | intergranular | | | - | |

Table 4.11 Definition of hydrothermally altered pyroclastic lithic types and occurrence in Kapowai Caldera Complex ignimbrites. Dash indicates occurrence of lithic type in ignimbrite. plag = plagioclase; qtz = quartz; opx = orthopyroxene; cpx = clinopyroxene; calc = calcite; chlor = chlorite; seri = sericite; recryst = recrystallised.

| Lithology | | Crystal Assemblage | Matrix | WES-1 | WES-4 | Oteao | Manuka | Webb Creek |
|---|---|---|---|---|---|---|---|---|
| Ignimbrite | WSI | plag opx cpx qtz Fe-Ti oxides | relict vitroclastic with recryst qtz | - | - | - | - | - |
| | SSI | plag opx cpx qtz Fe-Ti oxides | mosaic of recryst qtz seri | - | | | | |
| | WPI | plag calc opx cpx Fe-Ti oxides | relict vitroclastic recryst calc chlor qtz | - | - | | | |
| | SPI | plag calc opx cpx chlor Fe-Ti oxides | recryst calc chlor qtz | - | | | | |
| Tuff | PVT | plag calc opx cpx chlor Fe-Ti oxides | relict vitroclastic with recryst calc chlor qtz | - | | | | |

***Hydrothermally altered tuff***

Minor propylitic altered vitric tuff (PVT) lithics were sampled from WES-1 Ignimbrites. Alteration is observed in the crystals and also in the matrix. Plagioclase crystals are typically partially or completely altered to calcite or sericite. Pyroxene crystals are commonly altered to chlorite. Glass shards and pumice fragments in the matrix are altered to tridymite, cristobalite, kaolinite, or sericite (determined by XRD analysis). The original texture is either partially or completely destroyed, so that only in some instances can the original texture be recognised.

## 4.4 Provenance of KCC lithic fragments

Most KCC lithic fragments represent vent-derived lithologies and hence provide direct evidence for the composition of the volcanic pile and sub-volcanic crust. In most instances this volcanic dominance reflects a sampling bias such that youngest ignimbrites (typically those best exposed) have been sequentially restricted to excavating lithic fragments from the pre-existing volcanic pile. The dominance of volcanic lithologies over basement or plutonic fragments, implies a significant thickness of the volcanic pile and a relatively high fragmentation level (cf. Krippner et al., 1998).

The variety of lithic fragment lithologies in KCC ignimbrites attests to considerable heterogeneity in the volcanic pile. Numerous rhyolitic lava dome and dome complexes are inferred to be buried due to the high abundance of rhyolite fragments and additional mineralogical types compared to surface lavas. Several buried intracaldera welded ignimbrites are inferred, also because of their high abundance and distinct lithologies compared with the exposed ignimbrites.

Importantly, volcanic lithic fragments also provide evidence for the earliest volcanism at the KCC. As there is a considerable difference in age between the oldest rhyolite lava and the oldest rhyolitic ignimbrite, it is likely that the oldest pyroclastic deposits erupted at the KCC are not presently exposed. Abundant welded ignimbrite and lava lithics imply significant burial of volcanic units, and some of these are likely to represent some of the oldest KCC volcanic eruptions.

A lack of basement lithics in KCC lithic populations is not surprising, given that Mesozoic basement rocks do not outcrop within the central or southern CVZ (Skinner, 1986). The depth to basement in central CVZ is unknown, although the minimum depth is greater than 1100 m (Trotter, 1995). The consistent lack of Mesozoic greywacke basement and Tertiary sedimentary lithics in KCC ignimbrites implies that they lie at a considerable depth below the volcanic pile. No drillholes have been drilled within the caldera to establish this depth, although adjacent groundwater boreholes have drilled to depths of 220 m and have only struck a sequence of thick ignimbrites (up to 200 m) occasionally overlying pre-caldera andesite (Adams, 1992). It is likely that at the KCC, the depth to basement is > 1 km, given the minimum depth of

1100m (Trotter, 1995) and intracaldera thickness of 200 - 400 m for some ignimbrites (e.g. WES Ignimbrites).

Although rare, plutonic lithic fragments (micro-granodiorites) sampled from WES Ignimbrites are significant lithologies. Two possible sources for these lithics are likely to be either the crystallised margins of the WES magma chamber (i.e. cognate fragments), or pre-caldera granitic crust (e.g. Brown et al., 1998a). No geochemical data has been obtained to constrain the provenance of these fragments.

The source of sedimentary lithics is likely to be intracaldera siltstones and sandstones (i.e. Wainora Formation) interbedded within the volcanic pile. It is difficult to establish which member of the Wainora Formation these lithics are derived from, and they may in fact represent other buried lacustrine sequences. Importantly, these sedimentary lithics imply major periods of relative quiescence at the KCC.

# Chapter Five

# WHAREPAPA ERUPTIVE SEQUENCE

## 5.1 Introduction

Wharepapa Eruptive Sequence (WES) represents the final caldera collapse episode at the KCC. Multiple, large volume explosive eruptions produced a thick intracaldera succession of welded ignimbrites, vitric and crystal tuffs, and localised lithic lag breccias. Exocaldera correlatives to WES are the most widespread onland CVZ pyroclastics known. Consequently, this sequence is not only important in the evolution of the KCC, but is significant as a major pyroclastic unit in the CVZ.

This chapter documents the vertical and lateral variation of intracaldera WES and describes its petrology and geochemistry. Constraints are placed on the source vents, eruptive behaviour, and emplacement mechanisms of the sequence using lithic componentry and interbedded tuff thickness variation. The timing and mechanism for caldera collapse is also discussed. Potential exocaldera correlatives including onland CVZ ignimbrites and distal tephras in onshore and offshore sedimentary successions are described, and their variation with intracaldera units discussed. Stratigraphic relations of the WES to other KCC units, and WES radiometric dates determined in this study, are discussed fully in Chapter 3.

## 5.2 Intracaldera WES

WES was previously mapped as a single ignimbrite unit defined within the Wharepapa Ignimbrite Formation (Skinner, 1993; 1995). Wharepapa Ignimbrite, as previously defined, also included all other KCC ignimbrites, vitric and crystal tuffs, and basal lacustrine siltstones. This research has recognised several lithologically and compositionally distinctive ignimbrites present within the KCC. Each ignimbrite defined is unique and distinctive from the Wharepapa Ignimbrite (Chapters 3 and 6). Wharepapa Ignimbrite itself consists of a sequence of fall and flow deposits of similar composition and necessitates inclusion within a larger pyroclastic flow and fall sequence, and the term Wharepapa Eruptive Sequence (WES) is proposed to incorporate all of these eruptions.

Intracaldera WES has been established by compiling several sections in the Rangihau, Kauaeranga and Kapowai valleys. The initial deposit is a weakly welded ignimbrite (WES-1) with interbedded vitric tuffs (WES-1a). This ignimbrite is overlain by thick vitric and crystal tuffs (WES-2). Locally in the Slip Stream valley, these tuffs are overlain by lithic lag breccia (WES-3). A second major weakly welded ignimbrite (WES-4) overlies the lithic lag breccia in the Slip Stream valley. At other intracaldera localities WES-4 is seen to directly overlie tuffs (WES-2).

The WES is the main intracaldera unit exposed at the KCC. Its main volume consists of WES-1 Ignimbrite and to a much lesser extent WES-4 Ignimbrite. Significant outcrops of these ignimbrites are found at many localities (Figure 5.1).

A

B

C

Figure 5.1 Intracaldera WES outcrops. A, 15-25m bluffs of case-hardened and weakly silicified WES-1 Ignimbrite exposed in the western Kapowai valley. View south from T11/531688. B, 25 m bluff of WES-1 Ignimbrite in the Kapowai Valley (T11/552676). C, 45 m bluff of WES-1 Ignimbrite exposed in the upper Kauaeranga valley. WES forms the ridgeline extending from the left to upper centre. Taurauikau Andesite forms the ridge on the skyline (southern margin of Table Mountain). View NW from T12/481569.

## Lithology

WES consists of a conformable sequence of several pyroclastic fall and flow deposits. The lithology and mineralogy of each pyroclastic type is broadly similar (Table 5.1).

### *WES-1 Ignimbrite*

WES-1 is a light grey-light brown, pumice and lithic-rich, weakly welded rhyolitic ignimbrite. Two juvenile types are present. Type 1 is a grey, poorly vesicular, incipiently fibrous, incipiently lenticular, subrounded weakly phyric pumice. Phenocrysts consist of plagioclase, minor orthopyroxene, minor clinopyroxene, and Fe-Ti oxides. Maximum juvenile (MJ) sizes range up to 60 mm and abundances range up to 10 %. Type 2 is a cream, incipiently vesicular, moderately fibrous, incipiently lenticular, aphyric pumice. Phenocrysts are rare and consist of plagioclase, orthopyroxene, minor clinopyroxene, and Fe-Ti oxides. MJ sizes are consistently smaller (35 mm max.) and are less abundant (7 % max.) than Type 1 pumice.

The matrix crystal population consists of plagioclase, orthopyroxene, clinopyroxene, with minor quartz, biotite, and amphibole, and Fe-Ti oxides. Lithic fragments consist of welded ignimbrite (Webb Creek Ignimbrite, Trig Q Ignimbrite, and Oteao Ignimbrite), rhyolite lavas, andesite lavas (Maumaupaki Formation and Taurahuehue Andesite), vitric and crystal tuffs, volcaniclastic siltstones (Wainora Formation) and granodiorite. The matrix is typically fine ash, incipiently to moderately devitrified, and has a well developed vitroclastic texture. Silicification of the matrix occurs at some localities (i.e. Rangihau Rd, T11/496680; Wharepapa Rd, T11/524677).

### *WES-1a vitric tuffs*

Ash-fine lapilli vitric tuffs occur interbedded near the base of WES-1 Ignimbrite. Tuffs are cream, moderately sorted, coarse ash-fine lapilli vitric tuffs. Two juvenile varieties are present. Type 1 is grey, poorly vesicular, incipiently fibrous, incipiently lenticular, subrounded weakly phyric pumice. Phenocrysts (<1 %) consist of plagioclase, orthopyroxene, minor clinopyroxene and Fe-Ti oxides. MJ sizes range up to 8 mm (3 mm average) and have an abundance up to 7 %. Type 2 is cream, incipiently vesicular, moderately fibrous, incipiently lenticular, aphyric pumice. Phenocrysts are rare (< 0.5 %) and consist of plagioclase, orthopyroxene, minor clinopyroxene and Fe-Ti oxides. MJ sizes are consistently smaller (5 mm max.) and less abundant than Type 1 pumice.

Tuffs are weakly indurated. The sequence typically has a massive structure, although mm-scale shower bedding is present within parts of the sequence.

*WES-2 crystal and vitric tuffs*

Vitric and minor crystal fine lapilli-ash tuffs overlie WES-1 Ignimbrite and are locally overlain by WES-3 lithic lag breccia, or more commonly by WES-4 Ignimbrite. Tuffs are cream-dark grey and show variable grain size from dominantly fine lapilli to minor ash.

The juvenile component consists of two types. Type 1 is a light grey, poorly vesicular, incipiently fibrous, incipiently lenticular, subrounded weakly phyric pumice. Phenocrysts (< 1 %) consist of plagioclase, orthopyroxene, minor clinopyroxene, and Fe-Ti oxides. MJ sizes range up to 25 mm (mean: 15mm) and have an abundance up to 10 % (mean 5 %). Type 2 is a cream, incipiently vesicular, moderately fibrous, incipiently lenticular, aphyric pumice. Phenocrysts are rare and consist of plagioclase, orthopyroxene, minor clinopyroxene, and Fe-Ti oxides. MJ sizes are consistently smaller (12 mm max.) and are less abundant than Type 1 pumice.

Matrix crystal abundance is highly variable in tuffs. Abundances of 3-15 % are common, but this can increase up to 40 % in crystal-rich laminae. Crystals are dominated by subhedral to anhedral plagioclase, and Fe-Ti oxides. Mafic minerals are rare and can include orthopyroxene and clinopyroxene.

Pumice fragments and lesser glass shards form the bulk of the tuff matrix. Glass shard morphologies are dominated by cuspate and platey forms and typically have thin to moderate wall thickness and are small to moderately sized (up to 125 μm).

*WES-3 lithic lag breccia*

Clast supported, fines depleted lithic lag breccia locally occurs between WES-2 and WES-4 on the eastern WES structural boundary in the Slip Stream valley. Lithic blocks (2300 mm max.) are dominated by plagioclase-pyroxene phyric rhyolite lava (group I rhyolite lava), with minor plagioclase-pyroxene phyric andesite lava (Taurahuehue Andesite) and welded ignimbrite (Trig Q Ignimbrite; WES-1 Ignimbrite). Lithics are consistently angular-subangular implying, along with their size, a vent provenance (Buesch, 1992). The matrix (15 %) consists of ash sized pumice fragments, crystals (plagioclase, pyroxene, Fe-Ti oxides), and glass shards.

*WES-4 Ignimbrite*

The final unit in the WES is a light grey, pumice and lithic-rich, weakly welded rhyolitic ignimbrite. Two juvenile types are present. Type 1 is a grey, poorly vesicular, incipiently fibrous, incipiently lenticular, subrounded, weakly phyric pumice. Phenocrysts consist of plagioclase, orthopyroxene, minor clinopyroxene, and Fe-Ti oxides. MJ sizes range up to 50 mm and have an abundance up to 10 %. Type 2 is a cream, incipiently vesicular, moderately fibrous, incipiently lenticular, aphyric pumice. Phenocrysts are rare and consist of plagioclase, orthopyroxene, minor clinopyroxene, and Fe-Ti oxides. MJ sizes are smaller (up to 30 mm) and are less abundant than Type 1 pumice.

Table 5.1 Lithological summary of intracaldera WES units. plag = plagioclase; opx = orthopyroxene; cpx = clinopyroxene; qtz = quartz; biot = biotite; amph = amphibole.

| Unit | Juvenile | Matrix Mineralogy | Lithic population | Matrix |
|---|---|---|---|---|
| **WES-1 Ignimbrite** | (I) grey, poorly vesicular, incipiently fibrous, incipiently lenticular, plag cpx opx phyric pumice<br><br>(II) cream , incipiently vesicular, moderately fibrous, incipiently lenticular, plag cpx opx phyric pumice | plag + opx + cpx ± qtz ± biot ± amph | Trig Q Ignimbrite, Webb Creek Ignimbrite , Kapowai Rhyolite group , Rangihau Rhyolite group, Maumaupaki Formation, Taurahuehue Andesite, volcaniclastic siltstone and sandstone, vitric and crystal tuff, granodiorite | fine ash vitroclastic |
| **WES-1a vitric tuff** | (II) grey , moderately vesicular, moderately fibrous, incipiently lenticular, plag cpx opx phyric pumice | plag + opx + cpx | Kapowai Rhyolite group lavas, Taurahuehue Andesite | fine ash vitroclastic |
| **WES-2 vitric & crystal tuffs** | (II) light grey , moderately vesicular, moderately fibrous, incipiently lenticular, plag phyric pumice<br><br>(II) cream , incipiently vesicular, moderately fibrous, incipiently lenticular, plag phyric pumice | plag ± opx ± cpx | Kapowai Rhyolite group lavas, Rangihau Rhyolite group lavas, Taurahuehue Andesite lavas, welded ignimbrite | fine ash vitroclastic with abundant pumice fragments |
| **WES-3 lithic lag breccia** | II) grey , moderately vesicular, moderately fibrous, incipiently lenticular, plag cpx opx phyric pumice | | Kapowai Rhyolite group lava, Trig Q Ignimbrite, WES-1 Ignimbrite, Maumaupaki Formation, Taurahuehue Andesite | |
| **WES-4 Ignimbrite** | (II) grey, moderately vesicular, incipiently fibrous, non lenticular plag opx cpx phyric pumice<br><br>(II) cream, incipiently vesicular, moderately fibrous, incipiently lenticular plag opx cpx phyric pumice | plag + opx ± cpx ± qtz ± amph | Trig Q Ignimbrite, Webb Creek Ignimbrite, WES-1 Ignimbrite, Kapowai Rhyolite group , Rangihau Rhyolite group, Taurahuehue Andesite, volcaniclastic siltstone, crystal and vitric tuff | coarse ash vitroclastic |

The matrix crystal population consists of plagioclase and orthopyroxene, with minor clinopyroxene, and rare quartz and amphibole, and Fe-Ti oxides. Lithic fragments consist of welded ignimbrite (Webb Creek Ignimbrite and Trig Q Ignimbrite), rhyolite lavas and andesite lavas (Maumaupaki Formation and Taurahuehue Andesite). The matrix is typically non devitrified coarse ash, non-devitrified and displays a well developed vitroclastic texture.

### Stratigraphic variation

The thickness, and componentry size and abundance of intracaldera WES units varies throughout the caldera floor. Intracaldera variations are described here between proximal (or near vent) and medial sections. Proximal sections are defined by the presence of lithic lag breccia (WES-3) and thick (> 3 m) crystal and vitric tuffs (WES-2). Medial sections are those lacking lag breccia unit and have thin (< 0.5 m) crystal and vitric tuffs.

The most well exposed proximal section of WES occurs on the eastern escarpment of the Slip Stream valley (Figure 5.2). About 50 m of thick WES-1 Ignimbrite occurs at the base of the section. No basal contact is exposed. WES-1 Ignimbrite is overlain by thick (3-3.5 m variable) vitric and crystal ash tuffs (WES-2). These in turn are overlain by a 1.5-2 m thick lithic lag breccia (WES-3), which is overlain by a second ignimbrite (WES-4). Contacts are conformable as no indicators of erosion or soil development have been observed between units.

Three key medial localities, where contacts are exposed between WES units, occur in the upper Kauaeranga valley and Rangihau valley (Figure 5.3). WES-2 vitric and crystal tuffs vary in thickness, but are significantly thinner than in proximal localities. WES-1 and WES-4 Ignimbrite have similar characteristics to proximal localities, although thin (0.5-1 m) lithic concentration zones are more prevalent.

Basal WES-1 Ignimbrite has a sharp, planar contact with volcaniclastic lacustrine siltstone exposed at several intracaldera localities (see chapter 3). No distinctive grading and fines depletion, or sedimentary structures (i.e. convolute, dish and pillar structures) indicative of a subaqueous depositional environment (Cas and Wright, 1991) are observed, suggesting that the siltstone was lithified and exposed prior to ignimbrite emplacement (cf. CP-2 Ignimbrite, Chapter 3). No other basal contacts with other units have been observed. WES-1 Ignimbrite thickness varies from 30-60 m in the Rangihau valley to ca. 300 m in the Kapowai valley, and is the most common WES unit occurring in all KCC catchments.

Interbedded vitric tuffs (WES 1a) have a sharp basal and upper contact within WES-1 Ignimbrite (Figure 5.4). Limited exposures occur on the escarpment in the Haukawakawa Valley (T11/485642), lower Kapowai valley (T11/543687) and upper Kauaeranga Valley (T12/488583). Thickness varies from ca. 2 m in the Haukawakawa valley, to ca. 0.5 m in the lower Kapowai and upper Kauaeranga valleys. Tuffs

exposed in the lower Kapowai and upper Kauaeranga valley show evidence of post-emplacement deformation. In the lower Kapowai valley, tuffs exposed are tilted ca. 20° to the east, and in the upper Kauaeranga valley, tuffs appear to have been folded and tilted following deposition.

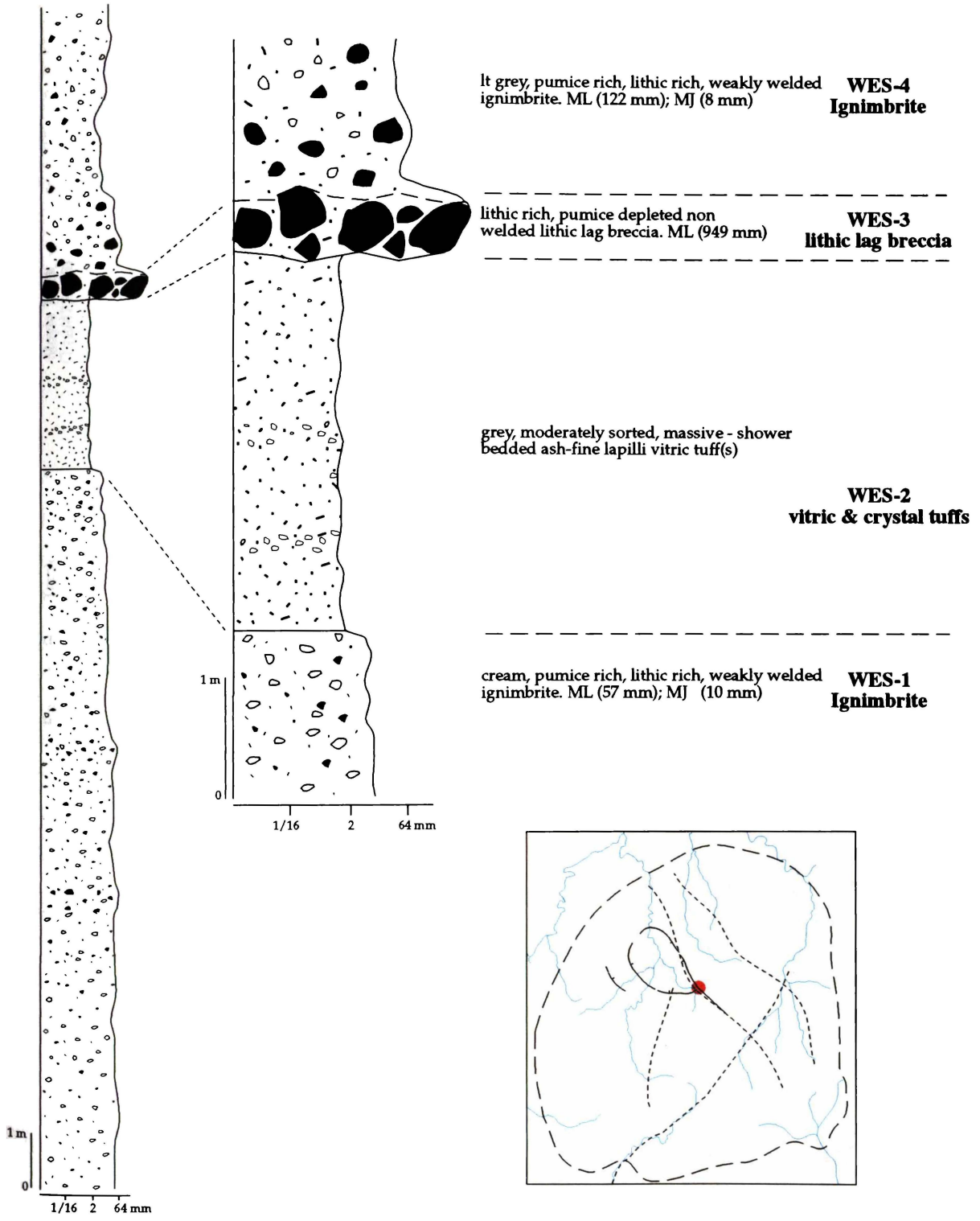


Figure 5.2 Proximal WES section exposed on the eastern escarpment of the Slip Stream valley (T11/511643). Inset shows location of section within the Kapowai Caldera Complex.

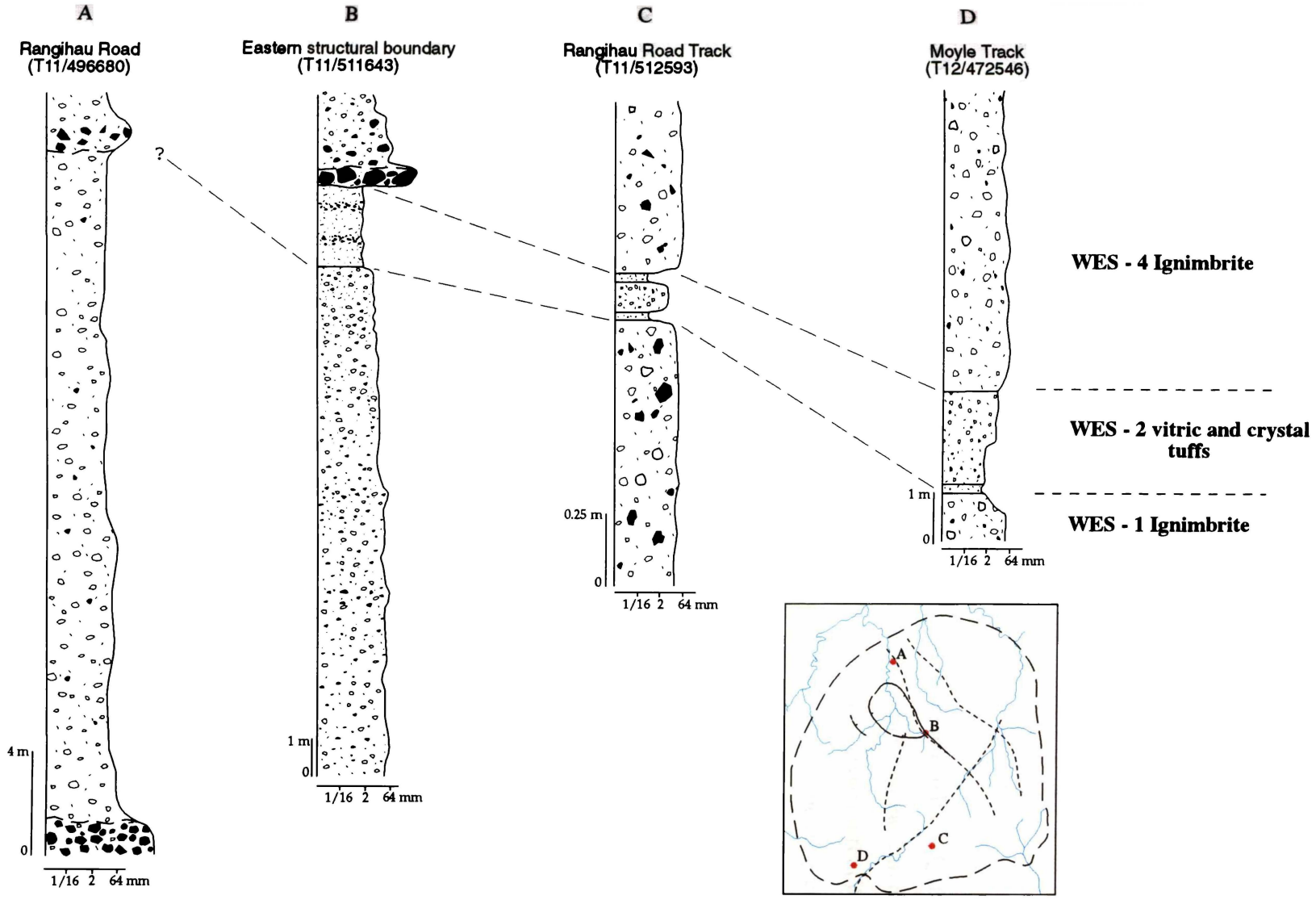


Figure 5.3 Stratigraphic variation in intracaldera WES. Sections represent medial localities (see inset) apart from the eastern structural boundary section. Dashed line indicates correlation of WES-2 vitric and crystal tuff.

WES-2 vitric and crystal tuffs overlie WES-1 Ignimbrite at several intracaldera localities. Along the Pinnacles-Rangihau Rd track (T12/512593), a thin (< 0.3 m) vitric tuff sequence occurs interbedded between WES-1 and WES-4 Ignimbrites. The tuff sequence consists of a central ca. 0.25 m bed of coarse ash vitric tuff with occasional pumice lapilli, and thinner (< 0.05 m) ash sized vitric tuffs above and below the middle tuff.

On Moyles Ridge (T12/472576) a ca. 1 m vitric tuff sequence is exposed. This consists of basal fine ash sized vitric tuff (0.1 m) and overlying coarse ash-fine lapilli vitric tuff (0.8 m). The contact between tuff beds is sharp and planar. On the eastern escarpment in the Slip Stream valley (T/11511643), a ca. 3 m thick vitric tuff is present, which has a sharp planar contact with underlying WES-1 Ignimbrite and overlying lithic lag breccia (WES-3).

Localised lithic lag breccia (WES-3) outcrops between WES-2 tuffs and WES-4 Ignimbrite on the escarpment in the eastern Rangihau valley. Breccia has a maximum thickness of ca. 2 m at T11/511643. Lag breccia has a sharp, irregular basal contact with underlying vitric and crystal tuffs (WES-2), but an irregular and gradational contact with overlying ignimbrite (WES-4). The restricted occurrence of the lithic lag breccias to the eastern escarpment, its fines depleted nature, and large clast size implies a vent source near this locality (cf. Wright and Walker, 1977; Walker; 1985).

WES-4 Ignimbrite outcrops sporadically in the KCC. As it has a similar appearance to WES-1 Ignimbrite, it is differentiated, where possible, on the basis of field relations with underlying WES units or based on relative elevation differences between WES-1 and WES-4 Ignimbrite. WES-4 Ignimbrite thickness varies from a few metres in the upper Kauaeranga valley to ca. 50 m in the plateau adjacent to the Slip Stream valley, and perhaps 80 m in parts of the Kapowai valley. No units are observed to overlie WES-4 Ignimbrite.

## Componentry

The componentry of all WES units is consistent in both fall and flow deposits. Limited geochemical (Table 5.2) and mineralogical (Table 5.3, 5.4, 5.5) data has been obtained for these components.

### *Juvenile*

Juvenile fragments consist of two types. Type 1 is grey, poorly vesicular, incipiently fibrous, incipiently lenticular, subrounded weakly phyric pumice. Phenocrysts consist of plagioclase ($An_{32-39}$), orthopyroxene, minor clinopyroxene and Fe-Ti oxides. MJ sizes range up to 60 mm and have an abundance up to 10 %. Type 2 is cream, incipiently vesicular, moderately fibrous, incipiently lenticular, aphyric pumice. Phenocrysts are rare and consist of plagioclase, orthopyroxene, minor clinopyroxene, and Fe-Ti oxides. MJ sizes are consistently smaller (up to 35 mm) and are less abundant than Type 1 pumice.

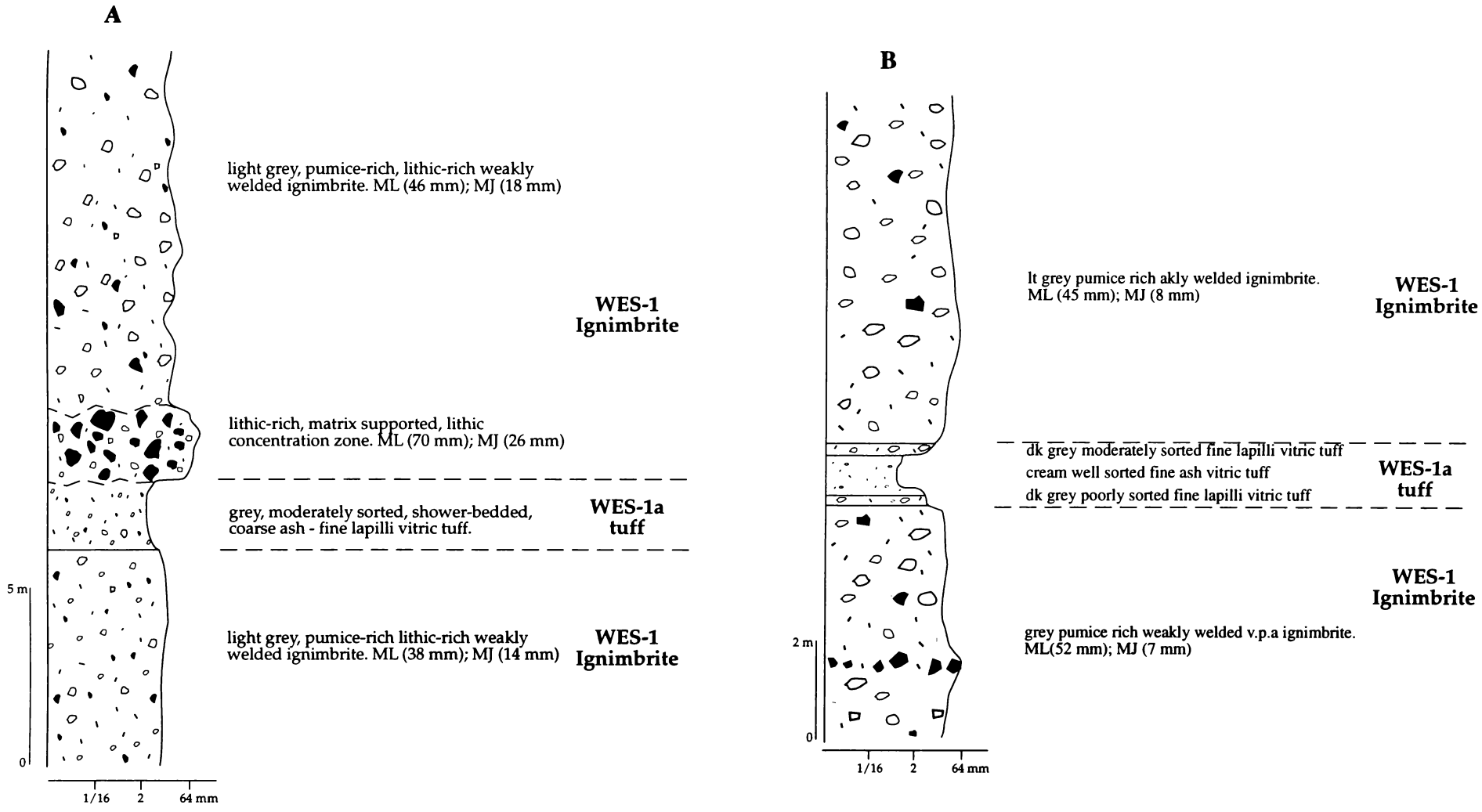


Figure 5.4 Interbedded WES-1a vitric tuffs in the: A, Haukawakawa Stream valley (T11/485642); and B, upper Kauaeranga River valley (T12/488583).

These two juvenile types define the magma composition, and their phenocryst assemblage defines the magma mineralogy (Lipman, 1967). Several XRF analyses of pumice clasts from WES ignimbrite have been obtained and although clasts appeared fresh in hand specimen, high LOI (7.8-9.5 wt.%) and $Al_2O_3$ (20.2-21.7 wt. %) values indicate that clasts have suffered from incipient weathering.

To augment pumice analyses, lithic-poor whole rock ignimbrite samples were then selected for XRF analysis. Any lithic fragments in the samples were removed during sample preparation. Glass shards have also been analysed from WES-1 and WES-4 Ignimbrites as a further means of establishing major element composition (Table 5.8).

Excluding pumice analyses with high LOI and wt. % $Al_2O_3$ values and taking the mean glass shard analysis, geochemical analyses indicate a calc-alkaline rhyolitic composition of ca. 72-77 wt. % $SiO_2$ (Figure 5.5). WES composition does not vary significantly from early erupted units to those erupted late in the sequence. However, the range in juvenile chemistry together with the two juvenile types suggests that the WES magma reservoir was compositionally zoned.

WES magmatic mineralogy is defined as plagioclase, orthopyroxene, with minor clinopyroxene, and Fe-Ti oxides. Juvenile clast mineralogy better defines magmatic mineralogy than the matrix assemblage because (i) crystals are typically concentrated in the matrix, as fine vitric grains are elutriated during transport; (ii) phenocrysts are mixed from different parts of magma chamber; and (iii) lithic fragments may supply crystals to the matrix.

Table 5.2 Whole rock and individual pumice clast major element (normalised to 100 %, volatile free) and trace element XRF analyses of WES-1 and WES-4 Ignimbrites. + total Fe as $Fe_2O_3$; *original totals.

| Sample | W99886 | W99614 | W99614 | W99922 | W99633 | W99952 | W99850 | W99973 | W99939 |
|---|---|---|---|---|---|---|---|---|---|
| Unit | WES-1 | WES-1 | WES-1 | WES-4 | WES-4 | WES-1 | WES-1 | WES-1 | WES-1 |
| Analysis | type 1 pumice | type 2 pumice | type 1 pumice | whole rock | whole rock | whole rock | whole rock | whole rock | whole rock |
| | wt.% | wt.% | wt.% | wt.% | wt.% | wt.% | wt.% | wt.% | wt.% |
| $SiO_2$ | 72.75 | 65.41 | 65.88 | 75.39 | 72.73 | 68.15 | 72.50 | 71.59 | 71.83 |
| $TiO_2$ | 0.38 | 1.01 | 1.02 | 0.34 | 0.55 | 0.63 | 0.53 | 0.49 | 0.47 |
| $Al2O_3$ | 15.05 | 20.21 | 21.67 | 13.98 | 16.45 | 18.02 | 16.26 | 16.46 | 15.14 |
| $Fe_2O_3$+ | 2.88 | 6.36 | 6.57 | 2.20 | 3.90 | 4.92 | 3.70 | 3.60 | 3.81 |
| MnO | 0.69 | 0.10 | 0.15 | 0.07 | 0.05 | 0.09 | 0.05 | 0.06 | 0.07 |
| MgO | 0.76 | 0.99 | 0.89 | 0.21 | 0.42 | 1.49 | 0.33 | 0.77 | 0.91 |
| CaO | 1.76 | 2.46 | 1.70 | 1.35 | 1.38 | 2.17 | 1.61 | 1.91 | 2.26 |
| Na2O | 2.88 | 1.85 | 1.12 | 2.92 | 1.87 | 2.21 | 1.96 | 2.62 | 2.62 |
| $K_2O$ | 2.80 | 1.48 | 0.90 | 3.50 | 2.61 | 2.24 | 3.02 | 2.46 | 2.81 |
| $P_2O_5$ | 0.04 | 0.14 | 0.10 | 0.03 | 0.03 | 0.09 | 0.03 | 0.03 | 0.07 |
| LOI * | 5.21 | 7.75 | 9.48 | 4.78 | 6.75 | 6.28 | 6.21 | 6.51 | 5.77 |
| Total * | 99.88 | 100.25 | 99.83 | 100.08 | 100.09 | 100.22 | 100.23 | 100.32 | 99.97 |
| Ba | 1426 | 656 | 438 | 688 | 606 | 1830 | 674 | 1186 | 2106 |
| Rb | 80 | 91 | 55 | 82 | 89 | 84 | 91 | 71 | 88 |
| Sr | 140 | 414 | 116 | 96 | 111 | 262 | 227 | 175 | 200 |
| Y | 94 | 18 | 38 | 45 | 38 | 32 | 48 | 35 | 46 |
| Zr | 244 | 228 | 171 | 272 | 218 | 186 | 235 | 248 | 225 |
| Nb | 5 | 4 | 6 | 8 | 7 | 6 | 7 | 8 | 7 |
| Th | 7 | 4 | 4 | 8 | 6 | 5 | 6 | 7 | 6 |
| Pb | 1 | 1 | 1 | 13 | 1 | 1 | 1 | 4 | 1 |
| Ga | 16 | 14 | 19 | 14 | 16 | 16 | 15 | 15 | 15 |
| Zn | 118 | 61 | 68 | 58 | 58 | 62 | 64 | 59 | 61 |
| Ni | 6 | 4 | 7 | 3 | 4 | 6 | 4 | 3 | 3 |
| V | 33 | 25 | 87 | 9 | 35 | 57 | 29 | 23 | 38 |
| Cr | 3 | 3 | 6 | 3 | 27 | 11 | 8 | 7 | 5 |
| La | 48 | 9 | 21 | 20 | 20 | 23 | 35 | 18 | 31 |
| Ce | 99 | 30 | 49 | 57 | 40 | 51 | 74 | 49 | 66 |
| Nd | 61 | 10 | 24 | 36 | 20 | 11 | 37 | 15 | 29 |
| K/Rb | 290 | 135 | 135 | 355 | 244 | 221 | 276 | 288 | 265 |
| Rb/Sr | 0.57 | 0.22 | 0.47 | 0.85 | 0.80 | 0.32 | 0.40 | 0.41 | 0.44 |

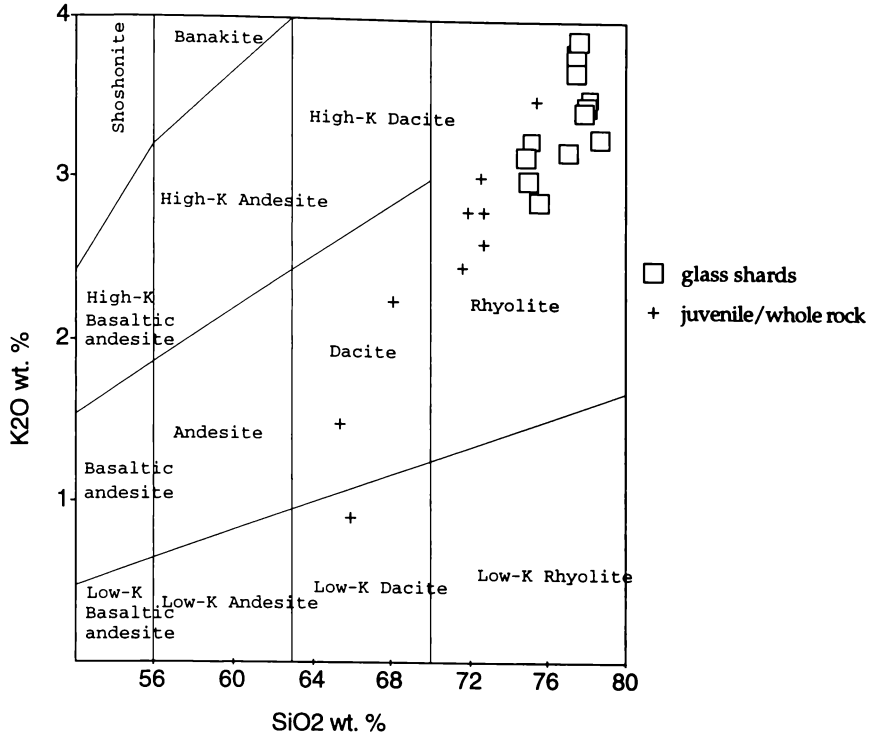


Figure 5.5 $K_2O$ vs $SiO_2$ plot of electron microprobe WES glass shard and XRF juvenile and whole rock analyses. Classification fields from Le Maitre (1989).

### *Matrix Crystals*

The matrix crystal assemblage in WES units consists of plagioclase ($An_{35-46}$), orthopyroxene ($En_{54}$), and clinopyroxene, with minor quartz, biotite, and amphibole, and Fe-Ti oxides (titanomagnetite and ilmenite). The variation in plagioclase compositions (Figure 5.6) reflects both magmatic (andesine) compositions and accidental plagioclase crystals (labradorite) probably derived from andesitic-dacitic lava or pyroclastic lithic fragments. Quartz, biotite and amphibole crystals are rare constituents and are not present in all samples. When present, they occur as discrete, fine grained (< 0.1 mm) crystals, and this suggests that they are accidental crystals scavenged from the substrate, or from comminuted lithic fragments.

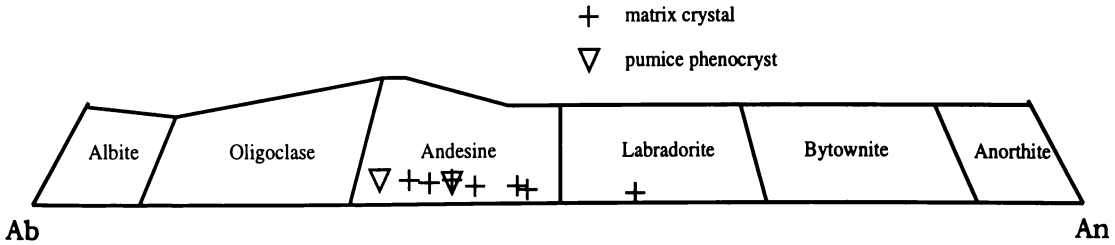


Figure 5.6 Variation in feldspar composition of pumice phenocrysts and matrix crystals in WES ignimbrites.

### *Lithics*

The lithic population in WES-1 and WES-4 Ignimbrites are very similar. Both populations are characterised by abundant welded ignimbrite (Webb Creek Ignimbrite, Trig Q Ignimbrite, and possibly Oteao Ignimbrite), rhyolite lavas (rhyolite lava group I and III only), and andesite lavas (Maumaupaki Formation and Taurahuehue Andesite). Volcaniclastic siltstone and sandstone fragments (Wainora Formation) occur in both but are most common in WES-1 Ignimbrite.

Table 5.3 Feldspar phenocryst and crystal compositions in WES-1 and WES-4 Ignimbrites.

| Sample | W99923 | W99923 | W99923 | W99923 | W99928 | W99928 | W99928 | W99614 | W99614 | W99614 |
|---|---|---|---|---|---|---|---|---|---|---|
| Analysis | matrix crystal | matrix crystal | matrix crystal | matrix crystal | matrix crystal | matrix crystal | matrix crystal | matrix crystal | pumice phenocryst | pumice phenocryst |
| Ignimbrite | WES-4 | WES-4 | WES-4 | WES-4 | WES-1 | WES-1 | WES-1 | WES-1 | WES-1 | WES-1 |
| | wt% | wt% | wt% | wt% | wt% | wt% | wt% | wt% | wt% | wt% |
| SiO2 | 58.75 | 54.50 | 58.96 | 70.19 | 57.73 | 55.01 | 58.11 | 58.24 | 58.11 | 60.20 |
| TiO2 | 0.20 | 0.24 | 0.26 | 1.42 | 0.18 | 0.12 | 0.07 | 0.11 | 0.12 | 0.19 |
| Al2O3 | 25.57 | 28.44 | 26.51 | 13.34 | 25.90 | 27.02 | 25.20 | 25.95 | 25.99 | 24.80 |
| FeO | 0.37 | 0.55 | 0.39 | 4.76 | 0.42 | 0.51 | 0.38 | 0.27 | 0.36 | 0.45 |
| MnO | 0.04 | 0.06 | 0.04 | 0.04 | 0.00 | 0.04 | 0.00 | 0.02 | 0.10 | 0.03 |
| MgO | 0.01 | 0.03 | 0.03 | 0.10 | 0.02 | 0.09 | 0.05 | 0.02 | 0.04 | 0.04 |
| CaO | 7.69 | 11.49 | 9.12 | 1.46 | 8.41 | 9.46 | 7.13 | 7.72 | 7.99 | 6.50 |
| Na2O | 7.07 | 4.73 | 5.92 | 3.62 | 6.45 | 5.92 | 7.16 | 6.50 | 6.69 | 7.43 |
| K2O | 0.34 | 0.15 | 0.31 | 2.88 | 0.30 | 0.25 | 0.40 | 0.41 | 0.33 | 0.39 |
| TOTAL | 100.02 | 100.19 | 101.52 | 97.81 | 99.39 | 98.42 | 98.49 | 99.25 | 99.73 | 100.02 |
| | | | | | | | | | | |
| Ab | 61.30 | 42.30 | 53.00 | 57.30 | 57.10 | 52.30 | 63.00 | 58.90 | 59.10 | 65.90 |
| An | 36.80 | 56.80 | 45.20 | 12.80 | 41.10 | 46.20 | 34.70 | 38.70 | 39.00 | 31.80 |
| Or | 1.90 | 0.90 | 1.80 | 29.90 | 1.80 | 1.50 | 2.30 | 2.40 | 1.90 | 2.30 |

Table 5.4 Orthopyroxene phenocryst and crystal compositions in WES-1 Ignimbrite.

| Sample | W99614 | W99614 |
|---|---|---|
| Analysis | matrix crystal | pumice phenocryst |
| Ignimbrite | WES-1 | WES-1 |
| | wt % | wt % |
| SiO2 | 51.36 | 52.09 |
| TiO2 | 0.21 | 0.57 |
| Al2O3 | 0.48 | 0.54 |
| FeO | 26.99 | 26.73 |
| MnO | 1.50 | 1.58 |
| MgO | 19.91 | 20.27 |
| CaO | 1.31 | 1.27 |
| Na2O | 0.05 | 0.12 |
| K2O | 0.24 | 0.10 |
| Cl | 0.06 | 0.07 |
| Cr2O3 | 0.05 | 0.03 |
| NiO | 0.05 | 0.00 |
| TOTAL | 102.21 | 103.36 |
| | | |
| Wo | 2.55 | 2.46 |
| En | 54.03 | 54.68 |
| Fs | 43.42 | 42.86 |

Table 5.5 Ilmenite compositions in WES-1 Ignimbrite.

| Sample | W99614 | W99614 | W99614 |
|---|---|---|---|
| Analysis | pumice phenocryst | pumice phenocryst | pumice phenocryst |
| Ignimbrite | WES-1 | WES-1 | WES-1 |
| | wt% | wt% | wt% |
| SiO2 | 0.21 | 0.20 | 1.25 |
| TiO2 | 46.30 | 45.88 | 39.33 |
| Al2O3 | 0.27 | 0.51 | 4.87 |
| FeO | 48.78 | 49.32 | 44.06 |
| MnO | 1.15 | 1.25 | 0.91 |
| MgO | 2.00 | 1.75 | 1.43 |
| CaO | 0.14 | 0.18 | 0.15 |
| Na2O | 0.01 | 0.11 | 0.21 |
| K2O | 0.32 | 0.14 | 0.15 |
| Cl | 0.05 | 0.08 | 0.11 |
| Cr2O3 | 0.00 | 0.01 | 0.05 |
| NiO | 0.03 | 0.09 | 0.00 |
| | | | |
| TOTAL | 99.24 | 99.51 | 92.52 |

Lithic fragments in WES fall deposits (i.e. WES-1a, WES-2) are much less abundant (< 1 %) and smaller (ash-very fine lapilli) compared with lithics in WES ignimbrites. Lithic fragments consist of several varieties and are dominated by group I rhyolite lavas, with minor volcaniclastic siltstone and welded ignimbrite fragments.

***Matrix***

The matrix texture in WES ignimbrites is consistently vitroclastic consisting of thick walled cuspate and platy glass shards, and small (< 0.2 mm) pumice fragments (Figure 5.7). Significantly there is a marked difference in glass shard size between WES-1 and WES-4 Ignimbrites. WES-4 typically contains larger and thicker glass shards than WES-1 Ignimbrite. Glass shards in WES-1 Ignimbrite are also more commonly devitrified, and the matrix typically vapour phase altered compared to WES-4 Ignimbrite.

Glass shards in WES fall deposits tend to be finer grained than in WES ignimbrite. Shards vary from non-devitrified to moderately devitrified, and have thin to moderate wall thickness. Cuspate and platey shard forms are common.

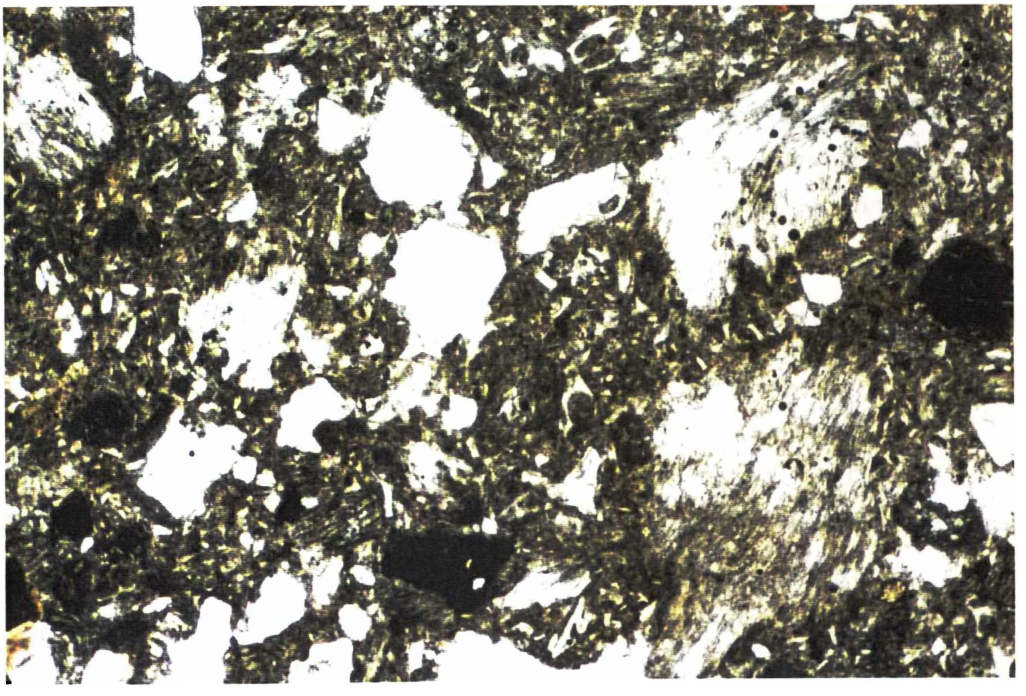

Figure 5.7 Photomicrographs of pumice rich WES-1 Ignimbrite with well defined vitroclastic texture (W99614). Field of view is 4mm across.

Juvenile, lithic, and matrix crystal abundances of WES ignimbrites and fall units varies throughout the KCC. Representative componentry abundances are presented in Table 5.6.

Table 5.6 Modal componentry of selected WES units.

| Unit | WES-1 Ignimbrite | | | WES-2 vitric & crystal tuffs | | | WES-4 Ignimbrite | | |
|---|---|---|---|---|---|---|---|---|---|
| Sample | W99614 | W99928 | W99856 | W99854 | W99677 | W99927 | W99678 | W99923 | W99922 |
| **Juvenile** | **34.3** | **16.3** | **30.0** | **26.6** | **4.3** | **3.6** | **14.6** | **22.6** | **3.0** |
| **Matrix Crystal** | | | | | | | | | |
| Plagioclase | 4.0 | 3.3 | 3.0 | 8.3 | 1.3 | 4.6 | 14.3 | 3.6 | 5.0 |
| Orthopyroxene | 1.0 | 0.1 | | 0.2 | | 0.2 | 1.0 | 0.1 | 0.1 |
| Clinopyroxene | | | | | | | 0.3 | 0.2 | |
| Amphibole | | | | | | | | | |
| Biotite | | | | | | | | | |
| Fe-Ti oxides(>0.05mm) | | | | 0.3 | 0.1 | | 0.3 | 0.6 | 0.3 |
| **Total Crystal** | **5.0** | **3.4** | **3.0** | **8.6** | **1.3** | **4.6** | **15.9** | **4.2** | **5.3** |
| **Lithic** | | | | | | | | | |
| Volcanic | 13.6 | 13.0 | | 3.0 | | 0.6 | 1.3 | 6.3 | 7.3 |
| Sedimentary | | | | | | | | | |
| **Matrix** | | | | | | | | | |
| Glass shard | 41.0 | 62.3 | 65.2 | 61.0 | 90.3 | 87.6 | 65.2 | 61.6 | 83.0 |
| Pumice fragment | 6.1 | 5.0 | 1.8 | 0.6 | 4.0 | 3.4 | 3.0 | 5.0 | 1.3 |
| **TOTAL** | **100.0** | **100.0** | **100.0** | **100.0** | **100.0** | **100.0** | **100.0** | **100.0** | **100.0** |

## Post-depositional modification

Following deposition several processes have occurred which have modified the lithology or structure of WES units. Processes include welding and vapour phase alteration of pyroclastic flow deposits, and deformation of the entire sequence.

### *Welding*

WES-1 and WES-4 Ignimbrites typically display little variation in welding. Both are weakly welded as they contain non to incipiently lenticular pumice clasts, exhibit no flattening of matrix glass shards, and there is a consistent lack of columnar cooling joints within outcrops. WES-1 and WES-4 Ignimbrite has an average density of 1.35 g $cm^{-3}$, consistent with a weak welding definition (cf. Briggs, 1976; Streck and Grunder, 1995). WES-2 vitric and crystal tuffs are non welded, but weakly indurated, and WES-3 lithic lag breccia is non-welded.

### *Vapour phase alteration*

Post-depositional vapour phase alteration of ignimbrites is a common process whereby the magmatic component (i.e. juvenile and glass shards), is pervasively altered to feldspar, tridymite, cristobalite, and zeolites by volatile phases passing upward through the cooling deposit (Briggs, 1976). The majority of WES ignimbrite and tuff outcrops are not vapour phase altered.

WES-1 Ignimbrite exhibits minor vapour phase alteration in the Rangihau valley (T11/496680). Tridymite, cristobalite, and zeolite record vapour phase crystallisation in pumice vesicles, and the original vitroclastic matrix is replaced with irregular, very fine grained cristobalite and K-feldspar (Figure 5.8). The overall colour of the ignimbrite appears buff or light pink, rather than light grey or cream observed for unaltered WES ignimbrites.

***Hydrothermal alteration***

Significant hydrothermal alteration of intracaldera WES units is not observed. All hydrothermally altered ignimbrites in the KCC pre-date the WES (see Chapter 8). Minor silicification of WES-1 Ignimbrite occurs in the lower Kapowai valley. WES-1 Ignimbrite glass shards are incipiently altered to very fine quartz crystals and the overall colour is whiter compared to non-silicified ignimbrite. Silicification has produced a series of 15-25 m high bluffs which have a fluted appearance (Figure 5.1a).

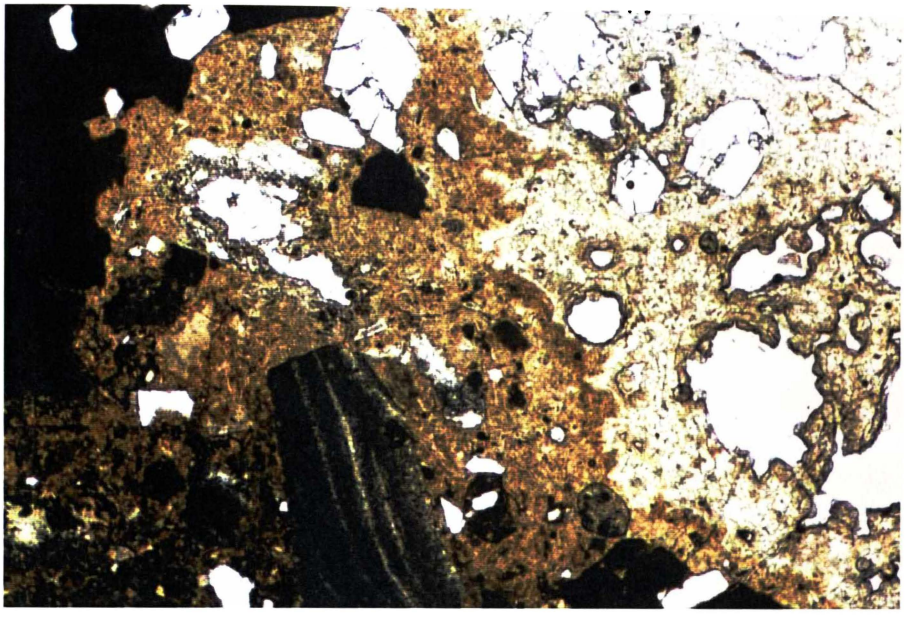

**Figure 5.8** Vapour phase altered WES-1 Ignimbrite with relict vitroclastic texture consisting of very fine cristobalite and K-feldspar (W99602). Pumice vesicles are infilled with tridymite, cristobalite and zeolite minerals. Field of view is 4mm across.

***Deformation***

Deformation of the WES is recognised on moderate to large intracaldera scales. Moderate scale fracturing and displacement of the sequence is implied by a clastic dike section in the lower Kapowai valley. Large scale tilting and uplift of WES blocks are observed at several localities within the KCC. These features together infer post-eruption deformation, although the exact timing is difficult to establish because of the discontinuous exposure of WES, and that post-WES units do not occur.

## Clastic dikes

In the lower Kapowai valley a section of clastic dikes intruding WES-1 Ignimbrite are exposed (Figure 5.9). This platform extends for 50 m along the bed of the Kapowai River and consists of at least 14 clastic dikes. Dikes are infilled with primary pyroclastic fall material including pumice, accretionary lapilli, lithic fragments, and crystals. Grains vary from ash to lapilli and lateral grading occurs in some thick dikes. Dike thickness varies from 8 to 450 mm, and dike length varies from 10 to 20 m across the exposed platform (Figure 5.10).

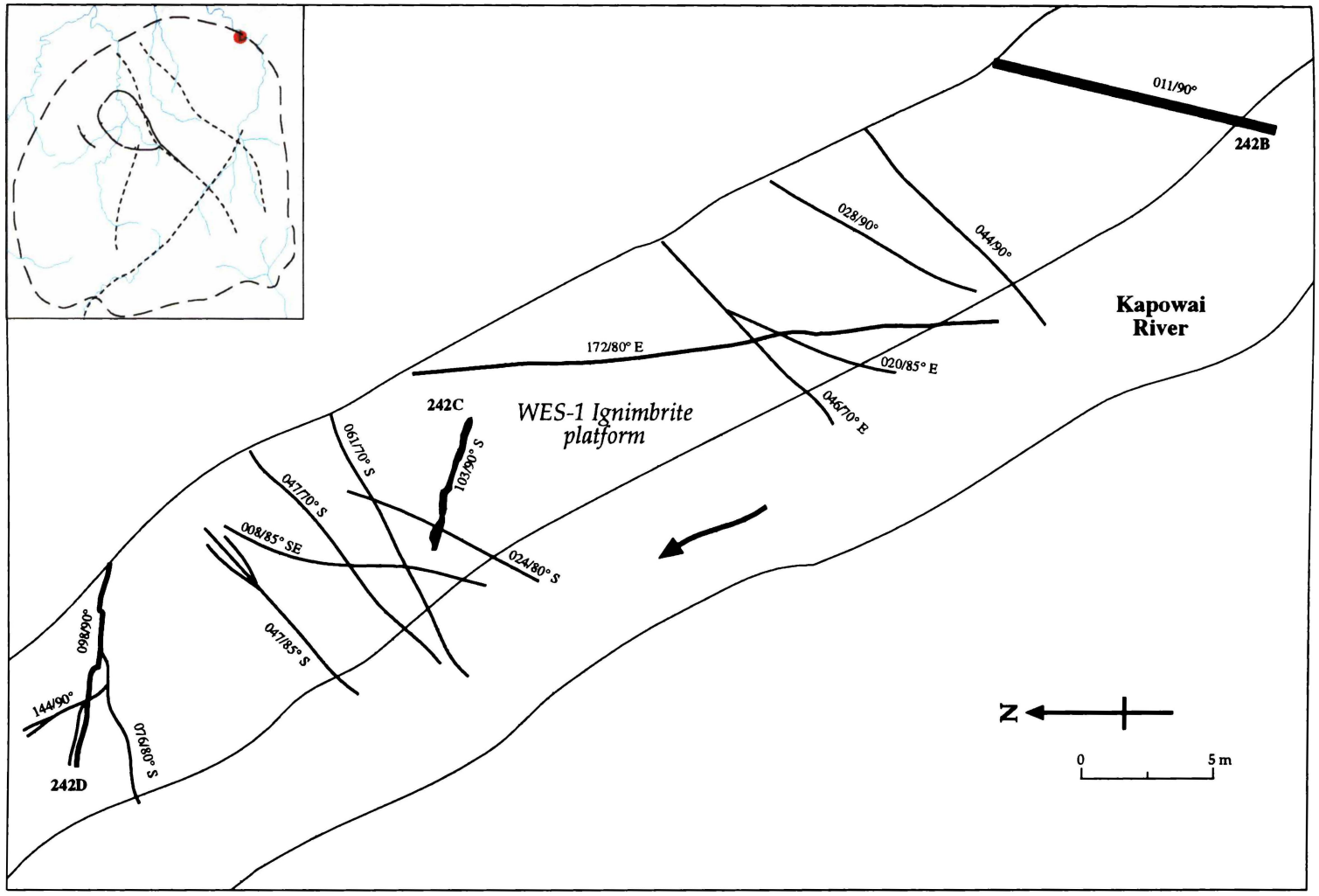


Figure 5.9 Map of clastic dikes within WES-1 Ignimbrite, lower Kapowai valley (T11/551679; see inset). Relative dike thickness indicated by line thickness. Inset shows location in the Kapowai Caldera Complex.

A B

**Figure 5.10 Clastic dikes deforming WES-1 Ignimbrite in the Kapowai valley (T11/551679). A, 40-45 cm wide cream, pumice-rich, lithic-poor, lapilli - ash clastic dike. B, 25-30 cm cream, pumice-rich faulted ash clastic dike. Hammer is 30 cm long.**

Dike orientations are dominated by NE-SW strikes (044-061), with NNE-SSW striking (008-024) clastic dikes the next most common trends (Figure 5.11). These two major clastic dike trends are similar to the regional structural pattern in central CVZ, which is dominated by NE and N-trending faults. Other minor dike trends vary significantly from E-W through to N-S. Dikes are typically inclined vertical or near vertical (70-85° dip), implying vertical fracturing through the ignimbrite, but the extent is unknown.

The relative timing of dike emplacement is difficult to establish for the entire exposed section. However, a multiple dike section in the northernmost part of the section provides some constraints on the relative timing of two dike trends (Figure 5.12b). Here, the major E-W striking dike is variably displaced (5-40 mm) by a series of offset NW striking faults. This would imply that E-trending dikes pre-date NW dikes, and that there was NW-SE displacement of part of the exposed section.

The presence of primary pyroclastic fall material (e.g. accretionary lapilli), suggests that the origin of the dikes is likely related to syn-eruptive fracturing and infilling from above (e.g. Keating and Valentine, 1988). Most dikes are massive and fine ash sized, although some dikes that exhibit grading from fine ash to lapilli possibly indicate that several pyroclastic fall phases occurred during deposition. Within graded dikes, early fall phases deposited ash sized material, but this changed to coarser (lapilli) grains in later

phases. Only significant extension (ca. 30-35 cm) of some dikes allowed the coarser material to be preserved.

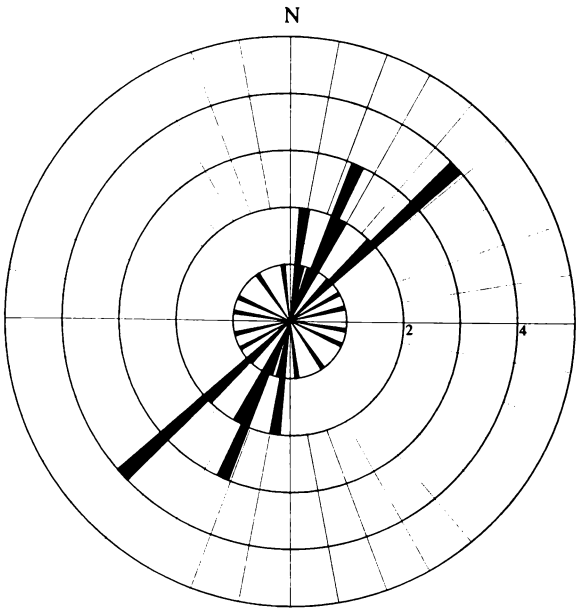


Figure 5.11. Rose diagram of clastic dikes within WES-1 Ignimbrite, lower Kapowai valley (T11/551679).

This is a similar origin proposed for clastic dikes observed at other localities in the CVZ (e.g. Bardebes, 1997). A Neptunian-dike model, where infilling dike material is derived from lithologies immediately below the ignimbrite, is not favoured because the infilling material is primary pyroclastic fall material, and that volcaniclastic siltstone is likely to underlie WES-1 Ignimbrite at this locality.

## Faulting and Tilting

Faulting and tilting of the WES sequence has occurred throughout the KCC. Tilting has been induced locally by caldera subsidence, intrusion of rhyolite lava domes or by faulting. On the eastern margin of the WES collapse zone (between Slip and Oteao Streams), the WES plateau has been tilted up to 10° towards the NNE. Tilting reflects normal faulting and block rotation of the footwall block probably during caldera subsidence. Approximately 20 m displacement of WES-1 Ignimbrite also occurs along a normal fault (Haukawakawa Fault) in the Haukawakawa valley, but tilting of the footwall at this location is unclear.

In the upper Kauaeranga valley (T/12489583), Kauaeranga Rhyolite dome intrudes the WES. Near the contact, WES-1 Ignimbrite is inclined by up to 20°. Displacement along the Kapowai Fault through the Kapowai and Kauaeranga valleys does not appear to have offset the WES, suggesting the fault has not been active since the WES eruption. All other intracaldera faults are concealed so that displacement of WES (if any) by these faults is not observed.

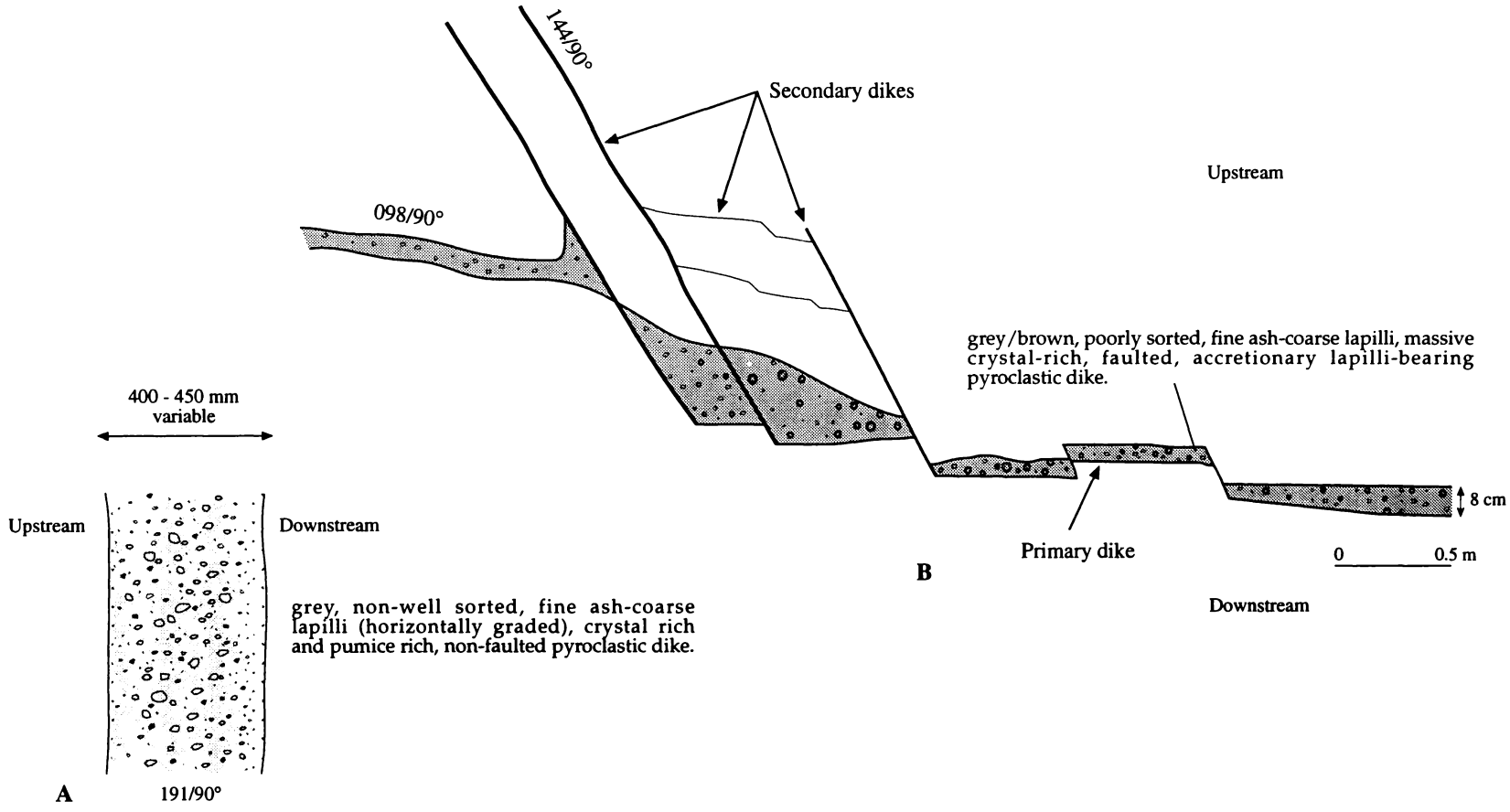


Figure 5.12 Detail of two major clastic dikes within WES-1 Ignimbrite, lower Kapowai valley (T11/551679). A, Non faulted, horizontally graded ash-lapilli vitric clastic dike. B, Faulted lensoidal, ash-fine lapilli clastic dike. Major E-trending dike (098 strike) is variably displaced (5-40 mm) by a series of NW-SE striking faults (ca. 144 strike).

## Source vent location

Locating source vents for explosively erupted units at caldera volcanoes is typically hampered by post-eruption modification of the vent (Lipman, 1984). These include infilling by younger eruptives, volcanic-tectonic induced deformation, and development of freshwater lakes. Constraining the source vent location of WES deposits utilises ML data for ignimbrites and thickness variations of the WES-2 tuff. Maximum juvenile (MJ) data shows no evidence of variation with distance and is therefore not useful for constraining source vents.

For intracaldera ignimbrites, well constrained lithic isopleths are seldom achieved from ML data. This is because ML often does not vary consistently due to the influence of numerous point source origins (i.e. multiple vents along arcuate ring fractures), and also because of topographic-induced grain size bias (Buesch, 1992). Importantly the other problem especially faced at the KCC, is the limited outcrop which means that it is difficult to establish the stratigraphic level when measuring ML. This is significant because ML can vary vertically through an ignimbrite, so that without stratigraphic control, the data can be mis-leading.

Discrete ML data is usually presented for outflow ignimbrite sheets (e.g. Carr, 1984), and this is the same approach taken here for the intracaldera WES ignimbrites (Figure 5.13). For WES ignimbrites, two features are present in the lateral variation of ML (Figure 5.14). For transects along a northern and northeastern direction from the eastern escarpment in Slip Stream valley, lithic sizes generally decrease. This implies that some WES pyroclastic flows were initiated from the central KCC area and travelled north and northeast.

Along a southern transect, ML increases towards the southern topographic boundary which is fundamentally different from the northern and northeastern transects (Figure 5.13). This variation may be related to significant topographic barriers (i.e. Taurauikau Andesite, Bulls Run Rhyolite) or depocentres present in the southern KCC sector during pyroclastic flow emplacement. Clasts transported by pyroclastic flows can be influenced by topographic barriers or depressions such that the dense lithic clasts may be detached from the pyroclastic flow and deposited (e.g. Buesch, 1992).

Another possibility, is that the ML data indicates the presence of a secondary vent for the WES in the southern KCC sector. However, no lithologic or structural evidence has been observed to indicate the presence of vents, although it is possible that rhyolite lava domes which post date the WES eruption (e.g. Kauaeranga rhyolite dome, Camp rhyolite dome, Tauranikau rhyolite dome) may have obscured WES source vents in this area.

MJ data for intracaldera WES ignimbrites typically is similar throughout the KCC. When plotted along similar transects as for ML (Figure 5.14), the MJ data generally shows no clear relationship between

proximity to vent and increasing clast size, which is a similar pattern found with other pyroclastic deposits (e.g. Suzuki-Kamata and Kamata, 1990).

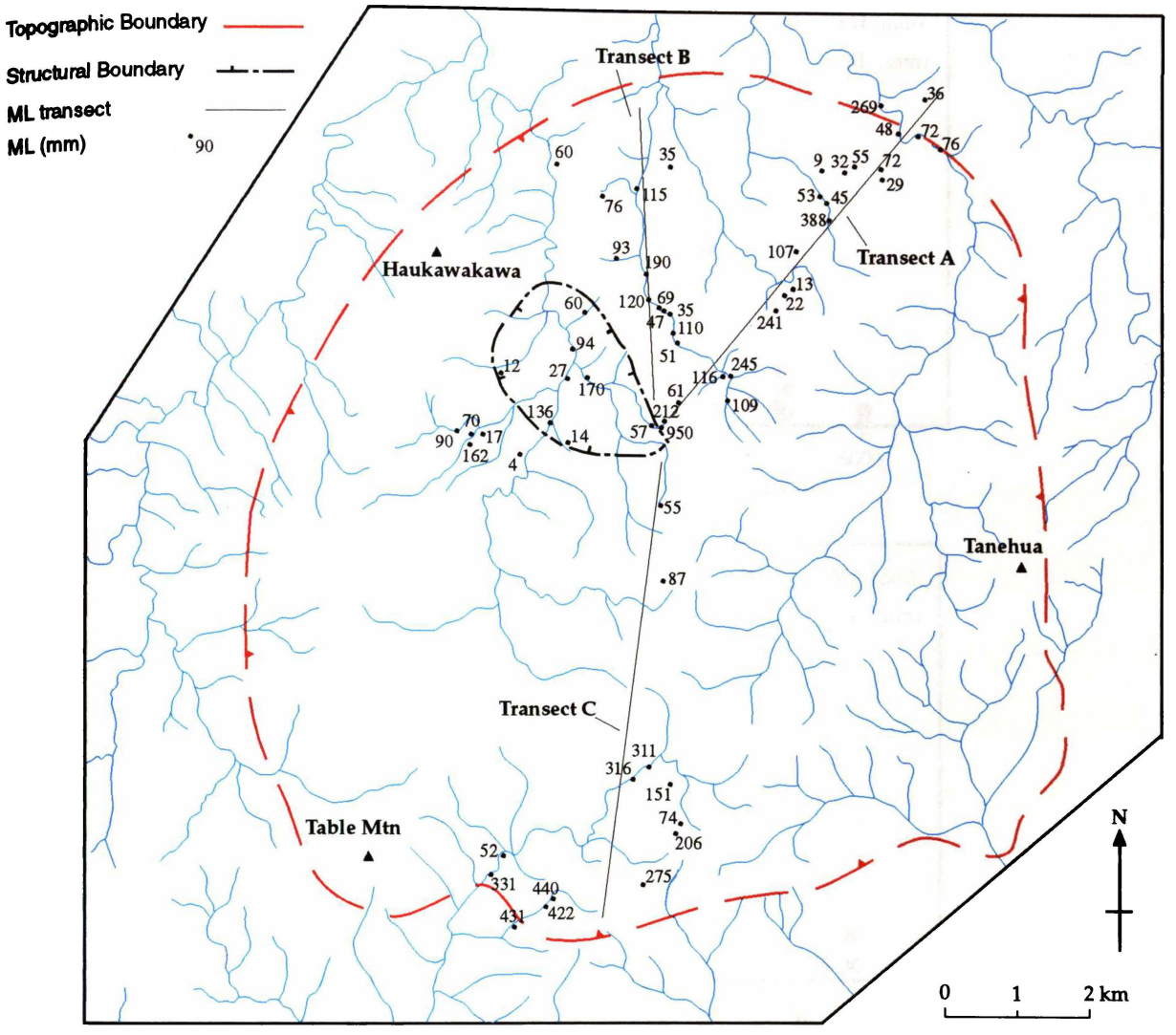


Figure 5.13 Maximum lithic size ($M_L$) data (mm) for intracaldera WES ignimbrites.

Conformable pyroclastic fall deposits interbedded between ignimbrites or lithic lag breccias can provide fundamental evidence for vent location (e.g. Self et al., 1986). WES-2 vitric and crystal tuff has a maximum thickness (ca. 3 m) on the eastern escarpment in the Slip stream valley (T11/511643). At other intracaldera localities, the thickness of WES-2 is less. In the southern sector of the KCC, WES-2 thickness varies from 0.25 to 0.5 m. Although limited, this data suggests that the likely source vent for WES-2 tuff is further north, perhaps in the Slip stream area.

Based upon the ML data and tuff thickness, coupled with interbedded lithic lag breccia and the presence of a ca. 3 $km^2$ collapse zone, it is highly likely that the source vent(s) for at least the WES-2 to WES-4 deposits, is located within the Slip Stream-Haukawakawa Stream area. Additional vents may have occurred near the southern topographic margin as suggested by ML data in that area. The source area for WES-1 Ignimbrite

is unknown because no lithological or structural features are observed associated with the ignimbrite to enable the area to be defined.

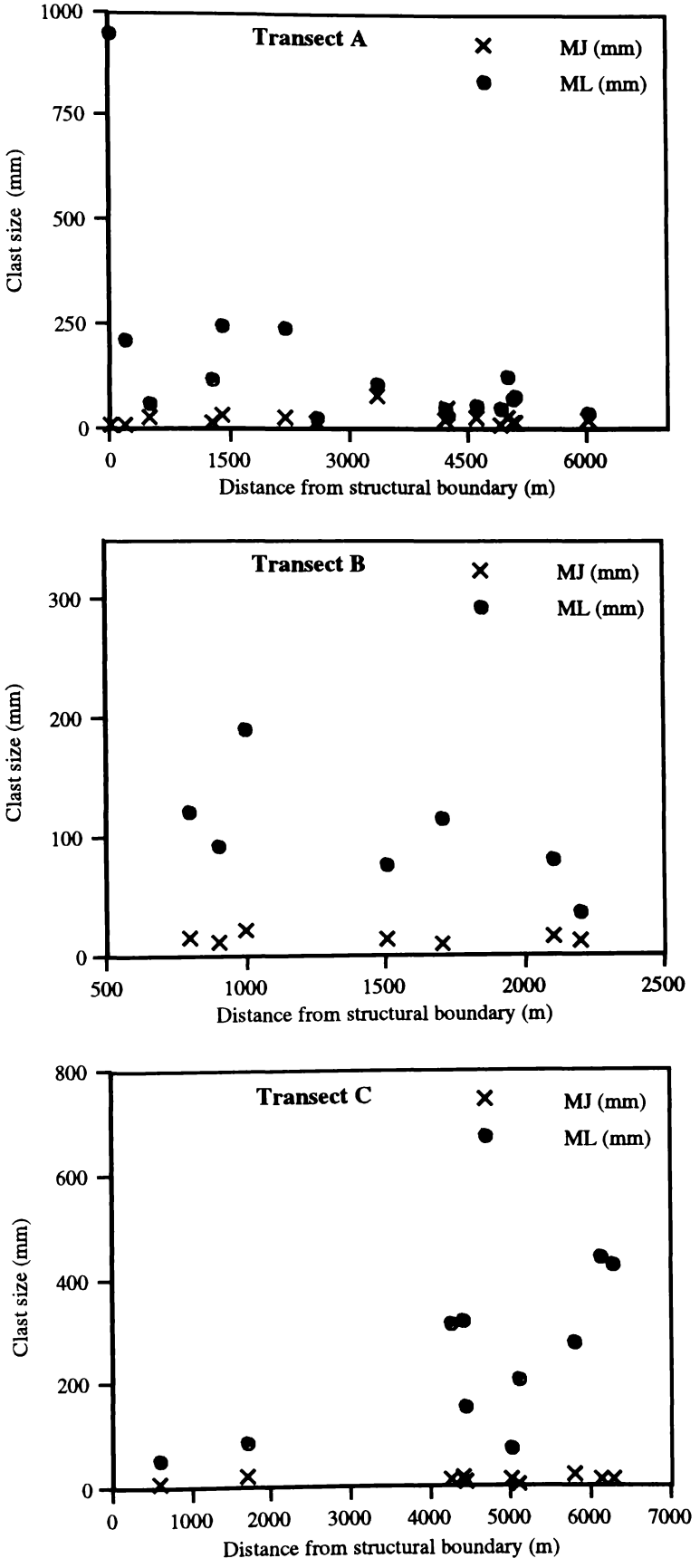


Figure 5.14 Variation in ML(mm) and MJ(mm) vs distance for WES ignimbrites. Transects extend from the WES structural boundary and are defined in Figure 5.13.

### Distribution

WES dominates the surficial intracaldera geology of the KCC. It is the most widespread and thickest unit exposed. WES is exposed throughout the KCC, aside from the western sector where it only forms sporadic, minor outcrops. WES-1 and WES-4 Ignimbrites are the largest units, with tuffs representing only a very minor volume.

Figure 5.15 Thick (up to 400 m) WES in the upper Kapowai valley.

Intracaldera WES outcrops predominantly in the northern, eastern and southern sectors of the KCC. Thickest exposures of the WES occur in the upper Kapowai valley where up to 400 m accumulated covering ca. 25 $km^2$ (Figure 5.15). A significant depocentre must have been present within the upper Kapowai valley area, prior to WES eruption to accommodate the thickness of WES pyroclastics.

One possible origin for the depocentre is that the area may represent an older caldera floor generated from a pre-WES eruption. Support for this includes several rhyolite lavas and domes (Kydd Rhyolite) which are overlain by the WES within the Kapowai valley floor and on its immediate margins. Another possible origin is that the area may also represent part of the WES caldera collapse zone, however there is no structural evidence to support this.

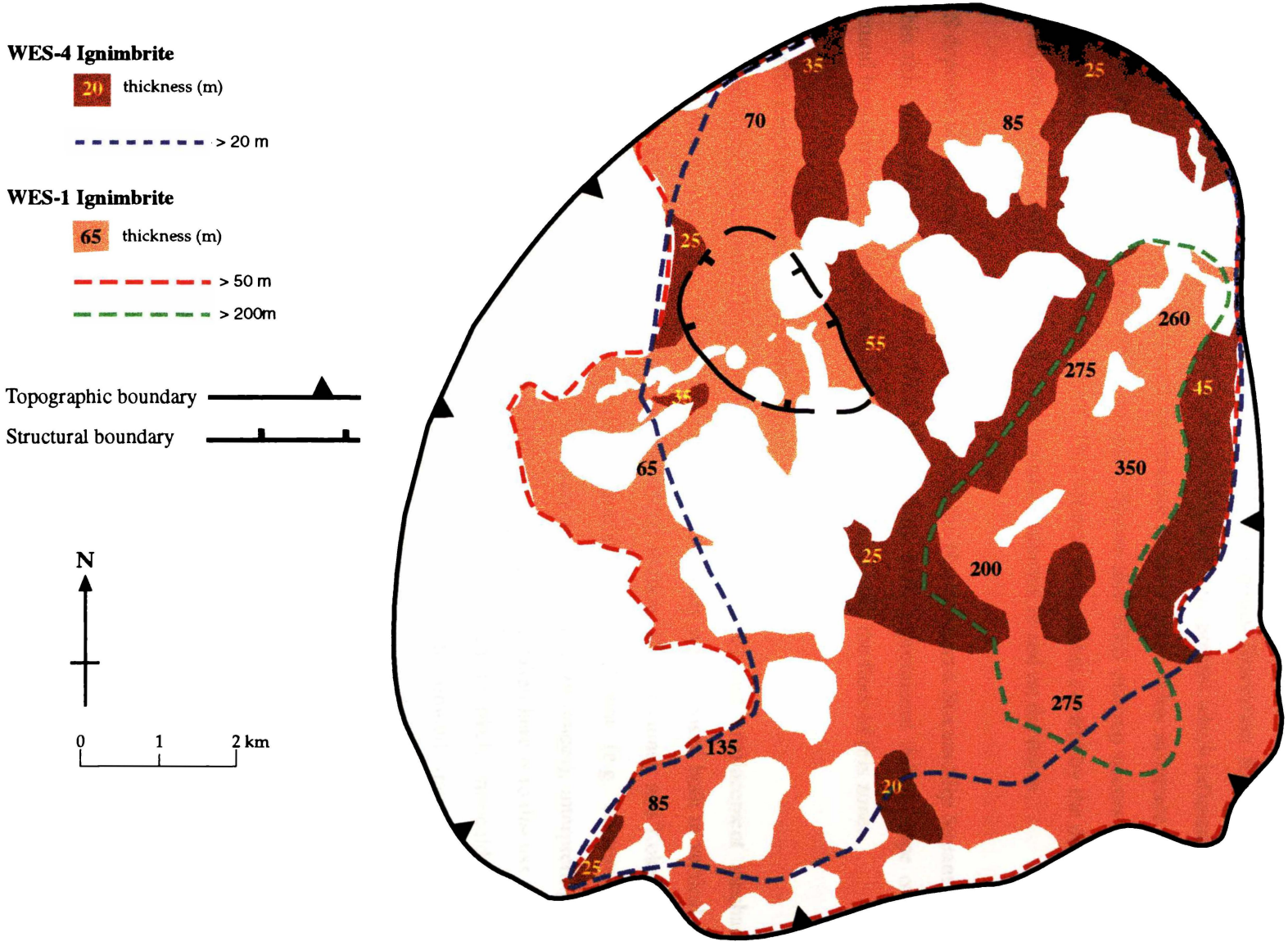


Figure 5.16 Intracaldera distribution and thickness(m) of WES-1 and WES-4 Ignimbrites.

Two key features influenced the intracaldera distribution of WES ignimbrites: (1) At the time of the WES eruption, significant topographic barriers were present on the western (Haukawakawa ridge), southwestern (Waiwawa range) and eastern (Tanehua-Ruahine ridge) margin influencing the outflow of WES ignimbrites. Thin veneer deposits of ignimbrite in these elevated areas are also likely to have been more rapidly eroded than valley-infilling deposits, therefore affecting the present distribution. (2) Several intracaldera rhyolite domes (e.g. Welcome Jack Rhyolite dome, Starvation Rhyolite dome, Bulls Run Rhyolite dome complex, and Kydd Rhyolite dome complex) were present which influenced the thickness of intracaldera WES ignimbrite which could accumulate in these areas. This influence is best seen on the margins of the Bulls Run Rhyolite dome complex. Sparse thin WES outcrop occurs on the southern and southwestern margins and on the dome itself. This reflects topographic control by the dome complex, such that only thin, easily erodable ignimbrite was deposited adjacent to and on the dome.

WES deposits are generally in situ, aside from within the Haukawakawa Stream-Slip Stream collapse zone. Within this zone distorted blocks of WES-1 Ignimbrite form a prominent debris slope on the western structural boundary margin. Numerous deformed blocks also infill the floor of this zone.

### Ignimbrite emplacement and facies

Most terminology describing flow geometries (e.g. aspect ratio) and emplacement mechanisms for ignimbrites relate to exocaldera ignimbrites which are commonly well exposed both in vertical and lateral profiles (Walker et al., 1981; Walker and Wilson, 1982; Walker, 1983; Branney and Kokelaar, 1992). As the depositional environment for intracaldera ignimbrites is different (e.g. numerous, immediate topographic barriers and local depocentres; relatively small transport distances), interpreting intracaldera WES ignimbrites using exocaldera models is difficult. The approach taken here is to discuss the lithological features observed, define general ignimbrite facies and relate them to likely intracaldera emplacement conditions. Flow geometries have not been reconstructed because of the limited outcrop.

Intracaldera WES-1 and WES-4 Ignimbrites consistently exhibit similar lithological features which allow some common constraints to be made on their emplacement mechanisms. A significant lack of gas segregation pipes, minor localised vapour phase alteration, preservation of cuspate and platey glass shards and the weakly welded nature, suggest that the ignimbrites were emplaced at relatively low temperatures and probably low velocities. They could therefore be regarded as low-grade ignimbrites (cf. Branney and Kokelaar, 1992).

Intracaldera WES ignimbrites show some lithic clast segregation which is mainly observed at medial localities, although minor segregation has also been observed at proximal sites (Figure 5.17). Segregation is typically restricted to certain vertical elevations which imply changes in the depositional and transport conditions (Branney and Kokelaar, 1992). No vertical grading or clast size variation with distance of

pumice clasts has been observed in WES ignimbrites, which contrasts with outflow ignimbrites (Palladino and Valentine, 1995; Streck and Grunder, 1995).

Detailed facies characterisation of intracaldera WES ignimbrites is difficult to establish, and only broad facies are used here. Thick WES ignimbrite originally infilled most of the KCC valleys (up to 400 m), and buried most of the pre-existing landscape. This formed broad plateaux which are now dissected, but are inferred to have covered most of the northern, eastern, and southern KCC upto a minimum of ca. 400m. Where topographic barriers occurred (i.e. Waiwawa range; Tanehua-Ruahine ridge) WES ignimbrites were emplaced as thin veneer deposits, which are now poorly preserved.

Proximal WES facies are defined as including interbedded lithic lag breccia (WES-3) and thick (up to 3 m) vitric and crystal tuffs (WES-2). Pyroclastic flows within these facies exhibit limited grain sorting or grading. Proximal facies appear to have a restricted distribution and are limited to the margins (< 0.5-1 km) of the collapse zone.

Medial facies are defined as those where ignimbrites exhibit some more obvious size and/or density segregation of clasts, thinner (< 0.5 m) interbedded vitric and crystal tuffs occur, and lithic lag breccias do not occur. Medial facies dominate the intracaldera distribution of WES-1 and WES-4 ignimbrites.

Figure 5.17 Lithic concentration zones (LCZ) in WES-1 Ignimbrite. Medial location, Oteao valley (T11/503674). Note normal grading in upper, broad LCZ and lower thin, non-graded LCZ.

## Eruptive evolution

Stratigraphic studies at the KCC have revealed a conformable composite pyroclastic sequence for the WES, which included both pyroclastic fall and flow deposits. The following interpretation of the eruptive history is based upon this intracaldera stratigraphy.

Initial explosive eruptions produced minor pyroclastic flows (WES-1 Ignimbrite). A change in eruptive style resulted in the deposition of fine lapilli-ash fall deposits, which were subsequently eroded in some parts by a large pyroclastic flow (WES-1 Ignimbrite). It is unclear whether there was a time break between the tuffs and ignimbrite due to the erosional contact. Significantly, no interbedded lithic lag breccias have been observed with WES-1 Ignimbrite. Conformable, relatively thick, weakly shower bedded vitric tuffs (WES-2) overlie WES-I Ignimbrite implying sustained pulses of explosive eruptions. These tuffs are ash-fine lapilli sized and moderately sorted, suggesting they are the product of vent-fed buoyant plumes, and do not represent co-ignimbrite tephra (Sparks and Walker, 1977).

Lithic lag breccia (WES-3) conformably overlying vitric tuffs (WES-2) indicate a significant change in eruptive behaviour. Lithic breccias are unstratified and form only a relatively thin (< 3 m) unit compared to other proximal lithic breccias reported, where thicknesses range up to > 30 m and compositional stratification is common (e.g. Aramaki, 1984; Druitt and Bacon, 1986; Beresford, 1997). Where lithic lag breccias are stratified or consist of multiple breccias types, this can be inferred to relate to several eruptive pulses or vent sources (e.g. Rosi, et al., 1996). Therefore the nature of WES-3 lithic lag breccia implies a single and dramatic change in eruptive behaviour. Breccias grade into ignimbrite (WES-4 Ignimbrite) inferring a gradual increase in magmatic material ejected, until the climatic ignimbrite event where eruption intensities peaked.

Therefore the eruptive process leading to caldera collapse is inferred by this gradation. It is likely that widening of the vent allowed larger grain sizes to be abraded and incorporated into the eruption column. These were deposited at proximal vent localities, as thin lithic lag breccias. Progressive vent flaring lead to catastrophic caldera collapse which produced a significant increase in the discharge rate. This ultimately lead to a collapse of the erupted column and development of pyroclastic flows (WES-4 ignimbrite).

## Collapse mechanism

Caldera subsidence is inferred to have taken place during the later eruption phases (i.e. from WES-2 to WES-4), as lithic lag breccia occurs interbedded between WES-2 vitric tuffs and WES-4 Ignimbrite. The source for this component of the WES is a subsidence zone, centred on the Rangihau valley and the term Rangihau Caldera is proposed for it. This has been established by ML data, thickness of interbedded WES-2 vitric tuff and the presence of interbedded lithic lag breccia. The source for the earlier component, i.e. WES-1 Ignimbrite, is difficult to establish because of the lack of basal tuffs and interbedded lithic lag breccia. No physical evidence is available to suggest that Rangihau Caldera is the source area for the WES-1 eruption.

Rangihau Caldera is well defined by a ca. 3 $km^2$ depressed area bounded by an almost complete set of arcuate ring faults (Figure 5.18). The zone is the only area affected by significant collapse (minimum of ca. 100 m displacement), although subsidence is inferred to extend outside the caldera, towards the southwest. Evidence for this is obtained from remote sensing lineations and an observed fault which occur to the southwest of the Rangihau Caldera (Figure 5.18).

A major ca. 3 km, arcuate lineation observed in both Landsat MSS and SAR from is centred on the NE margin of the Waiwawa range and relates to a significant escarpment at the head of the Haukawakawa valley. This escarpment may relate to mass wasting following subsidence to the NW and possibly defines the southwestern margin of subsidence associated with the WES eruption. A single fault (Haukawakawa Fault) is also observed outside the SW structural boundary, in the upper Haukawakawa valley. It displaces Haukawakawa Member and overlying WES-1 Ignimbrite by up to 20m. Therefore these two features suggest a zone of subsidence extending from the Rangihau Caldera SW to the NW Waiwawa range escarpment.

WES caldera collapse is therefore suggested to have occurred in a relatively small discrete zone (Rangihau Caldera), but subsidence appears to have affected a larger block extending to the Waiwawa range. Observed displacement only occurs within the Slip Stream-Haukawakawa Stream valleys. Maximum displacement occurred on the eastern structural boundary (ca. 100m minimum) and progressively less at the southwestern boundary (ca. 80 m minimum). Displacement of ca. 20 m on the Haukawakawa Fault occurs, but no other displacement is observed further to the SW. This suggests a differential displacement with minor subsidence in the upper Haukawakawa valley, increasing to major displacement and caldera collapse in the Slip Stream-lower Haukawakawa valley area.

This style of collapse has been described at other calderas (e.g. Silverton Caldera, Colorado; Snowdon Caldera, Wales) but on a larger scale (Steven and Lipman, 1976; Howells et al., 1986). The most appropriate model which incorporates these collapse features is termed trapdoor collapse (Lipman, 1997). This model describes a zone of major collapse coupled with an adjacent area where more minor subsidence has taken place (Lipman, 1997).

## 5.3 Exocaldera WES

WES was initially erupted over a wide area across the CVZ and northern New Zealand. Here, correlations to intracaldera WES are attempted for onland CVZ ignimbrites, ignimbrites in adjacent basins, and distal tuffs in onshore and offshore New Zealand. Correlating exocaldera units to intracaldera WES requires a stringent application of lithological characteristics (Hildreth and Mahood, 1985). Key features applied in WES correlation include juvenile morphology and mineralogy, and lithic population for ignimbrites, and major element glass shard chemistry for distal tuffs.

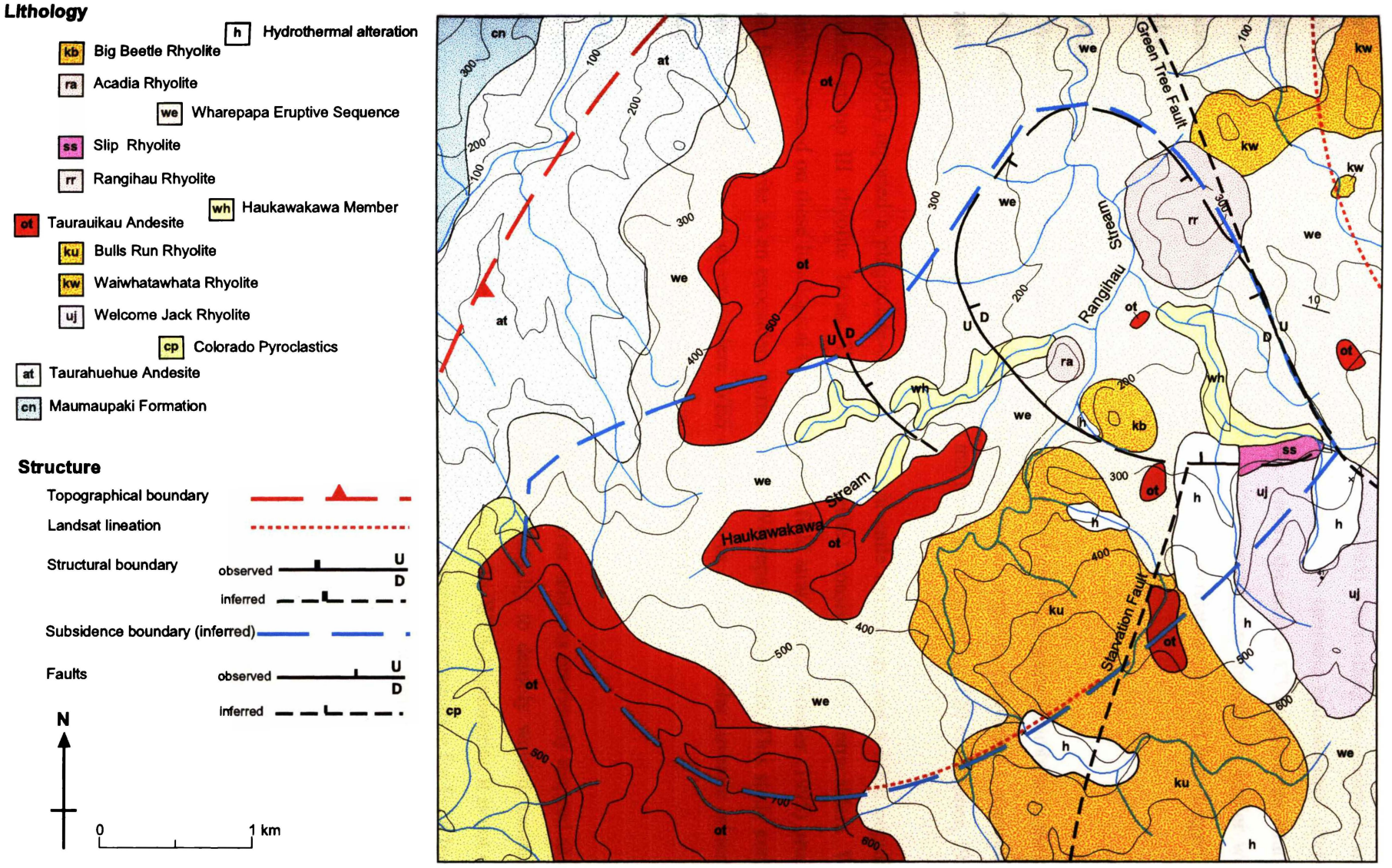


Figure 5.18 Geological map of upper Rangihau valley illustrating structural boundary and possible subsidence zone associated with the WES eruption.

## Central CVZ ignimbrites

Central CVZ is characterised by numerous thick ignimbrites erupted over a period of ca. 10-5 Ma (Aldrich, 1995; McGunnigle, 1995; Skinner, 1995; Trotter, 1995). Unravelling the ignimbrite stratigraphy in this area however, is hampered by discontinuity of exposure, sporadic hydrothermal alteration, and complex volcanic-tectonic deformation. This section reviews the central CVZ ignimbrite stratigraphy in light of the new intracaldera definition for WES. Surface correlatives mapped by earlier workers are discussed and revisions are suggested (Table 5.7). Subsurface correlations derived from logged boreholes are also discussed.

### *Hot Water Beach Ignimbrite*

Hot Water Beach Ignimbrite was mapped as a flow member of the Wharepapa Ignimbrite to the east of the KCC (Adams, 1992; Skinner, 1995). It is overlain by fluvial deposits (Taiwawe Conglomerate) and Pumpkin Rock Ignimbrite. Hot Water Beach has a maximum thickness of ca. 120 m (Skinner, 1993).

Skinner (1995) reported a plagioclase-orthopyroxene juvenile mineralogy and a lithic population (i.e. including group III rhyolite lavas, Tapuaetahi Andesite) consistent with intracaldera Wharepapa Ignimbrite. Based on these lithological features and the field stratigraphy, Skinner (1995) proposed Hot Water Beach ignimbrite as an exocaldera correlative to Wharepapa Ignimbrite. This study confirms Hot Water Beach Ignimbrite as an exocaldera WES correlative as it has a similar juvenile mineralogy and lithic population, and is overlain by the Pumpkin Rock Ignimbrite.

### *Pepe Ignimbrite*

Pepe Ignimbrite outcrops locally in Pepe Stream, SW of Tairua, and was previously mapped as a member of the Wharepapa Ignimbrite (Skinner, 1995). As it is partially to densely welded, contains highly lenticular pumice, overlies Tapuaetahi Andesite, and is overlain by WES-1 Ignimbrite, it is not considered to be a correlative outflow unit of WES ignimbrites. A more appropriate correlative for Pepe Ignimbrite is the Trig Q Ignimbrite, as these ignimbrite have similar highly lenticular pumice, and both pre-date the WES.

### *Mares Leg Ignimbrite*

Mares Leg Ignimbrite occurs in Stingray Bay-Cathedral Cove on the NE Coromandel coast, 2km north of Hahei (Rogers, 1994). Mares Leg Ignimbrite has a similar juvenile component and vitroclastic matrix compared with WES ignimbrites, and it underlies Pumpkin Rock Ignimbrite, which together suggest a correlation to WES. Mares Leg Ignimbrite lacks ferromagnesian minerals in the matrix, but this feature in itself can indicate that it is a distal deposit. Based on this evidence, Mares Leg Ignimbrite is considered to be a correlative to WES Ignimbrites.

Table 5.7 Summary of key marker ignimbrites in the central CVZ and potential correlation to intracaldera WES defined in this study. A correlation is suggested by "yes"; reason(s) for not correlating is given. plag = plagioclase; qtz = quartz; opx = orthopyroxene; amph = amphibole; biot = biotite. Sources: Adams (1992), Skinner (1995), McGunnigle (1995), Trotter (1995), Rogers (1994), and Bardebes (1997).

| Ignimbrite | Lithology (wt.% $SiO_2$) | Juvenile Mineralogy | Correlation* | K/Ar Age | Possible Source |
|---|---|---|---|---|---|
| Momoparaua | 2 juveniles(66-73%; 72-76%) | plag + amph + opx + biot + qtz | no: juvenile mineralogy | | dome-building pyroclastic |
| Ohui | 2 juveniles(76-77%) | plag + qtz + biot | no: juvenile mineralogy | | ? |
| Hikuai | 3 Juveniles(70-74%; 68-69%) | plag + qtz + opx + cpx | no: juvenile types, juvenile mineralogy | | Wharekawa Caldera |
| Pauanui | 2 juveniles(53-57%; 71-72%) | plag + cpx + opx + amph | no: juvenile mineralogy | | ? |
| Trig Q | 1 juvenile (%) | plag + opx | no: lenticular juvenile, partially welded | | ? |
| Ferry Landing | 1 juvenile | plag + opx | no: lenticular juvenile, partially welded | | ? |
| Flaxmill | 2 juvenile | plag | yes | | Kapowai Caldera Complex |
| Cathedral Cove | 2 juveniles(67-77%) | plag + qtz | yes | | Kapowai Caldera Complex |
| Mare's Leg | 2 juveniles(67-75%) | plag | yes | | Kapowai Caldera Complex |
| Hot Water Beach | - | plag + qtz | yes | | ? |
| Pumpkin Rock | 1 juvenile (74 -76%) | plag + opx + amph | no: age, mineralogy | 5.9 Ma | Whitianga Caldera Complex |
| Carina Rock | 1 juvenile | plag + opx + cpx + amph + qtz | no: age, mineralogy | 10 Ma | ? |

*Ferry Landing Ignimbrite*

Highly lenticular, partially welded Ferry Landing Ignimbrite occurs at Whakapanui Point, near Whitianga (Bardebes, 1997). Initially, this ignimbrite was mapped within the Wharepapa Ignimbrite Formation (Skinner, 1995), although the partially welded nature, highly lenticular pumice, and plagioclase-orthopyroxene juvenile mineralogy is more similar to Trig Q Ignimbrite.

A correlation with WES-1 or WES-4 Ignimbrite is not favoured as the juvenile mineralogy of WES ignimbrites typically also includes clinopyroxene. WES-1 and WES-4 Ignimbrites are also never observed more than weakly welded in the KCC or adjacent to the KCC, which also implies that they are not related to the Ferry Landing Ignimbrite.

*Flaxmill Ignimbrite*

Flaxmill Ignimbrite occurs on the southern margin of Maramaratotara Bay and is a light grey, pumice-rich (MJ: 38mm), lithic-rich (ML: 45 mm) weakly welded ignimbrite. Flaxmill Ignimbrite is considered a likely correlative to WES ignimbrites, as it has a similar juvenile type and mineralogy, and a similar relative age (Bardebes, 1997).

*Pauanui Borehole*

Several devitrified or hydrothermally altered ignimbrites were logged from a borehole drilled near Pauanui (Trotter, 1995). Between depths of 425 to 467 m, a strongly devitrified ignimbrite containing crystals of plagioclase, orthopyroxene, clinopyroxene, and rare quartz occurs. No other features including juvenile morphology and abundance, and matrix texture are reported, although the mineral assemblage is similar to that of WES-1 and WES-4 Ignimbrites. A correlation is difficult to establish on mineralogy alone, and more lithological data needs to be acquired to confirm a link between this ignimbrite and WES ignimbrites.

*Boreholes in the Coroglen - Whenuakite area*

Several boreholes drilled in the Coroglen-Whenuakite area record evidence of thick ignimbrites (> 200 m) overlying Taurahuehue Andesite or Tapuaetahi Andesite (Adams, 1992). Differentiation of ignimbrites was not achieved by Adams (1992), but the main ignimbrite identified was the Hot Water Beach Ignimbrite (considered in this study to be a WES correlative). It is also possible that other exocaldera WES ignimbrites were drilled and some of these may have been included within the Hot Water Beach Ignimbrite unit. However, no detailed lithological data is available.

*Central CVZ distribution*

The distribution of WES-correlative ignimbrite throughout onland central CVZ, as defined in this study, is therefore a modification from previous work (e.g. Skinner, 1993; 1995). The revised distribution emphasises three major areas of WES ignimbrite, in the northern, eastern, and southern central CVZ (Figure 5.19). No significant outcrops of WES-correlative ignimbrite have been defined in western CVZ. This is possibly because no major WES pyroclastic flows travelled to the west of the KCC, or if ignimbrite was deposited it has subsequently been eroded.

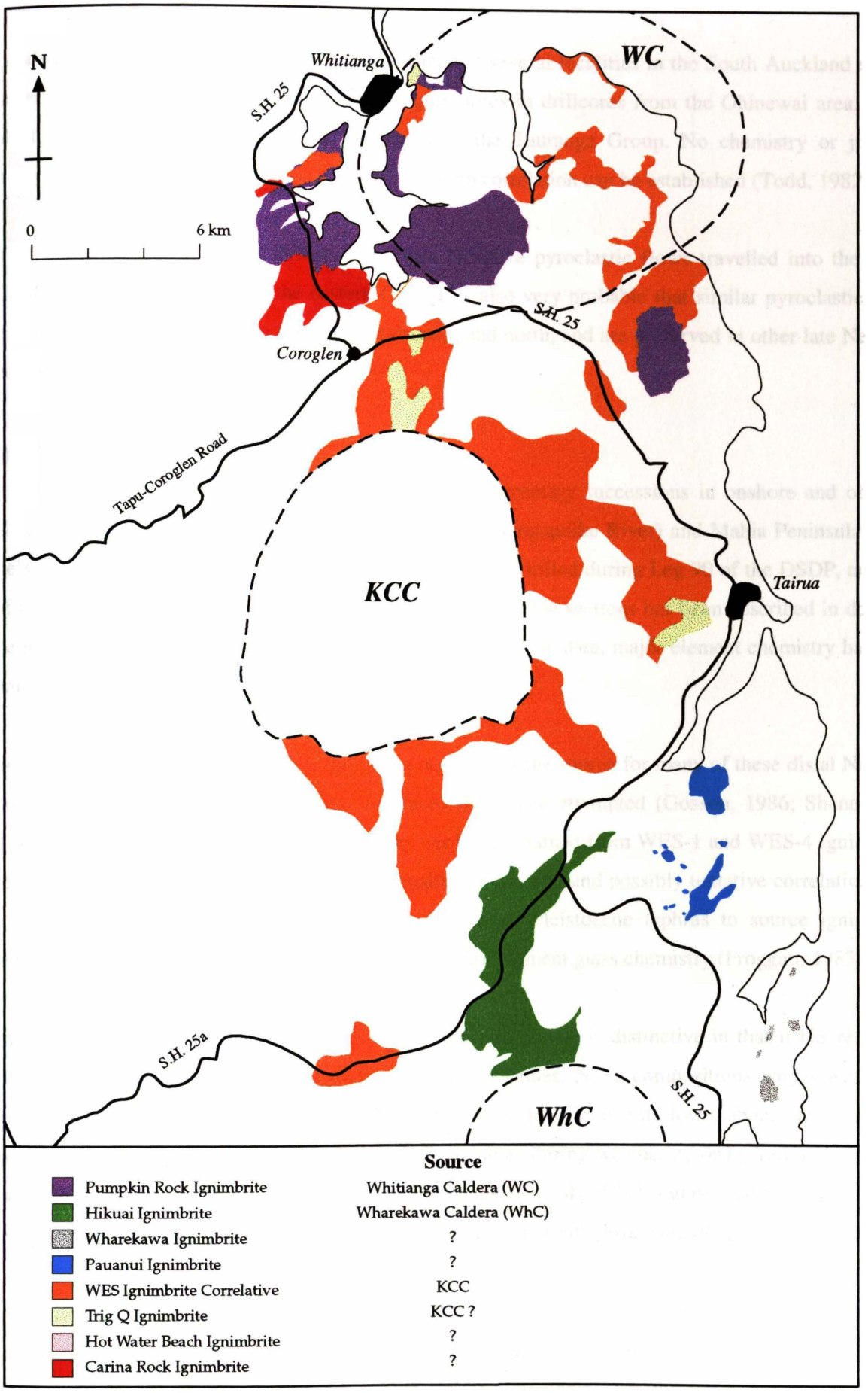


Figure 5.19 Map of exocaldera correlative WES ignimbrite and other major central CVZ ignimbrites. Compiled from Skinner (1986; 1993; 1995), Adams (1992), Rogers (1994), Trotter (1995), McGunnigle (1995), Aldrich (1995), Karl (1996), Briggs et al. (1998), and this study.

## Ignimbrites outside the CVZ

Several distal Neogene ignimbrites have been described at several localities in the South Auckland region. Nelson et al. (1988) reported three late Miocene ignimbrites in drillcores from the Ohinewai area. These ignimbrites occur in the Whangamarino Formation of the Tauranga Group. No chemistry or juvenile mineralogy has been described for these ignimbrites, so no correlation can be established (Todd, 1982).

However, these drillcores provide evidence that late Neogene pyroclastic flows travelled into the South Auckland region, most likely from the eastern CVZ. It is also very probable that similar pyroclastic flows derived from the eastern CVZ, also travelled south, east, and north, and are preserved in other late Neogene marine and terrestrial basins.

## Co-ignimbrite tephra correlation

Numerous distal Neogene tephras are found in several sedimentary successions in onshore and offshore New Zealand. Two onland sections at Tukemoike Stream (Mangapoike River) and Mahia Peninsula in the Hawke's Bay contain numerous silicic tephras. Offshore cores drilled during Leg 90 of the DSDP, and Leg 181 of the ODP also contain abundant distal tephras. Each of these sections has been described in detail or will be in the near future. Along with lithological and stratigraphic data, major element chemistry has been determined for most tephras at each locality.

Caldera volcanoes within the CVZ, have long been regarded as the source for many of these distal Neogene tephras, although no correlations to source volcanoes have been attempted (Gosson, 1986; Shane et al., 1998). In this study, major element glass chemistry has been obtained from WES-1 and WES-4 Ignimbrites (Table 5.8) from electron microprobe analysis to enable comparison and possibly tentative correlation to be made with distal Miocene-Pliocene tephras. Correlations of Pleistocene tephras to source ignimbrites derived from the TVZ have also been made also using major element glass chemistry (Froggatt, 1983).

The major element chemistry of glass shards from WES ignimbrites is distinctive in that it has relatively high FeO (1.73 mean wt. %) and $TiO_2$ (0.38 mean wt.%) values. $Na_2O$ compositions vary significantly between glass shards (2.05 mean wt. % $Na_2O$; 0.94 sd.dev) and have an overall lower abundance than distal tephras. This is most likely due to variations in alkali exchange during weathering or hydration of the glass shards (Scott, 1971; Shane et al., 1998). Major element analysis totals of WES glass shards are comparable to average silicic glass analyses from TVZ-derived pyroclastic deposits (Froggatt, 1983).

As ferromagnesian minerals and lithic fragments have very low abundances within distal tephras, any correlation is based solely upon comparing glass chemistry of the distal tuffs to the proximal WES. Such correlation has several inherent restrictions including: (i) glass shard and juvenile compositions vary in individual eruptives; (ii) multiple eruptives from a single volcano can have a similar composition; and (iii) analytical conditions vary for each dataset.

Table 5.8 Microprobe analyses of WES glass in pumice and glass shards normalised to 100% volatile free. All Fe calculated as FeO.

| Sample | W99614 | W99614 | W99614 | W99614 | W99614 | W99923 | W99923 | W99923 | W99923 | W99923 | W99923 | W99923 | Mean | (Sd.dev) |
|---|---|---|---|---|---|---|---|---|---|---|---|---|---|---|
| Analysis | shard | shard | pumice | shard | shard | shard | shard | shard | shard | shard | pumice | pumice | | |
| | wt.% | wt.% | wt.% | wt.% | wt.% | wt.% | wt.% | wt.% | wt.% | wt.% | wt.% | wt.% | | |
| SiO2 | 75.11 | 74.94 | 74.84 | 76.97 | 75.57 | 77.41 | 78.10 | 77.58 | 77.93 | 78.61 | 77.81 | 77.42 | 76.86 | 1.36 |
| TiO2 | 0.40 | 0.41 | 0.56 | 0.35 | 0.31 | 0.44 | 0.33 | 0.40 | 0.31 | 0.37 | 0.32 | 0.32 | 0.38 | 0.07 |
| Al2O3 | 13.83 | 13.85 | 13.42 | 13.50 | 15.04 | 13.51 | 12.94 | 13.48 | 13.02 | 12.79 | 13.13 | 13.92 | 13.54 | 0.60 |
| FeO | 1.57 | 1.64 | 1.97 | 1.67 | 1.86 | 1.66 | 1.72 | 1.65 | 1.73 | 1.68 | 1.78 | 1.81 | 1.73 | 0.11 |
| MnO | 0.09 | 0.06 | 0.01 | 0.21 | 0.04 | 0.02 | 0.08 | 0.12 | 0.02 | 0.13 | 0.18 | 0.11 | 0.09 | 0.06 |
| MgO | 0.27 | 0.19 | 0.24 | 0.27 | 0.24 | 0.13 | 0.18 | 0.20 | 0.24 | 0.24 | 0.21 | 0.14 | 0.21 | 0.05 |
| CaO | 1.63 | 1.47 | 1.41 | 1.32 | 1.30 | 1.27 | 1.26 | 1.27 | 1.21 | 1.01 | 1.14 | 1.01 | 1.28 | 0.18 |
| Na2O | 3.46 | 4.03 | 2.34 | 2.40 | 2.45 | 1.24 | 1.36 | 0.84 | 1.80 | 1.63 | 1.71 | 1.32 | 2.05 | 0.94 |
| K2O | 3.25 | 3.00 | 3.16 | 3.19 | 2.87 | 3.80 | 3.52 | 3.88 | 3.47 | 3.27 | 3.43 | 3.69 | 3.38 | 0.31 |
| Cl | 0.36 | 0.33 | 0.83 | 0.12 | 0.31 | 0.27 | 0.51 | 0.38 | 0.29 | 0.28 | 0.31 | 0.25 | 0.35 | 0.18 |
| Cr2O3 | 0.00 | 0.00 | 1.14 | 0.00 | 0.00 | 0.12 | 0.02 | 0.16 | 0.00 | 0.00 | 0.00 | 0.00 | 0.12 | 0.33 |
| NiO | 0.04 | 0.05 | 0.08 | 0.00 | 0.00 | 0.14 | 0.00 | 0.03 | 0.00 | 0.00 | 0.00 | 0.00 | 0.03 | 0.04 |
| H2O* | 7.71 | 6.80 | 4.14 | 8.92 | 8.72 | 7.75 | 9.36 | 10.34 | 6.52 | 6.96 | 9.75 | 9.32 | 8.02 | 1.74 |
| TOTAL** | 92.29 | 93.20 | 95.86 | 91.08 | 91.28 | 92.25 | 90.64 | 89.66 | 93.48 | 93.04 | 90.25 | 90.68 | | |

*by difference

**original total

Comparison of major element compositions is obtained by examining the ratio of the mean glass shard chemistry of a Neogene distal tephra with the mean WES glass shard composition (Sarna-Wojcicki et al., 1984). Chemically similar tephras will have ratios close to 1.00 for each element, whereas differences are shown by ratios greater or less than 1.00.

***Tukemokihi Stream - Mangapoike River section***

Tukemokihi Stream, in northern Hawke's Bay contains a significant onshore Neogene sequence (Gosson, 1986). The sequence is one of the main onland Neogene reference sections in New Zealand containing numerous biostratigraphic datums, providing a major paleomagnetic record, and containing numerous interbedded silicic tephra beds within the sequence (Wright, 1985; Gosson, 1986; Wright and Vella, 1988). Major element glass shard chemistry has been determined for most tephras (Gosson, 1986).

Comparison of the total data set of tephras to WES glass compositions yielded a subset of 12 tephras which had the closest composition (Figure 5.20). These tephras occur in the upper Tongaporutuan stage of the section, where the abundance of tephras increases significantly.

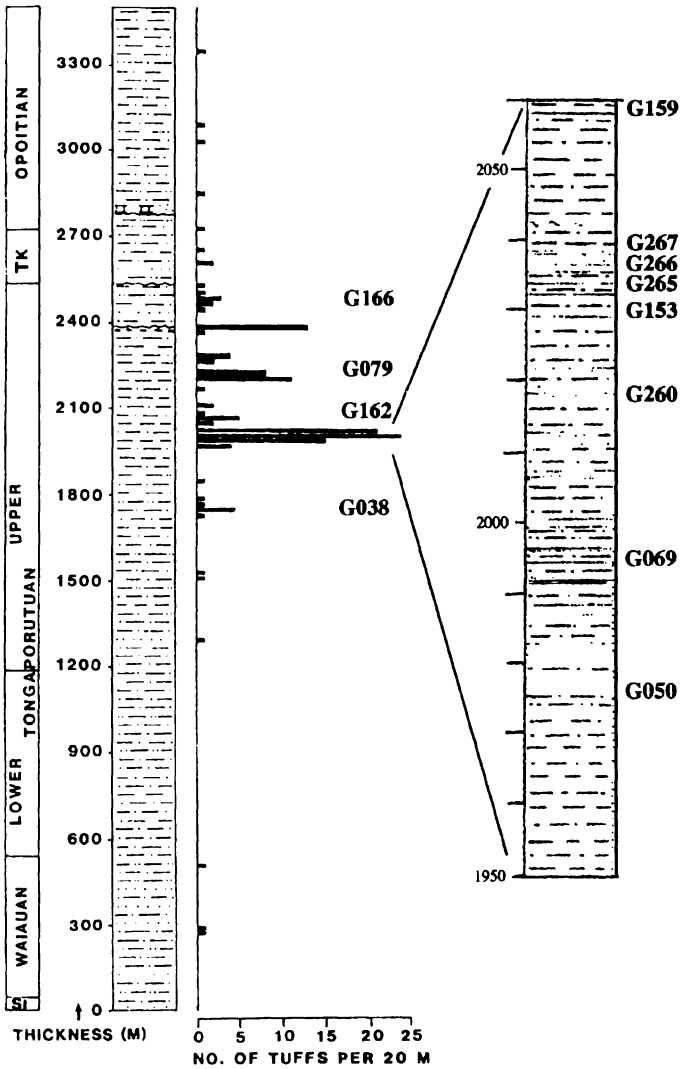


Figure 5.20 Tukemokihi Stream, Mangapoike River section. Tephras used in comparison are bolded. Adapted from Gosson (1986).

More detailed comparison of the initial 12 tephras indicated that 3 tephras (G267, G266 and G153) most closely matched the WES composition (Figure 5.21). These 3 tephras all occur at about the same stratigraphic level. Of note is tephra G265 which occurs between G266 and G153 and might be expected to have a similar composition. However, it is significantly different with higher FeO and CaO values and lower $TiO_2$ compared with tephras G266 and G153. This suggests that a distinctly different tephra was deposited between G266 and G153, and that tephras G266 and G153 are not related.

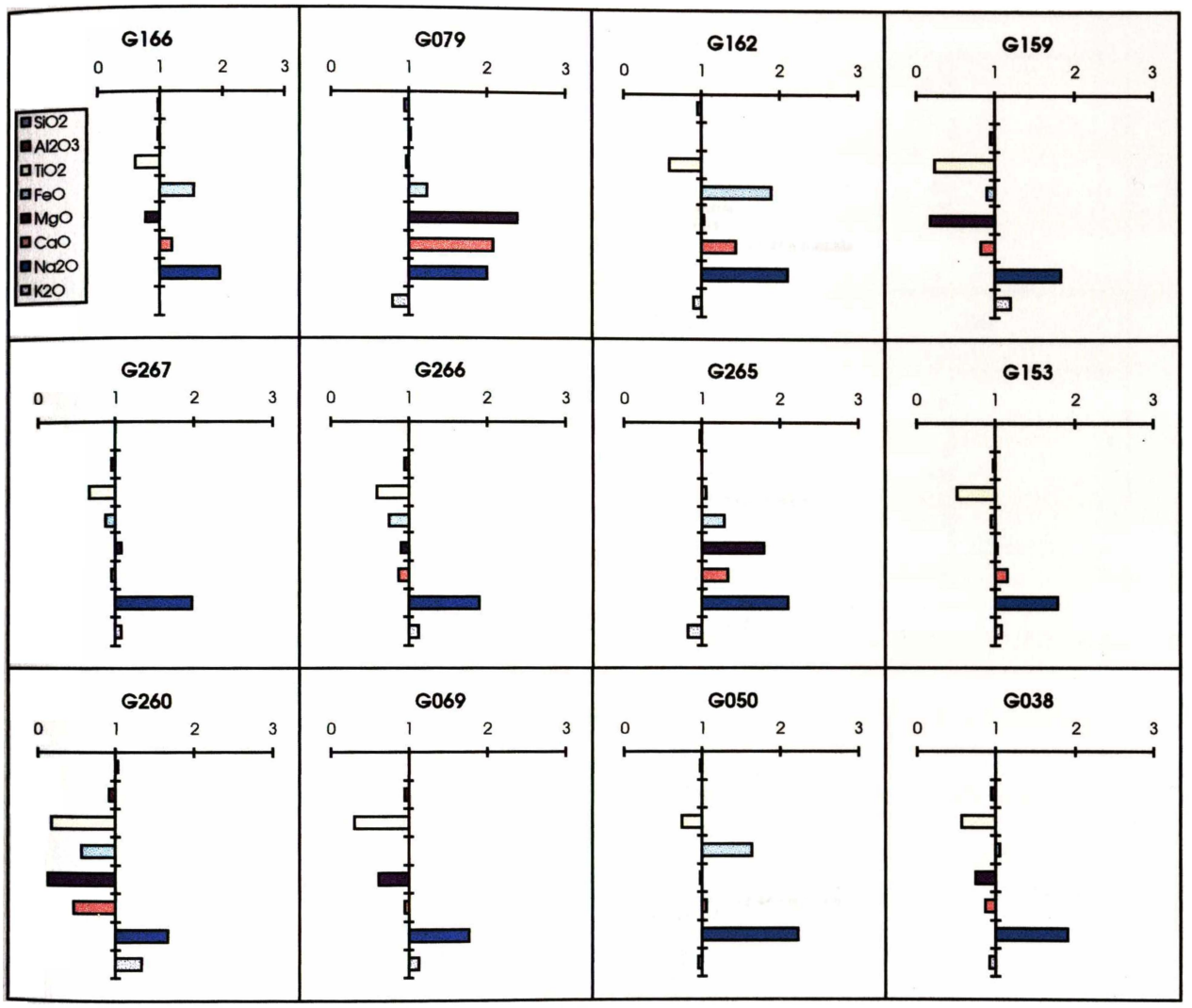


Figure 5.21. Comparison of WES glass chemistry to Tukemokihi Stream tephras. Tephra glass chemistry data from Gosson (1986).

### *Mahia Peninsula*

At least 71 medium-K, calc-alkaline rhyolitic (72-78 wt.% $SiO_2$) tephra beds are present within a ca. 600 m thick volcaniclastic mud-dominated Neogene sequence at Mahia Peninsula (Shane et al., 1998). Tephra units are dominated by glass shards and phenocrysts (typically > 80%) with minor felsic and rare ferromagnesian crystals. Shane et al. (1998) analysed the major element glass chemistry of all tephras and presented selected analyses. The full unpublished dataset was obtained for this comparison (P. Shane, pers comm. 1998).

All tephras were initially compared with the WES glass chemistry. A subset of 12 samples which have similar compositions were selected for further comparison (Figure 5.22). Of these the closest match in major element glass chemistry to the WES composition are tephras 426, 425 and 432 (Figure 5.23). Generally these tephras have a similar composition compared to the WES, apart from slight differences in $TiO_2$, MgO and MnO abundances. There is a significant difference (ca. 50 m) in stratigraphic position between tephra 432 and tephras 426/425, so it is unlikely that they are the same tephras.

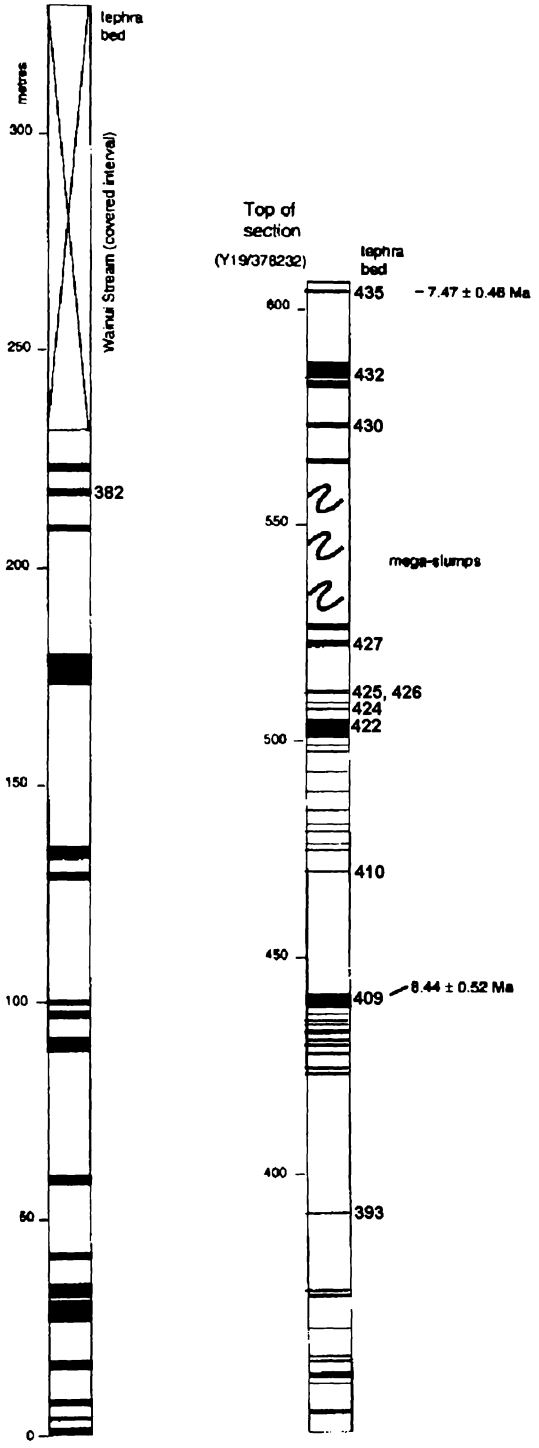


Figure 5.22 Stratigraphic column of the Mahia Peninsula tephra-bearing Neogene sequence, showing the position and relative thickness of macroscopic tephra beds (black). Tephras used for comparison are numbered. Adapted from Shane et al. (1998).

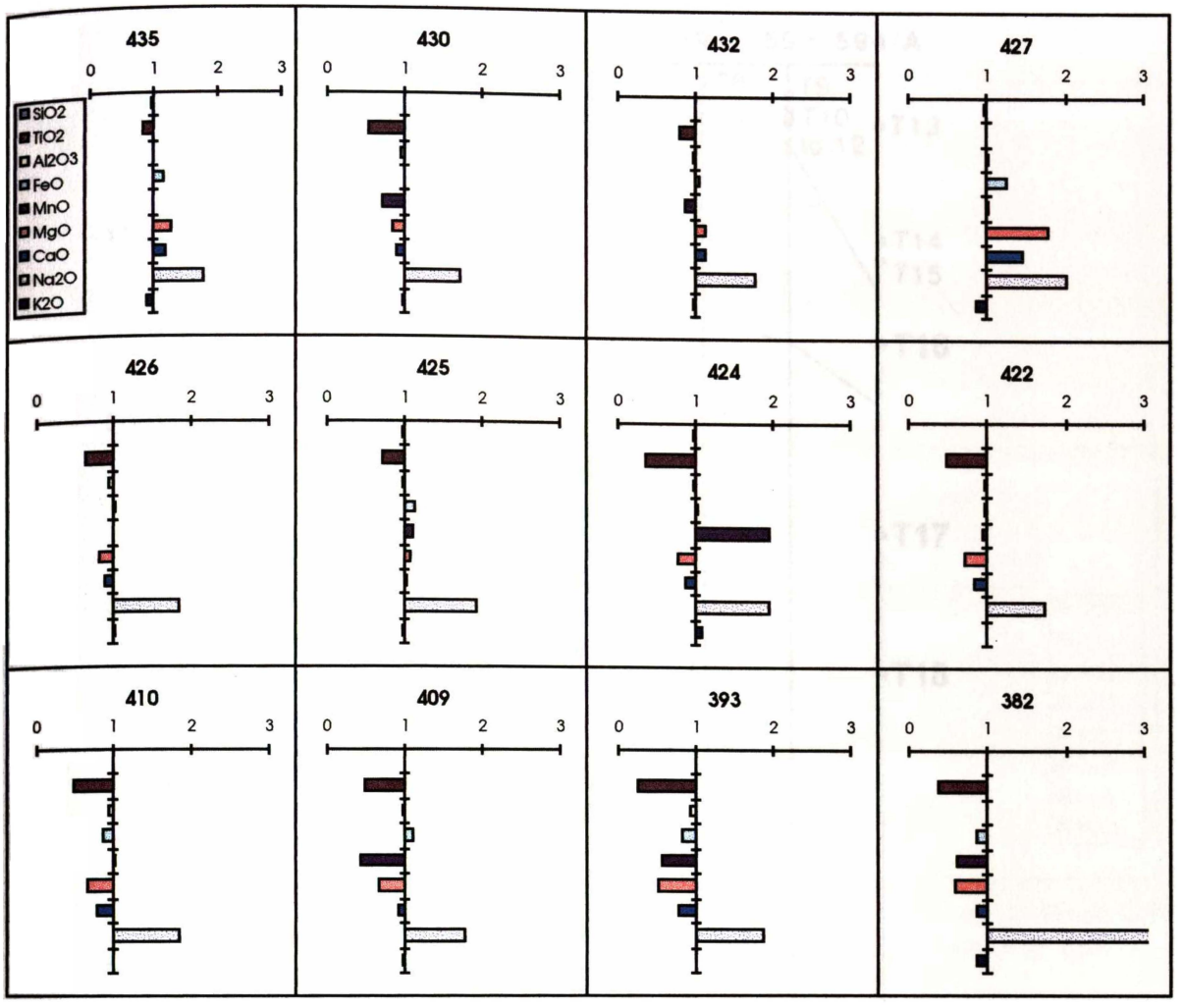


Figure 5.23 Mahia Peninsula tephras compared with WES ignimbrite glass shards. Tephra glass shard chemistry from P. Shane (pers comm. 1998).

***DSDP Leg 90***

18 thin (1-10 cm) megascopic vitric tephras of Neogene age were observed in cores drilled during Leg 90 of the Deep Sea Drilling Project (DSDP) (Nelson et al., 1986). Tephras are mainly rhyolitic (74-78 wt. % $SiO_2$) except for tephras T1-T3 which are basaltic. Glass shards are abundant, and minor felsic and mafic crystals also occur. Altered lithic fragments and pyrite were present in some tephras. The occurrence and relative age of tephras is indicated in Figure 5.24.

Major element glass chemistry was determined for all 18 tephras. A comparison of the glass chemistry of silicic Miocene-Pliocene tephras from Sites 590B, 591 and 594 with WES ignimbrite glass shard chemistry is illustrated in Figure 5.25. Most tephras show no or poor correlation to the WES composition. However, tephra T16 shows good correlation in all elements except $TiO_2$ and MgO, although it is of mid-Pliocene age. The mid-Pliocene age however, is questionable (C.S. Nelson pers comm.) because ages of T16 and other DSDP tephras were estimated using assumed constant rates of sedimentation, together with limited biostratigraphic or paleomagnetic age controls (Nelson et al., 1986). No radiometric ages for tephras have been determined.

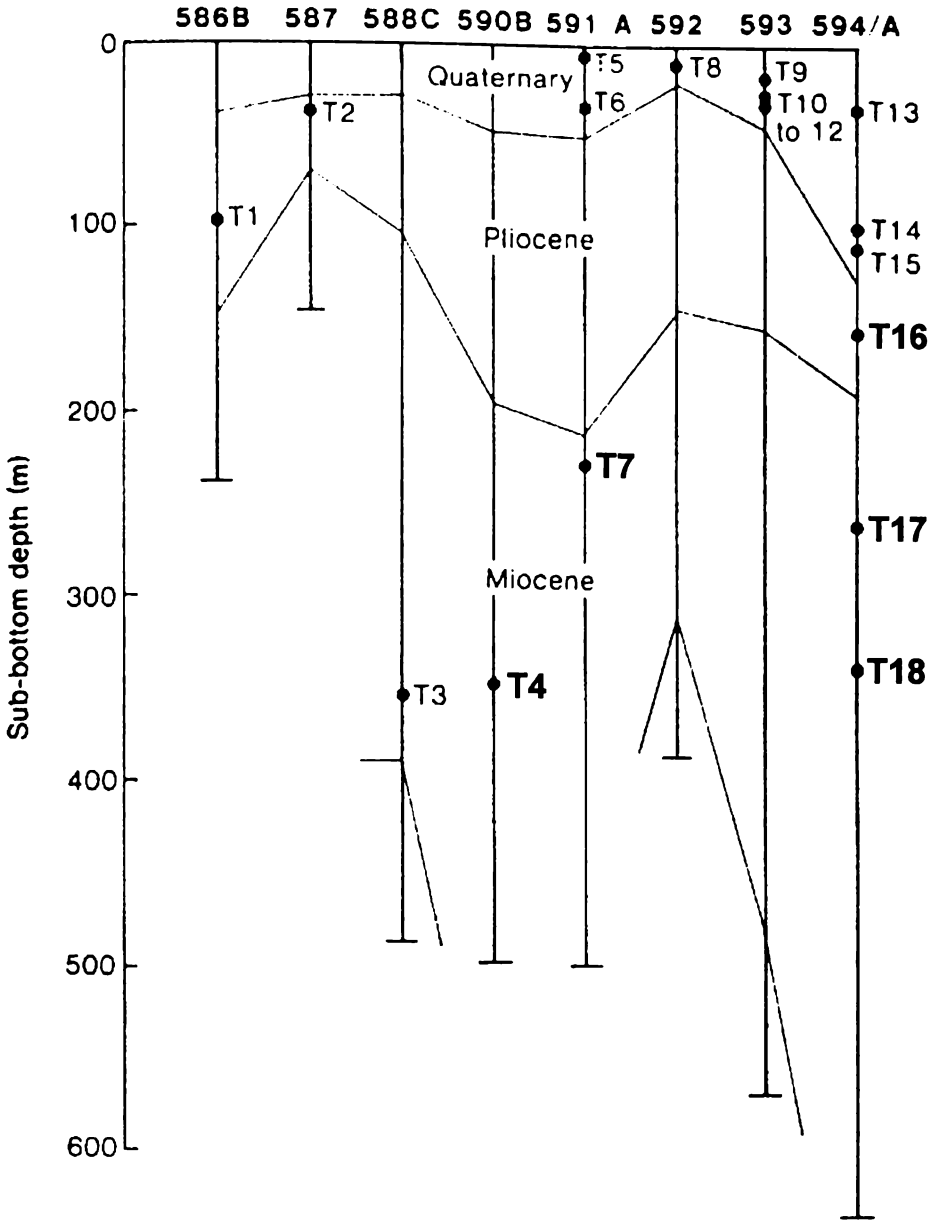


Figure 5.24 Megascopic tephras in DSDP Leg 90 cores. Adapted from Nelson et al. (1986).

***Correlations***

Any suggested correlations of WES ignimbrite to the three distal tephra localities is very much preliminary and requires more detailed geochemical and mineralogical analysis. Nevertheless, tentative correlations based on major element chemistry are inferred between WES ignimbrites and selected distal tephras observed at Tukemokihi Stream, Mahia Peninsula and sites 590B, 591 and 594 of DSDP Leg 90.

Tephras 425, 426, and 423 from the Mahia Peninsula section, T16 from DSDP Leg 90 Site 594A, and tephras G153, G266 and G267 from Tukemokihi Stream section have the closest compositions to WES glass shards (Figure 5.26). These tephras have a similar age to that of intracaldera WES of late Miocene to early Pliocene.

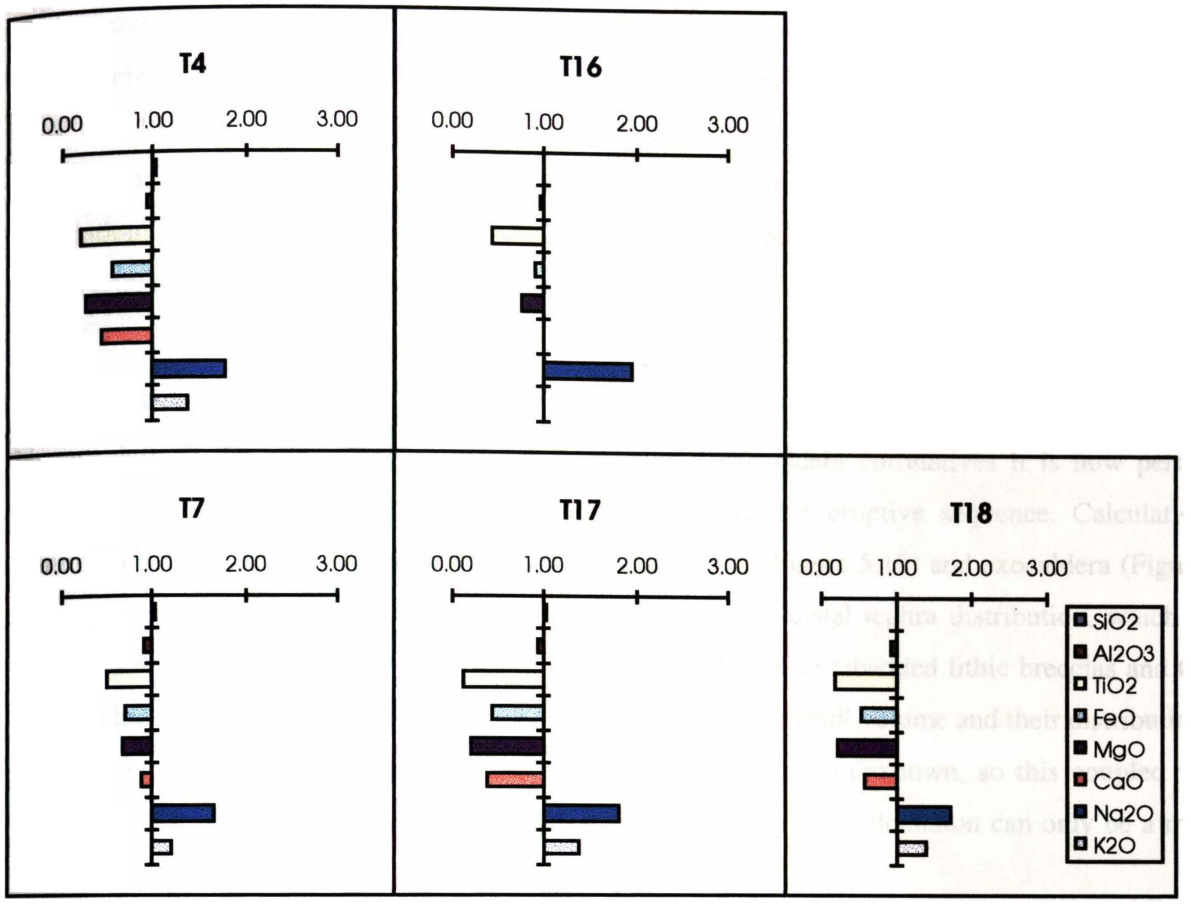


Figure 5.25 Comparison of WES glass shard major element chemistry with silicic Miocene-Pliocene tephras observed in DSDP Leg 90 cores. Tephra glass shard chemistry from Nelson et al. (1986).

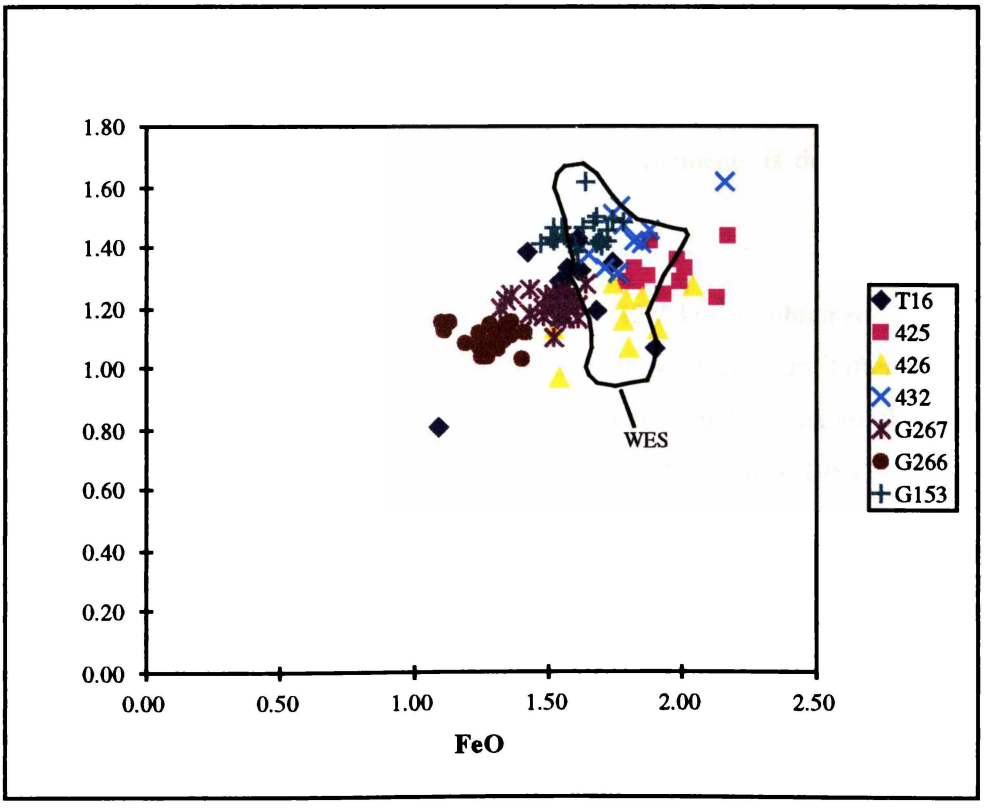


Figure 5.26 CaO-FeO plot of the closest matching Neogene tephra compositions compared with WES glass shard compositions. Field of WES glass shard compositions is indicated. Tephra data from Gosson (1986), Nelson et al. (1986), and P. Shane (pers comm. 1998).

To improve correlations, future work needs to utilise new geochemical analysis techniques (e.g. LA ICP-MS) to obtain trace element data, and establish additional tephra records including the recently drilled ODP Leg 181 cores. Ideally a dataset recording all geochemical and mineralogical data for distal tephras and compositions (preferably glass shards) of pyroclastic units in the CVZ should be established to enable correlations to be made. This record would be invaluable for reconstructing the CVZ explosive record of which only a small part is observable within the zone.

## 5.4 WES volume

Having defined the intracaldera distribution and revised exocaldera correlatives it is now pertinent to constrain the volume of magmatic material erupted during this eruptive sequence. Calculation of a minimum volume for the WES is based upon the intracaldera (Figure 5.16) and exocaldera (Figure 5.27) distribution of WES-1 and WES-4 Ignimbrites. It excludes the distal tephra distribution, which has not been established because correlations are, at best, only tentative. Interbedded lithic breccias and tuffs are also not included in the calculation because they represent a very small volume and their distribution is not well known. The amount of material eroded from the WES is also unknown, so this coupled with the exclusion of some interbedded units and distal tephra means that the calculation can only be a minimum estimate.

The average conservative thicknesses of WES-1 and WES-4 Ignimbrite are used to calculate the volume for a given intracaldera area. In the exocaldera region, the WES ignimbrites have not been distinguished, so the volume represents the total WES volume for a given thickness. Magmatic equivalent volume is then calculated using the ratio of ignimbrite density (average: 1.35 g $cm^{-3}$) to density of silicic magma (2.3 $cm^{-3}$) (Table 5.9). Finally the magma volume exclusive of lithic fragments is determined by assuming an average lithic abundance in WES ignimbrites of 10%.

From the calculation, a minimum estimated total volume of 42.7 $km^3$ is obtained (Table 5.9). Using a pyroclastic-magma ratio of 0.59, this equates to a magmatic volume of 22.7 $km^3$ (after 10% (i.e. 2.52 $km^3$) lithic fragment volume removed). Significantly, the exocaldera volume is larger than the intracaldera volume, which is similar compared with most caldera volcanoes (e.g. Lipman, 1984).

In the calculation, erosion has not been considered. Within the caldera WES must have infilled most of the valleys and submerged many of the lower lying rhyolite domes. Evidence for this is provided by the dissected WES ignimbrite plateaux which occur sporadically within the caldera and have elevations up to 400 m. Based on the present intracaldera distribution of WES ignimbrite plateaux, and the depth of valleys originally infilled by WES, perhaps up to half of the original intracaldera WES volume has been removed by erosion. The amount of exocaldera erosion may also be at a similar level, and therefore the calculated minimum volume of 42.7 $km^3$ may differ by a factor of 2, so that the true erupted volume may be closer to ca. 80-100 $km^3$.

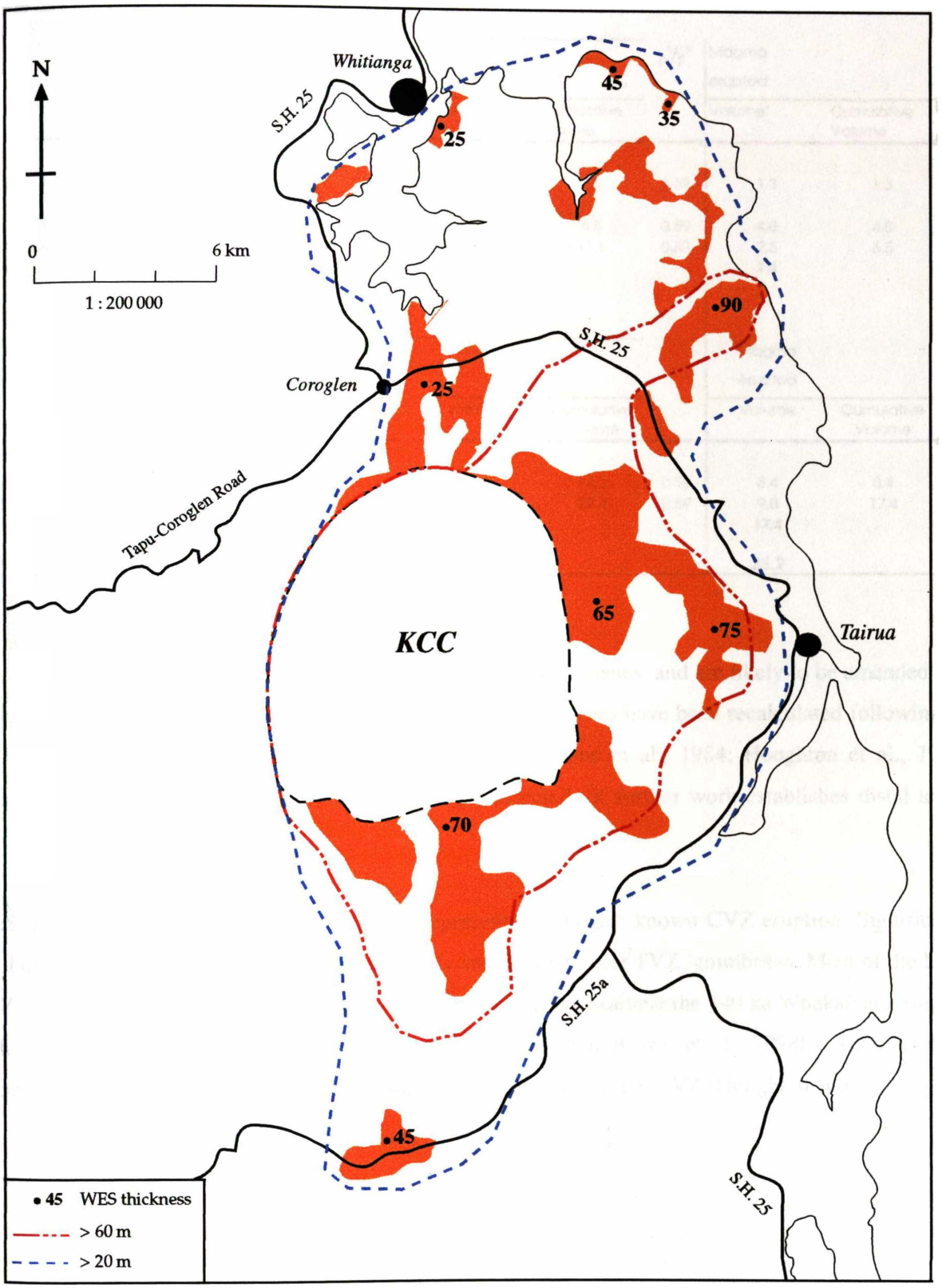


Figure 5.27 Isopach map of exocaldera correlative WES. Thickness data from this study and also from Adams (1992), Skinner (1993; 1995), and Karl (1996).

Table 5.9 Minimum volume calculation for the WES. $\rho^i/\rho^s$ = density of ignimbrite (mean: 1.35 g cm$^{-3}$)/ density of silicic magma (2.3 g cm$^{-3}$). * conservative average thickness used for volume calculation. + volume without lithic fragment volume deducted.

| **Intracaldera** | Area (km²) | | | Volume (km³) | | | | |
|---|---|---|---|---|---|---|---|---|
| | Area | Cumulative area | Th* (m) | Ignimbrite | | $\rho^i/\rho^s$ | Magma erupted | |
| | | | | Volume | Cumulative Volume | | Volume* | Cumulative Volume |
| Ignimbrite | | | | | | | | |
| WES-4 (>20m) | 73.6 | 73.6 | 30 | 2.2 | 2.2 | 0.59 | 1.3 | 1.3 |
| WES-1 (>50m) | 90.9 | 90.9 | 75 | 6.8 | 6.8 | 0.59 | 4.0 | 4.0 |
| WES-1 (>200m) | 15.7 | 106.6 | 275 | 4.3 | 11.1 | 0.59 | 2.5 | 6.5 |
| **Subtotal** | | | | **13.3** | | | **7.8** | |
| **Exocaldera** | Area (km²) | | | Volume (km³) | | | | |
| | Area | Cumulative area | Th* (m) | Ignimbrite | | | Magma erupted | |
| | | | | Volume | Cumulative Volume | | Volume | Cumulative Volume |
| Isopach | | | | | | | | |
| WES (>20m) | 405.9 | 405.9 | 35 | 14.2 | 14.2 | 0.59 | 8.4 | 8.4 |
| WES (>60m) | 202.9 | 608.8 | 75 | 15.2 | 29.4 | 0.59 | 9.0 | 17.4 |
| **Subtotal** | | | | **29.4** | | | **17.4** | |
| **TOTAL** | | | | **42.7** | | | **25.2** | |

It is important to appreciate that pyroclastic volumes are only estimates, and are likely to be amended over time. For example most early volume estimates for TVZ ignimbrites have been recalculated following the acquisition of new data or different interpretations (e.g. Wilson et al., 1984; Houghton et al., 1995). Therefore, this estimated volume is likely to change, especially if further work establishes distal tephra correlations.

WES is the most widespread CVZ unit and it represents the largest known CVZ eruption. Significantly this largest CVZ ignimbrite volume is considerably smaller than most TVZ ignimbrites. Most of the larger TVZ eruptions are in fact up to an order of magnitude larger, for example the 340 ka Whakamaru eruption with an estimated volume of 1000 km$^3$ (Houghton et al., 1995; Brown et al., 1998b). Small eruptive volumes relate to smaller caldera volcanoes in the CVZ compared to the TVZ (Houghton et al., 1995).

# Chapter Six

# PETROGRAPHY AND MINERALOGY OF KCC VOLCANIC ROCKS

## 6.1 Introduction

The intracaldera KCC geology is dominated by andesitic-rhyolitic pyroclastic deposits, lava domes and flows. Pre-caldera geology consists of andesitic-dacitic lava flows and dikes. This chapter documents the petrography and mineralogy of the caldera and pre-caldera lithologies. Petrological processes identified during petrographic and mineralogical studies are applied together with geochemical data (Chapter 7) to constrain the petrogenesis of erupted units.

Petrographic descriptions are augmented by modal mineral data and mineral chemistry for selected units. Modal data are based on 500 total point counts using a SWIFT point counter. Mineral analyses were obtained using a Jeol 733 Electron Microprobe at the Analytical Facility, Victoria University, Wellington. Elemental analysis was undertaken using an accelerating potential of 15kV, and beam current of 12 nA.

## 6.2 Petrography

### Andesite Lavas

Three andesitic to dacitic formations are present within the pre-caldera succession at the KCC: Maumaupaki Formation, Taurahuehue Andesite and Tapuaetahi Andesite. A caldera-related andesitic-dacitic formation (Taurauikau Andesite) was erupted sporadically during dominantly silicic volcanism at the KCC. Taurahuehue Andesite and Taurauikau Andesite have a similar two-pyroxene mineralogy, but the other formations have additional phases including amphibole, biotite and quartz (Figure 6.1). Modal mineral variations occur within all formations (Table 6.1).

*Maumaupaki Formation*

Maumaupaki Formation consists of andesite and lesser dacite lavas. Lavas are grey, hypocrystalline, medium grained, phaneritic and porphyritic. Phenocrysts (40 %) consist of plagioclase, amphibole, clinopyroxene, orthopyroxene, biotite, quartz, and Fe-Ti oxides. Phenocrysts occasionally occur as glomerocrysts of plagioclase, clinopyroxene and orthopyroxene.

Plagioclase phenocrysts (2.5 mm max.) are subhedral, prismatic or tabular and are typically embayed. Oscillatory zonation and polysynthetic twinning is common. Amphibole phenocrysts (3.7 mm max.) are subhedral, prismatic or stubby prismatic, and usually dark brown-dark green hornblende. Clinopyroxene phenocrysts (1.8 mm max.) are subhedral and tabular. Orthopyroxene phenocrysts (1.5 mm max.) are subhedral, prismatic and weakly pleochroic. Biotite (0.7 mm max.) is subhedral, flaky, and pleochroic from dark brown to pale yellow-brown. Quartz phenocrysts (1.6 mm max.) are anhedral, equant with

strongly embayed margins, and only occur in dacitic lavas. Fe-Ti oxides consist of titanomagnetite (anhedral, equant) and ilmenite (anhedral, prismatic).

Groundmass is typically very fine intersertal with interstitial amphibole, orthopyroxene, and Fe-Ti oxides in andesite lavas, although glassy or hyalopilitic textures can also occur.

***Taurahuehue Andesite***

Taurahuehue Andesite consists of grey, hypocrystalline, medium grained, porphyritic andesite lava. Phenocrysts (28 %) consist of plagioclase ($An_{59-85}$), orthopyroxene ($En_{61-70}$), clinopyroxene ($Wo_{41-45}$ $En_{40-48}$ $Fs_{9-19}$) and Fe-Ti oxides. Single, discrete phenocrysts are common, but may also occur as glomerocrysts of (i) orthopyroxene and clinopyroxene; and (ii) plagioclase.

Plagioclase phenocrysts (3.6 mm max.) are subhedral, prismatic or tabular. Compositional zonation is highly variable and includes normal, reversed, and oscillatory zoned phenocrysts, typically all within the same lava. Orthopyroxene, clinopyroxene, glass blebs, zircon and Fe-Ti oxide inclusions are common, but their abundance is highly variable. Orthopyroxene phenocrysts (3.5 mm max.) are subhedral, prismatic or stubby prismatic, and typically contain Fe-Ti oxide inclusions. Clinopyroxene phenocrysts (3.75 mm max.) are subhedral, prismatic, fragmented and contain inclusions of plagioclase, orthopyroxene and Fe-Ti oxides. In some lavas, orthopyroxene and clinopyroxene phenocrysts exhibit a partial or complete rim of very fine grained, pyroxene crystals. Fe-Ti oxide phenocrysts (0.5 mm max.) consist of anhedral, equant titanomagnetite and anhedral, prismatic ilmenite.

Groundmass is fine grained, pilotaxitic, hyalopilitic, or rarely intergranular, and contains variable abundances of plagioclase, pyroxene, zircon and Fe-Ti oxide crystals. Undifferentiated clays occur in some lavas within the groundmass or phenocryst fractures.

***Tapuaetahi Andesite***

Tapuaetahi Andesite consists of grey, hypocrystalline, medium phaneritic, porphyritic andesite and dacite lavas. Phenocrysts (35-40 %) consist of plagioclase ($An_{41-72}$), quartz, orthopyroxene ($En_{63-83}$), clinopyroxene ($Wo_{40-44}$ $En_{45-51}$ $Fs_{8-15}$), rare biotite ($Mg\#_{54-62}$) and Fe-Ti oxides.

Plagioclase phenocrysts (3 mm max.) are euhedral to subhedral, prismatic or tabular and many exhibit resorbed margins. Normal and oscillatory compositional zonation and polysynthetic twinning is common. Quartz phenocrysts (1.1 mm max.) are anhedral and equant, and typically exhibit strongly resorbed and embayed margins. Orthopyroxene phenocrysts (2.25 mm max.) are subhedral and prismatic. Clinopyroxene phenocrysts (0.25 mm max.) are typically subhedral and stubby prismatic. Biotite phenocrysts (1.5 mm max.) are subhedral, tabular or prismatic and typically corroded. Fe-Ti oxide phenocrysts (0.75 mm max.) consist of anhedral, equant titanomagnetite and ilmenite.

Groundmass is intersertal with devitrified interstitial glass and Fe-Ti oxides. Minor interstitial orthopyroxene and clinopyroxene crystals can also occur. Undifferentiated clays, produced by incipient weathering, infill fractures in some phenocrysts, or occur as irregular patches in the groundmass of some lavas.

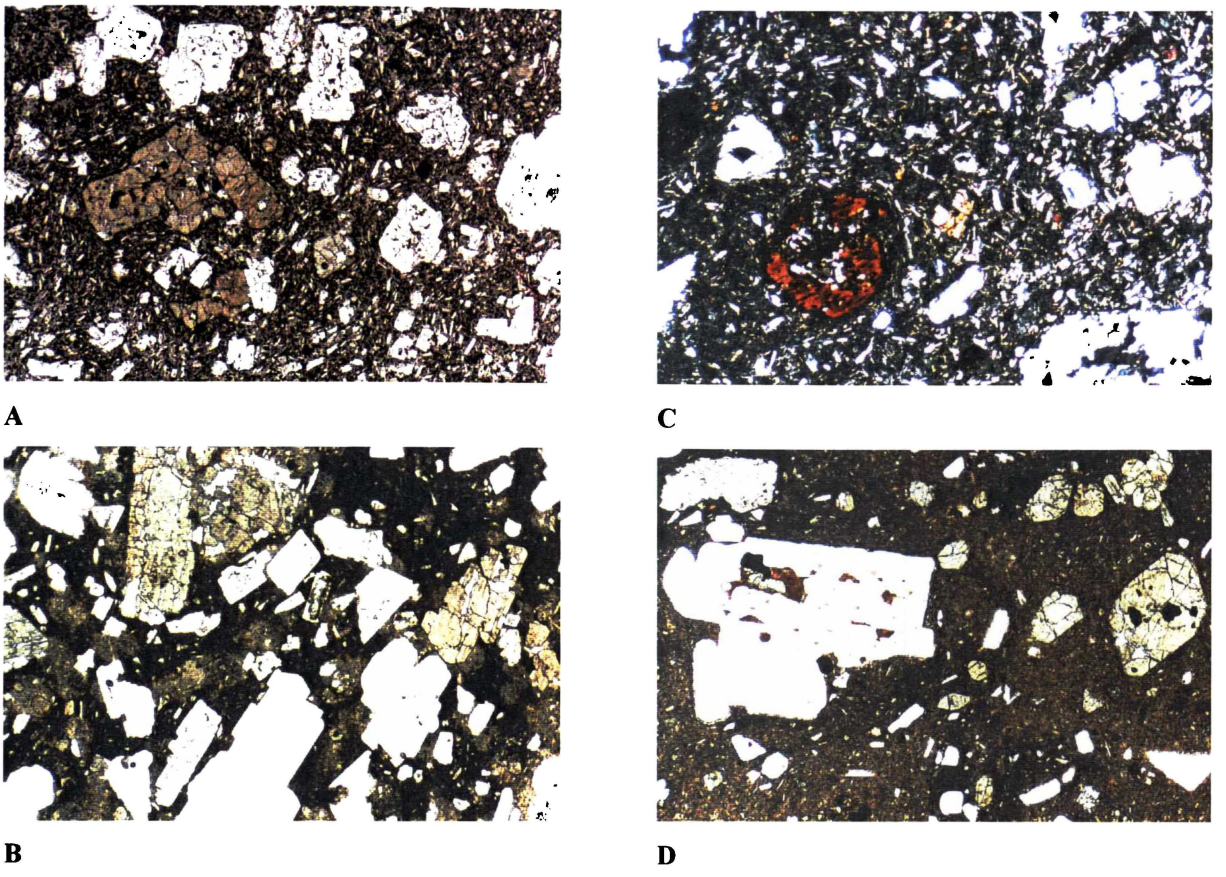


Figure 6.1 Photomicrographs of pre-caldera and caldera-related andesite lavas of the Kapowai Caldera Complex. A, Taurahuehue Andesite with plagioclase, orthopyroxene and clinopyroxene phenocrysts set in an intergranular groundmass (W99601). B, Taurahuehue Andesite with abundant phenocrysts of plagioclase, orthopyroxene and clinopyroxene set in a hyalopilitic groundmass (W99685). C, Tapuaetahi Andesite with strongly resorbed biotite and plagioclase phenocrysts set in an intergranular groundmass (W99951). D, Taurauikau Andesite with sieved and embayed plagioclase, orthopyroxene and clinopyroxene phenocrysts in a hyalopilitic groundmass (W99641). Field of view is 4 mm across.

### *Taurauikau Andesite*

Taurauikau Andesite consists of light grey, hypocrystalline, medium grained, porphyritic andesite lava. Phenocrysts (40-44 %) consist of plagioclase ($An_{47-57}$), orthopyroxene ($En_{61-75}$), clinopyroxene ($Wo_{42-45}$ $En_{40-42}$ $Fs_{16-17}$) and Fe-Ti oxides. Discrete, single phenocrysts occur as well as glomerocrysts of (i) plagioclase; and (ii) orthopyroxene and clinopyroxene.

Table 6.1 Modal mineralogy for selected pre-caldera and caldera-related andesite-dacite lavas.

| | Maumaupaki Formation | Tourahuehue Andesite | | | Tapuaetahi Andesite | | Tauraukau Andesite | | |
|---|---|---|---|---|---|---|---|---|---|
| | W991016 | W99601 | W99691 | W99692 | W99877 | W99951 | W99816 | W99796 | W99732 |
| **Phenocrysts** | | | | | | | | | |
| Plagioclase | 23.2 | 22.0 | 24.4 | 40.6 | 33.0 | 20.0 | 26.8 | 26.0 | 32.2 |
| Orthopyroxene | 3.2 | 2.6 | 9.2 | 4.6 | 7.3 | 4.0 | 9.2 | 6.3 | 5.4 |
| Clinopyroxene | 4.1 | 3.0 | 1.2 | 5.3 | 6.3 | | 7.2 | 3.6 | 2.4 |
| Amphibole | 8.6 | | | | | | | | |
| Biotite | | | | | | 3.4 | | | |
| Fe-Ti oxides (>0.05mm) | 1.5 | | 0.2 | 1.6 | 1.0 | | | 1.3 | 0.2 |
| Quartz Xenocrysts | 0.5 | | | | | | | | |
| **Total** | **41.1** | **27.6** | **35.0** | **52.1** | **47.6** | **37.8** | **43.2** | **37.2** | **40.2** |
| | | | | | | | | | |
| **Secondary Minerals** | | | | | | | | | |
| Undifferentiated clays | | | | | 7.6 | 10.4 | | 10.0 | |
| | | | | | | | | | |
| **Groundmass** | | | | | | | | | |
| Glass | 16.5 | 29.2 | 57.2 | 7.0 | 18.6 | 9.2 | 1.8 | 5.6 | 31.6 |
| Plagioclase laths | 35.7 | 21.0 | 6.8 | 22.3 | 22.6 | 37.4 | 50.8 | 27.3 | 9.0 |
| Granular Pyroxenes | 2.1 | 2.2 | | 6.0 | 1.0 | | | 9.3 | 0.4 |
| Fe-Ti oxides (<0.05mm) | 4.6 | 20.0 | 1.0 | 12.6 | 2.6 | 5.2 | 4.2 | 10.6 | 1.8 |
| Devitrified glass patches | | | | | | | | | 17.0 |
| **Total** | **58.9** | **72.4** | **65.0** | **47.9** | **44.8** | **51.8** | **56.8** | **52.8** | **59.8** |
| | | | | | | | | | |
| **TOTAL** | **100.0** | **100.0** | **100.0** | **100.0** | **100.0** | **100.0** | **100.0** | **100.0** | **100.0** |

Plagioclase phenocrysts (7.5 mm max.) are subhedral, prismatic or tabular. Compositional zonation is highly variable with most lavas containing a mixed population of normal, reverse, and oscillatory zoned phenocrysts. Twinning is also variable ranging from simple to polysynthetic. Zircon, glass, Fe-Ti oxides and pyroxene inclusions are common. Orthopyroxene phenocrysts (2.25 mm max.) are subhedral and prismatic, and most phenocrysts contain glass, plagioclase and Fe-Ti oxide inclusions. Some orthopyroxene phenocrysts are rimmed by very fine grained clinopyroxene crystals. Clinopyroxene phenocrysts (3.2 mm max.) are subhedral, tabular or stubby prismatic, and usually contain Fe-Ti oxide inclusions. Fe-Ti oxide phenocrysts (0.5 mm max.) consist of anhedral, equant titanomagnetite and ilmenite.

Groundmass is very fine, occasionally pilotaxitic and includes intergranular (orthopyroxene, clinopyroxene and Fe-Ti oxide crystals) and hyalopilitic varieties. Undifferentiated clays (produced from weathering), occur as irregular patches in the groundmass and occasionally infill fractures in some phenocrysts.

## Rhyolite lavas

Rhyolite lavas erupted at the KCC are divided into one of four rhyolite lava groups based on phenocryst mineralogy (Figure 6.2). These are group I (plagioclase-pyroxene phyric), group II (quartz-plagioclase-biotite phyric), group III (plagioclase-phyric), and group IV (plagioclase-amphibole phyric) rhyolite lavas. The petrology of each group is presented here. Apart from phenocryst variations, each rhyolite group also exhibits variations in modal mineralogy (Table 6.2 and 6.3).

### *Group I*

Group I rhyolite lavas are defined as plagioclase-pyroxene phyric rhyolite lavas. This is the dominant intracaldera rhyolite lava group at the KCC. Kapowai rhyolite lavas are typically light grey, fine grained, phaneritic and porphyritic. Phenocrysts (6-32 %) consist of plagioclase ($An_{21-62}$), orthopyroxene ($En_{44-63}$), clinopyroxene ($Wo_{41-43}$ $En_{42-43}$ $Fs_{15-20}$) and Fe-Ti oxides.

Plagioclase phenocrysts (3.2 mm max.) are subhedral, prismatic or tabular and typically contain zircon, Fe-Ti oxide and glass inclusions. Oscillatory or normal compositional zonation is present in some phenocrysts. Orthopyroxene phenocrysts (1.5 mm max.) are subhedral, prismatic and commonly contain Fe-Ti oxide inclusions. Clinopyroxene phenocrysts (0.75 mm max.) are subhedral, prismatic or tabular. Fe-Ti oxide phenocrysts (0.8 mm max.) are anhedral, equant titanomagnetite or subhedral, prismatic ilmenite.

Groundmass is very fine grained, devitrified and hyalopilitic. Macro- and micro-spherulites are common. Amygdules occur in some lavas, and infilling minerals include quartz, tridymite, biotite, and Fe-Ti oxides. Undifferentiated clays, produced from weathering, are present in some lavas, and occur as irregular patches in the groundmass, and occasionally within phenocryst fractures.

*Group II*

Group II rhyolite lavas are defined as quartz-plagioclase-biotite phyric rhyolite lavas. Group II lavas are light grey-grey, medium grained, phaneritic, and porphyritic. Phenocrysts (12-16 %) consist of quartz, plagioclase ($An_{26-37}$), biotite ($Mg\#_{25-43}$) and minor Fe-Ti oxides. Phenocrysts occur as discrete crystals or infrequently as glomerocrysts.

Quartz phenocrysts (1.25 mm max.) are anhedral, equant and commonly have embayed margins. Plagioclase phenocrysts (3.5 mm max.) are subhedral, prismatic or tabular. Oscillatory and normal compositional zonation is common. Some phenocrysts contain re-melted glass and Fe-Ti oxide inclusions. Biotite phenocrysts (1.25 mm max.) are subhedral, prismatic or stubby prismatic. Fe-Ti oxide phenocrysts (0.4 mm max.) are anhedral, equant titanomagnetite (typically with embayed margins), and subhedral, prismatic ilmenite. Accessory zircon crystals are rarely observed in thin section, although significant zircon crystals have been separated (using SPT heavy liquid) from the bulk rock. Of the constituent lavas, Ruahine Rhyolite has the highest zircon abundance (ca. 0.25-0.5 %) in this group, and also of all rhyolite lavas.

Groundmass is very fine, devitrified and hyalopilitic or pilotaxitic. Macro- and micro-spherulites occur in some lavas. Amygdules occur in some lavas, and infilling minerals include quartz, tridymite, biotite, and Fe-Ti oxides.

*Group III*

Group III rhyolite lavas are defined as plagioclase phyric rhyolite lavas. No ferromagnesian phenocrysts occur. Group III rhyolite lavas are typically light grey, fine grained, phaneritic, and porphyritic. Phenocrysts (5-6 %) consist of plagioclase ($An_{36-45}$) and minor Fe-Ti oxides. Phenocrysts occur as discrete crystals or in glomeroporphyritic clots.

Plagioclase phenocrysts (1.6 mm max.) are subhedral, stubby prismatic or euhedral, and display simple or polysynthetic twinning. Compositional zonation is variable and mixed populations of oscillatory and normal zoned phenocrysts are common. Some plagioclase phenocrysts contain glass and Fe-Ti oxide inclusions. Fe-Ti oxide phenocrysts (0.5 mm max.) are anhedral, equant titanomagnetite and subhedral, prismatic ilmenite.

Groundmass is very fine, devitrified, and hyalopilitic with microlites of plagioclase and Fe-Ti oxides.

*Group IV*

Group IV rhyolite lavas are defined as plagioclase-amphibole phyric rhyolite lavas. Group IV lavas are light grey, fine grained, phaneritic, and porphyritic. Phenocrysts (14-25 %) consist of plagioclase ($An_{47-53}$), amphibole ($Mg\#_{40-53}$), and Fe-Ti oxides. Phenocrysts occur as single, discrete crystals, and glomerocrysts are rare.

Table 6.2 Modal mineralogy for selected Group I rhyolite lavas of the Kapowai Caldera Complex.

| | Waiwhatawhata Rhyolite | Big Beetle Rhyolite | Kapowai Rhyolite | Precipice Rhyolite | Kokonga Rhyolite | Taurauniikau Rhyolite | Kauaeranga Rhyolite | Camp Rhyolite | Pinnacles Rhyolite | Atuatumoe Rhyolite | Bulls Run Rhyolite | Kydd Rhyolite |
|---|---|---|---|---|---|---|---|---|---|---|---|---|
| | W99623 | W99839 | W99894 | W99912 | W99989 | W99865 | W99876 | W99994 | W99995 | W991008 | W99746 | W99918 |
| **Phenocrysts** | | | | | | | | | | | | |
| Plagioclase | 6.2 | 10.4 | 29.2 | 17.4 | 6.8 | 10.8 | 7.6 | 12.0 | 14.8 | 7.8 | 9.0 | 5.6 |
| Quartz | | | | | | | | | | | | |
| Orthopyroxene | | | 2.2 | 0.2 | 0.4 | | | 1.8 | | 0.4 | | 0.2 |
| Clinopyroxene | | | | 0.4 | | | 0.8 | | 0.6 | | | |
| Amphibole | | | | | | | | | | | | |
| Biotite | | | | | | | | | | | | |
| Fe-Ti oxides (>0.05mm) | 0.2 | 0.2 | 1.0 | 0.6 | 0.2 | 0.4 | 0.6 | 0.8 | 1.0 | 1.0 | 2.0 | |
| **Total Phenocrysts** | **6.4** | **10.6** | **32.4** | **18.6** | **7.4** | **11.2** | **9.0** | **14.6** | **16.4** | **9.2** | **11.0** | **5.8** |
| | | | | | | | | | | | | |
| **Groundmass** | | | | | | | | | | | | |
| Devitrified glass | 84.2 | 84.0 | 56.8 | 78.4 | 89.4 | 79.8 | 91.0 | 85.4 | 81.4 | 71.6 | 48.8 | 72.6 |
| Plagioclase | 3.4 | 3.4 | 1.0 | 0.2 | 0.6 | 3.0 | | | 0.6 | 5.3 | 22.6 | |
| Fe-Ti oxides (<0.05mm) | | 1.4 | | | | | | | | 2.0 | | 2.3 |
| Tridymite | | | 1.8 | 2.8 | 0.4 | 4.2 | | | | 10.6 | | 19.3 |
| Undifferentiated clays | 6.0 | 0.6 | 8.0 | | | | | | 1.6 | 1.3 | 7.0 | |
| Glass | | | | | | 1.8 | | | | | 10.6 | |
| Vesicles | | | | | 2.2 | | | | | | | |
| **Total Groundmass** | **93.6** | **89.4** | **67.6** | **81.4** | **92.6** | **88.8** | **91.0** | **85.4** | **83.6** | **90.8** | **89.0** | **94.2** |
| | | | | | | | | | | | | |
| **TOTAL** | **100.0** | **100.0** | **100.0** | **100.0** | **100.0** | **100.0** | **100.0** | **100.0** | **100.0** | **100.0** | **100.0** | **100.0** |

Table 6.3 Modal mineralogy for selected Group II-IV rhyolite lavas of the Kapowai Caldera Complex.

| | Welcome Jack Rhyolite | | Ruahine Rhyolite | | Scots Rhyolite | Acadia Rhyolite | Rangihau Rhyolite | Slip Rhyolite | Miller Flat Rhyolite | |
|---|---|---|---|---|---|---|---|---|---|---|
| **Rhyolite Group** | II | II | II | II | II | III | III | IV | IV | IV |
| | W99834 | W99807 | W991005 | W991015 | W991006 | W99725 | W99600 | W99788 | W99976 | W99902 |
| **Phenocrysts** | | | | | | | | | | |
| Plagioclase | 6.4 | 6.6 | 6.4 | 4.1 | 9.3 | 5.2 | 5.4 | 11.2 | 13.0 | 23.3 |
| Quartz | 7.8 | 4.5 | 7.8 | 9.2 | | | | | | |
| Orthopyroxene | | | | | | | | | | |
| Clinopyroxene | | | | | | | | | | |
| Amphibole | | | | | | | | 1.0 | 3.0 | 1.3 |
| Biotite | 2.6 | 3.3 | 2.2 | 2.2 | 4.0 | | | | | |
| Fe-Ti oxides (>0.05mm) | 0.2 | | | | | 0.2 | 0.4 | 1.6 | 0.6 | |
| **Total Phenocrysts** | **16.8** | **14.4** | **16.4** | **15.5** | **13.3** | **5.4** | **5.8** | **13.8** | **16.6** | **24.6** |
| **Groundmass** | | | | | | | | | | |
| Devitrified glass | 83.2 | 84.0 | 80.2 | 81.5 | 85.7 | 78.8 | 84.2 | 82.0 | 71.3 | 53.9 |
| Plagioclase lath | | 1.6 | | | 1.0 | 4.2 | 6.6 | 2.4 | 9.5 | 13.3 |
| Tridymite | | | 3.4 | | | 7.6 | 3.4 | 1.4 | | 5.6 |
| Cristobalite | | | | | | 0.4 | | | | |
| Fe-Ti oxides (<0.05mm) | | | | 3.0 | | 3.6 | | 0.4 | 2.6 | 2.6 |
| **Total Groundmass** | **83.0** | **85.6** | **83.6** | **87.9** | **86.7** | **94.6** | **94.2** | **86.2** | **83.4** | **75.4** |
| **TOTAL** | **100.0** | **100.0** | **100.0** | **100.0** | **100.0** | **100.0** | **100.0** | **100.0** | **100.0** | **100.0** |

Plagioclase phenocrysts (3.1 mm max.) are subhedral, prismatic or tabular and some contain Fe-Ti oxide and glass inclusions. Compositional zoning is complex and populations of reverse, normal and oscillatory zoned plagioclase phenocrysts are common. Amphibole (1.4 mm max.) phenocrysts are subhedral, tabular or prismatic, dark green to brown pleochroic hornblende with some exhibiting lamellar twins. Fe-Ti oxides (0.3 mm max.) are anhedral, equant titanomagnetite, typically with embayed margins.

Groundmass is typically very fine, devitrified, flow banded, intersertal or pilotaxitic.

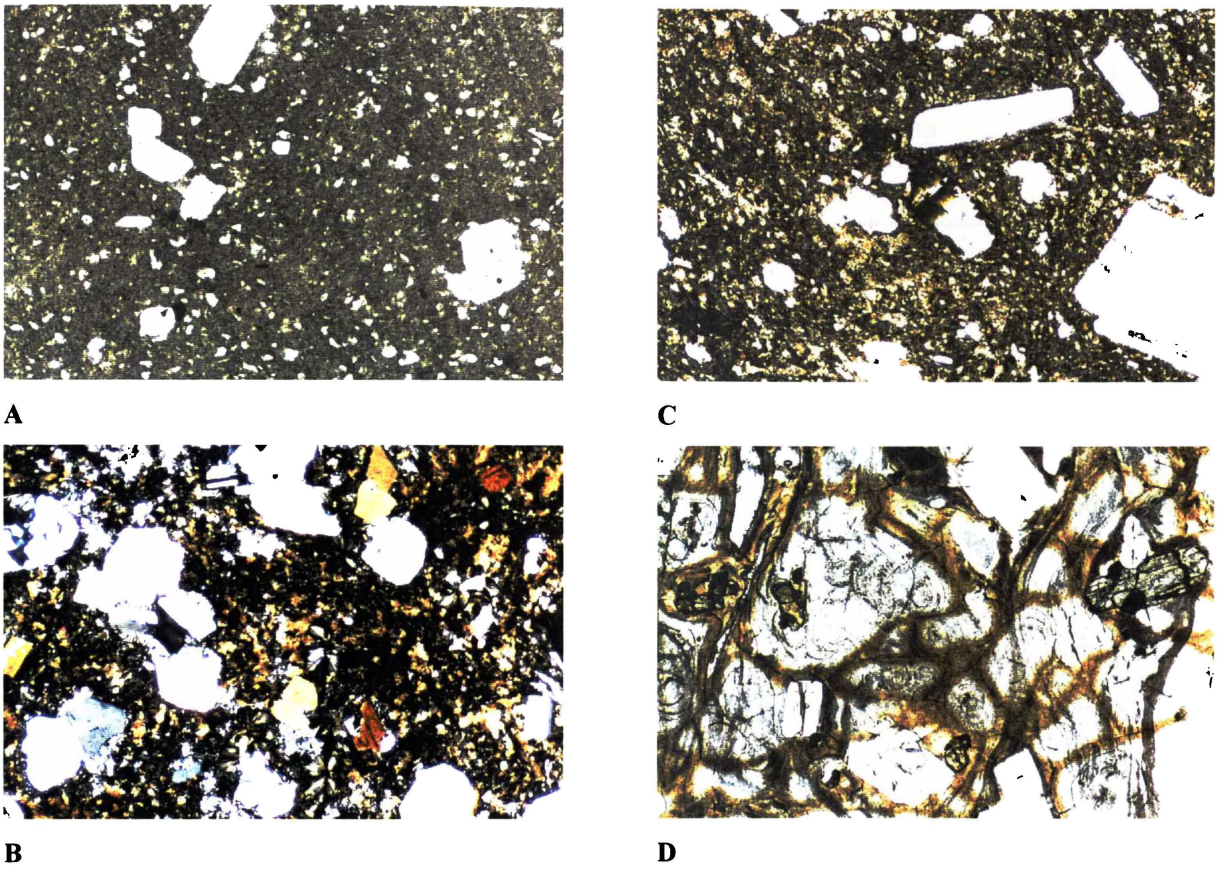


Figure 6.2 Photomicrographs of examples of the four Kapowai Caldera Complex rhyolite lava groups. A, Rangihau Rhyolite (group III) lava with phenocrysts of plagioclase set in a devitrified hyalopilitic groundmass (W99600). B, Welcome Jack Rhyolite lava (group II) with quartz, plagioclase, and biotite phenocrysts set in a hyalopilitic groundmass (W99806). C, Slip Rhyolite lava (group IV) with phenocrysts of plagioclase and hornblende set in a devitrified hyalopilitic groundmass (W99788). D, Precipice Rhyolite lava (group I) with phenocrysts of plagioclase, orthopyroxene and titanomagnetite set in a perlitic, glassy weakly devitrified groundmass (W99908). Field of view is 4 mm across.

## Ignimbrites

The petrography of the major KCC ignimbrites is presented here, except for the WES ignimbrites which are described separately in Chapter Five. Ignimbrites show significant variations in juvenile composition, morphology, and phenocryst mineralogy, matrix mineralogy (Table 6.4), and matrix texture.

Table 6.4 Modal componentry for selected Kapowai Caldera Complex ignimbrites.

| Ignimbrite | Webb Creek | | Trig Q | | Manuka | | Otoao |
|---|---|---|---|---|---|---|---|
| | W99693 | W99695 | W99988 | W99990 | W99890 | W99898 | W99612 |
| **Juvenile** | **42.3** | **14.0** | **22.6** | **28.3** | **34.6** | **51.6** | **21.3** |
| **Matrix Crystal** | | | | | | | |
| Plagioclase | 6.3 | 4.6 | 4.3 | 19.0 | 12.6 | 1.6 | 12.6 |
| Orthopyroxene | 0.2 | 0.6 | | | 0.3 | 1.3 | 3.0 |
| Clinopyroxene | | 0.3 | | | 0.3 | | 3.0 |
| Amphibole | | | | | | | |
| Biotite | | | | | | | |
| Fe-Ti oxides(>0.05mm) | 0.6 | 0.6 | 1.0 | 2.3 | | 1.6 | 0.3 |
| **Total Crystal** | **7.1** | **6.1** | **5.3** | **21.3** | **13.2** | **4.5** | **18.9** |
| **Lithic** | | | | | | | |
| Volcanic | | 12.3 | 1.6 | 2.6 | 3.0 | 2.0 | 3.0 |
| **Matrix** | | | | | | | |
| Glass Shard | 50.6 | 67.3 | 70.3 | 47.8 | 43.6 | 38.3 | 56.8 |
| Pumice Fragment | | 0.3 | 0.2 | | 5.6 | 3.6 | |
| **TOTAL** | **100.0** | **100.0** | **100.0** | **100.0** | **100.0** | **100.0** | **100.0** |

### *Webb Creek Ignimbrite*

Webb Creek Ignimbrite is light brown, pumice-rich and weakly welded (Figure 6.3). Juvenile clasts consist of light brown moderately fibrous, incipiently lenticular, incipiently vesicular, weakly porphyritic (<1 %) pumice. Phenocrysts consist of subhedral, prismatic plagioclase (0.75 mm max.), subhedral, stubby prismatic orthopyroxene (0.15 mm max.), euhedral, stubby prismatic zircon (< 0.05 mm), and anhedral equant or prismatic Fe-Ti oxides (0.05 mm max.).

Matrix crystals (6-7 %) consist of plagioclase, orthopyroxene, clinopyroxene, amphibole and Fe-Ti oxides. Plagioclase crystals (1.4 mm max.) are subhedral, prismatic or tabular. Normal and oscillatory zonation, polysynthetic twinning and sieve textures are common. Orthopyroxene crystals (0.75 mm max.) are subhedral and prismatic. Saw-toothed ends and Fe-Ti oxide inclusions occur in some crystals. Clinopyroxene crystals (0.4 mm max.) are subhedral and stubby prismatic. Amphibole crystals (0.75 mm max.) are subhedral, prismatic and pleochroic from green to yellow brown. Rare zircon crystals are very fine grained (< 0.05 mm), euhedral, and stubby prismatic. Fe-Ti oxide crystals (0.3 mm max.) are anhedral equant titanomagnetite.

The matrix is very fine grained, devitrified and has a poorly developed vitroclastic texture. Cuspate and platy glass shards are common.

### *Trig Q Ignimbrite*

Trig Q Ignimbrite is brown, crystal and pumice rich and weakly to partially welded (Figure 6.4). Juvenile clasts consist of brown, poor to moderately fibrous, incipiently to highly lenticular, incipiently to moderately vesicular, weakly porphyritic pumice. Phenocrysts (1 %) consist of plagioclase ($An_{43-44}$) (1.25 mm max.), rare zircon (< 0.05 mm) and Fe-Ti oxides (0.25 mm max.).

Matrix crystals (5-21 %) consist of plagioclase ($An_{48}$), orthopyroxene ($En_{76}$) and Fe-Ti oxides. Plagioclase crystals (1.0 mm max.) are subhedral, prismatic or tabular, and typically fragmented or broken. Reverse, normal, and oscillatory zonation, and polysynthetic twinning is common. Orthopyroxene crystals (0.25 mm max.) are subhedral and prismatic. Zircon crystals (<0.05 mm) are euhedral, stubby prismatic, and rare. Fe-Ti oxide crystals (0.2 mm max.) are anhedral equant titanomagnetite.

The matrix is very fine grained and devitrified, and varies from vitroclastic to glassy. Cuspate and platy shards are preserved in the weakly welded ignimbrite zone only (see Chapter 3).

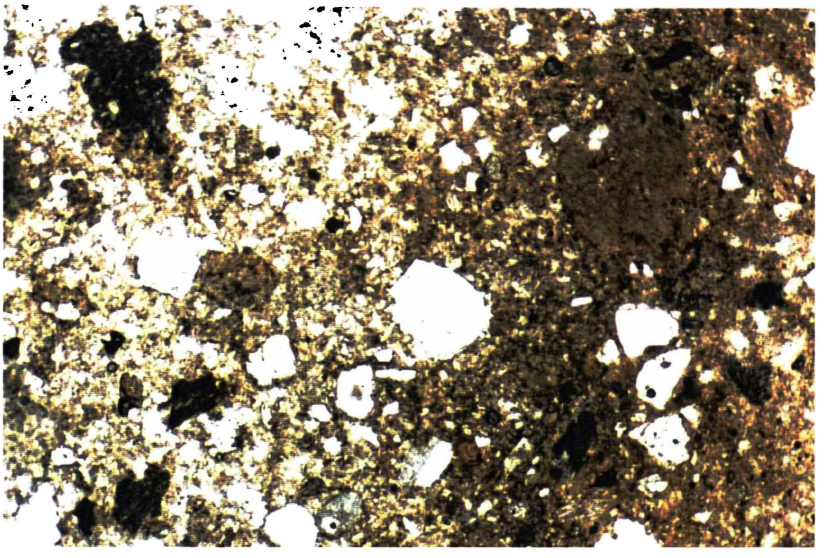

Figure 6.3 Photomicrograph of Webb Creek Ignimbrite (W99695). Note orthopyroxene and plagioclase crystals in matrix, and poorly developed relict vitroclastic matrix texture. Field of view is 4mm across.

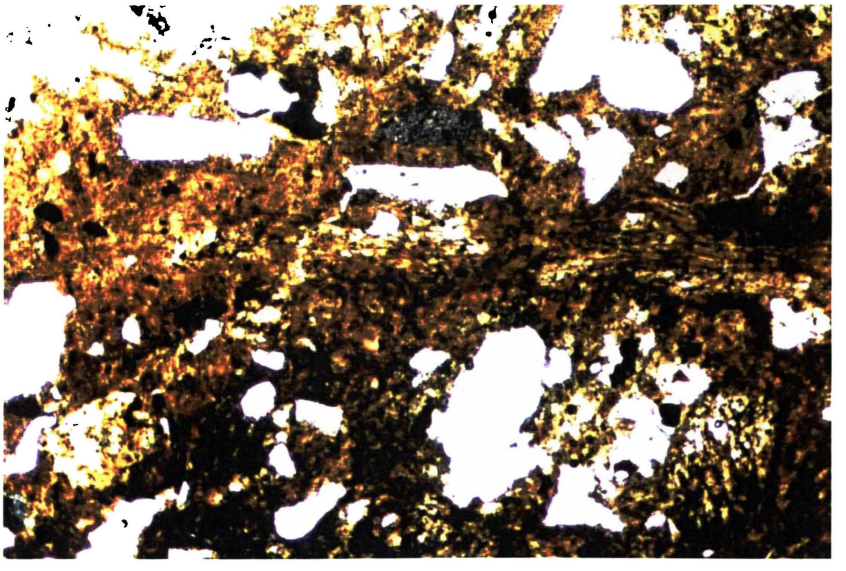

Figure 6.4 Photomicrograph of Trig Q Ignimbrite (W99989). Note lenticular pumice, abundant plagioclase crystals, and poorly developed vitroclastic matrix texture. Field of view is 4mm across.

***Manuka Ignimbrite***

Manuka Ignimbrite is light brown/pink, pumice-rich, lithic-rich, vapour phase altered and weakly welded (Figure 6.5). Juvenile clasts consist of cream, moderately fibrous, incipiently lenticular, moderately vesicular, weakly porphyritic pumice. Phenocrysts (1-3 %) consist of plagioclase (1.0 mm max.), amphibole (0.5 mm max.), and Fe-Ti oxides (0.25 mm max.).

Matrix crystals (5-13 %) consist of plagioclase, orthopyroxene, clinopyroxene, amphibole, and Fe-Ti oxides. Plagioclase crystals (1.6 mm max.) are subhedral, and tabular. Glass and Fe-Ti oxide inclusions are common. Orthopyroxene crystals (1.25 mm max.) are subhedral, stubby prismatic and typically have broken saw-tooth ends. Clinopyroxene (0.3 mm max.) crystals are subhedral, stubby prismatic. Amphibole crystals (0.3 mm max.) are subhedral, stubby prismatic green-brown hornblende. Fe-Ti oxide crystals (0.5 mm max.) consist of anhedral, equant titanomagnetite and anhedral, prismatic ilmenite. Embayed margins are common.

The matrix is very fine, devitrified, vapour phase altered, and has a relict vitroclastic texture. Occasional thin-walled, cuspate glass shards occur.

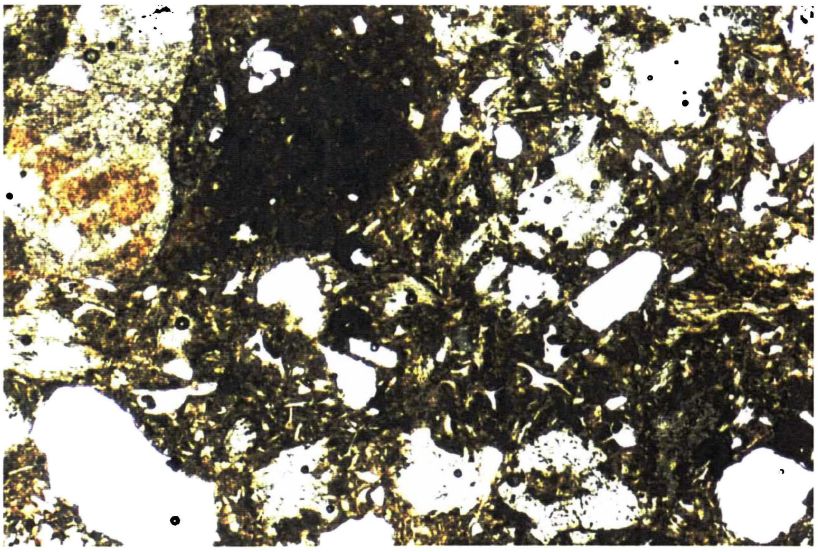

Figure 6.5 Photomicrograph of Manuka Ignimbrite (W99890). Note abundant volcanic lithic fragments and occasional cuspate glass shards. Field of view is 4mm across.

***Oteao Ignimbrite***

Oteao Ignimbrite is a scoria-rich, crystal-rich, weakly welded ignimbrite (Figure 6.6). Juvenile clasts consist of four types (scoria, pumice, mingled scoria-pumice and mixed scoria-pumice).

Scoria clasts are brown, moderately vesicular, poorly fibrous, incipiently lenticular, and moderately phyric. Phenocrysts (3-5 %) consist of subhedral, prismatic or tabular plagioclase ($An_{54-68}$) (1.0 mm max.), subhedral, prismatic orthopyroxene ($En_{51-66}$) (1.0 mm max.), subhedral, stubby prismatic clinopyroxene (0.25 mm max.), and anhedral, equant or prismatic Fe-Ti oxides (0.1 mm max.). Pumice clasts are light

brown, poorly vesicular, moderately fibrous, incipiently lenticular, and poorly phyric. Phenocrysts (1 %) consist of subhedral, prismatic or stubby prismatic plagioclase ($An_{33-38}$) (0.5 mm max.), subhedral, prismatic orthopyroxene ($En_{52-53}$) (0.3 mm max.), euhedral, stubby-prismatic zircon (< 0.05 mm), and anhedral, equant or prismatic Fe-Ti oxides (0.2 mm max.). Mingled scoria-pumice are grey/light brown streaked, moderately vesicular, poorly fibrous, moderately lenticular, and poorly phyric. Phenocrysts (1-3 %) consist of subhedral, tabular plagioclase (1.0 mm max.), subhedral prismatic orthopyroxene (0.75 mm max.), subhedral, stubby prismatic clinopyroxene (0.4 mm max.), and anhedral equant Fe-Ti oxides (0.2 mm max.). Mixed scoria-pumice are pale brown, poorly vesicular, non fibrous, non lenticular, and poorly phyric. Phenocrysts (1-3 %) consist of subhedral, tabular plagioclase (0.5 mm max.), subhedral prismatic orthopyroxene (0.5 mm max.), and anhedral equant Fe-Ti oxides (0.1 mm max.).

Matrix crystals (15-18 %) consist of plagioclase ($An_{26}$), orthopyroxene, clinopyroxene ($Wo_{40-42}$ $En_{41-44}$ $Fs_{16-17}$) and Fe-Ti oxides. Plagioclase crystals (1.5 mm max.) are subhedral and tabular. Sieve textures, resorbed margins, and broken or fragmented textures are common. Oscillatory, normal, and reverse compositional zonation are common. Orthopyroxene crystals (0.5 mm max.) are subhedral, prismatic or stubby prismatic and typically contain glass and Fe-Ti oxide inclusions. Clinopyroxene crystals (2 mm max.) are subhedral tabular or stubby prismatic. Zircon crystals (< 0.05 mm) are euhedral stubby prismatic, and rare. Fe-Ti oxides (1 mm max.) are anhedral, equant titanomagnetite and anhedral, prismatic ilmenite, and typically exhibit resorbed margins.

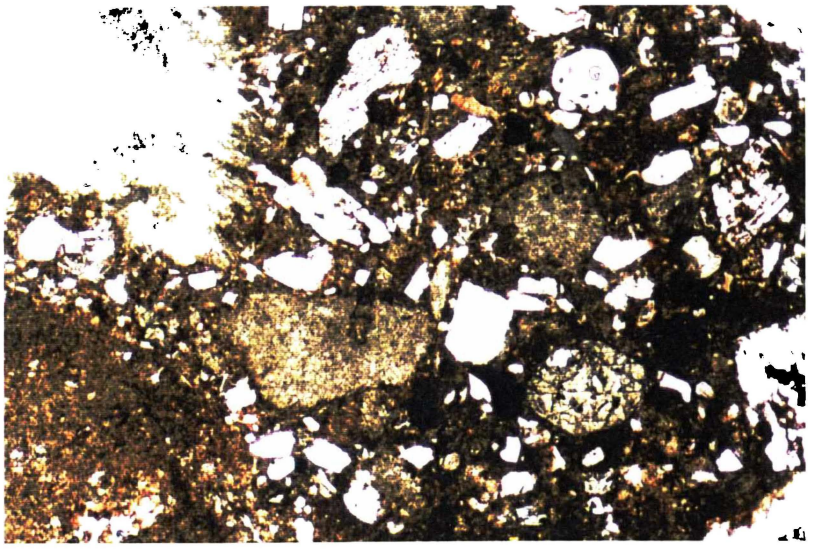

Figure 6.6 Photomicrograph of Oteao Ignimbrite (W99612). Note abundant plagioclase (some with sieve texture) and pyroxene crystals. Light brown pumice clasts in top left; dark brown scoria in bottom left. Field of view is 4mm across.

The matrix is very fine devitrified, and has a poorly developed vitroclastic texture. Rare cuspate and platy glass shards, typically with thin walls are common.

## 6.3 Mineralogy

Mineralogical data has been obtained for selected andesite and rhyolite lavas, and ignimbrites of the KCC by electron microprobe analysis. All data for plagioclase, pyroxene, amphibole, biotite and Fe-Ti oxide phenocrysts and crystals are presented in Appendix V.

***Feldspar***

Plagioclase feldspar is the most abundant felsic phase in KCC volcanic rocks. Quartz is the only other felsic phase to occur. K-feldspar, which is common in Whitianga Volcanic Centre rhyolites (Briggs et al., 1998), has not been observed or analysed in any unit. Plagioclase shows a wide variation in composition, with distinctive plagioclase compositions in andesite lavas, rhyolite lavas, and ignimbrites (Figure 6.7).

Plagioclase compositions range from dominantly sodic oligoclase to andesine in plagioclase phyric, plagioclase-pyroxene phyric, and quartz-plagioclase-biotite phyric rhyolite lavas, and rhyolitic ignimbrites. In andesite lavas, hornblende phyric rhyolite lavas, and mafic ignimbrites, compositions vary from calcic bytownite to labradorite.

Taurauikau Andesite and Taurahuehue Andesite lavas have a similar phenocryst mineralogy, but differ in that Taurauikau Andesite lavas have more sodic (labradorite) compositions than Taurahuehue Andesite lavas (bytownite). Reversely zoned plagioclase compositions are common in Taurahuehue Andesite lavas, but are less common in Taurauikau Andesite and Tapuaetahi Andesite. Normal and oscillatory zoned phenocrysts are common in all formations.

Significant differences are shown between group IV rhyolite lavas which have calcic compositions and group II rhyolite lavas with sodic compositions. There is also a significant range in composition for group I rhyolite lavas ranging from oligoclase (Tauranikau Rhyolite) to andesine to labradorite (Precipice Rhyolite). Between and within rhyolite lava groups there is a range of phenocryst compositional zonation. Normal, reverse and oscillatory zonation are common, and typically one or both of these dominant over the other(s).

Plagioclase compositions in ignimbrites range from andesine to labradorite and bytownite. Variable compositions in juvenile clasts are clearly apparent in the mixed andesitic-rhyolitic Oteao Ignimbrite. Andesine is present in pumice clasts, while in scoria, only labradorite has been determined. Rhyolitic ignimbrites show a more restricted compositional range (i.e. only andesine).

Similar compositions between plagioclase crystals in the matrix, and phenocrysts in juvenile clasts within ignimbrites, imply that the matrix crystals are juvenile (e.g. Manuka Ignimbrite). Differences between these suggest that in some instances (e.g. Manuka Ignimbrite; Trig Q Ignimbrite) matrix crystals are

derived from a more mafic source (e.g. pre-caldera andesitic lava lithic fragments) or possibly from unconsolidated surficial sediments, and would therefore represent xenocrysts (cf. Skinner, 1995).

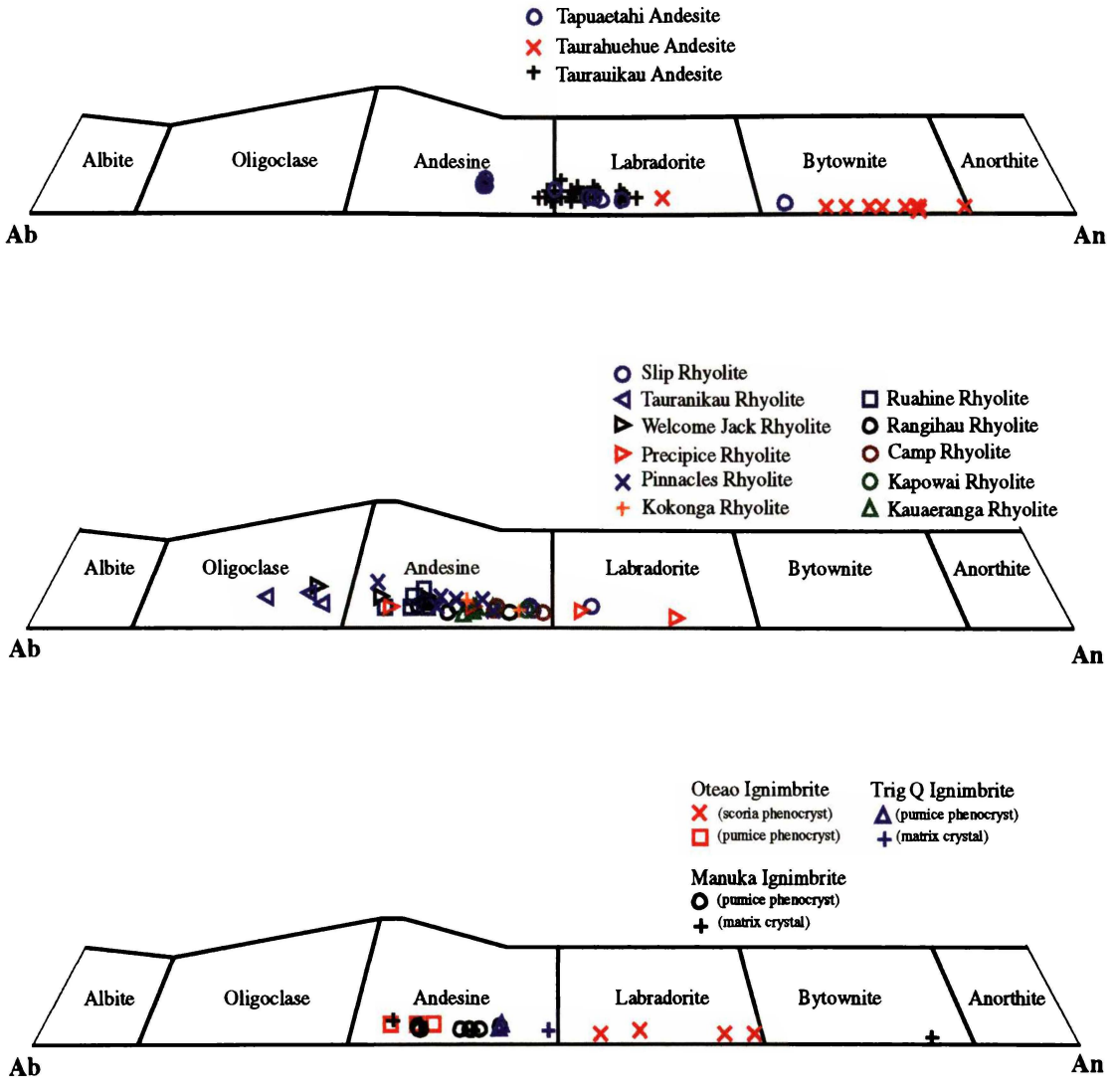


Figure 6.7 Plagioclase feldspar phenocryst and crystal compositions in volcanic units of the Kapowai Caldera Complex. A, Phenocrysts in andesite lavas; B, Phenocrysts in rhyolite lavas; C, Phenocrysts (in juvenile clasts) and crystals (matrix) in ignimbrites.

Reverse, normal and oscillatory zonation is observed in all ignimbrite plagioclase phenocrysts, although the abundance of each varies. Manuka Ignimbrite typically has the least variably population, and is dominated by normal zoned plagioclase with lesser oscillatory and rare reversely zoned phenocrysts. Reverse zonation appears more abundant than normal zonation in Trig Q Ignimbrite. Pumice clasts in Oteao ignimbrite contain reverse, normal and oscillatory zoned plagioclase. Variable plagioclase compositions in KCC ignimbrites implies a complex magmatic history for each magma. The presence of reverse zoning in all these ignimbrites suggests that disequilibrium conditions occurred in the magmas at certain stages of their crystallisation history.

***Pyroxene***

Orthopyroxene and clinopyroxene phases are present in all pre-caldera and caldera-related andesite lavas, group I rhyolite lavas, and most ignimbrites of the KCC. Compositions vary between units (Figure 6.8).

In andesite lavas, significant differences occur between Taurahuehue Andesite and Taurauikau Andesite clinopyroxene and orthopyroxene compositions. Clinopyroxene (augite) and orthopyroxene (clinoenstatite) phenocrysts are generally more Mg-rich in Taurahuehue Andesites than in Taurauikau Andesites. Clinopyroxene compositions in Tapuaetahi Andesite lavas are similar to Taurahuehue Andesite, although orthopyroxenes are highly variable, ranging from Mg-rich to Mg-poor clinoenstatite.

In most pre-caldera and caldera-related andesitic-dacitic lavas, some co-existing orthopyroxene and clinopyroxene phenocrysts have different Mg/Fe ratios. These disequilibrium compositions are indicative of mixing of two compositionally distinctive magmas (e.g. Sakuyama, 1979; Nixon, 1988).

Orthopyroxenes in rhyolite lavas are typically more Fe-rich than in andesite lavas. Within the group I lavas, there are some compositional differences, most notably that Kapowai Rhyolite orthopyroxene phenocrysts are more Mg-rich than Camp Rhyolite compositions. Disequilibrium compositions of co-existing orthopyroxene and clinopyroxene phenocrysts are also present, although only sufficient data for the Precipice Rhyolite lavas have been obtained to support this.

In KCC ignimbrites there is a wide range in orthopyroxene compositions from Mg-rich clinoenstatite (Trig Q Ignimbrite) to Mg-poor clinoenstatite (scoria phenocryst in Oteao Ignimbrite). Similar clinopyroxene compositions between juvenile phenocrysts and matrix crystals from the Oteao Ignimbrite suggest that some of the crystals are co-magmatic and not accidentally incorporated.

***Amphibole***

Amphiboles define one of the four rhyolite lava groups at the KCC (i.e. group IV rhyolite lavas). Amphibole phenocrysts analysed from the Slip Rhyolite lava are calcic hornblendes with edenitic-edenitic hornblende compositions (Leake et al., 1997). Other amphibole phenocrysts observed in the Miller Flat Rhyolite (another constituent group IV rhyolite lava) have a similar green-brown pleochroism and extinction angle to Slip Rhyolite, suggesting that they have similar compositions.

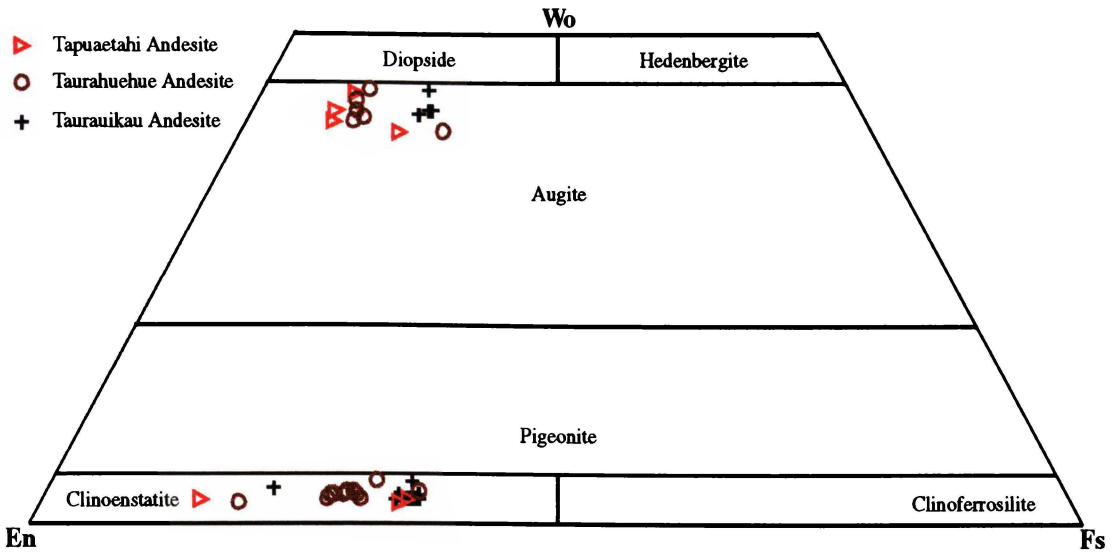


A

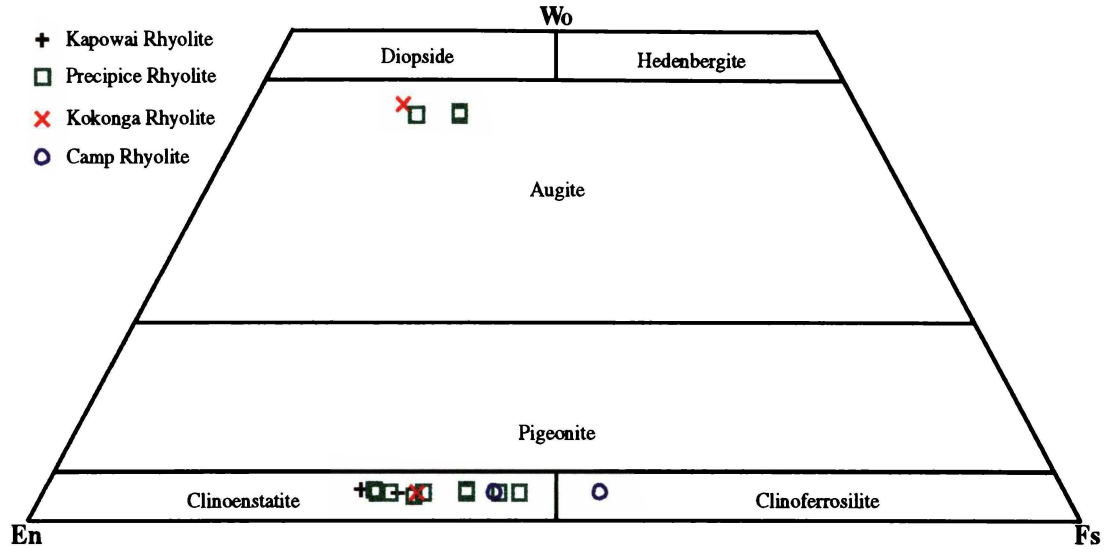


B

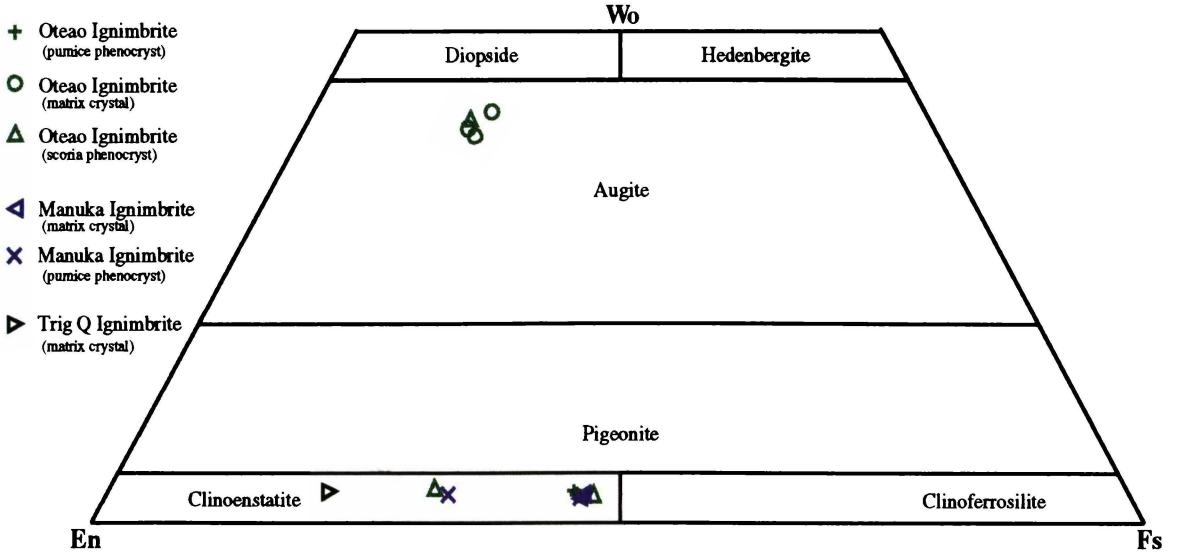


C

Figure 6.8 Pyroxene phenocryst and crystal compositions in volcanic units of the Kapowai Caldera Complex. A, Phenocrysts in andesite lavas. B, Phenocrysts in rhyolite lavas. C, Phenocrysts (juvenile) and crystals (matrix) in ignimbrites. Classification based upon Morimoto et al. (1988).

***Biotite***

Biotite phenocrysts have been analysed from Welcome Jack Rhyolite and Ruahine Rhyolite lavas (i.e. group II rhyolite lavas), and Tapuaetahi Andesite lavas. Significant compositional variations occur between these three lavas (Figure 6.9). Welcome Jack Rhyolite and Ruahine Rhyolite lavas have similar compositions, although some biotite phenocrysts from the Ruahine Rhyolite are more Fe-rich. Biotite in Tapuaetahi Andesite is more Mg-rich compared with biotite phenocrysts in either Ruahine Rhyolite or Welcome Jack Rhyolite lavas.

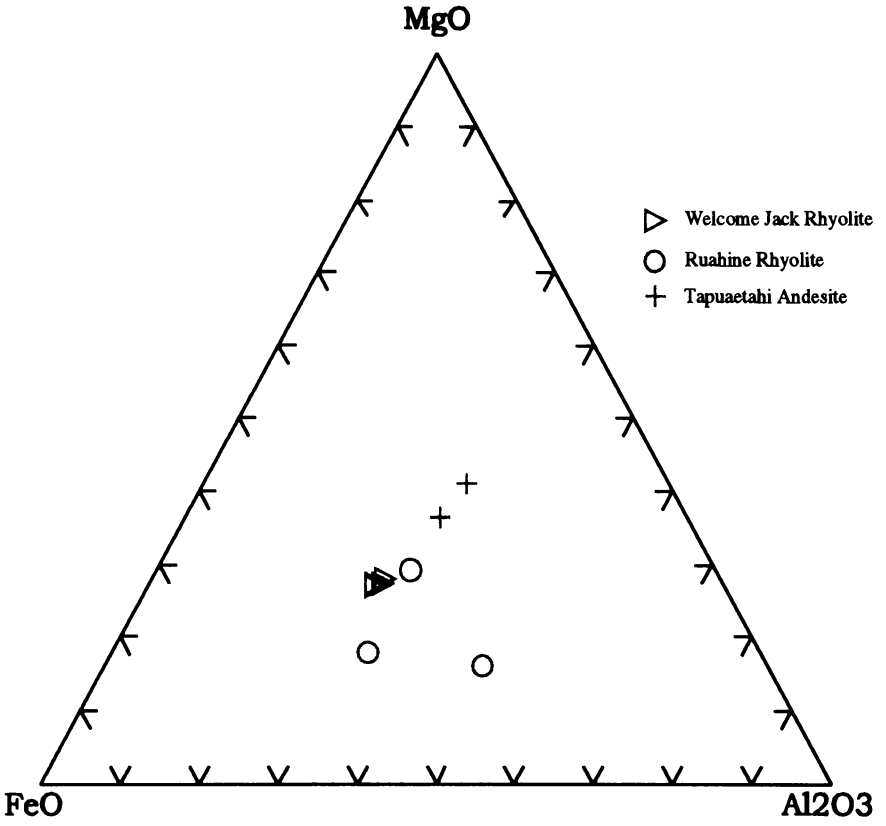


Figure 6.9 Biotite phenocryst compositions in volcanic units of the Kapowai Caldera Complex.

***Fe-Ti oxides***

Titanomagnetite and ilmenite phenocrysts were analysed from numerous KCC volcanic units. Compositions vary in both titanomagnetite and ilmenite phenocrysts for andesite and rhyolite lavas (Figure 6.10). Within some lavas there is significant variability in composition between either titanomagnetite (e.g. Taurauikau Andesite, Kapowai Rhyolite) or ilmenite (e.g. Tapuaetahi Andesite) suggesting that some lavas may contain co-existing Fe-Ti oxides which are not in equilibrium (Bacon and Hirschmann, 1988).

Estimates of magmatic crystallisation temperatures for igneous rocks can be obtained from co-existing titanomagnetite-ilmenite pairs (Buddington and Lindsey, 1964; Carmichael, 1967). However, equilibrium crystallisation for the pairs needs to be established, and this is achieved using compositional tie-lines (Figure 6.11) as defined by Bacon and Hirschman (1988).

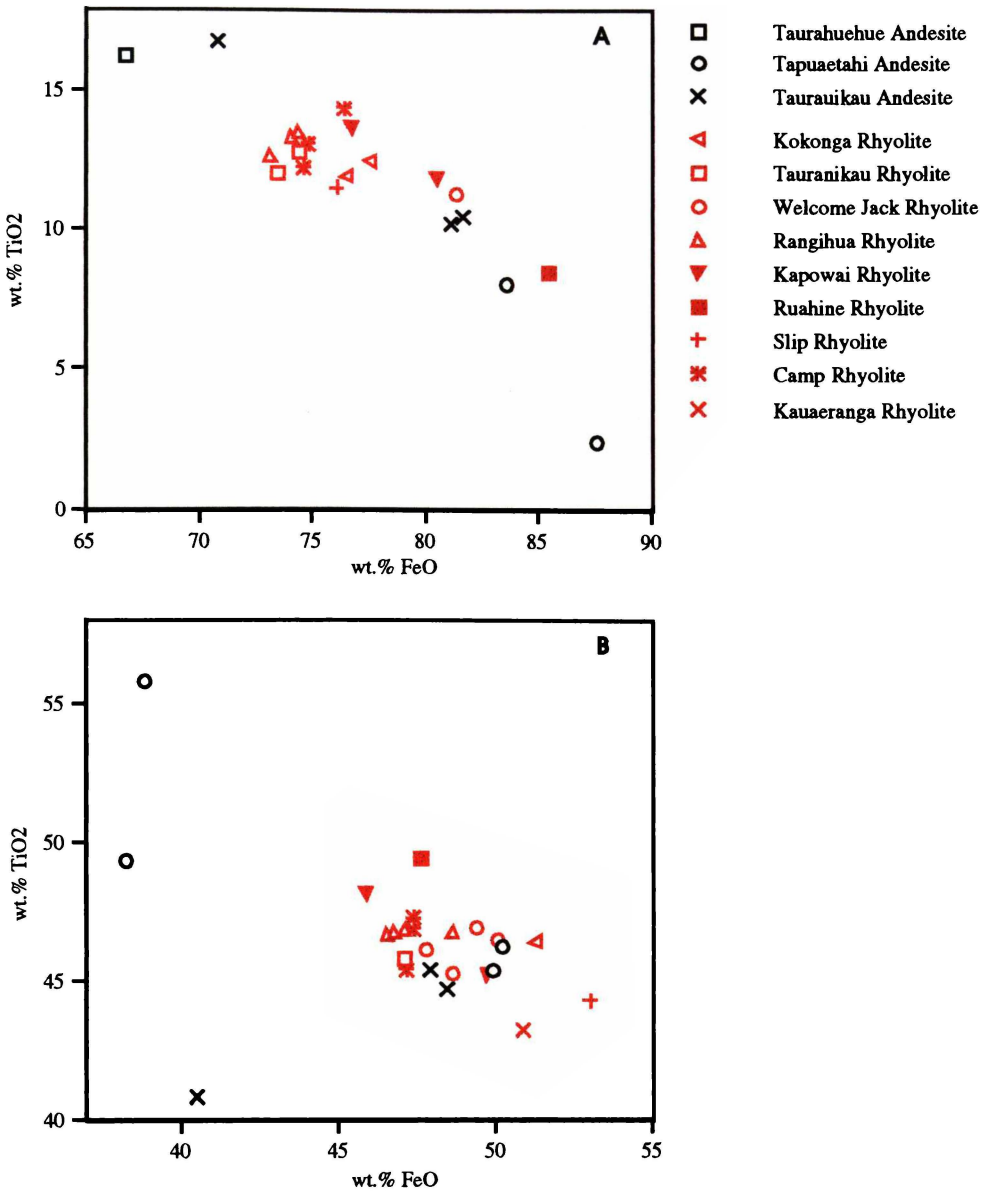


Figure 6.10 Variation in composition within titanomagnetite (A) and ilmenite (B) phenocrysts of pre-caldera and caldera-related lavas.

Calculated temperatures, using the method of Carmichael (1967), for selected rhyolite lavas vary from 823°C in Rangihau Rhyolite (plagioclase phyric) to 940°C in Kauaeranga Rhyolite (plagioclase-pyroxene phyric) (Figure 6.12). The calculated temperatures form a clear linear relationship between (log)oxygen fugacity and temperature, which provides confidence in the results. These results suggest a thermal gradient of low temperatures in plagioclase phyric rhyolite lavas to higher temperatures in pyroxene and amphibole bearing lavas.

The calculated temperatures are generally consistent for silicic magmas temperatures calculated in the CVZ (e.g. Blattner, 1996) and for silicic magmas in general (Hildreth, 1981). Differences in the calculated temperatures between Kauaeranga and Rangihau Rhyolites is probably associated with differences in whole rock composition, phenocryst mineral assemblage and volatile contents in these lavas (Hildreth, 1981).

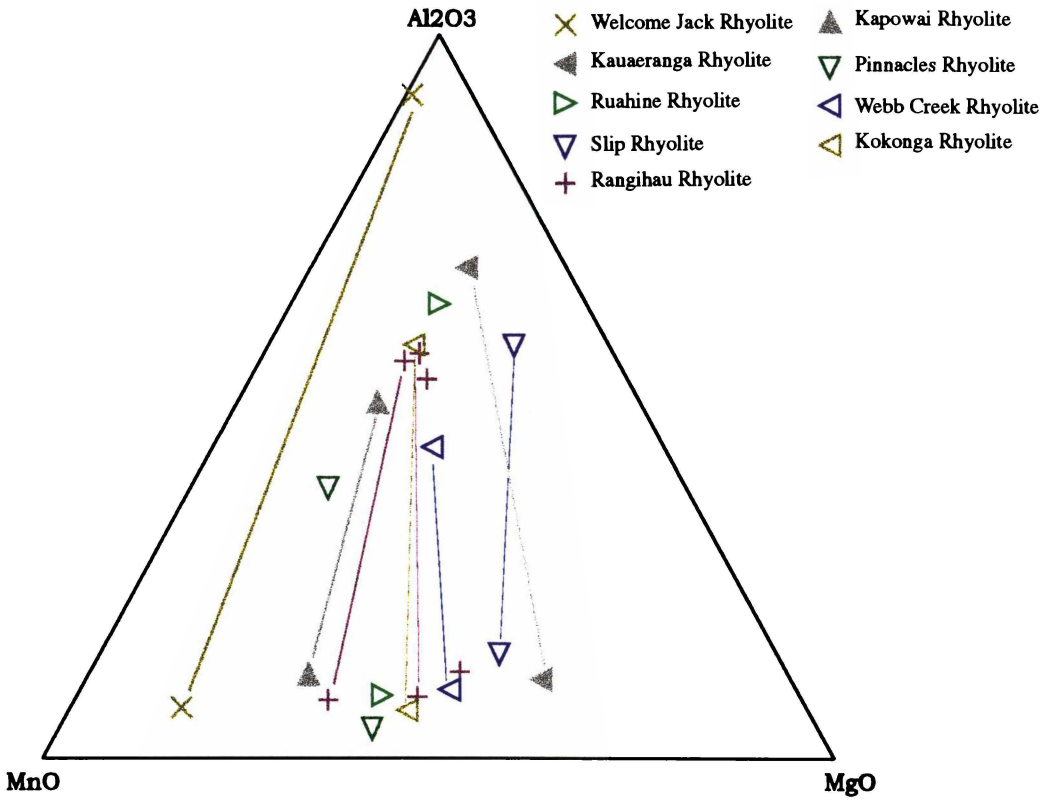


Figure 6.11 Partitioning of titanomagnetite and ilmenite pairs in the system MgO-MnO-Al203 for selected rhyolite lavas of the Kapowai Caldera Complex. Compositional tie-lines are indicated (Bacon and Hirschman, 1988).

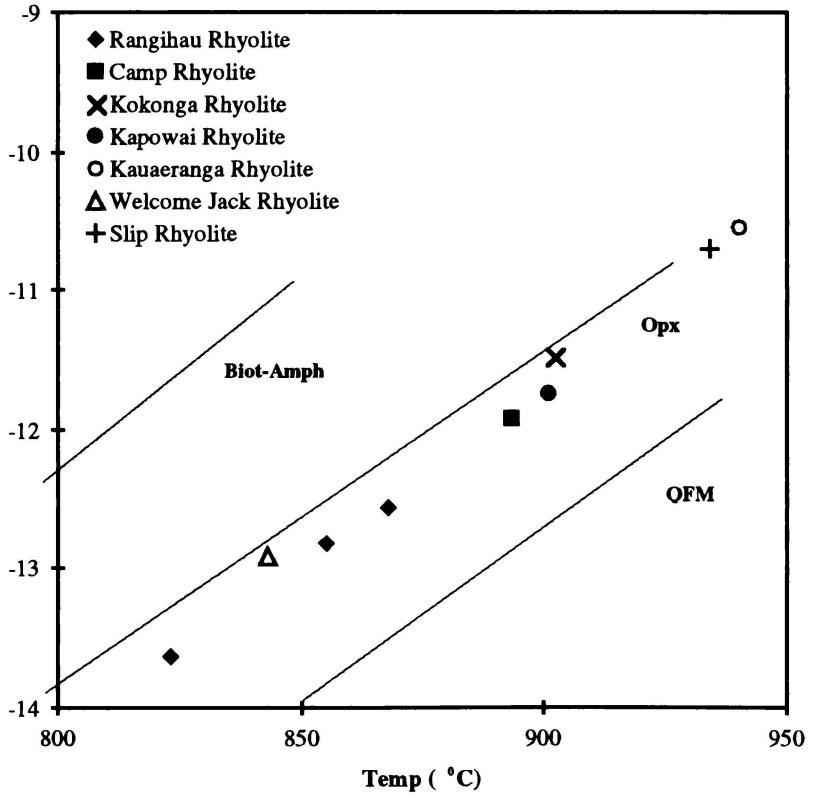


Figure 6.12 Calculated temperatures of selected rhyolite lavas of the Kapowai Caldera Complex based upon co-existing titanomagnetite and ilmenite phenocrysts. QFM, Opx, Biot-Amph are oxygen fugacity buffer curves for dacitic and rhyolitic compositions from Carmichael (1967).

## 6.4 Petrological processes

Numerous petrographic and mineralogical studies of volcanic sequences (particularly of intermediate composition) at subduction-related volcanoes have identified numerous complex magmatic processes that have occurred within these magma types (e.g. Sakuyama, 1979, Stamatelopoulou-Seymour et al., 1990; Stimac and Pearce, 1992; Clynne, 1999). Recently, these standard petrographic and mineralogical analyses, have been augmented by high resolution trace element and isotopic studies of phenocryst phases (e.g. Singer et al., 1995; Knesel et al., 1999; Tepley et al., 1999). These have further highlighted the complexity of phenocryst compositions and textures, and supported initial ideas that most subduction-related magmas have evolved in an intricate and highly variable manner.

From the petrographic and mineralogical analysis of pre-caldera and caldera-related volcanic rocks at the KCC, the presence of disequilibrium textures suggest that the development of these magmas was also variable and evolved via several major processes. These processes may include magma mixing and mingling, assimilation, oscillations within magma columns and magma replenishment (Tepley et al., 1999; Knesel et al., 1999).

Disequilibrium textures include (i) sieve textures in plagioclase phenocrysts/crystals; (ii) reverse and oscillatory compositional zonation in plagioclase phenocrysts/crystals; and (iii) occasional mantling of pyroxene phenocrysts by very fine grained pyroxene crystals. Most of these features are present in pre-caldera and caldera-related andesite lavas, although (i) and (ii) have been observed in rhyolite lavas and silicic ignimbrites.

Sieve textures present in plagioclase phenocrysts/crystals imply that incomplete melting of the phase has occurred prior to eruption (Hibbard, 1995). One possible reason is injection of a hotter more mafic magma into a pre-existing, cooler silicic magma chamber, with a resulting increase in the primary magma temperature and subsequent crystal melting. Sieve textures are common in intermediate composition lavas at the KCC, and are also typical of most subduction-related intermediate rocks (Gill, 1981).

Reverse and oscillatory compositional zonation may be indicative of progressive temperature increase (reverse) or fluctuating temperature (oscillatory) (Hibbard, 1995). This may also result from mixing of silicic magma with hotter mafic magma (e.g. Stimac and Pearce, 1992). Reverse, oscillatory and normal zonation are typically present in most pre-caldera andesite lavas implying a complex crystallisation history punctuated by magma interactions of different compositions.

Mantling of pyroxene phenocrysts by finer grained, granular pyroxene is another petrographic feature indicative of dynamic magmatic processes. Mantle contacts are generally irregular, suggesting that melting or resorption of the pyroxene phenocryst occurred followed by growth of secondary pyroxene (cf. Sakuyama, 1979).

Apart from mineralogical and petrographic evidence, limited lithological features clearly support magma mixing (and mingling) in at least one KCC volcanic unit. Oteao Ignimbrite contains a mixed juvenile assemblage of primary scoria and pumice clasts, mingled scoria and pumice, and mixed dacitic clasts. This assemblage clearly demonstrates that magma mixing and mingling was a significant process in the development of this magma.

Another magmatic process which can be inferred at the KCC, is crustal assimilation. In some rhyolite lavas (e.g. Kauaeranga Rhyolite, Kapowai Rhyolite) xenoliths of other rhyolite lavas and rarely andesite lavas have been observed. Rare lower crustal xenoliths have also been observed, including meta-quartzite in andesite lavas and others including quartz-orthopyroxene-plagioclase granulite and sillimanite hornfels have been reported in WES ignimbrites by other workers (Skinner, 1995). Crustal assimilation is a common process in the generation of subduction-related magmas (Graham and Hackett, 1987; Hildreth and Moorbath, 1988; Price et al., 1999).

# Chapter Seven

# GEOCHEMISTRY AND PETROGENESIS

## 7.1 Introduction

Volcanic rocks erupted at caldera volcanoes can provide an opportunity to study petrological features from a wide spectrum of magmatic compositions. Geochemical data obtained from caldera-derived volcanic rocks have provided direct evidence for compositional gradients and zonation of magma chambers (Hildreth, 1981; Boden, 1989; Duffield and Ruiz, 1992; Streck and Grunder, 1997), and interactions between mafic and silicic magmas (Hildreth et al., 1991; Blake et al., 1992). Spatial and temporal variations in magma composition can also be constrained (Lipman et al. 1978; Riciputi et al. 1995; Sutton et al., 1995), and petrogenetic models can be developed to explain magmatic variations at caldera volcanoes.

This chapter describes the geochemical characteristics of selected KCC volcanic rocks and lava lithic fragments. Major and trace element variations are presented, and broad magma types erupted are established for andesite and rhyolite compositions using bivariate and multi-element analysis. Finally, constraints are placed on the petrogenesis of andesitic and rhyolitic magmas erupted at the KCC.

Major, trace element and rare earth element (REE) chemistry of selected KCC lava and pyroclastic rocks and lithic fragments have been determined. Samples were chosen on the basis of freshness and lack of alteration.

Major and trace element XRF analyses were determined for 72 samples. These included pre-caldera and caldera-related andesitic-dacitic lavas, the four rhyolite lava groups, all major ignimbrites, and selected lava lithic fragments. In the first instance, the objective was to collect and compile a much larger dataset of XRF analyses, but severe problems were encountered in obtaining fresh samples, particularly unweathered and unaltered pumice clast samples in ignimbrites. Sampling of lavas was also restricted by deep weathering profiles, sporadic hydrothermal alteration, and lack of outcrop. These constraints also restricted the number of REE analyses that were undertaken. A subset of 26 samples from the 72 XRF analyses were analysed for REE abundances by ICP-MS.

## 7.2 Methodology

### XRF

Crushed powder samples were prepared using a tungsten-carbide ring-mill. Samples were analysed at the Department of Geological Sciences, University of Canterbury. Glass fusion beads (for major element analysis) were prepared following the general methods of Norrish and Hutton (1969), with modifications after Harvey et al. (1973) and Schroeder et al. (1980). Approximately 0.3g of rock powder was fused with 1.61g of flux ($Li_2B_4O_7$, $Li_2CO_3$ and $La_2O_3$ mixture) plus a few grains of oxidant ($NH_4NO_3$) at 1000°C for at

least 20 minutes in Pt/Au crucibles. Loss on ignition was calculated after fusion. Glass beads were then pressed using heated (approx. 150°C) polished aluminium platterns and plunger. 50 mm diameter pressed powder pellets (for trace element analysis) were prepared using approximately 15 g of rock powder and bound using polyvinyl alcohol solution (Norrish and Hutton, 1969).

Major and trace element abundances were determined using a Phillips PW 1400 automatic X-Ray Spectrometer coupled to a Hewlett Packard 300 computer. Pressed pellets were irradiated using a 3kW Au tube (at 60kV, 45mA) for analysis of Zr, Nb, Ba, Ni, Cr, V, La, Ce, Nd, and with a 3kW Mo tube (at 90kV, 30mA) for analysis of Rb, Sr, Y, Th and Ga. Fusion beads were irradiated using a 3kW Sc tube (at 50kV, 50mA) for determination of major element concentrations. Pressed pellets and fusion beads were prepared and analysed by Stephen Brown (technical officer). The full dataset of XRF results are presented in Appendix VI.

### ICP-MS

Crushed powder samples were prepared using a tungsten-carbide ring-mill. Samples were analysed by ICP-MS at Monash University. All wet chemistry was performed in "class 350" clean air cabinets. 50-100 mg samples of rock powder were dissolved in HF-$HNO_3$ mixture in high pressure bombs and then evaporated to dryness. They were then refluxed in aqua regia, and twice in concentrated $HNO_3$ to remove fluorides, then dissolved in 2% $HNO_3$. This solution was then diluted to 50ml of 2% $HNO_3$ (made with sub-boiled distilled concentrated $HNO_3$ and 18.2 M-ohm Millipore water). Aliquots of this solution were then taken and diluted to an appropriate dilution factor for presentation to the mass spectrometer. The final solution also contained 10 ppb indium to serve as an internal standard. One analytical blank and 4 standard solutions (based on 50 mg and 100 mg of digested U.S. Geological Survey standard BHVO-1) are typically prepared with each run. BHVO-1 was used as a check to monitor accuracy during the analysis procedure.

Diluted rock and acid samples were analysed by inductively-coupled plasma mass spectrometry (ICP-MS) using a high resolution Finnigan MAT *ELEMENT* magnetic sector ICP-MS. The transition metals and P were analysed in medium mode (resolution = 3000) which removed the effects of Cl interferences in these elements. Integrated count data from the instrument was reduced using a custom, off-line, spreadsheet-based program. Precision is better than 5% for each analysis. As described above, determination of analytical accuracy is based on analysis of the solution standards, and is typically better than 5% for most elements at the 95% confidence interval. The mass spectrometry and data reduction were performed by Louise Frick (Laboratory Manager). The full dataset of ICP-MS analyses are presented in Appendix VII.

## 7.3 Geochemical classification

The total alkalis-silica (TAS) scheme, defined by LeMaitre (1989), is used to geochemically classify the KCC volcanic rocks (Figure 7.1). Lavas analysed vary from basaltic andesite (56.1 wt.% $SiO_2$) to high silica andesite (60.0-61.8 wt.% $SiO_2$), to low silica dacite (63.3-64.6 wt.% $SiO_2$) to rhyolite (71.0-78.8

wt.% $SiO_2$; normalised values). Ignimbrite juvenile and whole rock compositions vary from low-silica andesite (57.2-59.3 wt.% $SiO_2$) to dacite (63.2-69.5 wt.% $SiO_2$) and low silica rhyolite (71.2-75.4 wt.% $SiO_2$). Lava lithic fragments show a similar trend compared with outcropping lavas analysed. Lithics vary in composition and form two compositional groups of high silica andesite to low silica dacite (61.4-64.1 wt. % $SiO_2$) and low to high silica rhyolite (70.5-77.2 wt. % $SiO_2$).

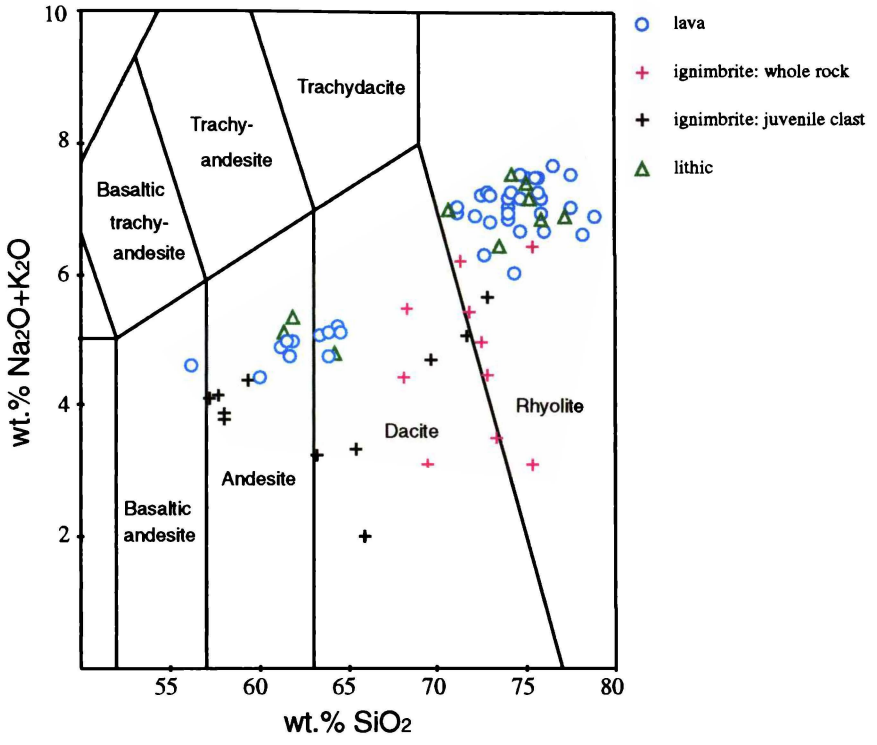


Figure 7.1 TAS classification of selected volcanic rocks (normalised to 100%, volatile free) from the Kapowai Caldera Complex. After Le Maitre (1989).

An apparent compositional gap from 65 to 70 wt.% $SiO_2$ is observed for KCC lavas. This may in part be caused by sampling bias, as some unanalysed dacite and andesite lava lithics sampled from intracaldera ignimbrites may have compositions that fall within this gap. Some ignimbrites analysed have compositions within these gaps, although some of these are considered to be dubious as incipient weathering (see below) has affected XRF values and totals, or because the analyses are whole-rock and not of juvenile clasts.

This compositional gap overlaps the gap of 68.0 to 73.0 wt.% $SiO_2$ identified by Adams et al. (1994) during a regional geochemical study of CVZ igneous rocks. Therefore, the compositional gap at the KCC does mimic the general lack of dacitic lavas erupted throughout the CVZ.

Subdivision of the volcanic rocks using $K_2O$ vs $SiO_2$ reveals a medium-K suite of rocks with some high-K rhyolites (Figure 7.2) which is similar to most of the central and southern CVZ volcanics (Adams et al., 1994). This is typical of the calc-alkaline (high alumina) magma series associated with subduction-related magmas (Wilson, 1989).

Initial sampling followed by petrographic analysis of KCC volcanic rocks revealed devitrification of groundmass glass in most silicic lavas, and in glass in juvenile clasts and matrix in some ignimbrites. Undifferentiated clays were observed mainly in andesite lavas (especially pre-caldera units). Only samples without observable weathering were analysed geochemically. No samples were analysed that showed any indication of hydrothermal alteration.

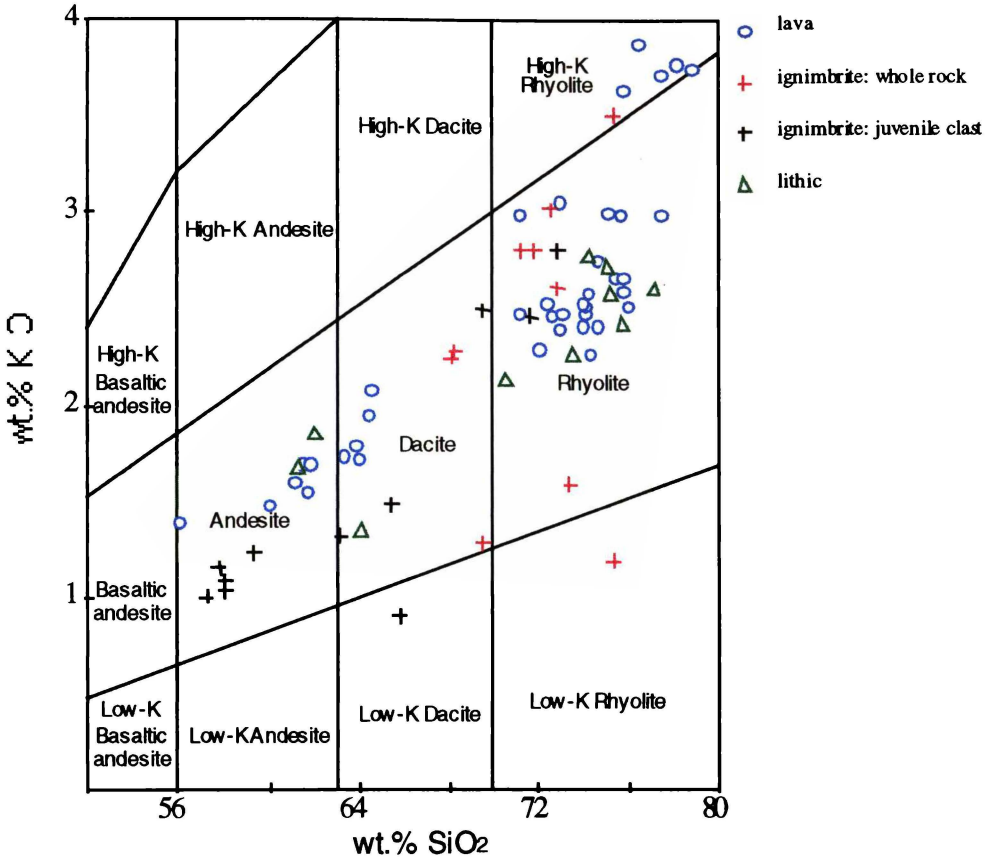


Figure 7.2 Subdivision of Kapowai Caldera Complex volcanic rocks into low-K, medium-K and high-K types (data normalised to 100% volatile free). After Le Maitre (1989).

Apart from devitrification, variable major and trace element abundances in some ignimbrite whole-rock and juvenile clast analyses implies that incipient weathering has affected these samples. This weathering is indicated by high LOI and $Al_2O_3$ values, scatter of $Na_2O$, and $K_2O$ (to a lesser extent) values, and enrichment in Ba. High LOI values are related to high volatile contents (especially $H_2O$) contained in weathering products (i.e. clay minerals). Variable $Na_2O$, and $K_2O$ are most likely due to alkali exchange of volcanic glass during incipient weathering or devitrification (Scott, 1971). CVZ volcanic rocks, and especially CVZ ignimbrites, typically have variable alkali abundances (Adams, et al. 1994). This is more pronounced in ignimbrites rather than lavas, reflecting the susceptibility of glass shards to weathering.

Trace element variations, particularly in Ba, are seen in samples with high LOI. An explanation for this could be that of Price et al. (1991) who suggested a two-stage process for Ba enrichment in weathered or hydrothermally altered basalts. During initial weathering, Ba is mobilised as the volcanic glass breaks

down, and is then fixed by substitution into, or adsorbed onto, secondary clay minerals (Price et al., 1991). No secondary Ba-bearing minerals have been determined petrographically in weathered samples, although it is possible that these may be present and act as a further enrichment of Ba.

Additional evidence for weathering is indicated by some low CaO values, high MnO and Y abundances in WES ignimbrites, low La and Ce abundances in Trig Q Ignimbrite, and high V in the Webb Creek Ignimbrite. Variations are probably related to mobilisation of elements during weathering and some possible enrichments as suggested for the Ba values.

As most ignimbrites appear to be affected by incipient weathering, these are not used in the definition of magma groups or in the discussion of the petrogenesis of andesite or rhyolite magmas at the KCC. Lavas analysed do not show any indication of weathering, and these form the basis of these discussions.

## 7.4 Major and trace element variation

Major and trace element variation diagrams are presented in Figures 7.3 and 7.4. Overall decreases in $TiO_2$, $Al_2O_3$, $Fe_2O_3$, MnO, MgO, CaO, and $P_2O_5$ with increasing $SiO_2$ indicates their compatible behaviour in the phenocryst and accessory phases (e.g. plagioclase feldspar, pyroxene, titanomagnetite, ilmenite, apatite) present in the volcanic suite. The increase in $K_2O$ abundance with increasing $SiO_2$ reflects its incompatible behaviour in phenocrysts. $Na_2O$ varies significantly and no general trend can be established.

With increasing $SiO_2$ content, Ba, Rb, Zr, Y, Nb, and Th increase reflecting their incompatible behaviour with respect to the observed phenocryst phases (i.e. plagioclase feldspar, pyroxene). The variable decrease in Sr, Zn, Ga, Ni, and V with increasing $SiO_2$ indicates the compatible behaviour of these elements in phenocryst phases (i.e. plagioclase feldspar, pyroxene, titanomagnetite). Pb and Cr contents are close to detection limits and trends are difficult to establish.

Within andesite-dacite lavas some differences in major and trace element variation are apparent. Taurahuehue Andesite has different trends for $TiO_2$, CaO, Zr, and Rb. Scoria clasts in the Oteao Ignimbrite have significantly lower Ni and Cr abundances compared with the general trend for Taurauikau Andesite, although scoria values do have a similar composition to the most primitive Taurahuehue Andesite, and therefore KCC lava.

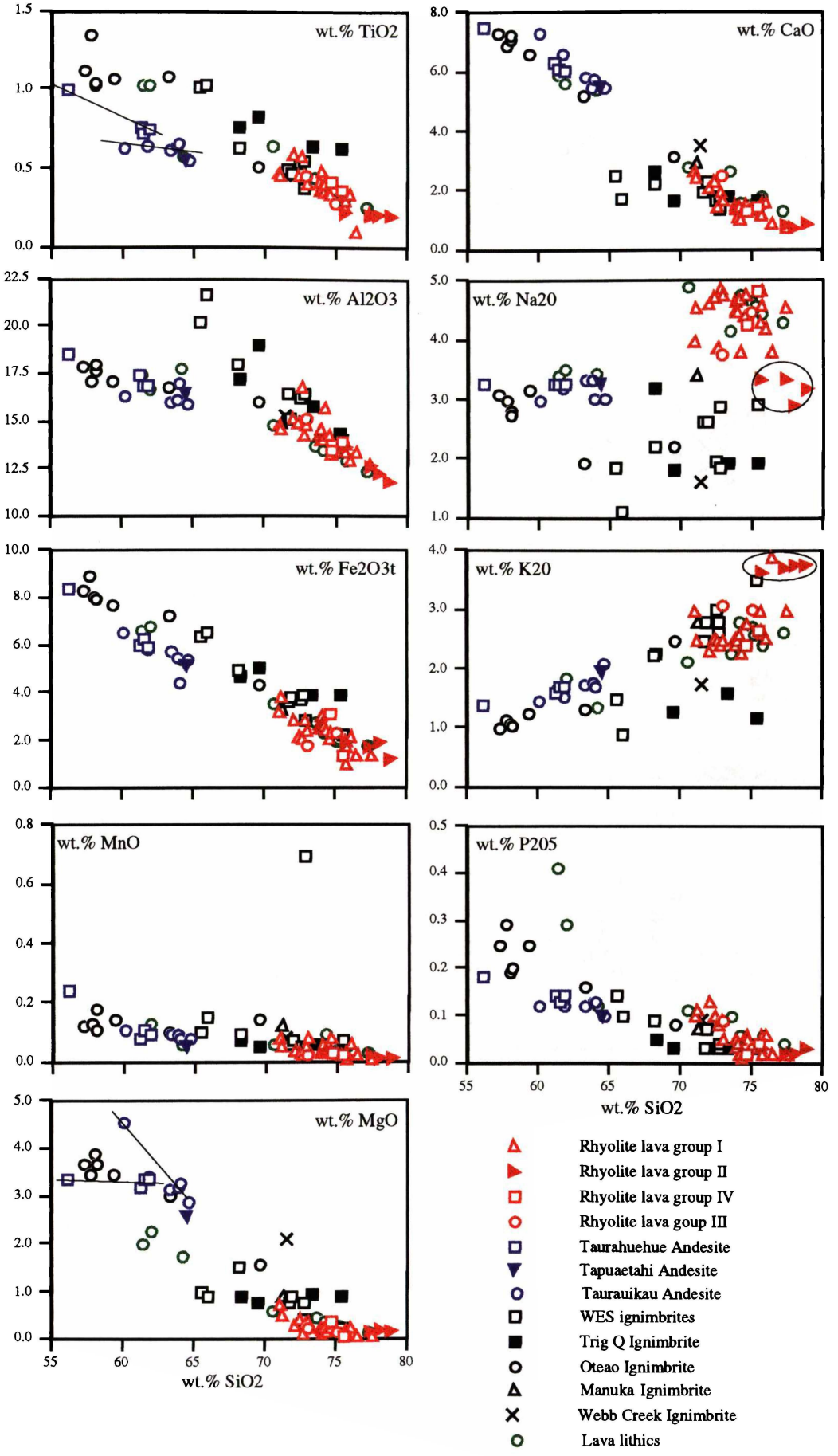


Figure 7.3 Major element variation diagrams for selected Kapowai Caldera Complex lavas, ignimbrites and lava lithic fragments.

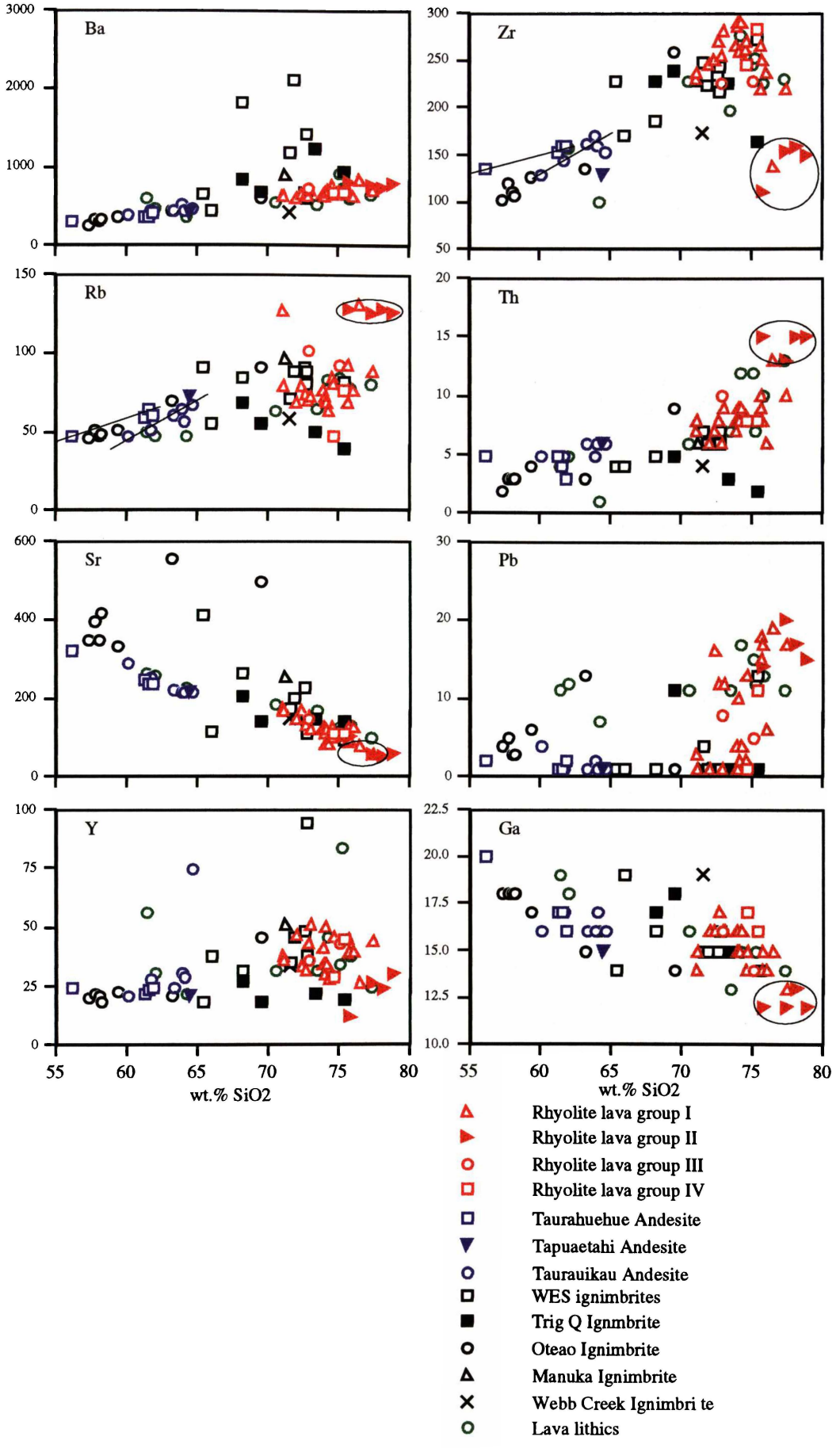


Figure 7.4 Trace element variation diagrams for selected Kapowai Caldera Complex lavas, ignimbrites and lava lithic fragments.

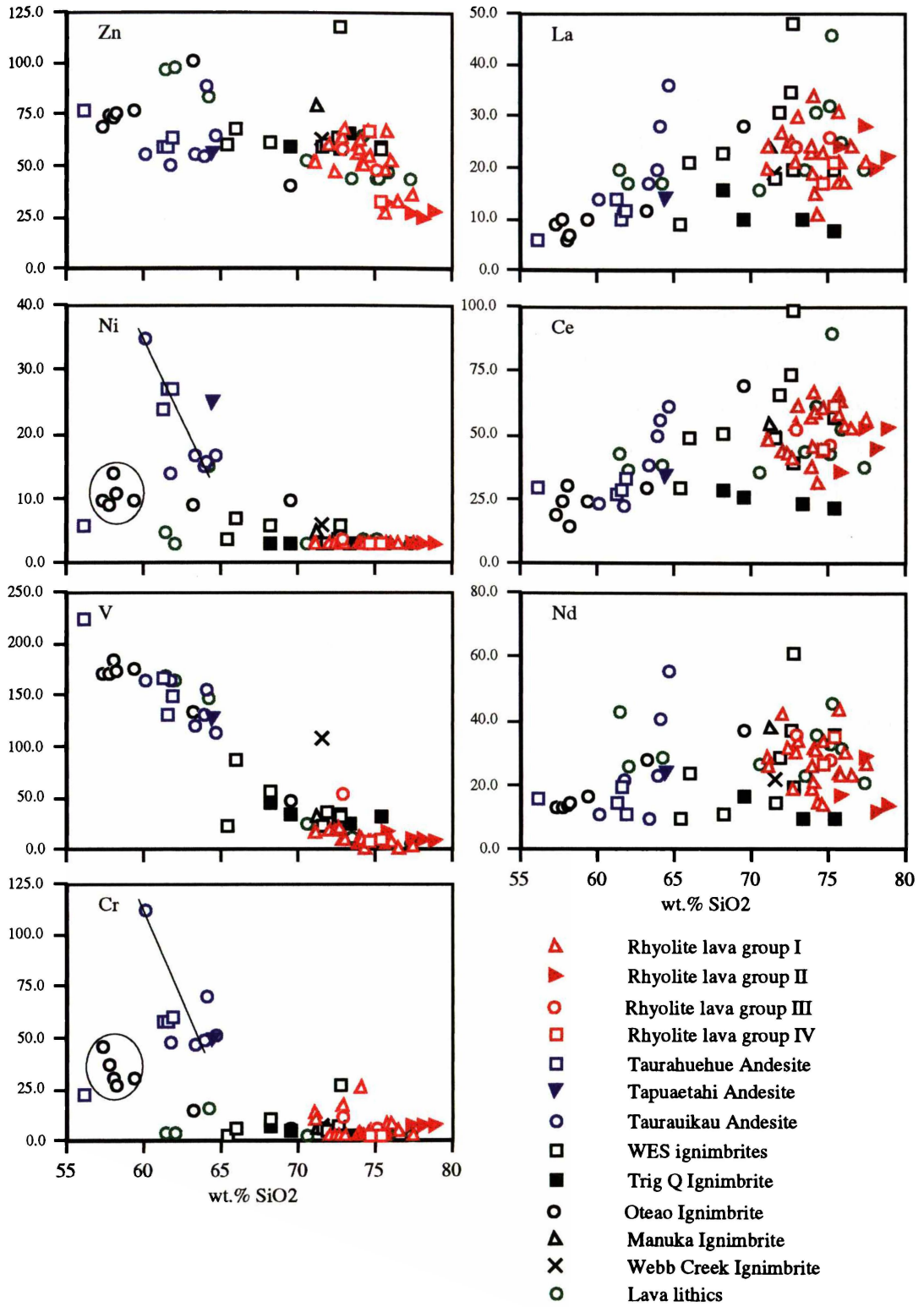


Figure 7.4 (Continued).

Within the rhyolite lava groups, there is considerable overlap in major and trace element abundances. However, group II rhyolite lavas (quartz-plagioclase-biotite phyric) typically cluster in a discrete group. This is particularly seen by high $K_2O$, Rb, and Th abundances, and by low $Al_2O_3$, $TiO_2$ and Sr, Zr, and Ga abundances. Together with the high $SiO_2$ values, this implies that this group is the most evolved or fractionated magma type generated at the KCC.

The major and trace element variations therefore imply crystal fractionation trends within some magma compositions (especially andesites). The lack of high silica dacitic magma (given that ignimbrite values are not considered because of weathering) and the variable trends within the andesitic and rhyolitic lavas suggests that there is no continuous differentiation mechanism linking the andesite and rhyolite lavas.

Although all lavas are related spatially, there are only limited temporal relationships between andesitic and rhyolitic magmas at the KCC. Taurauikau Andesite lavas were erupted prior to, during and following periods of explosive and effusive rhyolitic volcanism. Therefore these magmas could be potentially related to the silicic magmas. Oteao Ignimbrite contains both andesitic and rhyolitic juvenile clasts indicating a clear interaction of intermediate and silicic magmas. Andesitic scoria clasts within the ignimbrite are unweathered, unlike pumice clasts which typically are incipiently to moderately weathered. Hence, no detailed analysis of the magmatic relationships of contrasting juvenile compositions in this ignimbrite can be investigated.

## 7.5 Recognition of magma groups

Numerous andesite-dacite and rhyolite lavas have been erupted prior to or during volcanic activity at the KCC. These have been subdivided on the basis of phenocryst mineralogy or field stratigraphy into several groups. This section describes and compares the major and trace element (including REE) chemistry of each lava group to establish the major magma groups erupted at the KCC. As stated above, because most ignimbrites have been affected by incipient weathering, only lava chemistry is utilised.

***Andesitic - Dacitic magmas***

Two pre-caldera andesitic formations (Taurahuehue Andesite and Tapuaetahi Andesite) and one caldera-related andesitic formation (Taurauikau Andesite) have been analysed. Taurahuehue Andesite is older than Tapuaetahi Andesite, although this is only established from K/Ar dating and no field relationships are observed. Taurauikau Andesite lavas and dikes post-date these two units and were erupted periodically during silicic volcanism at the KCC.

There is general overlap in major and trace element composition between all three andesite lava formations, although some differences are apparent. Taurahuehue Andesite has an andesitic composition (56-62 wt.% $SiO_2$) compared to Tapuaetahi Andesite and Taurauikau Andesite which have high silica andesite to low silica dacite compositions (60-65 wt.% $SiO_2$). $Al_2O_3$ and $TiO_2$ contents are higher in pre-caldera andesite lavas.

Significant differences are observed in Sr, Ba, and Ce contents, where Taurahuehue Andesite and Tapuaetahi Andesite have low Ce (27-34 ppm) and low Ba/Rb values compared with high Ce (24-62) and high Ba/Rb values in the Taurauikau Andesite (Figure 7.5). However, these values may indicate incipient weathering as Ba and Ce are very mobile in CVZ andesite lavas (Fulton, 1988; Hunt, 1991). Taurauikau

Andesite also tends to have lower Sr (214-293 ppm) values than Taurahuehue Andesite and Tapuaetahi Andesite lavas (Figure 7.5d).

Analyses of constituent lavas within andesite formations show considerable compositional variation (e.g. spread of V and Zr values within Taurauikau Andesite, Figure 7.5c), and implies that these lavas are not closely genetically related. This is not surprising, as temporal variations in the composition of lavas erupted from stratovolcanoes or composite cones are common (e.g. Hildreth and Fierstein, 1997; Hobden et al., 1999). This reflects the short residence time and variations in the role of shallow level magmatic processes (e.g. assimilation, fractional crystallisation, and mingling) of these magma batches (Hobden et al., 1999).

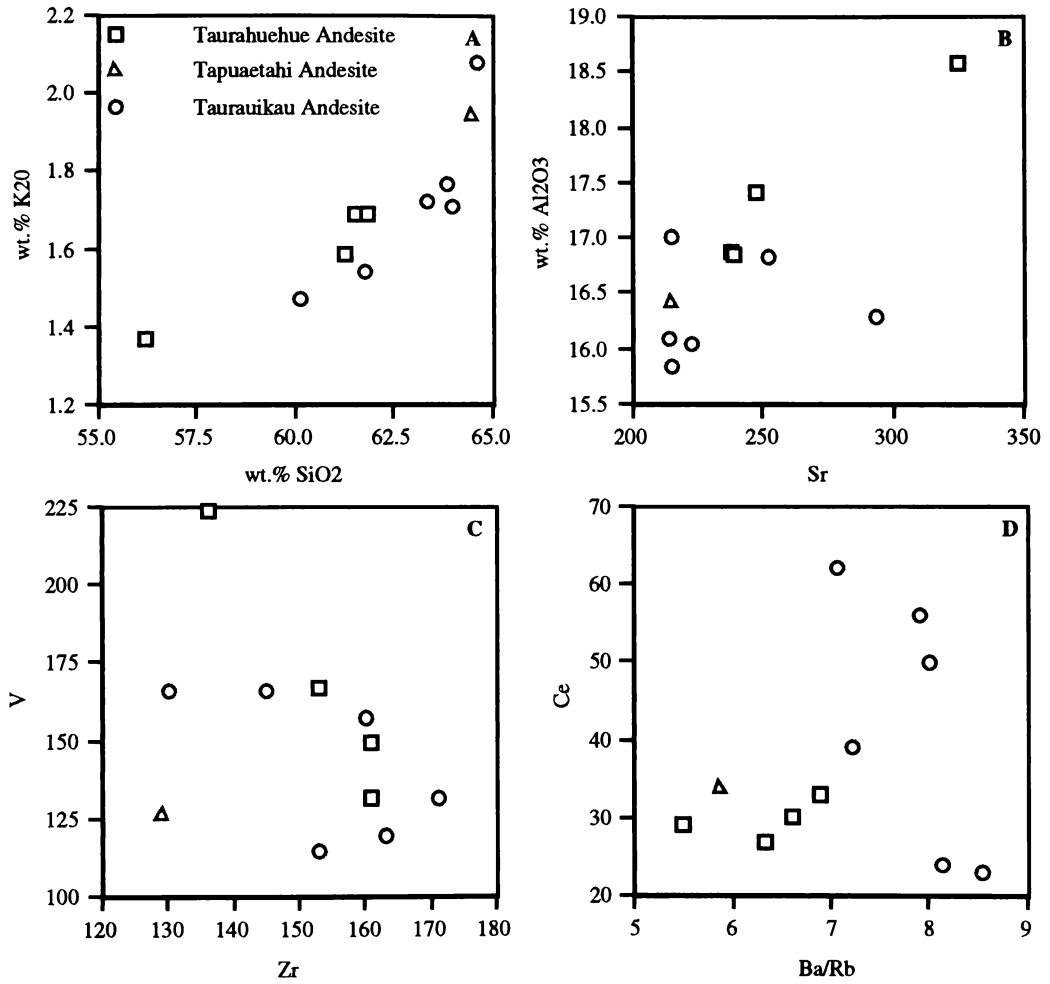


Figure 7.5 Bivariate plots of pre-caldera and caldera-related andesite lavas of the Kapowai Caldera Complex.

Multi-element variation diagrams (normalised to MORB) indicate that the andesite magmas have all been generated in a similar continental margin subduction setting. This is indicated by the negative Nb, P, and Ti anomalies, and depletion in HFSE relative to LILE (Thirwell et al., 1994; Pearce and Peate, 1995). All three andesite formations have a similar multi-element pattern, although there are some differences. Taurauikau Andesite tends to have more enriched LILE relative to Taurahuehue Andesite, and some lavas also have a larger negative Nb anomaly.

Both pre-caldera and caldera-related andesitic-dacitic lavas show a similar pattern of enriched LREE relative to HREE (Figure 7.7). HREE depletion is generally consistent ($La_N/Yb_N$ = 4.04-4.98 ) for all andesite lavas. Overall, the Taurahuehue Andesite shows a marked REE enrichment compared to both the Tapuaetahi and Taurauikau Andesite lavas. A minor negative Eu anomaly (0.77-0.88 Eu/Eu*) suggests that moderate plagioclase feldspar fractionation has occurred in all andesite lavas (e.g. Arth, 1980; Hanson, 1980).

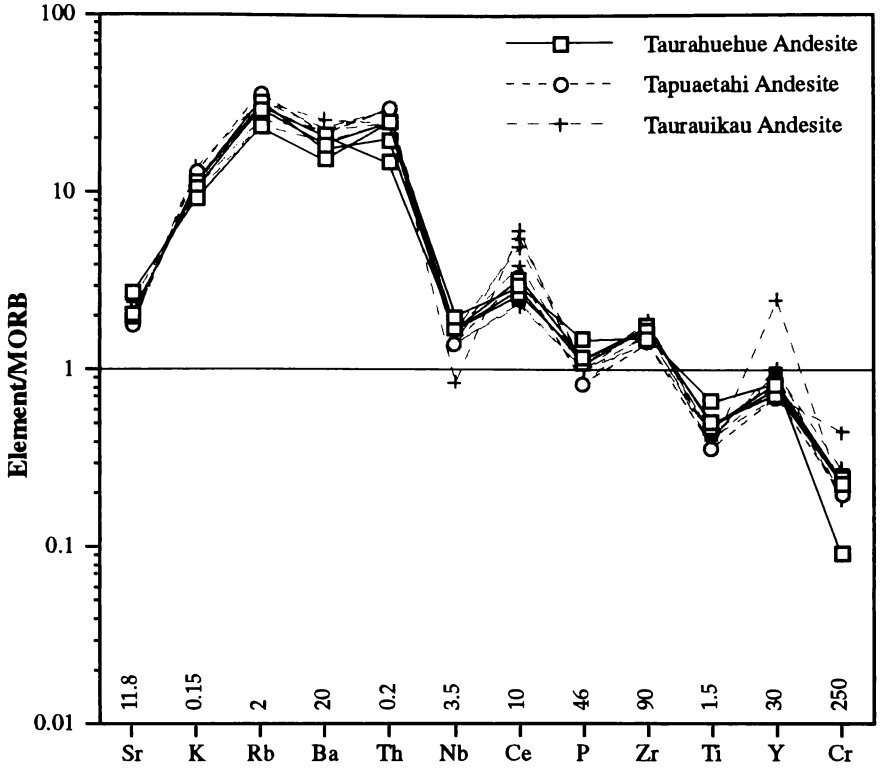


Figure 7.6 Multi-element diagram of pre-caldera and caldera-related andesite lavas of the Kapowai Caldera Complex. Normalising MORB data from Pearce (1983).

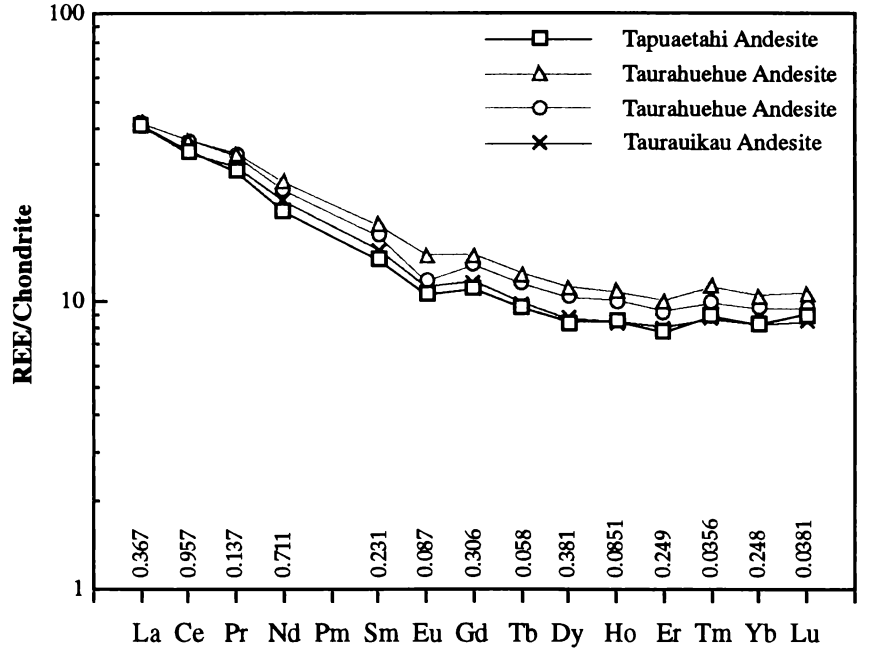


Figure 7.7 REE variations in pre-caldera and caldera andesite lavas of the Kapowai Caldera Complex. Normalising chondritic data from Taylor and McLennan (1985)

Therefore, major and trace element chemistry reveals that there are differences in composition between pre-caldera and caldera-related andesites at the KCC (Table 7.1). Pre-caldera andesite lavas typically have lower $SiO_2$ (56-64 wt.% $SiO_2$), Ba (311-428 ppm), Ce (27-34 ppm), and higher $Al_2O_3$ (16.4-18.59 wt.% $Al_2O_3$), and $TiO_2$ (0.55-1.0 wt. % $TiO_2$) contents compared to caldera-related andesites, although there is some overlap. Pre-caldera lavas have more enriched REE compared to caldera-related andesite lavas, which infers some difference in the petrogenesis of these two lava groups.

Pre-caldera and caldera-related andesitic magma compositions are not related by simple crystal fractionation, and are likely to have evolved via other magmatic processes (i.e. crustal assimilation, mixing). A discussion of the petrogenesis of pre-caldera andesitic magmas and andesitic magmas erupted within the KCC is presented later in this chapter.

Table 7.1 Summary phenocryst mineralogy and geochemistry of pre-caldera and caldera-related andesitic-dacitic magma types at the Kapowai Caldera Complex.

| Unit | Formation | Mineralogy | wt.% $SiO_2$ | wt.% $K_2O$ | K/Rb | Rb/Sr | $La_N/Yb_N$ | Eu/Eu*) |
|---|---|---|---|---|---|---|---|---|
| Pre-caldera | Taurahuehue Andesite | plag + opx + cpx + Fe-Ti oxides | 56.1-61.8 | 1.37-1.69 | 216-241 | 0.15-0.27 | 4.04-4.47 | 0.77-0.88 |
| | Tapuaetahi Andesite | plag + opx ± cpx + Fe-Ti oxides | 64.4 | 1.95 | 222 | 0.34 | 4.96 | 0.85 |
| Caldera-related | Taurauikau Andesite | plag + opx + cpx + Fe-Ti oxides | 60.0-64.6 | 1.47-2.08 | 227-258 | 0.16-0.31 | 4.98 | 0.84 |

***Rhyolitic magmas***

Four rhyolite lava groups have been defined at the KCC on the basis of phenocryst mineralogy. There is no temporal pattern apparent in these rhyolite lavas. The oldest rhyolite (Welcome Jack Rhyolite; rhyolite lava group II) is a quartz-plagioclase-biotite phyric rhyolite lava, and successive rhyolite lavas vary in mineralogy and include plagioclase-pyroxene phyric (rhyolite lava group I), plagioclase-amphibole phyric (rhyolite lava group IV), plagioclase phyric (rhyolite lava group III), and additional quartz-plagioclase-biotite phyric (rhyolite lava group II) rhyolite lavas. The youngest rhyolite lavas erupted are all rhyolite group I lavas, which have a similar composition to the final large scale explosive episode (i.e. WES).

These rhyolite groups have distinctive whole rock geochemical compositions. Compositions vary from low-silica to high-silica rhyolite (71.1-76.5 wt.% $SiO_2$) in group I lavas, to medium-silica rhyolite (72.9-75.4 wt.% $SiO_2$) in group III and IV, and high silica rhyolite (75.8-78.8 wt. % $SiO_2$) in group II lavas.

Bivariate diagrams indicate some overlap in composition between group I, III, and IV rhyolite lavas, although there are some significant differences (Figure 7.8). Group II consistently has the most distinct composition, with high $K_2O$ (3.63-3.76 wt. %), Ba (743-814 ppm), Rb (125-128 ppm), and low $Al_2O_3$

(11.79-13.62 wt .% $Al_2O_3$), and Sr (51-100 ppm) indicating that it is the most evolved group of rhyolite lavas. Rhyolite lava groups III and IV generally show discrete compositions, although this is limited to $K_2O$, Rb, and Ba abundances. Rhyolite lavas in Group I have the most diverse compositions, and there is generally some degree of overlap with the three other groups. Group I rhyolite lavas also contain lavas with the least evolved (i.e. lowest $K_2O$, Rb, and Ba values) rhyolitic compositions.

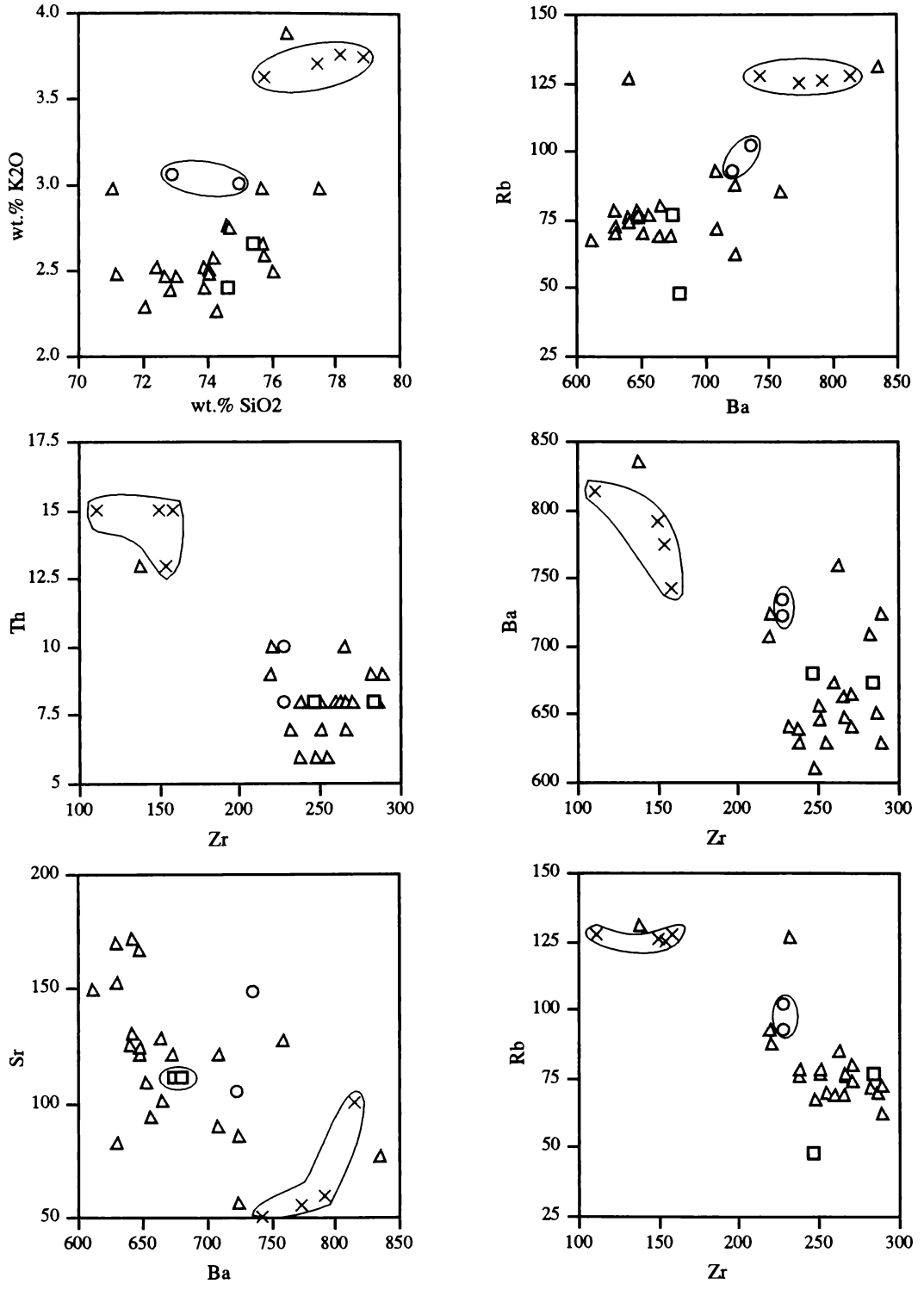


Figure 7.8 Bivariate plots of Kapowai Caldera Complex rhyolite lavas.

Groups III and IV rhyolite lava groups show minor inter-group compositional variations, whereas lavas in group I and group II exhibit considerable differences. For group I, this probably reflects the varying amount and type of pyroxene phase present in these lavas. In group II, it is apparent that the two constituent lavas (Welcome Jack Rhyolite and Ruahine Rhyolite) have significantly different chemistry, which is not reflected in the phenocryst type or abundance as they have similar mineralogy and modal mineral abundance.

Temporal variations are difficult to evaluate because not all lavas have been K/Ar dated. Interestingly, the oldest rhyolite lava dated (Welcome Jack Rhyolite), has the most evolved composition, with the highest $SiO_2$, $K_2O$, Ba, Rb, and lowest $Al_2O_3$, Sr and Zr abundances of all KCC rhyolites. Rhyolite lavas which post-date Welcome Jack Rhyolite contain considerably lower $SiO_2$, $K_2O$, Ba and Rb abundances, suggesting that younger silicic magmas generated at the KCC were less evolved than the oldest lavas. However, there appears to be no systematic variation in composition with time.

There is a limited spatial pattern to the composition of rhyolite lavas erupted at the KCC. Group III rhyolite lavas are restricted to within (Acadia Rhyolite) or on the boundaries of the WES collapse zone, near the central KCC. Rhyolite lavas of group II only occur in the central KCC (Welcome Jack Rhyolite) and on the eastern margin of the topographic boundary (Ruahine Rhyolite), suggesting some structural control on their location, or that they represent discrete magma reservoirs. Group III rhyolite lavas are the least voluminous rhyolite lava group and form small dikes and lava flows in the central and NE sector of the KCC. Rhyolite lavas of group I are the most voluminous group and are distributed throughout the KCC, but generally in the central, southern and NE sectors.

Multi-element variation diagrams (normalised to MORB) show a consistent depletion of HFSE relative to LILE punctuated by negative Nb, P and Ti anomalies (Figure 7.9). This pattern indicates that as with the pre-caldera and caldera-related andesite magmas, KCC rhyolite magmas have all been generated in a similar continental margin subduction setting (Thirwell et al., 1994; Pearce and Peate, 1995). However, it is also possible that the rhyolite magmas have been generated by partial melting of crust with a continental margin subduction setting composition (Hildreth, 1981).

Most rhyolite lavas have a similar multi-element pattern, although there are some differences. Group II rhyolite lavas have the greatest LILE abundances compared to the other three groups. Aside from that difference, lava groups have similar abundances in all other elements, except for $P_2O_5$, $TiO_2$ and Cr where there is considerable variation.

Rhyolite lavas show considerable variation in REE abundances (Figure 7.10a, b). All lavas show a consistent pattern of enriched LREE relative to HREE (15.03-4.08 $La_N/Yb_N$), with moderately steep LREE and flat HREE patterns. However, there are some significant differences in the degree of overall LREE

enrichment, and parallel but widely varying HREE. Most show negative Eu anomalies (apart from the Ruahine Rhyolite), which are more pronounced than in andesite lavas, implying significantly greater plagioclase fractionation in rhyolite magmas (Arth, 1980; Hanson, 1980). The negative Eu anomaly is highly variable (0.58-0.91 Eu/Eu*) within and between rhyolite groups implying varying degrees of plagioclase fractionation.

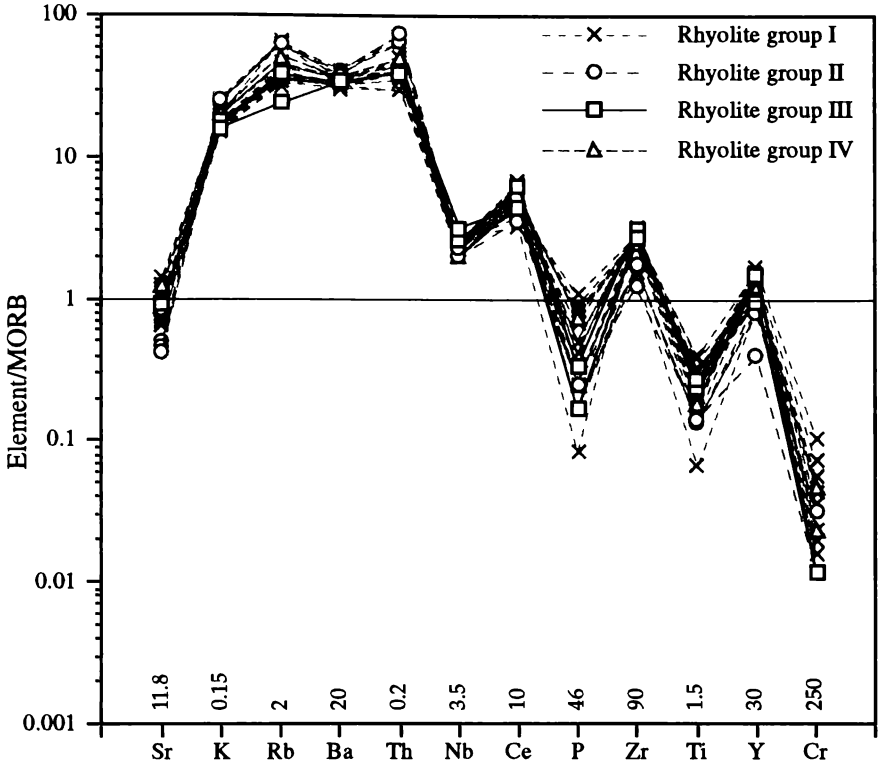


Figure 7.9 Multi-element diagram of rhyolite lavas of the Kapowai Caldera Complex. Normalising MORB data from Pearce (1983).

Group I rhyolite lavas exhibit the largest spread of REE abundances, which is consistent with the highly variable major and trace element composition of lavas within this group. Generally, all lavas within this group show a similar pattern of HREE depletion relative to LREE, but the extent of Eu and Ce anomalies and MREE and HREE depletion varies significantly. Precipice Rhyolite lava has the most depleted REE abundances of all KCC rhyolite lavas, which is consistent with its low-silica (i.e. 71.1 wt.% $SiO_2$) composition. Progressively more enriched REE abundances however, cannot be related by simple crystal fractionation, as increased REE enrichment is not matched by increasing silica composition. This implies that lavas in this group are not genetically related (cf. Woodhead, 1989). Wharepapa Rhyolite lava has a significant depletion in the MREE and HREE relative to other rhyolite lavas of this group and a strong negative Eu anomaly, implying that there has been significant plagioclase and zircon (see below) fractionation (Hanson, 1980).

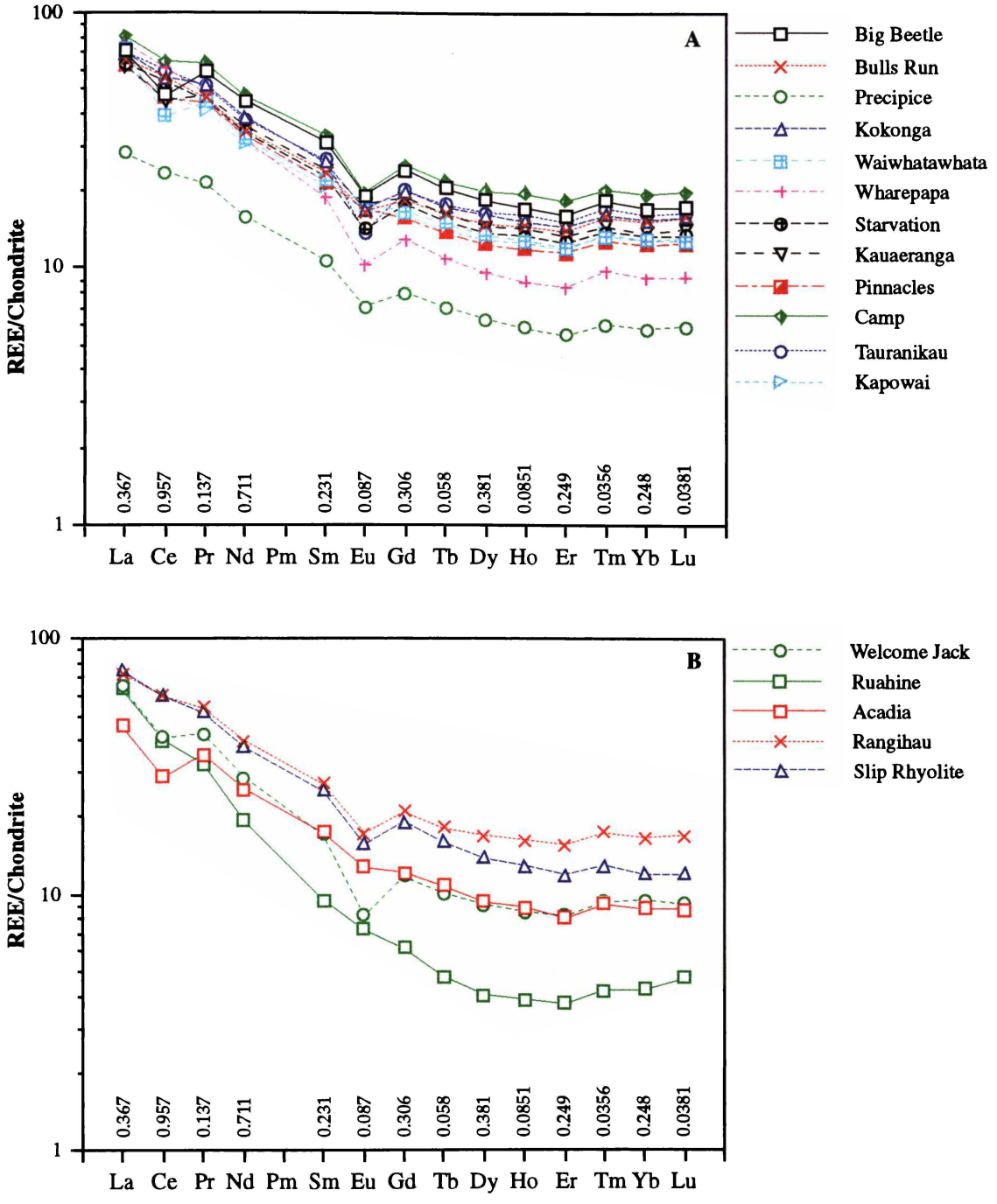


Figure 7.10 Chondrite normalised REE abundances for selected rhyolite lavas of the Kapowai Caldera Complex. A, Group I rhyolite lavas. B, Group II (green), III (red), and IV (blue) rhyolite lavas. Normalising chondritic data from Taylor and McLennan (1985).

Ruahine Rhyolite lava (rhyolite lava group II) contains the most strongly depleted MREE and HREE abundances ($La_N/Yb_N$ = 15.03) of all KCC rhyolite lavas, and has no Eu anomaly. Ruahine Rhyolite also has a distinctive mineralogy (high quartz/plagioclase ratio) and highly evolved major and trace element composition (i.e. wt.% $SiO_2$ = 75.8; wt.% $K_2O$ = 3.63; Zr = 111 ppm). Strong depletion in MREE and concave upward HREE abundances may be explained by fractionation of zircon (Hanson, 1980). Separation of zircon crystals from KCC rhyolite lavas revealed that Ruahine Rhyolite lavas had the most abundant zircon population (ca. 0.25-0.5 modal %), which supports its distinctive HREE depleted pattern. Other KCC rhyolite lavas (and ignimbrites) contain accessory zircon, but at much lower (< 0.1 %) abundances.

Welcome Jack Rhyolite which has a similar mineralogy, but different modal abundance (i.e. (lower quartz/plagioclase ratio) compared with Ruahine Rhyolite, has a strong negative Eu anomaly and flat MREE and HREE pattern implying that plagioclase fractionation has been a significant process in the genesis of this magma (Hanson, 1980).

Group III rhyolite lavas (i.e. Rangihau Rhyolite and Acadia Rhyolite) show different REE patterns. Acadia Rhyolite has the most depleted REE abundances, has a strongly negative Ce anomaly, and weakly negative Eu anomaly. In comparison, the Rangihau Rhyolite parallels, but is more enriched in LREE than the Acadia Rhyolite and has no Ce anomaly. MREE and HREE in the Rangihau Rhyolite are more enriched compared to the Acadia Rhyolite, suggesting that zircon fractionation was more prominent in the Acadia Rhyolite (Hanson, 1980). These REE patterns imply a petrogenetic relationship between these two magmas, which may be different degrees of fractionation. Differences in Ce anomalies may be related to incipient weathering.

Slip Rhyolite (group IV) has a similar pattern to most KCC rhyolite lavas of depleted HREE relative to LREE, and a negative Eu anomaly. Although amphibole is a major phenocryst phase in this rhyolite, there is only a weak depletion of MREE compared to the Rangihau Rhyolite which contains no amphibole. This indicates that in the evolution of the Slip Rhyolite magma, amphibole fractionation was minor compared with plagioclase fractionation.

Ce anomalies vary considerable between all rhyolite lavas from strongly negative (e.g. Big Beetle Rhyolite) to weakly negative (e.g. Kauaeranga Rhyolite) to no anomaly (e.g. Bulls Run Rhyolite). Negative Ce anomalies in arc magmas are inferred to be inherited from subducted oceanic sediments (Hole et al., 1984; Woodhead, 1989), but they may also be developed in volcanic rocks that have suffered from incipient weathering or hydrothermal alteration (Price et al., 1991; Briggs et al., 1993). As incipient weathering has affected KCC ignimbrites, it is also highly likely that some of these Ce anomalies are related to weathering of rhyolite lavas, even though there is no indication of weathering in thin sections.

Variable REE abundances in rhyolite lavas at the KCC reflects the differences in phenocryst and accessory phase mineralogy and abundance. This is similar to other rhyolitic volcanic centres in the CVZ and TVZ (Nairn, 1989; Sutton, et al., 1995; Briggs et al., 1998). REE compositions in particular compare favourably to some TVZ rhyolitic calderas where highly variable REE abundances are common (e.g. Briggs, et al. 1993). Importantly at the KCC, accessory zircon phenocrysts have a significant control on the REE element abundances in some rhyolitic magmas. Group II (quartz-plagioclase-biotite phyric) rhyolite lavas are the main type, although some pyroxene-phyric lavas (i.e. Wharepapa Rhyolite) are also likely to have similar REE patterns because of low Zr abundance (i.e. < 160 ppm) and occurrence of accessory zircon (< 0.5 %) (Figure 7.11).

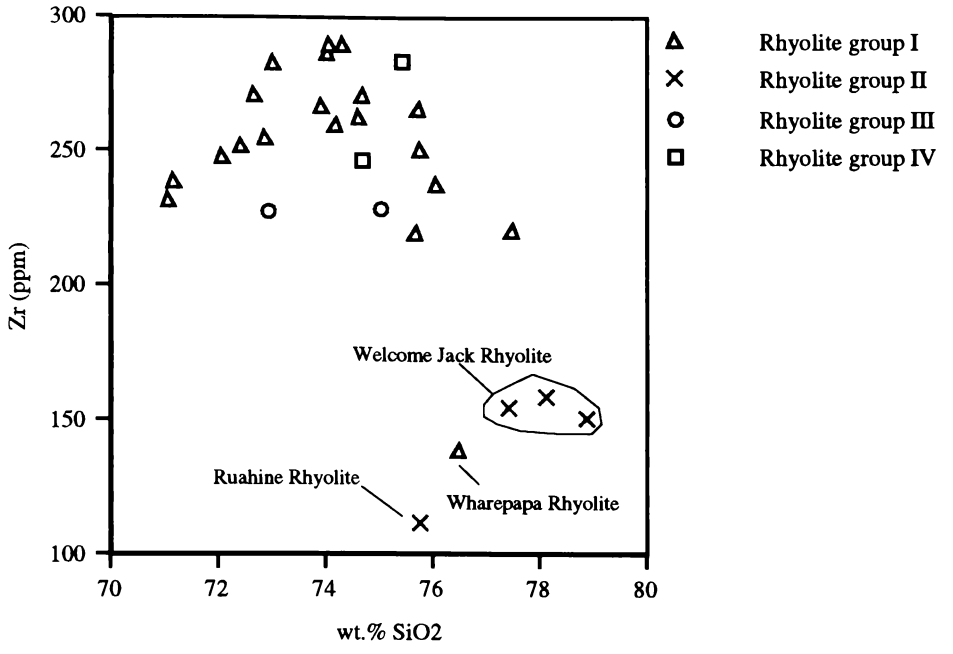


Figure 7.11 Zr-$SiO_2$ plot of Kapowai Caldera Complex rhyolite lavas, illustrating low Zr abundances in lavas which contain the highest abundance of accessory zircon, and the most depleted MREE and HREE abundances.

Although there are variations within groups, four broad rhyolite magma types can be defined at the KCC, combining both the mineralogy, and major element, trace element and REE chemistry, (Table 7.2).

Table 7.2 Summary phenocryst mineralogy and geochemistry of rhyolitic magma types at the Kapowai Caldera Complex.

| Rhyolite group | Phenocryst mineralogy | $SiO_2$ | $K_2O$ | K/Rb | Rb/Sr | $La_N/Yb_N$ | Eu/Eu*) |
|---|---|---|---|---|---|---|---|
| I | plag + opx ± cpx + Fe-Ti oxides ± zir ± apat | 71.0-77.5 | 2.26-3.88 | 195-320 | 0.45-1.70 | 4.08-8.24 | 0.59-0.93 |
| II | qtz + plag + biot + Fe-Ti oxides + zir + apat | 75.8-78.9 | 3.63-3.76 | 235-247 | 1.28-2.51 | 6.87-15.03 | 0.58-0.95 |
| III | plag + Fe-Ti oxides ± zir ± apat | 74.6-75.4 | 2.40-2.66 | 286-415 | 0.43-0.69 | 4.36-5.19 | 0.72-0.88 |
| IV | plag + amph + Fe-Ti oxides ± zir ± apat | 72.9-75.0 | 3.01-3.06 | 249-269 | 0.68-0.89 | 6.21 | 0.72 |

## 7.6 Comparison with central CVZ volcanic rocks

Central CVZ is a significant area of andesitic and rhyolitic volcanism in New Zealand. Numerous rhyolite domes of varying mineralogy have been erupted in the late Miocene-early Pliocene. Several volcanic centres have been defined where multiple lava domes or flows occur (Skinner, 1986). This section compares the composition of KCC volcanic rocks to selected central CVZ rocks using bivariate plots.

### Andesite-Dacite lavas

Andesitic-dacitic lavas erupted at or near the KCC, generally have dissimilar major and trace element chemistry compared with other intermediate composition lavas erupted in the central CVZ (Figure 7.12). Taurauikau Andesite has a more variable, but overall different composition compared with the closest analogous Omahine Subgroup andesite lava, which outcrops 10 km SE from the SE topographic margin of the KCC (McGunnigle, 1995). Compared to these Omahine Subgroup lavas, Taurauikau Andesite lavas typically have higher MgO, Ba and $Al_2O_3$ abundances.

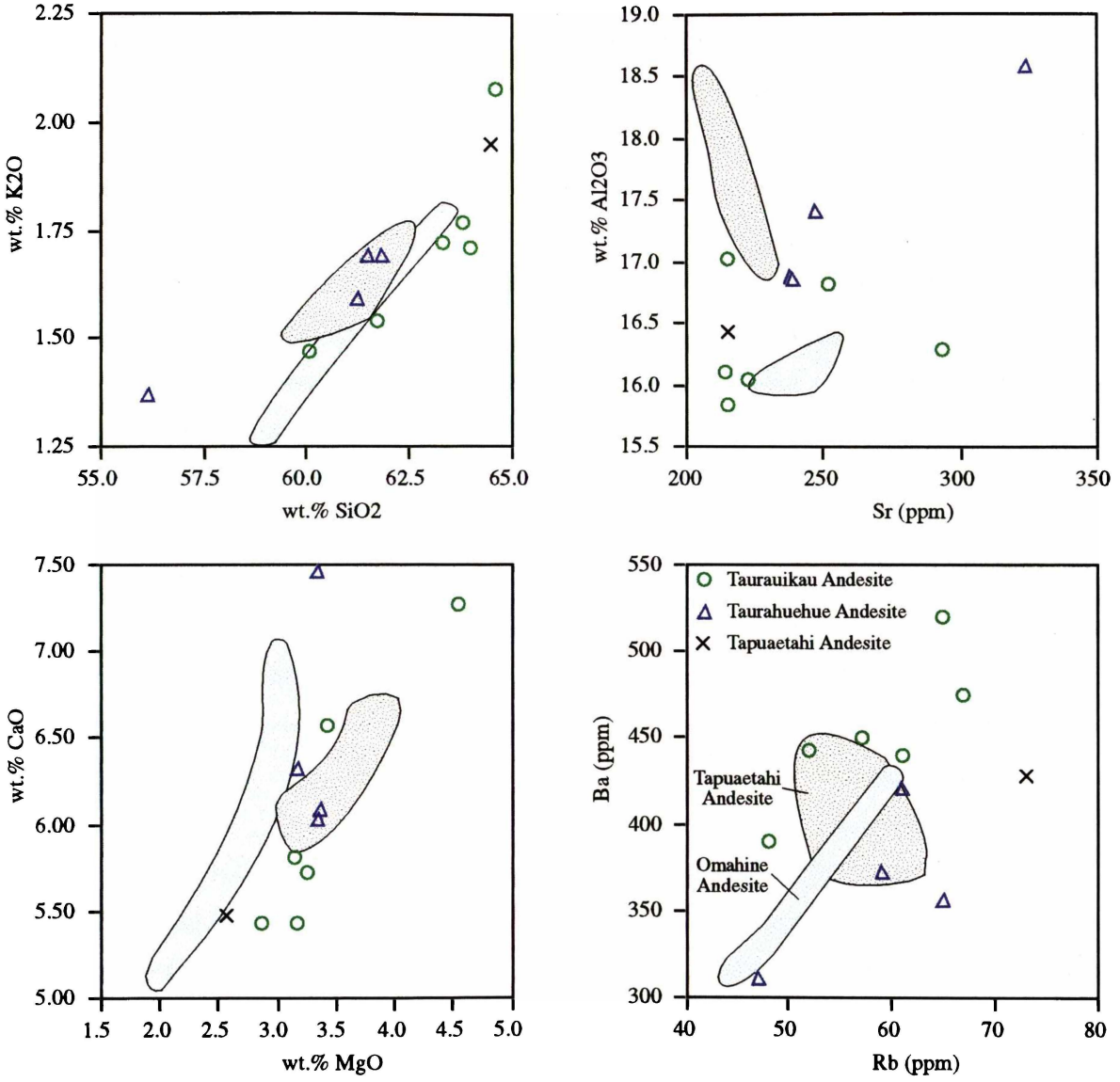


Figure 7.12 Bivariate diagrams comparing pre-caldera and caldera-related andesitic-dacitic lavas at the Kapowai Caldera Complex with other central CVZ andesitic-dacitic lavas. Fields established using data from Adams (1992) and McGunnigle (1995).

Tapuaetahi Andesite lavas erupted near the eastern margin of the KCC, have significantly different compositions to Tapuaetahi Andesite erupted between Tairua and Hot Water Beach, with higher Rb. $K_2O$ and lower MgO and CaO (Adams, 1992). No data are available to directly compare with Taurahuehue Andesite lavas from the KCC, although these KCC lavas do have some similar major element compositions compared with the Tapuaetahi Andesite from between Tairua and Hot Water Beach.

The differences in composition between these spatially different and in some cases (i.e. Omahine Subgroup lavas cf. Taurauikau Andesite) temporally different intermediate composition lavas is not surprising. Compositions typically vary within lavas erupted from the same composite cone or stratovolcano, and also between composite cones in the same volcanic arc. This is well documented for most volcanic arcs (e.g. Hildreth and Moorbath, 1988; Peate et al., 1997) and is clearly apparent in extinct and active North Island volcanic arcs (Adams et al., 1994, Graham et al., 1995).

### Rhyolite lavas

Rhyolite lavas erupted at the KCC generally have distinctive major and trace element chemistry compared with rhyolites erupted from other volcanic centres in the central CVZ (Figure 7.13). Although KCC lavas have a similar $SiO_2$ compositional range, they form a distinct low $K_2O$ series within all central CVZ rhyolite lavas.

Group I rhyolite lavas of the KCC are the most distinctive group with low $K_2O$, Rb, and high Zr abundances. There are some similarities in major and trace elements (i.e. CaO, MgO, $Al_2O_3$, and Sr) with the Motutapere and Cooks rhyolite lava domes at the Whitianga Volcanic Centre (Fisher, 1986; Rogers, 1994) and the Whenuakite and Pukekotare rhyolite lavas immediately north of the northern margin of the KCC topographic boundary (Adams, 1992; Guay, 1999).

Group II lavas show no major and trace element similarities with other central CVZ lavas. Significantly, they also differ from similar quartz-plagioclase-biotite phyric lavas which occur immediately to the east of the Ruahine Rhyolite (Skinner, 1995; Karl, 1996). The age relationship of these two lava sequences is unclear, so that no genetic relationship can be established, although their distinctive chemistry implies that although mineralogically similar, the bulk magma compositions were very different.

Compared to other central CVZ rhyolite lavas, Group III and IV rhyolite lavas also typically have distinctive major and trace element chemistry, although the data for these rhyolite groups is limited. As with the Ruahine Rhyolite lavas, similar mineralogy in both group IV rhyolite lavas and the Pukekotare Rhyolite (which occurs adjacent to the northern margin of the KCC) is not matched by any similarities in bulk chemistry (Guay, 1999). This further supports the model that rhyolite lavas erupted at the KCC and in other areas of the central CVZ represent compositionally discrete magma batches.

## 7.7 Petrogenesis of KCC magmas

Major and trace element geochemistry together with the basaltic andesite-andesite-rhyolite series confirm a calc-alkaline magmatic series for KCC volcanic rocks, which is consistent with most CVZ volcanic rocks (Adams et al., 1994). Calc-alkaline magmas are considered to be generated in an active continental margin where oceanic crust is subducted (Wilson, 1989).

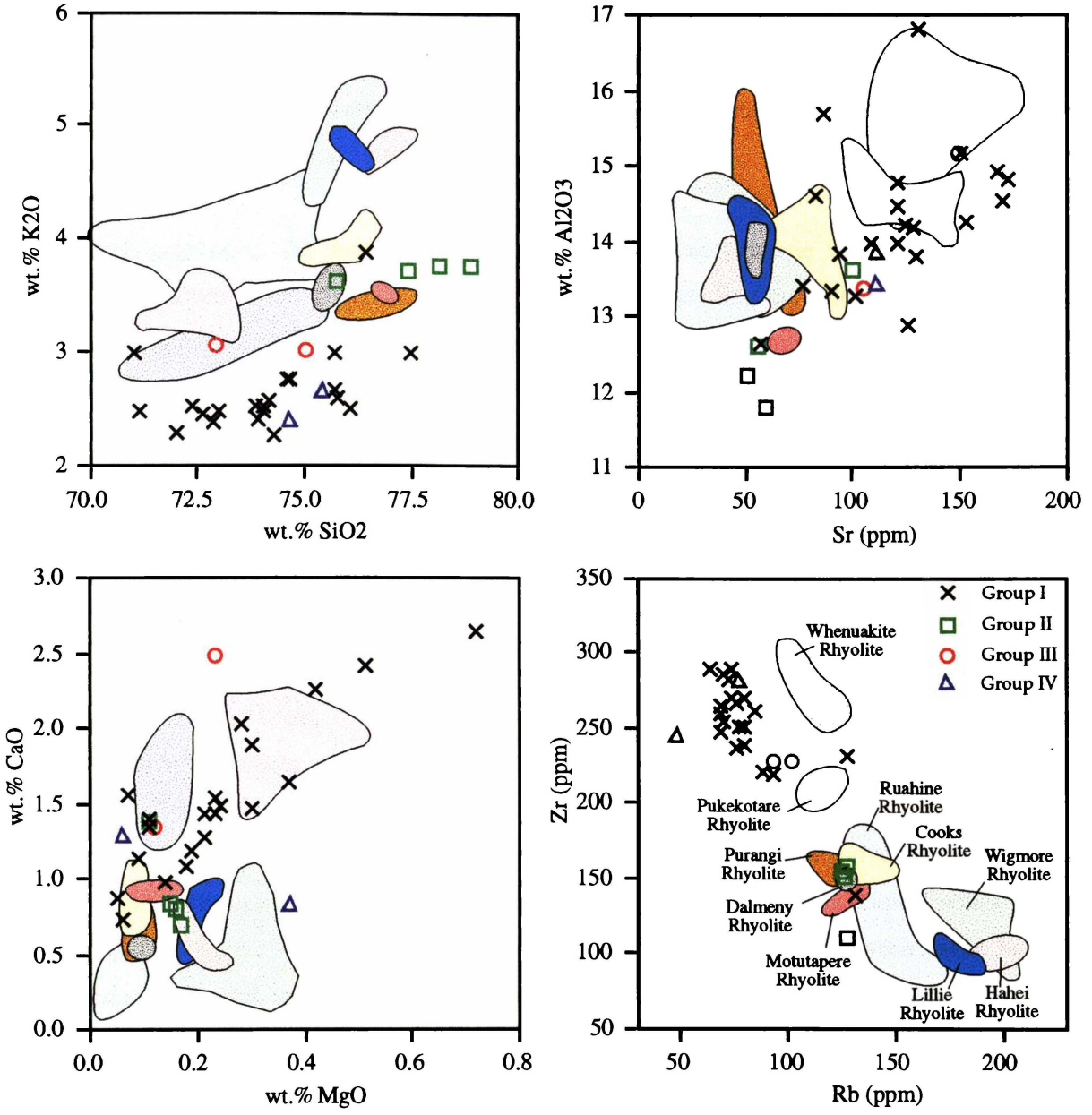


Figure 7.13 Comparison of group I-IV Kapowai Caldera Complex rhyolite lavas of this study with other central CVZ rhyolite lavas. Fields established using data from Fisher (1986), Adams (1992), Rogers (1994), Bardebes (1997), Karl (1996), and Guay (1999).

Petrogenetic models describing the generation of subduction-related continental arc magmas have been well established (Gill, 1981; Wilson, 1989). Generally, three major components are considered in these models, which are the: (i) subducting slab (i.e. oceanic crust and sediment veneer); (ii) mantle wedge (consisting of depleted asthenosphere and enriched subcontinental lithosphere); and (iii) the continental crust (lower and upper crust) (Wilson, 1989; Hawkesworth, 1991; Arculus, 1994; Pearce and Peate, 1995). Numerous processes have been postulated to occur within and between these components (e.g. Pearce and Peate, 1995).

Hydrous fluids released by dehydration from the subducting slab are considered to provide the primary impetus for melt generation (Peate et al., 1997). Variable element fractionation takes place during this transfer process, and as the fluid migrates through and equilibrates with the mantle wedge (Hawkesworth

et al., 1991; Pearce and Peate, 1995). Trace element anomalies (i.e. negative Ce, Nb anomalies) characteristic of arc magmas are considered to relate to this subducting slab component (Hole et al., 1984; Woodhead, 1989). Low Ce abundances in arc-related volcanic rocks may also result from weathering or hydrothermal alteration (Price et al., 1991; Briggs et al., 1993).

Following melt generation, the melt migrates up through the denser mantle wedge to the base of the continental crust. During this stage, melt-mantle interactions including crystallisation and assimilation within the subcontinental lithosphere and ponding at the base of the continental crust may take place (Pearce and Peate, 1995). Further upward migration may see magma assimilation, storage and homogenisation occurring at the base of the continental crust and assimilation-fractional crystallisation at shallower levels (Pearce and Peate, 1995).

This section focuses on the petrogenesis of the andesitic and rhyolitic magmas generated at the KCC, and attempts to establish any genetic relationship between them. Trace element data are used to constrain the nature of the source and, together with petrographic and mineralogic data, to establish the key magmatic processes which have occurred. No isotopic data have been obtained in this study, so establishing the source composition and role of crustal assimilation is restrictive.

Central to the arguments for determining petrogenetic processes, are the spatial and temporal relationships of magma batches. The suite of KCC volcanic rocks are spatially related, having erupted within or on the immediate margins of the caldera complex. However, temporal variations between lavas have been difficult to constrain, and consequently the genetic relationships between magma batches (e.g. crystal fractionation, assimilation, mixing) are not always simple to establish.

### Source characteristics

Sr, Nd, and Pb isotopic data are routinely used to constrain the source composition of magmas. However, as this data has not been obtained during this study, incompatible element ratio and element-element bivariate diagrams are drawn to approximate the ratio of the elements in the source region (Figure 7.14) (Sun and McDonough, 1989). The ratio of a pair of highly incompatible elements, whose bulk partition coefficients are similar, will not vary during fractional crystallisation and will vary little during partial melting, and will therefore indicate the ratio of their composition in the source (Woodhead, 1989; Rollinson, 1993).

KCC data plotted on the Y-Ho plot produces a strong linear relationship, but the same data plotted on other diagrams (i.e. U/Nb-U/Pb and Sm-Hf) is more scattered. This suggests that the source material has a heterogeneous composition (Bougault et al., 1980). Some data which plots away from the general trends also have elevated Ce and Y abundances implying incipient weathering of these samples.

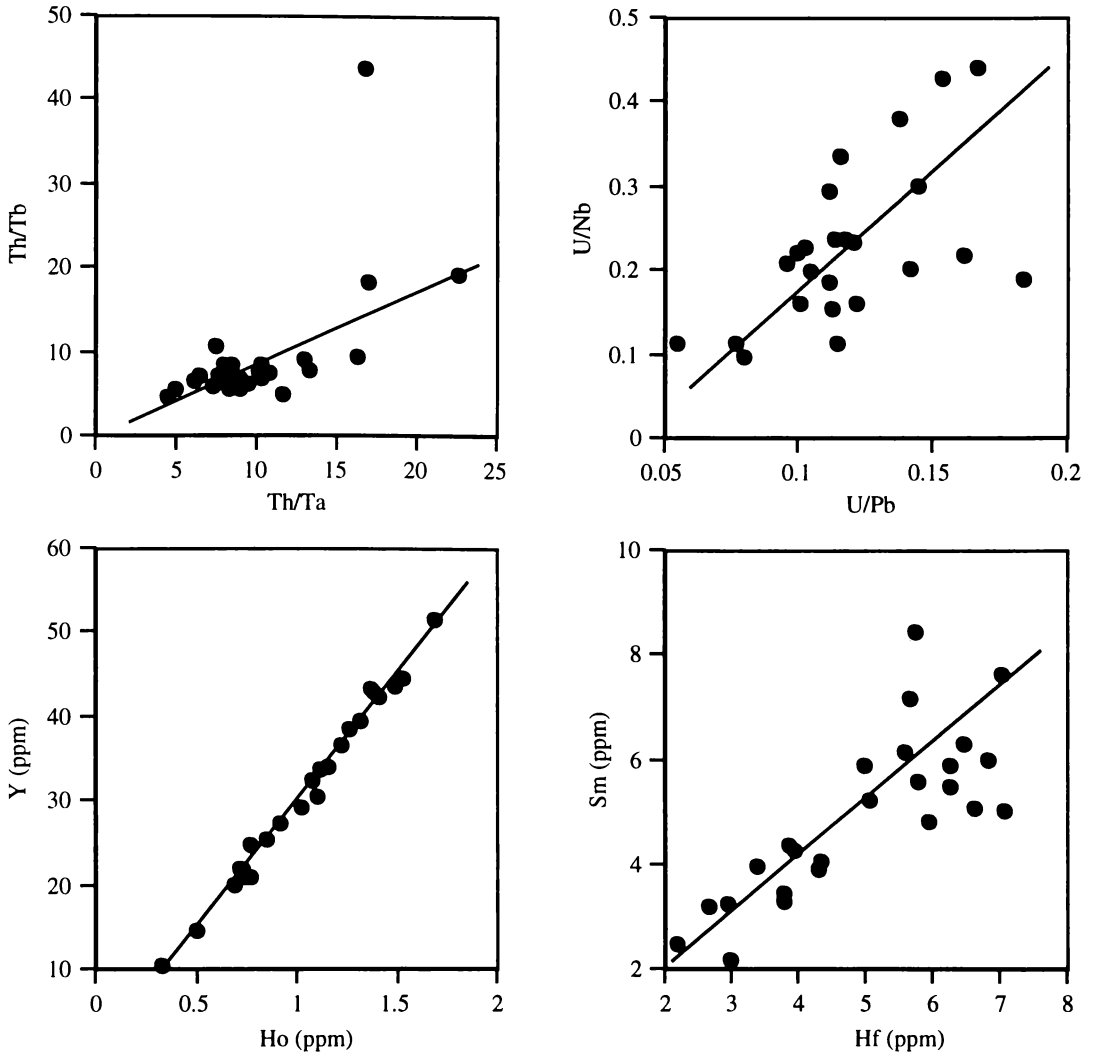


Figure 7.14. Highly incompatible element ratios and element bivariate diagrams for Kapowai Caldera Complex volcanic rocks. Only ICP-MS data are plotted.

A generally consistent trend of LREE enrichment relative to HREE for both andesite and rhyolite lavas (Figure 7.15), implies broadly similar petrogenetic pathways for intermediate and silicic magmas generated at the KCC, following melt generation (Wilson, 1989). Differences in composition have arisen because of the variable extent of processes (crystal fractionation, magma mixing, assimilation) within the melting column and lithosphere, and possibly due to variations in the source composition (Pearce and Peate, 1995).

## Crystal fractionation

As with most arc-related magmas, crystal fractionation is likely to be the major magmatic process which has influenced the petrogenesis of KCC magmas after the initial source melt was formed (Wilson, 1989). This is initially suggested by major and trace element variation diagrams, although most of these magmas are not temporally related and so direct fractionation between these magmas is not possible.

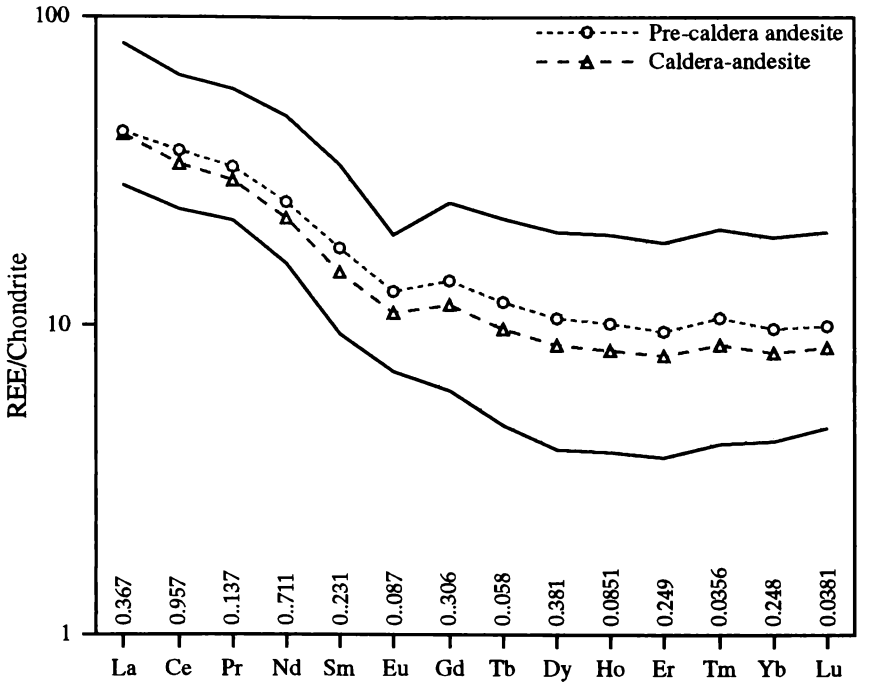


**Figure 7.15 Chondrite normalised REE diagram of pre-caldera and caldera-related andesite lavas compared to the range of REE abundances in Kapowai Caldera Complex rhyolite lavas (grey). Normalising chondritic data from Taylor and McLennan (1985).**

To confirm fractionation processes in some intermediate (i.e. Taurauikau Andesite, Taurahuehue Andesite) and silicic magma suites (i.e. Welcome Jack Rhyolite), one method is to utilise incompatible ratio-incompatible element plots (Allegre and Minster, 1978). If crystal fractionation is the dominant petrogenetic process, a constant, horizontal relationship is present. However, if a sloping line results, this may infer differing degrees of partial melting (Allegre and Minster, 1978). Incompatible elements are readily recognised for intermediate composition magmas (e.g. Zr, Rb, Ba), although the presence of additional mineral phases (e.g. biotite, hornblende, zircon, apatite) in silicic magmas means that these elements are not (Zr) or less incompatible (Ba, Rb) (Wilson, 1989).

Plots of Ba/Th-Th (Figure 7.16a) and Rb/Th-Th (Figure 7.16b) are generated to test for fractionation as these are the least incompatible elements for the compositions erupted at the KCC. In both of these plots there are no linear trends present within any intermediate or silicic lava groups, implying that these lavas are not related by crystal fractionation. Significantly, there is also a divergence in the overall slope of intermediate and silicic magmas (Figure 7.16a), implying that there is no petrogenetic relationship, even though the Taurauikau Andesite lavas were erupted at similar times to most of the rhyolite lavas at the KCC.

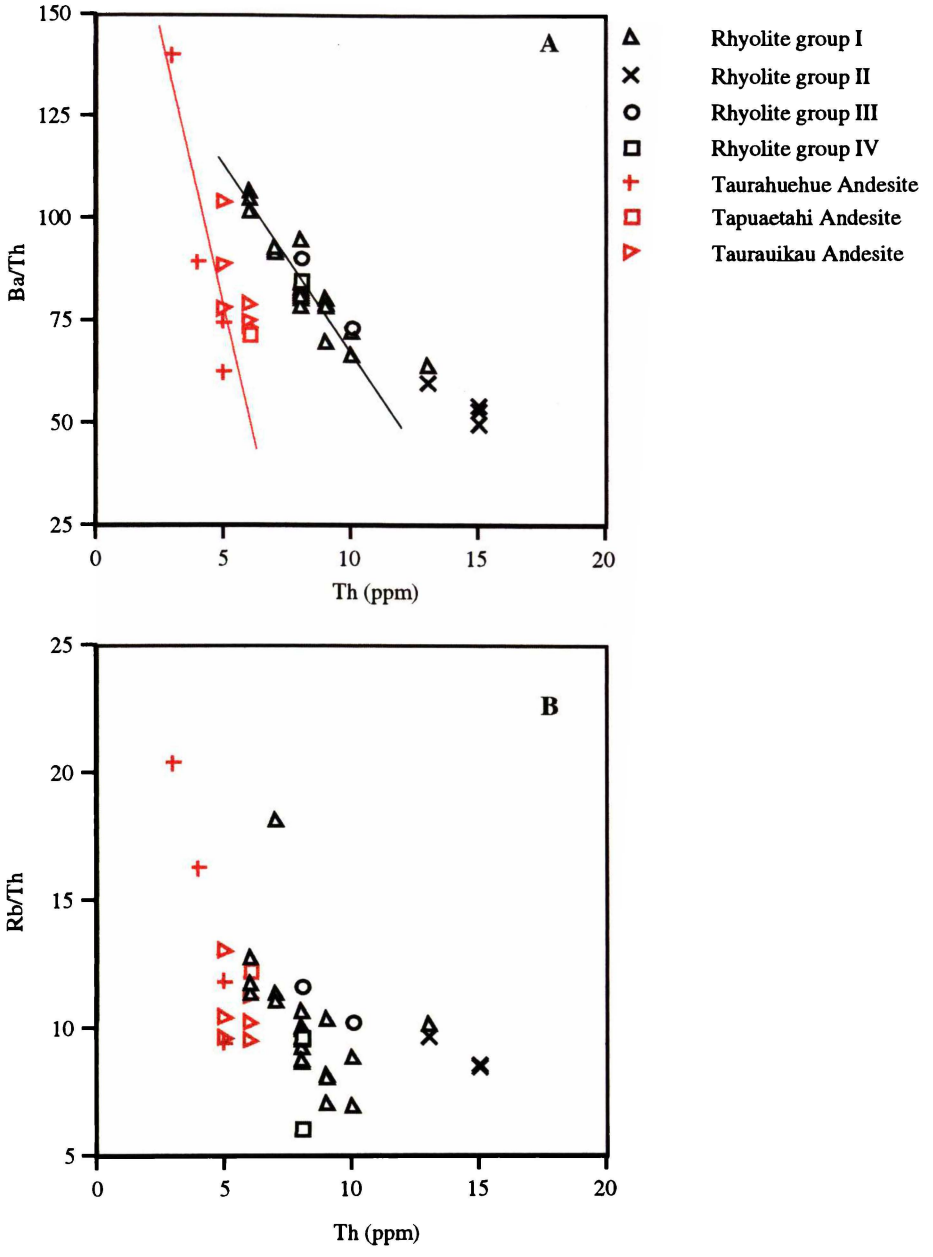


Figure 7.16 Bivariate incompatible ratio - incompatible element plots illustrating no crystal fractionation relationship between Kapowai Caldera Complex volcanic rocks. A, Ba/Th - Th. B, Rb/Th - Th.

## Magma mixing

Mixing of magmas is a process whereby discrete magma bodies interact and mix to form an intermediate or hybrid composition (Hibbard, 1995). Evidence for magma mixing and mingling (incomplete mixing of magmas) at the KCC is clearly indicated by the Oteao Ignimbrite. This ignimbrite contains both scoria and pumice juvenile clasts, as well as mingled scoria-pumice and mixed scoria and pumice, inferring a complex interaction between at least two mafic and silicic magmas.

There is also petrographic and mineralogical evidence of disequilibrium textures including: (i) reverse and oscillatory compositional zoning of phenocrysts and crystals; (ii) mantling of orthopyroxene and clinopyroxene phenocrysts by finer grained pyroxene; and (iii) the presence of co-existing orthopyroxene

and clinopyroxene phenocrysts with different Mg/Fe ratios in the same sample. These textures may indicate magma mixing, although other processes including magma replenishment and magma convection may also generate these textures. Most of these features are observed in the andesite lavas, which is not surprising given that most intermediate composition magmas generated at continental arcs characteristically show evidence of mixing (e.g. Graham and Hackett, 1987; Clynne, 1999).

Rhyolitic lavas and ignimbrites show limited evidence for mixing of silicic magmas and this includes occasional reversely zoned plagioclase phenocrysts, and multiple pumice types in some ignimbrites. Several pumice types in ignimbrites may indicate either mixing of discrete silicic magmas, or compositional zonation of a single silicic magma chamber. Incipient weathering of pumice clasts precludes more detailed geochemical investigation of these processes.

Geochemical data can be used to test for magma mixing by comparing the relationship of incompatible element-element ratios in bivariate plots (Langmuir et al., 1978). In these plots, data producing clear hyperbolic or curved relationships imply that mixing has been a major petrogenetic process (Langmuir et al., 1978). To discount the possibility that the mixing curve may be fortuitous, a second or companion plot is made consisting of the original ratio versus the denominator of the ratio. In this plot, mixing will be indicated by a linear relationship of all data (Langmuir et al., 1978). As previously mentioned, there are poor temporal constraints on most of the magmas generated at the KCC. Only some suites of andesite (Taurauikau Andesite, Taurahuehue Andesite) and silicic magmas (Welcome Jack Rhyolite) were erupted in a time (i.e. by field relationships or K/Ar dating) constrained sequence.

In a Rb-Rb/K diagram there is no hyperbolic relationship between KCC andesitic and rhyolitic magmas, indicating that mixing did not take place between these magmas (Figure 7.17a). On the companion diagram (1/K-Rb/K), there is also no linear relationship. However, within the Taurahuehue Andesite and the Taurauikau Andesite lavas there is an apparent linear relationship (Figure 7.17b), suggesting that mixing of less mafic and more mafic magmas within these two groups may have occurred.

### Crustal contamination

Contamination or assimilation of crustal lithologies into magmas can be an important process in the generation and diversification of magmas. Crustal lithologies (e.g. upper crustal greywacke, its metamorphosed equivalent, and lower crustal granulite) can be established from the recognition of crust-derived xenoliths, and can directly imply interactions between magmas and the crust (e.g. Graham et al., 1990). Crustal xenoliths have been observed in pre-caldera andesites, KCC lavas, and KCC ignimbrites, and include granulite (lower crust), hornfels, granodiorite and andesite lavas (upper crust), all of which infer that crustal assimilation has occurred in some KCC magmas.

In many calc-alkaline suites, assimilation coupled with fractional crystallisation (AFC) is considered to be an important component in the petrogenesis of magmas (DePaolo, 1980; Hildreth and Moorbath, 1988; Graham et al., 1995; Smith, et al., 1996). At the KCC and at other CVZ volcanic centres, AFC is likewise considered to be a potential petrogenetic process, although the data (i.e. Sr, Nd, Pb isotopic data) is yet to be acquired to fully test this (cf. Hawthorn, 1996).

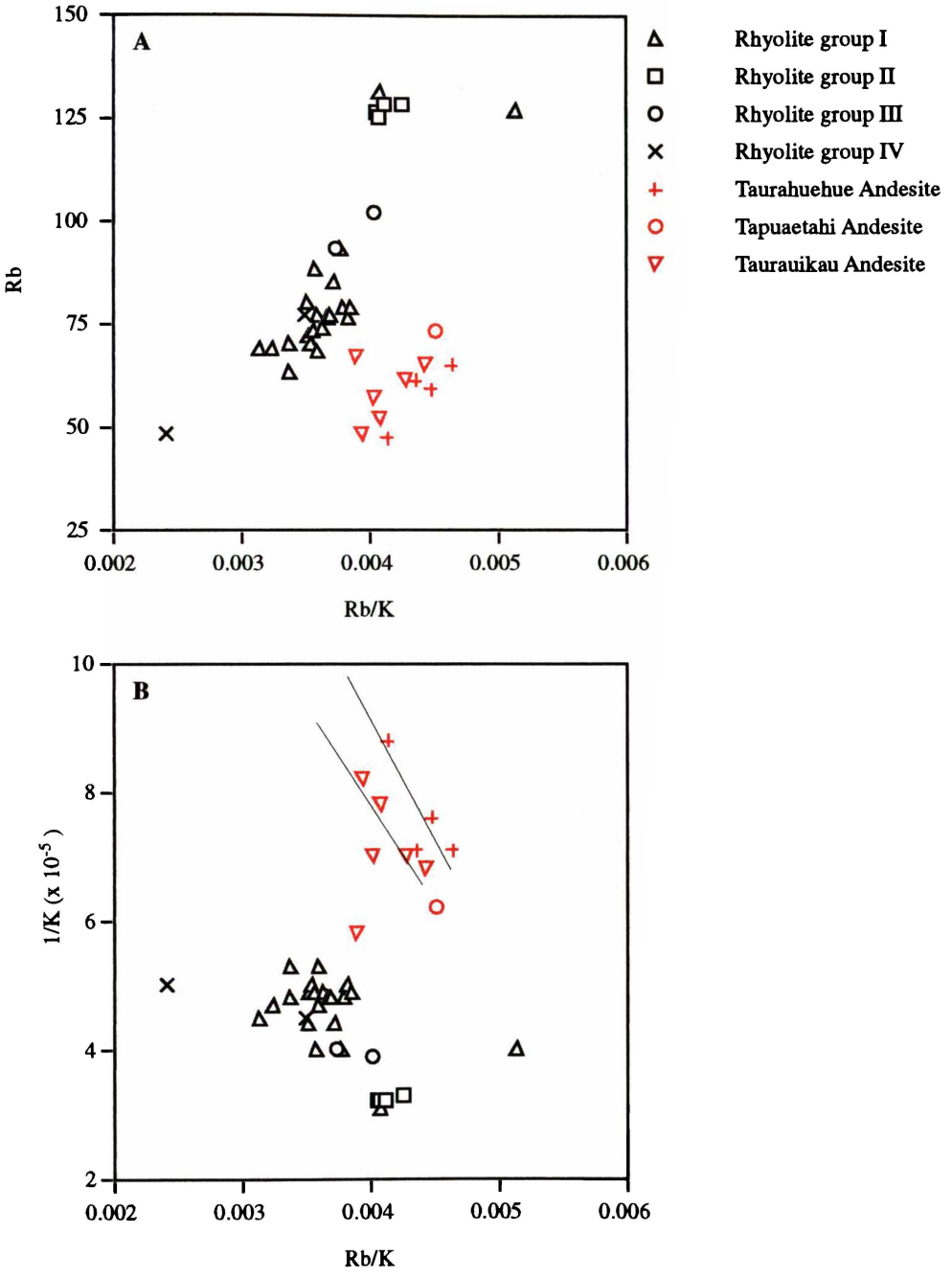


Figure 7.17 Incompatible element - element ratio diagrams of Kapowai Caldera Complex volcanic rocks as a test for magma mixing.

## Summary of petrogenesis

### *Pre-caldera and caldera-related andesitic-dacitic magmas*

KCC andesites and dacites show compositional characteristics similar to other intermediate continental arc lavas (Gill, 1981), and it is likely that they were generated by similar processes. These are dominated by fractionation of mantle-derived basaltic magmas, but also include crustal assimilation and magma mixing.

Andesitic-dacitic magmas generated at the KCC show broadly similar major and trace element (including REE) compositions implying that similar petrogenetic processes have occurred during their development. Crystal fractionation is the governing process and is inferred from major and trace element variation diagrams, and incompatible element ratio - incompatible element plots. Mixing of andesitic-dacitic magmas is also evident and includes a mixed/mingled andesitic ignimbrite (Oteao Ignimbrite), disequilibrium compositions of co-existing orthopyroxene and clinopyroxene phenocrysts, varying compositional zonation (reverse and oscillatory) of plagioclase phenocrysts, and sieve textures in plagioclase phenocrysts.

Basaltic lavas are rare at the KCC (cf. Skinner, 1995), so that a direct examination of possible fractionation of parental basaltic magma to generate andesitic magmas cannot be undertaken. However, basalts (Mercury Basalts Subgroup) are common on the eastern margin of the Kuaotunu Peninsula, 30 km NE of the KCC and calc-alkaline basalts from this area (i.e. Opito Bay Basalts) are used as a parental composition to test for fractionation (Hawthorn, 1996).

With crystal fractionation, it would be expected that the andesite lavas should show LILE enrichment relative to the basaltic composition (Wilson, 1989). LILE enrichment is apparent for $K_2O$, Ba and Th, although there is no enrichment in Sr or Rb (Figure 7.18). Significantly, KCC andesite lavas show the least Nb depletion compared to the basaltic lavas. This contrasts with the expected abundance relationship, where the greatest Nb depletion should be in the more evolved andesitic compositions, which are likely to have suffered more from crustal contamination (Wilson, 1989). Therefore, fractionation from a parental basaltic composition is possible, and probably the key process, although other process identified by petrographic and mineralogical analysis including magma mixing and assimilation are likely to be variably involved.

### *Rhyolitic magmas*

Rhyolitic magmagenesis in subduction-related continental arcs is a controversial process that has still to be resolved for many well studied large volume rhyolitic provinces (e.g. Graham et al., 1995). Several hypotheses have been suggested for the generation of rhyolitic magmas and include: (i) crustal fusion by massive transfer of heat from the mantle to the crust (Graham et al., 1992); (ii) fractionation from basaltic parental magma (Riciputi, 1995); and (iii) fractional crystallisation of basalt accompanied by crustal assimilation (Graham et al., 1995).

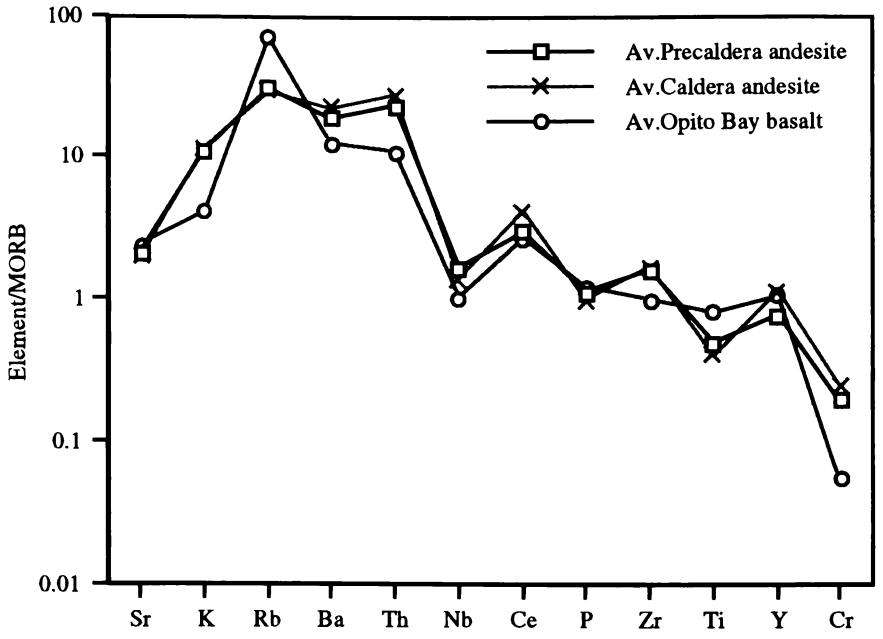


Figure 7.18 MORB normalised multi-element diagram comparing average pre-caldera and caldera-related Kapowai Caldera Complex andesite compositions with Mercury Basalt from Opito Bay, Kuaotunu Peninsula (data from Hawthorn, 1996). MORB normalising data from Pearce (1983).

Many of these models rely upon trace element and Sr, Nd, Pb and O isotopes of temporally related rhyolitic ignimbrites and lavas to evaluate petrogenetic processes (McCulloch et al., 1994; Sutton et al. 1995). Temporal constraints are poor at the KCC and radiogenic isotopes have not been obtained. However, key magmatic processes have been identified using trace element data.

Parental basaltic magmas of KCC rhyolitic magmas are likely to have a different composition to that of the Opito Bay basalt (Hawthorn, 1996), as a multi-element diagram indicates that the basalt and KCC rhyolites have distinctive and unrelated multi-element patterns (Figure 7.19). This implies that the KCC rhyolitic magmas evolved from a different parental magmatic composition compared to the pre-caldera and caldera-related andesitic magmas.

The lack of basalt erupted at the KCC, suggests that crystal fractionation of a basaltic magma alone is unlikely to produce the large volumes of rhyolite magmas erupted at the KCC. This volume argument has been considered at the TVZ, where it has been suggested that some of the parental basaltic magmas may pond at the base of the continental crust, fractionate, and assimilate continental crust to produce the large volumes of evolved rhyolitic magmas within this zone (Graham et al., 1995).

Major and trace element variations, and negative Eu anomalies in some rhyolite lavas imply that the major petrogenetic process generating rhyolite magmas at the KCC was crystal fractionation. There is some evidence, however, which indicates that rhyolitic magmas are not derived from compositions similar to pre-caldera or caldera-related andesite magmas. This includes distinctly different trace element characteristics of

andesite and rhyolite lavas, offset fractionation trends (Figure 7.20), an apparent compositional gap (i.e. 66-70 wt.% $SiO_2$) between the intermediate and silicic compositions, and a different parental basaltic magma composition. Therefore a different petrogenetic pathway must have been followed to generate the rhyolitic magmas.

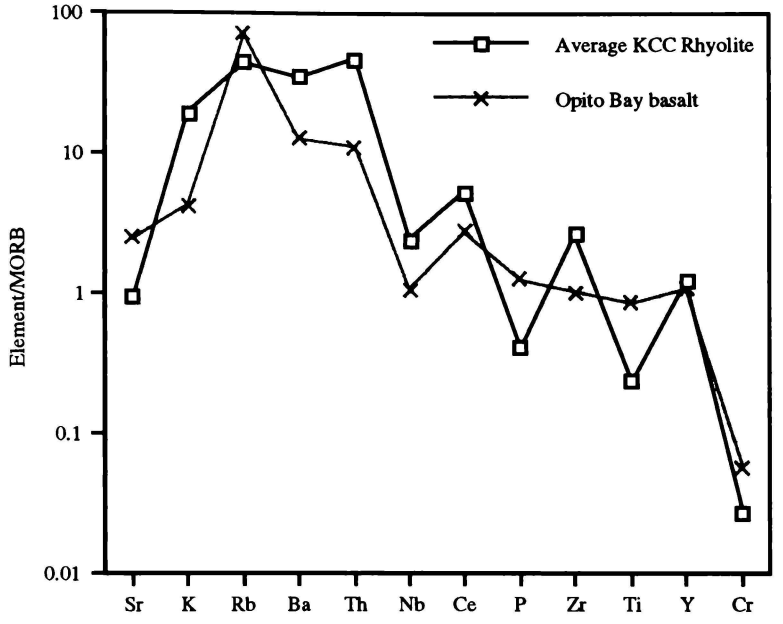


Figure 7.19 Multi-element diagram comparing possible basaltic parental composition (Opito Bay basalt) with average rhyolitic composition at the Kapowai Caldera Complex. Average andesite compositions are also indicated. MORB normalising data from Pearce (1983).

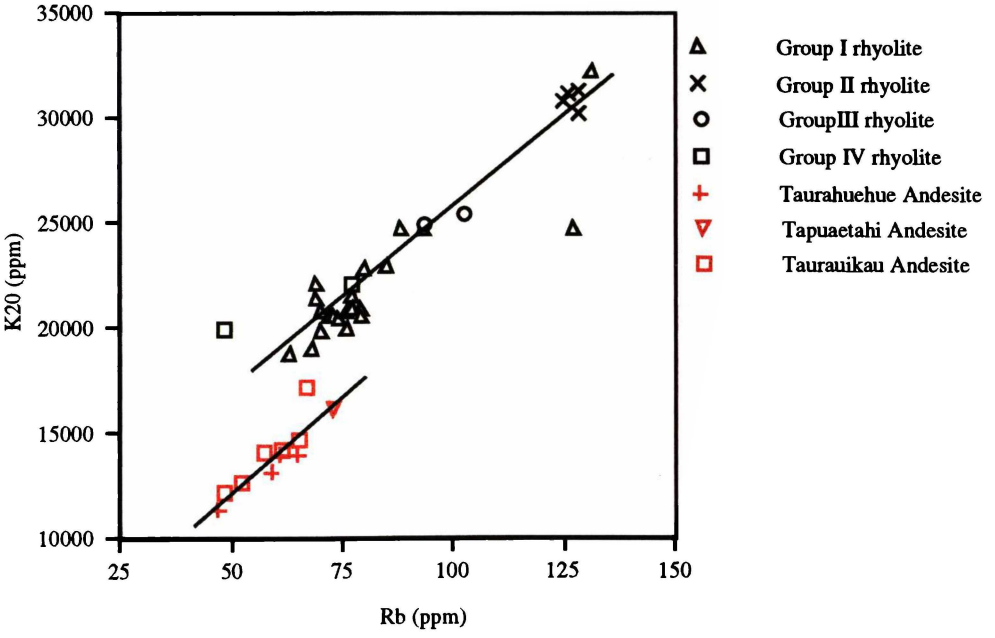


Figure 7.20 Plot of K vs Rb for Kapowai Caldera Complex andesitic and rhyolitic lavas.

Assimilation of crustal lithologies by rhyolitic magmas is a clear process at the KCC, with evidence provided by the presence of crustal xenoliths (e.g. granulite, hornfels, granodiorite, andesite lavas) in lavas

and ignimbrites. Assimilation is considered a fundamental component in the generation of subduction-related silicic magmas (Hildreth and Moorbath, 1988), and it is also considered here to be a crucial component in the genesis of KCC rhyolitic magmas. However, isotopic data for CVZ crustal lithologies and KCC volcanic rocks needs to be attained before an understanding of the extent of assimilation can be established.

There is some limited lithological and trace element evidence which suggests that mixing between low and high silica rhyolitic magmas may have occurred. Multiple pumice types in most KCC rhyolitic ignimbrites implies that individual magma reservoirs were either compositionally zoned prior to eruption, or that multiple silicic magma chambers were tapped during the eruptive phase. As the pumice clasts have been affected by incipient weathering, it is not possible to examine this further.

Therefore the petrogenesis of rhyolitic magmas erupted at the KCC follows a different pathway to that of the pre-caldera and caldera-related andesites. Initial basaltic magmas generated in the mantle wedge migrate to the base of the crust, where they pond, fractionate and assimilate lower crustal lithologies (e.g. granulite). Migration through the crust may follow where they continually evolve by additional crystal fractionation and assimilation (AFC). At a certain mid-crustal level, the high basaltic magma flux leads to melting of large volumes of crustal lithologies (i.e. crustal anatexis), which then further evolve and form high level silicic magma reservoirs.

Variable degrees of crystal fractionation and crustal assimilation are indicated by the variable major and trace element chemistry and non-parallel REE patterns of KCC rhyolite lavas, and implies that each lava represents a discrete silicic magma batch of unique composition. This is similar for silicic volcanic centres in the CVZ (e.g. Whitianga Volcanic Centre) and at most TVZ rhyolitic centres (Sutton et al., 1995; Briggs et al., 1998).

Therefore the genetic difference between andesitic-dacitic and rhyolitic magma suites may relate to whether (i) basaltic magmas pond at the base of the crust and migrate directly through the crust, and evolve by progressive fractionation, assimilation (AFC) and mixing to andesitic-dacitic compositions or (ii) high basaltic magma fluxes generate a heat source sufficient enough to melt crustal rocks which then evolve to rhyolitic compositions (Figure 7.21). Based upon the geochemical data obtained during this study the two suites evolved generally independent of each other, apart from limited hybridisation of andesitic-rhyolitic magmas (e.g. Oteao Ignimbrite)

A fundamental feature of this bi-modal system are the factors which control whether andesitic or rhyolitic magmas are ultimately generated. These factors most likely occur in the source region and include the physical nature of the initial (i.e. mantle wedge) melt, mantle wedge, and lower crust (Pearce and Peate, 1995).

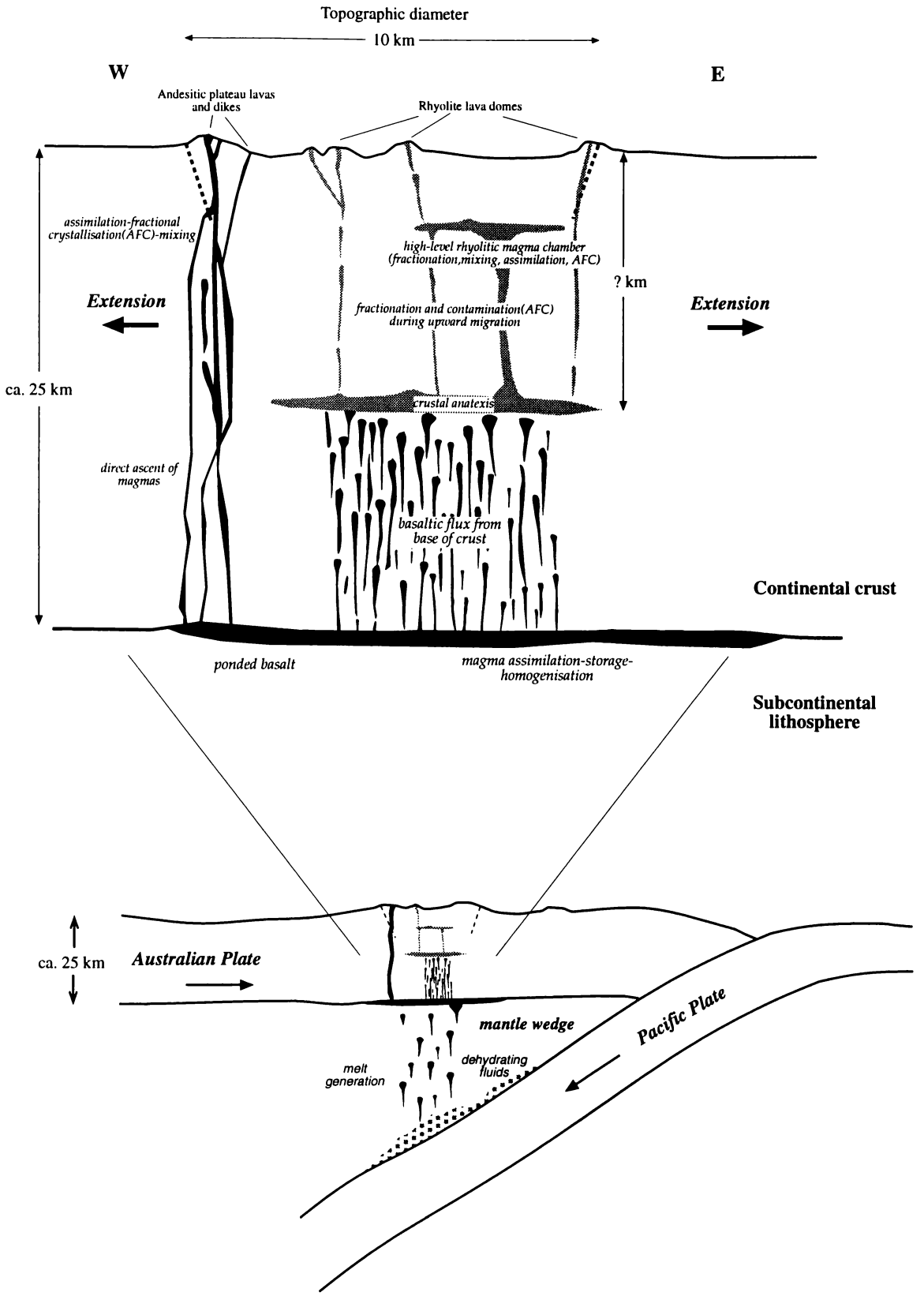


Figure 7.21 Simplified petrogenetic model (not to scale) for the generation of intermediate and silicic magmas erupted at the Kapowai Caldera Complex. Modified from Hildreth (1981) and Pearce and Peate (1995).

# Chapter Eight

# EPITHERMAL ALTERATION

## 8.1 Introduction

CVZ contains a significant epithermal gold province, known as the Hauraki Goldfield (Christie and Brathwaite, 1986). Epithermal-type gold-silver deposits are the most common forms of mineralisation and occur throughout the province (Christie and Brathwaite, 1986). The structural and stratigraphic settings, and geochemistry of deposits varies, although most are hosted by intermediate to silicic volcanic sequences, (e.g. Moore, 1976; Merchant, 1978; de Ronde, 1986). The KCC, like most other CVZ calderas, contains multiple zones of epithermal alteration (Skinner, 1995). However, unlike other CVZ calderas, epithermal gold-silver deposits are associated with some of the alteration zones at the KCC (cf. Briggs and Fulton, 1990; Briggs et al., 1998).

Silicic caldera volcanoes have been recognised as important sources of epithermal mineral deposits, especially in North America (e.g. Lipman et al., 1976; Slack and Lipman, 1979; Hedenquist, 1986; Mills et al., 1988), and recently, the influence of caldera structures in controlling the distribution of epithermal mineralisation has also been emphasised (Lipman, 1992; Elston, 1994; Rytuba, 1994). At the KCC, there is evidence to relate the location and timing of alteration zones and epithermal deposits to caldera structures and also the regional fault pattern.

This chapter discusses the characteristics, and temporal and spatial variation of epithermal alteration at the KCC. It then describes the influence of caldera and regional structures on the location and relative timing of epithermal systems.

Several of the epithermal Au-Ag bearing quartz vein systems and disseminated zones within the central KCC have been mined (Bell and Fraser, 1912; Downey, 1935). In this study, no attempt was made to investigate the nature of these mineralised zones, because access into the workings is considered unsafe. Several exploration companies have also described the ore structures and alteration in detail (Earth Scientists Ltd, 1973; Freeport of Australia Ltd, 1973; Couper, 1982; Robson et al., 1994).

Selected hydrothermally altered lavas and welded ignimbrites from throughout the KCC were analysed by X-ray powder diffraction (XRD) at the University of Waikato. Samples were powdered and then air-dried for 24 hours, prior to analysis. Samples were initially analysed as unorientated powder mounts in order to gain bulk mineral data. Representative samples were then treated with ethylene glycol followed by heating to 550°C to determine the clay minerals present. Representative XRD traces are included in this chapter and additional traces are presented in Appendix VIII.

## 8.2 Historical Au-Ag mining

Productive gold and silver mining from 1899 to 1933 was carried out from four sites in the Slip Stream tributary of the Rangihau Stream (Figure 8.1a, b) (Downey, 1935). The largest deposit was located on the northern flank of the Welcome Jack Rhyolite dome (Kapowai Mine; T11/509638). More than 4600 tonnes of ore was extracted, with a yield of 3500 oz of bullion (Table 8.1). A second, large deposit occurs 2 km south of the Kapowai Mine (Welcome Jack Mine; T11/511629). Other deposits were located on the northwestern (Big Beetle Mine; T11/503643) and western margins (Golden Reefs Mine; T11/506636) of the rhyolite dome.

A

B

Figure 8.1 A, Welcome Jack Rhyolite dome (right) host to the majority of epithermal Au-Ag deposits in central KCC, Slip Stream valley. Tailings from the Kapowai Mine adits can be seen on the foreground slope of the dome. The Big Slip to the left of the Welcome Jack dome resulted from rotational failure of hydrothermally altered rhyolite lava. View south from the Rangihau Rhyolite dome (T11/504653). B, Tailings (arrow) of the Welcome Jack Mine, central Kapowai Caldera Complex (T11/509627). Hydrothermally altered Welcome Jack Rhyolite lava (group II rhyolite) forms outcrops in foreground and centre left.

As was typical of the mining era, only high ore grades (ca. ~ 60g/t) were targeted for extraction. These ores were typically associated with E-W striking, south-dipping quartz vein structures located within or on the margins of the Welcome Jack Rhyolite Dome. Ore occurs as native gold and silver, or as inclusions within pyrite (Bell and Fraser, 1912). No other deposits were identified by prospectors during mining activity, or by subsequent exploration companies.

Modern exploration of the Welcome Jack deposits has included mapping of the mineralised structures, sampling for assay, and aeromagnetic surveying to examine structural relationships between ore deposits (Robson, 1989; Robson et al., 1994). Until recently, Heritage Mining Ltd. held a prospecting licence (PL 31-1844) over the mining area. However, this licence has now expired following government legislation (Crown Minerals Amendment Act (No.2) 1997) prohibiting prospecting and mining activities in central and northern Coromandel Peninsula.

Table 8.1 Production summary of Kapowai Caldera Complex gold-silver mines. Data from Bell and Fraser (1912), Downey (1935) and Robson (1989). Note bullion includes gold and silver.

| Mine | Period mined | Ore Mined (t) | Bullion Recovered (oz) | Host rock | Ore Structures |
|---|---|---|---|---|---|
| Kapowai | 1899-1933 | 4660 | 3524 | silicified rhyolitic tuffs | segregated veins/lenticular pipes within (090/45 S) mineralised band |
| Welcome Jack | 1899-1903 | 466 | 1628 | altered biotite rhyolite | veins/pipeclays within (088/>45 S) quartz reef |
| Big Beetle | 1899-1905 | 543 | 956 | silicified rhyolitic tuffs | disseminated (peppered) in flat lying reef (120/50 S) |
| Golden Reefs | 1902-1906 | 48 | 31 | altered rhyolitic tuffs | vein |

## 8.3 Epithermal alteration

Hydrothermal alteration is a general term encompassing the mineralogical, textural and chemical changes in rocks produced by percolating geothermal fluids (Heinrich et al., 1989). Where geothermal systems are hosted by silicic volcanics, alteration extends over 100's of metres and tends to have a plume form (Figure 8.2).

Epithermal alteration relates to fluid-rock interactions at temperatures below < 350°C (Lindgren, 1933; Heinrich et al., 1989). This thermal regime is initially recognised in the field by the presence of key alteration mineral assemblages. Additional analysis can be made to further constrain the temperature range, and also establish the physico-chemical conditions in which the assemblage was generated. Epithermal alteration and epithermal mineral deposits are common in the CVZ, and are considered equivalent to active geothermal systems in the TVZ (Christie and Brathwaite, 1986; Heinrich et al., 1989).

Epithermal alteration of rhyolitic and andesitic lavas, and ignimbrites occurs at several localities within the KCC (see below). Two rhyolite lava domes, Bulls Run Rhyolite (plagioclase-pyroxene phyric; group I rhyolite) and Welcome Jack Rhyolite (quartz-plagioclase-biotite phyric; group III rhyolite) have been altered. Several welded ignimbrites have been altered and some can be correlated to mapped intracaldera ignimbrites. Pre-caldera andesite (Taurahuehue Andesite) is locally altered. Numerous altered lava and pyroclastic lithic fragments have also been observed within several intracaldera ignimbrites.

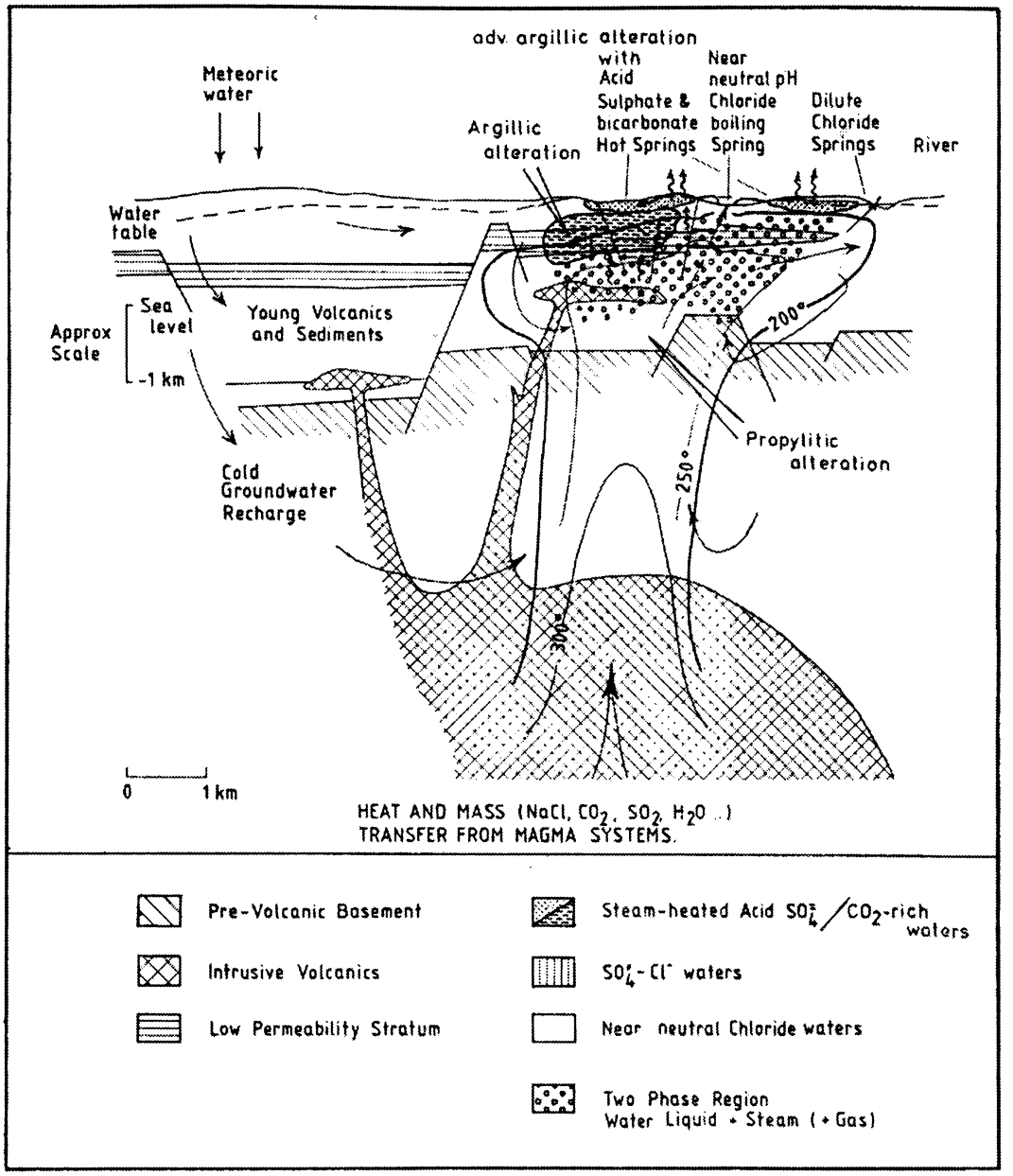


Figure 8.2 Hydrothermal system associated with silicic volcanism. Adapted from Henley, 1985.

## Alteration types

Two major alteration types are mapped at the KCC: propylitic and sericitic alteration. Propylitic alteration is defined by the presence of calcite and chlorite minerals (Heald et al., 1987). The presence of these minerals produces a green/white colouration. Propylitic alteration is especially common in welded ignimbrites and is rarely observed in rhyolite lavas.

Sericitic alteration is characterised by the presence of quartz and sericite/illite, adularia, and/or pyrite (Heald et al., 1987). The presence of quartz and sericite produces a strongly bleached/white colouration and hardness increases significantly compared with unaltered lithologies. Veinlets (typically < 2 mm width) infilled with quartz and pyrite are common in some altered rhyolite lavas.

Apart from these two main types, other alteration varieties also occur. Jasper and undifferentiated clays infill veinlets in pre-caldera (Taurahuehue Andesite) andesite lava. Minor argillic (kaolinite, pyrophyllite, dickite and alunite) alteration occurs sporadically in the central KCC (Figure 8.12c). No relict structures associated with geothermal systems (e.g. hydrothermal breccias, sinters or relict geysers) have been observed (cf. Moore, 1976).

## Mineral transformation

Mineralogical changes are important criteria for recognising hydrothermal alteration and defining alteration types in the field. Alteration assemblages have been established for many CVZ epithermal alteration zones and those definitions are generally applied here (e.g. Merchant, 1978; Haworth, 1993). Original pre-altered rock compositions are silicic-dominated, and include both lavas and welded ignimbrites. Alteration of intermediate composition (andesite-dacite) lavas occurs but is rare.

Primary minerals exhibit a distinct sequence of susceptibility to alteration: titanomagnetite > biotite > orthopyroxene > clinopyroxene > plagioclase feldspar > quartz. This is generally similar to sequences described for other epithermal alteration areas in the CVZ (e.g. Haworth, 1993; Aldrich, 1995).

General stability fields for both primary and secondary minerals are presented in Figure 8.3. Fields define several degrees of hydrothermal alteration. Incipient to weak alteration is defined by secondary chlorite ± calcite, and in some samples may also include leucoxene, pyrite, and quartz. Moderate alteration is defined by progressive alteration of plagioclase to calcite ± clays (illite) ± sericite. Orthopyroxene is completely replaced and clinopyroxene partially replaced by chlorite ± calcite. Strong alteration is characterised by complete replacement of plagioclase by quartz, clays, pyrite, or sericite.

### *Fe-Ti oxides*

Titanomagnetite and ilmenite are present in both welded ignimbrites and lavas. Typically these are the first minerals to be altered. Initially they are altered to an intermediate phase, leucoxene, and then progressively to pyrite.

### *Biotite*

Alteration of biotite to chlorite or more commonly illite occurs in incipiently altered Welcome Jack Rhyolite lavas. The original crystal form or a skeletal relict form may be retained in weakly altered lavas (Figure 8.8a).

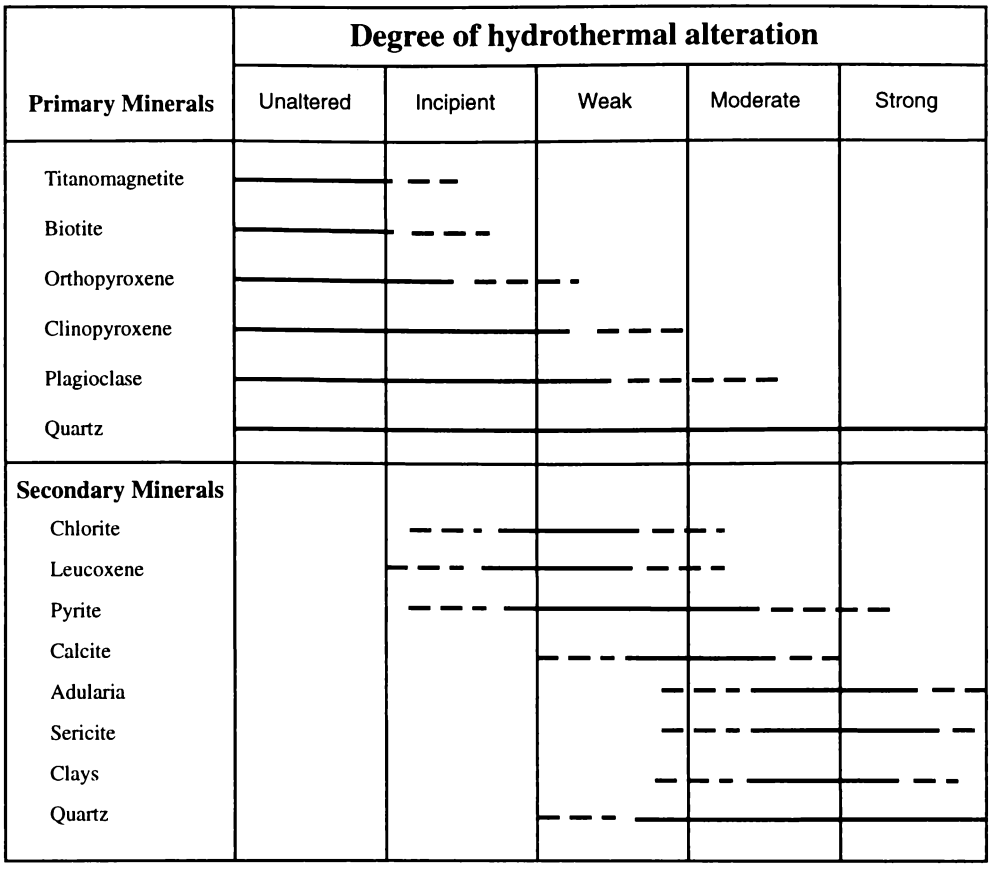


Figure 8.3 General stability fields for primary phenocrysts/crystals and alteration minerals in hydrothermally altered rocks of the Kapowai Caldera Complex.

***Pyroxene***

Pyroxene crystals and phenocrysts are ubiquitous in KCC volcanic rocks and are commonly incipiently altered to chlorite. With increased alteration chlorite can itself be altered to calcite, or sericite/illite minerals. Clinopyroxene and alteration products of clinopyroxene tend to be more resistant to alteration than orthopyroxene.

***Plagioclase***

Weakly altered plagioclase feldspar crystals/phenocrysts are replaced by calcite and illite. In strongly altered samples, calcite is replaced by very fine quartz, or quartz polymorphs, and/or adularia, and/or illite. Degrees of alteration are well expressed by the secondary minerals replacing plagioclase crystals, and its altered form, which varies from unaltered crystals (non - incipient alteration) to partially altered with alteration along cleavage planes (moderate alteration) to completely destroyed (strong alteration).

***Quartz***

Quartz is the least susceptible primary mineral affected by alteration. It retains its crystal form and composition, whilst other minerals and glass in the same rock are altered. Primary quartz is differentiated by secondary hydrothermal quartz by its occurrence as single, discrete crystals and typically larger crystal size.

*Glass*

The glassy groundmass of rhyolite lavas and vitroclastic matrix in ignimbrites is the most susceptible component to hydrothermal alteration and is the first component to be affected. In incipient alteration, glass is replaced by chlorite, and/or kaolinite, and/or illite/sericite. Increasing alteration can find the glass replaced by a very fine mosaic of quartz, and/or adularia and sericite. Unlike other areas in the CVZ, zeolites have not been observed replacing glass (cf. Aldrich, 1995).

## Alteration mineralogy

All primary minerals show a variety of secondary mineral replacements. Common replacement assemblages for ferromagnesian minerals, plagioclase feldspar and titanomagnetite have been reported from several epithermal alteration zones in the CVZ (e.g. Merchant, 1978; de Ronde, 1986; Haworth, 1993). At the KCC, similar assemblages occur and these together with likely chemical changes are presented in Figure 8.4. XRD analysis has been a fundamental technique in identifying alteration minerals. Representative XRD traces of a bulk sample and the clay fraction from several samples are presented in Figure 8.6 and 8.7 respectively.

*Chlorite*

Chlorite is an initial alteration mineral and commonly replaces ferromagnesian minerals (i.e. pyroxene, biotite). It is a common mineral in both welded ignimbrites and rhyolite lavas (Figure 8.5). Where it replaces a ferromagnesian crystal, the original crystal form is typically retained up until high levels of propylitic alteration (Figure 8.8d). Chlorite may be replaced at higher alteration grades by other minerals including calcite, clay or quartz. Although chlorite alteration is almost exclusive to ferromagnesian minerals, chlorite is also observed replacing plagioclase feldspar, and is inferred to replace pumice clasts and/or glass shards and glassy matrix.

Chlorite displays a wide variety of colours and pleochroism from dark green to green-yellow pleochroic to very pale green. Interference colours also vary from moderate second order interference colours to pale blue-grey. Optical variations are inferred to reflect compositional differences in chlorites. Differences are also suggested by varying intensities of chlorite peaks (see appendix VIII).

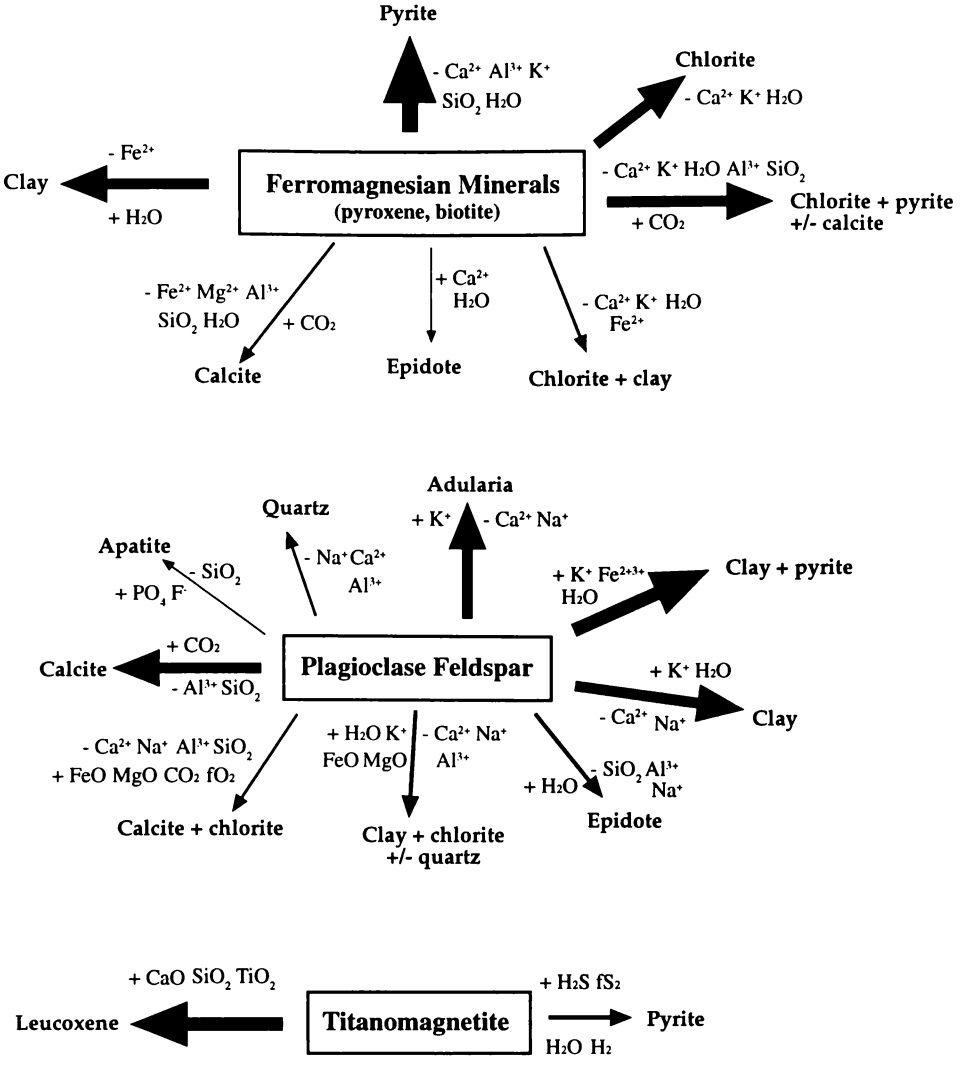


Figure 8.4 Secondary mineral replacements and associated chemical changes observed for altered rocks in the Kapowai Caldera Complex. Arrow size is proportional to relative abundance of replacement mineral(s). Modified from Merchant (1978) and de Ronde (1986).

### *Calcite*

Calcite alteration is common in welded ignimbrites and lavas, typically occurring only in weak to moderate alteration levels. Calcite is typically observed with chlorite, although it is commonly more abundant, and it may also occur with other secondary minerals including illite, adularia, quartz or leucoxene. Replacement by calcite occurs both within the groundmass or vitroclastic matrix and in phenocryst/crystal assemblages (Figure 8.8c, e).

Initially replacing secondary chlorite at weak alteration levels, calcite partially and then completely replaces plagioclase at progressively higher levels of alteration. Calcite is absent from strong alteration where quartz, adularia, sericite and clays dominate.

Calcite exhibits a variety of habits ranging from coarse (0.5-1 mm) anhedral-euhedral crystals replacing plagioclase phenocrysts to fine grained irregular aggregates replacing the groundmass. Cleavage in calcite

is variable and occasionally is well displayed. Calcite crystals commonly display characteristic high 3/4 order interference colours.

***Pyrite***

Pyrite crystals are common in most altered samples, forming characteristic fine grained cubic crystals, irregular masses, or lining veinlet walls (Figure 8.8b). Pyrite replaces biotite or pyroxenes or may completely replace titanomagnetite. Large amounts of pyrite are common in veined samples and is closely linked to quartz - sericite/illite alteration. Pyrite usually replaces leucoxene, an intermediate secondary mineral, which is only seen in occasional samples.

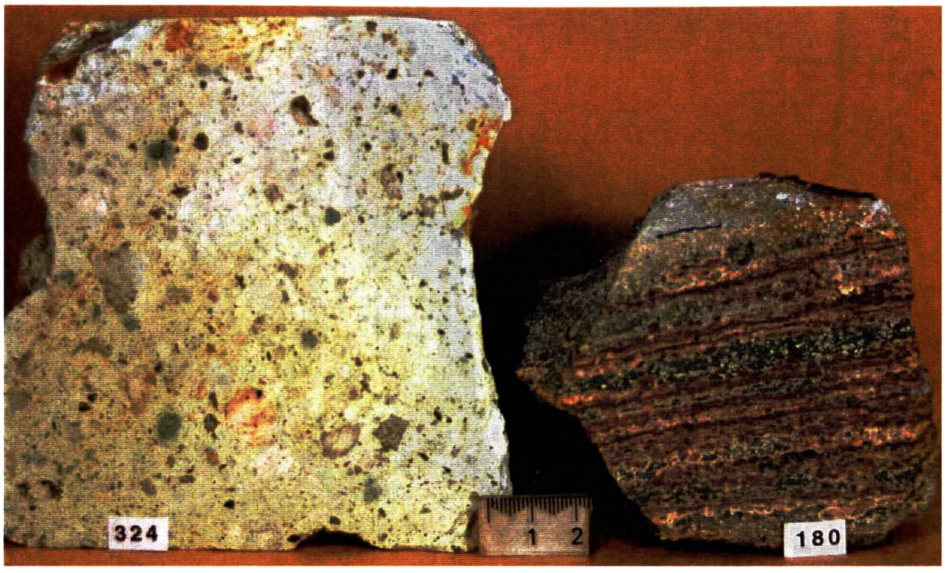


Figure 8.5 Chlorite present in propylitic altered rhyolite and ignimbrite. Very fine grained chlorite forms green flow bands in Welcome Jack Rhyolite (180; W99805) and irregular green patches replacing pumice in undifferentiated welded ignimbrite (324; W991001).

***Illite/sericite***

Confusion exists in the literature as to the definition of sericite (essentially a petrographic term for a white fine grained mica) and illite (Shelley, 1985). They have similar mineralogic and petrographic characteristics, although they differ in composition. Optically and in XRD analysis, they are treated as a similar entity.

Sericite is a key secondary mineral and together with quartz defines one of the major alteration types at the KCC. Sericite is common in moderately to strongly altered rhyolite and ignimbrite samples. It is difficult to determine optically, but generally is identified by its low relief, and granular, fine grained nature. It has been detected in most XRD traces of moderately to strongly altered samples.

***Kaolinite***

Kaolinite was detected in several samples using XRD analysis, although identification of kaolinite in thin section is difficult. It is common in both altered rhyolite and ignimbrite at moderate to strong alteration levels.

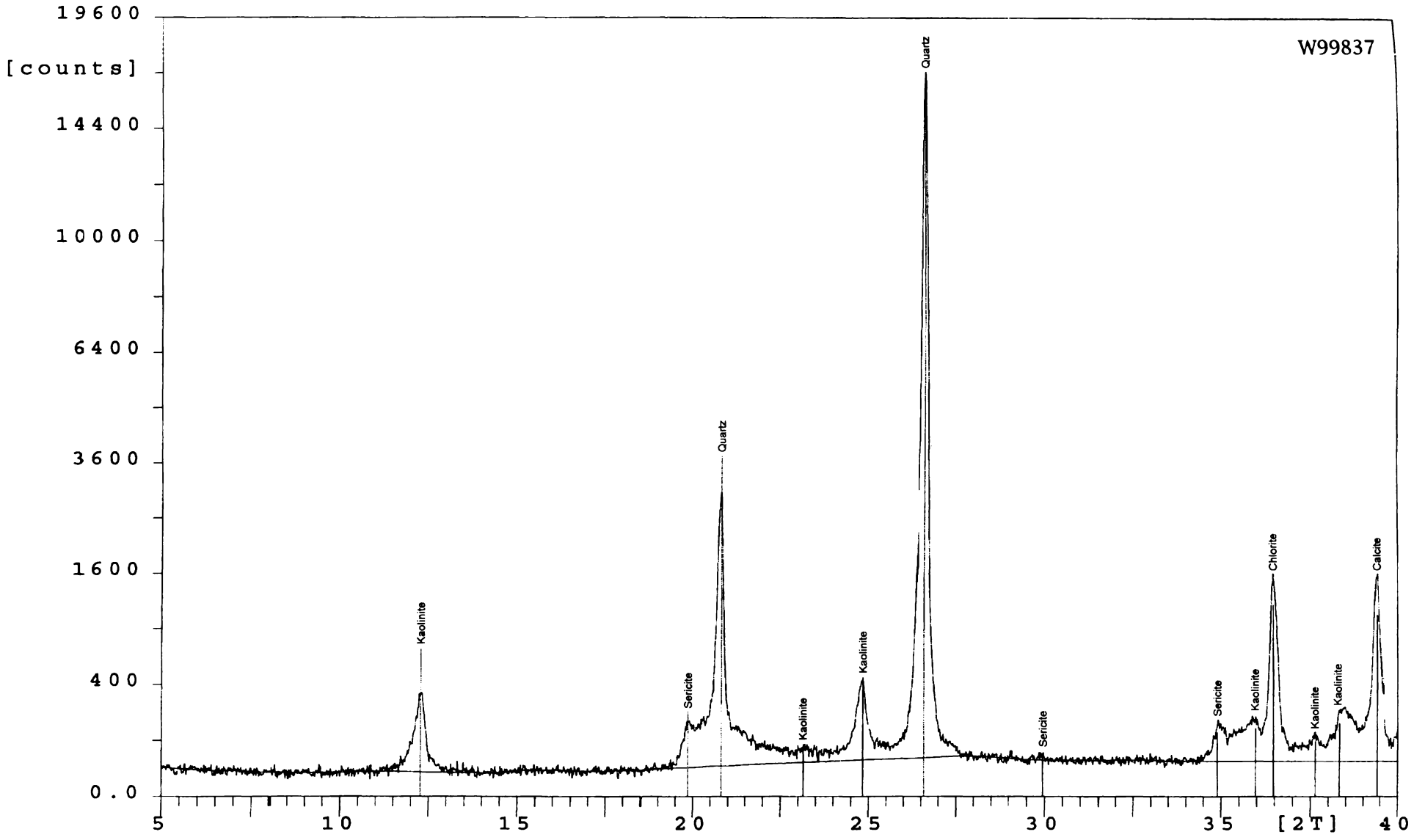


Figure 8.6 Bulk XRD trace of sericitic altered Welcome Jack Rhyolite lava (W99837).

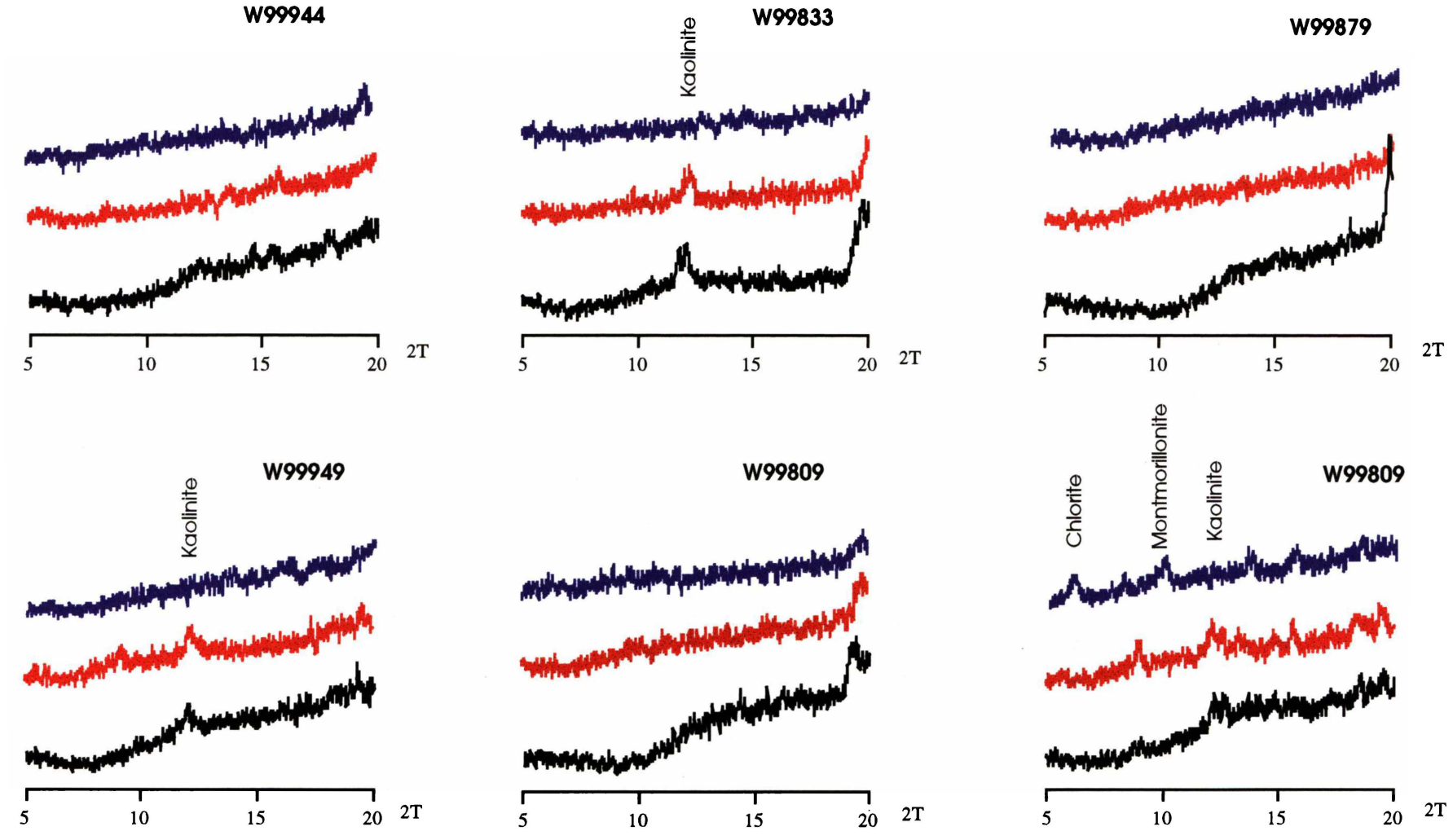


Figure 8.7 XRD traces of clay minerals from hydrothermally altered rocks from the Kapowai Caldera Complex. Black is untreated sample, red is sample treated with ethylene glycol, and blue is sample heated to 550°C.

***Epidote***

Epidote has only been observed optically in some samples, where it is a rare secondary phase. It displays characteristic high relief and anhedral form. Epidote occurs in moderate to strongly altered samples and typically replaces chlorite pseudomorphs of pyroxene. It has also been identified in XRD traces.

***Adularia***

No primary K-feldspar phase (i.e. sanidine) has been observed or analysed in KCC volcanic rocks. K-feldspar (adularia) has been determined by XRD analysis in some samples using peaks defined from Steiner (1970). Adularia replaces plagioclase feldspar at moderate to high alteration levels.

***Alunite***

Alunite has been tentatively identified by XRD analysis in several samples, but has not been observed optically.

***Dickite***

Dickite has been tentatively identified in some samples by XRD analysis. It has not been observed in thin section.

***Analcime***

Zeolites occur in altered samples, and also in unaltered rhyolite lavas of the KCC. Optical discrimination of zeolites in altered samples is difficult to establish, however analcime has been detected in several XRD traces. These samples correspond to very fine grained, very low relief, colourless zeolites observed in thin section.

***Pyrophyllite***

Pyrophyllite has been tentatively identified in several samples, but only from XRD traces. It has not been observed optically,

***Apatite***

Apatite has been observed optically in sericitc altered samples. It occurs as very fine grained, colourless, euhedral, prismatic crystals. Apatite has been tentatively identified by XRD analysis in corresponding samples.

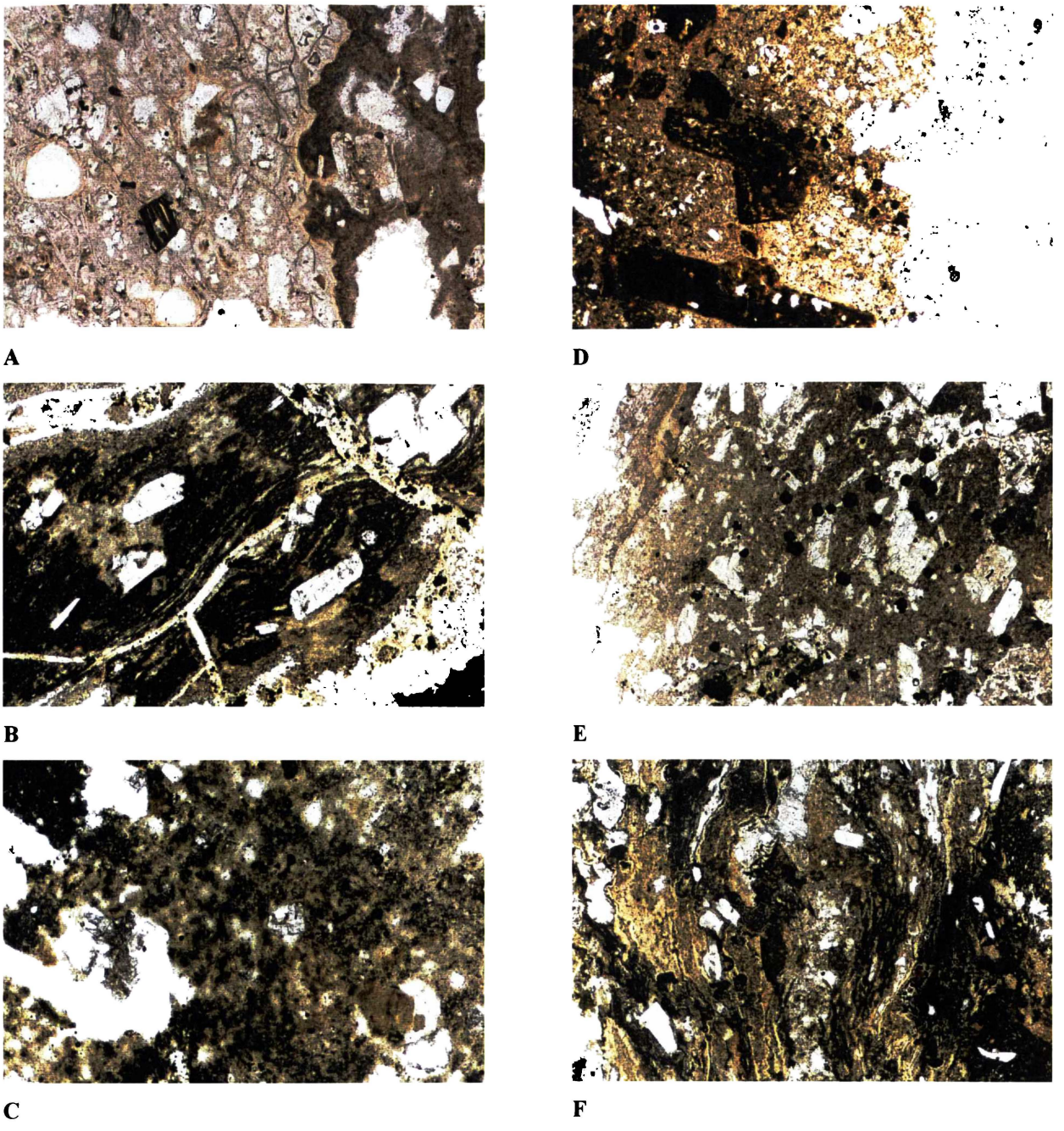


Figure 8.8 Photomicrographs of selected hydrothermally altered lava, pyroclastic and lithic fragments from the Kapowai Caldera Complex. A, Propylitic altered Welcome Jack Rhyolite lava (W99805) with skeletal biotite phenocryst replaced by illite and unaltered quartz phenocrysts. B, Sericitic altered Bulls Run Rhyolite lava (W99750) with numerous cross-cutting veinlets infilled by quartz and pyrite. C, Propylitic altered ignimbrite (W991001) with calcite and zeolite (analcime) infillng voids. D, Propylitic altered dacite lava lithic (W99892LB). Primary pyroxene phenocrysts replaced by chlorite and pyrite. E, Propylitic altered rhyolite lava lithic (W99955LE) with secondary calcite, chlorite and abundant pyrite. F, Silicified ignimbrite (W991001LD) with original vitroclastic texture replaced with very fine grained sericite or clays. Length of all photos is 4mm.

### *Quartz*

Secondary quartz crystals occur in weakly altered samples and increases in its abundance with increasing degree of alteration. Initial quartz replacement in weakly altered samples occurs as fine grained aggregates developed among chloritised or calcitised pyroxenes. With increased alteration, quartz completely replaces chlorite/calcite to produce an irregular patch of interlocking undulose quartz. Quartz also replaces plagioclase at moderate to strong alteration levels. Veinlets of quartz with pyrite, sericite, or adularia, and interlocking quartz is common in strongly altered samples (Figure 8.8 b).

### Textural changes

*Ignimbrites*

Pyroclastic textures in altered ignimbrites are generally recognised by relict pumice clasts, lithic fragments, and in incipiently altered samples by relict glass shard forms. Pumice clasts generally retain their form, but are replaced or their vesicles infilled by secondary minerals (e.g. sericite, quartz, illite). In incipiently altered ignimbrites the original vitroclastic matrix is either partially or completely destroyed and replaced with irregular and finer grained secondary minerals.

*Lavas*

Original porphyritic textures present in all rhyolite lavas are retained at low levels of alteration. However, with increased degree of alteration, phenocrysts are altered and their original form destroyed. In strongly altered samples the porphyritic texture is commonly replaced with a mosaic of fine to very fine grained secondary crystals including quartz, pyrite, adularia, and sericite. In these situations, an original porphyritic texture may only be inferred by comparison with the surrounding less altered country rock.

## 8.4 Distribution of alteration

Epithermal alteration occurs in three locations within the KCC: (i) central KCC; (ii) Kapowai valley, and (iii) Kauaeranga valley. Alteration zones are also inferred to be buried within the volcanic pile of the KCC as numerous altered lithic fragments have been observed within intracaldera ignimbrites.

### Central KCC

In the central KCC, between the Slip Stream valley and Starvation Creek, several sericitic and propylitic alteration zones occur (Figure 8.9). The alteration zones are sporadic, but are commonly associated with two rhyolite lava domes (Welcome Jack Rhyolite dome and Bulls Run Rhyolite dome).

Propylitic alteration of ignimbrite and rhyolite lava occurs on the western margin of the Welcome Jack Rhyolite dome. The ignimbrite is most likely pre-WES because of its limited outcrop and low lithic abundance. Propylitic alteration of rhyolite lava occurs near the entrance to the Welcome Jack Mine. Minor argillic alteration is present in isolated pockets on the western margin of the Welcome Jack dome (Figure 8.12c).

Sericitic alteration is restricted to the western and eastern margin of the Welcome Jack dome. Numerous silicified blocks of rhyolite lava form a substantial field on the western ridge of the Mine Creek valley. The parental lava mineralogy is unclear as primary phenocrysts have been destroyed.

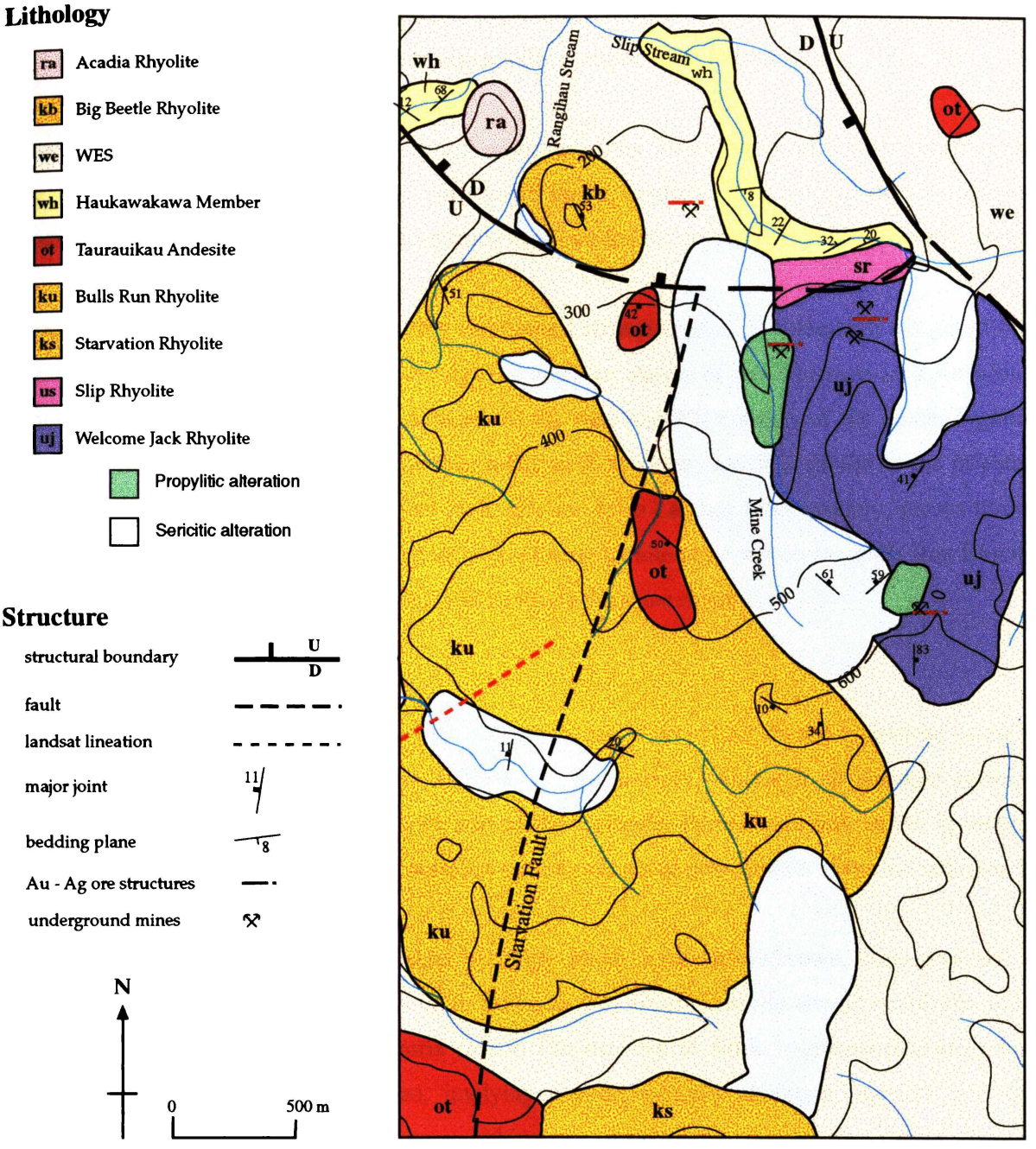


Figure 8.9. Distribution of epithermal alteration types and associated Au-Ag ore structures at the Welcome Jack Rhyolite dome, central Kapowai Caldera Complex.

Epithermal quartz veins/reefs and breccia pipes occur within the hydrothermally altered rhyolite lava and peripheral hydrothermally altered intracaldera ignimbrites. Structures typically strike E-W and have moderate dips (45-50°) to the south (Bell and Fraser, 1912; Robson, 1989). These major vein systems are not exposed at the surface, although quartz veinlets (typically 5-10 mm) have been observed in some lava outcrops.

Sericitic alteration occurs within and on the margins of the Bulls Run Rhyolite dome complex, to the west of the Welcome Jack Rhyolite dome (Figure 8.12d). In central and NE alteration zones, Bulls Run Rhyolite lava exhibits incipient to moderate sericitic alteration. Primary phenocrysts (plagioclase,

pyroxene) may remain, but the original glassy groundmass is altered to quartz and/or very fine sericite and clays (illite). Veinlets (typically < 4 mm) occasionally occur in some altered lavas.

Isolated, silicified rhyolite lava blocks (up to 2 m) occur on the southern margin. These typically consist of very fine grained mosaic quartz and occasional pyrite crystals. Primary phenocrysts (plagioclase, pyroxene, titanomagnetite) have been completely replaced and the original porphyritic texture destroyed.

Several intracaldera structures occur within this central alteration area. The southern margin of the WES structural boundary is inferred to pass through the northern margin of the Welcome Jack Rhyolite dome. Although it is concealed, it is present adjacent to the west and NE margins of the dome. Significantly, where it is inferred to pass through the dome, it has an E-W strike, which is similar to the orientation of ore structures. A NNE-trending concealed fault, inferred from Landsat MSS imagery, passes through the Bulls Run Rhyolite. This may control the location of sericitic alteration within the Bulls Run Rhyolite and also andesite dikes (Taurauikau Andesite) which intrude the same rhyolite.

### Upper Kapowai valley

In the floor of the upper Kapowai valley, at least two areas of propylitic altered ignimbrite occur (Figure 8.10). The two areas cover ca. 600 $m^2$ and 700 $m^2$ respectively. Although an absolute correlation is difficult, the ignimbrite(s) are likely to be part of the Colorado Pyroclastics unit as the ignimbrites are overlain by the WES, and Colorado Pyroclastics ignimbrites occur downstream of the altered ignimbrites.

The two ignimbrites appear similar in their lithology which is pale green/brown, lithic-poor and weakly welded. Juvenile pumice clasts are difficult to define as they are consistently altered to chlorite and calcite and closely resemble the ignimbrite matrix colour. The majority of lithic fragments (including both lava and pyroclastic lithologies) are altered, implying post-depositional alteration together with the host ignimbrite. Veins or veinlets are not present within these ignimbrites.

Propylitic altered ignimbrites are restricted to the Kapowai valley floor and lie along the strike of the Kapowai Fault. The location of alteration also coincides with the intersection of intracaldera faults (Precipice Fault and Green Tree Fault) and the Kapowai Fault implying significant structural control on the location of alteration.

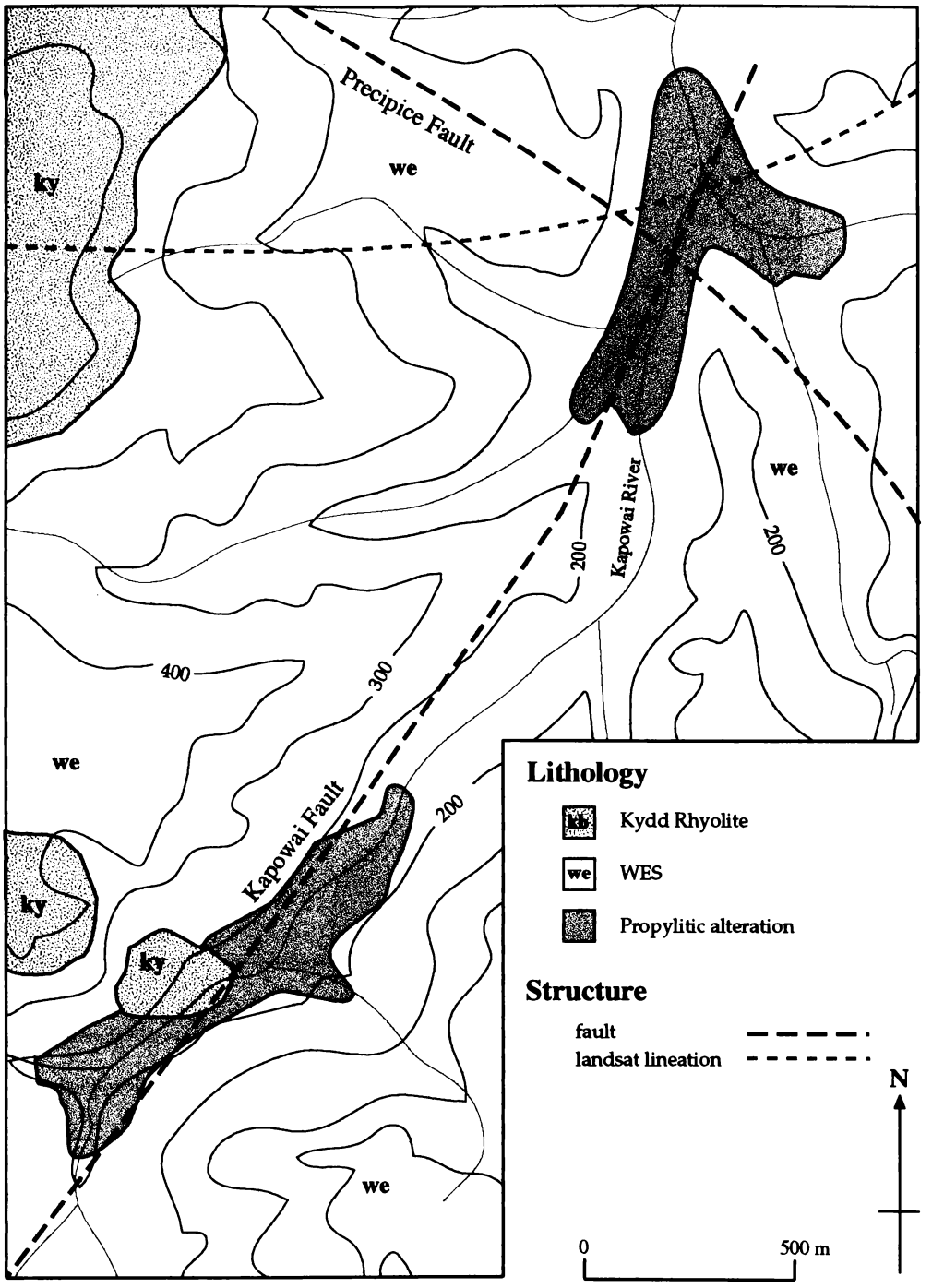


Figure 8.10. Zones of propylitic altered welded ignimbrite in the Kapowai valley. No veins have been observed in the areas of alteration.

## Upper Kauaeranga valley

In the upper Kauaeranga valley (Figure 8.11), a small (< 200 $m^2$) area of propylitic altered ignimbrite occurs. Although it is difficult to fully establish, Webb Creek Ignimbrite is the most likely ignimbrite as it outcrops immediately downstream of this locality. The altered ignimbrite displays a distinctive hummocky surface, and is variably coloured from pale green to green-brown (Figure 8.12a). Juvenile clasts are completely altered to chlorite and calcite, although most lithic fragments are unaltered. Rare quartz and chalcedony veinlets are also present. Veinlets are irregular, typically thin (5-20 mm width) and generally continuous up to ca. 1-2 m in length (Figure 8.12b).

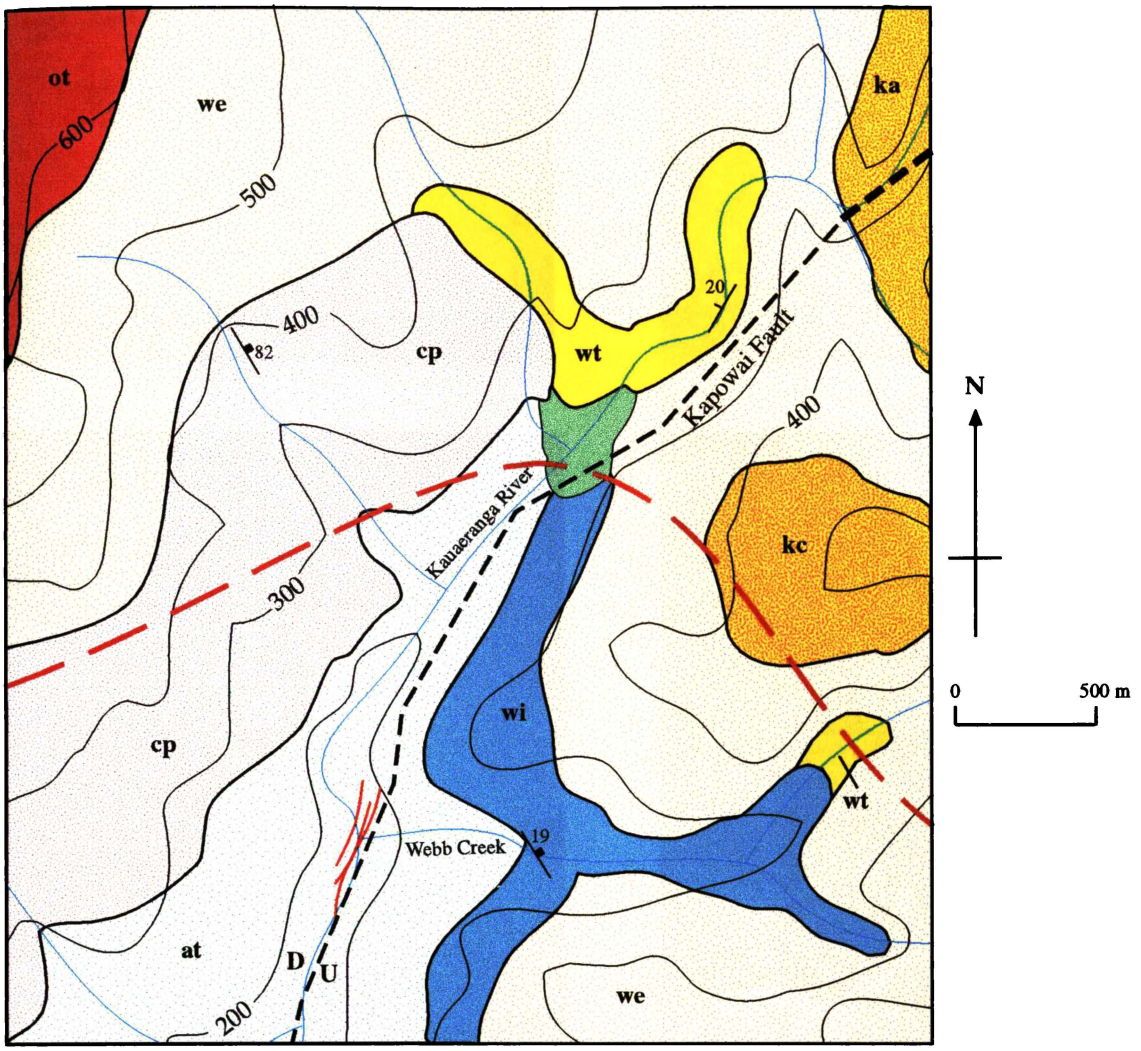


Figure 8.11. Location of propylitic alteration and jasper-infilling veinlets, upper Kauaeranga valley.

Alteration of pre-caldera Taurahuehue Andesite lava also occurs in the upper Kauaeranga valley, ca. 0.8 km downstream of the altered Webb Creek Ignimbrite. The alteration zone covers ca. 100 $m^2$ and is confined to the valley floor. Alteration consists of several thin (< 10 mm), irregular, typically continuous veinlets which can be traced for up to 12 m. Jasper infills all veinlets, with minor undifferentiated clays also present.

Alteration zones occur within the floor of the Kauaeranga valley, along the strike of the Kapowai Fault. Propylitic altered ignimbrite is located at the intersection of the fault with the inferred topographic boundary.

A

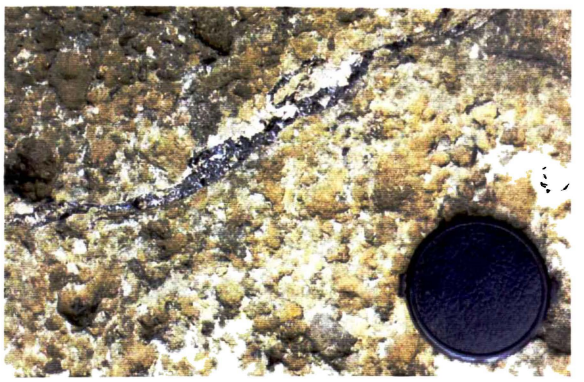

B

C

D

Figure 8.12 Outcrops of hydrothermally altered Kapowai Caldera Complex lavas and ignimbrite. A, Propylitic altered Webb Creek Ignimbrite in the Kauaeranga valley (T12/487581). B, Close up of propylitic altered Webb Creek Ignimbrite (A). Note green-brown, hummocky surface and quartz - chalcedony vein. C, Argillic altered Bulls Run Rhyolite lava in Mine Creek Valley (T11/506627). D. Sericitic altered Bulls Run Rhyolite lava in the upper Rangihau River (T11/494619). Boulder in foreground right is 1 m high.

## Altered lithic fragments

Altered lithic fragments are a variable component of the lithic population in KCC ignimbrites (Chapter 4). Sericitic and propylitic alteration of both lava and pyroclastic lithic lithologies is present, and these have been divided on the basis of degree of alteration (Table 4.10, 4.11).

As these lithics (and most other lithic fragments) typically represent vent-derived fragments excavated at depth (up to ca. 500 m depth), they infer the presence of buried alteration zones. Alteration mineral assemblages are generally similar to surficial zones implying similar chemical and physical conditions between buried and surficial alteration zones. The genetic relationship between altered lithics and surficial alteration zones is unclear, although it is likely that some altered lithics represent distinct alteration zones possibly older than those exposed, given that some are found in the older intracaldera ignimbrites (e.g. Colorado Pyroclastics; Manuka Ignimbrite).

## 8.5 Structural control

The distribution of epithermal mineral deposits and associated alteration zones are commonly controlled by shallow (ca. < 1 km) crustal structures (Sillitoe, 1993). Structures provide crucial paths for geothermal fluids to migrate to the surface and for meteoric waters to recharge the system (Hedenquist, 1986).

In epithermal deposits, structures relate to both the regional tectonic pattern (i.e. normal and reverse faults), localised volcanic structures (e.g. lava domes, structural boundary faults, faults related to resurgent doming) or a combination of both (Rytuba, 1994; Elston, 1994). Structures associated with epithermal systems are typically highly variable in number, orientation, dimension, and age. Although they may control the location of active geothermal systems or the distribution of alteration in fossil systems, not all structures may host precious metal mineralisation (Hayba et al., 1985). Therefore, structural analysis and interpretation is fundamental to evaluating not only the structural setting of epithermal deposits, but for focusing on prospective targets.

At the KCC, two fundamental structural elements control the distribution of alteration zones and possibly mineral deposits associated with alteration. These are structures related to caldera volcanism and larger scale faults associated with the regional central CVZ fault pattern (Figure 8.13). Also apparent is the interaction of these two sets of structures.

### Caldera structures

Intracaldera rhyolite lava domes and intracaldera faults impart a significant control on the location of most alteration zones and associated precious metal mineralisation at the KCC.

Following emplacement of the rhyolite lava domes, epithermal systems were established soon after, which altered the core and margins of the domes. The inferred Starvation Fault may also be associated with alteration in the central KCC. Sericitic alteration occurs along the trend of the fault and interestingly unaltered Taurauikau Andesite dikes also lie and strike parallel to the fault. Bell and Fraser (1912) implied a continuation of the mineral deposit veins in the Welcome Jack area as extending along an E-W strike towards the Bulls Run area. This could not be confirmed, although it does add to the implied E-W control on ore structures.

NW-trending intracaldera faults (i.e. Green Tree Fault and Precipice Fault) intersect propylitic altered ignimbrite in the upper Kapowai valley. These faults are interpreted as intracaldera faults as they (i) never extend beyond the topographic boundary, (ii) have a trend which is significantly different from the regional fault trend, and (iii) in part they intersect and define the structural collapse boundary for the WES (i.e. Green Tree Fault). Alteration is only observed at the SE extent of these faults, although, the Green Tree Fault may also influence alteration on the eastern margin of the Welcome Jack Rhyolite dome.

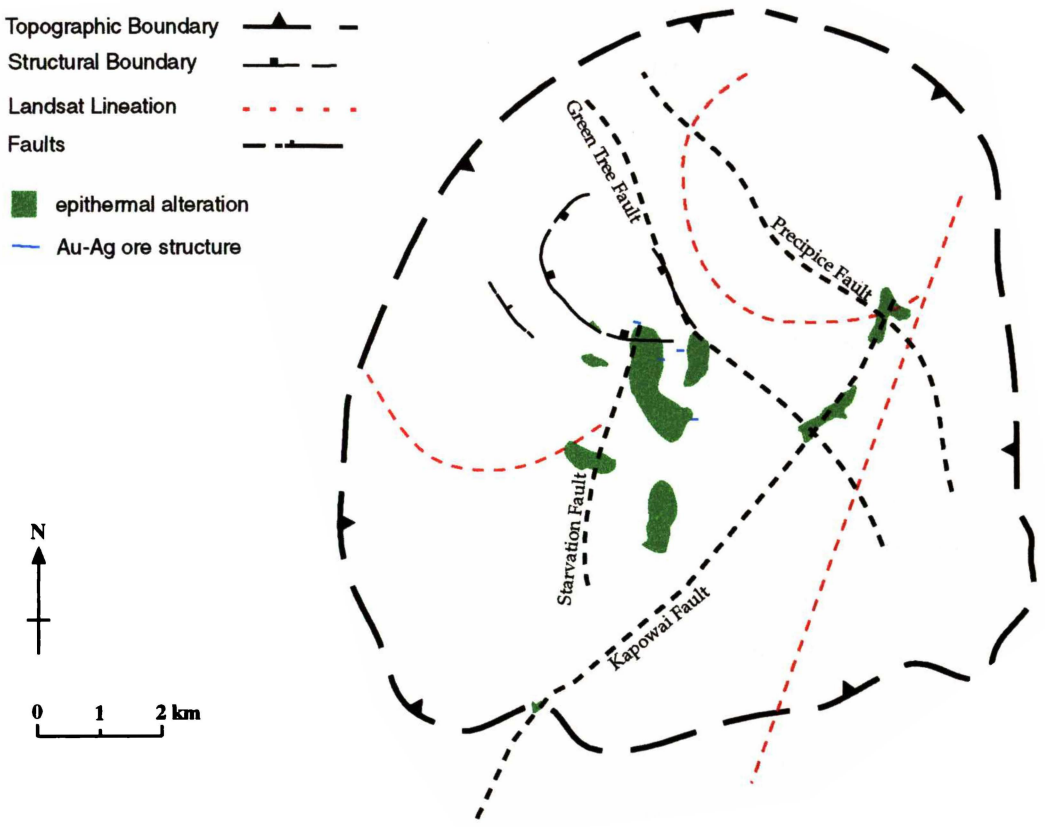


Figure 8.13 Summary of structural elements and epithermal alteration zones at the Kapowai Caldera Complex.

## Regional structural influence

The only apparent influence of the regional structure on the epithermal alteration pattern, is the NE-trending Kapowai Fault which extends through the Kapowai and Kauaeranga valleys. It has a similar NE-SW orientation to the faults mapped within the central CVZ region (Skinner, 1986; Belliss and Christie, 1994), and extends across the topographic boundary, implying that it is related to the regional structural pattern and is not a caldera structure.

Propylitic alteration occurs sporadically along the Kapowai Fault. Alteration zones in the upper Kapowai valley are located where intracaldera faults intersect with the Kapowai Fault. This suggests that interaction between regional and intracaldera faults may have controlled the location of alteration and possibly mineralisation.

Propylitic alteration of Webb Creek Ignimbrite in the upper Kauaeranga valley is located at the intersection of the topographic boundary and the Kapowai Fault. Altered pre-caldera andesite lava occurs along the Kapowai Fault, but south of the topographic boundary. As in the Kapowai valley, there is a suggestion that the Kapowai Fault and the topographic boundary appear to control the location of alteration in the upper Kauaeranga valley.

The influence of both caldera and regional faults in controlling the location of epithermal alteration/mineralisation is not reported elsewhere in the CVZ, although it is described at several epithermal deposits in North America (e.g. Mills et al., 1988). Interaction is variable in time and space and results in only some structures hosting alteration and/or mineralisation.

## 8.6 Timing of alteration

The timing of all epithermal alteration in the KCC pre-dates the WES. No WES units or rhyolite lavas which post-date WES, show any evidence of alteration. Only certain ignimbrites and rhyolite lava domes host alteration.

In the central KCC, alteration and mineralisation occurred post-emplacement of the Welcome Jack and Bulls Run Rhyolite domes, but the exact timing is difficult to establish from the field stratigraphy. Furthermore, it is difficult to establish whether there was one large epithermal system which affected both rhyolite domes, or that two or more smaller independent systems occurred.

Alteration along the Kapowai Fault pre-dates the WES eruption, but any age relationship with nearby rhyolite domes is difficult to establish. Alteration is likely to have occurred following development of the Precipice Fault and Green Tree Fault, and their subsequent intersection with the Kapowai Fault.

## 8.7 Characteristics of KCC epithermal system(s)

From the distribution of the alteration zones, it can be inferred that several epithermal systems were periodically active at the KCC. These systems are variable in their present surface extent, but all appear to be localised and controlled by caldera and regional faults. Aside from the central alteration zone, where mineralisation is known, other alteration zones may or may not indicate mineral deposits at depth.

Based on the dominance of sericite and adularia, and the relatively large areal extent covered by ore structures and alteration zones, the central KCC hydrothermal system(s) can be classified as a low-sulphidation, adularia-sericite type (Heald et al., 1987). Other alteration zones in the Kapowai and Kauaeranga valleys are also likely to be of this type based on their similar alteration mineralogy. Low-sulphidation type epithermal systems are common in the Coromandel Peninsula and most of the economic deposits are of this type (Christie and Brathwaite, 1986; Brathwaite et al. 1989).

To fully evaluate the chemical and temperature conditions of hydrothermal fluids within the KCC epithermal systems, fluid inclusion and stable isotope studies on vein material would need to be obtained. This has not been attempted here for reasons mentioned in this chapter's introduction, although some constraints can be placed using the alteration mineral assemblages observed in the host rocks.

The alteration mineralogy consists of three major assemblages: (i) propylitic consisting of chlorite, calcite, quartz, illite, sericite, adularia, analcime, and apatite; (ii) sericitic consisting of quartz, sericite, illite, pyrite, epidote; and (iii) argillic composed of kaolinite, alunite, dickite, and pyrophyllite. Propylitic and sericitc assemblages are typical of chloride fluids (Henley, 1985; Hedenquist, 1986). The argillic assemblage is considered to relate to an acid-sulphate fluid, or as reported in other CVZ locations, it may also reflect a late overprinting by a lower temperature chloride fluid (e.g. Christie and Brathwaite, 1986).

Stability fields for hydrothermal alteration assemblages have been determined based upon thermodynamic data for individual constituent minerals (Inoue, 1993). These diagrams provide some constraints on the chemical conditions and interactions in hydrothermal fluids (Figure 8.14). The presence of certain minerals can also provide controls on fluid temperatures. For example, the presence of epidote in some central KCC alteration zones, implies a fluid temperature of at least 240 °C (Hedenquist, 1986).

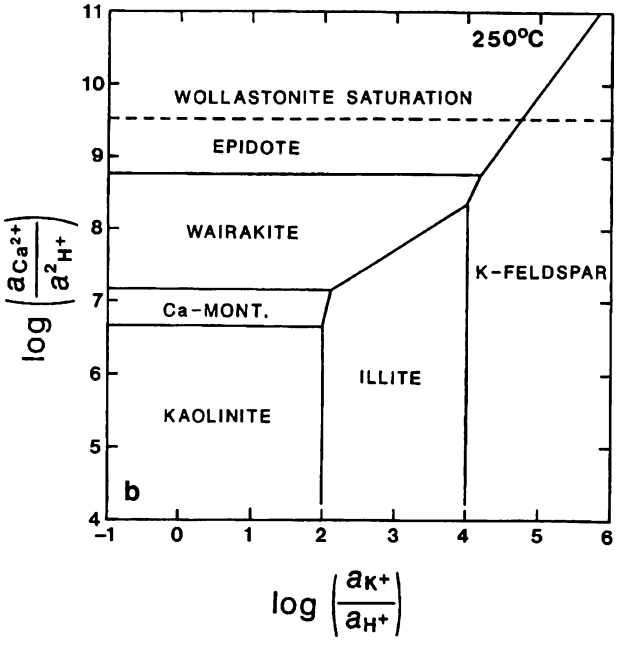


Figure 8.14 Calculated stability relations among common alteration minerals at the Kapowai Caldera Complex. Relations are a function of cation activity ratios in a coexisting solution at constant temperature and pressure. Adapted from Inoue (1995).

## 8.8 Comparison with other calderas

### TVZ calderas

Known CVZ caldera volcanoes are consistently smaller (5-12 km) and have erupted much less volcanic material than TVZ calderas (average caldera diameter ~ 20 km) (Wilson et al., 1995). However, structural relations between epithermal systems and calderas in the two zones are similar. The location of present day geothermal systems in the TVZ is variable (Figure 8.15), but generally reflects structural control from both the regional NE-trending fault pattern and localised caldera structures (Hedenquist, 1986). Interactions between regional faults and caldera structures have also controlled the location of several systems (e.g. Whakarewarewa, Waiotapu and Wairakei) (Thompson, 1974; Cole, 1990).

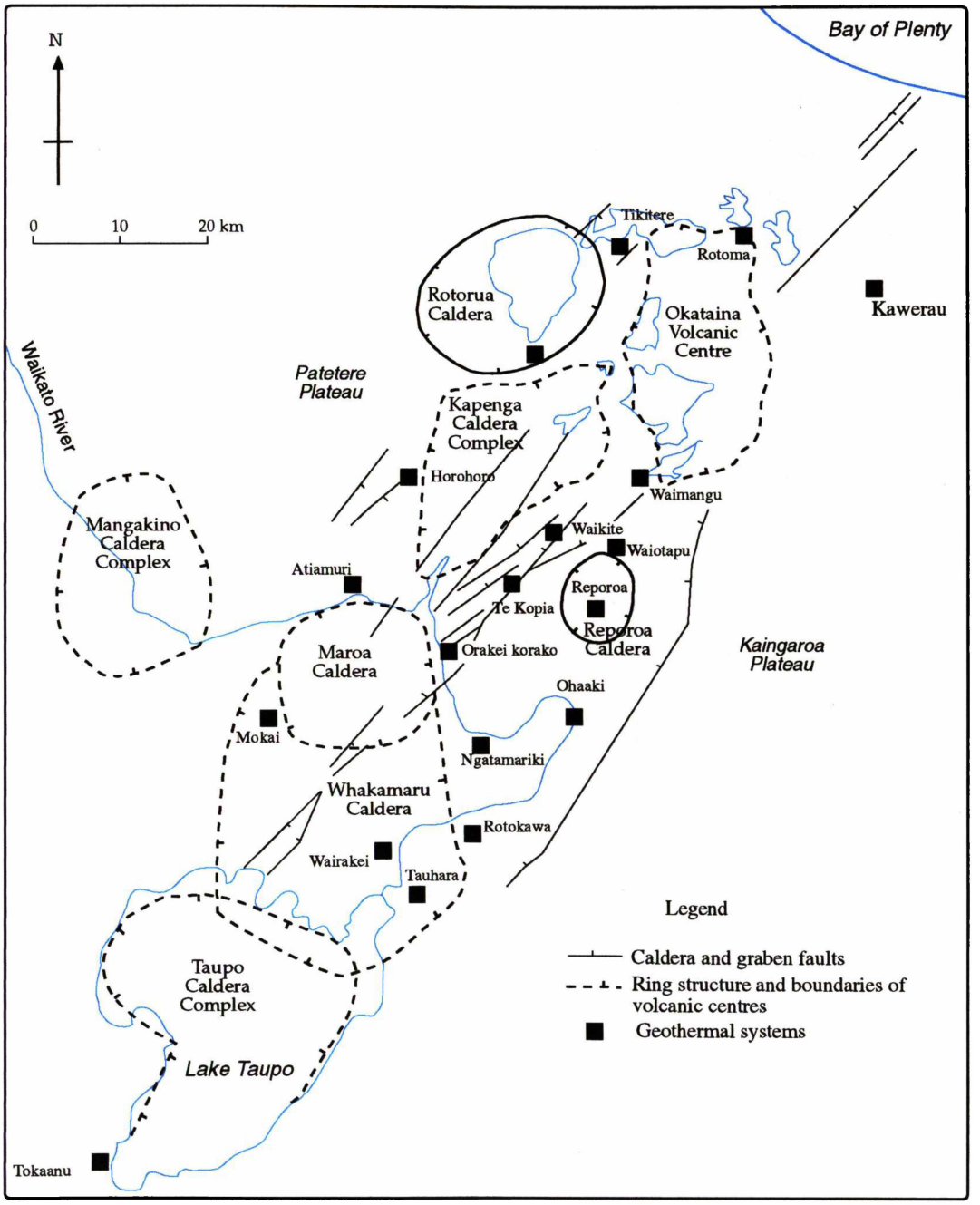


Figure 8.15 Location of active geothermal systems in the TVZ compared to the regional structural pattern and caldera structures. Adapted from Hedenquist (1986) and Wilson et al. (1995).

TVZ calderas thus provide good analogues for understanding epithermal alteration patterns and associated mineralisation at CVZ calderas. This is particularly pertinent when for most CVZ calderas, the structural and stratigraphic history remains poorly known.

## Mineralised calderas/caldera complexes

Many precious metal deposits associated with caldera volcanoes have been described from North America. Most of the calderas hosting mineral deposits are Tertiary or Mesozoic in age and subsequently more eroded than CVZ calderas. Typically this allows greater exposure, and hence a better understanding of the relationships between mineral deposits and alteration zones with both caldera and regional structures.

Significant work relating deposits to caldera structures and caldera evolution, has focused on calderas in the San Juan Mountains (Lipman et al., 1976), but studies have also been undertaken on calderas in other areas including Arizona (Lipman and Sawyer, 1985), New Mexico (Goff and Gardner, 1994), and Nevada (Mills et al., 1988). Aside from highlighting structural controls on mineralisation (Figure 8.16), work in North America has also emphasised the episodic nature of geothermal systems developed following several episodes of dome emplacement, caldera collapse or resurgence (Lipman et al., 1976; Slack and Lipman, 1979).

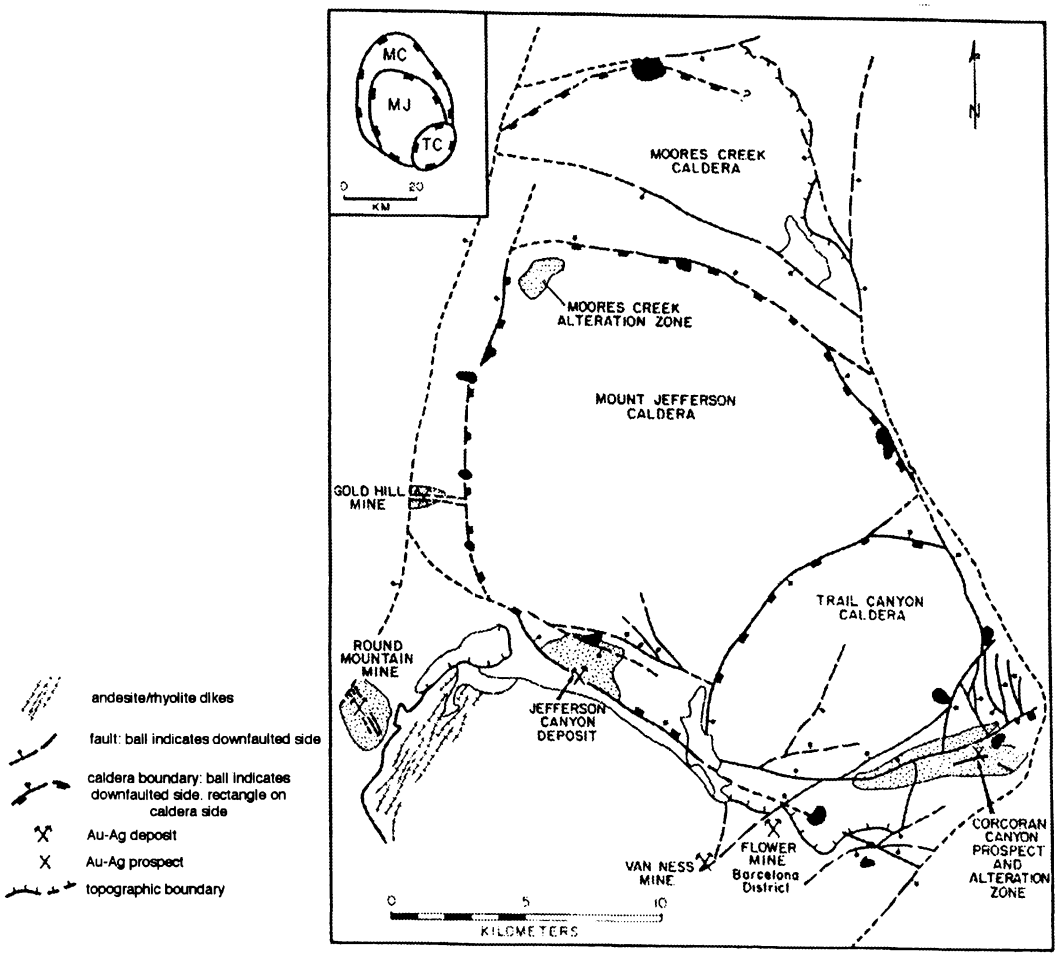


Figure 8.16 Structural map of the Toquima caldera complex highlighting control of alteration and mineralisation by major faults, and volcanic structures. Modified from Mills et al. (1988).

Numerous epithermal deposits related to calderas or ring/arcuate structures have been reported from many other locations (e.g. Eaton and Setterfield, 1993; Arribas et al., 1995; van Thournout et al., 1996; Milesi et al., 1999). Significant structural, mineralogic, geochemical and stratigraphic variability is present between these locations, although links between caldera structures and/or regional tectonic corridors and mineralisation are consistent.

The influence by either caldera structures or regional faults, or both, on alteration and/or mineralisation is highly variable. Control by both a structural boundary and conjugate regional strike-slip faults occurs at the Pongkor (Indonesia) Au-Ag-(Mn) epithermal deposit (Milesi et al., 1999), and at the Tavua Caldera where numerous areas of alteration and mineralisation occur both on the caldera margins and in the central caldera, associated with a regional shear zone (Figure 8.17) (Eaton and Setterfield, 1993). At the epithermal deposit at Portovelo, Ecuador, the major structural influence on alteration and mineralisation is by the regional fault corridor (van Thournout et al., 1996).

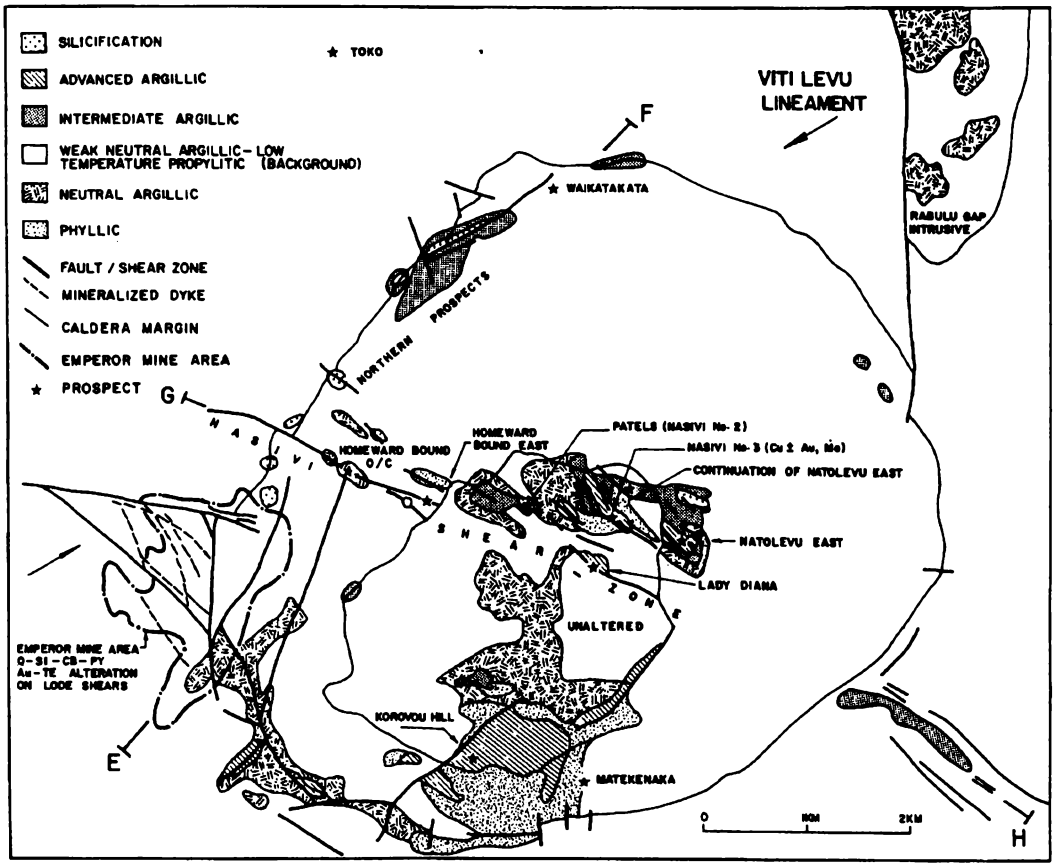


Figure 8.17 Variable distribution of alteration and mineralisation at Tavua caldera, Fiji. After Eaton and Setterfield, 1993.

In comparison with these and other mineralised calderas, the KCC varies in its dimensions, structural features, and age. However, there are similarities in the strong control by caldera structures and regional fault corridors on the location of mineral deposits and the timing and periodic nature of mineralisation. As prospecting within the KCC has only focused on central historic deposits, it is pertinent that any further investigations also include additional alteration zones identified here.

# Chapter Nine

# CALDERA FACIES AND EVOLUTION OF THE KAPOWAI CALDERA COMPLEX

## 9.1 Introduction

Modern approaches to understanding the complexity of geological processes and sequences at ancient caldera volcanoes have utilised the facies model concept. This incorporates the physical, lithologic, and compositional features of deposits and relates them to an environment of formation and deposition (Cas and Wright, 1987).

Evolutionary models for caldera volcanoes are commonly presented to summarise the volcanic, structural and petrological development of the volcano (e.g. Lipman, 1975; Elston, 1984; Leat, 1984; Chesner and Rose, 1991). Typically, subdivision of the model can be made based on evidence of significant periods of volcanism (effusive or explosive) or quiescence (lacustrine or fluvial sedimentary sequences) at the caldera.

This chapter presents a caldera facies model for the KCC, and describes both intracaldera and exocaldera facies associations. The evolution of the KCC is then described which incorporates discussion on its lithological, structural and petrological development. Finally, comparisons are made of the morphology, caldera longevity, and the structural and volcanological evolution of the KCC with Quaternary calderas and caldera complexes within the TVZ.

## 9.2 Caldera facies

Facies concepts for volcanoes and volcaniclastic sequences have only recently been developed (Cas and Wright, 1987). They were established based upon facies concepts developed for sedimentary sequences (Middleton, 1978; Walker, 1984). In both realms, the facies concept links the physical characteristics (e.g. lithology, geometry, composition) of sequences to geological processes and enables paleogeographic and/or paleoenvironmental reconstructions to be developed (Walker, 1984).

Conceptual facies models have been developed for caldera volcanoes (e.g. Lipman, 1984; Cas and Wright, 1987) and have been used as a basis for the recognition of extinct silicic centres or calderas (e.g. Orth et al., 1989; Briggs and Fulton, 1990). Facies models for caldera volcanoes are unique, as they focus predominantly on the emplacement of large scale pyroclastic flows, dispersal of large scale (i.e. plinian and phreatoplinian) fall deposits, and emplacement of lavas domes and flows, all from a common source area. Associated with these volcanic facies, other facies including lacustrine, fluvial, mass wasting, plutonic and hydrothermal alteration facies may also occur (e.g. Briggs and Fulton, 1990; O'Halloran and Gaul, 1997). Depositional environments are variable and can include both subaerial or subaqueous deposition within proximal - medial (typically intracaldera) and distal (exocaldera) localities (Cas and Wright, 1987).

Typically the record of extinct and highly eroded silicic caldera volcanoes is only preserved in the volcaniclastic record (Riggs and Busby-Spera, 1991). In these cases, facies models of modern active volcanoes provide the framework for the interpretation of volcaniclastic sequences and allow the location of silicic volcanic centres to be constrained (e.g. McPhie, 1986; Orth et al., 1989).

Intracaldera and exocaldera facies associations are described for the KCC, and these are separated by the present topographic boundary. Effusive facies which cross this boundary, are included within the intracaldera facies association because they either have source vents within the boundary (e.g. Taurauikau Andesite) or have source vents inferred to occur along the boundary (e.g. Ruahine Rhyolite; Kokonga Rhyolite; Camp Rhyolite).

## Intracaldera facies association

The intracaldera facies association includes all facies which occur within the topographic boundary. These consist of a diverse assemblage of caldera infilling facies, and are dominated by pyroclastic, effusive, and lacustrine facies (Figure 9.1). Minor, but significant hydrothermal alteration and mass wasting facies are also present. The majority of facies were deposited within a subaerial setting, although some such as the lacustrine facies and some constituents within the older pyroclastic facies were deposited within local subaqueous environments.

Intracaldera facies have a restricted distribution and complex geometry. This arises because of the periodic explosive and effusive eruptions within the caldera, partial burial by younger volcanic eruptions, and deformation of units by volcano-tectonic events, e.g. caldera subsidence, faulting, and resurgence (Lipman, 1984; Orth et al., 1989). Consequently, facies analysis is biased towards the well exposed younger sequences, with limited analysis of the older, partially exposed sequences.

### Pyroclastic facies

Pyroclastic deposits form the major infilling facies at the KCC and include many ignimbrites and tuff deposits erupted during volcanic activity at the KCC. These can be divided into two chronostratigraphic sequences of pyroclastic flow and fall deposits (Facies P1 and P2). Proximal and medial subfacies are identified for the youngest (P2) facies, but similar division cannot be established for the older (P1) sequence because of limited exposure.

The oldest succession (Facies P1) consists of several sporadically outcropping ignimbrites and tuffs, all of which pre-date the WES. These have variable component abundance and morphology, and are typically of silicic composition, although some are of mixed (andesitic-rhyolitic) composition (e.g. Oteao Ignimbrite). Most ignimbrite units are generally weakly welded, although some grade from weakly to densely welded (e.g. Trig Q Ignimbrite).

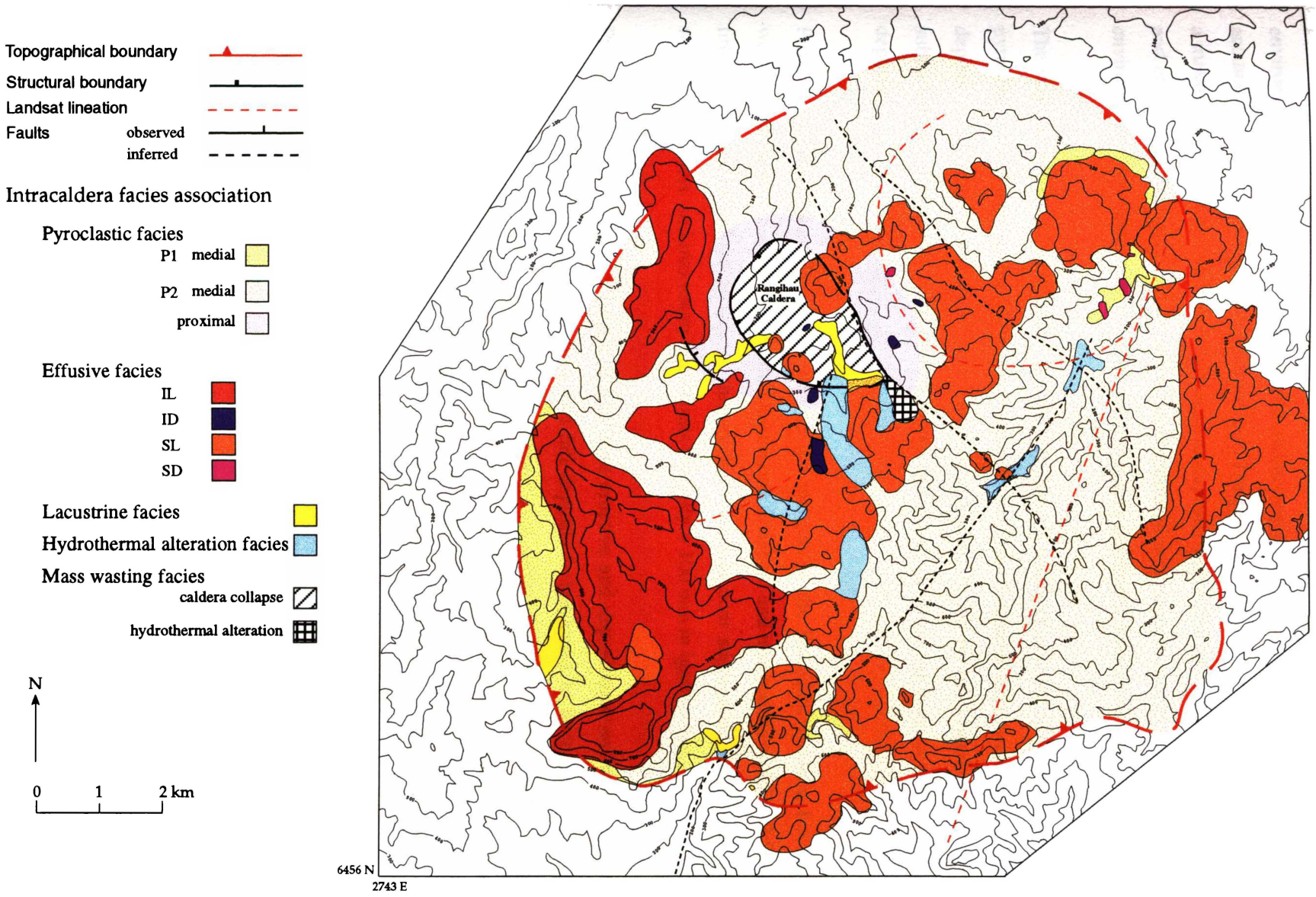


Figure 9.1 Distribution of intracaldera facies at the Kapowai Caldera Complex. P1 - pre-WES pyroclastics; P2 - WES pyroclastics; IL - intermediate lavas; ID - intermediate dikes; SL - silicic lavas; SD - silicic dikes.

Facies P1 outcrops in sporadic, small areas within the KCC. Facies thickness varies from ca. 2-3 m to 75 m (Webb Creek Ignimbrite), with this exposure dependent on deformation (e.g. faulting) and burial by younger pyroclastics. Most constituent pyroclastic deposits within this facies were deposited in a subaerial environment, probably on the eroded flanks and/or ring-plain of the pre-caldera andesite composite cones, or accumulated within the subsided, caldera floor. The presence of convolute and dish and pillar structures, and a massive, fine grained texture present in some deposits (e.g. CP-2 Ignimbrite), suggests that in some areas and at certain times, pyroclastic material was deposited in a subaqueous environment. Possible subaqueous environments (e.g. lakes, river systems) were probably developed within older collapse zones.

The younger pyroclastic succession (Facies P2) consists solely of a single eruptive sequence, the WES. No pyroclastic units overlie this sequence. Facies P2 consists of several large scale pyroclastic flow and fall deposits, with flow deposits the major component. Facies P2 can be subdivided into proximal and medial subfacies (see Chapter 5) based on the presence or lack of lithic lag breccia and thick interbedded fall deposits.

Proximal subfacies have been identified on the margins of the Rangihau Caldera, but especially on the western and eastern margins where lithic lag breccia (0.5-1 m) and interbedded tuff (1- 3.5 m) occurs. Other lithological features characteristic of this subfacies include poor segregation of juvenile and lithic clasts within ignimbrites, and maximum lithic clasts typically > 100 mm in ignimbrites.

Proximal subfacies record changes in near vent eruptive and depositional environments (see Chapter 5). Deposition and accumulation of flow and fall deposits is suggested to have occurred within a zone of eruption column deflation (Walker, 1985). Depostional surfaces varied from an initial irregular landscape consisting of locally elevated (e.g. rhyolite lava domes) and gently sloped plateaux (older ignimbrites) to a gently outward sloping pyroclastic apron consisting of WES deposits, constructed during accumulation of pyroclastic material.

The medial subfacies of P2 facies is more widespread than proximal facies, and occurs throughout the KCC, where it varies in thickness from ca. < 10 m to up to 400 m. Significant lithological differences compared with proximal deposits include greater ignimbrite thickness, and more pronounced clast segregation and smaller lithic clast sizes within ignimbrites (typically < 100 mm).

All components within the medial subfacies were deposited within a subaerial environment. In contrast with proximal subfacies, medial depositional environments were characterised by a highly variable landscape which included multiple rhyolite lava domes and dome complexes, thick sporadic ignimbrite plateaux (formed by older P1 facies ignimbrites), and major collapse or depositional zones (e.g. Kapowai valley). There is no evidence of subaqueous deposition at the base of the WES sequence, even though it contacts

with lacustrine facies in several areas. This implies that the lacustrine sequences were lithified and exposed prior to WES eruption.

The thickness and infilling nature of medial subfacies implies that the intracaldera environment was strongly influenced by the eruption and deposition of multiple sequences of pyroclastic flow and fall deposits. As the distribution of the older P1 facies is poorly known, and no proximal subfacies are exposed, the scale of the older sequences cannot be clearly defined. However, some of the P1 constituent deposits may be of a similar volume (i.e. < 100 $km^3$) to the WES.

**Effusive facies**

Effusive facies form a significant component of the intracaldera facies association at the KCC. Intermediate and silicic lavas and dikes form two subfacies, and within these there is considerable variability in age, geometry, minimum volume and composition. Most of these lavas were emplaced entirely within the KCC, although some older lavas do cross the youngest (i.e. present) topographic boundary.

### Intermediate lavas and dikes

Intermediate lava flow facies (Facies IL) and intermediate dike facies (Facies ID) occur mainly in the western sector of the KCC. Lava flow members of Facies IL vary in thickness from ca. 2-4 m for individual flows and up to 150 m for composite flows. This latter thickness reflects ponding of multiple lava flows within a major basin (i.e. Table Mountain). Most lava flows are poorly defined, eroded and dissected by fluvial systems, which limits the extent of their original lengths. Most exposed lava flows are in the range of ca. 0.5 - 1 km in length. Dikes are also observed, and in some instances infer the location of source vents (Skinner, 1993, 1995).

Based upon the geometry of lava flows and the occurrence of dikes, several vents for intermediate lavas are inferred within the western sector. At least two occurred along the Haukawakawa ridge at Haukawakawa Trig (T11/480666) and to the south at T11/476649. Several vents also occurred within the Waiwawa Range and probably include Mt. Rowe (T11/478592) and within Table Mountain. Younger K/Ar (i.e. 7.6 Ma) ages of lava flows erupted from northern (i.e. Haukawakawa ridge) vents compared with southern vents (i.e. Table Mountain, 8.5-8.1 Ma) indicates a migration of andesitic eruptions to the north.

Based on the lengths and thicknesses of lava flows, and the occurrence of dikes, these represent a near vent or proximal facies assemblage, although interbedded welded fall facies are rare (cf. Cole et al., 1986). Lava flows were deposited on steep slopes or between ridges on the upper flanks of composite cones, similar to modern environments (e.g. Tongariro volcanic complex; Cole et al., 1986).

Intermediate dike facies (Facies ID) consist of several andesitic dikes of variable width (ca. 1-5 m), orientation (e.g. N-S, NE-SW), age and location. They can be divided into those that: (i) are associated with

proximal composite cone vent facies; and (ii) those which occur some distance (ca. 1-2 km) from intermediate vents and intrude silicic lava facies or pyroclastic facies.

Intermediate dikes associated with proximal vent facies are rarely observed (cf. Skinner, 1993, 1995). These were emplaced either during or following eruptive activity at the composite cones. Intermediate dikes which intrude silicic lava facies or pyroclastic facies post-date those associated with vent facies. All intermediate dikes have a broadly similar mineralogy and composition to the lava facies.

### Silicic lavas and dikes

Silicic lava domes (Facies SL) and dikes (Facies SD) occur on the southern and eastern topographic boundaries, and throughout the caldera. Both facies consist of low-silica to high silica rhyolite compositions. Facies SL includes several rhyolite dome complexes and many individual rhyolite lava domes of variable volume.

Lava domes and dome complexes consist of lava, autoclastic breccia and obsidian lithofacies which are highly variable in distribution and occurrence within each lava dome or dome complex. Most exposed outcrops are deeply eroded and only include one or rarely two of these lithofacies, which contrasts with younger rhyolite lava flows, where multiple lithofacies can be recognised (e.g. Fink, 1983; Fink and Manley, 1987). Based on the lack of brecciated lava margins, and absence of reworked rhyolitic volcaniclastic material, a subaerial environment of emplacement is inferred for rhyolite lava domes at the KCC.

The distribution of the silicic lava and dike facies at the KCC is suggested to be related to caldera structures (e.g. structural boundaries, faults), although there is limited evidence because most intracaldera structures are buried. An example of emplacement control by a structural boundary is given by the Big Beetle and Acadia Rhyolite domes which were erupted along the southwestern margin of the WES structural boundary. Alignment of some rhyolite lava domes may be related to either intracaldera faults (e.g. Rangihau Rhyolite dome, Waiwhatawhata Rhyolite dome and Wharepapa Rhyolite dome aligned NE in northeastern sector) or regional faults (e.g. Tauranikau Rhyolite dome and Kauaeranga Rhyolite dome in the southern sector).

Silicic lava dikes (Facies SD) have only been observed to outcrop in the Kapowai River valley where they intrude either silicic lavas (Kapowai Rhyolite) or pyroclastics (Colorado Pyroclastics). Dikes are variable in width (ca. 2-5 m), composition (low to medium silica rhyolite), and age. Some dikes have K/Ar dates of 5.12-5.19 Ma, clearly younger than WES (i.e. 5.8 Ma), although no contacts have been observed.

Emplacement of dikes occurred in both shallow, water-saturated, and deeper, water-free zones of the volcanic pile. Intrusion into water-saturated strata is inferred by irregular brecciated, glassy dike margins in some dikes (e.g. Precipice Rhyolite dike A, Figure 3.26). Water-free intrusions are inferred by sharp, planar contacts.

**Lacustrine facies**

Lacustrine facies occur in several restricted, valley floor-confined areas. These are mainly within the KCC, although some cross the SW margin of the present topographic boundary. Thicknesses range from ca. 35 m to 50 m. Three sequences have been divided mainly by relative age and to a lesser extent by internal lithofacies and occur in the (i) Waiwawa River-Wainora Stream area (Waiwawa Member); (ii) upper Kauaeranga valley (Tarawaere Member); and (iii) Haukawakawa Stream-Slip Stream area (Haukawakawa Member) (see Chapter 3).

Four major siltstone lithofacies, occurring within these sequences have been defined and are: (i) massive; (ii) carbonaceous (iii) mm-horizontal laminated; and (iv) mm-horizontal laminated with interbedded laminae or beds of primary or reworked pyroclastic material. These facies vary in thickness, abundance and distribution within the sequences. Minor lithofacies include carbonaceous sandstones and conglomerates (in Waiwawa Member), and massive or bedded volcaniclastic sandstones (in Haukawakawa Member). Contacts between facies are also variable and include both sharp and gradational boundaries. All lacustrine facies are deformed by faulting and/or subsidence, and this is best observed in the Haukawakawa Member.

Variable environments of deposition within freshwater lakes are indicated by the four lithofacies. Massive siltstone and mm-horizontal laminated siltstone lithofacies are the most common types and represent the background, suspension-fallout sedimentation (Larsen and Crossey, 1996). Horizontally laminated, coarse volcaniclastic beds indicate terrestrial input of pyroclastic fall material into the lake system, or eroded pyroclastic material washed into the lake. Multiple volcaniclastic beds are common and represent periodic inputs of pyroclastic material. Carbonaceous beds are less common and thinner than other beds. These beds represent periods of organic accumulation within the lake floor.

As a whole the lacustrine facies represent periods of quiescence between large-scale explosive eruptions, although smaller scale explosive events within the KCC or distal eruptions are recorded. Sequences are all terminated by large scale pyroclastic flow deposits, although the nature of the contact varies from sharp and erosive on exposed lacustrine facies (e.g. Haukawakawa Member) to gradational from a subaqueous to subaerial environment (Waiwawa Member).

Based upon the exposed lacustrine sequences, at least three major freshwater lakes were present during the evolution of the KCC. Freshwater lakes are common within modern calderas (e.g. Nelson et al., 1994) and intracaldera volcaniclastic lacustrine facies are known for many extinct calderas (e.g. Fritz et al., 1990; Larsen and Crossey, 1996). At the KCC and at other calderas, lakes are likely to have developed within several types of basins including fault-bounded depressions or caldera collapse structures.

### Mass wasting facies

Mass wasting facies are a minor, but important component of the intracaldera facies association. This facies consists of post-collapse landslide breccias associated with the WES eruption (i.e. infilling the Rangihau Caldera), and minor slope failures throughout the KCC. Typically this facies consists of chaotic, poorly consolidated breccias of variable lithology (e.g. ignimbrite, hydrothermally altered rhyolite lava) and clast size (typically > block size for large volume breccias).

Generation of these breccias are related to mechanisms which generate hill slope instability and include caldera collapse (Rangihau Caldera) and hydrothermal alteration (The Big Slip). Formation of the Rangihau Caldera and associated steeply inward dipping fault scarps lead to the development of landslide breccias which infilled most of the caldera floor. Hydrothermal alteration of rhyolite lava domes at the head of the Slip Stream valley lead to failure of the dome's northern slope and generation of a major translational slide which extends for ca. 1 km.

### Hydrothermal alteration facies

Hydrothermal alteration forms a significant facies within the KCC. Three main areas of alteration are defined in: (i) the central KCC; (ii) the Kapowai valley; and (iii) in the upper Kauaeranga valley. Sericitic alteration and propylitic alteration occurs within the central KCC, but only propylitic alteration occurs within the Kapowai and Kauaeranga valleys. Gold and silver deposits are only associated with the central KCC alteration zone. The distribution of these facies is closely related to the location or intersection of intracaldera (e.g. Precipice Fault, Green Tree Fault) and/or regional faults (e.g. Kapowai Fault).

Alteration zones are variable in their geometry, age and host rock lithology. Most zones cover small areas (i.e. < 0.5 $km^2$), although some composite zones in the central CVZ cover up to 1 $km^2$. Host rocks include silicic lavas (e.g. Welcome Jack Rhyolite) and welded ignimbrites (e.g. Webb Creek Ignimbrite) of varying ages. The different host rocks and the presence of hydrothermally altered lithic fragments in intracaldera ignimbrites, implies different ages for hydrothermal alteration, and hence multiple geothermal systems within the caldera.

Propylitic and sericitic alteration assemblages and the unaltered surrounding country rock indicates that geothermal systems were active in a subaerial environment.

## Exocaldera facies association

The exocaldera facies association incorporates all facies genetically related to the KCC, which occur outside of its topographic boundary. This includes several outflow pyroclastic facies that form a heavily dissected ignimbrite shield to the north, east and south of the caldera.

Exocaldera facies are typically more geometrically and lithologically simple, have better continuity of exposure, and suffer less from hydrothermal alteration compared with intracaldera facies (Cas and Wright, 1987). Exocaldera facies may be intercalated with exocaldera facies from other adjacent volcanic centres within the ignimbrite shield, or may infill calderas (e.g. Lipman et al., 1996). Exocaldera facies may also extend beyond the ignimbrite shield to distal terrestrial and marine environments (e.g. O'Halloran and Gaul, 1997).

**Outflow pyroclastic facies**

Outflow pyroclastic facies at the KCC include several pyroclastic sequences that have been derived (e.g. WES ignimbrites), or inferred to have been derived (e.g. Trig Q Ignimbrite) from the KCC. Sequences are dominated by ignimbrites, with lesser interbedded tuffs. Compared with intracaldera equivalents, exocaldera pyroclastic facies are typically thinner and contain smaller juvenile and lithic clasts, but have a larger distribution (Figure 9.2). Exocaldera ignimbrites display more evidence of clast segregation or grading and are less affected by hydrothermal alteration. Tuffs in outflow facies are also finer grained and thinner than intracaldera tuffs, and have a wider distribution. Two subfacies are defined based on key lithologic or geometric differences. These are (i) the caldera rim subfacies, and (ii) the coastal or distal subfacies.

Caldera rim subfacies (CR) includes all exocaldera ignimbrites and tuffs which occur on or near to (typically < 5 km) the topographic boundary of the KCC. By definition, ignimbrites in this facies have thicknesses greater than 30 m (typically up to 70-80 m) and contain maximum juvenile and lithic components greater than 20 mm within their vertical profile. This subfacies consists of several weakly to densely welded ignimbrites (WES-1, WES-4, Trig Q Ignimbrites) and minor fall deposits. These vary in their component abundance, morphology and welding, although they are all of silicic composition.

CR subfacies have an asymmetric distribution to the north, east and south of the KCC. Major valley systems between eroded pre-caldera andesitic-dacitic volcanic edifices, must have been present for the pyroclastic material to accumulate in these areas. Significantly there are rare or no outcrops of this facies to the west of the KCC, presumably due to the topographic highs present prior to and during deposition. Thin, veneer-type ignimbrites which were presumably deposited upon these highs, were subsequently rapidly eroded.

For CR facies, a subaerial environment of deposition is indicated because of the (i) lack of fluvial (i.e. cross-bedding, clast imbrication) and lacustrine (i.e. horizontal laminations, well sorted, very fine grain size) features of the primary deposits; (ii) lack of interbedded fluvial/lacustrine beds or reworked volcaniclastic material; and (iii) variation in welding (i.e. weak to dense welding) typical of subaerially deposited ignimbrites. Initial and subsequent pyroclastic flow and fall deposits, which constitute this subfacies, generated a thick ignimbrite shield over the eroded pre-caldera andesitic-dacitic composite cones.

Coastal or distal subfacies (CD) consists of correlative CR subfacies pyroclastics, although minor interbedded conglomerate and sandstone beds are present also. In contrast to the CR subfacies, CD subfacies are defined where pyroclastic thicknesses are less than 35 m and a maximum juvenile and lithic component of less than 20mm occurs within the vertical profile. Exceptions to this definition occur, for example major depocentres where thicknesses range up to 90 m (Adams, 1992), but these areas are considered distal rather than caldera rim localities based upon the small pyroclastic clast size and more pronounced clast segregation compared with CR subfacies.

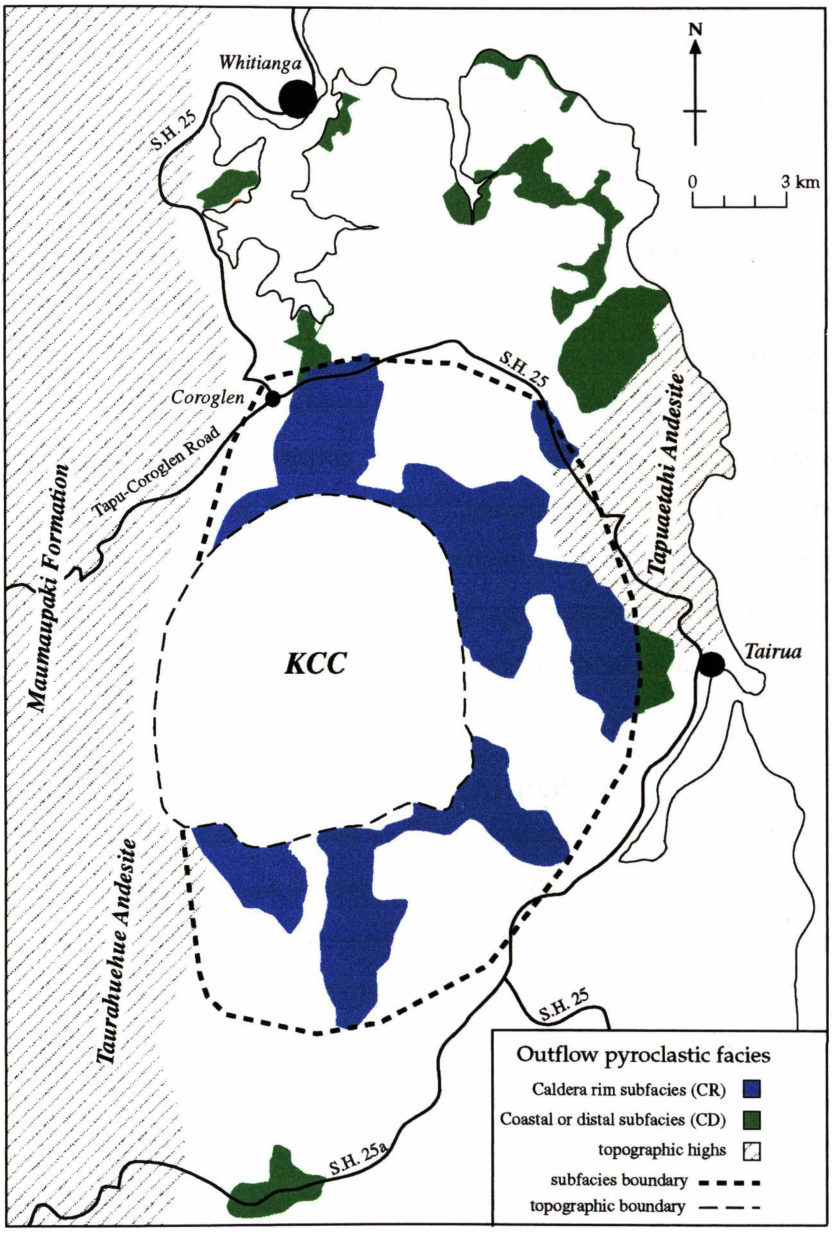


Figure 9.2 Distribution of exocaldera facies derived from the Kapowai Caldera Complex, and location of topographic highs (i.e. pre-caldera andesite-dacite formations).

CD subfacies covers a much larger area than facies CR, occurring throughout most of the northern, eastern and southern sectors of onland central CVZ. Lithologies vary within this subfacies between coastal exposures and inland areas, although the differences are highly variable. Coastal exposures in the north and east tend to be more affected by local deformation associated with the Whitianga Volcanic Centre, which

has resulted in truncation or erosion of sequences, faulting, and formation of clastic dikes (Rogers, 1994; Bardebes, 1997). Onland exposures to the east and south of the KCC tend to be are less affected by local deformation, and more complete sequences are exposed.

Subfacies CD was deposited mostly in a subaerial environment, although there is evidence that in some areas, pyroclastic flow and fall material was deposited and later reworked in local fluvial settings (e.g. Adams, 1992; Skinner, 1995). Evidence includes (i) thin (0.1-1.5 m) interbedded fluvial conglomerate or sandstone units within ignimbrite sequences, and (ii) thick (up to 5 m) pyroclastic flow and fall deposits with interbedded reworked volcaniclastic beds (Adams, 1992). Mixed subaqueous and subaerial environments are commonly reported for distal outflow facies from other silicic volcanic centres (e.g. McPhie, 1983; O'Halloran and Gaul, 1997).

A different landscape is envisaged for deposition of the CD subfacies compared with the CR subfacies. In contrast with the caldera rim area, the depositional surface consisted of a typically less dissected, gentler sloped landscape bounded by major topographic highs to the west and east. Two major topographic highs which bound this area are the eroded pre-caldera andesite-dacite composite cones to the west and southwest of the Waiwawa River (Maumaupaki Formation, Taurahuehue Andesite), and composite cones to the east of the KCC between Hot Water Beach and Pumpkin Hill (Tapuaetahi Andesite). These topographic highs acted as impediments to pyroclastic flow movement, and probably influenced the transport directions of post-depositional volcanogenic sediments. Some major basins were present within this landscape (e.g. west of Hot Water Beach) and acted as sites for significant pyroclastic accumulation.

## 9.3 Evolution of the Kapowai Caldera Complex

Most evolutionary models for caldera volcanoes incorporate the caldera cycle model initially developed for North American calderas (Smith and Bailey, 1968; Lipman, 1984). This cycle highlights the major structural and volcanological processes which have occurred during a single collapse cycle and includes: (i) pre-caldera volcanism and regional tumescence; (ii) large-scale eruption and caldera collapse; (iii) resurgence and extrusion of intracaldera lava domes; and (iv) late stage hydrothermal alteration and mineralisation.

In the case of a caldera complex, the partial or complete cycle has occurred several times, usually within overlapping or nested areas of the volcano (e.g. Lipman, 1975; Cole et al., 1998). Typically, evidence for early collapse cycles is buried by deposits or structures associated with younger collapse events, and may only be indicated by sporadic inliers, or by lithic fragments within ignimbrites (Lipman et al., 1996; Cole et al., 1998).

At the KCC, there is evidence to support several caldera collapse cycles. The most recent cycle, associated with the WES is indicated by a 3 $km^2$ oblong collapse zone (Rangihau Caldera) in the Haukawakawa-Slip Stream area which may be part of a larger subsidence area which extends to the northern margin of the

Waiwawa Range. Structural boundaries of the collapse zone consist of high-angle normal faults with thick pyroclastic flow and fall deposits, including proximal lithic lag breccia on the footwall. Other older caldera collapse events are suggested by: (i) circular features (up to 4.5 km diameter) on remote sensing imagery; (ii) accumulation of thick (up to 400 m) ignimbrites and tuffs in zones within the KCC; and (iii) the presence of several intracaldera welded ignimbrites and numerous welded ignimbrite lithics which pre-date the WES.

At least three caldera collapse events have occurred at the KCC based on the structural features and deposits described above. The temporal and spatial relationships between these events is poorly constrained, apart from the caldera collapse cycle associated with the WES, which is the youngest. WES deposits have infilled major depocentres within the KCC, which most likely related to older collapse zones, and therefore concealed the structural features and deposits associated with these zones, and also their stratigraphic relations.

K/Ar dating of the intracaldera sequence indicates that the volcanic succession was erupted from ca. 8.5 to 4.9 Ma. However, volcaniclastic lacustrine sequences derived from the KCC pre-date this oldest age. The intracaldera sequence can be divided into four major periods:

Period I: incorporates initial silicic volcanism (explosive and effusive) from before ca. 8.5 Ma to 8.0 Ma.

Period II: represents a change to dominantly effusive volcanism, and intermittent lake systems from ca. 7.6 Ma to prior to the WES eruption.

Period III: records the WES pyroclastic eruptions at ca. 5.8 Ma.

Period IV: records the final period of effusive volcanism following the WES until ca. 4.9 Ma.

The following sections discuss the petrologic evolution of the KCC during these periods. It is important to emphasise that these discussions are hampered by: (i) the poor exposure of pre-WES pyroclastics; (ii) paucity of intracaldera contacts; and (iii) limited radiometric dates. Summaries of the major volcanic lithologies erupted at the KCC are presented in Tables 9.1 and 9.2, and a schematic model for the evolution of the KCC is presented in Figure 9.3.

Together with variations in the types and styles of volcanism, and environments of deposition, structural elements at the KCC have also varied with time. Structures identified in this study include intracaldera structural boundaries, caldera floors, faults and intrusions, and structures (i.e. faults) associated with the regional fault pattern (see Chapter 2 for detail). These have influenced the distribution of primary volcanic deposits, alteration zones and the location of basins within the caldera. Temporal changes in structural elements at the KCC have been discussed in chapter 2. They are not repeated in this chapter, except where relevant.

Table 9.1 Summary of the lithology, composition, and mineralogy for intracaldera ignimbrites at the Kapowai Caldera Complex.

| Period | Ignimbrite | Lithology | Composition (wt.% $SiO_2$) | Juvenile | Juvenile Mineralogy | Matrix Mineralogy | Matrix |
|---|---|---|---|---|---|---|---|
| I | Webb Creek | light grey pumice and lithic-rich weakly welded ignimbrite | 71.5 | one pumice type | plag±qtz±opx±cpx±amph | plag±qtz±opx±cpx±amph | fine ash, devitrified poorly vitroclastic |
| | Trig Q | light brown-black pumice and crystal-rich weakly to partially welded ignimbrite | 68.2-75.4 | one pumice type | plag+cpx | plag+cpx | fine ash devitrified glassy poorly vitroclastic |
| II | Manuka | cream/pink pumice and lithic-rich weakly vapour phase altered welded ignimbrite | 71.2 | one pumice type | plag+cpx±opx±qtz | plag+cpx±opx±qtz | fine ash devitrified relict vitroclastic |
| | Oteao | dark grey juvenile and crystal-rich weakly welded ignimbrite | 57.3-69.6 | scoria, pumice, mingled and mixed types | plag+cpx+opx | plag+cpx+opx | fine ash devitrified poorly vitroclastic |
| III | WES-1 | light grey pumice and lithic-rich weakly welded ignimbrite | 71.6-72.8 | two pumice types | plag+opx±cpx±qtz±amph | plag+opx±cpx±qtz±amph | coarse ash non devitrified vitroclastic |
| | WES-4 | light grey pumice and lithic-rich weakly welded ignimbrite | 72.7-75.4 | two pumice types | plag+opx+cpx±qtz±biot±amph | plag+opx+cpx±qtz±biot±amph | fine ash incipiently devitrified vitroclastic |

Table 9.2 Summary of the lithology, composition, volume, and age of rhyolite lavas and dikes at the Kapowai Caldera Complex. Caldera floor is defined as the area bounded by the present topographic boundary.

| Period | Unit | Lithology | Composition (wt.% $SiO_2$) | Volume ($km^3$) | K/Ar age (Ma) | Location |
|---|---|---|---|---|---|---|
| I | Welcome Jack Rhyolite dome | qtz+plag+biot fine grained rhyolite lava | 77.4-78.9 | 0.8 | 8.42 ± 0.22 | caldera floor |
| | Moss Creek Rhyolite dome | plag+biot phyric fine grained rhyolite lava | | | | caldera floor |
| | Atuatumoe Rhyolite dome | plag+opx phyric fine grained rhyolite lava | | 0.4 | | southern topographic boundary |
| II | Scots Rhyolite lava | plag+biot phyric fine grained rhyolite lava | | | | caldera floor |
| | Rangihau Rhyolite dome | plag phyric fine grained rhyolite lava | 75.4 | 0.25 | 6.89 ± 0.37 | caldera floor |
| | Waiwhatawhata Rhyolite dome | plag+opx+cpx phyric fine grained rhyolite lava | 72.6-74.2 | 0.25 | | caldera floor |
| | Kydd Rhyolite dome complex | plag+opx±cpx phyric medium grained rhyolite lava | 74.7 | 1.2 | | caldera floor |
| | Wharepapa Rhyolite dome complex | plag phyric fine grained rhyolite lava | 76.4 | 0.1 | | caldera floor |
| | Kapowai Rhyolite dome | plag+opx+cpx±qtz±amph phyric medium grained rhyolite lava | 72.4-75.7 | 0.35 | | caldera floor |
| | Kokonga Rhyolite dome | plag+opx+cpx phyric fine grained rhyolite lava | 73.9 | 0.6 | 6.51 ± 0.36 | caldera floor |
| | Bulls Run Rhyolite dome complex | plag+opx+cpx phyric fine grained rhyolite lava | 74.6-76.1 | 1.0 | | caldera floor |
| | Starvation Rhyolite dome | plag+opx+cpx phyric fine grained rhyolite lava | 75.8 | 0.1 | | caldera floor |
| | Ruahine Rhyolite dome complex | qtz+plag+biot phyric fine grained rhyolite lava | 75.8 | 4.5 | 5.86 ± 0.31 | eastern topographic boundary |
| | Slip Rhyolite dike | plag+amph phyric fine grained rhyolite lava | 72.9 | | | caldera floor |
| | Miller Flat Rhyolite lava | plag+amph phyric fine grained rhyolite lava | 75.0 | | | caldera floor |
| III | Acadia Rhyolite dome | plag+opx phyric fine grained rhyolite lava | 74.6 | 0.015 | | caldera floor |
| | Big Beetle Rhyolite dome | plag+opx+cpx phyric fine grained rhyolite lava | 72.0 | 0.02 | | caldera floor |
| IV | Precipice Rhyolite dikes | plag+opx+cpx phyric fine grained rhyolite lava | 71.1 | - | 5.12 ± 0.28 | caldera floor |
| | Kauaeranga Rhyolite dome | plag+opx+cpx phyric fine grained rhyolite lava | 72.9 | 0.5 | 4.90 ± 0.60 | caldera floor |
| | Camp Rhyolite dome complex | plag+opx+cpx phyric fine grained rhyolite lava | 73.0-74.0 | 0.2 | 5.30 ± 0.30 | southern topographic boundary |
| | Tauranikau Rhyolite dome | plag+opx+cpx phyric fine grained rhyolite lava | 74.3-77.5 | 0.35 | | caldera floor |
| | Pinnacles Rhyolite dome | plag+opx+cpx phyric fine grained rhyolite lava | 74.0 | 0.5 | | southern topographic boundary |

***Period I (pre 8.5 - ca. 8.0 Ma): Initial explosive silicic volcanism***

Prior to silicic volcanism in the Rangihau-Kauaeranga-Kapowai area, andesitic-dacitic volcanoes and their products dominated the landscape. Intermediate composition lava flows, breccias and tuffs were deposited throughout this area. In the Waiwawa River -Wainora Stream area, a thick (up to 35 m) lacustrine sequence overlying andesitic lava flows and breccias indicates that a freshwater lake was present after intermediate volcanism. This lake was probably surrounded by eroding extinct, or active composite cones or stratovolcanoes, similar to modern day analogues in the Tongariro Volcanic Centre (i.e. Lake Rotoaira).

This freshwater lake may have developed by several processes including: (i) damming of stream drainage by lava flows or landslides; (ii) depressions generated by collapse or explosion craters; or (iii) as fault bound depressions (Lowe and Green, 1992). The extent of this lake is recorded by the presence of lacustrine deposits which cover an area of ca. 1 $km^2$. No other correlative sequences have been observed within or on the margins of the KCC, although it is likely that other lakes and fluvial systems occurred within the area during this time.

Silicic volcanic glass within this sequence indicates that moderate to large scale explosive rhyolitic eruptions were occurring at the KCC or from other buried CVZ silicic volcanic centres during this time. The increasing abundance and size of volcaniclastic grains in the upper sequence may indicate that KCC-derived material was dominant. If so, then this is the first sign of silicic volcanism in the Kapowai-Rangihau-Kauaeranga area.

The freshwater lake environment in the Waiwawa-Wainora area was ultimately destroyed by the first large scale rhyolitic pyroclastic flow eruptions from the KCC. This initial eruption deposited ignimbrite (Webb Creek Ignimbrite) and tuff throughout the Rangihau-Kauaeranga-Kapowai area, although modern exposures are restricted to the upper Kauaeranga valley. Webb Creek Ignimbrite is considered to be derived from a southern KCC source based upon its thickness (up to 75 m) and ML (up to 573 mm) in the Kauaeranga valley.

Prior to or soon after deposition of the Webb Creek Ignimbrite, rhyolite lava domes were erupted in the central KCC (Welcome Jack Rhyolite). There are no basal contacts observed, so any relationship with Webb Creek Ignimbrite can not be constrained. Epithermal mineralisation is associated with, and controlled by, emplacement of the Welcome Jack Rhyolite dome, although the only temporal constraint on mineralisation is that it occurred following emplacement of the lava dome.

Other rhyolite domes were erupted in the upper Waiwawa valley (Moss Creek Rhyolite) and further south in the upper Kauaeranga valley (Atuatumoe Rhyolite). These may have been associated with explosive silicic eruptions in the southern KCC (e.g. Webb Creek Ignimbrite). Atuatumoe Rhyolite lava dome overlies Webb Creek Ignimbrite and so may have been erupted as a late stage dome following the explosive eruptions.

A period of general quiescence in other areas of the KCC is recorded by volcaniclastic lacustrine sequences (Tarawaere Member) which overlie Webb Creek Ignimbrite in the upper Kauaeranga valley. Compared with Waiwawa Member, the distribution of this sequence is more sporadic and discontinuous. This is mainly due to post-depositional faulting and tilting associated with the Kapowai Fault and probably also by emplacement of younger rhyolite lava domes (e.g. Camp Rhyolite dome complex). The lacustrine sequence in the upper Kauaeranga valley is overlain in turn by a complex sequence of multiple pyroclastic fall and flow deposits and interbedded sporadic reworked volcaniclastic lacustrine and fluvial beds (Colorado Pyroclastics). These occur in the upper Kauaeranga valley and also extend to the NW along the present western margin of the Waiwawa range. This mixed sequence records a period of multiple moderate scale explosive silicic eruptions from the KCC, which was deposited in a variable subaqueous-subaerial environment.

One of the larger explosive eruptions preserved during this period is the Trig Q Ignimbrite. This outcrops only in the northern margin of the KCC, although correlative lithic fragments have been sampled from younger intracaldera ignimbrites, and floats of correlative ignimbrite have been observed in southern (e.g. Wainora Stream valley) catchments. A northern KCC source is favoured based upon the limited distribution (i.e. northern sector) and thickness (up to ca. 30 m) of the ignimbrite.

The final phase within Period I incorporated eruption and emplacement of andesitic-dacitic lava flows and sporadic dikes in the Waiwawa range-Table Mountain area (Taurauikau Andesite). Thick lava flows were erupted during this phase and some of these accumulated (up to ca. 150 m) in a major basin, which has subsequently undergone topographic inversion, forming the erosion-resistant Table Mountain. This basin was possibly generated by either a major valley system developed within eroding pyroclastics (e.g. Colorado Pyroclastics, Trig Q Ignimbrite) or by tectonic activity (e.g. fault-bound depression).

The primary distribution of these andesitic-dacitic lava flows is unclear because of subsequent erosion and intracaldera activity. The timing of cessation of volcanism in the Waiwawa range - Table Mountain area is also unclear, but based upon K/Ar age data, it must have ended prior to andesitic eruptions along the Haukawakawa Ridge.

***Period II (pre 7.6 Ma - 5.9 Ma): Multiple rhyolite and andesite lavas, and ignimbrites***

Period II is characterised by a major phase of explosive and effusive andesitic-rhyolitic volcanism within the Rangihau-Kauaeranga-Kapowai area. Its initial stages were marked by renewed andesitic volcanism from several vents along the Haukawakawa Ridge. Multiple lava flows and dikes were erupted and emplaced along the area of this ridge up until ca. 7.6 Ma. Further eruptions of andesitic-dacitic lava flows occurred south of the Haukawakawa Ridge in the upper Haukawakawa valley at ca. 6.6 Ma.

During this period numerous rhyolite domes and dome complexes were erupted mainly in the central KCC (Bulls Run Rhyolite dome complex; Rangihau Rhyolite dome, 6.9 Ma), but also in the northeastern

(Kokonga Rhyolite dome, 6.5 Ma; Kydd Rhyolite dome complex) and eastern sectors (Ruahine Rhyolite dome complex, 5.9 Ma). Rhyolite lava mineralogy and compositions are highly varied during this period and there are no clear temporal relationships between domes.

Several ignimbrites (Manuka Ignimbrite, Oteao Ignimbrite) were also erupted from the KCC during this period. These ignimbrites only outcrop in the northeastern sector of the KCC, although they most likely had a wider initial distribution. No caldera collapse zones can be defined unequivocally for these ignimbrites because of the paucity of outcrop and hence lack of ML data. However, a potential collapse zone in the northeastern sector is identified by remote sensing imagery (see Chapter 2 for detail). This zone is infilled by younger WES pyroclastics, which matches the field relationships of the ignimbrites (i.e. WES younger than Manuka Ignimbrite or Oteao Ignimbrite).

A quiescent phase at the end of this period was marked by the accumulation of volcaniclastic lacustrine siltstones (Haukawakawa Member) in the Haukawakawa Stream-Slip Stream area. These siltstones record the presence of a large (ca. 4 $km^2$) lake within the centre of the caldera complex. This lake may have developed within a depression associated with an earlier caldera collapse event or by impeded drainage caused by surrounding andesite (Taurauikau Andesite) and rhyolite (Bulls Run Rhyolite, Welcome Jack Rhyolite) lava flows. Andesitic volcanic glass or clasts are not observed within this lacustrine sequence indicating that the lake developed following cessation of andesitic volcanism along the Haukawakawa Ridge.

This central lake was eventually destroyed by initiation of the WES eruptive episode. The lacustrine sequence is highly deformed, uplifted and eroded which indicates that tumescence (associated with the ascending WES magma chamber) probably occurred within this area prior to the WES eruption.

***Period III (ca. 5.8 Ma): WES caldera collapse cycle***

Wharepapa Eruptive Sequence (WES) represents the most complete and largest magnitude pyroclastic sequence exposed at the KCC. It is the only KCC pyroclastic deposit which can be unequivocally related to a caldera collapse episode. WES consists of a conformable succession of thick ignimbrites, tuffs and localised lithic lag breccia erupted at ca. 5.8 Ma (averaged K/Ar ages).

No pre-cursor effusive volcanic activity is recognised, although regional tumescence is suggested by deformed and uplifted lacustrine siltstones (Haukawakawa Member) in the eventual caldera collapse zone (i.e. Haukawakawa Stream-Slip Stream area). Initial explosive eruptions deposited a widespread ignimbrite (WES-1 Ignimbrite) which infilled valleys and previous collapse zones within the KCC, before overtopping the caldera rim and travelling to the north, east and south. Eruption rates diminished and moderate-scale periodic explosive eruptions and co-ignimbrite fallout deposited thick (up to 3.5 m) beds of crystal and vitric tephra within and adjacent to the caldera. Continued explosive eruptions lead to erosion of the

conduit(s) and instability of the country rock, resulting in the eventual catastrophic collapse of the magma chamber roof. This phase is marked by lithic lag breccias (WES-3 lithic lag breccia) near the source. Subsequent increases in the discharge rate due to vent-widening produced energetic pyroclastic flows which emplaced ignimbrite (WES-4 Ignimbrite) throughout the caldera, and onto the adjacent landscape.

Post-eruptive tumescence or resurgence is not recognised within the caldera, although post-WES effusive volcanism occurred within the main collapse zone (Rangihau Caldera). Big Beetle Rhyolite dome and Acadia Rhyolite dome were erupted and emplaced along the southwestern margin of the Rangihau Caldera structural boundary.

***Period IV (post 5.8 Ma - 4.9 Ma): Post-WES effusive volcanism***

Following the WES eruption, no further large-scale explosive eruptions occurred from the KCC. However, several rhyolite lava domes (including Kauaeranga Rhyolite, 4.9 Ma; Tauranikau Rhyolite) and dome complexes (Camp Rhyolite dome complex; 5.3 Ma) were erupted on its southern margin. These erupted through thick pyroclastics of Period I (i.e. Webb Creek Ignimbrite, Colorado Pyroclastics) and the WES. Rhyolite lava dikes (Precipice Rhyolite, 5.19 Ma) were emplaced in the Kapowai valley and intruded Kapowai Rhyolite and Colorado Pyroclastics.

Associated with these late stage rhyolitic eruptions, several andesitic dikes (Taurauikau Andesite) were intruded through the WES succession in the central KCC. The exact timing of emplacement of these dikes is unclear, and presently can only be constrained to post-WES. Following volcanic activity at the KCC, the major focus of silicic volcanism shifted to the south (Wharekawa Volcanic Centre; Skinner, 1986), although major effusive silicic activity also occurred on the margins of the KCC (i.e. Whenuakite Volcanic Centre; Adams, 1992) and to the north at the Whitianga Volcanic Centre (Skinner, 1995).

## Compositional evolution

Compositions of volcanic rocks erupted at the KCC have varied during the evolution of the caldera. Prior to silicic volcanism, low-silica andesites to low-silica dacitic volcanic rocks were erupted (Maumaupaki Formation; Taurahuehue Andesite; Tapuaetahi Andesite) along the CVZ volcanic arc. This precursor intermediate volcanism is similar to other silicic provinces and silicic calderas (Colucci et al., 1991; Petterson et al., 1992; Cole et al., 1998).

With development of an extensional tectonic regime, rhyolitic magmas were developed in the Rangihau-Kauaeranga-Kapowai area after ca. 9.0 Ma. Eruption of these silicic magmas occurred from this time up until ca. 4.9 Ma and, significantly, andesitic magmas also continued to be generated and erupted. Bi-modal andesitic-rhyolitic magmatism at the KCC, appears to be a unique situation compared with other CVZ calderas (e.g. Briggs and Fulton, 1990; Briggs et al., 1998) and is distinctive from TVZ calderas where only bi-modal basaltic-rhyolitic magmatism is known (Wilson et al., 1995).

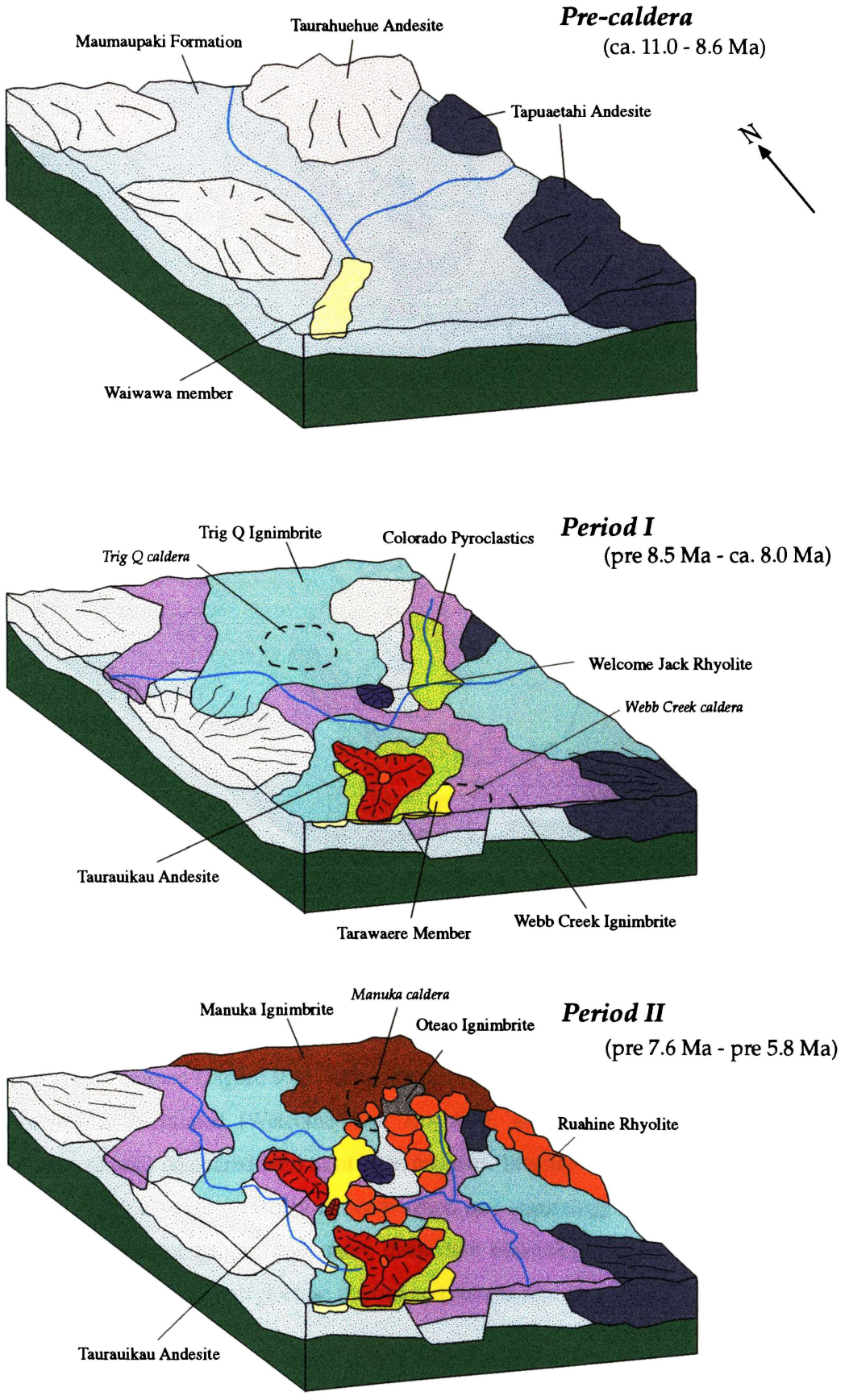


Figure 9.3 Simplified schematic reconstruction of the major phases in the evolution of the Kapowai Caldera Complex. Not to scale.

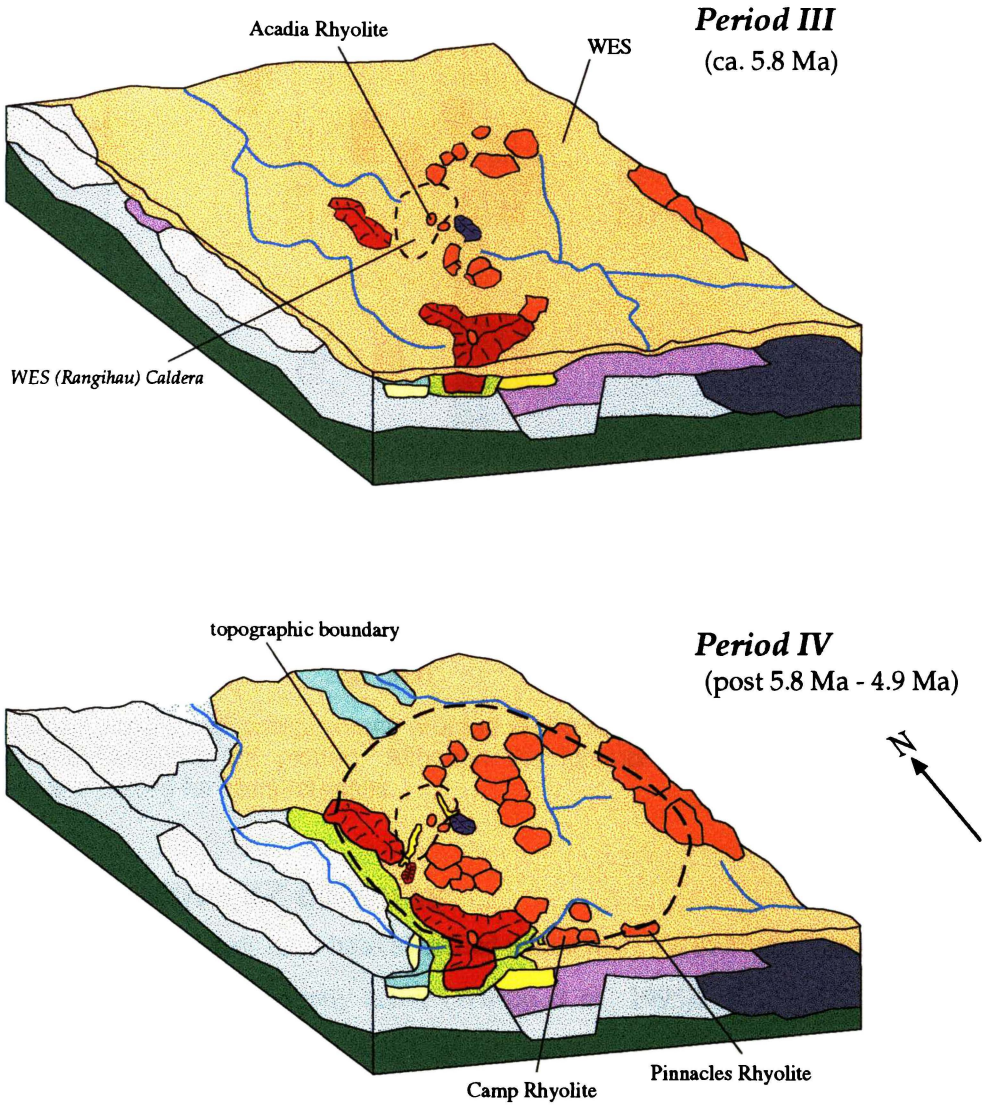


Figure 9.3 Continued.

During the period of activity at the KCC there was significant variation in the composition of both rhyolite and andesite magmas erupted (Figure 9.4). Although there are limited data, early silicic magmas of Period I were more highly differentiated (Welcome Jack Rhyolite), and mineralogically distinctive (i.e. quartz-plagioclase-biotite phyric) compared with most later magmas. Eruptions of silicic magmas during periods II-IV are characterised by a broad similarity in composition and mineralogy (i.e. plagioclase-pyroxene phyric), with occasional eruptions of magma with more distinctive mineralogy (e.g. plagioclase-amphibole phyric; quartz-plagioclase-biotite phyric; plagioclase phyric) and composition (e.g. Ruahine Rhyolite).

Andesitic magmas erupted during the same period of silicic volcanism, show a more consistent mineralogy and bulk composition compared with the silicic magmas. Early caldera-related andesites (Taurauikau Andesite) were typically of low-silica (60 wt.% $SiO_2$) andesite and this shifted to more silica-rich (62 wt.% $SiO_2$) andesites and low-silica (63-64 wt.% $SiO_2$) dacites with time.

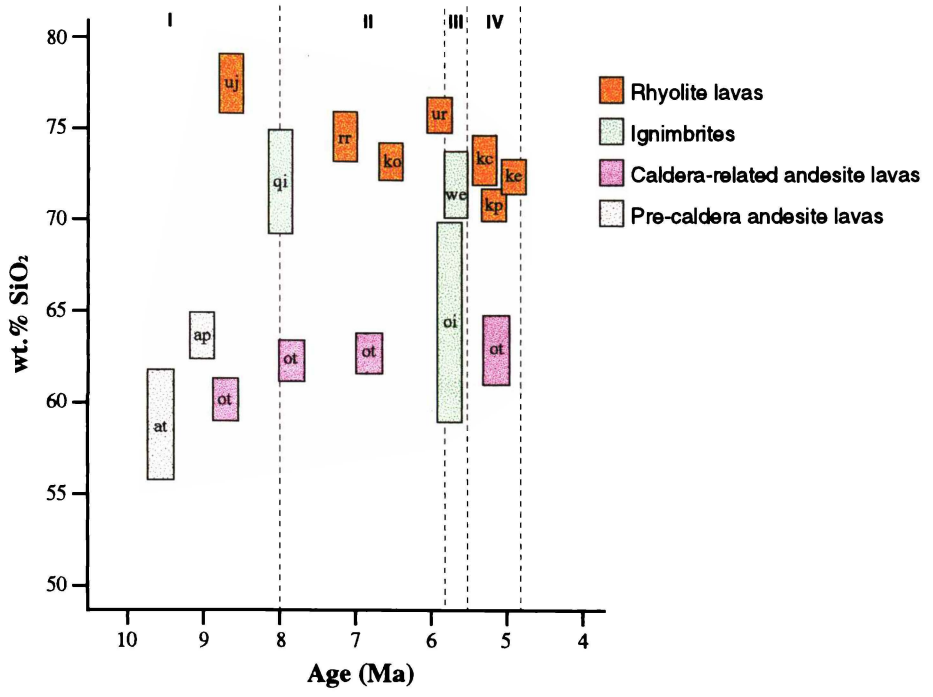


**Figure 9.4** Temporal variation of compositions erupted at the Kapowai Caldera Complex. Only units with a K/Ar age and XRF analysis are plotted. Although the ignimbrite $SiO_2$ abundances are affected by weathering, they are plotted for completeness.

## 9.4 Comparison with TVZ calderas

Eight Quaternary caldera volcanoes have been identified within the TVZ in North Island, New Zealand, two of which (i.e. Taupo, Okataina) are currently active (Wilson et al., 1995). Compared with these calderas, the KCC shows some similarities and differences in longevity, dimension, morphology and evolution.

It is important to note that ideas on the nature, structure and evolution of TVZ calderas have continuously evolved over the last 30 years of research (e.g. Wilson et al., 1984; Wilson et al., 1995). Modern radiometric dating (K/Ar and Ar/Ar) coupled with higher resolution geophysical surveys and geological mapping has advanced the understanding of these calderas (Bibby et al., 1995; Cole et al., 1995; Houghton et al., 1995). Individual TVZ calderas have unique features, but they can be grouped into apparently single collapse structures (e.g. Reporoa), and those where multiple, spatially-related collapse events have occurred (e.g. Mangakino, Taupo) (Cole et al., 1998).

A fundamental difference between TVZ calderas and the KCC, is that the intracaldera sequence is better exposed at the KCC, compared with any TVZ caldera. As mentioned previously, this is because of infilling by younger pyroclastic deposits or by the presence of freshwater lakes at TVZ calderas. The exocaldera record however, is better known for the TVZ calderas because of: (i) well exposed outflow ignimbrite stratigraphy (Bailey and Carr, 1994); (ii) numerous geothermal drillholes which have revealed the subsurface stratigraphy for several calderas (Browne, 1978; Grindley and Mumme, 1991); and (iii) a well documented onshore and offshore distal tephra record for TVZ silicic volcanism (Nelson et al., 1986; Froggatt and Lowe, 1990),

## Dimension and morphology

KCC covers a total area of ca. 110 $km^2$ in central CVZ. It is sub-circular in shape, with the major length (11 km) along a N-S trend and a minor length (10 km) orientated E-W. In comparison with most TVZ calderas, it is considerably smaller (Figure 9.5), although its dimensions are similar to the recently recognised Reporoa caldera (15 x 10 km) (Nairn et al., 1994).

The smaller size of the KCC compared with TVZ calderas in general, is also paralleled by differences in eruptive volumes. Although there are limited volumetric data for all KCC-derived ignimbrites, the minimum calculated volume (ca. 40 $km^3$) for the largest known KCC ignimbrite eruption (i.e. WES) is smaller compared with the largest magnitude (i.e. 100 to > 300 $km^3$) TVZ caldera-derived eruptions (Wilson et al., 1995).

As would be expected for individual volcanoes, there are differences in the morphology of the KCC and TVZ calderas. Most of the caldera complexes of the TVZ have an irregular form due to multiple eruptions from overlapping centres within the volcano and subsequent caldera wall modification, or in some instances (e.g. Kapenga) the morphology is also influenced by the regional fault pattern. KCC also has an irregular sub-circular form developed by multiple caldera collapse events within the caldera.

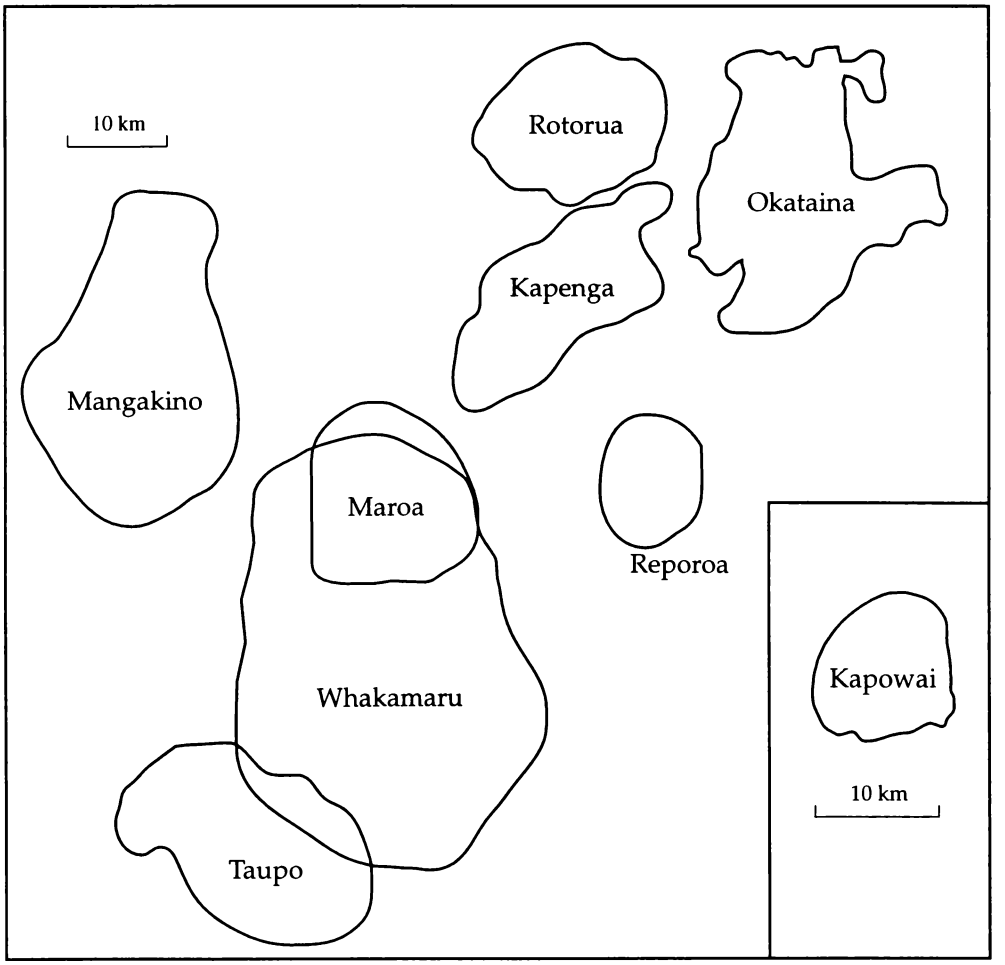


Figure 9.5 Comparison of the dimension and morphology of the Kapowai Caldera Complex with known calderas of the TVZ. Caldera boundaries for TVZ calderas adapted from Nairn et al. (1994).

## Longevity

Volcanic activity (andesitic and rhyolitic) at the KCC spans a period of at least 3.5 Ma based upon the oldest (i.e. Taurauikau Andesite; 8.5 Ma) and youngest (Kauaeranga Rhyolite; 4.9 Ma) K/Ar dated units. This is considerably longer than some extinct TVZ calderas (e.g. ca. 0.8 Ma for Mangakino Caldera Complex; Briggs et al., 1993), although the range is comparable with other caldera volcanoes in North America (Boden, 1986; Heiken et al., 1986), and is less than the period for many extinct rhyolitic volcanic fields (e.g. Steven and Lipman, 1976; Gibbons and Young, 1999).

The longer period of activity at the KCC compared with extinct TVZ calderas must relate to differences in the rate and longevity of magmagenesis between these continental margin subduction systems. Rates of magmagenesis at subduction settings are controlled primarily by the rate of subduction (Hochstein et al., 1995), but other factors which may influence it include: (i) the orientation (e.g. dip angle, angle of convergence) of the subducting plate; (ii) structural complexity of the continental crust; and (iii) the rate of crustal extension. The lifespan of magmagenesis is fundamentally influenced by the period of subduction, which is affected by the orientation and movement rates of constituent tectonic plates in the subduction system.

Differences in the longevity and magma production rates in the CVZ and TVZ subduction systems therefore relate to the character of the subduction settings. The TVZ currently has one of the world's highest heat flows for an extensional area (i.e. > 860 $Wm^2$; Stern, 1985) and rates of subduction are ca. 50 mm/year (Walcott, 1978). For the CVZ volcanic arc during the period ca. 9 - 4.9 Ma there are no constraints on the heat flow or rates or subduction, so no direct comparison can be made. However, based upon much less magma volumes erupted and a longer period of volcanic activity, the CVZ subduction zone system was significantly different to the present TVZ arc (Wilson, 1996).

## Evolution

A similar pre-caldera pattern is present for both TVZ calderas and the KCC. Pre-caldera intermediate volcanics outcrop to the west and north of the KCC, and andesitic-dacitic lava lithic fragments are observed in most intracaldera ignimbrites. Although there are only limited outcrops of older andesite volcanoes on the margins of TVZ calderas (e.g. Titiraupenga, Pureora), abundant andesite lava lithic fragments in TVZ caldera derived ignimbrites (Krippner et al., 1998; Cole et al., 1998) and andesite lava flows intersected by geothermal drillholes (Browne, et al. 1992) indicate that intermediate volcanics were widespread prior to silicic volcanism in central TVZ. This suggests a progressive change from intermediate-dominant to silicic-dominant volcanism in the CVZ arc system and within the central TVZ arc systems (Adams et al., 1994). Within the transition zone (i.e. Tauranga area) between these two volcanic provinces, a similar trend from early andesitic-dominant volcanism (3-4 Ma) to later silicic-dominant volcanism (2.5-2.0 Ma) also occurs (Briggs et al., 1996).

Caldera-related volcanic activity at the KCC is characterised by cyclic effusive and explosive volcanism of both andesitic and rhyolitic magmas. Similar cyclic effusive and explosive volcanism is common at several TVZ calderas (e.g. Okataina, Taupo), although major caldera-related andesitic eruptions are not known (Nairn, 1981; Sutton et al., 1995). Bi-modal magmatism has occurred within Okataina and Taupo calderas, but is bi-modal in terms of basaltic-rhyolitic compositions (Wilson et al., 1995).

Quiescence periods between major explosive eruptions are marked by several volcaniclastic lacustrine sequences at the KCC. The record of quiescence at TVZ calderas is poorly known because of the lack of intracaldera exposure, although drillholes have revealed lacustrine and fluvial sequences within several calderas. For example, a thick (up to 135 m) volcaniclastic lacustrine sequence infills the Mangakino Caldera Complex (Grindley and Mumme, 1991), and multiple sporadic fluvio-lacustrine sequences intercalated with primary volcanic deposits have been reported in drill-logs from the Okataina Caldera Complex (Nairn, 1989).

A fundamental feature of the KCC, and also of most other CVZ and TVZ calderas, is that post-eruption caldera resurgence has not occurred (cf. Nairn, 1981). This is generally similar compared to other circum-Pacific calderas, but contrasts with some North American calderas (e.g. most large San Juan Mountains calderas/caldera complexes; Valles Caldera; Yellowstone) and western South American calderas where resurgence has been recognised as a key structural element in their evolution (Smith and Bailey, 1968; Lipman, 1984).

Resurgent American calderas and CVZ/TVZ calderas are related to a common tectonic setting (i.e. subduction-related), although there is a major difference in crustal thickness and age. CVZ/TVZ calderas have developed in relatively thin (ca. 15-25 km thick) Mesozoic continental crust (Beanland and Haines, 1998), compared to resurgent American calderas where Precambrian-Paleozoic continental crust ranges in thicknesses from ca. 40-75 km (Zandt et al., 1995; Beck et al., 1996).

Although there are some exceptions, major caldera resurgence appears to be favoured in regions of thicker and much older continental crust (Lipman, 1984). This favours development of large magma chambers which evolve over longer time periods (Houghton et al., 1995) and leads to more significant structural upwelling or resurgence. As the crust is younger and thinner (due to higher extension rates - especially in the central TVZ), resurgence has not occurred in CVZ calderas and is not likely to occur in active TVZ calderas.

Following cessation of volcanic activity at the KCC, the major focus of Coromandel volcanism progressively migrated to the south, although activity also occurred on its northern margin (i.e. Whenuakite Volcanic Centre) and further to the north (i.e. Whitianga Volcanic Centre) (Skinner, 1995). Several younger (i.e. < 5 Ma) rhyolitic volcanic centres occurred south of the KCC at Wharekawa, Tunaiti (Briggs and

Fulton, 1990), near Waihi (Brathwaite and Christie, 1996) and at Tauranga (Briggs et al., 1996). Although the caldera structures and deposits are obscured, multiple distal tephras in offshore marine sequences (i.e. ODP Site 1124), during this period indicate that large magnitude rhyolitic eruptions occurred from these centres.

Migration of volcanism within the TVZ has also clearly occurred; silicic volcanism (ca. 1.6-0.6 Ma) initiated at Mangakino and later Kapenga calderas, but later activity (0.6 Ma-present) has shifted to the central TVZ (Houghton et al., 1995).

# Chapter Ten

# SUMMARY AND IMPLICATIONS

## 10.1 Introduction

This chapter presents a summary of the thesis and discusses the implications of the study.

## 10.2 Summary

1. The Kapowai Caldera Complex (KCC) was initially defined in the central Coromandel Volcanic Zone (CVZ) by remote sensing imagery which delineated the topographic boundary and intracaldera structures. This was further supported by a negative gravity anomaly (52 mgal), low amplitude magnetic anomalies, and the presence of lithofacies (e.g. thick infilling pyroclastics, numerous rhyolite lavas domes, and lacustrine sequences) attributable to caldera-forming eruptions. These features define the KCC as a subcircular caldera complex covering an area of ca. 110 $km^2$.

Intracaldera structures recognised in this study include: (i) structural boundaries observed for one collapse episode (i.e. Wharepapa Eruptive Sequence; WES), and inferred (based on remote sensing and geological analysis) for others; (ii) N and NW-trending faults, most of which are inferred by remote sensing, but supported by the location of rhyolite lava domes, andesite dikes or zones of hydrothermal alteration; and (iii) intrusive rhyolite and andesite dikes. Most of these intracaldera structural elements were developed in association with caldera collapse cycles, and few (e.g. Kapowai Fault) are influenced by the dominant NE-trending regional fault pattern.

2. KCC was a major andesitic-rhyolitic volcano, active during the late Neogene (ca. 8.5-4.9 Ma), following major andesitic-dacitic volcanism throughout the central CVZ. The intracaldera volcanic succession is dominated by moderate to large-scale rhyolitic and andesitic ignimbrites and rare tuffs, numerous rhyolitic lava domes, dome complexes and dikes, and andesite lavas and dikes. Intercalated with this sequence are minor volcaniclastic to carbonaceous lacustrine sequences, and landslide breccias.

Six intracaldera ignimbrites have been defined on the basis of composition, mineralogy, and component abundance and morphology. Most ignimbrites are of rhyolitic composition, although some (e.g. Oteao Ignimbrite) are of mixed andesitic-rhyolitic composition. Older ignimbrites (e.g. Trig Q Ignimbrite and Webb Creek Ignimbrite) form sporadic outcrops as they are commonly buried by the youngest and largest rhyolitic pyroclastic sequence (i.e. WES).

Rhyolitic lava domes have been subdivided on the basis of phenocryst mineralogy into four groups (group I: plagioclase-pyroxene phyric; group II: quartz-plagioclase-biotite phyric; group III: plagioclase phyric;

and group IV: plagioclase-amphibole phyric). There are no systematic temporal or spatial relationships between or within these rhyolite groups. Andesite lavas and dikes were erupted or emplaced in the western sector of the KCC, during three major periods: (i) following initial explosive silicic eruptions (i.e. at ca. 8.5 Ma); (ii) contemporaneous with rhyolitic effusive eruptions (7.6 - 6.4 Ma); and (iii) after eruption of the WES (< 5.8 Ma).

K/Ar dating of the intracaldera volcanic rocks implies a younger and longer period (ca. 3.6 Ma age span, i.e. from 8.5 to 4.9 Ma) of volcanic activity at the KCC, than previously thought (cf. Skinner, 1995). The oldest dated intracaldera volcanic unit (Taurauikau Andesite; 8.5 Ma) overlies a sequence of rhyolitic pyroclastic flow and fall deposits, and volcaniclastic lacustrine units, and therefore provides only a minimum age for the inception of volcanism at the KCC.

3. Lithic fragment populations in intracaldera KCC ignimbrites are highly variable and include volcanic lithologies (rhyolite, andesite, and dacite lavas, welded ignimbrite, breccias, and welded tuff), although sedimentary (lacustrine siltstone and sandstones) and rare plutonic (granodiorite) lithologies have been observed. The majority of lithic fragments are shallow upper crustal lithologies and are considered to be vent-derived. They therefore provide some additional stratigraphic constraints on the intracaldera succession, and also an indication of the composition of the volcanic pile and sub-volcanic crust at the KCC. Several volcanic lithic lithologies which do not outcrop provide evidence for older explosive and effusive eruptive events.

4. The intracaldera succession is dominated by a thick (up to 400 m) conformable sequence (Wharepapa Eruptive Sequence; WES) of pyroclastic flow and fall deposits, associated with a large scale rhyolitic explosive episode. Intracaldera WES deposits vary from proximal deposits of thick ignimbrite with interbedded lithic lag breccia (ML: 950 mm) and thick (up to 3.5 m) vitric and crystal tuffs, to medial deposits of thick ignimbrites which show some clast segregation, lack lithic lag breccias and contain thinner (< 0.5 m) interbedded crystal and vitric tuffs. Exocaldera deposits have been correlated to the north, east and south of the KCC in central CVZ, and consist mainly of ignimbrites, with occasional interbedded thin tuffs.

An estimated bulk minimum volume of ca. 43 $km^3$ for the WES has been calculated based upon the distribution and thickness of intracaldera ignimbrites and exocaldera correlatives in central CVZ. The true volume is considered to be at least twice this value, based upon the tentative correlation of distal WES tuffs in onshore and offshore marine sequences, and the deep post-depositional erosion which has occurred within and outside the caldera.

5. Volcanic rocks erupted are of the calc-alkaline magma series. The range of magma compositions is divided into a low-silica andesite to low-silica dacite group, and high-silica dacite to high-silica rhyolite

group. There are major and trace element compositional differences within these groups, which broadly parallel the mineralogical differences. Caldera-related andesitic to low-silica dacitic lavas differ from pre-caldera andesitic-dacitic lavas by having higher $SiO_2$, Ba, Ce and K/Rb values. Rhyolite lava groups overlap in their major and trace element chemistry, although group II (quartz-plagioclase-biotite phyric) lavas are distinguished by having the highest $SiO_2$, $K_2O$, and Rb/Sr values and the most distinctive REE abundances ($La_N/Yb_N$ = 6.87-15.03).

Magmatic processes have been identified based upon petrographic, mineralogical, and geochemical analysis. Crystal fractionation is probably a major process whereby these magmas have differentiated, and the presence of disequilibrium textures present in some lavas and ignimbrites (i.e. reverse zoning in plagioclase phenocrysts; disequilibrium pyroxene compositions; crustal xenoliths), imply that other magmatic processes (e.g. magma mixing, crustal assimilation, AFC) also occurred during the development of these magmas. Magma mixing and mingling is clearly apparent in the products of some KCC magmas (e.g. mixed andesitic-rhyolitic composition of Oteao Ignimbrite),

6. Two distinctive magma suites were erupted at the KCC; (i) andesite to low-silica dacite, and (ii) low to high-silica rhyolite. These two suites are unrelated by differentiation as they have significantly different trace element compositions, and also because a large compositional gap (i.e. moderate to high-silica dacite) occurs between them. The two suites probably represent two separate magma lineages which followed different petrogenetic pathways within the same continental margin-subduction zone setting.

For the intermediate suite, melts were generated by fluids or melts from the subducted slab that migrated into the overlying mantle wedge and ponded at the base of the continental crust. During ponding and subsequent migration through the crust they differentiated from primary basaltic magmas to intermediate compositions. Differentiation processes probably included crystal fractionation, crustal assimilation, AFC, and magma mixing and mingling.

The origin of the silicic magmas is more contentious. Parental magmas were probably generated by crustal melting (possibly of previous subduction-related lithologies) and then differentiated by processes including fractional crystallisation and assimilation in upper crustal levels. Crystal fractionation involved phenocryst phases (i.e. plagioclase, pyroxene, amphibole, biotite, titanomagnetite, ilmenite) although accessory phases (especially zircon) influenced some magmas.

7. Numerous geothermal systems were active during periods of volcanic activity at the KCC. These are indicated by several areas of hydrothermal alteration (propylitic and sericitic) and associated mineralisation present within the KCC, and by hydrothermally altered lithic fragments in intracaldera ignimbrites. Degrees of alteration, host rock lithology and mineralised zones vary within the KCC,

although there is a common control on the location of alteration zones by both caldera structures and regional NW-trending faults.

Central KCC areas (i.e. Rangihau Stream-Slip Stream area) of propylitic and sericitic alteration and mineralisation are controlled by an E-trending structural collapse boundary and a N-trending intracaldera fault (Starvation Fault). Propylitic alteration zones in the Kapowai valley are controlled by the intersection of intracaldera faults (Precipice Fault and Green Tree Fault) and NE-trending regional faults (Kapowai Fault). In the upper Kauaeranga valley, a small area of propylitic alteration also lies on the trend of the Kapowai Fault.

8. Intracaldera and exocaldera facies associations are recognised at the KCC using models for active caldera volcanoes. Intracaldera facies are dominated by thick widespread infilling pyroclastic and effusive (rhyolite and andesite) facies, with minor lacustrine, hydrothermal alteration, and mass wasting facies occurring in smaller areas. Facies vary in their geometry, distribution, thickness and composition but are all linked to active and passive processes associated with caldera volcanism. Most volcanic facies and all hydrothermal facies were deposited in a subaerial environment, although localised subaqueous environments (freshwater lakes and fluvial systems) are indicated by the presence of lacustrine facies and some reworked pyroclastics.

The exocaldera facies association consists of outflow pyroclastic flow and fall lithologies. These have been divided into caldera rim and distal subfacies. Both subfacies thin away from the KCC, and presently form a strongly dissected ignimbrite apron to the north, east and south of the caldera. However, the distribution of pyroclastics deposited within the caldera rim facies were less influenced by topographic highs and localised depocentres compared with the more distal facies. Also, caldera rim pyroclastics were deposited predominantly within subaerial environments, whereas both subaerial and subaqueous (fluvial or lacustrine) depositional environments are recognised for distal facies.

## 10.3 Implications

KCC is characterised by: (i) its relatively small dimensions (10 x 11 km); (ii) small magmatic volumes (< 30 $km^3$) erupted over a long time interval (ca. 3.6 Ma); and (iii) bi-modal andesite-rhyolite eruptions. These features have several implications for the nature of the CVZ subduction system during the late Miocene (ca. 8.5-4.9 Ma) in comparison with the present Hikurangi subduction system (TVZ arc) in the North Island (Table 10.1), and with models for caldera development based upon North American examples.

Table 10.1 Comparison of the nature of the subduction systems and calderas within the CVZ and onland TVZ. Data from Walcott (1978), Darby and Williams (1991); Briggs and Fulton (1990); Adams et al. (1994), Wilson et al. (1995), Beanland and Haines (1998) are used in the comparison.

| | Coromandel Volcanic Zone | Taupo Volcanic Zone |
|---|---|---|
| **Calderas** | | |
| 1. No. of identified silicic centres | 8 during 8 Ma period | 8 during 1.6 Ma period |
| 2. Age span of silicic calderas | 2 - 3.6 Ma | 0.8 Ma present max. |
| 3. Average caldera diameter | 6 - 8 km | 18 - 20 km |
| 4. Average magma volumes erupted | < 30 $km^3$ | 100 - 300 $km^3$ |
| 5. Compositions erupted | bi-modal andesite/rhyolite (basalts rare), with precursor andesites. In some centres (not KCC), voluminous late-stage andesitic plateau lavas | bi-modal basalt/rhyolite with precursor andesites, and andesites to NE and SW |
| 6. Epithermal mineralisation | fossil, deep level (200 - 500 m) Au-Ag deposits | active geothermal fields |
| **Subduction system** | | |
| 1. Age span | intermediate dominant: 18 Ma - 9 Ma<br>silicic dominant: 10 Ma - 2 Ma | intermediate dominant: 2.2 Ma - ca. 1.8 Ma<br>silicic dominant: 1.6 Ma - present |
| 2. Rate of subduction | ? < 50 mm/year | ~ 50 mm/yr |
| 3. Rate of crustal extension | ? 3 - 6 mm/yr | 7 - 18 mm/yr |
| 4. Crustal thickness | ~25 km | ~15 km |
| 5. Regional structural trends | NNE & NE-trending, 15 km wide extensional fault zones (e.g. KOST, WTFZ)<br>- smaller throws and heaves cf. TFB | NE-trending, 30 km wide Taupo Fault Belt (TFB)<br>- large throws and heaves on extensional faults |

***CVZ - TVZ comparison***

Relatively small caldera dimensions and small silicic eruptive volumes at the KCC compared with TVZ calderas (average ca. 18-20 km diameter; 100-300 $km^3$ volumes) implies that smaller volume silicic magma reservoirs occurred within the CVZ crust. Residence times for some TVZ calderas have been estimated, and include time scales of ca. $10^4$ to $10^5$ yrs (e.g. Taupo Caldera Complex, Houghton et al., 1995; Sutton et al., 1995; Whakamaru Caldera, Brown and Fletcher, 1999). No comparison in residence times can be made with KCC magmas as their residence times remain unknown because of the incomplete volcanic record, and limited age control for erupted units.

Bi-modal andesite-rhyolite magmagenesis at the KCC contrasts with most TVZ calderas where bi-modal basalt-rhyolite is common (Graham et al., 1995). Eruption of basaltic magmas suggests relatively rapid ascent from the lower crust via deep-seated faults, whereas differentiated andesitic magmas are likely to develop by slower ascent, greater crustal interaction, and storage within high-level reservoirs (Wilson, 1989). Therefore, this infers significant differences in the structural nature and thickness of crust between the two subduction systems.

Significantly CVZ and TVZ calderas share a similar relationship with regard to precious metal deposits. Epithermal Au-Ag deposits at CVZ caldera volcanoes are suggested from this study to be strongly influenced by intracaldera and, to a lesser extent, regional structures. Although no similar deposits have been discovered in the TVZ, the locations of active geothermal systems within the zone are also influenced by intracaldera and regional structures (Cole, 1990).

Apart from comparing caldera features, other fundamental differences are known for the CVZ and TVZ arc system. The crust in both arcs is of a similar age (i.e. Mesozoic), but thinner (ca. 15 km) in the TVZ compared with the CVZ (ca. 25 km) (Beanland and Haines, 1998). The main factor controlling this difference is likely to be the high crustal extension rates (ca. 7-18 mm/yr) in the TVZ (Darby and Williams, 1991). Although there are no direct data, it is likely based upon smaller dimensions of CVZ calderas (ca. 5-11 km diameter), smaller magmatic volumes erupted (< 30 $km^3$, KCC), and longer lifespans (3.6 Ma, KCC) compared with TVZ calderas, that extension rates in the CVZ were probably considerably lower during the late Miocene.

The Hikurangi subduction system which generates the TVZ continental arc presently consists of oblique subduction of the Pacific Plate beneath the Australian plate at rates of ca. 50 mm/yr (Walcott, 1978; Cole, 1990). For the CVZ subduction system there is no comparable data published, although the contrasting features of the KCC compared with TVZ calderas, and differences in crustal thickness and extension rates in these zones implies a significant difference in North Island subduction system configurations (e.g. subduction rates, dip of the subducting plate, subduction orientation) during the late Miocene (CVZ) compared with the Quaternary (TVZ).

*North American Caldera model*

Most current models which describe the structural and volcanic evolution of caldera volcanoes (i.e. caldera cycle) were developed based on North American calderas (e.g. Smith and Bailey, 1968; Steven and Lipman, 1976; Lipman, 1984). This was because North American calderas are typically well exposed and deeply eroded which allows detailed analysis of their evolution to be undertaken. Apart from the general caldera cycle, several fundamental concepts including the relationship between ignimbrites and caldera collapse, compositional zonation of silicic magma chambers, caldera resurgence, and relationships of porphyry/epithermal mineralisation to caldera structures were developed and refined based on these calderas (Steven and Ratte, 1965; Smith, 1979; Hildreth, 1981; Lipman, 1984).

Although the general caldera model has been widely accepted and applied outside of North America (e.g. Druitt and Sparks, 1984), there are fundamental differences between it and features observed at the KCC, as well as most other CVZ and TVZ calderas. Differences between the KCC and North American calderas include contrasting magma volumes, eruption rates, caldera dimensions, single vs. multiple magma chambers, and caldera resurgence (Table 10.2).

At the KCC, silicic magma batches erupted are typically much smaller (ca. < 30 $km^3$) compared with the majority of North American calderas (ca. 100-3000 $km^3$) (Lipman, 1984). This also leads directly to differences in caldera dimensions with the KCC having a smaller diameter (i.e. 11 km) compared with North American calderas (i.e. 12-40 km diameters) (Lipman, 1984).

Table 10.2 Comparison of the Kapowai Caldera Complex with North American calderas/caldera complexes. Data for comparison derived from Lipman (1984). * typical diameters.

| | **Kapowai Caldera Complex** | **North American Calderas** |
|---|---|---|
| Caldera diameter | 11 km | 12 - 40 km* |
| Eruptive volumes | < 30 $km^3$ | 100 - 3000 $km^3$ |
| Magma | bi-modal andesite-rhyolite | variable, but typically bi-modal basalt-rhyolite |
| Crustal thickness | 25 km | 40-75 km |
| Crustal age | Mesozoic | Precambrian-Paleozoic |
| Rates of extension | high (ca. 3-6 mm/yr) | low |
| Evolution | multiple, small scale (< 4 km diameter) caldera collapse episodes | multiple, large scale (>10 km) caldera collapse episodes |
| Mineralisation | structurally controlled epithermal mineralisation | structurally controlled porphyry/epithermal mineralisation |
| Resurgence | none | common |

Multiple magma chambers within CVZ and TVZ calderas have been recognised (e.g. Briggs et al., 1993; McGunnigle, 1995) and this is also found at the KCC (e.g. Oteao Ignimbrite). Although multiple magma chambers have also been recognised for some North American calderas, it is more common for North American calderas to be associated with compositionally zoned magma chambers (Hildreth, 1979).

As well as these general volume differences, there is also a contrast in the total volume of material erupted during a caldera cycle. At North American calderas, only a small proportion of the total magma chamber volume is inferred to be erupted, with the remainder cooling and crystallising to form a high-level plutonic body (e.g. Fiske and Tobisch, 1994). In comparison, at the KCC and TVZ/CVZ calderas, the bulk of the magma chamber is evacuated mainly during explosive phases of an eruptive cycle, and the remainder by numerous pre- or post-collapse effusive silicic lava domes (Nairn, 1989; Wilson et al., 1995). Evidence for this is that the suceeding magma batch has a different composition and is derived from a discrete source (Sutton et al., 1995; Briggs et al., 1998).

Associated with this feature is the significant lack of major intrusive bodies (batholith, ring-dikes) present at the KCC, compared with North American calderas. At the KCC, intrusive structures exposed include lava (andesite/rhyolite) dikes, but no hypabyssal or plutonic intrusives outcrop, and no buried plutonic bodies can be implied because there is no significant volume of plutonic or hypabyssal lithic fragments. In contrast, caldera cycles at North American calderas typically incorporate late-stage crystallisation of voluminous batholiths and ring-dike systems (Lipman, 1975; Elston, 1984; Lipman, 1984), and lithic populations of some ignimbrites contain significant proportions of plutonic and hypabyssal lithologies (e.g. Hildreth and Mahood, 1986).

As discussed in Chapter 9, a further fundamental difference between the KCC, together with other CVZ/TVZ calderas, and North American calderas (e.g. most large San Juan Mountains calderas/caldera complexes; Valles Caldera; Yellowstone Caldera) is that caldera resurgence has not occurred at New Zealand calderas. Resurgence is considered to be a fundamental structural element in the evolution of most North American calderas (Smith and Bailey, 1968; Lipman, 1984).

The contrasts between caldera features mentioned above most likely relate to fundamental differences in crustal thickness and age, and extension rates between North American and New Zealand caldera settings. Although the general model for caldera evolution based on North American examples is valid and has been used as a basis for the interpretation of CVZ and TVZ calderas, it is important to realise and appreciate the fundamental differences between the two regions.

## 10.3 Future studies

To advance the understanding of the KCC, future studies should focus on several key areas.

(1) Higher resolution geophysical surveying, focusing on the KCC (cf. Malengreau et al., 1997 -who focused on high resolution gravity surveys across regional CVZ), especially including gravity surveying, is needed to define the boundaries of collapse zones that have been inferred in this study by remote sensing or geological mapping These may also improve the delineation of the topographic boundary (especially in

the western and northern margins) and constrain the geophysical character of the subvolcanic crust and volcanic pile.

(2) Additional radiometric dating (preferably using K/Ar) of volcanic units not dated in this work is required to further refine the intracaldera volcanic stratigraphy. Radiometric dating and geochemical analysis of late Neogene distal tephras recently discovered during the ODP Leg 181 will provide a more reliable record of the widespread silicic KCC eruptives. K/Ar dating of correlated exocaldera WES units is also required to constrain regional central CVZ stratigraphy. Detailed palynological and biostratigraphic dating of the intracaldera lacustrine sequences is required, since three stratigraphically distinct units are now recognised (cf. Skinner, 1995), but only one of these has a biostratigraphic age.

(3) The petrogenesis of KCC volcanic rocks is poorly constrained by limited major and trace element, REE and Sr, Nd, and Pb isotopic data for volcanic rocks and potential crustal contaminants (e.g. Mesozoic greywacke). There are obvious difficulties in resolving this because of deep weathering profiles, sporadic hydrothermal alteration, and variable temporal relationships. However, isotopic data focusing on the andesite and rhyolite lavas, augmented by further major and trace element analyses, will better constrain the petrogenesis of KCC magmas and allow further comparison with other central CVZ centres (e.g. Whitianga Volcanic Centre; Briggs et al., 1998) and the active TVZ.

# References

Abrahamson, L. 1987. Aspects of late Quaternary stratigraphy and evolution of some coastal embayments on the east Coromandel Peninsula. Unpublished MSc thesis, University of Waikato.

Adams, C.J. Graham, I.J. Seward, D. and Skinner, D.N.B. 1994. Geochronological and geochemical evolution of Late Cenozoic volcanism in the Coromandel Peninsula, New Zealand. New Zealand Journal of Geology and Geophysics 37: 359-379.

Adams, J.C. 1992. A facies approach to the geology of the Hot Water Beach-Whenuakite region, Coromandel Volcanic Zone. Unpublished MSc thesis, University of Waikato.

Aldrich, S.M. 1995. Volcanic geology and hydrothermal alteration of the Onemana Area, Eastern Coromandel Peninsula. Unpublished MSc thesis, University of Waikato.

Allegre, C.J. and Minster, J.-F. 1978. Quantitative models of trace element behaviour in magmatic processes. Earth and Planetary Science Letters 38: 1-25.

Aramaki, S. 1984. Formation of the Aira Caldera, Southern Kyushu, 22, 000 years ago. Journal of Geophysical Research 89: 8485-8501.

Arculus, R.J. 1994. Aspects of magma genesis in arcs. Lithos 33: 189-208.

Arribas, A., Cunningham, C.G., Rytuba, J.J., Rye, R.O., Kelly, W.C., Podwysocki, M.H., McKee, E.H. and Tosdal, R.M. 1995. Geology, geochronology, fluid inclusions, and isotope geochemistry of the Rodalquilar gold alunite deposit, Spain. Economic Geology 90: 795-822.

Arth, J.G. 1980. Rare earth element geochemistry of the island-arc volcanic rocks of Rabaul and Talasea, New Britain. Geological Society of America Bulletin 92: 858-863.

Backshall, D.T. 1982. A microearthquake study of the Hauraki Rift. Unpublished MSc thesis, University of Auckland.

Bacon, C.R. and Hirschman, M.M. 1988. Mg/Mn partitioning as a test for equilibrium between co-existing Fe-Ti oxides. American Mineralogist 73: 57-61.

Bailey, R.A. and Carr, R.G. 1994. Physical geology and eruptive history of the Matahina Ignimbrite, Taupo Volcanic Zone, North Island, New Zealand. New Zealand Journal of Geology and Geophysics 37: 319-344.

Ballance, P.F. 1976. Evolution of the upper Cenozoic magmatic arc and plate boundary in northern New Zealand. Earth and Planetary Science Letters 28: 356-370.

Ballance, P.F. 1988. Late Cenozoic time-lines and calc-alkaline volcanic arcs in northern New Zealand - further discussion. Journal of the Royal Society of New Zealand 18: 347-358.

Bardebes, P.A. 1997. Volcanic geology of the rhyolitic rocks of the Cooks Beach - Whitianga Harbour Region, Coromandel Volcanic Zone. Unpublished MSc thesis, University of Waikato.

Bassett, P.B. 1998. Influence of weathering and hydrothermal alteration on engineering characteristics of eastern Coromandel rocks. Unpublished MSc thesis, University of Waikato.

Beanland, S. and Haines, J. 1998. The kinematics of active deformation in the North Island, New Zealand, determined from geological strain rates. New Zealand Journal of Geology and Geophysics 41: 311-323.

Beck, S.L., Zandt, G., Myers, S.C., Wallace, T.C., Silver, P.G. and Drake, L. 1996. Crustal-thickness variations in the central Andes. Geology 24: 407-410.

Bell, J.M. and Fraser, C. 1912. The geology of the Waihi-Tairua Subdivision, Hauraki Division. New Zealand Geological Survey Bulletin No. 15, 192p.

Belliss S.E. and Christie, A.B. 1994. Processing of Japan Earth Resources-1 Synthetic Aperture Radar data to aid geological mapping in the central Coromandel Peninsula. Proceedings of the 28th Annual Conference, New Zealand Branch, Australasian Institute of Mining and Metallurgy, p 33-49.

Beresford, S.W. 1997. Volcanology and geochemistry of the Kaiangaroa Ignimbrites. Unpublished PhD thesis, University of Canterbury.

Bibby, H.M., Caldwell, T.G., Davey, F.J. and Webb, T.H. 1995. Geophysical evidence on the structure of the Taupo Volcanic Zone and its hydrothermal circulation. Journal of Volcanology and Geothermal Research 68: 29-58.

Black, P.M., Briggs, R.M., Itaya, T., Dewes, E.R., Dunbar, H.M., Kawasaki, K., Kuschel, E., Smith, I.E.M. 1992. K-Ar age data and geochemistry of the Kiwitahi Volcanics, western Hauraki Rift, North Island, New Zealand. New Zealand Journal of Geology and Geophysics 35: 403-413.

Black, P.M., Doi, M., Itaya, T. and Smith, I.E.M. 1995. The Northland volcanic arc: age range and variation in magma type with time. Geological Society of new Zealand Miscellaneous Publication 81A, p 82.

Blake, S., Wilson, C.J.N., Smith, I.E.M. and Walker, G.P.L. 1992. Petrology and dynamics of the Waimihia mixed magma eruption, Taupo Volcano, New Zealand. Journal of the Geological Society, London 149: 193-207.

Blattner, P. 1996. Temperature and isotopic evolution of silicic magmas, Taupo Volcanic Zone and Coromandel Volcanic Zone, New Zealand. New Zealand Journal of Geology and Geophysics 39: 353-362.

Boden, D.R. 1986. Eruptive history and structural development of the Toquima caldera complex, central Nevada. Geological Society of America Bulletin 97: 61-74.

Boden, D.R. 1989. Evidence for step-function zoning of magma and eruptive dynamics, Toquima Caldera Complex. Journal of Volcanology and Geothermal Research 37: 39-57.

Bougault, H., Joron, J.L. and Treuil, M. 1980. The primordial chondritic nature and large scale heterogeneities in the mantle: evidence from high and low partition coefficient elements in oceanic basalts. Philosophical Transactions of the Royal Society of London. A 297: 203-213.

Branney, M.J. 1995. Downsag and extension at calderas: new perspectives on collapse geometries from ice-melt, mining, and volcanic subsidence. Bulletin Volcanology 57: 303-318.

Branney, M.J. and Kokelaar, P. 1992. A reappraisal of ignimbrite emplacement: progressive aggradation and changes from particulate to non-particulate flow during emplacement of high-grade ignimbrite. Bulletin of Volcanology. 54: 504-520.

Brathwaite, R.L., Christie, A.B. and Skinner, D.N.B. 1989. The Hauraki goldfield - regional setting, mineralisation and recent exploration, In Kear, D. (ed) Mineral deposits of New Zealand: Australasian Institute of Mining and Metallurgy Monograph 13, p 45-56.

Brathwaite, R.L. and Christie, A. B. 1996. Geology of the Waihi area. scale 1:50000. Institute of Geological and Nuclear Sciences, Lower Hutt, geological map 21.

Briggs, N.D. 1976. Welding and crystallisation zonation in Whakamaru Ignimbrite, central North Island, New Zealand. New Zealand Journal of Geology and Geophysics 19: 189-212.

Briggs, R.M. and Fulton, B.W.J. 1990. Volcanism, structure and petrology of the Whiritoa-Whangamata coastal section, Coromandel Volcanic Zone, New Zealand: facies model evidence for the Tunaiti Caldera. New Zealand Journal of Geology and Geophysics 33: 623-633.

Briggs, R.M., Gifford, M.G., Moyle, A.R., Taylor, S.R., Norman, M.D., Houghton, B.F. and Wilson, C.J.N. 1993. Geochemical zoning and eruptive mixing in ignimbrites from Mangakino volcano, Taupo Volcanic Zone, New Zealand. Journal of Volcanology and Geothermal Research 56: 175-203.

Briggs, R.M., Hall, G.J., Harmsworth, G.R., Hollis, A.G., Houghton, B.F., Hughes, G.R., Morgan, M.D., and Whitbread-Edwards, A.R. 1996. Geology of the Tauranga Area, Occasional Report No. 22, Department of Earth Sciences, University of Waikato, New Zealand.

Briggs, R.M., Rogers, J., Adams, J.C., Bardebes, P.A., Price, R.C. and Maas, R. 1998. Rhyolitic volcanics of the Whitianga Volcanic Centre, a late Miocene caldera complex, eastern Coromandel. Geological Society of New Zealand Miscellaneous Publication 101A.

Bromley, C.J. and Brathwaite, R.L. 1991. Waihi Basin structure in light of recent geophysical surveys. Proceedings of the 25th Annual Conference 1991, New Zealand Branch of the Australasian Institute of Mining and Metallurgy, p 225-238.

Brothers, R.N. 1984. Subduction regression and oceanward migration of volcanism, North Island, New Zealand. Nature 309: 698-700.

Brothers, R.N. 1986. Upper Tertiary and Quaternary volcanism and subduction zone regression, North Island, New Zealand. Journal of the Royal Society of New Zealand 16: 275-298.

Brown, S.J.A., Burt, R.M., Cole, J.W., Krippner, S.J.P., Price, R.C. and Cartwright, I. 1998a. Plutonic lithics in ignimbrites of Taupo Volcanic Zone, New Zealand; sources and conditions of crystallisation. Chemical Geology 148: 21-41.

Brown, S.J.A., Wilson C.J.N., Cole J.W. and Wooden J. 1998b. The Whakamaru group ignimbrites, Taupo Volcanic Zone, New Zealand - evidence for reverse tapping of a zoned silicic magmatic system. Journal of Volcanology and Geothermal Research 84:1-37.

Brown, S.J.A. and Fletcher, I.R. 1999. SHRIMP U-Pb dating of the pre-eruption growth history of zircons from the 340 ka Whakamaru Ignimbrite, New Zealand; evidence for >250 k.y. magma residence times. Geology 27: 1035-1038.

Browne, P.R.L. 1978. Petrological logs of drillholes, Kawerau geothermal field. New Zealand Geological Survey Report 84: 1-57.

Browne, P.R.L., Graham, I.J., Parker, R.J. and Wood, C.P. 1992. Subsurface andesite lavas and plutonic rocks in the Rotokawa and Ngatamariki geothermal systems, Taupo Volcanic Zone, New Zealand. Journal of Volcanology and Geothermal Research 51: 199-215.

Bryan, S.E., Cas, R.A.F. and Marti, J. 1998. Lithic breccias in intermediate volume phonolitic ignimbrites, Tenerife (Canary Islands): constraints on pyroclastic flow depositional processes. Journal of Volcanology and Geothermal Research 81: 269-296.

Buesch, D.C. 1992. Incorporation and redistribution of locally derived lithic fragments within a pyroclastic flow. Geological Society of America Bulletin 104: 1193-1207.

Buddington, A.F. and Lindsley, D.H. 1964. Iron-titanium oxide minerals and synthetic equivalents. Journal of Petrology 5: 310-357.

Burns, B. 1984. Kapowai ecological area. Auckland Conservancy dedicated areas report No. 3. New Zealand Forest Service, Auckland, 22p.

Burns, B. 1985. Te Tipi ecological area. Auckland Conservancy dedicated areas report No. 6. New Zealand Forest Service, Auckland, 27p.

Campos-Enriquez, J.O. and Garduno-Monroy, V.H. 1995. Los Azufres silicic center (Mexico): inference of caldera structural elements from gravity, aeromagnetic, and geoelectric data. Journal of Volcanology and Geothermal Research 67: 123-152.

Carmichael, I.S.E. 1967. The iron-titanium oxides of salic volcanic rocks and their associated ferromagnesian silicates. Contributions to Mineralogy and Petrology 14: 36-64.

Carr, R.G. 1984. The Matahina Ignimbrite: its evolution including its eruption and post-depositional changes. Unpublished PhD thesis, University of Auckland.

Cas, R.A.F and Wright, J.V. 1987. Volcanic successions, modern and ancient: a geological approach to processes, products, and successions. Allen and Unwin, London, 528p.

Chesner, C.A. and Rose, W.I. 1991. Stratigraphy of the Toba tuffs and the evolution of the Toba caldera complex, Sumatra, Indonesia. Bulletin of Volcanology 53: 343-356.

Christiansen, R.L. 1984. Quaternary and Pliocene volcanism of the Yellowstone Rhyolite Plateau region of Wyoming, Idaho and Montana. United States Geological Survey Professional Paper 729.

Christie, A.B. and Brathwaite, R.L. 1986. Epithermal gold-silver and porphyry copper deposits of the Hauraki Goldfield - a review. In: Henley, R.W., Hedenquist, J.W. and Roberts, P.J.(eds), Guide to the active epithermal(geothermal) systems and precious metal deposits of New Zealand. Monograph series on mineral deposits 26: 129-145, Gebruder Borntraeger, Berlin-Stuttgart.

Christie A.B. Belliss, S.E. and Brathwaite, R.L. 1994. Use of remote sensing data to aid geological mapping of the Waihi 1:50000 scale map sheet, Coromandel region. Proceedings of the 28th Annual Conference, New Zealand Branch, Australasian Institute of Mining and Metallurgy, p 51-65.

Clarke, D.S., Sporli, K.B., Smith, I.E.M., Locke, C.A., Kobe, H.W., Black, P.M. and Ballance, P.F. 1990. The geological setting of gold deposits in the Coromandel Volcanic Zone. Proceedings from the 1990 PACRIM Conference, Auckland.

Clynne, M.A. 1999. A complex magma mixing origin for rocks erupted in 1915, Lassen Peak, California. Journal of Petrology 40: 105-132.

Cochrane, G.R. and Wan, T.F. 1983. Interpretation of structural characteristics of the Taupo Volcanic Zone, New Zealand, from Landsat Imagery. International Journal of Remote Sensing 4: 111-128.

Cole, J.W. 1978. Distribution, petrography and chemistry of Kiwitahi and Maungatautari Volcanics, North Island, New Zealand. New Zealand Journal of Geology and Geophysics 21: 143-154.

Cole, J.W. 1979. Structure, petrology and genesis of Cenozoic volcanism, Taupo Volcanic Zone, New Zealand - a review. New Zealand Journal of Geology and Geophysics 22: 631-657.

Cole, J.W. 1986. Distribution and tectonic setting of late Cenozoic volcanism in New Zealand. In: Smith, I.E.M. (ed), Late Cenozoic volcanism in New Zealand. The Royal Society of New Zealand Bulletin 23: 7-20.

Cole, J.W. 1990. Structural control and origin of volcanism in the Taupo Volcanic Zone, New Zealand. Bulletin of Volcanology 52: 445-459.

Cole, J.W. and Lewis, K.B. 1981. Evolution of the Taupo-Hikurangi subduction system. Tectonophysics 72: 1-21.

Cole, J.W., Graham, I.J., Hackett, W.R. and Houghton, B.F. 1986. Volcanology and petrology of the Quaternary composite volcanoes of Tongariro Volcanic Centre, Taupo Volcanic Zone. In: Smith, I.E.M. (ed), Late Cenozoic volcanism in New Zealand. The Royal Society of New Zealand Bulletin 23: 224-250.

Cole, J.W., Darby, D.J. and Stern, T.A. 1995. Taupo Volcanic Zone and Central Volcanic Region-backarc structures of North Island, New Zealand. In: Taylor, B. (ed), Backarc basins: tectonics and magmatism. Plenum Press, New York, 425p.

Cole, J.W., Brown, S.J.A., Burt, R.M., Beresford, S.W. and Wilson, C.J.N. 1998. Lithic types in ignimbrites as a guide to the evolution of a caldera complex, Taupo Volcanic Centre, New Zealand. Journal of Volcanology and Geothermal Research 80: 217-237.

Colucci, M.T., Dungan, M.A. and Ferguson, K.M. 1991. Precaldera lavas of the southeastern San Juan Volcanic field: parent magmas and crustal interactions. Journal of Geophysical Research 96: 13413-13434.

Couper, P.G. 1982. Final report on the Kapowai Prospect, Coromandel Peninsula, New Zealand PL 31-458. Amoco Minerals N.Z. Ltd open file company report, No. 123.

Darby, D.J. and Williams, R.O. 1991. A new geodetic estimate of deformation in the Central Volcanic Region of the North Island, New Zealand. New Zealand Journal of Geology and Geophysics 34: 127-136.

Davy, B.W. and Caldwell, T.G. 1998. Gravity, magnetic and seismic surveys of the caldera complex, Lake Taupo, North Island, New Zealand. Journal of Volcanology and Geothermal Research 81: 69-89.

DePaolo, D.J. 1980. Trace element and isotopic effects of combined wallrock assimilation and fractional crystallisation. Earth and Planetary Science Letters 53: 189-202.

de Ronde, C.E.J. 1986. The Golden Cross gold-silver deposit. In: Henley, R.W., Hedenquist, J.W. and Roberts, P.J. (eds), Guide to the active epithermal(geothermal) systems and precious metal deposits of New Zealand. Monograph series on mineral deposits 26: 165-183, Gebruder Borntraeger, Berlin-Stuttgart.

Downey, J.F. 1935. Goldmines of the Hauraki District, New Zealand. Government Printer, Wellington, 305p.

Druitt, T.H. 1985. Vent evolution and lag breccia formation during the Cape Riva eruption of Santorini, Greece. Journal of Geology 93: 439-454.

Druitt, T.H. and Sparks, R.S.J. 1984. On the formation of calderas during ignimbrite eruptions. Nature 310: 679-681.

Druitt, T.H. and Bacon, C.R. 1986. Lithic breccia and ignimbrite erupted during the collapse of Crater Lake Caldera, Oregon. Journal of Volcanology and Geothermal Research 29: 1-32.

Duffield, W.A. and Ruiz, J. 1992. Compositional gradients in large reservoirs of silicic magma as evidenced by ignimbrites versus Taylor Creek rhyolite. Contributions to Mineralogy and Petrology 110: 192-210.

Earth Scientists Ltd, 1973. Gumtown prospects, Kapowai, Coromandel Peninsula. Prepared for JBL Exploration (NZ) Ltd, Open file report 313, Ministry of Commerce.

Eaton, P.C. and Setterfield, T.N. 1993. The relationship between epithermal and porphyry hydrothermal systems within the Tavua caldera, Fiji. Economic Geology 88: 1053-1083

Eichelberger, J.C. and Koch, F.G. 1979. Lithic fragments in the Bandelier Tuff, Jemez Mountains, New Mexico. Journal of Volcanology and Geothermal Research 5: 115-134.

Elston, W.E. 1984. Mid-Tertiary ash-flow tuff cauldrons, southwestern New Mexico. Journal of Geophysical Research 89: 8733-8750.

Elston, W.E. 1994. Siliceous volcanic centers as guides to mineral exploration: review and summary. Economic Geology 89: 1662-1686.

Fenaughty, K.F. 1986. Sheet 282, Coromandel. Gravity anomaly map, Coastal series, 1:250 000, Department of Scientific and Industrial Research, Wellington.

Fink, J. H. 1983. Structure and emplacement of a rhyolitic obsidian flow: Little Glass Mountain, Medicine Lake Highland, northern California. Geological Society of America Bulletin 94: 362-380.

Fink, J.H. and Manley, C.R. 1987. Origin of pumiceous and glassy textures in rhyolite domes and flows. In: Fink, J. (ed), The emplacement of silicic domes and lava flows. Geological Society of America Special Paper 212: 77-88.

Fisher, G.D. 1986. Geological aspects of an area near Whitianga, Coromandel Peninsula. Unpublished MSc thesis, University of Auckland.

Fisher, R.V. 1961. Proposed classification of volcano-clastic sediments and rocks. Geological Society of America Bulletin 72: 1409-1414.

Fisher, R.V. 1966. Rocks composed of volcanic fragments and their classification. Earth Science Reviews 1: 287-298.

Fisher, R.V. and Schmincke, H.-U. 1984. Pyroclastic Rocks. Springer-Verlag, Berlin, 472p.

Fiske, R.S. and Tobisch, O.T. 1994. Middle Cretaceous ash-flow tuff and caldera deposit in the Minarets Caldera, east-central Sierra Nevada, California. Geological Society of America Bulletin 106: 582-593.

Fraser, C. 1910. The geology of the Thames Subdivision, Hauraki, Auckland. New Zealand Geological Survey Bulletin No. 10, 136p.

Freeport of Australia Ltd, 1973. Report on reconnaissance of Kapowai area. Open file report 309, Ministry of Commerce, New Zealand.

Fritz, W.J., Howells, M.F., Reedman, A.J. and Campbell, S.D.G. 1990. Volcaniclastic sedimentation in and around an Ordovician subaqueous caldera, lower Rhyolitic Tuff Formation, north Wales. Geological Society of America Bulletin 102: 1246-1256.

Froggatt, P.C. 1983. Toward a comprehensive upper Quaternary tephra and ignimbrite stratigraphy in New Zealand using electron microprobe analysis of glass shards. Quaternary Research 19: 188-200.

Froggatt, P.C. and Gosson, G.J. 1982. Techniques for the preparation of tephra samples for mineral and chemical analysis and radiometric dating. Victoria University of Wellington, Wellington, 12p.

Froggatt, P.C. and Lowe, D.J. 1990. A review of late Quaternary silicic and some other tephra formations from New Zealand: their stratigraphy, nomenclature, distribution, volume and age. New Zealand Journal of Geology and Geophysics 33: 89-109.

Fulton, B.W.J. 1988. The volcanic geology of the Whiritoa-Whangamata area. Unpublished MSc thesis, University of Waikato.

Gadsby, M.R., Sporli, K.B. and Clarke, D.S. 1990. Structural elements in epithermal gold deposits of the Coromandel Peninsula, New Zealand. Annual Conference 1990, Australasian Institute of Mining and Metallurgy, p 145-151.

Gibbons, W. and Young, T.P. 1999. Mid-Caradoc magmatism in central Llyn, rhyolite petrogenesis, and the evolution of the Snowdonia volcanic corridor in NW Wales. Journal of the Geological Society, London 156: 301-316.

Gill, J.B. 1981. Orogenic andesites and plate tectonics. Springer-Verlag, Berlin, 358p.

Goff, F. and Gardner, J.N. 1994. Evolution of a mineralised geothermal system, Valles caldera, New Mexico. Economic Geology 89: 1803-1832.

Gosson, G.J. 1986. Miocene and Pliocene silicic tuffs in marine sediments of the East Coast Basin, New Zealand. Unpublished PhD thesis, Victoria University of Wellington.

Graham, I.J. and Hackett, W.R. 1987. Petrology of calc-alkaline lavas from Ruapehu volcano and related vents. Journal of Petrology 28: 531-567.

Graham, I.J. Gulson, B.L., Hedenquist, J.W. and Mizon, K. 1992. Petrogenesis of late Cenozoic volcanic rocks from the Taupo Volcanic Zone, New Zealand, in light of new lead isotope data. Geochimica et Cosmochimica Acta 56: 2797-2819.

Graham, I.J., Cole, J.W., Briggs, R.M., Gamble, J.A. and Smith, I.E.M. 1995. Petrology and petrogenesis of volcanic rocks from the Taupo Volcanic Zone: a review. Journal of Volcanology and Geothermal Research 68: 59-87.

Grindley, G.W. and Mumme, T.C. 1991. Magnetic stratigraphy and correlation of ignimbrite eruptions of the Mangakino basin and Tokoroa plateau. New Zealand Geological Survey Record 43: 25-36.

Guay, C.M.Y. 1999. Volcanic geology and geochemistry of the Coroglen-Whenuakite area, eastern Coromandel Peninsula, New Zealand. Unpublished MSc thesis, University of Waikato.

Hanson, G.N. 1980. Rare earth elements in petrogenetic studies of igneous systems. Annual Reviews of Earth and Planetary Sciences 8: 371-406.

Harvey, P.K., Taylor, D.M., Hendry, R.D. and Bancroft, F. 1973. An accurate fusion method for the analysis of rocks and chemically related materials by X-ray fluorescence spectrometry. X ray Spectrometry 2: 33-44.

Hawkesworth, C.J., Hergt, J. M., Ellam, R.M., and McDermott, F. 1991. Element fluxes associated with subduction related magmatism. Philosophical Transactions of the Royal Society of London. Series A 335: 393-405.

Haworth, A.V. 1993. Volcanic geology and hydrothermal alteration of the lower Waitekauri Valley, Waihi, New Zealand. Unpublished MSc(Tech) thesis, University of Waikato.

Hawthorn, B.M. 1996. Volcanic geology of the Opito Bay region, northern Coromandel Peninsula. Unpublished MSc thesis, University of Waikato.

Hayba, D.O., Bethke, P.M., Heald, P. and Foley, N.K. 1985. Geologic, mineralogic, and geochemical characteristics of volcanic-hosted epithermal precious-metal deposits. In: Berger, B.R. and Bethke, P.M. (eds) Reviews in Economic Geology Vol. 2, p 129-167.

Hayward, B.W. 1971. The geology and eruptive history of the Table Mountain region, Coromandel Peninsula. Unpublished BSc(Hons) project, University of Auckland.

Hayward, B.W. 1973. Upper Tertiary freshwater mussel fossils from the Coromandel volcanic sequence. Journal of the Royal Society of New Zealand 3: 61-69.

Hayward, B.W. 1974a. Whitianga Group sediments of the Table Mountain area, Coromandel Peninsula. Journal of the Royal Society of New Zealand 4: 161-176.

Hayward, B.W. 1974b. Geology and eruptive history of Table Mountain area, Coromandel Peninsula. New Zealand Journal of Geology and Geophysics 17: 403-422.

Hayward, B.W. 1978. Kauaeranga Kauri - a pictorial history of the Kauri timber industry in the Kauaeranga Valley, Thames. Lodestar Press, Auckland, 48p.

Hayward, B.W. 1979. Eruptive history of the early to mid-Miocene Waitakere Volcanic Arc, and paleogeography of the Waitemata Basin, northern New Zealand. Journal of the Royal Society of New Zealand 9: 297-320.

Hayward, B.W. 1993. The tempestuous 10 Million year life of a double arc and intra-arc basin - New Zealand's Northland basin in the early Miocene. In: Ballance, P.F. (ed), South Pacific Sedimentary Basins. Sedimentary Basins of the World, 2. Elsevier, Amsterdam, p 113-142.

Heald, P., Foley, N.K., Hayba, D.O. 1987. Comparative anatomy of volcanic-hosted epithermal deposits: acid-sulphate and adularia-sericite types. Economic Geology 82: 1-26

Hedenquist, J.W. 1986. Geothermal systems in the Taupo Volcanic Zone: their characteristics and relation to volcanism and mineralisation. In: Smith, I.E.M.(ed), Late Cenozoic volcanism in New Zealand. The Royal Society of New Zealand Bulletin 23, p 134-168.

Heiken, G. and McCoy, F. 1984. Caldera development during the Minoan eruption, Thira, Cyclades, Greece. Journal of Geophysical Research 89: 8441-8462.

Heiken, G., Goff, F., Stix, J., Tamanyu, S. Shafiqullah, M., Garcia, S. and Hagan, R. 1986. Intracaldera volcanic activity, Toledo Caldera and embayment, Jemez Mountains, New Mexico. Journal of Geophysical Research. 91: 1799-1815.

Heinrich, C.A., Henley, R.W. and Seward, T.M. 1989. Hydrothermal systems. Australian Mineral Foundation, Adelaide, 74p.

Henley, R.W. 1985. The geothermal framework of epithermal deposits. In: Berger, B.R. and Bethke, P.M.(eds), Reviews in Economic Geology Vol. 2, p 1-24.

Herzer, R.H. 1995. Seismic stratigraphy of a buried volcanic arc, Northland, New Zealand and implications for Neogene subduction. Marine and Petroleum Geology 12: 511-531.

Hibbard, M.J. 1995. Petrography to petrogenesis. Prentice Hall, New Jersey, 587p.

Hildreth, W. 1979. The Bishop Tuff: evidence for the origin of compositional zonation in silicic magma chambers. Geological Society of America Special Paper 180, p 43-75.

Hildreth, W. 1981. Gradients in silicic magma chambers: implications for lithospheric magmatism. Journal of Geophysical Research 86: 10153-10192.

Hildreth, W. and Mahood, G.A. 1985. Correlation of ash-flow tuffs. Geological Society of America Bulletin 96: 968-974.

Hildreth, W. and Mahood, G.A. 1986. Ring fracture eruption of the Bishop Tuff. Geological Society of America Bulletin 97: 396-403.

Hildreth, W. and Moorbath, S. 1988. Crustal contributions to arc magmatism in the Andes of central Chile. Contributions to Mineralogy and Petrology 98: 455-489.

Hildreth, W., Halliday, A.N. and Christiansen, R.L. 1991. Isotopic and chemical evidence concerning the genesis and contamination of basaltic and rhyolitic magma beneath the Yellowstone plateau volcanic field. Journal of Petrology 32: 63-138.

Hildreth, W. and Fierstein, J. 1997. Recent eruptions of Mount Adams, Washington Cascades, USA. Bulletin of Volcanology 58: 472-490.

Hobden, B.J., Houghton, B.F., Davidson, J.P. and Weaver, S.D. 1999. Small and short-lived magma batches at composite volcanoes: time windows at Tongariro volcano, New Zealand. Journal of the Geological Society 156: 865-868.

Hochstein, M.P. 1995. Crustal heat transfer in the Taupo Volcanic Zone (New Zealand): comparison with other volcanic arcs and explanatory heat source models. Journal of Volcanology and Geothermal Research 68: 117-151.

Hochstein, M.P. and Nixon, I.M. 1979. Geophysical study of the Hauraki Depression, North Island, New Zealand. New Zealand Journal of Geology and Geophysics 22: 1-19.

Hochstein, M.P. and Ballance, P.F. 1993. Hauraki Rift: a young, active, intra-continental rift in a back-arc setting. In: Ballance, P.F. (ed), South Pacific sedimentary basins, Sedimentary Basins of the world, 2. Elsevier Science Publishers B.V., Amsterdam, p 295-305.

Hogg, A.G, and McCraw, J.D. 1983. Late Quaternary tephras of Coromandel Peninsula, North Island, New Zealand: a mixed peralkaline and calc-alkaline tephra sequence. New Zealand Journal of Geology and Geophysics 26: 163-188.

Hole, M.J., Saunders, A.D., Marriner, G.F. and Tarney, J. 1984. Subduction of pelagic sediments: implications for the origin of Ce-anomalous basalts from the Mariana Islands. Journal of the Geological Society 141: 453-472.

Houghton, B.F. and Cuthbertson, A.S. 1989. Kaimai: sheet T14 BD. Geological Map of New Zealand, 1: 50 000, New Zealand Geological Survey, Wellington.

Houghton, B.F. and Wilson, C.J.N. 1991. A vesicularity index for pyroclastic deposits. Bulletin of Volcanology 51: 451-462.

Houghton, B.F. Wilson, C.J.N., McWilliams, M.O., Lanphere, M.A., Weaver, S.D., Briggs, R.M. and Pringle, M.S. 1995. Chronology and dynamics of a large silicic magmatic system: central Taupo Volcanic Zone, New Zealand. Geology 23: 13-16.

Howells, M.F., Reedman, A.J. and Campbell, D.G. 1986. The submarine eruption and emplacement of the Lower Rhyolitic Tuff Formation (Ordovician), North Wales. Journal of the Geological Society, London 143: 411-423.

Hunt, P. 1991. The volcanic geology of the Whiritoa Hill area. Unpublished MSc thesis, University of Waikato.
Hunt, T.M. and Syms, M.C. 1977. Sheet 3, Auckland (1st ed). Magnetic map of New Zealand, 1:250 000, Total Force Anomalies. Department of Scientific and Industrial Research, Wellington.

Inoue, A. 1995. Formation of clay minerals in hydrothermal environments. In: Velde, B.(ed) Origin and mineralogy of clays. Springer-Verlag, Berlin, p 268-321.

Itaya, T., Nagao, K., Inoue, K., Honjou, Y., Okada, T. and Ogata, A. 1991. Argon isotope analysis by a newly developed mass spectrometric system for K-Ar dating. Mineralogical Journal 15: 203-221.

Jackson, J.A. and White, N.J. 1989. Normal faulting in the upper continental crust: observations from regions of active extension. Journal of Structural Geology 11: 15-36.

Kamp, P.J.J. 1984. Neogene and Quaternary extent and geometry of the subducted plate beneath North Island, New Zealand: implications for Kaikoura tectonics. Tectonophysics 108: 241-266.

Kamp, P.J.J. 1988. Tectonic geomorphology of the Hikurangi margin: surface manifestations of different modes of subduction. Zeitshrift Geomorphologie N.F. Suppl-Bd, 69: 55-67.

Karl, M.L. 1996. Volcanic geology of the Tairua Region, Eastern Coromandel Peninsula. Unpublished MSc thesis, University of Waikato.

Kear, D. 1955. Mesozoic and lower Tertiary stratigraphy and limestone deposits, Torehina, Coromandel. New Zealand Journal of Science and Technology 37: 107-114.

Kear, D. 1994. A "least-complex" dynamic model for late Cenozoic volcanism in the North Island, New Zealand. New Zealand Journal of Geology and Geophysics 37:223-236.

Keating, G. N. and Valentine, G.A. 1998. Proximal stratigraphy and syn-eruptive faulting in rhyolitic Grants Ridge Tuff, New Mexico, USA. Journal of Volcanology and Geothermal Research 81: 37-49.

Knesel, K.M., Davidson, J.P. and Duffield, W.A. 1999. Evolution of silicic magma through assimilation and subsequent recharge: evidence from Sr isotopes in sanidine phenocrysts, Taylor Creek Rhyolite, New Mexico. Journal of Petrology 40: 773-786.

Krippner, S.J.P., Briggs, R.M., Wilson, C.J.N. and Cole, J.W. 1998. Petrography and geochemistry of lithic fragments in ignimbrites from the Mangakino Volcanic Centre: implications for the composition of the subvolcanic crust in western Taupo Volcanic Zone, New Zealand. New Zealand Journal of Geology and Geophysics 41: 187-199.

Larsen, D. and Crossey, L.J. 1996. Depositional environments and paleolimnology of an ancient caldera lake: Oligocene Creede Formation, Colorado. Geological Society of America Bulletin 108: 526-544.

Langmuir, C.H., Vocke, R.D., Hanson, G.N. and Hart S.R. 1978. A general mixing equation with applications to icelandic basalts. Earth and Planetary Science Letters 37: 380-392.

Leake, B.E., Woolley, A.R., Arps, C.E.S., Birch, W.D., Gilbert, M.C., Grice, J.D., Hawthorne, F.C., Kato, A., Kisch, H.J., Krivovichev, V.G., Linthout, K., Laird, J., Mandarino, J., Maresch, W.V., Nickel, E.H., Rock, N.M.S., Schumacher, J.C., Stephenson, N.C.N., Ungaretti, L., Whittaker, E.J.W. and Youzhi, G. 1997. Nomenclature of amphiboles: report of the subcommittee on amphiboles of the International Mineralogical Association Commission on New Minerals and Mineral Names. Mineral Magazine 61: 295-321.

Leat, P.T. 1984. Geological evolution of the trachytic caldera volcano Menengai, Kenya Rift Valley. Journal of the Geological Society, London 141: 1057-1069.

Le Maitre, R.W. (ed) 1989. A classification of igneous rocks and glossary of terms. Blackwell Scientific Publications, Oxford, 193p.

Lindgren, W. 1933. Mineral deposits, 4th Ed. New York, McGraw-Hill, 933p.

Lipman, P.W. 1967. Mineral and chemical variations within an ash-flow sheet from Aso caldera, southwestern Japan. Contributions to Mineralogy and Petrology 16: 300-327.

Lipman, P.W. 1975. Evolution of the Platoro caldera complex and related volcanic rocks, southeastern San Juan Mountains, Colorado. United States Geological Survey Professional Paper 852, 128p.

Lipman, P.W., Doe, B.R., Hedge, C.E. and Steven, T.A. 1978. Petrologic evolution of the San Juan volcanic field, southwestern Colorado: Pb and Sr isotope evidence. Geological Society of America Bulletin 89: 59-82.

Lipman, P.W. 1984. The roots of ash-flow calderas in western North America: windows into the tops of granitic batholiths. Journal of Geophysical Research 89: 8801-8841.

Lipman, P.W. 1992. Ash Flow calderas as structural controls of ore deposits-recent work and future problems. United States Geological Survey Bulletin 2012.

Lipman, P.W. 1997. Subsidence of ash-flow calderas: relation to caldera size and magma-chamber geometry. Bulletin of Volcanology 59: 198-218.

Lipman, P.W., Fisher, F.S., Mehnert, H.H., Naeser, C.W., Luedke, R.G. and Steven, T.A. 1976. Multiple ages of mid-Tertiary mineralisation and alteration in the western San Juan mountains, Colorado. Economic Geology 71: 571-588.

Lipman, P.W. and Sawyer, D.A. 1985. Mesozoic ash-flow caldera fragments in southeastern Arizona and their relation to porphyry copper deposits. Geology 13: 652-656.

Lipman, P.W., Dungan, M.A., Brown, L.L., Deino, A. 1996. Recurrent eruption and subsidence at the Platoro Caldera Complex, southeastern San Juan volcanic field, Colorado: New tales from old tuffs. Geological Society of America Bulletin 108: 1039-1055.

Lowe, D.J. and Green, J.D. 1992. Lakes. In: Soons, J.M. and Selby, M.J. (eds), Landforms of New Zealand. Longman Paul, Auckland, 531p.

Malengreau, B., Hochstein, M.P. and Bromley, C.J. 1997. Revised gravity map of Coromandel Peninsula, New Zealand. Geological Society of New Zealand Miscellaneous Publication 91A, p117.

Marti, J., Mitjaila, J. and Arana, V. 1994. Stratigraphy, structure and geochronology of the Canadas caldera (Tenerife, Canary Islands). Geological Magazine 131: 715-727.

McCulloch, M.T., Keyser, T.K., Woodhead, J.D. and Kinsley, L. 1994. Pb-Sr-Nd-O isotopic constraints on the origin of rhyolites from the Taupo Volcanic Zone of New Zealand: evidence for assimilation followed by fractionation of basalt. Contributions to Mineralogy and Petrology 115: 303-312.

McGunnigle, N. 1995. Volcanic geology of the Hikuai region, eastern Coromandel Peninsula. Unpublished MSc thesis, University of Waikato.

McPhie, J. 1983. Outflow ignimbrite sheets from late Carboniferous calderas, Currabubula Formation, New South Wales, Australia. Geological Magazine 120: 487-503.

McPhie, J. 1986. Primary and redeposited facies from a large-magnitude, rhyolitic, phreatomagmatic eruption: Cana Creek tuff, late Carboniferous, Australia. Journal of Volcanology and Geothermal Research 28: 319-350.

Merchant, R.J. 1978. Metallogenesis in the Thames-Tapu area, Coromandel Peninsula, New Zealand. Unpublished PhD thesis, University of Auckland.

Merchant, R.J., Corbett, G.J. and Smith, M.J. 1988. The Ohui prospect, prospecting licence 31-874, Coromandel Peninsula, New Zealand-status report. Unpublished report for Austpac Gold Exploration, New Zealand Ltd.

Metz, J.M. and Mahood, G.A. 1985. Precursors to the Bishop Tuff eruption: Glass Mountain, Long Valley, California. Journal of Geophysical Research 90: 11121-11126.

Middleton, G.V. 1978. Facies. In: Fairbridge, R.W. and Bourgeois, J. (eds), Encyclopaedia of sedimentology. Hutchinson and Ross, New York, 901p.

Milesi, J.P., Marcoux, E., Sitorus, T., Simandjuntak, M., Leroy, J. and Bailly, L. 1999. Pongkor (west Java, Indonesia): a Pliocene supergene-enriched epithermal Au-Ag-(Mn) deposit. Mineralium Deposita 34: 131-149.

Mills, B.A., Boden, D.R. and Sander, M.V. 1988. Alteration and precious metal mineralisation associated with the Toquima Caldera Complex, Nye County, Nevada. In: Schafer, R.W., Cooper, J.J. and Vikre, P.G. (eds), Bulk Mineable Precious metal deposits of the Western United States, Symposium Proceedings, Geological Society of Nevada, p 303-331.

Moore, C.R. 1976. Gold-silver mineralisation of the Broken Hills area, Hikuai. Unpublished MSc thesis, University of Auckland.

Morimoto, N., Fabries, J., Ferguson, A.K., Ginzburg, I.V., Ross, M., Seifert, F.A, Zussman, J., Aoki, K. and Gottardi, G. 1988. Nomenclature of pyroxenes. American Mineralogist 73: 1123-1133.

Nairn, I.A. 1981. Some studies of the geology, volcanic history, and geothermal resources of the Okataina volcanic centre, Taupo Volcanic Zone, New Zealand. Unpublished PhD thesis, Victoria University of Wellington.

Nairn, I.A. 1989. Sheet V16AC-Mount Tarawera. Geological map of New Zealand 1: 50 000. Map, 1 sheet, and notes. Department of Scientific and Industrial Research, Wellington.

Nairn, I.A. and Cole, J.W. 1981. Basalt dikes in the 1886 Tarawera Rift. New Zealand Journal of Geology and Geophysics 24: 585-592.

Nairn, I.A., Wood, C.P. and Bailey, R.A. 1994. The Reporoa Caldera, Taupo Volcanic Zone: source of the Kaingaroa Ignimbrites. Bulletin of Volcanology 56: 529-537.

Nelson C.H., Bacon, C.R., Robinson, S.W., Adam, D.P., Bradbury, J.P., Barber, J.H., Schwartz, D., Vagenas, G. 1994. The volcanic, sedimentologic, and paleolimnologic history of the Crater Lake caldera floor, Oregon: evidence for small caldera evolution. Geological Society of America Bulletin 106: 684-704.

Nelson, C.S., Froggatt, P.C. and Gosson, G.J. 1986. Nature, chemistry, and origin of late Cenozoic megascopic tephras in Leg 90 cores from the southwest Pacific. In: Kennett, J.P. et al. (ed), Initial reports of the Deep Sea Drilling Project 90. Washington, United States Government Printing Office, p 1161-1173.

Nelson, C.S., Mildenhall, D.C., Todd, A.J. and Pocknall, D.T. 1988. Subsurface stratigraphy, paleoenvironments, palynology, and depositional history of the late Neogene Tauranga Group at Ohinewai, Lower Waikato lowland, South Auckland, New Zealand. New Zealand Journal of Geology and Geophysics 31: 21-40.

Nelson, C.S., Kamp, P.J.J. and Mildenhall, D.C. 1989. Late Pliocene distal silicic ignimbrites, Port Waikato, New Zealand: implications for volcanism, tectonics and sea level changes in South Auckland. New Zealand Journal of Geology and Geophysics 32: 357-370.

New Zealand Seismological Observatory, 1970. New Zealand Seismological Report 1970. Geophysics Division, Department of Scientific and Industrial Research, Wellington.

Norrish, K. and Hutton, J.T. 1969. An accurate X-ray spectrograph method for the analysis of a wide range of geological samples. Geochimica et Cosmochimica Acta 33: 431-453.

Nixon, G.T. 1988. Petrology of the younger andesites and dacites of Iztaccihuatl volcano, Mexico: I. Disequilibrium phenocryst assemblages as indicators of magma chamber processes. Journal of Petrology 29: 213-264.

O'Leary, G.P. 1978. A geophysical study of the Whitianga Graben. BSc(Hons) project, University of Auckland.

O'Halloran, G.J. and Gaul, A.J. 1997. Sedimentary responses to sub-aerial felsic volcanism from the Late Devonian-Early Carboniferous northern Macalister Synclinorium, southeastern Australia. Sedimentary Geology 109: 209-232.

Orth, K., Cas, R.A.F. and Wright, J.V. 1989. Facies analysis and facies associations in the recognition of volcanic centres in silicic terranes: an example from the early Devonian of Australia. Australian Journal of Earth Sciences 36: 167-188.

Palladino, D.M. and Valentine, G.A. 1995. Coarse-tail vertical and lateral grading in pyroclastic flow deposits of the Latera Volcanic Complex (Vulsini, central Italy): origin and implications for flow dynamics. Journal of Volcanology and Geothermal Research 69: 343-364.

Peate, D.W., Pearce, J.A., Hawkesworth, C.J. Colley, H., Edwards, C.M.H., Hirose, K. 1997. Geochemical variations in Vanuatu arc lavas: the role of subducted material and a variable mantle wedge composition. Journal of Petrology 38: 1331-1358.

Pearce, J.A. 1983. Role of the sub-continental lithosphere in magma genesis at active continental margins. In: Hawkesworth, C.J. and Norry, M.J.(eds), Continental basalts and mantle xenoliths. Shiva, Natwich, p 230-249.

Pearce, J.A. and Peate, D.W. 1995. Tectonic implications of the composition of volcanic arc magmas. Annual Reviews of Earth and Planetary Sciences 23: 251-285.

Petterson, M.G., Beddoe-Stephens, B., Millward, D. and Johnson, E.W. 1992. A pre-caldera plateau-andesite field in the Borrowdale Volcanic Group of the English lake district. Journal of the Geological Society 149: 889-906.

Potter, D.B. and Oberthal, C.M. 1987. Vent sites and flow directions of the Otowi ash flows (lower Bandelier Tuff), New Mexico. Geological Society of America Bulletin 98: 66-76.

Price, R.C., Gray, C.M., Wilson, R.E., Frey, F.A., Taylor, S.R. 1991. The effects of weathering on rare-earth elements, Y and Ba abundances in Tertiary basalts from southern Australia. Chemical Geology 93: 245-265.

Price, R.C., Stewart, R.B., Woodhead, J.D. and Smith, I.E.M. 1999. Petrogenesis of high-K arc magmas: evidence from Egmont volcano, North Island, New Zealand. Journal of Petrology 40: 167-197.

Rabone, S.D.C. 1991. Residual total force magnetic anomaly map, Coromandel region, 1:100 000. New Zealand Geological Survey Report M183.

Reid, A.H. 1953. The story of the Kauri. A.H. & A.W. Reed, Wellington, 439p.

Riciputi, L.R., Johnson, C.M., Sawyer, D.A. and Lipman, P.W. 1995. Crustal and magmatic evolution in a large multicyclic caldera complex: isotopic evidence from the central San Juan volcanic field. Journal of Volcanology and Geothermal Research 67: 1-28.

Riggs, N.R. and Busby-Spera, C.J. 1991. Facies analysis of an ancient, dismembered, large caldera complex and implications of intra-arc subsidence: middle Jurassic strata of Cobre Ridge, southern Arizona, USA. Sedimentary Geology 74: 39-68.

Robson, R.N. 1989. PLA 31-1844: preliminary reconnaissance report. Heritage Mining N.L., closed file report.

Robson, R.N., Stevens, M.R. and Haworth, T. 1994. Technical report for the three year period ending 19 April 1994, PL 31-1844, Kapowai. Heritage Mining Ltd.

Rogers, J. 1994. Rhyolite volcanics of the Cooks Beach/Hahei region, eastern Coromandel Peninsula. Unpublished MSc thesis, University of Waikato.

Rollinson, H. 1993. Using geochemical data: evaluation, presentation and interpretation. Longman Group, Essex, 352p.

Rosi, M., Vezzoli, L., Aleotti, P. and De Censi, M. 1996. Interaction between caldera collapse and eruptive dynamics during the Campanian Ignimbrite eruption, Phlegraean Fields, Italy. Bulletin of Volcanology 57: 541-554.

Rytuba, J.J. 1994. Evolution of volcanic and tectonic features in caldera settings and their importance in the localisation of ore deposits. Economic Geology 89: 1687-1696.

Sarna-Wojcicki, A., Bowman, H.W. and Russell, P.C. 1979. Chemical correlation of some late Cenozoic tuffs of northern and central California by neutron activation analysis of glass and comparison with X-ray fluorescence analysis. United States Geological Survey Professional Paper 1147.

Sakuyama, M. 1979. Evidence of magma mixing: petrological study of Shirouma-Oike calc-alkaline andesite volcano, Japan. Journal of Volcanology and Geothermal Research 5: 179-208.

Schmid, R. 1981. Descriptive nomenclature and classification of pyroclastic deposits and fragments: recommendations of the IUGS Subcommission on the Systematics of Igneous Rocks. Geology 9: 41-43.

Schofield, J.C. 1967. Sheet 3 Auckland. Geological Map of New Zealand 1:250 000. Department of Scientific and Industrial Research, Wellington.

Schroeder, B., Thompson, G., Sulanowska, M. and Ludden, J.N. 1980. Analysis of geologic materials using an automated X-ray fluorescence system. X-ray spectrometry 9: 198-205.

Scott, R.B. 1971. Alkali exchange during devitrification and hydration of glasses in ignimbrite cooling units. Journal of Geology 79: 100-110.

Self, S., Goff, F., Gardner, J.N., Wright, J.V. and Kite, W.M. 1986. Explosive rhyolitic volcanism in the Jemez Mountains: vent locations, caldera development and relation to regional structure. Journal of Geophysical Research 91: 1779-1798.

Shane, P., Black, T., Eggins, S. and Westgate, J. 1998. Late Miocene marine tephra beds: recorders of rhyolitic volcanism in North Island, New Zealand. Journal of Geology and Geophysics 41: 165-178.

Shelley, D. 1985. Optical Mineralogy (2nd ed). Elsevier, New York, 321p.

Sillitoe, R.H. 1993. Epithermal models: Genetic types, geometric controls and shallow features. In: Kirkham, R.V., Sinclair, W.D., Thorpe, R.I. and Duke, J.M. (eds), Mineral Deposit Modelling. Geological Association of Canada, Special Paper 40: 403-417.

Simpson, C.J. 1999. Landslide analysis for Thames and the Kauaeranga valley, New Zealand. Unpublished MSc thesis, University of Waikato.

Singer, B.S., Dungan, M.A., and Layne, G.D. 1995. Textures and Sr, Ba, Mg, Fe, K and Ti compositional profiles in volcanic plagioclase: clues to the dynamics of calc-alkaline magma chambers. American Mineralogist 80: 776-798.

Skilling, I.P. 1993. Incremental caldera collapse of Suswa volcano, Gregory Rift Valley, Kenya. Journal of the Geological Society, London 150: 885-896.

Skinner, D.N.B. 1969. Colville Formation-a new formation possibly correlative with the Waitemata Group. New Zealand Journal of Geology and Geophysics 12: 349-360.

Skinner, D.N.B. 1972. Subdivision and petrology of the Mesozoic rocks of Coromandel (Manaia Hill Group). New Zealand Journal of Geology and Geophysics 15: 203-227.

Skinner, D.N.B. 1976. Sheet N40 and pts N35, N36, N39 Northern Coromandel. Geological map of New Zealand 1: 63 360. Department of Scientific and Industrial Research, Wellington.

Skinner, D.N.B. 1983. Ring rhyolites round Rangihau. New Zealand Geological Society Miscellaneous Publication 30A.

Skinner, D.N.B. 1986. Neogene volcanism of the Hauraki Volcanic Region, In: Smith, I.E.M.(ed), Late Cenozoic volcanism in New Zealand. The Royal Society of New Zealand Bulletin 23: 21-47

Skinner, D.N.B. 1993. Geology of the Coromandel Harbour area. scale 1:50000. Institute of Geological and Nuclear Sciences, Lower Hutt, geological map 4.

Skinner, D.N.B. 1995. Geology of the Mercury Bay area. scale 1: 50 000. Institute of Geological and Nuclear Sciences, Lower Hutt, geological map 17.

Slack, J.F. and Lipman, P.W. 1979. Chronology of alteration, mineralization, and caldera evolution in the Lake City area, western San Juan Mountains, Colorado. In: Ridge, J.D. (ed), Papers on mineral deposits of western North America; proceedings of the Fifth Quadrennial Symposium of the International Association on the Genesis of Ore Deposits; Volume 2. Report - Nevada Bureau of Mines and Geology, p 151-157.

Smith, R.D., Cameron, K.L., McDowell, F.W. Niemeyer, S. and Sampson, D.E. 1996. Generation of voluminous silicic magmas and formation of mid-Cenozoic crust beneath north-central Mexico: evidence from ignimbrites, associated lavas, deep crustal granulites, and mantle pyroxenites. Contributions to Mineralogy and Petrology 123: 375-389.

Smith, R.L. 1979. Ash flow magmatism. Geological Society of America Special Paper 180, p 5-27.

Smith, R.L. and Bailey, R.A. 1968. Resurgent cauldrons. In: Coats, R.R., Hay, R.L. and Anderson, C.A. (eds), Studies in volcanology. Geological Society of America memoir 116: 613-662.

Soengkeno, S., Hochstein, M.P., Smith, I.E.M. and Itaya, T. 1992. Geophysical evidence for widespread reversely magnetised pyroclastics in the western Taupo Volcanic Zone (New Zealand). New Zealand Journal of Geology and Geophysics 35: 47-55.

Sollas, W.J. and McKay, A. 1905. Rocks of the Cape Colville Peninsula, New Zealand. Volumes 1 and 2. Government Printer, Wellington.

Sparks, R.S.J. and Walker, G.P.L. 1977. The significance of vitric-enriched air-fall ashes associated with crystal-enriched ignimbrites. Journal of Volcanology and Geothermal Research 2: 329-341.

Stamatelopoulou-Seymour, K., Vlassopoulos, D., Pearce, T.H. and Rice, C. 1990. The record of magma chamber processes in plagioclase phenocrysts at Thera volcano, Aegean Volcanic Arc, Greece. Contributions to Mineralogy and Petrology 104: 73-84.

Steiger, R.H. and Jager, E. 1977. Subcommission on geochronology: convention on the uses of decay constants in geochrononology and cosmochronology. Earth and Planetary Science Letters 36: 359-362.

Steiner, A. 1970. Genesis of hydrothermal K-feldspar (adularia) in an active geothermal environment at Wairakei, New Zealand. Mineralogical Magazine 37: 916-922.

Stern, T.A. 1985. A back-arc basin formed within continental lithosphere: the Central Volcanic Region of New Zealand. Tectonophysics 112:385-409.

Steven, T.A. and Ratte, J.C. 1965. Geology and structural controls of ore deposition in the Creede district, San Juan Mountains, Colorado. United States Geological Survey Professional Paper 487.

Steven, T.A. and Lipman, P.W. 1976. Calderas of the San Juan volcanic field, south-western Colorado. United States Geological Survey Professional Paper 958.

Stimac, J.A. and Pearce, T.H. 1992. Textural evidence of mafic-felsic magma interaction in dacite lavas, Clear Lake, California. American Mineralogist 77: 795-809.

Streck, M.J. and Grunder, A.L. 1995. Crystallization and welding variations in a widespread ignimbrite sheet; the Rattlesnake Tuff, eastern Oregon, USA. Bulletin of Volcanology 57: 151-169.

Streck, M.J. and Grunder, A.L. 1997. Compositional gradients and gaps in high-silica rhyolites of the Rattlesnake Tuff, Oregon. Journal of Petrology 38: 133-163.

Sun, S.S. and McDonough W.F. 1989. Chemical and isotopic systematics of oceanic basalts: implications for mantle composition and processes. In: Saunders, A.D. and Norry, M.J.(eds), Magmatism in Ocean Basins. Geological Society of London Special Publication 42, p 429-448.

Sutton, A.N., Blake, S. and Wilson, C.J.N. 1995. An outline geochemistry of rhyolite eruptives from Taupo volcanic centre, New Zealand. Journal of Volcanology and Geothermal Research 68:153-175.

Suzuki-Kamata, K. 1988. The ground layer of the Ata pyroclastic flow deposit, southwestern Japan-evidence for the capture of lithic fragments. Bulletin of Volcanology 50: 119-129.

Suzuki-Kamata, K. and Kamata, H. 1990. The proximal facies of the Tosu pyroclastic flow deposit erupted from Aso caldera, Japan. Bulletin of Volcanology 52: 325-333

Suzuki-Kamata, K., Kamata, H. and Bacon, C.R. 1993. Evolution of the caldera-forming eruption at Crater Lake, Oregon, indicated by component analysis of lithic fragments. Journal of Geophysical Research 98: 14059-14074.

Takagi, M. 1995. Miocene-Pliocene arc volcanism of the Hauraki region in North Island, New Zealand. Unpublished MSc thesis, Hiruzen Research Institute, Okayama, Japan.

Taylor, S.R. and McLennan, S.M. 1985. The continental crust: its composition and evolution. Blackwell, Oxford, 312p.

Tepley, F.J., Davidson, J.P. and Clynne, M.A. 1999. Magmatic interactions as recorded in plagioclase phenocrysts of Chaos Crags, Lassen Volcanic Centre. Journal of Petrology 40: 787-806.

Thirwell, M.F., Smith, T.E., Graham, A.M., Theodorou, N., Hollings, P., Davidson, J.P. and Arculus, R.P. 1994. High field strength element anomalies in arc lavas: source or process?. Journal of Petrology 35: 819-838.

Thompson, B.N. 1974. Geology of the Rotorua Geothermal District. In: Geothermal resources survey - Rotorua Geothermal District. Department of Industrial and Scientific Research, Lower Hutt, 120p.

Todd, A.J. 1982. Subsurface stratigraphy of late Cenozoic sediments at Ohinewai, lower Waikato Basin. Unpublished MSc thesis, University of Waikato.

Trotter, W.M. 1995. The volcanic geology of the Pauanui-Opoutere Beach region, eastern Coromandel Volcanic Zone. Unpublished MSc thesis, University of Waikato.

van Thournout, F., Salemink, J., Valenzuela, G., Merlyn, M., Boven, A. And Muchez, P. 1996. Portovelo: a volcanic-hosted epithermal vein-system in Ecuador, South America. Mineralium Deposita 31: 269-276.

Walcott, R.I. 1978. Tectonics and late Cenozoic evolution of New Zealand. Geophysical Journal of the Royal Astronomical Society 52: 137-164.

Walcott, R.I. 1984. Reconstructions of the New Zealand region for the Neogene. Paleogeography, Paleoclimatology, Paleoecology 46: 217-231.

Walker, G.P.L. 1983. Ignimbrite types and ignimbrite problems. Journal of Volcanology and Geothermal Research 17: 65-88.

Walker, G.P.L. 1984. Downsag calderas, ring faults, caldera sizes, and incremental caldera growth. Journal of Geophysical Research 89: 8407-8416.

Walker, G.P.L. 1985. Origin of coarse lithic breccias near ignimbrite source vents. Journal of Volcanology and Geothermal Research 25: 157-171.

Walker, G.P.L., Self, S. and Froggatt, P.C. 1981. The ground layer of the Taupo Ignimbrite: a striking example of sedimentation from a pyroclastic flow. Journal of Volcanology and Geothermal Research 10: 1-11.

Walker, G.P.L. and Wilson, C.J.N. 1982. Ignimbrite depositional facies: the anatomy of a pyroclastic flow. Journal of the Geological Society, London 139: 581-592.

Walker, R.G. (ed) 1984. Facies models, 2nd edition. Geological Association of Canada, Geosciences Canada Reprint Series 1, 317p.

Wilson, C.J.N. 1996. Taupo's atypical arc. Nature 379: 27-28.

Wilson, C.J.N., Rogan, A.M., Smith, I.E.M., Northey, D.J., Nairn, I.A. and Houghton, B.F. 1984. Caldera volcanoes of the Taupo Volcanic Zone, New Zealand. Journal of Geophysical Research 89: 8463-8484.

Wilson, C.J.N., Houghton, B.F., McWilliams, M.O., Lanphere, M.A., Weaver, S.D. and Briggs, R.M. 1995. Volcanic and structural evolution of Taupo Volcanic Zone: a review. Journal of Volcanology and Geothermal Research 68: 1-28.

Wilson, M. 1989. Igneous Petrogenesis, a global tectonic approach. Unwin Hyman Ltd., London, 466p.

Woodhead, J.D. 1989. Geochemistry of the Mariana arc (western Pacific): source composition and processes. Chemical Geology 76: 1-24.

Woodward, D.J. 1971. Sheet 3 Auckland, Gravity map of New Zealand 1: 250 000, Bouguer Anomalies. Department of Scientific and Industrial Research, Wellington.

Wright, I.C. 1985. Mangapoike River: a late Miocene magnetostratigraphic reference column for New Zealand. In: Cooper, R.(ed.), Hornibrook Symposium, extended abstracts. New Zealand Geological Survey Record 9, p 105-107.

Wright, I.C. and Vella, P.P. 1988. A New Zealand late Miocene magnetostratigraphy: glacioeustatic and biostratigraphic correlations. Earth and Planetary Science Letters 87: 193-204.
Wright, J.V. and Walker, G.P.L. 1977. The ignimbrite source problem: significance of a co-ignimbrite lag-fall deposit. Geology 5: 729-732.

Zandt, G., Myers, S.C., Wallace, T.C. 1995. Crust and mantle structure across the Basin and Range-Colorado Plateau boundary at 37°N latitude and implications for Cenozoic extensional mechanism. Journal of Geophysical Research 100: 10529-10548.

# Appendix I

## Sample Catalogue

### *Mapping Units*

Hydrothermally altered ignimbrite/rhyolite lava (h)

| | |
|---|---|
| Colorado Pyroclastics | (cp) |
| Webb Creek Ignimbrite | (wi) |
| Trig Q Ignimbrite | (qi) |
| Manuka Ignimbrite | (mi) |
| Oteao Ignimbrite | (oi) |
| Wharepapa Eruptive Sequence | (wes) |
| Acadia Rhyolite | (ra) |
| Rangihau Rhyolite | (rr) |
| Slip Rhyolite | (ss) |
| Miller Flat Rhyolite | (sm) |
| Ruahine Rhyolite | (ur) |
| Welcome Jack Rhyolite | (uj) |
| Moss Creek Rhyolite | (um) |
| Scots Rhyolite | (us) |
| Precipice Rhyolite | (kd) |
| Wharepapa Rhyolite | (kh) |
| Bulls Run Rhyolite | (ku) |
| Kapowai Rhyolite | (kk) |
| Kokonga Rhyolite | (kg) |
| Pinnacles Rhyolite | (kp) |
| Atuatumoe Rhyolite | (ka) |
| Tauranikau Rhyolite | (kt) |
| Camp Rhyolite | (kc) |
| Kauaeranga Rhyolite | (ku) |
| Starvation Rhyolite | (ks) |
| Big Beetle Rhyolite | (kb) |
| Waiwhatawhata Rhyolite | (kw) |
| Kydd Rhyolite | (ky) |
| Moyles Rhyolite | (ko) |
| Taurauikau Andesite | (ot) |
| Tapuaetahi Andesite | (ap) |
| Taurahuehue Andesite | (at) |
| Maumaupaki Formation | (cn) |
| Waiwawa Member | (ww) |
| Tarawaere Member | (wt) |
| Haukawakawa Member | (wh) |

### *Lithic Types*

| | |
|---|---|
| Plagioclase-pyroxene phyric rhyolite lava lithic | (RPP) |
| Plagioclase phyric rhyolite lava lithic | (RP) |
| Plagioclase-amphibole phyric rhyolite lava lithic | (RPA) |
| Plagioclase-pyroxene phyric dacite lava lithic | (DPP) |
| Plagioclase-quartz phyric dacite lava lithic | (DPQ) |
| Plagioclase-amphibole phyric dacite lava lithic | (DPA) |
| Plagioclase-pyroxene phyric andesite lava lithic | (APP) |
| Plagioclase-amphibole phyric andesite lava lithic | (APA) |
| Webb Creek welded ignimbrite type | (WEB) |
| Trig Q welded ignimbrite type | (TRI) |
| Brown welded ignimbrite type | (MAN) |
| Vapour phase altered ignimbrite type | (VAP) |
| Undifferentiated welded ignimbrite type | (UND) |
| Rhyolitic crystal tuff | (RCT) |
| Rhyolitic vitric tuff | (RVT) |
| Volcanic breccia lithic | (BRE) |
| Plutonic lithic | (PLU) |
| Volcaniclastic siltstone lithic | (VSI) |
| Volcaniclastic sandstone lithic | (VSA) |
| Volcaniclastic breccia lithic | (VBR) |
| Sericitic altered rhyolite lava lithic | (SRL) |
| Propylitic altered rhyolite lava lithic | (PRL) |
| Sericitic altered dacite lava lithic | (SDL) |
| Silicified andesite lava lithic | (SAL) |
| Weakly silicified welded ignimbrite lithic | (WSI) |
| Strongly silicified welded ignimbrite lithic | (SSI) |
| Weakly propylitic welded ignimbrite lithic | (WPI) |
| Strongly propylitic welded ignimbrite lithic | (SPI) |
| Propylitic altered tuff lithic | (PT) |

W No. are numbers assigned to samples stored in the Department of Earth Sciences Rock Store. Grid References are based upon the NZMS 260 (1: 50 000) topographic maps T12 and T11.
T= thin section; M= modal analysis; P= electron microprobe analysis; F = XRF analysis; D = XRD analysis; I = ICP-MS analysis; K = K/Ar age determined.

| W No. | Lithology | Unit | Location | Grid Ref. | T | M | P | F | D | I | K |
|---|---|---|---|---|---|---|---|---|---|---|---|
| W99600 | blue/grey fine phyric rhyolite lava | rr | Rangihau Stm | T11/499654 | T | M | P | F | | I | K |
| W99601 | dk grey fine phyric andesite lava | at | Rangihau Rd | T11/493687 | T | M | P | F | | I | |
| W99602 | cream v.p.a lith. r weakly welded ignimbrite | wes-1 | Rangihau Rd | T11/496680 | T | | | | | | |
| W99603 | cream v.p.a lith. r weakly welded ignimbrite | wes-1 | Rangihau Rd | T11/496680 | T | | | | | | |
| W99604 | cream v.p.a pum r weakly welded ignimbrite | wes-1 | Rangihau Rd | T11/496680 | T | | | | | | |
| W99605 | cream lith r weakly welded ignimbrite | wes-1 | Rangihau Rd | T11/496680 | T | | | | | | |
| W99606 | cream weakly welded ignimbrite | wes-1 | Rangihau Rd | T11/496680 | | | | | | | |
| W99606LA | brown welded ignimbrite lithic | UND | Rangihau Rd | T11/496680 | T | | | | | | |
| W99606LB | grey cry r lith r ignimbrite lithic | UND | Rangihau Rd | T11/496680 | T | | | | | | |
| W99606LC | grey fine-phyric rhyolite lava lithic | RPP | Rangihau Rd | T11/496680 | T | | | | | | |
| W99606LD | dk grey lith r welded ignimbrite lithic | UND | Rangihau Rd | T11/496680 | T | | | | | | |
| W99606LE | pink/red v.p.a. welded ignimbrite lithic | VPA | Rangihau Rd | T11/496680 | T | | | | | | |
| W99607 | dk grey crs phyric andesite lava | ot | Rangihau Rd | T11/496662 | T | | | | | | |
| W99608 | cream vitric tuff | wes-2 | Rangihau Rd Track | T11/496662 | T | | | | | | |
| W99609 | cream/white silicified rhyolite lava | h | Rangihau Rd Track | T11/504628 | T | | | | | | |
| W99610 | pink pum r cry r v.p.a weakly welded ignimbrite | mi | Oteao Rd | T11/537681 | | | | | | | |
| W99611 | cream/grey pum r cry r weakly welded ignimbrite | wes-4 | Oteao Rd | T11/537681 | | | | | | | |
| W99612 | dk grey pum r cry r weakly welded andesitic ignimbrite | oi | Oteao Rd | T11/534670 | T | M | P | F | | I | K |
| W99613 | devitrified rhyolite lava | ky | Miller's Flat Rd | T11/536658 | T | | | | | | |
| W99614 | lt grey pum r weakly welded ignimbrite | wes-1 | McGoram Road | T11/542683 | T | M | P | F | | | K |
| W99615 | pink/orange cry r, lith p weakly welded ignimbrite | mi | Oteao Rd | T11/540680 | T | | | | | | |
| W99615LA | brown/red fine phyric rhyolite lava lithic | RPP | Oteao Rd | T11/540680 | T | | | | | | |
| W99615LB | grey spher fine phyric rhyolite lava lithic | rpa | Oteao Rd | T11/540680 | T | | | F | | | |
| W99615LC | grey welded ignimbrite lithic | WPI | Oteao Rd | T11/540680 | T | | | | | | |
| W99615LD | lt grey f-band fine phyric rhyolite lava lithic | RPP | Oteao Rd | T11/540680 | T | | | | | | |
| W99615LE | grey med phyric incip. vesicular andesite lava lithic | APP | Oteao Rd | T11/540680 | T | | | | | | |
| W99615LF | grey f-band fine phyric rhyolite lava lithic | RPP | Oteao Rd | T11/540680 | T | | | | | | |
| W99615LG | grey med phyric andesite lava lithic | APP | Oteao Rd | T11/540680 | T | | | | | | |
| W99616 | cream pum r cry p weakly welded ignimbrite | mi | Oteao Rd | T11/541679 | T | | | | | | |
| W99617 | pink pum r silicified v.p.a weakly welded ignimbrite | oi | Oteao Rd | T11/539679 | T | | | | | | |
| W99618 | grey/pink fine phyric rhyolite lava | kh | Oteao Rd | T11/528664 | T | | | F | | I | |
| W99619 | cream lith r pum r weakly welded ignimbrite | wes-4 | Oteao Rd | T11/527661 | T | | | | | | |
| W99619LA | red/brown pheno p fine phyric rhyolite lava lithic | RPP | Oteao Rd | T11/527661 | T | | | | | | |
| W99619LB | grey glassy pum r welded ignimbrite lithic | UND | Oteao Rd | T11/527661 | T | | | | | | |
| W99619LC | cream pum r lithic p welded ignimbrite lithic | UND | Oteao Rd | T11/527661 | T | | | | | | |
| W99620 | brown/red weath fine phyric rhyolite lava | ky | Oteao Rd | T11/526662 | | | | | | | |
| W99621 | green/cream lith r pum p silicified ignimbrite | h | Oteao Rd | T11/527663 | T | | | | | | |
| W99622 | dk pink/grey med phyric rhyolite lava | ky | Oteao Rd | T11/517660 | T | | | F | | I | |
| W99623 | blue/lt grey fine phyric rhyolite lava | kw | Oteao No.2 dome | T11/513663 | T | M | | | | | |
| W99624 | blue/lt grey fine phyric rhyolite lava | ky | Oteao Rd | T11/516660 | | | | | | | |
| W99625 | blue/lt grey fine phyric rhyolite lava | ky | Oteao Rd | T11/517663 | | | | | | | |
| W99626 | lt grey/pale pink pum r lith r weakly welded ignimbrite | wes-4 | Oteao Rd | T11/526660 | T | | | | | | |
| W99626LA | grey fine phyric rhyolite lava lithic | RPP | Oteao Rd | T11/526660 | T | | | | | | |
| W99627 | lt brown/grey pum r lith r partially welded ignimbrite | wes-4 | Wharepapa Rd | T11/530668 | T | | | | | | |
| W99628 | deeply weath. ignimbrite | wes | Wharepapa Rd | T11/ 532674 | | | | | | | |
| W99629 | lt brown pum r cry p weakly welded ignimbrite | wes | Manuka Rd | T11/533678 | T | | | | | | |
| W99630 | lt brown pum r lith p weakly welded ignimbrite | wes-1 | off Manuka Rd | T11/533677 | T | | | F | | | |
| W99630LA | grey fine phyric andesite lava lithic | APP | off Manuka Rd | T11/533677 | T | | | | | | |
| W99630LA | grey spher rhyolite lava lithic | RPP | off Manuka Rd | T11/533677 | T | | | | | | |
| W99630LA | grey med phyric dacite lava lithic | RPP | off Manuka Rd | T11/533677 | T | | | | | | |
| W99631 | lt grey pum r lith p weakly welded ignimbrite | wes-1 | 100m from Manuka Rd end | T11/534677 | T | | | | | | |
| W99631LA | cream/green pum r welded ignimbrite lithic | SPI | 100m from Manuka Rd end | T11/534677 | T | | | | | | |
| W99631LB | grey fine phyric rhyolite lava lithic | RPP | 100m from Manuka Rd end | T11/534677 | | | | | | | |
| W99632 | brown cry r pum p partially welded ignimbrite | wes-4 | Wharepapa Stm/Oteao Rd | T11/535668 | T | | | | | | |
| W99632LA | grey/lt blue weath rhyolite lava lithic | DPA | Wharepapa Stm/Oteao Rd | T11/535668 | T | | | | | | |
| W99633 | grey pum r lith p weakly welded ignimbrite | wes-4 | Oteao Rd, 30m from culvert | T11/534668 | T | | | | | | |
| W99634 | purple/grey deeply weath. rhyolite lava | kk | S 361 Spot Height | T11/543672 | T | | | | | | |
| W99635 | purple/grey deeply weath. rhyolite lava | kk | east side of S 361 s.h. | T11/545668 | T | | | | | | |
| W99636 | purple/grey deeply weath. rhyolite lava | kk | hill 250m SW of S361 | T11/542668 | T | | | | | | |
| W99637 | purple/grey deeply weath. rhyolite lava | kk | ridgeline SW of W99636 | T11/539667 | | | | | | | |
| W99638 | grey/pink deeply weath. rhyolite lava | ky | Miller Flat Rd | T11/532653 | | | | | | | |
| W99639 | dk grey med phyric andesite lava | ot | Waiora Stm tributary | T12/453581 | | | | | | | |
| W99640 | lt. brown massive lacustrine siltstone | ww | Waiora Stm | T12/452580 | | | | | | | |
| W99641 | black crs phyric andesite lava | ot | near s.h. 377 | T12/455572 | T | | | | | | |
| W99642 | brown reworked cry r weakly welded ignimbrite | cp | waterfall near Waiora Track | T12/455584 | T | | | | | | |
| W99642LA | cream/grey weath med phyric andesite lava lithic | APA | waterfall near Waiora Track | T12/455584 | T | M | | | | | |
| W99642LB | cream/grey weath med phyric andesite lava lithic | APA | waterfall near Waiora Track | T12/455584 | | | | | | | |
| W99642LC | cream/grey weath fine phyric andesite lava lithic | APA | waterfall near Waiora Track | T12/455584 | | | | | | | |
| W99642LD | cream/grey weath med phyric andesite lava lithic | APA | waterfall near Waiora Track | T12/455584 | | | | | | | |
| W99642LE | cream/grey weath med phyric andesite lava lithic | APA | waterfall near Waiora Track | T12/455584 | | | | | | | |
| W99643 | grey pum p weakly welded ignimbrite | h | Webb Creek | T12/489573 | | | | | | | |
| W99643LA | cream pum r lith r welded ignimbrite lithic | SPI | Webb Creek | T12/489573 | T | | | | | | |
| W99644 | brown pum p lith r weakly welded ignimbrite | wes-1 | Pinnacles Track | T12/494577 | T | | | | | | |
| W99644LA | black porphyritic glassy med phyric rhyolite lava lithic | RPP | Pinnacles Track | T12/494577 | T | | | | | | |
| W99645 | brown silicified weath ignimbrite | wes-1 | Billy Goat Track | T12/497576 | | | | | | | |
| W99646 | purple/grey rhyolite volcanic breccia | kc | Billy Goat Track | T12/495574 | T | | | | | | |
| W99647 | grey pum r incipiently welded ignimbrite | wes-1 | Billy Goat Track | T12/495570 | | | | | | | |
| W99647LA | pink/grey fine phyric rhyolite lava lithic | RPP | Billy Goat Track | T12/495570 | | | | | | | |
| W99647LB | pink/grey fine phyric rhyolite lava lithic | RPP | Billy Goat Track | T12/495570 | | | | | | | |
| W99648 | cream fine ash accretionary lapilli tuff | wes-4 | Billy Goat Track | T12/495570 | T | | | | | | |
| W99649 | cream/brown pum r lith p weakly welded ignimbrite | wes-4 | Billy Goat Track | T12/495562 | T | | | | | | |
| W99650 | grey lith p weakly welded ignimbrite | wes-4 | Billy Goat Track | T12/493565 | T | | | | | | |
| W99651 | grey/brown autoclastic andesite lava breccia | ot | Hihi Stm | T12/445507 | | | | | | | |
| W99652 | grey/brown autoclastic andesite lava breccia | ot | Hihi Stm | T12/446508 | | | | | | | |
| W99653 | green/brown andesite lava breccia | ot | Hihi Stm Track | T12/453510 | | | | | | | |
| W99654 | cream/lt grey weakly welded ignimbrite | ot | Hihi Stm | T12/455511 | | | | | | | |
| W99655 | grey lith r weakly welded ignimbrite | h | Hihi Stm | T12/472517 | | | | | | | |
| W99656 | grey med phyric dacite lava | ot | Hihi Stm | T12/472517 | | | | | | | |

| W No. | Lithology | Unit | Location | Grid Ref. | T | M | P | F | D | I | K |
|---|---|---|---|---|---|---|---|---|---|---|---|
| W99657 | black med phyric andesite lava | ot | Hihi Stm-Junction Stm | T12/473518 | | | | | | | |
| W99658 | red/brown deeply weath med phyric andesite lava | ot | Hihi Stm | T12/448507 | | | | | | | |
| W99659 | brown lith r weakly welded ignimbrite | wes | Hihi Stm | T12/472517 | | | | | | | |
| W99660 | dk grey med phyric andesite lava | ot | Whangaiterenga Stm | T12/441553 | | | | | | | |
| W99661 | brown matrix-supported conglomerate | ot | Colorado Stm | T12/471565 | | | | | | | |
| W99662 | grey fine phyric andesite lava clast | ot | Colorado Stm | T12/471565 | | | | | | | |
| W99663 | grey/brown med phyric andesite lava clast | ot | Colorado Stm | T12/471565 | | | | | | | |
| W99664 | brown massive lacustrine siltstone | ww | Colorado Stm | T12/469567 | | | | | | | |
| W99665 | grey pum p cry r lith p incipiently welded ignimbrite | cp | Colorado Stm tributary | T12/469568 | | | | | | | |
| W99666 | blue/grey deeply weath. rhyolite lava | ko | Colorado Stm | T12/467572 | | | | | | | |
| W99667 | dk grey massive lacustrine siltstone | wt | Colorado Stm | T12/468574 | | | | | | | |
| W99668 | dk grey pum r lith r weakly welded ignimbrite | cp | Colorado Stm | T12/468574 | T | | | | | | |
| W99668LA | grey fine phyric andesite lava lithic | APP | Colorado Stm | T12/468574 | T | | | | | | |
| W99668LB | grey fine phyric andesite lava lithic | APP | Colorado Stm | T12/468574 | T | | | | | | |
| W99668LC | grey fine phyric dacite lava lithic | DPP | Colorado Stm | T12/468574 | T | | | | | | |
| W99668LD | grey fine phyric rhyolite lava lithic | RPP | Colorado Stm | T12/468574 | T | | | | | | |
| W99669 | brown massive lacustrine siltstone | wt | Colorado Stm | T12/469574 | | | | | | | |
| W99670 | brown cry r pum p weakly welded ignimbrite | cp | Colorado Stm | T12/469574 | | | | | | | |
| W99671 | brown cry r weakly welded ignimbrite | cp | Colorado Stm | T12/468574 | T | | | | | | |
| W99672 | brown weath. fine phyric andesite lava | at | Moyle Track | T12/476567 | T | | | | | | |
| W99673 | cry r lith p pum p ignimbrite | cp | Moyle Track | T12/472572 | T | | | | | | |
| W99673LA | grey med phyric andesite lava lithic | APP | Moyle Track | T12/472572 | T | | | | | | |
| W99674 | cry r lith p pum p ignimbrite | cp | Moyle Track | T12/472573 | T | | | | | | |
| W99674LA | grey fine phyric andesite lava lithic | APP | Moyle Track | T12/472573 | T | | | | | | |
| W99674LB | grey med phyric andesite lava lithic | APP | Moyle Track | T12/472573 | T | | | | | | |
| W99675 | pum r lith p cry r ignimbrite | cp | Moyle Track | T12/472574 | T | | | | | | |
| W99675LA | grey fine phyric andesite lava lithic | APP | Moyle Track | T12/472574 | T | | | | | | |
| W99676 | grey pum r lith p weakly welded ignimbrite | wes-1 | Moyle Track | T12/472575 | T | | | | | | |
| W99677A | grey lith p pum r weakly welded ignimbrite | wes-1 | Moyle Track | T12/472576 | T | | | | | | |
| W99677 | grey fine ash bedded vitric tuff | wes-2a | Moyle Track | T12/472576 | T | M | | | | | |
| W99678 | grey pum r lith p weakly welded ignimbrite | wes-4 | Moyle Track | T12/472576 | T | M | | | | | |
| W99679 | red/brown matrix supported andesitic breccia | ot | Kid Stream | T12/481578 | | | | | | | |
| W99680 | grey/brown med phyric weath andesitIC breccia clast | ot | Kid Stream | T12/481578 | | | | | | | |
| W99681 | dk grey med phyric andesite lava | at | Kid Stream | T12/479582 | T | | | F | | | |
| W99682 | dk grey med phyric andesite lava | at | Webb Creek | T12/485572 | T | | | | | | |
| W99683 | lt grey fine ash vitric tuff | at | Webb Creek | T12/485572 | | | | | | | |
| W99684 | dk grey medium phyric andesite lava | at | Webb Creek | T12/485572 | T | | | | | | |
| W99685 | dk grey med phyric andesite lava | at | Webb Creek | T12/484572 | T | | | | | | |
| W99686 | red/brown matrix supported andesitic breccia | at | Webb Creek | T12/483572 | | | | | | | |
| W99687 | dk grey med phyric andesite lava clast | at | Webb Creek | T12/483572 | | | | | | | |
| W99688 | dk grey med phyric andesite lava clast | at | Webb Creek | T12/483572 | | | | | | | |
| W99689 | dk grey med phyric andesite lava clast | at | Webb Creek | T12/483572 | | | | | | | |
| W99690 | grey med phyric autoclastic andesitic breccia | at | Webb Creek | T12/483572 | T | | | | | | |
| W99691 | dk grey med phyric andesite lava | at | Webb Creek | T12/482572 | T | M | P | F | | | K |
| W99692 | dk grey med phyric autoclastic andesitic breccia | at | Webb Creek | T12/485572 | T | M | | | | | |
| W99693 | grey lith r pum r weakly welded ignimbrite | wi | Webb Creek | T12/486572 | T | M | | F | | | K |
| W99693LA | lt blue/grey amygdaloidal fine phyric rhyolite lava lithic | RPP | Webb Creek | T12/486572 | T | M | | | | | |
| W99693LB | grey fine phyric rhyolite lava lithic | RPP | Webb Creek | T12/486572 | T | | | | | | |
| W99693LC | lt blue/grey amygdaloidal fine phyric rhyolite lava lithic | RPP | Webb Creek | T12/486572 | T | | | | | | |
| W99693LD | grey amygdaloidal fine phyric rhyolite lava lithic | RPP | Webb Creek | T12/486572 | T | | | | | | |
| W99693LE | grey/brown fine phyric rhyolite lava lithic | RPP | Webb Creek | T12/486572 | T | | | | | | |
| W99693LF | grey fine phyric dacite lava lithic | DPP | Webb Creek | T12/486572 | T | | | | | | |
| W99693LG | grey med phyric andesite lava lithic | APP | Webb Creek | T12/486572 | T | | | | | | |
| W99693LH | grey crs f band fine phyric rhyolite lava lithic | PRL | Webb Creek | T12/486572 | T | | | | | | |
| W99693LI | blue/grey med phyric rhyolite lava lithic | RPP | Webb Creek | T12/486572 | T | | | | | | |
| W99693LJ | lt grey/lt blue glassy med phyric dacite lava lithic | DPP | Webb Creek | T12/486572 | T | | | | | | |
| W99693LK | grey glomeroporphyritic fine phyric rhyolite lava lithic | RPP | Webb Creek | T12/486572 | T | | | | | | |
| W99693LL | lt grey glassy incip vesicular rhyolite lithic | RPP | Webb Creek | T12/486572 | | | | | | | |
| W99693LM | dk grey/blue med phyric rhyolite lava lithic | RP | Webb Creek | T12/486572 | T | | | | | | |
| W99693LN | brown med phyric vesicular rhyolite lava lithic | RPP | Webb Creek | T12/486572 | T | | | | | | |
| W99693LO | blue/grey amygdaloidal fine phyric rhyolite lava lithic | RPP | Webb Creek | T12/486572 | | | | | | | |
| W99694 | grey lith r pum r ignimbrite | wi | Webb Creek | T12/487572 | T | | | | | | |
| W99694LA | blue/grey med phyric rhyolite lava lithic | RPP | Webb Creek | T12/487572 | T | | | F | | | |
| W99694LB | blue/grey f band med phyric rhyolite lava lithic | RPP | Webb Creek | T12/487572 | T | | | | | | |
| W99694LC | grey med phyric dacite lava lithic | DPP | Webb Creek | T12/487572 | T | | | | | | |
| W99694LD | grey med phyric andesite lava lithic | APP | Webb Creek | T12/487572 | T | M | | | | | |
| W99694LE | grey med phyric andesite lava lithic | APP | Webb Creek | T12/487572 | T | | | | | | |
| W99694LF | pale green cry p lith p pum r vitric tuff lithic | RVT | Webb Creek | T12/487572 | T | | | | | | |
| W99694LG | dk grey f band med phyric andesite lava lithic | APP | Webb Creek | T12/487572 | T | | | | | | |
| W99694LH | brown/red fine phyric rhyolite lava lithic | RPA | Webb Creek | T12/487572 | T | M | | | | | |
| W99695 | grey lith r pum r weakly welded ignimbrite | wi | Webb Creek | T12/489572 | T | M | | | | | |
| W99695LA | dk grey cry r pum r lenticular welded ignimbrite lithic | WSI | Webb Creek | T12/489572 | T | | | | | | |
| W99695LB | dk grey fine phyric rhyolite lava lithic | RPP | Webb Creek | T12/489572 | T | | | | | | |
| W99695LC | dk grey med phyric rhyolite lava lithic | RPP | Webb Creek | T12/489572 | T | | | | | | |
| W99695LD | red/brown med phyric rhyolite lava lithic | RPP | Webb Creek | T12/489572 | | | | | | | |
| W99695LE | grey med phyric rhyolite lava lithic | RPP | Webb Creek | T12/489572 | T | | | | | | |
| W99695LF | blue/grey med phyric rhyolite lava lithic | RPP | Webb Creek | T12/489572 | T | | | | | | |
| W99695LG | dk grey med phyric dacite lava lithic | DPP | Webb Creek | T12/489572 | T | | | | | | |
| W99695LH | black porphyritic obsidian lithic | RPP | Webb Creek | T12/489572 | T | | | | | | |
| W99696 | grey cry r pum r ltih r weakly-partially welded ignimbrite | wt | Webb Creek | T12/489572 | T | | | | | | |
| W99697 | grey well sorted massive fractured siltstone | wt | Webb Creek | T12/489572 | T | | | | | | |
| W99698 | cream mod sorted cry r normal graded ash crystal/vitric tuff | wt | Webb Creek | T12/489572 | T | | | | | | |
| W99699 | grey well sorted massive volcaniclastic siltstone | wt | Webb Creek | T12/489572 | T | | | | | | |
| W99700 | grey mod sorted mm-bedded ash vitric tuff | wt | Webb Creek | T12/489572 | T | | | | | | |
| W99701 | black mod sorted massive carbonaceous siltstone | wt | Webb Creek | T12/489572 | T | | | | | | |
| W99702 | lt grey pum r poorly sorted fine lapilli vitric tuff | wt | Webb Creek | T12/489572 | T | | | | | | |
| W99703 | grey pum r lith p incipiently welded ignimbrite | cp | Rowe Stm | T12/482592 | | | | | | | |
| W99704 | blue/grey pum p lith p incipiently welded ignimbrite | cp | Rowe Stm | T12/482592 | | | | | | | |
| W99705 | lt grey pum p lith r mod sorted lapilli vitric tuff | cp | Rowe Stm | T12/482592 | | | | | | | |

| W No. | Lithology | Unit | Location | Grid Ref. | T | M | P | F | D | I | K |
|---|---|---|---|---|---|---|---|---|---|---|---|
| W99706 | grey med phyric andesite lava | ot | Moss Creek Track | T12/484596 | T | | | F | | I | K |
| W99707 | grey poorly sorted coarse ash fine lapilli vitric tuff | cp | Derek's Stm | T12/484572 | | | | | | | |
| W99708 | grey/brown pum r cry r lith p weakly welded ignimbrite | cp | Derek's Stm | T12/485572 | | | | | | | |
| W99709 | brown pum r cry r lith r reworked ignimbrite | cp | Derek's Stm | T12/485572 | | | | | | | |
| W99710 | brown mod sorted cm-laminated volcaniclastic sandstone | cp | Derek's Stm | T12/485572 | | | | | | | |
| W99711 | lt brown poor sorted cm-laminated volcaniclastic sandstone | cp | Derek's Stm | T12/485572 | | | | | | | |
| W99712 | brown/grey matrix supported andesitic breccia | ot | Derek's Stm | T12/483583 | | | | | | | |
| W99713 | brown pum r lith r ignimbrite | cp | Derek's Stm | T12/483583 | | | | | | | |
| W99714 | cream/white v.p.a. lith r ignimbrite | wes-1 | Rangihau Stm | T11/496648 | T | | | | | | |
| W99714LA | grey fine phyric rhyolite lava lithic | RPP | Rangihau Stm | T11/496648 | T | | | | | | |
| W99714LB | brown cry r lith p pum r weakly welded ignimbrite lithic | UND | Rangihau Stm | T11/496648 | T | | | | | | |
| W99714LC | brown/cream welded ignimbrite lithic | UND | Rangihau Stm | T11/496648 | | | | | | | |
| W99715 | grey well sorted laminated volcaniclastic siltstone | wh | Haukawakawa Stm | T11/492646 | | | | | | | |
| W99716 | grey well sorted laminated volcaniclastic siltstone | wh | Haukawakawa Stm | T11/489645 | | | | | | | |
| W99717 | cream weath vitric lapilli tuff | wh | Haukawakawa Stm | T11/489645 | | | | | | | |
| W99718 | brown well sorted laminated volcaniclastic siltstone | wh | Haukawakawa Stm | T11/488644 | | | | | | | |
| W99719 | brown/black well sorted carbonaceous volcaniclastic siltstone | wh | Haukawakawa Stm | T11/488644 | | | | | | | |
| W99720 | blue/grey vitric lapilli tuff | wh | Haukawakawa Stm | T11/486643 | | | | | | | |
| W99721 | brown well sorted laminated volcaniclastic siltstone | wh | Haukawakawa Stm | T11/485643 | | | | | | | |
| W99722 | brown well sorted laminated volcaniclastic siltstone | wh | Haukawakawa Stm | T11/482643 | | | | | | | |
| W99723 | blue/grey pum r lith p ignimbrite | wes-1 | Haukawakawa Stm | T11/482643 | T | | | | | | |
| W99724 | blue/grey pum r lith p ignimbrite | wes-1 | Haukawakawa Stm | T11/482643 | | | | | | | |
| W99724LA | grey/blue spher fine phyric rhyolite lava lithic | RP | Haukawakawa Stm | T11/482643 | T | | | | | | |
| W99724LB | blue/grey fine phyric f band rhyolite lava lithic | RPP | Haukawakawa Stm | T11/482643 | T | | | | | | |
| W99724LC | grey/lt blue fine phyric rhyolite lava lithic | RPP | Haukawakawa Stm | T11/482643 | T | | | | | | |
| W99724LD | grey well sorted lith p pum p vitric ash tuff lithic | RVT | Haukawakawa Stm | T11/482643 | T | | | | | | |
| W99724LE | grey fine phyric rhyolite lava lithic | RPP | Haukawakawa Stm | T11/482643 | T | | | | | | |
| W99725 | grey flow b rhyolite lava | ra | W flank of 246 S.H. | T11/493646 | T | M | | F | | I | |
| W99726 | brown massive well sorted volcaniclastic siltstone | wh | tributary of Haukawakawa Stm | T11/485642 | | | | | | | |
| W99727 | lt grey moderately sorted vitric lapilli tuff | wes-1a | W side of waterfall | T11/485642 | T | | | | | | |
| W99728 | cream pum r lith r weakly welded ignimbrite | wes-1 | on ridgeline SW of waterfall | T11/484642 | T | | | | | | |
| W99728LA | grey silicified med phyric rhyolite lava lithic | RP | on ridgeline SW of waterfall | T11/484642 | T | | | | | | |
| W99728LB | brown silicified massive volcaniclastic lacustrine siltstone lithic | VSI | on ridgeline SW of waterfall | T11/484642 | T | | | | | | |
| W99728LC | grey silicified vitric ash tuff | RVT | on ridgeline SW of waterfall | T11/484642 | T | | | | | | |
| W99728LD | grey glassy incip vesicular fine phyric rhyolite lava lithic | RPP | on ridgeline SW of waterfall | T11/484642 | T | | | | | | |
| W99729 | grey/cream cry r pum r ignimbrite | wes-1 | Haukawakawa Stm | T11/483641 | T | | | | | | |
| W99729LA | grey cry r lith r silicified welded ignimbrite lithic | WSI | Haukawakawa Stm | T11/483641 | T | | | | | | |
| W99729LB | grey fine phyric glassy rhyolite lava lithic | RPP | Haukawakawa Stm | T11/483641 | T | | | | | | |
| W99730 | brown moderately sorted volcaniclastic siltstone | wh | Haukawakawa Stm | T11/483640 | | | | | | | |
| W99731 | brown moderately sorted volcaniclastic siltstone | wh | Haukawakawa Stm | T11/482638 | T | | | | | | |
| W99732 | dk grey crs phyric andesite lava | ot | ridgeline NW of Haukawakawa Stm | T11/481637 | T | M | P | F | | | |
| W99733 | dk grey crs phyric andesite lava | ot | ridge NW of Rangihau Stm | T11/484636 | T | | | | | | K |
| W99734 | dk grey crs phyric andesite lava | ot | 200m E along ridge | T11/485637 | T | | | | | | |
| W99735 | grey glassy flow b rhyolite lava | ku | S side of Rangihau valley | T11/487635 | T | | | | | | |
| W99736 | grey cry r lith r weakly welded ignimbrite | wes-1 | E side of Rangihau Stm | T11/496645 | T | | | | | | |
| W99737 | lt grey fine-phyric rhyolite lava | ku | Rangihau Stm | T11/494642 | T | M | | F | | I | |
| W99738 | grey flow b devit rhyolite lava | ku | Rangihau Stm | T11/493640 | T | | | | | | |
| W99739 | cream v.p.a. pum p lith p weakly welded ignimbrite | wes-1 | Rangihau Stm | T11/493640 | | | | | | | |
| W99740 | cream silicified pum r ignimbrite | wes-1 | ridgeline W of Rangihau Stm | T11/492640 | | | | | | | |
| W99740LA | cream silicified fine phyric rhyolite lava lithic | SRL | ridgeline W of Rangihau Stm | T11/492640 | T | | | | | | |
| W99741 | dk grey crs phyric andesite lava | ot | ridgeline W of Rangihau Stm | T11/491639 | T | | | | | | |
| W99742 | cream moderately sorted vitric ash tuff | wes-2 | W ridge above Rangihau Stm | T11/491638 | T | | | | | | |
| W99743 | grey flow b lithoidal rhyolite lava | ku | Rangihau Stm | T11/492637 | T | | | F | | | |
| W99744 | grey flow b fine phyric rhyolite lava | ku | Rangihau Stm | T11/492637 | T | | | | | | |
| W99745 | brown/blue flow b rhyolite lava | ku | Rangihau-tributary confluence | T11/493636 | T | | | F | | | |
| W99746 | grey/brown flow b rhyolite lava | ku | Rangihau-tributary confluence | T11/493636 | T | M | | | | | |
| W99747 | dk grey med phyric andesite lava | ot | ridgeline SE of Rangihau Stm | T11/493635 | T | | | | | | |
| W99748 | dk grey crs phyric andesite lava | ot | tributary of Rangihau Stm | T11/495636 | T | | | | | | |
| W99749 | cream pum r lith p ignimbrite | wes-1 | tributary of Rangihau Stm | T11/494637 | | | | | | | |
| W99750 | green/grey altered rhyolite lava | h | tributary of Rangihau Stm | T11/493637 | T | | | | D | | |
| W99751 | lt grey fine phyric f band rhyolite lava | ku | ridgeline SE of Rangihau Stm | T11/495640 | T | | | | | | |
| W99752 | cream/white altered rhyolite lava | h | 640 s.h. | T11/506621 | T | | | | | | |
| W99753 | grey/cream fine phyric spher silicified rhyolite lava | h | Rangihau Rd Track | T11/506619 | T | | | | | | |
| W99754 | grey weath med phyric rhyolite lava | h | tributary of Rangihau Stm | T11/498620 | T | | | | D | | |
| W99755 | grey/cream weath rhyolite lava | h | tributary of Rangihau Stm | T11/498619 | T | | | | D | | |
| W99756 | cream silicified rhyolite lava | h | tributary of Rangihau Stm | T11/494619 | | | | | | | |
| W99757 | cream weathered rhyolite lava | h | tributary of Rangihau Stm | T11/492621 | T | | | | D | | |
| W99758 | lt grey pum r lith r weath ignimbrite | wes-1 | tributary of Rangihau Stm | T11/489622 | | | | | | | |
| W99758LA | grey vesicular weath andesite lava lithic | APP | tributary of Rangihau Stm | T11/489622 | | | | | | | |
| W99758LB | grey poorly sorted indurated volcaniclastic breccia lithic | VBR | tributary of Rangihau Stm | T11/489622 | | | | | | | |
| W99758LC | grey med phyric andesite lava lithic | APP | tributary of Rangihau Stm | T11/489622 | | | | | | | |
| W99759 | lt grey med phyric rhyolite lava | ku | tributary of Rangihau Stm | T11/486626 | | | | | | | |
| W99760 | grey/brown flow b fine phyric rhyolite lava | ku | Rangihau Stm | T11/486632 | T | | | | | | |
| W99761 | cream fine phyric rhyolite lava | ku | ridgeline SE of Rangihau Stm | T11/491630 | | | | | | | |
| W99762 | brown/grey lith r weakly welded (LCZ) ignimbrite | wes-1 | E side of Rangihau Stm | T11/497655 | T | | | | | | |
| W99762LA | dk green silicified lith r welded ignimbrite lithic | SSI | E side of Rangihau Stm | T11/497655 | T | | | | | | |
| W99762LB | grey fine phyric weak silicified rhyolite lava lithic | SRL | E side of Rangihau Stm | T11/497655 | T | | | | | | |
| W99762LC | green silicified lith r welded ignimbrite lithic | SSI | E side of Rangihau Stm | T11/497655 | T | | | | | | |
| W99762LD | lt grey med phyric andesite lava lithic | APP | E side of Rangihau Stm | T11/497655 | | | | | | | |
| W99762LE | lt blue/grey fine phyric rhyolite lava lithic | RPP | E side of Rangihau Stm | T11/497655 | T | | | | | | |
| W99762LF | blue/grey fine phyric rhyoltie lava lithic | RPP | E side of Rangihau Stm | T11/497655 | T | | | | | | |
| W99762LG | brown cry r pum p welded ignimbrite lithic | OA | E side of Rangihau Stm | T11/497655 | T | | | | | | |
| W99762LH | grey cry r pum r silicified welded ignimbrite lithic | WSI | E side of Rangihau Stm | T11/497655 | T | | | | | | |
| W99762LI | grey cry r lith r silicified welded ignimbrite lithic | WSI | E side of Rangihau Stm | T11/497655 | T | | | | | | |
| W99762LJ | cream/orange silicified lentic pum welded ignimbrite lithic | WSI | E side of Rangihau Stm | T11/497655 | T | | | | | | |
| W99762LK | grey med phyric f band glassy rhyolite lava lithic | RPP | E side of Rangihau Stm | T11/497655 | T | | | | | | |
| W99763 | grey cry r pum p weakly welded ignimbrite | wes-1 | E side of Rangihau Stm | T11/497655 | T | | | | | | |
| W99763LA | grey silicified welded ignimbrite lithic | WSI | E side of Rangihau Stm | T11/497655 | T | | | | | | |
| W99763LB | lt blue/grey f band fine phyric amygd rhyolite lava lithic | RPP | E side of Rangihau Stm | T11/497655 | T | | | | | | |

| W No. | Lithology | Unit | Location | Grid Ref. | T | M | P | F | D | I | K |
|---|---|---|---|---|---|---|---|---|---|---|---|
| W99763LC | brown/cream pum r lith r welded ignimbrite lithic | UND | E side of Rangihau Stm | T11/497655 | T | | | | | | |
| W99763LD | lt grey med phyric dacite lava lithic | DPP | E side of Rangihau Stm | T11/497655 | T | | | | | | |
| W99763LE | lt grey fine phyric dacite lava lithic | DPP | E side of Rangihau Stm | T11/497655 | T | | | | | | |
| W99763LF | green silicified lith r welded ignimbrite lithic | WSI | E side of Rangihau Stm | T11/497655 | T | | | | | | |
| W99763LG | brown/cream pum r lith r welded ignimbrite lithic | UND | E side of Rangihau Stm | T11/497655 | T | | | | | | |
| W99763LH | lt blue/grey f band fine phyric rhyolite lava lithic | RPP | E side of Rangihau Stm | T11/497655 | T | | | | | | |
| W99763LI | lt blue/grey weak vesic fine phyric rhyolite lava lithic | RPP | E side of Rangihau Stm | T11/497655 | T | | | | | | |
| W99763LJ | lt blue/grey f band fine phyric rhyolite lava lithic | RPP | E side of Rangihau Stm | T11/497655 | T | | | | | | |
| W99763LK | grey silicified lith r welded ignimbrite lithic | WSI | E side of Rangihau Stm | T11/497655 | T | | | | | | |
| W99763LL | lt grey med phyric dacite lava lithic | DPP | E side of Rangihau Stm | T11/497655 | T | | | | | | |
| W99763LM | lt grey med phyric rhyolite lava lithic | RPP | E side of Rangihau Stm | T11/497655 | T | | | | | | |
| W99763LN | grey fine phyric rhyolite lava lithic | RPP | E side of Rangihau Stm | T11/497655 | T | | | | | | |
| W99764 | brown lith p weakly welded ignimbrite | wes-1 | E side of Rangihau Stm | T11/497655 | T | | | | | | |
| W99764LA | lt blue/grey fine phyric rhyolite lava lithic | RPP | E side of Rangihau Stm | T11/497655 | T | | | | | | |
| W99764LB | lt blue/grey cry r lith r welded ignimbrite lithic | WPI | E side of Rangihau Stm | T11/497655 | T | | | | | | |
| W99765 | grey cry r pum r weakly welded ignimbrite | wes-1 | E side of Rangihau Stm | T11/497655 | T | | | | | | |
| W99765LA | grey pum r welded ignimbrite lithic | UND | E side of Rangihau Stm | T11/497655 | T | | | | | | |
| W99765LB | lt blue/grey fine phyric rhyolite lava lithic | RPP | E side of Rangihau Stm | T11/497655 | T | | | | | | |
| W99765LC | lt blue/grey fine phyric rhyolite lava lithic | RPP | E side of Rangihau Stm | T11/497655 | T | | | | | | |
| W99765LD | grey/lt blue med phyric dacite lava lithic | DPP | E side of Rangihau Stm | T11/497655 | T | | | | | | |
| W99765LE | brown/cream vitric tuff lithic | RVT | E side of Rangihau Stm | T11/497655 | T | | | | | | |
| W99765LF | grey/brown cry r pum p welded ignimbrite lithic | UND | E side of Rangihau Stm | T11/497655 | T | | | | | | |
| W99766 | grey mod sorted pum r mm-laminated volcaniclastic siltstone | wh | Rangihau-Slip Stm confluence | T11/498652 | T | | | | | | |
| W99767 | brown lacustrine siltstone | wh | Slip Stm | T11/501648 | | | | | | | |
| W99768 | brown lacustrine siltstone | wh | Slip Stm | T11/503647 | | | | | | | |
| W99769 | grey pum r vitric tuff | wh | Slip Stm | T11/499650 | T | | | | | | |
| W99770 | grey/brown pum r welded ignimbrite | wes-1 | N side of Slip Stm | T11/498652 | T | | | | | | |
| W99771 | grey pum r welded ignimbrite | wes-1 | N side of Slip Stm | T11/498652 | T | | | | | | |
| W99772 | grey pum p bedded welded ignimbrite | wes-1 | N side of Slip Stm | T11/498652 | T | | | | | | |
| W99772LA | grey/blue spher fine phyric rhyolite lava lithic | RPP | N side of Slip Stm | T11/498652 | T | | | | | | |
| W99772LB | lt grey/lt blue fine phyric silicified rhyolite lava lithic | RPP | N side of Slip Stm | T11/498652 | T | | | | | | |
| W99772LC | blue/grey fine phyric rhyolite lava lithic | RPP | N side of Slip Stm | T11/498652 | T | | | | | | |
| W99772LD | brown/cream silicified incip welded ignimbrite lithic | WSI | N side of Slip Stm | T11/498652 | T | | | | | | |
| W99772LE | grey spher fine phyric rhyolite lava lithic | RPP | N side of Slip Stm | T11/498652 | T | | | | | | |
| W99772LF | grey spher fine phyric rhyolite lava lithic | RPP | N side of Slip Stm | T11/498652 | T | | | F | | | |
| W99772LG | brown silicified vitric tuff lithic | RVT | N side of Slip Stm | T11/498652 | T | | | | | | |
| W99772LH | lt blue/grey fine phyric rhyolite lava lithic | RPP | N side of Slip Stm | T11/498652 | T | | | | | | |
| W99773 | ceram pum r lith p weakly welded ignimbrite | wes-1 | Rangihau Stm | T11/497650 | T | | | | | | |
| W99773LA | grey/cream lith r pum r welded ignimbrite lithic | WEB | Rangihau Stm | T11/497650 | T | M | | | | | |
| W99773LB | grey/lt blue med phyric dacite lava lithic | DPP | Rangihau Stm | T11/497650 | T | | | | | | |
| W99773LC | blue/grey fine phyric rhyolite lava lithic | RPP | Rangihau Stm | T11/497650 | T | | | | | | |
| W99773LD | grey/brown med phyric rhyolite lava lithic | RPP | Rangihau Stm | T11/497650 | T | | | | | | |
| W99773LE | brown pum r welded ignimbrite lithic | UND | Rangihau Stm | T11/497650 | T | | | | | | |
| W99773LF | grey med phyric rhyolite lava lithic | RP | Rangihau Stm | T11/497650 | T | | | | | | |
| W99773LG | grey fine phyric rhyolite lava lithic | RPP | Rangihau Stm | T11/497650 | T | | | | | | |
| W99774 | cream pum r weakly welded ignimbrite | wes-1 | E side of Haukawakawa Stm | T11/486642 | T | | | | | | |
| W99775 | cream volcaniclastic lacustrine siltstone | wh | tributary of Haukawakawa Stm | T11/487646 | | | | | | | |
| W99776 | grey pum r weakly welded ignimbrite | wes-1 | N side of stm | T11/487644 | T | | | | | | |
| W99777 | lt grey pum r lith p weakly welded ignimbrite | wes-1 | N side of stm | T11/487644 | T | | | | | | |
| W99778 | brown massive lacustrine siltstone | wh | NW side of Haukawakawa Stm | T11/487643 | | | | | | | |
| W99779 | pink/grey med phyric rhyolite lava | uj | end of Welcome Jack Track | T11/512622 | T | | | | | | |
| W99780 | lt grey pum r weakly welded ignimbrite | wes-4 | Welcome Jack Track | T11/510622 | T | | | | | | |
| W99780LA | lt grey crs f band fine phyric rhyolite lava lithic | RP | Welcome Jack Track | T11/510622 | T | | | | | | |
| W99780LB | pink/grey fine phyric rhyolite lava-crystal tuff lithic | RP | Welcome Jack Track | T11/510622 | T | | | | | | |
| W99780LC | grey/cream f band fine phyric rhyolite lava lithic | rpb | Welcome Jack Track | T11/510622 | T | | | | | | |
| W99780LD | grey/green weak silicified pum r welded ignimbrite lithic | WEB | Welcome Jack Track | T11/510622 | T | | | | | | |
| W99780LE | black glassy med phyric obsidian lithic | RP | Welcome Jack Track | T11/510622 | T | M | | F | | | |
| W99781 | white/cream silicified rhyolite lava | h | on Rangihau Rd Track | T11/616506 | T | | | | D | | |
| W99782 | grey/brown altered rhyolite lava | ks | on Moss Creek Hut Track | T11/504604 | T | | | | | | |
| W99783 | brown/grey med. phyric rhyolite lava | ks | on Rangihau Rd Track | T11/505608 | T | | | F | | I | |
| W99784 | cream weath med. phyric rhyolite lava | ks | SE of 716m s.h., on Rangihau Rd Track | T11/506611 | T | | | | | | |
| W99785 | cream/white silicified rhyolite lava | h | on Rangihau Rd Track | T11/506613 | T | | | | D | | |
| W99786 | grey crs ash sized vitric tuff | wes-1a | Slip Stream Track | T11/507643 | T | | | | | | |
| W99787 | cream mm-laminated lacustrine siltstone | wh | Slip Stm | T11/508641 | T | | | | | | |
| W99788 | grey med phyric rhyolite lava | ss | Slip Stm | T11/508641 | T | M | P | F | | I | |
| W99789 | grey massive lacustrine siltstone | wh | Slip Stm | T11/507641 | T | | | | | | |
| W99790 | brown massive lacustrine siltstone | wh | 20 m downstm of W99789; Slip Stm | T11/507641 | T | | | | | | |
| W99791 | grey/black carbonaceous bedded lacustrine siltstone | wh | Slip Stm | T11/507641 | T | | | | | | |
| W99792 | grey laminated-massive lacustrine siltstone | wh | Slip Stm | T11/506641 | T | | | | | | |
| W99793 | brown pum r cry r lacustrine siltstone | wh | 30 m downstm of W99792; Slip Stm | T11/505642 | T | | | | | | |
| W99794 | lt grey massive well sorted volcaniclastic siltstone | wh | downstm of Slip Stm-Mine Ck confluence | T11/505643 | T | | | | | | |
| W99795 | well laminated-massive lacustrine siltstone | wh | downstm of W99794 | T11/504643 | | | | | | | |
| W99796 | dk grey crs phyric andesite lava dike | ot | on Rangihau Rd Track | T11/497648 | T | M | | | | | |
| W99797 | dk grey crs phyric andesite lava dike | ot | on Rangihau Rd Track | T/11499638 | T | | | F | | | |
| W99798 | grey weath crs phyric andesite lava | ot | on Rangihau Rd Track | T11/501627 | T | | | | | | |
| W99799 | dk grey crs phyric andesite lava | ot | on Rangihau Rd Track | T11/501625 | T | | | F | | | |
| W99800 | grey hydro alt. pum r lith p ignimbrite | h | Mine Creek tributary | T11/506625 | T | | | | | | |
| W99801 | cream silicified rhyolite lava | h | Mine Creek tributary | T11/506626 | | | | | | | |
| W99802 | grey/cream hydro alt. rhyolite lava | h | Welcome Jack Battery track | T11/506627 | T | | | | D | | |
| W99803 | pink/grey weakly silicified rhyolite lava | h | Welcome Jack Battery track | T11/507627 | | | | | | | |
| W99804 | lithoidal rhyolite lava | uj | 30m upstm of Welcome Jack battery | T11/508627 | | | | | | | |
| W99805 | grey flow b mineralised fine phyric rhyolite lava | h | ridgeline NW of Welcome Jack mine | T11/509627 | T | | | | | | |
| W99806 | grey med phyric rhyolite lava | uj | ridgeline N of Welcome Jack mine | T11/509629 | T | | | | | | |
| W99807 | pink/cream fine phyric rhyolite lava | uj | ridgeline NW of Welcome Jack mine | T11/508632 | T | M | | F | | | |
| W99808 | grey weath silicified rhyolite lava | uj | small waterfall, on Slip Stm | T11/510633 | | | | | | | |
| W99809 | grey weakly welded pum r ignimbrite | h | 50 m downstm of W99808, Slip Stm | T11/511633 | | | | | D | | |
| W99809LA | grey incip vesic fine phyric hydro. alt. rhyolite lava | h | 50 m downstm of W99808, Slip Stm | T11/511633 | | | | | | | |
| W99809LB | grey/cream mottled hydro. atl. fine phyric rhyolite lava | h | 50 m downstm of W99808, Slip Stm | T11/511633 | | | | | | | |
| W99809LC | grey/green altered mod sorted crystal tuff | PVT | 50 m downstm of W99808, Slip Stm | T11/511633 | | | | | | | |

| W No. | Lithology | Unit | Location | Grid Ref. | T | M | P | F | D | I | K |
|---|---|---|---|---|---|---|---|---|---|---|---|
| W99809LD | grey silicified fine phyric rhyolite lava | SRL | 50 m downstm of W99808, Slip Stm | T11/511633 | | | | | | | |
| W99810 | weath spher rhyolite lava | h | 10 downstm of W99809, Slip Stm | T11/511633 | | | | | | | |
| W99811 | blue/grey fine phyric rhyolite lava | h | Slip Stm | T11/512635 | T | | | | D | | |
| W99812 | brown massive basal lacustrine sed | wh | on Farm Track | T11/487650 | | | | | | | |
| W99813 | grey/lt brown lith r lapilli crystal tuff | wh | on Farm Track | T11/487650 | T | | | | | | |
| W99814 | grey massive lacustrine siltstone | wh | on Farm Track | T11/487650 | | | | | | | |
| W99815 | lt grey pum r lith p weakly welded ignimbrite | wes-l | 10m up Farm track from WW99812 | T11/487650 | T | | | | | | |
| W99816 | dk grey crs phyric andesite lava | ot | upper Farm paddock | T11/484647 | T | M | P | F | | | K |
| W99817 | dk grey crs phyric andesite lava | ot | head of tributary stm | T11/479648 | T | | | | | | |
| W99818 | grey massive well sorted volcaniclastic siltstone | wh | 50m downstm of W99817 | T11/479647 | | | | | | | |
| W99819 | grey massive well sorted volcaniclastic siltstone | wh | confluence of two tributary stms | T11/478644 | | | | | | | |
| W99820 | cream massive well sorted volcaniclastic siltstone | wh | 35m upstm of W99819 | T11/478644 | | | | | | | |
| W99821 | grey pum r weakly welded ignimbrite | wes | 35m upstm of W99819 | T11/478644 | T | | | | | | |
| W99822 | grey weath cry r lith r pum p weakly welded ignimbrite | wes | 35m upstm of W99819 | T11/478644 | T | | | | | | |
| W99823 | cream/grey cataclaysite | wes | 35m upstm of W99819 | T11/478644 | | | | | | | |
| W99824 | brown pum r lith p mod. sheared weakly welded ignimbrite | wes | 35m upstm of W99819 | T11/478644 | T | | | | | | |
| W99825 | grey crs ash mod sorted vitric tuff | wes | waterfall upstm of W99820, tributary stm | T11/477645 | T | | | | | | |
| W99826 | brown moderately sorted volcaniclastic siltstone | wh | tributary stm | T11/476641 | T | | | | | | |
| W99827 | lacustrine siltstone | wh | tributary stm | T11/478642 | | | | | | | |
| W99828 | brown moderately sorted silicified volcaniclastic siltstone | wh | 80m downstm of tributary confluence | T11/480642 | | | | | | | |
| W99829 | grey massive volcaniclastic siltstone | wh | 50m downstm of W99828, tributary stm | T11/481642 | | | | | | | |
| W99830 | lt grey massive volcaniclastic siltstone | wh | downstm of W99829, tributary stm | T11/481642 | | | | | | | |
| W99831 | grey pum r lith r weakly welded ignimbrite | wes-l | 30m upstm of waterfall; tributary stm | T11/482642 | T | | | | | | |
| W99831LA | cream indurated moderately sorted vitric tuff lithic | RVT | 30m upstm of waterfall; tributary stm | T11/482642 | T | | | | | | |
| W99831LB | grey fine phyric incip vesic glassy rhyolite lava lithic | RPP | 30m upstm of waterfall; tributary stm | T11/482642 | T | | | | | | |
| W99831LC | grey pum r welded ignimbrite lithic | UND | 30m upstm of waterfall; tributary stm | T11/482642 | T | | | | | | |
| W99831LD | cream incip silicified welded ignimbrite lithic | WSI | 30m upstm of waterfall; tributary stm | T11/482642 | T | | | | | | |
| W99831LE | grey pum r welded ignimbrite lithic | UND | 30m upstm of waterfall; tributary stm | T11/482642 | T | | | | | | |
| W99831LF | brown lith r welded ignimbrite lithic | UND | 30m upstm of waterfall; tributary stm | T11/482642 | T | | | | | | |
| W99831LG | grey glassy fine phyric rhyolite lava lithic | RPP | 30m upstm of waterfall; tributary stm | T11/482642 | T | | | | | | |
| W99831LH | dk grey scoria r welded ignimbrite lithic | UND | 30m upstm of waterfall; tributary stm | T11/482642 | T | | | | | | |
| W99831LI | grey glassy incip vesic fine phyric rhyolite lava lithic | RPP | 30m upstm of waterfall; tributary stm | T11/482642 | T | M | | | | | |
| W99832 | grey/pink fine phyric silicified rhyolite lava | ku | on Rangihau Rd Track | T11/504622 | | | | | | | |
| W99833 | grey/pink fine phyric silicified rhyolite lava | ku | on Rangihau Rd Track | T11/506621 | T | | | | D | | |
| W99834 | lt grey well jointed fine phyric rhyolite lava | uj | 30m S of 691m s.h. | T11/511623 | T | M | P | F | | I | |
| W99835 | grey med phyric rhyolite lava | uj | 691m s.h. | T11/511623 | T | | | F | | | K |
| W99836 | grey/pink spher fine phyric rhyolite lava | uj | ridgeline to E of 691m S.H. | T11/512623 | T | | | | | | |
| W99837 | lt grey/cream silicified rhyolite lava | h | ridgeline to SW of the Big Slip | T11/513630 | | | | | D | | |
| W99838 | cream hydro alt. rhyolite lava | h | debris flow below the Big Slip | T11/513637 | T | | | | D | | |
| W99839 | grey/blue med phyric rhyolite lava | kb | E side of rhyolite | T11/497642 | T | M | | F | | I | |
| W99840 | grey/blue med phyric rhyolite lava | kb | tributary of Rangihau river | T11/497641 | T | | | | | | |
| W99841 | grey/blue pum r lith p weakly welded ignimbrite | h | tributary of Rangihau Stm | T11/497641 | T | | | | | | |
| W99841LA | cream fine phyric silicified rhyolite lava lithic | h | tributary of Rangihau Stm | T11/497641 | | | | | | | |
| W99841LB | lt grey mod indurated volcaniclastic siltstone lithic | VSI | tributary of Rangihau Stm | T11/497641 | | | | | | | |
| W99841LC | grey fine phyric weath dacite lava lithic | DPP | tributary of Rangihau Stm | T11/497641 | | | | | | | |
| W99841LD | grey weath fine phyric dacite lava lithic | DPP | tributary of Rangihau Stm | T11/497641 | | | | | | | |
| W99842 | brown massive mod sorted vitric tuff | h | tributary of Rangihau Stm | T11/495641 | | | | | | | |
| W99843 | cry r pum p lith p weakly welded ignimbrite | h | tributary of Rangihau Stm | T11/495642 | | | | | | | |
| W99844 | pum r weakly welded ignimbrite | h | tributary of Rangihau Stm | T11/495642 | | | | | | | |
| W99845 | lt grey lith r pum r v.p.a weakly welded ignimbrite | wes-l | Rangihau Stm | T11/494643 | T | | | | | | |
| W99845LA | cream lith r welded ignimbrite lithic | UND | Rangihau Stm | T11/494643 | T | | | | | | |
| W99845LB | grey med grained equigranular micro-granodiorite lithic | PLU | Rangihau Stm | T11/494643 | T | | | | | | |
| W99845LC | cream/brown lith p silicified welded ignimbrite lithic | WSI | Rangihau Stm | T11/494643 | T | | | | | | |
| W99845LD | cream lith r pum r welded ignimbrite lithic | UND | Rangihau Stm | T11/494643 | | | | | | | |
| W99845LE | cream vitric tuff lithic | RVT | Rangihau Stm | T11/494643 | T | | | | | | |
| W99845LF | lt brown/cream lith p vitric tuff lithic | RVT | Rangihau Stm | T11/494643 | | | | | | | |
| W99845LG | cream/brown weath welded ignimbrite lithic | UND | Rangihau Stm | T11/494643 | | | | | | | |
| W99845LH | cream silicified rhyolite lava lithic | SRL | Rangihau Stm | T11/494643 | T | | | | | | |
| W99845LI | cream/brown fine phyric silicified rhyolite lava lithic | SRL | Rangihau Stm | T11/494643 | | | | | | | |
| W99845LJ | cream pum r welded ignimbrite lithic | WSI | Rangihau Stm | T11/494643 | T | | | | | | |
| W99845LK | cream mod indurated volcaniclastic siltstone lithic | VSI | Rangihau Stm | T11/494643 | | | | | | | |
| W99845LL | grey/cream fine phyric rhyolite lava lithic | SRL | Rangihau Stm | T11/494643 | T | | | | | | |
| W99845LM | cream/brown lith r welded ignimbrite lithic | UND | Rangihau Stm | T11/494643 | T | | | | | | |
| W99845LN | cream pum r welded ignimbrite lithic | UND | Rangihau Stm | T11/494643 | | | | | | | |
| W99845LO | cream pum r welded ignimbrite lithic | MAN | Rangihau Stm | T11/494643 | T | | | | | | |
| W99846 | lt grey lith r pum r weakly welded ignimbrite | wi | Webb Creek | T12/488573 | T | | | | | | |
| W99846LA | dk grey med phyric rhyolite lava lithic | RPP | Webb Creek | T12/488573 | T | | | | | | |
| W99846LB | grey lith r incip silicified welded ignimbrite lithic | WSI | Webb Creek | T12/488573 | T | | | | | | |
| W99846LC | dk grey amygda spheru silici med phyric rhyolite lava lithic | RPP | Webb Creek | T12/488573 | T | | | | | | |
| W99846LD | grey silicified lith r cry p welded ignimbrite lithic | WSI | Webb Creek | T12/488573 | T | | | | | | |
| W99846LE | grey glassy fine phyric rhyolite lava lithic | RPP | Webb Creek | T12/488573 | T | | | | | | |
| W99846LF | grey glassy incip vesic fine phyric rhyolite lava lithic | RPP | Webb Creek | T12/488573 | T | | | | | | |
| W99846LG | pink/brown cry r pum p vitric tuff lithic | RVT | Webb Creek | T12/488573 | T | | | | | | |
| W99846LH | red/brown pum r lith r lentic welded ignimbrite lithic | MAN | Webb Creek | T12/488573 | T | M | | | | | |
| W99846LI | dk brown cry r welded ignimbrite lithic | WSI | Webb Creek | T12/488573 | T | | | | | | |
| W99847 | cream/grey weak laminated lacustrine siltstone | wt | Webb Creek | T12/488573 | | | | | | | |
| W99848 | lt grey lith r pum r cry r weakly welded ignimbrite | wes-l | 15 m off Track, in Webb Creek | T12/495577 | T | | | | | | |
| W99848LA | grey med phyric rhyolite lava lithic | RPP | 15 m off Track, in Webb Creek | T12/495577 | T | | | | | | |
| W99848LB | dk grey med phyric andes ite lava lithic | DPP | 15 m off Track, in Webb Creek | T12/495577 | T | | | | | | |
| W99848LC | grey pum r welded ignimbrite lithic | WSI | 15 m off Track, in Webb Creek | T12/495577 | | | | | | | |
| W99848LD | cream massive vitric ash tuff lithic | RVT | 15 m off Track, in Webb Creek | T12/495577 | T | | | | | | |
| W99848LE | grey med phyric dacite lava lithic | DPP | 15 m off Track, in Webb Creek | T12/495577 | T | | | | | | |
| W99848LF | grey mm f band fine phyric rhyolite lava lithic | RPP | 15 m off Track, in Webb Creek | T12/495577 | T | | | | | | |
| W99848LG | red/orange poor vesic fine phyric andesite lava lithic | APP | 15 m off Track, in Webb Creek | T12/495577 | T | M | | | | | |
| W99849 | lt grey lith r pum r weakly welded ignimbrite | wes-l | off Track, in Webb Creek | T12/495578 | T | | | | | | |
| W99849LA | cream bedded well sorted vitric tuff lithic | RVT | off Track, in Webb Creek | T12/495578 | T | | | | | | |
| W99849LB | black med phyric dacite lava lithic | DPP | off Track, in Webb Creek | T12/495578 | T | | | | | | |
| W99849LC | grey spher med phyric rhyolite lava lithic | RPP | off Track, in Webb Creek | T12/495578 | T | | | F | | | |
| W99849LD | red/brown med phyric rhyolite lava lithic | RPP | off Track, in Webb Creek | T12/495578 | T | | | | | | |

| W No. | Lithology | Unit | Location | Grid Ref. | T | M | P | F | D | I | K |
|---|---|---|---|---|---|---|---|---|---|---|---|
| W99849LE | orange v.p.a pum r lith p weakly welded ignimbrite lithic | UND | off Track, in Webb Creek | T12/495578 | T | | | | | | |
| W99849LF | cream/lt brown mod sort bedded vitric ash tuff lithic | RVT | off Track, in Webb Creek | T12/495578 | T | | | | | | |
| W99849LG | cream poorly sorted vitric tuff lithic | RVT | off Track, in Webb Creek | T12/495578 | T | | | | | | |
| W99849LH | brown/orange pum r lith r welded ignim lithic | MAN | off Track, in Webb Creek | T12/495578 | T | M | | | | | |
| W99849LI | lt grey pum r welded ignimbrite lithic | WEB | off Track, in Webb Creek | T12/495578 | T | M | | | | | |
| W99849LJ | lt grey indurated pum p lith r cry r sandstone lithic | VSA | off Track, in Webb Creek | T12/495578 | T | | | | | | |
| W99849LK | lt grey lith r pum r incip silicified welded ignimbrite lithic | WSI | off Track, in Webb Creek | T12/495578 | T | | | | | | |
| W99850 | lt grey pum r lith r weakly welded ignimbrite | wes-1 | Rangihau Rd Track | T12/512586 | T | | | F | | | |
| W99850LA | cream/lt grey fine phyric rhyolite lava lithic | RPP | Rangihau Rd Track | T12/512586 | T | | | | | | |
| W99850LB | lt blue/pink med phyric dacite lava lithic | RP | Rangihau Rd Track | T12/512586 | T | | | | | | |
| W99850LC | red/brown med phyric rhyolite lava lithic | RPP | Rangihau Rd Track | T12/512586 | T | | | | | | |
| W99850LD | lt blue/grey med phyric rhyolite lava lithic | RPP | Rangihau Rd Track | T12/512586 | T | | | | | | |
| W99850LE | lt blue/grey cry r vitric tuff lithic | RVT | Rangihau Rd Track | T12/512586 | T | | | | | | |
| W99850LF | lt blue/grey med phyric rhyolite lava lithic | RPP | Rangihau Rd Track | T12/512586 | T | | | | | | |
| W99851 | lt grey/cream pum r weakly welded ignimbrite | wes-1 | Rangihau Rd Track | T12/512593 | T | | | | | | |
| W99851LA | dk grey med phyric rhyolite lava lithic | RPP | Rangihau Rd Track | T12/512593 | T | | | | | | |
| W99851LB | lt blue/grey med phyric rhyolite lava lithic | RPP | Rangihau Rd Track | T12/512593 | T | | | | | | |
| W99851LC | grey/cream pum p lith r welded ignimbrite lithic | WEB | Rangihau Rd Track | T12/512593 | T | | | | | | |
| W99852 | lt grey/cream pum r weakly welded ignimbrite | wes-4 | Rangihau Rd Track | T12/512593 | T | | | | | | |
| W99852LA | grey/lt blue med phyric rhyolite lava lithic | RPP | Rangihau Rd Track | T12/512593 | T | | | | | | |
| W99852LB | brown/red med phyric rhyolite lava lithic | RPP | Rangihau Rd Track | T12/512593 | | | | | | | |
| W99852LC | lt blue/grey fine phyric rhyolite lava lithic | RPP | Rangihau Rd Track | T12/512593 | T | | | | | | |
| W99852LD | lt blue/grey med phyric rhyolite lava lithic | RPP | Rangihau Rd Track | T12/512593 | T | | | | | | |
| W99853 | brown well sorted lithified ash sized vitric tuff | wes-2 | Rangihau Rd Track | T12/512593 | T | | | | | | |
| W99854 | cream pum r crs ash tuff | wes-2 | Rangihau Rd Track | T12/512593 | T | M | | | | | |
| W99855 | grey well sorted ash tuff | wes-2 | Rangihau Rd Track | T12/512593 | T | | | | | | |
| W99856 | lt grey pum r cry r weakly welded ignimbrite | wes-1 | Rangihau Rd Track | T12/512593 | T | M | | | | | |
| W99856LA | lt blue/grey med phyric rhyolite lava lithic | RPP | Rangihau Rd Track | T12/512593 | T | | | | | | |
| W99856LB | brown spher glassy fine phyric rhyolite lava lithic | RPP | Rangihau Rd Track | T12/512593 | T | | | | | | |
| W99856LC | red/brown med phyric rhyolite lava lithic | RPP | Rangihau Rd Track | T12/512593 | T | | | | | | |
| W99856LD | brown/red fine phyric rhyolite lava lithic | RPP | Rangihau Rd Track | T12/512593 | T | | | | | | |
| W99856LE | brown/red fine phyric f band rhyolite lava lithic | RPP | Rangihau Rd Track | T12/512593 | T | | | | | | |
| W99856LF | lt blue/grey med phyric rhyolite lava lithic | RPP | Rangihau Rd Track | T12/512593 | | | | | | | |
| W99856LG | grey pum r lenticular welded ignimbrite lithic | WSI | Rangihau Rd Track | T12/512593 | T | | | | | | |
| W99856LH | grey med phyric rhyolite lava lithic | RPP | Rangihau Rd Track | T12/512593 | T | | | | | | |
| W99857 | grey/pink mm scale flow b amyg rhyolite lava | kt | Rangihau Rd Track | T12/512593 | T | | | | | | |
| W99858 | grey flow b fine phyric rhyolite lava | kt | Rangihau Rd Track | T12/511594 | T | M | | F | | | |
| W99859 | grey pum r weakly welded ignimbrite | wes-1 | Kauaeranga River | T12/508596 | T | | | | | | |
| W99859LA | grey/lt blue med phyric rhyolite lava lithic | RPP | Kauaeranga River | T12/508596 | T | | | | | | |
| W99859LB | brown pum r lith r welded ignimbrite lithic | MAN | Kauaeranga River | T12/508596 | T | | | | | | |
| W99859LC | dk grey glassy fine phyric rhyolite lava lithic | RPP | Kauaeranga River | T12/508596 | T | | | F | | | |
| W99859LD | grey glassy fine phyric rhyolite lava lithic | RPP | Kauaeranga River | T12/508596 | T | | | | | | |
| W99859LE | grey/brown incip vesicular fine phyric rhyolite lava lithic | RPP | Kauaeranga River | T12/508596 | T | | | | | | |
| W99859LF | grey incip vesicular glassy fine phyric rhyolite lava lithic | RPP | Kauaeranga River | T12/508596 | T | | | | | | |
| W99859LG | grey glassy fine phyric rhyolite lava lithic | RPP | Kauaeranga River | T12/508596 | T | | | | | | |
| W99859LH | lt grey glassy fine phyric rhyolite lava lithic | RPP | Kauaeranga River | T12/508596 | T | | | | | | |
| W99860 | lt grey pum r weakly welded ignimbrite | wes-1 | Kauaeranga River | T12/507595 | T | | | | | | |
| W99860LA | grey med phyric f band rhyolite lava lithic | RP | Kauaeranga River | T12/507595 | T | | | | | | |
| W99860LB | lt grey vesicular fine phyric rhyolite lava lithic | RPP | Kauaeranga River | T12/507595 | T | | | | | | |
| W99860LC | cream indurated lith p vitric tuff lithic | RVT | Kauaeranga River | T12/507595 | T | | | | | | |
| W99861 | lt grey pum r lithic r weakly welded ignimbrite | wes-1 | Kauaeranga River | T12/505594 | T | | | | | | |
| W99861LA | grey/lt blue med phyric dacite lava lithic | DPP | Kauaeranga River | T12/505594 | T | | | | | | |
| W99861LB | red/grey med phyric rhyolite lava lithic | RPP | Kauaeranga River | T12/505594 | T | | | | | | |
| W99861LC | brown pum r welded ignimbrite lithic | MAN | Kauaeranga River | T12/505594 | T | | | | | | |
| W99861LD | cream indurated fine - crs ash vitric tuff | RVT | Kauaeranga River | T12/505594 | T | | | | | | |
| W99861LE | grey/lt blue f-band fine phyric rhyolite lava lithic | RPP | Kauaeranga River | T12/505594 | T | | | | | | |
| W99861LF | cream mod indurated vitric tuff lithic | RVT | Kauaeranga River | T12/505594 | T | | | | | | |
| W99861LG | grey/lt blue med phyric rhyolite lava lithic | RPP | Kauaeranga River | T12/505594 | T | | | | | | |
| W99861LH | grey/rustic fine phyric rhyolite lava lithic | RPP | Kauaeranga River | T12/505594 | T | | | | | | |
| W99861LI | grey/lt blue med phyric rhyolite lava lithic | RPP | Kauaeranga River | T12/505594 | T | | | | | | |
| W99861LJ | grey/blue med phyric rhyolite lava lithic | RPP | Kauaeranga River | T12/505594 | T | | | | | | |
| W99862 | lt grey pum r lithic r weakly welded ignimbrite | wes-1 | Kauaeranga River | T12/500586 | T | | | | | | |
| W99862LA | grey/lt blue med phyric rhyolite lava lithic | RPP | Kauaeranga River | T12/500586 | T | | | | | | |
| W99862LB | grey/pink fine phyric rhyolite lava lithic | RPP | Kauaeranga River | T12/500586 | T | | | | | | |
| W99862LC | cream indurated vitric tuff lithic | RVT | Kauaeranga River | T12/500586 | T | | | | | | |
| W99862LD | lt brown/cream lith r crs ash lithic tuff lithic | RLT | Kauaeranga River | T12/500586 | T | | | | | | |
| W99862LE | grey/lt blue med phyric dacite lava lithic | DPP | Kauaeranga River | T12/500586 | T | M | | | | | |
| W99862LF | green/grey silicified pum p welded ignimbrite lithic | SSI | Kauaeranga River | T12/500586 | T | | | | | | |
| W99863 | lt grey pum r weakly welded ignimbrite | wes-1 | Pinnacles Track | T12/490573 | T | | | | | | |
| W99863LA | green silicified lithic r welded ignimbrite lithic | WSI | Pinnacles Track | T12/490573 | T | | | | | | |
| W99863LB | lt blue/grey fine phyric dacite lava lithic | DPP | Pinnacles Track | T12/490573 | T | | | | | | |
| W99863LC | llu/gry med hyi rhyolite lava lithic | RPP | Pinnacles Track | T12/490573 | T | | | | | | |
| W99863LD | green/grey silicified pum p welded ignimbrite lithic | WSI | Pinnacles Track | T12/490573 | | | | | | | |
| W99863LE | grey/lt blue med phyric rhyolite lava lithic | RPP | Pinnacles Track | T12/490573 | T | | | | | | |
| W99863LF | cream mod sorted weakly indurated vitric tuff | RVT | Pinnacles Track | T12/490573 | | | | | | | |
| W99863LG | cream pum r lith p welded ignimbrite lithic | UND | Pinnacles Track | T12/490573 | T | | | | | | |
| W99863LH | red/brown fine phyric rhyolite lava lithic | RPP | Pinnacles Track | T12/490573 | T | | | | | | |
| W99863LI | green/brown silicified pum p welded ignimbrite lithic | SSI | Pinnacles Track | T12/490573 | T | | | | | | |
| W99864 | lt grey/cream pum r lith r weakly weld ignimbrite | wes-1 | 10m off Pinnacles Track | T12/506589 | T | | | | | | |
| W99864LA | grey/lt blue fine phyric rhyolite lava lithic | RPP | 10m off Pinnacles Track | T12/506589 | T | | | | | | |
| W99864LB | grey pum r lentic welded ignimbrite lithic | UND | 10m off Pinnacles Track | T12/506589 | T | | | | | | |
| W99864LC | grey/lt blue fine phyric rhyolite lava lithic | RPP | 10m off Pinnacles Track | T12/506589 | T | | | | | | |
| W99864LD | grey/lt blue fine phyric rhyolite lava lithic | RPP | 10m off Pinnacles Track | T12/506589 | T | | | | | | |
| W99864LE | lt grey glassy fine phyric rhyolite lava lithic | RP | 10m off Pinnacles Track | T12/506589 | T | | | | | | |
| W99864LF | cream/lt grey lith r welded ignimbrite lithic | WEB | 10m off Pinnacles Track | T12/506589 | T | | | | | | |
| W99865 | grey/pink fine-phyric rhyolite lava | kt | tributary stm, Kauaeranga River | T12/507582 | T | M | P | F | | I | |
| W99866 | grey pum r lith r weakly welded ignimbrite | wes-1 | tributary stm, Kauaeranga River | T12/506582 | T | | | | | | |
| W99866LA | grey med phyric rhyolite lava lithic | RPP | tributary stm, Kauaeranga River | T12/506582 | T | | | | | | |
| W99866LB | brown lith r welded ignimbrite lithic | UND | tributary stm, Kauaeranga River | T12/506582 | T | | | | | | |

| W No. | Lithology | Unit | Location | Grid Ref. | T | M | P | F | D | I | K |
|---|---|---|---|---|---|---|---|---|---|---|---|
| W99866LC | pink/grey med phyric rhyolite lava lithic | RPP | tributary stm, Kauaeranga River | T12/506582 | T | | | | | | |
| W99866LD | lt blue/grey fine phyric rhyolite lava lithic | RPP | tributary stm, Kauaeranga River | T12/506582 | T | | | | | | |
| W99866LE | red/brown fine phyric rhyolite lava lithic | RPP | tributary stm, Kauaeranga River | T12/506582 | T | | | | | | |
| W99866LF | brown pum r welded ignimbrite lithic | MAN | tributary stm, Kauaeranga River | T12/506582 | T | | | | | | |
| W99866LG | lt blue/grey fine phyric rhyolite lava lithic | RPP | tributary stm, Kauaeranga River | T12/506582 | T | | | | | | |
| W99867 | lt grey pum r lith r weakly welded ignimbrite | wi | 30m downstm of W99866 | T12/506582 | T | | | | | | |
| W99867LA | lt grey silicified lith r welded ignimbrite lithic | SSI | 30m downstm of W99866 | T12/506582 | T | | | | | | |
| W99867LB | grey/red fine phyric dacite lava lithic | DPP | 30m downstm of W99866 | T12/506582 | T | M | | | | | |
| W99867LC | grey silicified lith r welded ignimbrite lithic | SSI | 30m downstm of W99866 | T12/506582 | T | | | | | | |
| W99867LD | lt grey pum r lith r welded ignimbrite lithic | WEB | 30m downstm of W99866 | T12/506582 | T | M | | | | | |
| W99867LE | grey/brown med phyric rhyolite lava lithic | RPP | 30m downstm of W99866 | T12/506582 | T | | | | | | |
| W99867LF | grey/lt blue fine phyric rhyolite lava lithic | RPP | 30m downstm of W99866 | T12/506582 | T | | | | | | |
| W99867LG | grey fine phyric dacite lava lithic | DPP | 30m downstm of W99866 | T12/506582 | | | | | | | |
| W99867LH | brown pum r lenticular welded ignimbrite lithic | MAN | 30m downstm of W99866 | T12/506582 | T | | | | | | |
| W99867LI | grey/blue fine phyric dacite lava lithic | DPP | 30m downstm of W99866 | T12/506582 | T | | | | | | |
| W99867LJ | grey/lt blue fine phyric rhyolite lava lithic | DPP | 30m downstm of W99866 | T12/506582 | T | | | | | | |
| W99867LK | grey/blue med phyric rhyolite lava lithic | DPP | 30m downstm of W99866 | T12/506582 | T | | | | | | |
| W99867LL | grey/lt blue med phyric rhyolite lava lithic | RPP | 30m downstm of W99866 | T12/506582 | T | | | | | | |
| W99867LM | brown pum r cry r v.p.a welded ignimbrite lithic | TRI | 30m downstm of W99866 | T12/506582 | | | | | | | |
| W99867LN | black med phyric rhyolite lava lithic | DPP | 30m downstm of W99866 | T12/506582 | T | | | | | | |
| W99868 | grey/green pum r lith r silicified weakly welded ignimbrite | h | Kauaeranga River | T12/487581 | T | | | | | | |
| W99868LA | grey/brown silicified lith r welded ignimbrite lithic | WSI | Kauaeranga River | T12/487581 | T | | | | | | |
| W99868LB | brown/grey cry r welded ignimbrite lithic | UND | Kauaeranga River | T12/487581 | T | | | | | | |
| W99868LC | dk grey fine phyric dacite lava lithic | DPP | Kauaeranga River | T12/487581 | T | | | | | | |
| W99868LD | grey/lt blue mm f band spher fine phyric rhyolite lava lithic | RPP | Kauaeranga River | T12/487581 | T | | | | | | |
| W99868LE | grey lith p indurated vitric tuff lithic | RVT | Kauaeranga River | T12/487581 | T | | | | | | |
| W99868LF | blue/grey lith r silicified welded ignimbrite lithic | SSI | Kauaeranga River | T12/487581 | T | | | | | | |
| W99868LG | blue/green silicified med phyric andesite lava lithic | SAL | Kauaeranga River | T12/487581 | T | | | | | | |
| W99868LH | blue/grey silicified welded ignimbrite lithic | SSI | Kauaeranga River | T12/487581 | T | | | | | | |
| W99868LI | grey glassy med phyric andesite lava lithic | APP | Kauaeranga River | T12/487581 | T | | | | | | |
| W99868LJ | grey altered lith p welded ignimbrite lithic | WPI | Kauaeranga River | T12/487581 | T | | | | | | |
| W99869 | brown massive indurated lacustrine siltstone | wt | E bank of Kauaeranga River | T12/488583 | | | | | | | |
| W99870 | lt grey pum r weakly welded ignimbrite | wes-1 | 200m downstm of Kauaeranga Gorge | T12/488583 | T | | | | | | |
| W99870LA | black glassy fine phyric rhyolite lava lithic | RPP | 200m downstm of Kauaeranga Gorge | T12/488583 | T | | | | | | |
| W99870LB | red/brown fine phyric rhyolite lava lithic | RPP | 200m downstm of Kauaeranga Gorge | T12/488583 | T | | | | | | |
| W99870LC | grey f band fine phyric rhyolite lava lithic | RPP | 200m downstm of Kauaeranga Gorge | T12/488583 | T | | | | | | |
| W99870LD | grey/green silicified lacustrine siltstone lithic | VSI | 200m downstm of Kauaeranga Gorge | T12/488583 | T | | | | | | |
| W99871 | dk grey well sorted alternat. cry r/pum r vitric ash tuff | wes-1 | 200m downstm of Kauaeranga Gorge | T12/488583 | T | | | | | | |
| W99872 | lt grey well sorted massive vitric ash tuff | wes-1 | 200m downstm of Kauaeranga Gorge | T12/488583 | T | | | | | | |
| W99873 | dk grey well sorted vitric ash tuff | wes-1 | 200m downstm of Kauaeranga Gorge | T12/488583 | T | | | | | | |
| W99874 | grey pum r weakly welded ignimbrite | wes-1 | 200m downstm of Kauaeranga Gorge | T12/488583 | T | | | | | | |
| W99874LA | grey fine phyric rhyolite lava lithic | RPA | 200m downstm of Kauaeranga Gorge | T12/488583 | T | | | | | | |
| W99874LB | grey silicified pum r welded ignimbrite lithic | SSI | 200m downstm of Kauaeranga Gorge | T12/488583 | T | | | | | | |
| W99874LC | grey med phyric andesite lava lithic | APP | 200m downstm of Kauaeranga Gorge | T12/488583 | T | | | | | | |
| W99874LD | brown/grey fine phyric andesite lava lithic | APA | 200m downstm of Kauaeranga Gorge | T12/488583 | T | M | | F | | | |
| W99874LE | grey spheru amygda fine phyric rhyolite lava lithic | RPP | 200m downstm of Kauaeranga Gorge | T12/488583 | T | | | | | | |
| W99874LF | lt brown altered pum r lith p welded ignimbrite lithic | WPI | 200m downstm of Kauaeranga Gorge | T12/488583 | T | | | | | | |
| W99874LG | lt brown pum r lith r silicified vitric tuff lithic | RVT | 200m downstm of Kauaeranga Gorge | T12/488583 | T | | | | | | |
| W99874LH | cream/grey lith r cry r volcaniclastic sandstone lithic | VSA | 200m downstm of Kauaeranga Gorge | T12/488583 | T | | | | | | |
| W99874LI | brown pum r lith r welded ignimbrite lithic | TRI | 200m downstm of Kauaeranga Gorge | T12/488583 | T | | | | | | |
| W99874LJ | grey f band amygda fine phyric rhyolite lava lithic | RPP | 200m downstm of Kauaeranga Gorge | T12/488583 | T | | | | | | |
| W99874LK | cream well sorted vitric tuff lithic | RVT | 200m downstm of Kauaeranga Gorge | T12/488583 | T | | | | | | |
| W99875 | cream/lt grey well sorted massive volcaniclastic siltstone | wt | 200m downstm of Kauaeranga Gorge | T12/488583 | | | | | | | |
| W99876 | pink/grey fine phyric rhyolite lava | ku | downstm side of Kauaeranga Gorge | T12/489583 | T | M | P | F | | I | K |
| W99877 | dk grey fine phyric andesite lava | at | Kauaeranga River | T12/483578 | T | M | | F | | I | |
| W99878 | green/grey pum r weakly welded ignimbrite | h | tributary stm of Kapowai River | T11/545643 | T | | | | D | | |
| W99878LA | green/grey propylitic alter. fine phyric rhyolite lava lithic | PRL | tributary stm of Kapowai River | T11/545643 | T | | | | | | |
| W99879 | green/grey cry r weakly welded ignimbrite | h | Precipice Stm-Kapowai River conflu. | T11/548643 | T | | | | D | | |
| W99880 | buff/grey fine phyric pheno r lithoidal rhyolite lava | ky | Kapowai River | T11/545651 | T | | | | | | |
| W99881 | blue/grey fine phyric devitrified rhyolite lava | kg | Kapowai River | T11/552661 | T | | | | | | |
| W99882 | grey fine phyric pheno r rhyolite lava | kg | Kapowai River | T11/552661 | T | | | | | | |
| W99883 | lt grey weakly welded pum r ignimbrite | wes-1 | Kapowai River | T11/546683 | T | | | | | | |
| W99883LA | grey/pink spheru amygda fine phyric rhyolite lava lithic | RPP | Kapowai River | T11/546683 | T | | | | | | |
| W99883LB | dk grey med phyric andesite lava lithic | APP | Kapowai River | T11/546683 | T | | | | | | |
| W99883LC | cream/lt brown pum p v.p.a welded ignimbrite lithic | MAN | Kapowai River | T11/546683 | T | | | | | | |
| W99883LD | brown pum r lith r welded ignimbrite lithic | TRI | Kapowai River | T11/546683 | T | | | | | | |
| W99883LE | grey glassy poor vesic rhyolite lava lithic | RPP | Kapowai River | T11/546683 | T | | | | | | |
| W99883LF | grey med phyric andesite lava lithic | APP | Kapowai River | T11/546683 | T | | | | | | |
| W99884 | lt grey pum r weakly welded ignimbrite | wes-1 | Kapowai River | T11/548682 | T | | | | | | |
| W99884LA | grey f band f phyric rhyolite lava lithic | RPP | Kapowai River | T11/548682 | T | | | | | | |
| W99884LB | grey/pink fine phyric f band rhyolite lava lithic | RPP | Kapowai River | T11/548682 | T | | | | | | |
| W99884LC | grey cry r lith r pum p welded ignimbrite lithic | UND | Kapowai River | T11/548682 | T | | | | | | |
| W99885 | lithified tuff layers (interbedded with W99884) | wes-1a | Kapowai River | T11/548682 | | | | | | | |
| W99886 | lt brown/grey pum r lith r weakly welded ignimbrite | wes-1 | Kapowai River | T11/551679 | T | | | F | | I | K |
| W99886LA | grey/pink f band amygda f phyric rhyolite lava lithic | RPP | Kapowai River | T11/551679 | T | | | | | | |
| W99886LB | grey/pink f band amygda f phyric rhyolite lava lithic | RPP | Kapowai River | T11/551679 | T | | | | | | |
| W99886LC | lt brown med phyric andesite lava lithic | APP | Kapowai River | T11/551679 | T | | | | | | |
| W99886LD | brown med phyric andesite lava lithic | APP | Kapowai River | T11/551679 | T | | P | | | | |
| W99886LE | brown cry r pum p lith p welded ignimbrite lithic | TRI | Kapowai River | T11/551679 | T | | | | | | |
| W99886LF | green/grey pum r lith p silicified welded ignimbrite lithic | WSI | Kapowai River | T11/551679 | T | | | | | | |
| W99886LG | cream pum r silicified vitric tuff lithic | RVT | Kapowai River | T11/551679 | T | | | | | | |
| W99886LH | brown fine phyric dacite lava lithic | DPP | Kapowai River | T11/551679 | T | M | | | | | |
| W99886LI | grey/pink fine phyric rhyolite lava lithic | RPP | Kapowai River | T11/551679 | T | | | | | | |
| W99886LJ | pink lith p partially welded ignimbrite lithic | VAP | Kapowai River | T11/551679 | T | M | | | | | |
| W99886LK | grey med phyric andesite lava lithic | APP | Kapowai River | T11/551679 | T | | | | | | |
| W99886LL | brown/grey fine phyric andesite lava lithic | APP | Kapowai River | T11/551679 | T | | | | | | |
| W99886LM | pink/grey fine phyric rhyolite lava lithic | RPP | Kapowai River | T11/551679 | T | | | | | | |
| W99886LN | green/grey pum r silicified welded ignimbrite lithic | SSI | Kapowai River | T11/551679 | T | | | | | | |
| W99886LO | green/grey lith r silicified welded ignimbrite lithic | SSI | Kapowai River | T11/551679 | T | | | | | | |

| W No. | Lithology | Unit | Location | Grid Ref. | T | M | P | F | D | I | K |
|---|---|---|---|---|---|---|---|---|---|---|---|
| W99886LP | brown pum r lith p welded ignimbrite lithic | WEB | Kapowai River | T11/551679 | T | | | | | | |
| W99886LQ | cream pum r welded ignimbrite lithic | UND | Kapowai River | T11/551679 | T | | | | | | |
| W99886LR | cream welded ignimbrite lithic | SPI | Kapowai River | T11/551679 | T | | | | | | |
| W99887 | brown/cream pum r crs ash-lapilli pyroclastic dike | wes-1 | Kapowai River | T11/551679 | T | | | | | | |
| W99888 | cream pum r ash pyroclastic dike | wes-1 | Kapowai River | T11/551679 | T | | | | | | |
| W99889 | cream chaloziodite bearing ash pyroclastic dike | wes-1 | Kapowai River | T11/551679 | T | | | | | | |
| W99890 | pink pum r weakly welded ignimbrite | mi | Kapowai River | T11/553673 | T | M | | | | | |
| W99890LA | pink pum r welded ignimbrite lithic | VAP | Kapowai River | T11/553673 | T | | | | | | |
| W99890LB | grey/brown fine phyric f band rhyolite lava lithic | RPP | Kapowai River | T11/553673 | T | | | | | | |
| W99890LC | grey f band fine phyric rhyolite lava lithic | RPP | Kapowai River | T11/553673 | T | | | | | | |
| W99890LD | brown/grey fine phyric pheno r dacite lava lithic | DPP | Kapowai River | T11/553673 | T | | | | | | |
| W99890LE | pink/orange welded ignimbrite lithic | VAP | Kapowai River | T11/553673 | T | | | | | | |
| W99890LF | pink silicified welded ignimbrite lithic | WSI | Kapowai River | T11/553673 | T | | | | | | |
| W99891 | pink/brown cry r pum p lith p v.p.a. weakly welded ignimbrite | mi | Kapowai River | T11/553673 | T | | | | | | |
| W99891LA | brown fine phyric dacite lava lithic | DPP | Kapowai River | T11/553673 | T | | | | | | |
| W99891LB | grey f band fine phyric rhyolite lava lithic | RPA | Kapowai River | T11/553673 | T | M | | | | | |
| W99891LC | brown/grey med phyric poor vesic andesite lava lithic | APP | Kapowai River | T11/553673 | T | | | | | | |
| W99891LD | pink pum r welded ignimbrite lithic | UND | Kapowai River | T11/553673 | T | | | | | | |
| W99891LE | lt brown pum r lith p v.p.a welded ignimbrite lithic | VPA | Kapowai River | T11/553673 | T | | | | | | |
| W99891LF | lt grey fine phyric weak silicified rhyolite lava lithic | SRL | Kapowai River | T11/553673 | T | | | | | | |
| W99891LG | brown pum r v.p.a silicified welded ignimbrite lithic | WSI | Kapowai River | T11/553673 | T | | | | | | |
| W99891LH | grey/brown fine phyric dacite lava lithic | DPP | Kapowai River | T11/553673 | T | | | | | | |
| W99891LI | grey/pink fine phyric rhyolite lava lithic | RPP | Kapowai River | T11/553673 | T | | | | | | |
| W99892 | grey/brown lith r pum p weakly welded ignimbrite | mi | E bank of Kapowai River | T11/554672 | T | | | | | | |
| W99892LA | grey fine phyric silicified dacite lava lithic | SDL | E bank of Kapowai River | T11/554672 | T | | | | | | |
| W99892LB | green/brown altered med phyric dacite lava lithic | PDL | E bank of Kapowai River | T11/554672 | T | | | | | | |
| W99892LC | pink pum r silicified welded ignimbrite lithic | WSI | E bank of Kapowai River | T11/554672 | T | | | | | | |
| W99892LD | pink/cream pum r lith p v.p.a welded ignimbrite lithic | VPA | E bank of Kapowai River | T11/554672 | T | | | | | | |
| W99892LE | brown/cream pum r lith p v.p.a welded ignimbrite lithic | VAP | E bank of Kapowai River | T11/554672 | T | | | | | | |
| W99892LF | dk grey med phyric andesite lava lithic | APP | E bank of Kapowai River | T11/554672 | T | | | | | | |
| W99892LG | brown silicified welded ignimbrite lithic | WSI | E bank of Kapowai River | T11/554672 | T | | | | | | |
| W99892LH | grey f band fine phyric rhyolite lava lithic | RPP | E bank of Kapowai River | T11/554672 | T | | | | | | |
| W99892LI | grey/pink amygda fine phyric rhyoltie lava lithic | RPP | E bank of Kapowai River | T11/554672 | T | | | | | | |
| W99892LJ | brown pum r silicified welded ignimbrite lithic | WSI | E bank of Kapowai River | T11/554672 | T | | | | | | |
| W99892LK | grey f band fine phyric rhyolite lava lithic | RPP | E bank of Kapowai River | T11/554672 | T | | | | | | |
| W99892LL | grey amygda fine phyric rhyolite lava lithic | RPP | E bank of Kapowai River | T11/554672 | T | | | | | | |
| W99893 | grey/brown pum r lith r silicified ignimbrite | mi | upstm of tributary; Kapowai River | T11/553671 | T | | | | | | |
| W99893LA | grey/pink f band fine phyric rhyolite lava lithic | RPP | upstm of tributary; Kapowai River | T11/553671 | T | | | | | | |
| W99893LB | grey glassy fine phyric rhyolite lava lithic | RP | upstm of tributary; Kapowai River | T11/553671 | T | | | | | | |
| W99893LC | dk grey fine phyric dacite lava lithic | DPP | upstm of tributary; Kapowai River | T11/553671 | T | | | | | | |
| W99894 | pink/grey med phyric pheno r rhyolite lava | kk | W bank of Kapowai River | T11/553671 | T | M | | F | | | |
| W99895 | grey mod sorted cry r pum p volcaniclastic siltstone | wh | W bank of Kapowai River | T11/553671 | T | | | | | | |
| W99896 | lt grey pum r lith r weakly welded ignimbrite | wes-1 | W bank of Kapowai River | T11/553671 | T | | | | | | |
| W99896LA | grey glassy poor vesic fine phyric rhyolite lava lithic | RPP | W bank of Kapowai River | T11/553671 | T | | | | | | |
| W99896LB | grey vesicular fine phyric rhyolite lava lithic | RPP | W bank of Kapowai River | T11/553671 | | | | | | | |
| W99896LC | cream v.p.a pum r welded ignimbrite lithic | VPA | W bank of Kapowai River | T11/553671 | T | | | | | | |
| W99896LD | grey fine phyric dacite lava lithic | DPP | W bank of Kapowai River | T11/553671 | T | M | | | | | |
| W99896LE | cream well sorted pum p lith p vitric tuff lithic | RVT | W bank of Kapowai River | T11/553671 | T | | | | | | |
| W99896LF | cream silicified rhyoltie lava lithic | SRL | W bank of Kapowai River | T11/553671 | T | | | | | | |
| W99896LG | brown med phyric dacite lava lithic | DPP | W bank of Kapowai River | T11/553671 | T | | | | | | |
| W99896LH | brown med phyric dacite lava lithic | DPP | W bank of Kapowai River | T11/553671 | T | | | | | | |
| W99896LI | grey glassy fine phyric rhyolite lava lithic | RPP | W bank of Kapowai River | T11/553671 | T | | | | | | |
| W99896LJ | pink/brown pum r lith r v.p.a welded ignimbrite lithic | MAN | W bank of Kapowai River | T11/553671 | T | | | | | | |
| W99896LK | brown fine phyric dacite lava lithic | DPP | W bank of Kapowai River | T11/553671 | T | | | | | | |
| W99897 | lt brown lith r weakly welded ignimbrite | mi | E bank of Kapowai River | T11/553670 | T | | | | | | |
| W99897LA | grey glassy fine phyric rhyolite lava lithic | RPP | E bank of Kapowai River | T11/553670 | T | | | | | | |
| W99897LB | pink/brown pum r welded ignimbrite lithic | MAN | E bank of Kapowai River | T11/553670 | T | | | | | | |
| W99897LC | grey glassy perlitic med phyric rhyolite lava lithic | RPP | E bank of Kapowai River | T11/553670 | T | | P | | | | |
| W99897LD | grey med phyric andesite lava lithic | APP | E bank of Kapowai River | T11/553670 | T | | P | | | | |
| W99897LE | grey glassy fine phyric rhyolite lava lithic | RPP | E bank of Kapowai River | T11/553670 | | | | | | | |
| W99897LF | grey glasy perlitic med phyric rhyolite lava lithic | RPP | E bank of Kapowai River | T11/553670 | | | | | | | |
| W99897LG | cream/pink pum r v.p.a welded ignimbrite lithic | MAN | E bank of Kapowai River | T11/553670 | T | | | | | | |
| W99898 | pink/grey pum r weakly welded ignimbrite | mi | Kapowai River | T11/552676 | T | M | P | F | | | |
| W99898LA | cream/lt grey silicified welded ignimbrite lava lithic | WSI | Kapowai River | T11/552676 | T | | | | | | |
| W99898LB | lt blue/grey fine phyric rhyolite lava lithic | RPP | Kapowai River | T11/552676 | T | | | | | | |
| W99898LC | cream/pink fine phyric rhyolite lava lithic | RP | Kapowai River | T11/552676 | T | M | | | | | |
| W99898LD | grey med phyric andesite lava lithic | APP | Kapowai River | T11/552676 | T | | | | | | |
| W99898LE | grey med phyric dacite lava lithic | DPP | Kapowai River | T11/552676 | T | | | | | | |
| W99898LF | brown fine phyric andesite lava lithic | APP | Kapowai River | T11/552676 | T | | | | | | |
| W99898LG | cream/orange silicified andesite? lava lithic | SAL | Kapowai River | T11/552676 | T | | | | | | |
| W99898LH | grey fine phyric f band rhyolite lava lithic | RPP | Kapowai River | T11/552676 | T | | | | | | |
| W99898LI | grey/pink fine phyric dacite lava lithic | DPP | Kapowai River | T11/552676 | T | | | | | | |
| W99898LJ | grey/brown f band fine phyric rhyolite lava lithic | RPP | Kapowai River | T11/552676 | T | | | | | | |
| W99898LK | brown med phyric altered andesite lava lithic | SAL | Kapowai River | T11/552676 | T | | | | | | |
| W99899 | lt grey/brown pum r lith p weakly welded ignimbrite | wes-1 | Kapowai River | T11/553678 | T | | | | | | |
| W99899LA | grey fine phyric rhyolite lava lithic | RPP | Kapowai River | T11/553678 | T | | | | | | |
| W99899LB | grey med phyric andesite lava lithic | APP | Kapowai River | T11/553678 | T | M | | | | | |
| W99899LC | lt grey fine phyric rhyolite lava lithic | RPP | Kapowai River | T11/553678 | T | | | | | | |
| W99899LD | grey fine phyric glomero f band rhyolite lava lithic | RPP | Kapowai River | T11/553678 | T | | | | | | |
| W99899LE | lt brown cry r lith r welded ignimbrite lithic | WSI | Kapowai River | T11/553678 | T | | | | | | |
| W99899LF | lt grey fine phyric mod silicified rhyolite lava lithic | RPP | Kapowai River | T11/553678 | T | | | | | | |
| W99899LG | grey med phyric mod silicified dacite lava lithic | SDL | Kapowai River | T11/553678 | T | | | | | | |
| W999(X) | lt grey lith p weakly welded ignimbrite | wes-1 | Kapowai River | T11/552678 | T | | | | | | |
| W99901 | lt grey lith p weakly welded ignimbrite | wes-1 | 50m from Ford, off Parakau Rd | T11/543683 | T | | | | | | |
| W99901LA | grey fine phyric andesite lava lithic | APP | 50m from Ford, off Parakau Rd | T11/543683 | T | | | | | | |
| W99901LB | grey fine phyric rhyolite breccia lithic | BRE | 50m from Ford, off Parakau Rd | T11/543683 | T | | | | | | |
| W99901LC | grey f band fine phyric rhyolite lava lithic | RPP | 50m from Ford, off Parakau Rd | T11/543683 | T | | | | | | |
| W99901LD | grey fine phyric dacite lava lithic | DPP | 50m from Ford, off Parakau Rd | T11/543683 | T | | | | | | |
| W99901LE | grey/pink silicified fine phyric rhyolite lava lithic | SRL | 50m from Ford, off Parakau Rd | T11/543683 | T | | | | | | |

| W No. | Lithology | Unit | Location | Grid Ref. | T | M | P | F | D | I | K |
|---|---|---|---|---|---|---|---|---|---|---|---|
| W99901LF | brown cry r lith r volcaniclastic sandstone lithic | VSA | 50m from Ford, off Parakau Rd | T11/543683 | T | | | | | | |
| W99901LG | brown lith r silicified welded ignimbrite lithic | WSI | 50m from Ford, off Parakau Rd | T11/543683 | T | | | | | | |
| W99901LH | dk grey/brown med phyric andesite lava lithic | APP | 50m from Ford, off Parakau Rd | T11/543683 | T | M | | | | | |
| W99901LI | brown/red med phyric rhyolite lava lithic | RPP | 50m from Ford, off Parakau Rd | T11/543683 | T | | | | | | |
| W99901LJ | grey fine phyric rhyolite lava lithic | RPP | 50m from Ford, off Parakau Rd | T11/543683 | T | | | | | | |
| W99901LK | grey fine phyric dacite lava lithic | DPP | 50m from Ford, off Parakau Rd | T11/543683 | T | | | | | | |
| W99901LL | dk grey med phyric andesite lava lithic | APP | 50m from Ford, off Parakau Rd | T11/543683 | T | | | | | | |
| W99901LM | grey/blue fine phyric rhyolite lava lithic | RPP | 50m from Ford, off Parakau Rd | T11/543683 | T | | | | | | |
| W99901LN | grey glassy fine phyric rhyolite lava lithic | RPP | 50m from Ford, off Parakau Rd | T11/543683 | T | | | | | | |
| W99901LO | dk grey fine phyric andesite lava lithic | APP | 50m from Ford, off Parakau Rd | T11/543683 | T | | | | | | |
| W99901LP | black glassy fine phyric obsidian lithic | RPP | 50m from Ford, off Parakau Rd | T11/543683 | T | | | | | | |
| W99901LQ | grey fine phyric rhyolite lava lithic | RPP | 50m from Ford, off Parakau Rd | T11/543683 | T | M | | | | | |
| W99902 | grey/pink med phyric devitrified rhyolite lava | sm | Kapowai River | T11/553668 | T | M | | | | | |
| W99903 | lt brown pum r lith r weakly welded ignimbrite | cp | Kapowai River | T11/553668 | T | | | | | | |
| W99903LA | cream weath v.p.a welded ignimbrite lithic | UND | Kapowai River | T11/553668 | | | | | | | |
| W99903LB | grey glassy fine phyric rhyolite lava lithic | RPP | Kapowai River | T11/553668 | | | | | | | |
| W99903LC | cream/brown v.p.a pum r welded ignimbrite lithic | VPA | Kapowai River | T11/553668 | T | | | | | | |
| W99903LD | grey glassy fine phyric rhyolite lava lithic | RPP | Kapowai River | T11/553668 | T | | | | | | |
| W99903LE | cream/brown pum r welded ignimbrite lithic | MAN | Kapowai River | T11/553668 | T | | | | | | |
| W99903LF | grey glassy fine phyric rhyolite lava lithic | RPP | Kapowai River | T11/553668 | | | | | | | |
| W99903LG | brown fine phyric incip vesic andesite lava lithic | APP | Kapowai River | T11/553668 | T | | | | | | |
| W99903LH | brown med phyric incip vesic andesite lava lithic | APP | Kapowai River | T11/553668 | T | | | | | | |
| W99903LI | grey med phyric perlitic rhyolite lava lithic | RPP | Kapowai River | T11/553668 | T | | | | | | |
| W99903LJ | grey glassy fine phyric rhyolite lava lithic | RPP | Kapowai River | T11/553668 | | | | | | | |
| W99903LK | grey fine phyric rhyolite lava lithic | RPP | Kapowai River | T11/553668 | T | | | | | | |
| W99903LL | dk brown fine phyric vesic andesite lava lithic | APP | Kapowai River | T11/553668 | T | | | | | | |
| W99903LM | cream/brown pum r v.p.a welded ignimbrite lithic | VAP | Kapowai River | T11/553668 | T | | | | | | |
| W99904 | blue/grey med phyric pheno r dacite lava | kk | Kapowai River | T11/553666 | T | | | | | | |
| W99905 | purple/grey fine phyric dacite lava | kk | W bank of Kapowai River | T11/552665 | T | M | P | F | | I | |
| W99906 | blue/grey fine phyric dacite lava | kk | E bank of Kapowai River | T11/552664 | T | | | | | | |
| W99907 | blue/grey med phyric rhyolite lava | kk | both banks of Kapowai River | T11/551663 | T | | | | | | |
| W99908 | dk grey med phyric glassy rhyolite lava dike | kd | W bank of Kapowai River | T11/552660 | T | | | F | | | K |
| W99909 | dk grey med phyric glassy rhyolite lava dike | kd | W bank of Kapowai River | T11/552660 | | | | | | | |
| W99910 | lt grey weakly welded ignimbrite | cp | W bank of Kapowai River | T11/552660 | T | | | | | | |
| W99910LA | grey f band fine phyric rhyolite lava lithic | RPP | W bank of Kapowai River | T11/552660 | T | | | | | | |
| W99910LB | cream well sorted vitric tuff lithic | RVT | W bank of Kapowai River | T11/552660 | T | | | | | | |
| W99910LC | dk grey fine phyric andesite lava lithic | APP | W bank of Kapowai River | T11/552660 | T | | | | | | |
| W99910LD | brown cry r lith r crystal tuff lithic | RCT | W bank of Kapowai River | T11/552660 | T | | | | | | |
| W99910LE | cream/brown lith p welded ignimbrite lithic | UND | W bank of Kapowai River | T11/552660 | T | | | | | | |
| W99910LF | pink/cream cry r silicified welded ignimbrite lithic | WSI | W bank of Kapowai River | T11/552660 | T | | | | | | |
| W99910LG | dk grey med phyric andesite lava lithic | APP | W bank of Kapowai River | T11/552660 | T | | | | | | |
| W99910LH | grey/brown med phyric incip vesic andesite lava lithic | APP | W bank of Kapowai River | T11/552660 | T | | | | | | |
| W99910LI | lt grey lithic r pum p ignimbrite lithc | UND | W bank of Kapowai River | T11/552660 | | | | | | | |
| W99911 | cream lith r pumr weakly welded ignimbrite | cp | 60m upstm of W99910 | T11/552659 | T | | | | | | |
| W99912 | dk grey fine phyric dacite lava | kd | 60m upstm of W99910 | T11/552660 | T | M | P | F | | I | K |
| W99913 | lt grey pum r lith r weakly welded ignimbrite | wes-4 | Oteao track | T11/512645 | T | | | | | | |
| W99913LA | black fine phyric andesite lava lithic | APP | Oteao track | T11/512645 | T | | | | | | |
| W99913LB | dk grey/black med phyric andesite lava lithic | APP | Oteao track | T11/512645 | T | | | | | | |
| W99913LC | lt cream/brown welded ignimbrite lithic | UND | Oteao track | T11/512645 | T | | | | | | |
| W99913LD | lt grey glassy fine phyric rhyolite lava lithic | RP | Oteao track | T11/512645 | T | | | | | | |
| W99913LE | red/brown med phyric vesic basaltic andesite lava lithic | bpp | Oteao track | T11/512645 | T | | | | | | |
| W99913LF | grey glassy fine phyric rhyolite lava lithic | RPP | Oteao track | T11/512645 | | | | | | | |
| W99913LG | grey/pink mm f band fine phyric rhyolite lava lithic | RPP | Oteao track | T11/512645 | T | | | | | | |
| W99913LH | black med phyric andesite lava lithic | APP | Oteao track | T11/512645 | T | | | | | | |
| W99913LI | grey med phyric dacite lava lithic | DPA | Oteao track | T11/512645 | T | M | | | | | |
| W99913LJ | grey f band glassy fine phyric rhyolite lava lithic | RP | Oteao track | T11/512645 | T | | | | | | |
| W99913LK | brown/red fine phyric andesite lava lithic | APP | Oteao track | T11/512645 | | | | | | | |
| W99913LL | grey med phyric altered andesite lava lithic | SAL | Oteao track | T11/512645 | T | | | | | | |
| W99913LM | lt grey med phyric glassy andesite lava lithic | APP | Oteao track | T11/512645 | | | | | | | |
| W99913LN | grey amygda fine phyric rhyolite lava lithic | RPP | Oteao track | T11/512645 | T | | | | | | |
| W99914A | dk grey med phyric andesite lava | ot | crest of ridge, Oteao track | T11/513644 | T | | | F | | | |
| W99914 | grey lith r weakly welded ignimbrite | wes-4 | tributary of Oteao Stm | T11/519645 | | | | | | | |
| W99915 | lt grey mod sorted lithified tuff | wes-2 | tributary of Oteao Stm | T11/519645 | | | | | | | |
| W99916 | grey pum p lith p weakly welded ignimbrite | wes-4 | tributary of Oteao Stm | T11/519647 | T | | | | | | |
| W99917 | brown/grey pum r lith r weakly welded ignimbrite | wes-4 | confluence of tributary stms | T11/519648 | T | | | | | | |
| W99917LA | grey fine phyric rhyolite lava lithic | RPP | confluence of tributary stms | T11/519648 | T | | | | | | |
| W99917LB | black fine phyric obsidian lava lithic | RPP | confluence of tributary stms | T11/519648 | T | | | | | | |
| W99917LC | grey/pink mm f band fine phyric rhyolite lava lithic | RPP | confluence of tributary stms | T11/519648 | T | | | | | | |
| W99917LD | grey/pink fine phyric rhyolite lava lithic | RPP | confluence of tributary stms | T11/519648 | T | | | | | | |
| W99918 | purple/pink weak flow b fine phyric rhyolite lava | ky | 20m upstm of tributary confluence | T11/520648 | T | M | | | | | |
| W99919 | pum p lith p weakly welded ignimbrite | wes-4 | downstm of tributary confluence | T11/519648 | T | | | | | | |
| W99920 | black porphyritic obsidian lava | ky | Oteao Stm | T11/519649 | T | | | F | | | |
| W99921 | lt grey pum r lith r weakly welded ignimbrite | wes-4 | Oteao Stm | T11/519650 | T | | | | | | |
| W99921LA | brown poor sorted rhyolite breccia lithic | BRE | Oteao Stm | T11/519650 | T | | | | | | |
| W99921LB | brown/red fine phyric rhyolite lava lithic | RPP | Oteao Stm | T11/519650 | | | | | | | |
| W99921LC | brown fine phyric rhyolite lava lithic | RPP | Oteao Stm | T11/519650 | T | | | | | | |
| W99921LD | grey/blue med phyric rhyolite lava lithic | RPP | Oteao Stm | T11/519650 | T | | | | | | |
| W99921LE | grey mm f band fine phyric rhyolite lava lithic | RPP | Oteao Stm | T11/519650 | T | | | | | | |
| W99921LF | dk grey poor sorted rhyolite breccia lithic | BRE | Oteao Stm | T11/519650 | | | | | | | |
| W99921LG | grey spher amygda fine phyric rhyolite lava lithic | RPP | Oteao Stm | T11/519650 | T | | | | | | |
| W99921LH | pink pum r lith p welded ignimbrite lithic | VPA | Oteao Stm | T11/519650 | T | | | | | | |
| W99922 | lt grey pum p lith p weakly welded ignimbrite | wes-4 | top of waterfall, Slip Stm tributary | T11/511643 | T | | | F | | I | |
| W99922LA | dk grey fine phyric rhyolite lava lithic | RPP | top of waterfall, Slip Stm tributary | T11/511643 | T | | | | | | |
| W99923 | lt grey weakly welded ignimbrite | wes-4 | waterfall section, Slip Stm tributary | T11/511643 | T | | P | | | | |
| W99923LA | dk grey pum r cry r lenticular welded ignimbrite lithic | TRI | waterfall section, Slip Stm tributary | T11/511643 | T | M | | | | | |
| W99923LB | lt green lith r mod silicified welded ignimbrite lithic | WSI | waterfall section, Slip Stm tributary | T11/511643 | T | | | | | | |
| W99923LC | grey pum r lenticular welded ignimbrite lithic | TRI | waterfall section, Slip Stm tributary | T11/511643 | T | | | | | | |
| W99923LD | dk grey f band spher fine phyric rhyolite lava lithic | RPP | waterfall section, Slip Stm tributary | T11/511643 | T | | | | | | |
| W99923LE | grey fine phryic rhyolite lava lithic | RPP | waterfall section, Slip Stm tributary | T11/511643 | T | | | | | | |

| W No. | Lithology | Unit | Location | Grid Ref. | T | M | P | F | D | I | K |
|---|---|---|---|---|---|---|---|---|---|---|---|
| W99924 | multilithologic lithic lag breccia | wes-3 | waterfall section, Slip Stm tributary | T11/511643 | | | | | | | |
| W99925 | grey massive -shower bedded vitric tuff(top) | wes-2 | waterfall section, Slip Stm tributary | T11/511643 | T | | | | | | |
| W99926 | grey massive vitric tuff & poorly sorted flow(base) | wes-2 | waterfall section, Slip Stm tributary | T11/511643 | T | | | | | | |
| W99927 | lt grey pum r weakly welded ignimbrite | wes-1 | waterfall section, Slip Stm tributary | T11/511643 | T | M | | | | | |
| W99927LA | brown/pink fine phyric rhyolite lava lithic | RPP | waterfall section, Slip Stm tributary | T11/511643 | T | | | | | | |
| W99927LB | lt grey crs f band fine phyric rhyolite lava lithic | RP | waterfall section, Slip Stm tributary | T11/511643 | T | | | | | | |
| W99928 | lt grey pum r weakly welded ignimbrite | wes-1 | waterfall section, Slip Stm tributary | T11/511643 | T | M | P | | | | |
| W99928LA | brown poorly sorted volcaniclastic lacustrine sandstone lithic | VSA | waterfall section, Slip Stm tributary | T11/511643 | T | | | | | | |
| W99928LB | grey fine phyric rhyolite lava lithic | RPP | waterfall section, Slip Stm tributary | T11/511643 | T | | | | | | |
| W99928LC | grey glassy fine phyric crs f band rhyolite lava lithic | RPP | waterfall section, Slip Stm tributary | T11/511643 | T | | | | | | |
| W99928LD | dk grey glassy fine phyric f band rhyolite lava lithic | RPP | waterfall section, Slip Stm tributary | T11/511643 | T | | | | | | |
| W99929 | purple/grey fine phyric rhyolite lava | kw | Oteao Stm | T11/508661 | T | | | | | | |
| W99930 | grey rhyolite lava breccia | kw | Oteao Stm | T11/508661 | | | | | | | |
| W99931 | lt grey pum r weakly welded ignimbrite | wes-1 | Oteao Stm | T11/509660 | T | | | | | | |
| W99931LA | brown f band fine phyric rhyolite lava lithic | RP | Oteao Stm | T11/509660 | T | | | | | | |
| W99931LB | lt grey glassy fine phyric rhyolite lava lithic | RP | Oteao Stm | T11/509660 | T | | | | | | |
| W99931LC | brown poorly sorted volcaniclastic sandstone lithic | VSA | Oteao Stm | T11/509660 | T | | | | | | |
| W99931LD | grey/brown fine phyric dacite lava lithic | DPP | Oteao Stm | T11/509660 | T | | | | | | |
| W99931LE | grey/brown fine phyric rhyolite lava lithic | RPP | Oteao Stm | T11/509660 | T | | | | | | |
| W99931LF | grey fine phyric rhyolite lava lithic | RP | Oteao Stm | T11/509660 | T | | | | | | |
| W99931LG | dk grey med phyric dacite lava lithic | DPP | Oteao Stm | T11/509660 | T | M | | | | | |
| W99931LH | red/brown incip vesic andesite lava lithic | APP | Oteao Stm | T11/509660 | T | | | | | | |
| W99931LI | grey glassy fine phyric rhyolite lava lithic | RPP | Oteao Stm | T11/509660 | T | | | | | | |
| W99931LJ | grey/lt blue fine phyric rhyolite lava lithic | RPP | Oteao Stm | T11/509660 | T | | | | | | |
| W99931LK | grey/brown fine phyric rhyolite lava lithic | RPP | Oteao Stm | T11/509660 | T | | | | | | |
| W99931LL | grey fine phyric pheno p rhyolite lava lithic | RPP | Oteao Stm | T11/509660 | T | | | | | | |
| W99932 | lt grey/brown pum r lith p weakly welded ignimbrite | wes-1 | Oteao Stm | T11/511659 | T | | | | | | |
| W99932LA | brown fine phyric rhyolite lava lithic | RPP | Oteao Stm | T11/511659 | T | | | | | | |
| W99932LB | brown/red fine phyric rhyolite lava lithic | RPP | Oteao Stm | T11/511659 | T | | | | | | |
| W99932LC | grey/brown fine phyric rhyolite lava lithic | RPP | Oteao Stm | T11/511659 | T | | | | | | |
| W99932LD | brown fine phyric rhyolite lava lithic | RPP | Oteao Stm | T11/511659 | T | | | | | | |
| W99932LE | brown cry r lith r rhyolite breccia lithic | BRE | Oteao Stm | T11/511659 | T | | | | | | |
| W99933 | lt grey/brown pum r lith p weakly welded ignimbrite | wes-1 | Oteao Stm | T11/511658 | T | | | | | | |
| W99934 | lt grey pum r weakly welded ignimbrite | wes-1 | Oteao Stm | T11/512658 | T | | | | | | |
| W99935 | dk grey andesite breccia | ot | Oteao Stm | T11/512658 | T | | | | | | |
| W99936 | lt grey/brown pum r lith p weakly welded ignimbrite | wes-1 | 60 m upstm of W99936, Oteao Stm | T11/512658 | T | | | | | | |
| W99936LA | grey fine phyric rhyolite lava lithic | RP | 60 m upstm of W99936, Oteao Stm | T11/512658 | T | | | | | | |
| W99936LB | grey/lt grey fine phyric rhyolite lava lithic | RP | 60 m upstm of W99936, Oteao Stm | T11/512658 | T | | | | | | |
| W99936LC | brown/grey med phyric rhyolite lava lithic | RP | 60 m upstm of W99936, Oteao Stm | T11/512658 | T | | | | | | |
| W99936LD | brown med phyric andesite lava lithic | APP | 60 m upstm of W99936, Oteao Stm | T11/512658 | T | | | | | | |
| W99936LE | grey fine phyric rhyolite lava lithic | RP | 60 m upstm of W99936, Oteao Stm | T11/512658 | T | | | | | | |
| W99936LF | red/black weath med phyric andesite lava lithic | APP | 60 m upstm of W99936, Oteao Stm | T11/512658 | T | | | | | | |
| W99936LG | dk grey med phyric dacite lava lithic | DPP | 60 m upstm of W99936, Oteao Stm | T11/512658 | T | | | | | | |
| W99936LH | brown fine phyric rhyolite lava lithic | RP | 60 m upstm of W99936, Oteao Stm | T11/512658 | T | | | | | | |
| W99936LI | brown lith r welded ignimbrite lithic | MAN | 60 m upstm of W99936, Oteao Stm | T11/512658 | T | | | | | | |
| W99936LJ | grey fine phyric rhyolite lava lithic | RP | 60 m upstm of W99936, Oteao Stm | T11/512658 | T | | | | | | |
| W99937 | purple/grey weath fine phyric rhyolite lava | kw | Oteao Stm | T11/512657 | T | | | | | | |
| W99938 | lt grey/brown pum r lith p weakly welded ignimbrite | wes-1 | 50m upstm of W99938, Oteao Stm | T11/512657 | T | | | | | | |
| W99938LA | brown cry r pum r welded ignimbrite lithic | VAP | 50m upstm of W99938, Oteao Stm | T11/512657 | T | M | | | | | |
| W99938LB | grey/brown fine phyric rhyolite lava lithic | RP | 50m upstm of W99938, Oteao Stm | T11/512657 | T | M | | | | | |
| W99938LC | brown cry r pum r welded ignimbrite lithic | VAP | 50m upstm of W99938, Oteao Stm | T11/512657 | | | | | | | |
| W99938LD | grey/lt blue fine phyric rhyolite lava lithic | RPA | 50m upstm of W99938, Oteao Stm | T11/512657 | T | | | | | | |
| W99938LE | brown med phyric andesite lava lithic | APP | 50m upstm of W99938, Oteao Stm | T11/512657 | T | | | | | | |
| W99939LF | grey/brown fine phyric rhyolite lava lithic | RPP | 50m upstm of W99938, Oteao Stm | T11/512657 | T | | | | | | |
| W99940 | lt grey pum r lith p weakly welded ignimbrite | wes-4 | Oteao Stm | T11/513654 | T | | | | | | |
| W99940LA | pink/grey fine phyric rhyolite lava lithic | RPP | Oteao Stm | T11/513654 | T | | | | | | |
| W99940LB | brown/grey med phyric rhyolite lava lithic | RPP | Oteao Stm | T11/513654 | T | | | | | | |
| W99940LC | dk grey/red fine phyric andesite lava lithic | APP | Oteao Stm | T11/513654 | T | | | | | | |
| W99940LD | grey glassy fine phyric rhyolite lava lithic | RPP | Oteao Stm | T11/513654 | T | | | | | | |
| W99940LE | grey/pink fine phyric rhyolite lava lithic | RPP | Oteao Stm | T11/513654 | | | | | | | |
| W99941 | brown poorly sorted volcanic breccia | kw | 30m upstm of W99921, Oteao Stm | T11/519650 | T | | | | | | |
| W99942 | purple/grey fine phyric rhyolite lava | kw | downstm of Oteao-tribut. confluence | T11/519651 | T | | | | | | |
| W99943 | lt grey pum r weakly welded ignimbrite | wes-4 | confluence of Oteao-tributary stm | T11/518651 | T | | | | | | |
| W99943LA | grey-brown fine phyric rhyolite lava lithic | RPP | confluence of Oteao-tributary stm | T11/518651 | T | | | | | | |
| W99943LB | grey med phyric andesite lava lithic | APP | confluence of Oteao-tributary stm | T11/518651 | T | M | | | | | |
| W99943LC | red/brown fine phyric andesite lava lithic | APP | confluence of Oteao-tributary stm | T11/518651 | T | | | | | | |
| W99943LD | dk grey fine phyric glassy dacite lava lithic | DPP | confluence of Oteao-tributary stm | T11/518651 | T | | | | | | |
| W99943LE | grey/pink fine phyric rhyolite lava lithic | RPP | confluence of Oteao-tributary stm | T11/518651 | T | | | | | | |
| W99943LF | grey fine phyric amygda rhyolite lava lithic | RPP | confluence of Oteao-tributary stm | T11/518651 | T | | | | | | |
| W99943LG | dk grey fine phyric andesite lava lithic | APP | confluence of Oteao-tributary stm | T11/518651 | T | | | | | | |
| W99943LH | grey fine phyric rhyolite lava lithic | RPP | confluence of Oteao-tributary stm | T11/518651 | T | | | | | | |
| W99944 | purple/grey fine phyric rhyolite lava | kw | tributary of Oteao Stm | T11/508660 | T | | | | | | |
| W99945 | purple/grey fine phyric rhyolite lava | kw | Oteao Stm | T11/508662 | T | | | F | | | |
| W99946 | lt blue/grey fine phyric rhyolite lava | kw | ridgeline in Oteao valley | T11/510662 | T | | | | | | |
| W99947 | lt grey lith r weakly welded ignimbite | wes-1 | paddock to SE of farm track | T11/499658 | T | | | | | | |
| W99948LA | dk grey/brown fine phyric andesite lava lithic | APP | paddock to SE of farm track | T11/499658 | T | | | | | | |
| W99948LB | dk grey fine phyric andesite lava lithic | APP | paddock to SE of farm track | T11/499658 | T | | | | | | |
| W99948LC | green relict fine phyric altered andesite lava lithic | APP | paddock to SE of farm track | T11/499658 | T | | | | | | |
| W99948LD | lt grey glassy fine phyric incip vesic rhyolite lava lithic | RP | paddock to SE of farm track | T11/499658 | T | | | | | | |
| W99948LE | lt grey fine phyric rhyolite lava lithic | RPP | paddock to SE of farm track | T11/499658 | T | | | | | | |
| W99949 | grey well sorted massive volcaniclastic siltstone | wh | Kapowai River | T11/543687 | | | | | | | |
| W99950 | lt grey lith r pum r weakly welded ignimbrite | wes-1 | E bank of Kapowai River | T11/542688 | T | | | F | | | |
| W99950LA | brown/orange pum r silicified welded ignimbrite lithic | MAN | E bank of Kapowai River | T11/542688 | T | | | | | | |
| W99950LB | brown/grey fine phyric rhyolite lava lithic | RPP | E bank of Kapowai River | T11/542688 | T | | | | | | |
| W99950LC | cream med phyric rhyolite lava lithic | RP | E bank of Kapowai River | T11/542688 | T | | | | | | |
| W99950LD | grey/pink f band fine phyric rhyolite lava lithic | RPP | E bank of Kapowai River | T11/542688 | T | | | | | | |
| W99950LE | black poor vesic fine phyric andesite lava lithic | APP | E bank of Kapowai River | T11/542688 | T | | | F | | | |
| W99950LF | grey glassy med phyric andesite lava lithic | APA | E bank of Kapowai River | T11/542688 | T | M | | | | | |
| W99950LG | grey/pink amygda spher fine phyric rhyolite lava lithic | RPP | E bank of Kapowai River | T11/542688 | T | | | | | | |

| W No. | Lithology | Unit | Location | Grid Ref. | T | M | P | F | D | I | K |
|---|---|---|---|---|---|---|---|---|---|---|---|
| W99950LH | grey med phyric dacite lava lithic | APP | E bank of Kapowai River | T11/542688 | T | | | | | | |
| W99950LI | brown/orange pum r cry r welded ignimbrite lithic | MAN | E bank of Kapowai River | T11/542688 | T | | | | | | |
| W99950LJ | grey glassy crs phyric dacite lava lithic | DPQ | E bank of Kapowai River | T11/542688 | T | M | | | | | |
| W99950LK | green silicified pum r welded ignimbrite lithic | SPI | E bank of Kapowai River | T11/542688 | T | | | | | | |
| W99950LL | pink/grey pum r cry r welded ignimbrite lithic | UND | E bank of Kapowai River | T11/542688 | T | | | | | | |
| W99950LM | grey med phyric dacite lava lithic | DPQ | E bank of Kapowai River | T11/542688 | T | | | | | | |
| W99950LN | grey fine phyric andesite lava lithic | APP | E bank of Kapowai River | T11/542688 | T | | | | | | |
| W99950LO | green/grey silicified pum r welded ignimbrite lithic | WSI | E bank of Kapowai River | T11/542688 | T | | | | | | |
| W99950LP | brown/orange lith r welded ignimbrite lithic | MAN | E bank of Kapowai River | T11/542688 | T | | | | | | |
| W99950LQ | brown cry r welded ignimbrite lithic | TRI | E bank of Kapowai River | T11/542688 | T | | | | | | |
| W99950LR | brown pum r lentic cry r welded ignimbrite lithic | TRI | E bank of Kapowai River | T11/542688 | T | M | | | | | |
| W99950LS | lt brown well sorted coarse ash vitric tuff lithic | RVT | E bank of Kapowai River | T11/542688 | T | | | | | | |
| W99951 | dk grey med-phyric andesite lava | ap | Kapowai River | T11/542689 | T | M | P | F | | I | |
| W99952 | lt grey pum r weakly welded ignimbrite | wes-4 | scarp to E of Parakau Rd | T11/546688 | T | | | F | | | |
| W99952LA | grey fine phyric silic/altered andesite lava lithic | SAL | scarp to E of Parakau Rd | T11/546688 | T | | | | | | |
| W99952LB | grey/cream silicified rhyolite lava lithic | SRL | scarp to E of Parakau Rd | T11/546688 | T | | | | | | |
| W99952LC | blue/grey fine phyric rhyolite lava lithic | RPP | scarp to E of Parakau Rd | T11/546688 | T | | | | | | |
| W99952LD | brown/grey f band fine phyric rhyolite lava lithic | RPP | scarp to E of Parakau Rd | T11/546688 | T | | | | | | |
| W99952LE | brown silicified lith r welded ignimbrite lithic | WSI | scarp to E of Parakau Rd | T11/546688 | T | | | | | | |
| W99952LF | lt brown pum r welded ignimbrite lithic | UND | scarp to E of Parakau Rd | T11/546688 | T | | | | | | |
| W99953 | lt brown deeply weath pum r weakly welded ignimbrite | wes-1 | either side of foresty road | T11/551692 | | | | | | | |
| W99954 | lt grey pum r lith r weakly-partially welded ignimbrite | h | Kapowai River | T11/530623 | T | | | | | | |
| W99954LA | grey mm f band altered rhyolite lava lithic | RPP | Kapowai River | T11/530623 | T | | | | | | |
| W99954LB | grey/brown fine phyric dacite lava lithic | DPP | Kapowai River | T11/530623 | T | | | | | | |
| W99954LC | grey glassy incip vesic fine phyric rhyolite lava lithic | RPP | Kapowai River | T11/530623 | T | | | | | | |
| W99954LD | brown lith r welded ignimbrite lithic | UND | Kapowai River | T11/530623 | | | | | | | |
| W99955 | grey/green pum r hydro alt. weakly welded ignimbrite | h | Kapowai River | T11/532625 | T | | | | D | | |
| W99955LA | grey fine phyric rhyolite lava lithic | RPP | Kapowai River | T11/532625 | T | | | | | | |
| W99955LB | grey fine phyric hydro alt. rhyolite lava lithic | PRL | Kapowai River | T11/532625 | T | | | | | | |
| W99955LC | grey pum r welded ignimbrite lithic | SPI | Kapowai River | T11/532625 | T | | | | | | |
| W99955LD | grey fine phyric rhyolite lava lithic | RPP | Kapowai River | T11/532625 | T | | | | | | |
| W99955LE | dk grey/brown fine phyric veined/miner. lava lithic | PRL | Kapowai River | T11/532625 | T | | | | | | |
| W99955LF | grey glassy fine phyric hydro alt. rhyolite lava lithic | PRL | Kapowai River | T11/532625 | T | | | | | | |
| W99955LG | cream pum r altered welded ignimbrite lithic | SPI | Kapowai River | T11/532625 | T | | | | | | |
| W99955LH | grey glassy fine phyric rhyolite lava lithic | PRL | Kapowai River | T11/532625 | T | | | | | | |
| W99956 | grey/green lith r pum p weakly welded ignimbrite | h | 80m downstm of W99955, Kapowai River | T11/532625 | T | | | | | | |
| W99957 | brown lith r weakly welded ignimbrite | wes-1 | 20m downstm of W99956, Kapowai River | T11/532626 | T | | | | | | |
| W99958 | brown lith r pum r weakly welded ignimbrite | h | Kapowai River | T11/542640 | T | | | | | | |
| W99958LA | red/brown spher f band fine phyric rhyolite lava lithic | PRL | Kapowai River | T11/542640 | T | | | | | | |
| W99958LB | grey fine phyric andesite lava lithic | APP | Kapowai River | T11/542640 | T | | | | | | |
| W99958LC | grey/brown altered lith r welded ignimbrite lithic | SPI | Kapowai River | T11/542640 | T | | | | | | |
| W99958LD | pink/green f band med phyric rhyolite lava lithic | DPP | Kapowai River | T11/542640 | T | | | | | | |
| W99958LE | lt brown/cream indurated fine ash vitric tuff lithic | RVT | Kapowai River | T11/542640 | T | | | | | | |
| W99958LF | grey f band fine phyric rhyolite lava lithic | RPP | Kapowai River | T11/542640 | T | | | | | | |
| W99959 | purple/grey hydro. alt. weakly welded ignimbrite | h | Kapowai River-tributary confluence | T11/542641 | T | | | | D | | |
| W99960 | grey/green lith p weakly welded hydro alt. ignimbrite | h | Kapowai River-tributary confluence | T11/542641 | T | | | | D | | |
| W99961 | lith r weakly welded hydro. alt. ignimbrite | h | Kapowai River | T11/542642 | T | | | | | | |
| W99962 | brown weath pum r hydro alt. weakly welded ignimbrite | h | E bank, Kapowai River | T11/547651 | T | | | | | | |
| W99963 | blue/grey fine phyric hydro alt. rhyolite lava | h | Kapowai River-tributary confluence | T11/549654 | T | | | | D | | |
| W99964 | pale brown/buff pum r lith p weakly welded ignimbrite | wes-4 | upstm of 5m waterfall, Wharepapa Stm | T11/532676 | T | | | | | | |
| W99964LA | brown/red med phyric dacite lava lithic | DPP | upstm of waterfall, Wharepapa Stm | T11/532676 | T | | | | | | |
| W99964LB | grey spher fine phyric rhyolite lava lithic | RPP | upstm of waterfall, Wharepapa Stm | T11/532676 | T | | | | | | |
| W99964LC | grey spher flow b fine phyric rhyolite lava lithic | RPP | upstm of waterfall, Wharepapa Stm | T11/532676 | T | | | | | | |
| W99964LD | lt grey med phyric rhyolite lava lithic | RPP | upstm of waterfall, Wharepapa Stm | T11/532676 | T | | | | | | |
| W99965 | lt brown weath pum r lith p weakly welded ignimbrite | wes-4 | Wharepapa Stm | T11/533675 | T | | | | | | |
| W99965LA | grey med phyric rhyolite lava lithic | RPP | Wharepapa Stm | T11/533675 | T | | | | | | |
| W99965LB | grey mm f band fine phyric rhyolite lava lithic | RP | Wharepapa Stm | T11/533675 | T | | | | | | |
| W99965LC | grey f band med phyric rhyolite lava lithic | RPP | Wharepapa Stm | T11/533675 | T | | | | | | |
| W99965LD | grey mm f band fine phyric rhyolite lava lithic | RP | Wharepapa Stm | T11/533675 | T | | | | | | |
| W99965LE | grey mm f band spher fine phyric rhyolite lava lithic | RPP | Wharepapa Stm | T11/533675 | T | | | | | | |
| W99966 | lt grey pum r weakly welded ignimbrite | wes-4 | Wharepapa Stm | T11/533674 | T | | | | | | |
| W99966LA | grey glassy incip vesic fine phyric rhyolite lava lithic | RPP | Wharepapa Stm | T11/533674 | T | | | | | | |
| W99966LB | grey f band glassy fine phyric rhyolite lava lithic | RPP | Wharepapa Stm | T11/533674 | T | | | | | | |
| W99967 | grey pum r lith r weakly welded ignimbrite | wes-4 | Wharepapa Stm | T11/533673 | T | | | | | | |
| W99967LA | grey/pink mm f band fine phyric dacite lava lithic | DPP | Wharepapa Stm | T11/533673 | T | | | | | | |
| W99967LB | grey fine phyric rhyolite lava lithic | RPP | Wharepapa Stm | T11/533673 | T | M | | | | | |
| W99967LC | grey spher fine phyric dacite lava lithic | DPP | Wharepapa Stm | T11/533673 | T | | | | | | |
| W99967LD | grey fine phyric dacite lava lithic | DPP | Wharepapa Stm | T11/533673 | T | | | | | | |
| W99968 | brown weakly welded ignimbrite | wes-4 | 60m upstm of W99967, Wharepapa Stm | T11/533673 | | | | | | | |
| W99969 | brown pum r weakly welded ignimbrite | wes-4 | 60m upstm of W99968, Wharepapa Stm | T11/533672 | T | | | | | | |
| W99970 | lt grey pum r weakly welded ignimbrite | wes-4 | 12m waterfall, tributary of Oteao Stm | T11/504666 | T | | | | | | |
| W99970LA | grey spher fine phyric rhyolite lava lithic | RPP | 12m waterfall, tributary of Oteao Stm | T11/504666 | T | | | | | | |
| W99970LB | grey/pink fine phyric rhyolite lava lithic | RPP | 12m waterfall, tributary of Oteao Stm | T11/504666 | T | | | | | | |
| W99970LC | grey/pink fine phyric rhyolite lava lithic | RPP | 12m waterfall, tributary of Oteao Stm | T11/504666 | T | | | | | | |
| W99970LD | grey fine phyric rhyolite lava lithic | RPP | 12m waterfall, tributary of Oteao Stm | T11/504666 | T | | | | | | |
| W99970LE | black med phyric poorly vesicular andesite lava lithic | APP | 12m waterfall, tributary of Oteao Stm | T11/504666 | T | | | | | | |
| W99971 | purple/pink fine phyric rhyolite lava | kw | 100m+ waterfall, Oteao Stm | T11/508663 | T | | | F | | | |
| W99972 | lt grey pum r weakly welded ignimbrite | wes-1 | 100m downstm of waterfall | T11/508664 | | | | | | | |
| W99972LA | brown/grey spher flow b fine phyric rhyolite lava lithic | RPP | 100m downstm of waterfall | T11/508664 | T | | | | | | |
| W99972LB | grey/blue fine phyric rhyolite lava lithic | RPP | 100m downstm of waterfall | T11/508664 | T | | | | | | |
| W99972LC | grey/blue amyg fine phyric rhyolite lava lithic | RPP | 100m downstm of waterfall | T11/508664 | T | | | F | | | |
| W99972LD | grey med phyric andesite lava lithic | APP | 100m downstm of waterfall | T11/508664 | T | | | | | | |
| W99972LE | lt brown fine phyric andesite lava lithic | APP | 100m downstm of waterfall | T11/508664 | T | | | | | | |
| W99972LF | red/brown med phyric andesite lava lithic | APP | 100m downstm of waterfall | T11/508664 | T | M | | | | | |
| W99972LG | grey/brown fine phyric flow b rhyolite lava lithic | RPP | 100m downstm of waterfall | T11/508664 | T | | | | | | |
| W99973 | lt grey lith p weakly welded ignimbrite | wes-1 | E side of ridgeline | T11/511678 | T | | | F | | | |
| W99974 | lt grey pum r weakly welded ignimbrite | wes-1 | confluence of Oteao Stm and trib. | T11/507675 | | | | | | | |
| W99974LA | brown/red amygda fine phyric rhyolite lava lithic | RPP | confluence of Oteao Stm and trib. | T11/507675 | T | | | | | | |
| W99974LB | grey fine phyric andesite lava? lithic | APP | confluence of Oteao Stm and trib. | T11/507675 | T | | | | | | |

| W No. | Lithology | Unit | Location | Grid Ref. | T | M | P | F | D | I | K |
|---|---|---|---|---|---|---|---|---|---|---|---|
| W99974LC | grey med phyric andesite lava lithic | APP | confluence of Oteao Stm and trib. | T11/507675 | T | M | | | | | |
| W99974LD | grey med phyric andesite lava lithic | APP | confluence of Oteao Stm and trib. | T11/507675 | T | | | | | | |
| W99974LE | brown/red glassy fine phyric rhyolite lava lithic | RPP | confluence of Oteao Stm and trib. | T11/507675 | T | | | | | | |
| W99974LF | brown/red spher fine phyric rhyolite lava lithic | RPP | confluence of Oteao Stm and trib. | T11/507675 | T | | | | | | |
| W99974LG | grey med phyric andesite lava lithic | APP | confluence of Oteao Stm and trib. | T11/507675 | T | | P | F | | I | |
| W99975 | lt grey lith r weakly welded ignimbrite | wes-1 | ridgeline west of Oteao valley | T11/503674 | | | | | | | |
| W99975LA | grey fine phyric rhyolite lava lithic | RP | ridgeline west of Oteao valley | T11/503674 | T | | | | | | |
| W99975LB | grey mm-scale flow b fine phyric rhyolite lava lithic | RPP | ridgeline west of Oteao valley | T11/503674 | T | | | | | | |
| W99975LC | black fine phyric incip vesicular andesite lava lithic | APP | ridgeline west of Oteao valley | T11/503674 | T | | | F | | | |
| W99975LD | grey fine phyric glassy rhyolite lava lithic | RPP | ridgeline west of Oteao valley | T11/503674 | T | | | | | | |
| W99975LE | grey fine phyric rhyolite lava lithic | RPP | ridgeline west of Oteao valley | T11/503674 | T | M | | | | | |
| W99975LF | grey/brown spher fine phyric rhyolite lava lithic | RPP | ridgeline west of Oteao valley | T11/503674 | T | | | | | | |
| W99975LG | brown/orange silicified pum r welded ignimbrite lithic | WSI | ridgeline west of Oteao valley | T11/503674 | T | | | | | | |
| W99975LH | grey/brown fine phyric rhyolite lava lithic | RP | ridgeline west of Oteao valley | T11/503674 | T | M | | | | | |
| W99976 | purple/grey med phyric rhyolite lava | sm | Wharepapa Stm | T11/535665 | T | M | | F | | | |
| W99977 | cream/grey lith r pum r weakly welded ignimbrite | wes-4 | 10m downstm of W99976 | T11/535665 | T | | | | | | |
| W99977LA | grey glassy med phyric rhyolite lava lithic | RPP | 10m downstm of W99976 | T11/535665 | | | | | | | |
| W99977LB | grey glassy med phyric rhyolite lava lithic | RPP | 10m downstm of W99976 | T11/535665 | T | | | | | | |
| W99977LC | dk grey glassy med phyric andesite lava lithic | APP | 10m downstm of W99976 | T11/535665 | T | | | | | | |
| W99977LD | grey glassy med phyric rhyolite lava lithic | RPP | 10m downstm of W99976 | T11/535665 | T | | | | | | |
| W99977LE | grey glassy fine phyric incip. vesic rhyolite lava lithic | RPP | 10m downstm of W99976 | T11/535665 | T | | | | | | |
| W99977LF | dk grey glassy med phyric andesite lava lithic | APP | 10m downstm of W99976 | T11/535665 | T | | | | | | |
| W99978 | lt grey pum p lith p mod sorted vitric ash tuff | wes-4 | 15m downstm of W99977 | T11/535665 | T | | | | | | |
| W99979 | lt grey lith p vitric ash tuff | wes-4 | 15m downstm of W99978 | T11/535665 | T | | | | | | |
| W99980 | grey poorly sorted volcaniclastic lacustrine sandstone | wes-4 | 10m downstm of W99979 | T11/535665 | | | | | | | |
| W99981 | cream/grey pum r lith p silicified ignimbrite | wes-4 | 20m downstm of W99980 | T11/535665 | | | | | | | |
| W99982 | brown cry r pum r ignimbrite | wes-4 | 15m downstm of W99981 | T11/535665 | | | | | | | |
| W99983 | cream/grey cry r weakly welded ignimbrite | wes-4 | 60m downstm of W99982 | T11/534668 | | | | | | | |
| W99984 | yellow/cream pum p lith p massive lacustrine siltstone | wes-4 | Wharepapa Stm | T11/534679 | | | | | | | |
| W99985 | purple/grey fine phyric rhyolite lava | kk | intersection of forestry tracks | T11/541669 | T | | | | | | |
| W99986 | pale brown pum r weakly welded ignimbrite | cp | Trig Q section | T11/515701 | T | | | F | | | |
| W99986LA | cream/grey well sorted massive volcaniclastic sandstone lithic | VSA | Trig Q section | T11/515701 | T | | | | | | |
| W99986LB | dk grey incip vesic glassy fine phyric dacite lava lithic | DPP | Trig Q section | T11/515701 | T | | | | | | |
| W99986LC | grey fine phyric rhyolite lava lithic | RP | Trig Q section | T11/515701 | T | | | | | | |
| W99986LD | brown/orange pum r welded ignimbrite lithic | UND | Trig Q section | T11/515701 | T | | | | | | |
| W99986LE | brown/grey cry r welded ignimbrite lithic | UND | Trig Q section | T11/515701 | T | | | | | | |
| W99987 | cream/pink pum r lith p weakly welded ignimbrite | qi | Trig Q section | T11/515701 | T | | | | | | |
| W99988 | lt brown pum r weakly welded ignimbrite | qi | Trig Q section | T11/515701 | T | M | | F | | | |
| W99989 | dk grey cry r lith p weakly welded ignimbrite | qi | Trig Q section | T11/515701 | T | | | F | | | |
| W99990 | dk grey cry r lith p high lentic partially welded ignimbrite | qi | Trig Q section | T11/515701 | T | M | P | F | | | |
| W99991 | brown pum r lith r weakly welded ignimbrite | wes-1 | W side of ridgeline | T11/512720 | T | | | | | | |
| W99991LA | grey/pink amygda fine phyric rhyolite lava lithic | RP | W side of ridgeline | T11/512720 | T | | | | | | |
| W99991LB | black cry r welded ignimbrite lithic | UND | W side of ridgeline | T11/512720 | T | | | | | | |
| W99991LC | grey f band fine phyric rhyolite lava lithic | RPP | W side of ridgeline | T11/512720 | T | | | | | | |
| W99991LD | brown pum r cry r welded ignimbrite lithic | UND | W side of ridgeline | T11/512720 | T | | | | | | |
| W99991LE | brown poor vesic fine phyric dacite lava lithic | DPP | W side of ridgeline | T11/512720 | T | | | | | | |
| W99991LF | grey devit fine phyric rhyolite lava lithic | RP | W side of ridgeline | T11/512720 | T | | | | | | |
| W99991LG | brown glassy fine phyric rhyolite lava lithic | RPP | W side of ridgeline | T11/512720 | T | | | | | | |
| W99991LH | lt grey/brown med phyric rhyolite lava lithic | RPP | W side of ridgeline | T11/512720 | T | | | | | | |
| W99992 | lt grey pum r lith r weakly welded ignimbrite | wes-1 | W side of ridgeline | T11/512720 | T | | | | | | |
| W99993 | grey/blue fine phyric pheno r rhyolite lava | kc | off Pinnacles Track | T12/502577 | T | | | F | | | |
| W99994 | lt grey glassy med phyric rhyolite lava | kc | Pinnacles Track | T12/504578 | T | M | P | F | | I | K |
| W99995 | grey fine phyric rhyolite lava | kp | The Pinnacles | T12/518579 | T | M | P | F | | I | |
| W99996 | grey fine phyric rhyolite lava | us | Pinnacles Track | T12/512583 | T | | | | | | |
| W99997 | grey fine phyric rhyolite lava | h | Pinnacles Track | T12/493576 | T | | | | | | |
| W99998 | cream/white silicified rhyolite lava | h | Welcome Jack Track | T11/495628 | T | | | | D | | |
| W99999 | grey/yellow silicified rhyolite lava | h | Welcome Jack Track | T11/496629 | T | | | | D | | |
| W9991000 | cream silicified rhyolite lava | h | Welcome Jack Track | T11/498627 | T | | | | | | |
| W9991001 | pale green lith r weakly welded hydro.alt. ignimbrite | h | Mine Creek | T11/495633 | T | | | | D | | |
| W9991001LA | cream fine phyric silicified rhyolite lava lithic | SRL | Mine Creek | T11/495633 | T | | | | | | |
| W9991001LB | cream fine phyric silicified dacite lava lithic | SDL | Mine Creek | T11/495633 | T | | | | | | |
| W9991001LC | cream med phyric silicified rhyolite lava lithic | PRL | Mine Creek | T11/495633 | T | | | | | | |
| W9991001LD | cream/green altered welded ignimbrite lithic | SPI | Mine Creek | T11/495633 | T | | | | | | |
| W9991002 | grey/pink fine phyric rhyolite lava | kg | Top of waterfall, trib. of Kapowai | T11/556654 | T | M | P | F | | I | K |
| W9991003 | grey pum r lith p weakly welded ignimbrite | wes-4 | knob on ridgeline | T/11561651 | T | | | | | | |
| W9991004 | cream bleached lith r weakly welded ignimbrite | wes-4 | forestry track | T11/523672 | | | | | | | |
| W9991005 | lt grey med phyric biotite rhyolite | ur | ridgeline w of Kokonga stream | T11/565648 | T | M | P | F | | | K |
| W9991006 | grey fine phyric rhyolite lava | us | Pinnacles Track | T12/512583 | T | M | | | | | |
| W9991007 | grey/pink fine phyric rhyolite lava | kc | Billy Goat Track | T12/496570 | T | | | | | | |
| W9991008 | grey/blue fine phyric rhyolite lava | ka | Billy Goat Track | T12/491557 | T | | | | | | |
| W9991009 | dark grey fine phyric andesite lava | at | Atuatumoe Stream | T12/481564 | T | | | | | | |
| W9991010 | dark grey fine phyric andesite lava | at | Atuatumoe Stream | T12/484562 | T | | | | | | |
| W9991011 | dark grey fine phyric andesite lava | at | Phil's Stream | T12/452592 | T | | | | | | |
| W9991012 | dark grey fine phyric andesite lava | at | Waiwawa River | T12/456594 | T | | | | | | |
| W9991013 | lt brown horiz. laminated volcaniclastic sandstone | ww | Waiwawa River | T12/460594 | T | | | | | | |
| W9991014 | dark grey fine phyric andesite lava | at | Waiwawa River | T12/453596 | T | | | | | | |
| W9991015 | cream medium phyric rhyolite lava | ur | Paul Rd Track | T11/576633 | T | M | | | | | |
| W9991016 | grey medium phyric andesite lava | cn | McGorman Rd | T11/527693 | T | M | | | | | |

# Appendix II

## Lithologic parameters for pyroclastic deposits

Several parameters are used to describe the physical nature of pyroclastic deposits or the components (juvenile clasts, lithic fragments) within the deposits. This appendix defines those parameters used to describe KCC pyroclastic deposits.

### Welding

Welding parameters used in this study (Table II.1) are based upon the definitions of Streck and Grunder (1995).

Table II.1 Definition of welding terms applied to Kapowai Caldera Complex ignimbrites. Adapted from Streck and Grunder (1995).

| Welding | density | clast adhesion | clast deformation | |
|---|---|---|---|---|
| | | | juvenile | shards |
| densely | high | complete | moderate-strong | strong |
| partially | moderate-high | strong | moderate | slight |
| weakly | moderate | moderate | slight | slight |
| incipiently | moderate-low | slight | none | none |
| non-welded | low | none | none | none |

### Vesicularity

Juvenile clast vesicularity is defined (Table II.2) using the definitions of Houghton and Wilson (1989). Vesicularity is estimated in the field, and the vesicularity of individual juvenile clasts has not been measured in the laboratory.

Table II.2 Vesicularity of juvenile clasts in Kapowai Caldera Complex pyroclastic deposits. From Houghton and Wilson (1989).

| Description | % vesicularity |
|---|---|
| non vesicular | 0-5 |
| incipiently vesicular | 5-20 |
| poorly vesicular | 20-40 |
| moderately vesicular | 40-60 |
| highly vesicular | 60-80 |
| extremely vesicular | >80 |

### Fibrousity

The internal form or fibrousity of juvenile clasts is described by examining the size and shape of vesicles, and the length and spacing of glass fibres. No fibrousity parameters are known in the literature, and so in

this study fibrousity is defined on the basis of vesicle shape and relative distance between glass shards (Table II.3).

Table II.3 Definition of juvenile clast fibrousity for Kapowai Caldera Complex pyroclastic deposits.

| Fibrousity | internal form | vesicle shape | distance between glass strands |
|---|---|---|---|
| non | open framework | circular | large |
| poorly | semi-closed | ellipsoidal | moderate |
| moderately | closed | cigar-shaped | small |
| highly | glass stringers | tubular | negligible |

## Lenticularity

Lenticularity is used to describe the external shape of juvenile clasts. External shape is influenced by (i) deformation of the clast by abrasion and welding, and (ii) by the internal vesicle morphology. Lenticularity is typically defined on the basis of a flattening ratio where the major clast axis (length) is compared to the minor clast axis (width). This approach is adopted, together with the external clast morphology to define lenticularity in this study (Table II.4).

Table II.4 Definition of juvenile clast lenticularity for Kapowai Caldera Complex pyroclastic deposits.

| Lenticularity | external form | Flattening ratio (l/w) |
|---|---|---|
| non | circular | 1:1 |
| incipiently | oblong | 1-2:1 |
| poorly | oblong-cigar | 2-4:1 |
| moderately | cigar shaped | 4-6:1 |
| highly | finger-like | >7:1 |

## Component abundance

A common approach in describing the relative abundance of pyroclastic components is to use relative terms. Terms used in this study are presented in Table II.5.

Table II.5 Abundance terms used to qualify relative proportions of pyroclastic components in Kapowai Caldera Complex pyroclastic deposits

| Component | relative abundance term | |
|---|---|---|
| | poor | rich |
| Juvenile(pumice/scoria) | <3% | >15% |
| Lithics | <3% | >10% |
| Crystals | <1% | >15% |

## Grain size limits

Pyroclastic grain sizes (Table II.6) have been established by Fisher (1961, 1966) and these have been further endorsed and recommended for use by Schmid (1981).

Table II.6 Pyroclastic grain size limits

| grainsize (mm) | pyroclastic fragment | |
|---|---|---|
| | coarse | |
| 256 | | bombs/blocks |
| | fine | |
| 64 | | |
| | | lapilli |
| 2 | | |
| | coarse | |
| 1/16 | | ash |
| | fine | |

## Maximum clast size

Maximum clast size is a key parameter used to quantify the largest clast incorporated and transported by a pyroclastic flow or dispersed by a pyroclastic fall deposit. It is defined here for both juvenile (pumice and scoria) and lithic components.

The maximum juvenile size (MJ) is defined as the mean long axis length of six juvenile fragments. The maximum lithic size (ML) is defined as the mean long axis length of six lithic fragments. All sizes are recorded in millimetres.

# Appendix III

## K-Ar dating: sample preparation and K & Ar analysis

### Sample Preparation

Sixteen samples (8 rhyolite lavas, 4 andesite lavas and 4 ignimbrites) were selected for K-Ar dating (Table III.1). Samples were selected on the basis of crystal freshness and lack of visible weathering. No samples chosen showed any evidence of hydrothermal alteration.

For lava samples, whole rock was used. For ignimbrites, whole rock was also used, but prior to crushing, lithic fragments were removed.

Separates of plagioclase and biotite crystals from lavas and ignimbrite samples were collected using the following methodology.

#### *Crushing/Washing*

Initially any weathered zones or organic matter was removed from the whole rock by a combination of trimming with a rock-saw and chipping with a geological hammer followed by washing in water. Samples were then dried overnight prior to crushing.

Samples were first coarsely crushed with a mechanical steel jaw-crusher. Approximately 2-3kg of sample was crushed, depending upon the abundance of plagioclase or biotite in the sample. Crushed rock was then fed into a (Bico) mill crusher with a gap set at approximately 350μm. Samples were then washed individually to remove the clay and silt fraction. Samples were placed in a bucket, saturated with water and the floating clay and silt particles were washed away. This was repeated until the water was clear. Samples were then dried overnight by placing in an oven at 100°C.

#### *Sieving*

Dried samples were dry sieved into three fractions; (i) > 1.0ϕ (>500 μm); (ii) 1.0ϕ - 1.75ϕ (500μm - 300μm); and (iii) < 1.75ϕ (< 300μm).

#### *Vertical magnetic separation*

Typically, only 1.0ϕ - 1.75ϕ sieved fractions were selected for heavy liquid density separations. Prior to density separations, sieved fractions were passed through a vertical magnet. Here magnetic minerals (pyroxenes, Fe-Ti oxides) were removed from the sample. Both the non-magnetic fraction and magnetic fraction were retained.

Table III.1. Sample numbers, location (+ grid reference) and lithology of Kapowai Caldera Complex volcanic rocks dated by the K/Ar method at the Hiruzen Research Institute, Japan, and at the Institute of Geological and Nuclear Sciences (IGNS), Lower Hutt, Wellington.

| Hiruzen Lab. | | | | | | | | | |
|---|---|---|---|---|---|---|---|---|---|
| **Sample** | **Lab No.** | **Lithology** | **Unit** | **Mineral** | **Location** | **Grid Reference** | **K wt.%** | **rad. 40Ar** | **Age** |
| W99614 | S36-151 | rhyolitic ignimbrite | WES-1 Ignimbrite | plag | 20 m east of Oteao Rd | T11/511643 | 0.262±0.013 | 5.48±0.12 | 5.38±0.29 |
| W99886 | S36-153 | rhyolitic ignimbrite | WES-1 Ignimbrite | plag | Kapowai River bed | T11/551679 | 0.345±0.017 | 8.29±0.18 | 6.18±0.34 |
| W99612 | S36-156 | andesitic ignimbrite | Oteao Ignimbrite | plag | eastern bank adjacent to Oteao Rd | T11/534670 | 0.240±0.012 | 5.30±0.14 | 5.68±0.32 |
| W99693 | S36-154 | rhyolitic ignimbrite | Webb Creek Ignimbrite | plag | Pinnacles Track - Webb Creek Stream | T12/486572 | 0.294±0.015 | 6.16±0.20 | 5.39±0.32 |
| W99600 | S36-155 | rhyolite lava | Rangihau Rhyolite | plag | eastern bank of Rangihau Stream | T11/499654 | 0.281±0.014 | 7.52±0.15 | 6.89±0.37 |
| W99912 | S36-152 | rhyolite lava dike | Precipice Rhyolite | plag | western bank of Kapowai River | T11/522660 | 0.211±0.011 | 4.20±0.08 | 5.12±0.28 |
| W99908 | S36-149 | rhyolite lava dike | Precipice Rhyolite | plag | western bank of Kapowai River | T11/522660 | 0.254±0.013 | 5.12±0.33 | 5.19±0.42 |
| W991002 | S36-150 | rhyolite lava | Kokonga Rhyolite | plag | head of waterfall in tributary steam of Kapowai River | T11/556654 | 0.221±0.011 | 5.60±0.14 | 6.51±0.36 |
| W991005 | S36-148 | rhyolite lava | Ruahine Rhyolite | plag | northern margin of Tanehua-Ruahine ridge | T11/565648 | 0.400±0.020 | 9.09±0.15 | 5.86±0.31 |
| W99835 | S36-157 | rhyolite lava | Welcome Jack Rhyolite | biot | 691 m s.h. | T11/511623 | 6.128±0.123 | 200.8±3.4 | 8.42±0.22 |
| **IGNS Lab.** | | | | | | | | | |
| **Sample** | **Lab No.** | **Lithology** | **Unit** | **Min** | | **Grid Reference** | **K wt.%** | **rad. 40Ar** | **Age** |
| W99876 | 22254 | rhyolite lava | Kauaeranga Rhyolite | plag | southern margin of Kauaeranga Gorge | T12/489583 | 0.22 | 0.042 | 4.9±0.6 |
| W99994 | 22255 | rhyolite lava | Camp Rhyolite | plag | southern outcrop adjacent to Pinnacles Track | T12/504578 | 0.29 | 0.060 | 5.3±0.3 |
| W99706 | 22256 | andesite lava | Taurauikau Andesite | plag | at crest of Moss Creek Track | T12/484596 | 0.29 | 0.096 | 8.5±0.6 |
| W99816 | 22257 | andesite lava | Taurauikau Andesite | plag | outcrop in farm paddock | T11/484647 | 0.31 | 0.092 | 7.6±0.5 |
| W99691 | 22258 | andesite lava | Taurahuehue Andesite | plag | 20m downstm of andesite-ignimbrite contact, Webb Creek Stream | T12/482572 | 0.28 | 0.072 | 6.6±0.3 |
| W99733 | 22259 | andesite lava | Taurauikau Andesite | plag | outcrop exposed on eastern side of ridge, Rangihau valley | T11/484636 | 0.29 | 0.072 | 6.4±0.4 |

***Plagioclase Separation***

### Density Separation

Separation of plagioclase and biotite crystals from glass was obtained by a heavy liquid density separation. Sodium polytungstate (SPT) was used as the separation agent. For the best separation, density of the SPT was set using a disc float of 2.51g/cm$^3$ and disc sink of 2.58g/cm$^3$. With the correct density achieved, the liquid was placed into a separation funnel, followed by the sample. Following initial and subsequent stirring, plagioclase and biotite (+ quartz) sank to the funnel bottom and glass floated. The sink and the float were separately removed, washed to remove all SPT and retained.

### Inclined Magnetic Separation

With the plagioclase/quartz fraction, the three minerals were separated on an inclined magnetic separator. Initially, settings were chute angle 15°, and magnet 1 amp to remove any residual volcanic glass. To separate quartz and plagioclase, settings were chute angle 3-5°, and magnet at 2 amp. (Froggatt and Gosson, 1982).

### Hand-picking

Further purification of each plagioclase separate was attained by hand-picking to remove residual quartz or glass grains.

***Biotite Separation***

Following initial sample preparation, biotite crystals were separated using either an inclined board or hand-picking. SPT heavy liquid was not used to separate crystals.

## K and Ar analysis

Analysis of mineral separates were undertaken by the Institute of Geological Sciences, Wellington (6 samples) and the Hiruzen Research Institute, Japan (10 samples). Approximately 0.5 g of biotite and 1-2 g of plagioclase separate were prepared.

Analytical methods for the IGNS lab are presented below. For the Hiruzen Research lab, details of the K and Ar analysis method and error can be found in Itaya et al. (1991).

***Institute of Geological and Nuclear Sciences (IGNS), Wellington.***

### Argon Analysis

Argon is extracted in vacuo in a stainless steel/pyrex UHV system. Approximately 300mg is accurately weighed into a tantalum crucible and packed in a quartz wool 'cocoon'. Pumping and bakeout of the system at 100°C for twelve hours achieves initial vacuum of 5 x $10^{-8}$ torr. The sample is fused by RF

heating at about 1400 - 1500°C for five minutes. Immediately prior to fusion, an aliquot of Ar-38 tracer gas or 'spike' (about 2nL NTP) is dispensed into the system from an all metal precision gas pipette. A Ti/Zr getter and titanium sublimation pump are used to clean the gas, which is then analysed on a modified AEI MS10 mass spectrometer.

Mass spectrometer discrimination is frequently monitored using atmospheric argon standard (obsidian from Mayor Island) and samples are run in conjunction with the USGS biotite standard, LP6, radiogenic argon 43.09 nL/g.

### Potassium analysis

Potassium content is determined by XRF using a SRS-303 spectrometer, fitted with end-window rhodium tube. All major oxides are determined for correction of matrix effects on potassium. Results are the mean of three replicate determinations using fused discs and are expressed as weight % on oven-dried basis.

### Age Determination.

A radiometric K/Ar age was determined for each IGNS sample using the decay constants of (Steiger and Jager, 1977), and are 0.581 x $10^{-10}$ $yr^{-1}$ and 0.4962 x $10^{-9}$ $yr^{-1}$ for $^{40}K$ to $^{40}Ar$ and $^{40}Ca$, respectively, and 0.0001167 for $^{40}K$ content in potassium.

### Errors

Errors in the K content is ± 0.01% for all K values. For the radiogenic argon values, error consists of the precision of the total $^{40}Ar$, and error in the atmospheric argon correction. The latter is widely variable, independent of the % of radiogenic argon with respect to the total %. It varies from 1% up to about 20% for very low radiogenic argon.

# Appendix IV

## Pyroclastic componentry data

Table IV.1 Component (juvenile, lithic, and crystal) size and abundance for intracaldera Kapowai Caldera Complex ignimbrites.

| Sample | Grid Ref. | Ignimbrite | 6 Max. Juvenile (mm) | MJ(mm) | Total Juv % | Juvenile % | 6 Max. Lithic (mm) | ML(mm) | Lithic % | Crystal % |
|---|---|---|---|---|---|---|---|---|---|---|
| W99606 | T11/496680 | wes-1 | type (i) 19, 18, 16 ,16, 12,11 | 15 | 25 | 25 | 120, 94, 90, 73, 56, 51 | 80 | 5 | 5 |
| W99630 | T11/533677 | wes-1 | type (i) 86, 75, 33, 32, 26, 22 | 46 | 45 | 32 | 12, 10, 10, 9, 7, 7 | 9 | <1 | <3 |
| | | | type (ii) 58, 22, 21, 16, 14, 11 | 24 | | 13 | | | | |
| W99631 | T11/534679 | wes-1 | type (i) 46, 40, 19, 17, 16, 14 | 25 | 40 | 26 | 65, 32, 28, 26, 22, 20 | 32 | <3 | <1 |
| | | | type (ii) 8, 6, 6, 6, 5, 4 | 6 | | 14 | | | | |
| W99633 | T11/534668 | wes-4 | type (i) 35, 30, 26, 24, 20, 19 | 26 | 20 | 11 | 49, 45, 39, 36, 30, 29 | 38 | <3 | 3 |
| | | | type (ii) 16, 14, 13, 11, 11, 8 | 12 | | 9 | | | | |
| W99645 | T12/498576 | wes-1 | type (i) 43, 38, 38, 36, 32, 22 | 36 | 5 | 5 | 113, 92, 85, 81, 67, 63 | 84 | 3 | 7 |
| | | | type (ii) 18, 15, 15, 12, 11, 10 | 14 | | | | | | |
| W99649 | T12/495562 | wes-4 | type (i) 32, 27, 26, 19, 18, 16 | 138 | 20 | 20 | 89, 85, 77, 61, 40, 29 | 63 | 5 | <3 |
| W99650 | T12/493565 | wes-4 | type (i) 39, 36, 34, 30, 28, 21 | 31 | 10 | 7 | 82, 75, 71, 51, 43, 40 | 60 | <1 | 3 |
| | | | type (ii) 17, 16, 12, 12, 11, 9 | 13 | | 3 | | | | |
| W99677A | T12/472576 | wes-1 | type (i) 17, 13, 14, 10, 8, 4, 2 | 11 | 5 | 5 | 33, 30, 28, 26, 21, 21 | 26 | <3 | 3 |
| W99714 | T11/496648 | wes-1 | type (i) 12, 8, 8, 7, 6, 6 | 8 | 12 | 12 | 40, 33, 30, 24, 23, 12 | 27 | 15 | 5 |
| W99723 | T11/482643 | wes-1 | type (i) 48, 42, 40, 39, 37, 33 | 40 | 25 | 20 | 21, 18, 18, 16, 12, 10 | 16 | 3 | 7 |
| | | | type (ii) 22, 20, 19, 19, 18, 16 | 19 | | 5 | | | | |
| W99728 | T11/484642 | wes-1 | type (i) 33, 30, 27, 24, 22, 19 | 26 | 25 | 25 | 127, 81, 72, 51, 49, 42 | 70 | 15 | 5 |
| W99729 | T11/483641 | wes-1 | type (i) 17, 10, 9, 8, 8, 6 | 10 | 15 | 15 | 570, 110, 95, 73, 61, 60 | 162 | 10 | 3 |
| W99763 | T11/497655 | wes-1 | type (i) 17, 14, 14, 13, 12, 12 | 14 | 20 | 20 | 46, 46, 37, 35, 29, 23 | 36 | 5 | 5 |
| | | | | | | | LCZ-1: 124, 108, 62, 59, 46, 41 | 73 | 20 | |
| | | | | | | | LCZ-2: 226, 87, 78, 61, 56, 54 | 94 | 30 | |
| | | | | | | | LCZ-3: 122, 96, 74, 63, 62, 43 | 77 | 27 | |
| W99770 | T11/498652 | wes-1 | type (i) 36, 31, 30, 27, 24, 24 | 29 | 15 | 15 | LCZ: 418, 320, 98, 71, 62, 53 | 170 | 20 | <1 |
| W99774 | T11/486642 | wes-1 | type (i) 10, 9, 7, 6, 5, 5 | 7 | 20 | 3 | 25, 25, 16, 15, 12, 7 | 17 | 3 | 10 |
| | | | type (ii) 19, 18, 12, 11, 11, 11 | 14 | | 17 | | | | |
| W99780 | T11/510622 | wes-4 | type (i) 33, 25, 19, 15, 15, 12 | 20 | 25 | 25 | 182, 93, 66, 62, 60, 56 | 87 | 10 | 5 |

Table IV.1 continued.

| Sample | Grid Ref. | Ignimbrite | 6 MJ (mm) | MJ(mm) | Total Juv % | Juvenile % | 6 ML (mm) | ML(mm) | Lithic % | Crystal % |
|---|---|---|---|---|---|---|---|---|---|---|
| W99815 | T11/487650 | wes-1 | type (i) 25, 16, 14, 12, 12, 8 | 15 | 25 | 12 | 64, 58, 52, 50, 43, 41 | 51 | <1 | 5 |
| | | | type(ii) 26, 21, 19, 18, 17, 16 | 20 | | 13 | | | | |
| W99831 | T11/482643 | wes-1 | type (i) 9, 7, 7, 6, 5, 5 | 7 | 30 | 10 | 193, 87, 71, 65, 62, 62 | 90 | 20 | 5 |
| | | | type (ii) 32, 17, 10, 8, 8, 7 | 14 | | 20 | | | | |
| W99845 | T11/494643 | wes-1 | type (i) 42, 35, 22, 11, 10, 10 | 22 | 25 | 20 | 192, 167, 136, 127, 113, 82 | 136 | 15 | 5 |
| | | | type (ii) 4, 3, 3, 3, 3, 2 | 3 | | 5 | | | | |
| W99848 | T12/495577 | wes-1 | type (i) 18, 15, 11, 11, 10, 10 | 13 | 25 | 20 | 761, 482, 423, 421, 237, 228 | 422 | 15 | 15 |
| | | | type (ii) 8, 7, 7, 6, 5, 5 | 6 | | 5 | | | | |
| W99849 | T12/495578 | wes-1 | type (i) 13, 12, 12, 12, 10, 9 | 11 | 25 | 22 | 520, 502, 498, 432, 361, 328 | 440 | 20 | 10 |
| | | | type (ii) 3, 2, 2, 2, 1, 1 | 2 | | 3 | | | | |
| W99850 | T12/512586 | wes-1 | type (i) 6, 5, 5, 4, 4, 2 | 4 | 15 | 10 | 392, 342, 161, 152, 118, 72 | 206 | 15 | 5 |
| | | | type (ii) 9, 4, 3, 3, 2, 2 | 4 | | 5 | | | | |
| W99851 | T12/512587 | wes-1 | type (i) 12, 11, 10, 10, 8, 7 | 10 | 20 | 15 | 108, 86, 71, 62, 59, 57 | 74 | 15 | 3 |
| | | | type (ii) 10, 6, 3, 3, 3, 2 | 5 | | 5 | | | | |
| W99852 | T12/512593 | wes-4 | type (i) 12, 8, 7, 7, 7, 6 | 8 | 20 | 12 | 210, 192, 159, 112, 92, 68 | 139 | 7 | 15 |
| | | | type (ii) 6, 5, 3, 2, 2, 2 | 3 | | 8 | | | | |
| W99856 | T12/512593 | wes-1 | type (i) 10, 10, 9, 9, 8, 7 | 9 | 25 | 20 | 420, 132, 122, 86, 74, 72 | 151 | 7 | 15 |
| | | | type (ii) 4, 3, 3, 3, 2, 2 | 3 | | 5 | | | | |
| W99859 | T12/508596 | wes-1 | type (i) 14, 12, 12, 10, 9, 7 | 11 | 17 | 15 | 410, 380, 342, 273, 270, 189 | 311 | 10 | <3 |
| | | | type (ii) 4, 3, 3, 3, 2, 2 | 3 | | 2 | | | | |
| W99861 | T12/505594 | wes-1 | type (i) 20, 19, 18, 16, 16, 15 | 17 | 15 | 10 | 531, 382, 302, 290, 261, 127 | 316 | 15 | 5 |
| | | | type (ii) 15, 10, 10, 9, 8, 8 | 10 | | 5 | | | | |
| W99863 | T12/490573 | wes-1 | type (i) 13, 12, 11, 10, 10, 10 | 9 | 17 | 15 | 165, 120, 112, 109, 102, 86 | 116 | 5 | 3 |
| | | | type (ii) 5, 4, 2, 2, 2, 2 | 3 | | <2 | | | | |
| W99864 | T12/506589 | wes-1 | type (i) 29, 23, 20, 19, 17, 15 | 21 | 25 | 22 | 420, 375, 362, 201, 192, 102 | 275 | 12 | 10 |
| | | | type (ii) 9, 5, 4, 3, 3, 2 | 4 | | 3 | | | | |
| W99870 | T12/488583 | wes-1 | type (i) 12, 10, 8, 7, 7, 6 | 8 | 20 | 17 | 83, 52, 40, 37, 33, 24 | 45 | 7 | 5 |
| | | | type (ii) 6, 5, 4, 4, 3, 2 | 4 | | <3 | | | | |

Table IV.1 continued.

| Sample | Grid Ref. | Ignimbrite | 6 MJ (mm) | MJ(mm) | Total Juv % | Juvenile % | 6 ML (mm) | ML(mm) | Lithic % | Crystal % |
|---|---|---|---|---|---|---|---|---|---|---|
| W99874 | T12/488583 | wes-1 | type (i) 10, 8, 7, 7, 6, 6 | 7 | 15 | 13 | lithic pod: 73, 55, 41, 32, 30, 24 | 43 | 75 | 5 |
| | | | type (ii) 4, 3, 3, 3, 2, 2 | 3 | | 2 | matrix: 73, 62, 59, 54, 35, 29 | 52 | 7 | |
| W99883 | T11/683546 | wes-1 | type (i) 11, 10, 9, 9, 8, 8 | 9 | 20 | 12 | 113, 76, 74, 70, 57, 43 | 72 | 7 | 5 |
| | | | type (ii) 6, 5, 5, 3, 3, 2 | 4 | | 8 | | | | |
| W99884 | T11/548682 | wes-1 | type (i) 14, 12, 11, 10, 10, 9 | 11 | 20 | 10 | 115, 86, 81, 77, 52, 43 | 76 | 5 | 5 |
| | | | type (ii) 6, 6, 5, 5, 4, 3 | 5 | | 10 | | | | |
| W99886 | T11/551679 | wes-1 | type (i) 27, 26, 24, 22, 21, 19 | 23 | 25 | 15 | 168, 143, 124, 117, 108, 92 | 125 | 15 | 7 |
| | | | type (ii) 16, 8, 7, 6, 5, 5 | 8 | | 10 | | | | |
| W99899 | T11/553678 | wes-1 | type (i) 52, 37, 36, 30, 29, 27 | 35 | 30 | 28 | 69, 42, 36, 32, 22, 19 | 37 | <1 | 7 |
| | | | type (i) 8, 7, 6, 5, 4, 4 | 6 | | <2 | | | | |
| W99990 | T11/552678 | wes-4 | type (i) 13, 12, 10, 10, 9, 7 | 10 | 7 | 5 | 14, 3, 3, 3, 4, 2 | 5 | >1 | 7 |
| | | | type (ii) 10, 9, 8, 8, 7, 5 | 8 | | 2 | | | | |
| W99901 | T11/543683 | wes-4 | type (i) 9, 8, 8, 7, 7, 6 | 8 | 7 | 5 | 66, 59, 44, 42, 41, 38 | 48 | 3 | 5 |
| | | | type (i) 4, 3, 3, 2, 2, 2 | 3 | | 2 | | | | |
| W99913 | T11/512645 | wes-4 | type (i) 39, 37, 19, 18, 16, 14 | 8 | 25 | 22 | 172, 79, 39, 36, 22, 16 | 61 | 15 | 5 |
| | | | type (ii) 5, 4, 4, 3, 3, 2 | 4 | | <3 | | | | |
| W99922 | T11/511643 | wes-4 | type (i) 3, 3, 3, 2, 2, 2 | 3 | <3 | 10 | matrix: 42, 29, 24, 19, 18, 15 | 25 | <3 | 5 |
| | | | | | | | LCZ: 350, 245, 242, 218, 122, 96 | 212 | 30 | |
| W99923 | T11/511643 | wes-4 | type (i) 9, 9, 8, 8, 7, 6 | 8 | 7 | 6 | 2200, 1300, 950, 529, 430, 289 | 950 | 5 | 5 |
| | | | type (ii) 2, 2, 1, 1, 1, 1 | 1 | | <1 | | | | |
| W99927 | T11/511643 | wes-1 | type (i) 18, 17, 16, 16, 14, 12 | 16 | 20 | 15 | 79, 68, 61, 53, 49, 42 | 59 | 5 | 5 |
| | | | type (ii) 3, 3, 2, 2, 2, 2 | 2 | | 5 | | | | |
| W99928 | T11/511643 | wes-1 | type (i) 10, 9, 9, 8, 8, 6 | 10 | 15 | 12 | 82, 73, 61, 53, 43, 31 | 57 | 7 | 5 |
| | | | type (ii) 14, 10, 6, 5, 4, 4 | 7 | | 3 | | | | |
| W99931 | T11/509660 | wes-1 | type (i) 18, 16, 16, 15, 14, 12 | 15 | 15 | 12 | 175, 149, 132, 102, 90, 74 | 120 | 7 | 5 |
| | | | type (ii) 9, 5, 4, 4, 3, 3 | 5 | | <3 | | | | |
| W99934 | T11/512658 | wes-1 | type (i) 12, 10, 10, 9, 9, 9 | 10 | 15 | 12 | 61, 42, 36, 31, 22, 19 | 35 | 5 | 7 |
| | | | type (ii) 5, 4, 4, 3, 3, 3 | 4 | | <3 | | | | |

Table IV.1 continued.

| Sample | Grid Ref. | Ignimbrite | 6 MJ (mm) | MJ(mm) | Total Juv % | Juvenile % | 6 ML (mm) | ML(mm) | Lithic % | Crystal % |
|---|---|---|---|---|---|---|---|---|---|---|
| W99943 | T11/518651 | wes-4 | type (i) 16, 14, 12, 11, 10, 9<br>type (ii) 6, 5, 4, 4, 3, 3 | **12**<br>**4** | **20** | **17**<br>**3** | 149, 124, 118, 107, 103, 92 | **116** | **5** | **5** |
| W99947 | T11/499656 | wes-1 | type (i) 12, 12, 11, 10, 10, 9<br>type (ii) 10, 8, 7, 7, 6, 5 | **11**<br>**7** | **12** | **10**<br>**<2** | 72, 68, 64, 58, 51, 49 | **60** | **15** | **5** |
| W99950 | T11/542688 | wes-1 | type (i) 39, 30, 27, 25, 22, 19<br>type (ii) 3, 2, 2, 2, 2, 1 | **27**<br>**2** | **17** | **16**<br>**<1** | 369, 329, 292, 225, 214, 182 | **269** | **15** | **5** |
| W99952 | T11/546688 | wes-4 | type (i) 20, 16, 15, 14, 13, 13<br>type (ii) 16, 14, 11, 10, 9, 8 | **15**<br>**11** | **20** | **15**<br>**5** | 47, 44, 37, 32, 28, 26 | **36** | **10** | **3** |
| W99966 | T11/533674 | wes-4 | type (i) 14, 12, 11, 10, 9, 9<br>type (ii) 28, 19, 17, 16, 15, 14 | **11**<br>**18** | **25** | **5**<br>**20** | 122, 41, 33, 28, 24, 22 | **45** | **5** | **5** |
| W99967 | T11/533673 | wes-4 | type (i) 39, 22, 18, 17, 17, 16<br>type (ii) 27, 26, 19, 12, 10, 8 | **22**<br>**17** | **30** | **15**<br>**5** | 671, 581, 379, 262, 241, 194 | **388** | **20** | **5** |
| W99968 | T11/504666 | wes-4 | type (i) 12, 11, 10, 9, 8, 8<br>type (ii) 11, 11, 10, 7, 7, 6 | **10**<br>**9** | **15** | **10**<br>**5** | 110, 96, 93, 91, 84, 82 | **93** | **7** | **7** |
| W99972 | T11/508664 | wes-1 | type (i) 27, 22, 19, 18, 18, 17<br>type (ii) 10, 10, 9, 9, 8, 8 | **20**<br>**9** | **20** | **15**<br>**5** | 516, 168, 134, 131, 99, 89 | **190** | **5** | **5** |
| W99973 | T11/511678 | wes-1 | type (i) 11, 10, 10, 9, 9, 8<br>type (ii) 8, 8, 8, 7, 6, 6 | **10**<br>**7** | **10** | **6**<br>**4** | 42, 41, 39, 38, 28, 24 | **35** | **3** | **5** |
| W99974 | T11/507675 | wes-1 | type (i) 10, 9, 9, 8, 8, 7<br>type (ii) 7, 6, 6, 5, 5, 5 | **9**<br>**6** | **20** | **17**<br>**3** | 169, 122, 118, 101, 94, 83 | **115** | **7** | **5** |
| W99975 | T11/503674 | wes-1 | type (i) 15, 13, 10, 10, 9, 6 | **10** | **15** | **15** | LCZ: 104, 89, 74, 69, 62, 60 | **76** | **30** | **7** |
| W99977 | T11/535665 | wes-4 | type (i) 13, 12, 12, 11, 10, 10 | **11** | **25** | **25** | 271, 242, 216, 210, 194, 183 | **219** | **7** | **5** |
| W99979 | T11/535665 | wes-4 | type (i) 7, 7, 6, 6,6, 5 | **6** | **3** | **3** | 12, 10, 8, 8, 7, 7 | **9** | **3** | **7** |
| W991003 | T11/556654 | wes-4 | type (i) 46, 39, 37, 31, 28, 26 | **35** | **10** | **10** | 750, 620, 489, 459, 412, 320 | **508** | **20** | **3** |
| W99862 | T12/500586 | wes-1 | type (i) 18, 16, 13, 11, 10, 9<br>type (ii) 8, 4, 4, 3, 3, 2 | **13**<br>**4** | **15** | **12**<br>**3** | 287, 218, 210, 192, 146, 143 | **200** | **15** | **7** |

Table IV.1 continued.

| Sample | Grid Ref. | Ignimbrite | 6 MJ (mm) | MJ(mm) | Total Juv % | Juvenile % | 6 ML (mm) | ML(mm) | Lithic % | Crystal % |
|---|---|---|---|---|---|---|---|---|---|---|
| W99896 | T11/553671 | wes-1 | type (i) 31, 25, 24, 23, 21, 19<br>type (ii) 4, 4, 3, 3, 2, 2 | **24**<br>**3** | **15** | **12**<br>**3** | 352, 183, 110, 94, 92, 73 | **151** | **15** | **7** |
| W99619 | T11/527661 | wes-4 | type(i) 15, 13, 12, 10, 9, 8 | **11** | **30** | **30** | 32, 25, 22, 21, 18, 15 | **22** | **30** | **5** |
| W99626 | T11/526660 | wes-4 | type(i) 24, 23, 22, 21, 20, 18<br>type(ii) 20, 18, 13, 11, 10, 9 | **21**<br>**13** | **35** | **10**<br>**25** | 530, 367, 220, 168, 120, 42 | **241** | **10** | **7** |
| W99627 | T11/530668 | wes-4 | type (i) 89, 84, 80, 72, 62, 59 | **74** | **40** | **40** | 163, 121, 113, 84, 82, 79 | **107** | **25** | **7** |
| W99921 | T11/519650 | wes-4 | type (i) 17, 16, 15, 12, 11, 10<br>type (ii) 13, 9, 8, 7, 6, 6 | **14**<br>**8** | **30** | **25**<br>**5** | 429, 247, 218, 214, 189, 175 | **245** | **20** | **5** |
| W99932 | T11/511659 | wes-1 | type (i) 69, 49, 45, 35, 28, 24 | **42** | **35** | **35** | 95, 79, 67, 65, 59, 50 | **69** | **<3** | **3** |
| W99933 | T11/511658 | wes-1 | type (i) 91, 52, 38, 36, 33, 30 | **47** | **45** | **45** | 38, 33, 28, 26, 22, 17 | **27** | **<3** | **5** |
| W99936 | T11/512658 | wes-1 | type (i) 33, 22, 19, 18, 18, 17 | **21** | **35** | **35** | 227, 149, 110, 97, 92, 86 | **127** | **<1** | **7** |
| W99938 | T11/512657 | wes-1 | type (i) 37, 26, 20, 18, 18, 15 | **22** | **30** | **30** | 245, 162, 89, 61, 57, 45 | **110** | **<1** | **5** |
| W99940 | T11/513654 | wes-4 | type (i) 14, 13, 12, 12, 12, 11<br>type (ii) 24, 19, 12, 12, 10, 10 | **12**<br>**15** | **20** | **15**<br>**5** | 81, 67, 48, 42, 39, 29 | **51** | **<3** | **5** |
| W99917 | T11/519648 | wes-4 | type (i) 4, 3, 3, 3, 3, 2<br>type (ii) 3, 3, 3, 2, 2, 2 | **3**<br>**3** | **<3** | **<2**<br>**<1** | LCZ: 133, 127, 119, 104, 89, 82<br>matrix: 62, 51, 48, 44, 41, 39 | **109**<br>**48** | **35**<br>**<3** | **5** |
| W99953 | T11/551692 | wes-1 | type (i) 12, 11, 10, 10, 9, 9 | **10** | **15** | **15** | 349, 268, 213, 191, 189, 174 | **231** | **5** | **5** |
| W99964 | T11/532676 | wes-4 | type (i) 15, 12, 10, 10, 10, 9<br>type (ii) 11, 9, 8, 8, 7, 6 | **11**<br>**8** | **25** | **23**<br>**<2** | 104, 68, 41, 39, 34, 32 | **53** | **3** | **5** |
| W99965 | T11/533675 | wes-4 | type (i) 25, 24, 22, 21, 19 | **19** | **25** | **25** | 94, 57, 49, 41, 39, 33 | **52** | **3** | **5** |
| W99970 | T11/533673 | wes-4 | type (i) 18, 12, 11, 11, 10, 9 | **12** | **7** | **7** | 19, 18, 18, 17, 16, 16 | **17** | **3** | **5** |
| W99676 | T12/472575 | wes-1 | type (i) 22, 18, 10, 8, 7, 6<br>type (ii) 12, 6, 4, 4, 4, 3 | **12**<br>**6** | **16** | **15**<br>**<1** | 29, 25, 22, 16, 15, 14 | **121** | **<1** | **5** |
| W99673 | T12/472572 | cp | type (i) 7, 7, 6, 6, 5, 4 | **6** | **<1** | **<1** | 22, 11, 10, 6, 6, 5 | **10** | **<3** | **7** |

Table IV.1 continued.

| Sample | Grid Ref. | Ignimbrite | 6 MJ (mm) | MJ(mm) | Total Juv % | Juvenile % | 6 ML (mm) | ML(mm) | Lithic % | Crystal % |
|---|---|---|---|---|---|---|---|---|---|---|
| W99675 | T12/472574 | cp | type (i) 42, 36, 33, 27, 26, 24 | 31 | 20 | 20 | 62, 41, 37, 33, 30, 26 | 38 | 3 | 15 |
| W99703 | T12/482592 | cp | type (i) 7, 6, 6, 5, 5, 4 | 5 | 15 | 8 | 23, 21, 19, 16, 16, 12 | 18 | 10 | 3 |
| | | | type (ii) 7, 7, 7, 6, 6, 4 | 6 | | 7 | | | | |
| W99642 | T12/455584 | cp | type (i) 51, 46, 42, 40, 39, 37 | 42 | 7 | 7 | 46, 39, 36, 33, 32, 22 | 35 | <3 | 25 |
| W99668 | T12/468574 | cp | type(i) 17, 14, 12, 10, 9, 8 | 12 | 5 | 5 | 160, 158, 140, 125, 103, 89 | 129 | 30 | 3 |
| W99986 | T11/515701 | cp | type (i) 15, 12, 12, 10, 10, 9 | 11 | 20 | 20 | 31, 30, 29, 25, 22, 19 | 26 | 7 | 15 |
| W99903 | T11/553668 | cp | type (i) 26, 22, 21, 21, 20, 17 | 21 | 15 | 15 | 423, 291, 165, 119, 92, 84 | 196 | 15 | 7 |
| W99910 | T11/552660 | cp | type (i) 9, 8, 8, 7, 7, 6 | 8 | 12 | 7 | 159, 95, 89, 69, 62, 51 | 88 | 5 | 7 |
| | | | type (ii) 5, 5, 4, 4, 4, 3 | 4 | | 5 | | | | |
| W99621 | T11/527663 | h | type(i) 12, 10, 9, 8, 8, 7 | 9 | 12 | 12 | 18, 16, 15, 13, 8, 8 | 13 | 35 | <10 |
| W99809 | T11/511633 | h | type (i)12, 9, 7, 7, 7, 6 | 8 | 10 | 10 | 95, 86, 51, 48, 47, 32 | 55 | 5 | 5 |
| W99841 | T11/497641 | h | type (i) 19, 18, 14, 12, 10, 8 | 14 | 15 | 15 | 32, 22, 18, 14, 13, 12 | 18 | 3 | 1 |
| W99868 | T12/487581 | h | type (i) 25, 16, 15, 15, 12, 11 | 16 | 15 | 15 | 523, 380, 328, 289, 281, 182 | 331 | 25 | 7 |
| W99953 | T11/532625 | h | type (i) 24, 19, 15, 14, 13, 13 | 16 | 10 | 10 | 133, 74, 51, 46, 39, 33 | 63 | 7 | 7 |
| W99958 | T11/542640 | h | type (i) 140, 69, 66, 61, 53, 42 | 72 | 20 | 20 | 718, 622, 215, 163, 149, 142 | 335 | 15 | 3 |
| W99959 | T11/542641 | h | type (i) 12, 10, 10, 10, 9, 8 | 10 | 10 | 10 | 169, 89, 71, 62, 41, 29 | 77 | <3 | 5 |
| W99953 | T11/530623 | h | type (i) 17, 14, 13, 12, 11, 10 | 13 | 15 | 15 | 792, 469, 367, 244, 211, 189 | 379 | 15 | 3 |
| W99962 | T11/547651 | h | type (i) 14, 13, 12, 11, 10, 10 | 12 | 15 | 15 | 45, 42, 39, 32, 29, 25 | 35 | 5 | 5 |
| W99693 | T12/486572 | wi | type (i) 11, 10, 8, 7, 6, 6 | 8 | 25 | 15 | matrix: 470, 275, 242, 227, 211, 127 | 259 | 20 | 5 |
| | | | type (ii) 13, 9, 8, 8, 7, 7 | 9 | | 10 | LCZ1: 385, 361, 329, 318, 261, 241 | 316 | 80 | |
| | | | | | | | LCZ2: 113, 97, 72, 64, 62, 47 | 76 | 80 | |
| W99695 | T12/489573 | wi | type (i) 10, 9, 9, 6, 6, 5 | 8 | 15 | 12 | 721, 662, 628, 541, 493, 394 | 573 | 17 | 5 |
| | | | type (ii) 19, 16, 15, 14, 14, 12 | 15 | | 3 | | | | |

Table IV.1 continued.

| Sample | Grid Ref. | Ignimbrite | 6 MJ (mm) | MJ(mm) | Total Juv % | Juvenile % | 6 ML (mm) | ML(mm) | Lithic % | Crystal % |
|---|---|---|---|---|---|---|---|---|---|---|
| W99846 | T12/488573 | wi | type (i) 8 , 8, 7, 7, 6, 5 | 7 | 20 | 10 | 781, 662, 365, 352, 241, 206 | 431 | 30 | 5 |
| | | | type (ii) 15, 15, 13, 12, 10, 9 | 12 | | 10 | | | | |
| W99866 | T12/506582 | wi | type (i) 12, 12, 11, 11, 10, 10 | 11 | 15 | 15 | 487, 262, 237, 161, 149, 102 | 233 | 15 | 7 |
| W99867 | T12/506582 | wi | type (i) 27, 24, 20, 19, 16, 15 | 20 | 25 | 20 | 389, 323, 319, 256, 179, 135 | 267 | 10 | 7 |
| | | | type (ii) 12, 6, 4, 3, 2, 2 | 5 | | 5 | | | | |
| W99893 | T11/553671 | mi | type (i) 112, 97, 84, 77, 75, 67 | 85 | 17 | 17 | 67, 55, 42, 36, 29, 26 | 43 | 15 | 10 |
| W99890 | T11/553673 | mi | type (i) 75, 40, 33, 32, 31, 27 | 40 | 20 | 20 | 194, 178, 96, 92, 69, 55 | 114 | 7 | 7 |
| W99891 | T11/553673 | mi | type (i) 9, 8, 8, 7, 6, 5 | 7 | 3 | 3 | 52, 49, 30, 29, 21, 18 | 33 | <3 | 15 |
| W99892 | T11/554672 | mi | type (i) 7, 6, 5, 5, 4, 4 | 5 | 3 | 3 | 81, 78, 73, 61, 60, 54 | 68 | 20 | 5 |
| | | | type (ii) 4, 3, 3, 3, 2, 2 | 3 | | <1 | | | | |
| W99897 | T11/553670 | mi | type (i) 10, 9, 8, 8, 6, 5 | 7 | 7 | 7 | 721, 562, 349, 210, 184, 149 | 363 | 15 | 7 |
| W99898 | T11/552676 | mi | type (i) 59, 45, 44, 42, 32, 27 | 42 | 17 | 16 | 106, 79, 72, 57, 46, 45 | 68 | 5 | 7 |
| | | | type (i) 16, 14, 9, 8, 7, 6 | 10 | | <1 | | | | |
| W99615 | T11/540680 | mi | type(i) 31, 23, 22, 20, 19, 18 | 22 | 40 | 25 | 14, 13, 12, 12, 11, 10 | 12 | <5 | 15 |
| | | | type(ii) 18, 15, 12, 11, 10, 10 | 13 | | 15 | | | | |
| W99616 | T11/541679 | mi | type(i) 42, 41, 37, 36, 35, 32 | 37 | 30 | 15 | 46, 32, 28, 27, 25, 18 | 29 | 10 | 20 |
| | | | type(ii) 12, 11, 10, 10, 8, 7 | 10 | | 10 | | | | |
| | | | type (iii) 24, 22, 21, 20, 18, 16 | 20 | | 5 | | | | |
| W99988 | T11/515701 | qi | 48, 36 ,35, 30, 27, 22 | 33 | 40 | 40 | 18, 15, 15, 12, 10, 8 | 13 | 3 | 7 |
| W99989 | T11/515701 | qi | 81, 62, 56, 54, 51, 43 | 58 | 30 | 30 | 12, 11, 9, 7, 7, 7 | 9 | 2 | 10 |
| W99990 | T11/515701 | qi | 71, 67, 59, 58, 48, 35 | 56 | 25 | 25 | 10, 9, 8, 8, 7, 5 | 8 | 3 | 10 |
| W99612 | T11/534671 | oi | type(i) 110, 88, 65, 55, 50, 55 | 71 | 40 | 25 | 44, 10, 6, 5, 4, 3 | 12 | 3 | 5 |
| | | | type (ii) 37, 34, 32, 30, 26, 16 | 29 | | 15 | | | | |

# Appendix V

## Electron microprobe data

Table V.1 Electron microprobe analyses and calculated end member compositions of feldspar phenocrysts and crystals in Kapowai Caldera Complex volcanic units. p-core = phenocryst core; p-rim = phenocryst rim.

| Sample | W99601 | W99601 | W99601 | W99691 | W99601 | W99601 | W99601 | W99601 | W99601 | W99601 | W99601 | W99601 | W99601 |
|---|---|---|---|---|---|---|---|---|---|---|---|---|---|
| Analysis | p-core | p-core | p-core | p-core | p-core | p-rim | p-core | p-rim | p-core | p-rim | p-core | p-core | p-rim |
| Unit | Taurahuehue Andesite | Taurahuehue Andesite | Taurahuehue Andesite | Taurahuehue Andesite | Taurahuehue Andesite | Taurahuehue Andesite | Taurahuehue Andesite | Taurahuehue Andesite | Taurahuehue Andesite | Taurahuehue Andesite | Taurahuehue Andesite | Taurahuehue Andesite | Taurahuehue Andesite |
| | wt% | wt% | wt% | wt% | wt. % | wt. % | wt. % | wt. % | wt. % | wt. % | wt. % | | |
| SiO2 | 46.95 | 46.02 | 46.17 | 53.37 | 48.25 | 49.17 | 46.07 | 47.18 | 50.11 | 48.83 | 47.30 | 48.25 | 47.18 |
| TiO2 | 0.15 | 0.13 | 0.06 | 0.06 | 0.04 | 0.08 | 0.10 | 0.06 | 0.02 | 0.04 | 0.11 | 0.04 | 0.06 |
| Al2O3 | 33.95 | 34.34 | 33.29 | 29.54 | 32.85 | 32.80 | 34.60 | 33.59 | 32.27 | 32.81 | 34.05 | 32.85 | 33.59 |
| FeO | 0.62 | 0.60 | 0.53 | 0.55 | 0.63 | 0.57 | 0.52 | 0.60 | 0.47 | 0.59 | 0.47 | 0.63 | 0.6 |
| MnO | 0.05 | 0.01 | 0.00 | 0.02 | 0.05 | 0.02 | 0.00 | 0.08 | 0.09 | 0.09 | 0.03 | 0.05 | 0.08 |
| MgO | 0.09 | 0.11 | 0.08 | 0.09 | 0.09 | 0.14 | 0.04 | 0.09 | 0.11 | 0.05 | 0.03 | 0.09 | 0.09 |
| CaO | 17.35 | 17.71 | 16.68 | 12.40 | 17.47 | 16.01 | 18.09 | 17.33 | 15.49 | 16.43 | 17.31 | 17.47 | 17.33 |
| Na2O | 1.71 | 1.72 | 2.08 | 4.46 | 2.18 | 2.45 | 1.14 | 1.67 | 2.64 | 2.23 | 1.83 | 2.18 | 1.67 |
| K2O | 0.12 | 0.09 | 0.11 | 0.30 | 0.08 | 0.09 | 0.12 | 0.07 | 0.14 | 0.09 | 0.13 | 0.08 | 0.07 |
| TOTAL | 100.99 | 100.73 | 98.98 | 100.79 | 101.65 | 101.33 | 100.67 | 100.68 | 101.34 | 101.15 | 101.25 | 101.65 | 100.68 |
| | | | | | | | | | | | | | |
| Ab | 15.00 | 14.90 | 18.30 | 38.70 | 18.3 | 21.6 | 10.2 | 14.8 | 23.4 | 19.6 | 15.9 | 18.3 | 14.8 |
| An | 84.30 | 84.60 | 81.10 | 59.50 | 81.2 | 77.9 | 89.1 | 84.8 | 75.8 | 79.9 | 83.3 | 81.2 | 84.8 |
| Or | 0.70 | 0.50 | 0.60 | 1.70 | 0.5 | 0.5 | 0.7 | 0.4 | 0.8 | 0.5 | 0.7 | 0.5 | 0.4 |

Table V.1 continued.

| Sample | W99732 | W99732 | W99732 | W99732 | W99732 | W99732 | W99732 | W99732 | W99732 | W99816 | W99816 | W99816 | W99732 |
|---|---|---|---|---|---|---|---|---|---|---|---|---|---|
| Analysis | p-core | p-rim | p-core | p-core | p-rim | p-core | p-rim | p-core | p-rim | p-core | p-core | p-core | p-core |
| Unit | Tauraukau Andesite | Tauraukau Andesite | Tauraukau Andesite | Tauraukau Andesite | Tauraukau Andesite | Tauraukau Andesite | Tauraukau Andesite | Tauraukau Andesite | Tauraukau Andesite | Tauraukau Andesite | Tauraukau Andesite | Tauraukau Andesite | Tauraukau Andesite |
| | wt. % | wt. % | wt. % | wt. % | wt. % | wt. % | wt. % | wt. % | wt. % | wt% | wt% | wt% | wt. % |
| SiO2 | 55.04 | 54.12 | 53.61 | 53.57 | 55.55 | 52.63 | 50.32 | 54.86 | 51.85 | 54.15 | 54.29 | 55.44 | 56.52 |
| TiO2 | 0.03 | 0.13 | 0.07 | 0.02 | 0.09 | 0.20 | 0.06 | 0.02 | 0.09 | 0.10 | 0.17 | 0.13 | 0.05 |
| Al2O3 | 29.01 | 29.30 | 28.49 | 29.06 | 29.05 | 30.91 | 34.93 | 29.11 | 29.99 | 27.87 | 28.06 | 28.29 | 27.40 |
| FeO | 0.36 | 0.42 | 0.45 | 0.69 | 0.64 | 0.43 | 0.38 | 0.45 | 0.45 | 0.57 | 0.50 | 0.57 | 0.58 |
| MnO | 0.09 | 0.06 | 0.03 | 0.08 | 0.14 | 0.00 | 0.07 | 0.00 | 0.02 | 0.05 | 0.01 | 0.11 | 0.18 |
| MgO | 0.06 | 0.08 | 0.06 | 0.04 | 0.10 | 0.07 | 0.06 | 0.07 | 0.04 | 0.05 | 0.07 | 0.09 | 0.04 |
| CaO | 10.20 | 10.30 | 11.32 | 11.71 | 9.94 | 10.09 | 9.57 | 9.85 | 10.18 | 11.11 | 10.74 | 10.91 | 9.90 |
| Na2O | 5.23 | 5.31 | 4.83 | 4.66 | 5.28 | 5.19 | 4.78 | 5.51 | 5.06 | 4.71 | 5.28 | 5.14 | 5.63 |
| K2O | 0.25 | 0.42 | 0.30 | 0.30 | 0.61 | 0.28 | 0.44 | 0.25 | 0.35 | 0.40 | 0.34 | 0.46 | 0.29 |
| TOTAL | 100.28 | 100.13 | 99.17 | 100.13 | 101.41 | 99.80 | 100.59 | 100.12 | 98.04 | 99.00 | 99.45 | 101.12 | 100.58 |
| | | | | | | | | | | | | | |
| Ab | 47.4 | 47.1 | 42.8 | 41.1 | 47.3 | 47.4 | 46.1 | 49.6 | 46.4 | 42.40 | 46.20 | 44.80 | 49.9 |
| An | 51.1 | 50.5 | 55.4 | 57.1 | 49.1 | 50.9 | 51.1 | 49 | 51.5 | 55.30 | 51.90 | 52.50 | 48.4 |
| Or | 1.5 | 2.5 | 1.8 | 1.7 | 3.6 | 1.7 | 2.8 | 1.5 | 2.1 | 2.40 | 1.90 | 2.70 | 1.7 |

Table V.1 continued.

| Sample | W99732 | W99816 | W99601 | W99601 | W99601 | W99601 | W99601 | W99601 | W99951 | W99951 | W99951 | W99951 | W99951 |
|---|---|---|---|---|---|---|---|---|---|---|---|---|---|
| Analysis | p-rim | p-core | p-rim | p-core | p-rim | p-core | p-rim | p-core | phenocryst | p-rim | p-core | p-core | p-rim |
| Unit | Tauraulkau Andesite | Tauraulkau Andesite | Tauraulkau Andesite | Tauraulkau Andesite | Tauraulkau Andesite | Tauraulkau Andesite | Tauraulkau Andesite | Tauraulkau Andesite | Tapuaetahi Andesite | Tapuaetahi Andesite | Tapuaetahi Andesite | Tapuaetahi Andesite | Tapuaetahi Andesite |
| | wt. % | wt. % | wt. % | wt. % | wt. % | wt. % | wt. % | wt. % | wt% | wt. % | wt. % | wt. % | wt. % |
| SiO2 | 55.42 | 55.18 | 57.00 | 55.92 | 56.52 | 56.34 | 56.42 | 54.40 | 50.01 | 58.45 | 54.67 | 57.29 | 58.09 |
| TiO2 | 0.09 | 0.07 | 0.01 | 0.05 | 0.09 | 0.02 | 0.07 | 0.01 | 0.05 | 0.01 | 0.15 | 0.00 | 0.13 |
| Al2O3 | 28.68 | 28.37 | 27.72 | 28.37 | 27.63 | 27.78 | 27.38 | 28.86 | 32.54 | 26.24 | 28.53 | 27.89 | 26.42 |
| FeO | 0.44 | 0.63 | 0.55 | 0.46 | 0.57 | 0.59 | 0.55 | 0.55 | 0.27 | 0.38 | 0.29 | 0.23 | 0.15 |
| MnO | 0.16 | 0.15 | 0.13 | 0.00 | 0.00 | 0.01 | 0.00 | 0.01 | 0.05 | 0.01 | 0.16 | 0.00 | 0.14 |
| MgO | 0.06 | 0.06 | 0.04 | 0.08 | 0.07 | 0.08 | 0.04 | 0.07 | 0.03 | 0.02 | 0.03 | 0.01 | 0.03 |
| CaO | 10.77 | 10.51 | 10.11 | 11.07 | 9.94 | 10.42 | 10.07 | 11.57 | 14.71 | 8.46 | 10.97 | 10.31 | 8.64 |
| Na2O | 5.27 | 5.34 | 5.92 | 5.12 | 5.33 | 5.56 | 5.68 | 4.86 | 3.11 | 6.13 | 5.16 | 5.70 | 6.29 |
| K2O | 0.23 | 0.33 | 0.30 | 0.41 | 0.40 | 0.32 | 0.41 | 0.36 | 0.16 | 0.61 | 0.29 | 0.44 | 0.57 |
| TOTAL | 101.10 | 100.64 | 101.79 | 101.47 | 100.55 | 101.12 | 100.63 | 100.70 | 100.92 | 100.30 | 100.25 | 101.88 | 100.47 |
| | | | | | | | | | | | | | |
| Ab | 46.3 | 47.0 | 50.6 | 44.5 | 48.1 | 48.2 | 49.3 | 42.3 | 27.40 | 54.7 | 45.2 | 48.8 | 55.0 |
| An | 52.3 | 51.1 | 47.7 | 53.2 | 49.5 | 49.9 | 48.3 | 55.6 | 71.70 | 41.7 | 53.1 | 48.8 | 41.7 |
| Or | 1.3 | 1.9 | 1.7 | 2.3 | 2.4 | 1.8 | 2.3 | 2.1 | 0.90 | 3.6 | 1.7 | 2.5 | 3.3 |

Table V.1 continued.

| Sample | W99951 | W99951 | W99951 | W99951 | W99951 | W99600 | W99600 | W99600 | W99600 | W99600 | W99600 | W99905 | W99912 |
|---|---|---|---|---|---|---|---|---|---|---|---|---|---|
| Analysis | p-core | p-core | p-rim | p-core | p-core | p-core | p-core | p-core | p-core | p-core | p-core | p-core | p-core |
| Unit | Tapuaetahi Andesite | Tapuaetahi Andesite | Tapuaetahi Andesite | Tapuaetahi Andesite | Tapuaetahi Andesite | Rangihau Rhyolite | Rangihau Rhyolite | Rangihau Rhyolite | Rangihau Rhyolite | Rangihau Rhyolite | Rangihau Rhyolite | Kapowai Rhyolite | Precipice Rhyolite |
| | wt% | wt. % | wt. % | wt. % | wt. % | wt% | wt% | wt% | wt% | wt% | wt% | wt% | wt% |
| SiO2 | 54.87 | 54.02 | 58.18 | 55.68 | 58.93 | 59.62 | 57.39 | 57.03 | 57.93 | 56.00 | 58.28 | 56.11 | 52.87 |
| TiO2 | 0.12 | 0.04 | 0.00 | 0.06 | 0.04 | 0.15 | 0.06 | 0.14 | 0.08 | 0.11 | 0.20 | 0.09 | 0.16 |
| Al2O3 | 28.98 | 29.09 | 26.49 | 28.58 | 26.54 | 26.00 | 25.59 | 25.79 | 25.77 | 27.19 | 26.35 | 26.86 | 28.30 |
| FeO | 0.39 | 0.39 | 0.21 | 0.29 | 0.23 | 0.40 | 0.50 | 0.29 | 0.39 | 0.47 | 0.38 | 0.39 | 0.72 |
| MnO | 0.09 | 0.01 | 0.00 | 0.03 | 0.01 | 0.01 | 0.10 | 0.05 | 0.07 | 0.06 | 0.07 | 0.07 | 0.21 |
| MgO | 0.05 | 0.05 | 0.06 | 0.01 | 0.05 | 0.01 | 0.04 | 0.06 | 0.01 | 0.03 | 0.04 | 0.02 | 0.08 |
| CaO | 10.95 | 11.49 | 8.77 | 10.93 | 8.71 | 8.13 | 7.57 | 7.64 | 7.41 | 9.05 | 8.00 | 9.33 | 11.01 |
| Na2O | 5.01 | 4.89 | 6.30 | 5.32 | 6.32 | 6.52 | 6.97 | 7.15 | 6.61 | 5.89 | 6.67 | 5.71 | 5.36 |
| K2O | 0.24 | 0.25 | 0.48 | 0.30 | 0.46 | 0.33 | 0.45 | 0.39 | 0.41 | 0.24 | 0.26 | 0.29 | 0.28 |
| TOTAL | 100.67 | 100.23 | 100.50 | 101.20 | 101.29 | 101.16 | 98.66 | 98.54 | 98.68 | 99.04 | 100.24 | 98.86 | 98.99 |
| | | | | | | | | | | | | | |
| Ab | 44.6 | 42.9 | 55.0 | 46.0 | 55.3 | 58.1 | 60.9 | 61.5 | 60.3 | 53.3 | 59.2 | 51.6 | 46.1 |
| An | 53.9 | 55.7 | 42.3 | 52.3 | 42.1 | 40.0 | 36.5 | 36.3 | 37.3 | 45.3 | 39.3 | 46.6 | 52.3 |
| Or | 1.4 | 1.5 | 2.7 | 1.7 | 2.7 | 1.9 | 2.6 | 2.2 | 2.4 | 1.4 | 1.5 | 1.7 | 1.6 |

Table V.1 continued.

| Sample | W99912 | W99912 | W99912 | W991002 | W991002 | W99865 | W99865 | W99865 | W99834 | W99834 | W99834 | W991005 | W991005 |
|---|---|---|---|---|---|---|---|---|---|---|---|---|---|
| Analysis | p-core | p-core | p-rim | p-core | p-core | p-core | p-core | p-core | p-core | p-core | p-core | p-core | p-core |
| Unit | Precipice Rhyolite | Precipice Rhyolite | Precipice Rhyolite | Kokonga Rhyolite | Kokonga Rhyolite | Tauranikau Rhyolite | Tauranikau Rhyolite | Tauranikau Rhyolite | Welcome Jack Rhyolite | Welcome Jack Rhyolite | Welcome Jack Rhyolite | Ruahine Rhyolite | Ruahine Rhyolite |
| | wt% | wt. % | wt. % | wt% | wt% | wt% | wt% | wt% | wt% | wt% | wt% | wt% | wt% |
| SiO2 | 55.12 | 52.92 | 59.97 | 55.18 | 56.56 | 59.58 | 62.80 | 63.67 | 60.74 | 57.96 | 58.05 | 60.25 | 59.03 |
| TiO2 | 0.20 | 0.19 | 0.03 | 0.16 | 0.20 | 0.14 | 0.10 | 0.15 | 0.13 | 0.28 | 0.09 | 0.12 | 0.00 |
| Al2O3 | 26.41 | 29.83 | 25.30 | 27.47 | 26.39 | 23.39 | 23.22 | 22.39 | 22.27 | 24.35 | 25.89 | 25.23 | 25.62 |
| FeO | 0.33 | 0.61 | 0.35 | 0.54 | 0.28 | 0.24 | 0.21 | 0.31 | 0.21 | 0.25 | 0.32 | 0.22 | 0.22 |
| MnO | 0.10 | 0.04 | 0.04 | 0.08 | 0.04 | 0.13 | 0.05 | 0.04 | 0.06 | 0.01 | 0.08 | 0.07 | 0.12 |
| MgO | 0.04 | 0.07 | 0.03 | 0.08 | 0.05 | 0.00 | 0.06 | 0.04 | 0.00 | 0.06 | 0.03 | 0.10 | 0.04 |
| CaO | 8.74 | 12.58 | 6.88 | 9.37 | 8.43 | 5.32 | 5.14 | 4.07 | 5.04 | 6.50 | 7.67 | 7.12 | 7.14 |
| Na2O | 6.53 | 4.25 | 7.23 | 5.85 | 6.52 | 7.73 | 7.97 | 7.97 | 7.51 | 7.22 | 6.85 | 6.52 | 6.86 |
| K2O | 0.33 | 0.15 | 0.36 | 0.28 | 0.48 | 0.42 | 0.58 | 0.51 | 0.73 | 0.53 | 0.48 | 0.61 | 0.57 |
| TOTAL | 97.79 | 100.63 | 100.17 | 98.99 | 98.95 | 96.95 | 100.14 | 99.14 | 96.66 | 97.15 | 99.46 | 100.23 | 99.59 |
| | | | | | | | | | | | | | |
| Ab | 56.4 | 37.6 | 64.1 | 52.2 | 56.7 | 70.6 | 71.2 | 75.5 | 69.7 | 64.7 | 60.0 | 60.0 | 61.4 |
| An | 41.7 | 61.5 | 33.7 | 46.2 | 40.5 | 26.9 | 25.4 | 21.3 | 25.8 | 32.2 | 37.2 | 36.2 | 35.3 |
| Or | 1.9 | 0.9 | 2.1 | 1.6 | 2.7 | 2.5 | 3.4 | 3.2 | 4.4 | 3.1 | 2.8 | 3.7 | 3.3 |

Table V.1 continued.

| Sample | W99788 | W99788 | W99788 | W99982 | W99982 | W99982 | W99982 | W99982 | W99982 | W99876 | W99876 | W99876 | W99876 |
|---|---|---|---|---|---|---|---|---|---|---|---|---|---|
| Analysis | p-core | p-core | p-core | p-core | p-core | p-core | p-core | p-core | p-core | p-core | p-core | p-core | p-core |
| Unit | Slip Rhyolite | Slip Rhyolite | Slip Rhyolite | Pinnacles Rhyolite | Pinnacles Rhyolite | Pinnacles Rhyolite | Pinnacles Rhyolite | Pinnacles Rhyolite | Pinnacles Rhyolite | Kaueranga Rhyolite | Kaueranga Rhyolite | Kaueranga Rhyolite | Kaueranga Rhyolite |
| | wt% | wt% | wt% | wt% | wt% | wt% | wt% | wt% | wt% | wt% | wt% | wt% | wt% |
| SiO2 | 53.96 | 56.16 | 53.15 | 57.38 | 57.41 | 56.31 | 55.27 | 56.88 | 59.15 | 56.05 | 56.80 | 56.13 | 57.16 |
| TiO2 | 0.19 | 0.22 | 0.19 | 0.88 | 1.57 | 0.14 | 0.11 | 0.10 | 0.10 | 0.13 | 0.13 | 0.11 | 0.18 |
| Al2O3 | 27.64 | 28.24 | 28.43 | 25.42 | 25.92 | 25.89 | 25.99 | 25.63 | 24.34 | 26.05 | 25.75 | 25.83 | 26.43 |
| FeO | 0.42 | 0.28 | 0.56 | 0.35 | 0.44 | 0.38 | 0.38 | 0.33 | 0.40 | 0.39 | 0.36 | 0.35 | 0.42 |
| MnO | 0.08 | 0.01 | 0.01 | 0.07 | 0.07 | 0.06 | 0.00 | 0.09 | 0.09 | 0.01 | 0.12 | 0.05 | 0.10 |
| MgO | 0.09 | 0.07 | 0.05 | 0.01 | 0.04 | 0.01 | 0.03 | 0.05 | 0.07 | 0.06 | 0.03 | 0.01 | 0.06 |
| CaO | 9.80 | 10.63 | 9.50 | 8.57 | 7.38 | 8.04 | 8.70 | 7.74 | 6.39 | 8.38 | 8.08 | 8.18 | 8.74 |
| Na2O | 5.79 | 5.03 | 5.70 | 6.17 | 6.34 | 6.42 | 6.01 | 6.66 | 7.31 | 6.25 | 6.24 | 6.16 | 6.06 |
| K2O | 0.31 | 0.33 | 0.31 | 0.48 | 0.50 | 0.47 | 0.28 | 0.33 | 0.80 | 0.32 | 0.22 | 0.29 | 0.31 |
| TOTAL | 98.29 | 100.96 | 97.90 | 99.32 | 99.66 | 97.73 | 96.88 | 97.82 | 98.66 | 97.64 | 97.74 | 97.10 | 99.46 |
| | | | | | | | | | | | | | |
| Ab | 50.7 | 45.2 | 51.1 | 55.0 | 59.0 | 57.5 | 54.6 | 59.7 | 64.3 | 56.4 | 57.5 | 56.6 | 54.6 |
| An | 47.5 | 52.8 | 47.1 | 42.2 | 38.0 | 39.8 | 43.7 | 38.3 | 31.1 | 41.7 | 41.1 | 41.6 | 43.5 |
| Or | 1.8 | 2.0 | 1.9 | 2.8 | 3.1 | 2.8 | 1.7 | 2.0 | 4.6 | 1.9 | 1.3 | 1.7 | 1.9 |

Table V.1 continued.

| Sample | W99876 | W99612 | W99612 | W99612 | W99612 | W99612 | W99612 | W99612 | W99612 | W99990 | W99990 | W99990 |
|---|---|---|---|---|---|---|---|---|---|---|---|---|
| Analysis | p-core | scoria p-core | matrix c-core | scoria p-core | scoria p-core | scoria p-core | pumice p-core | pumice p-core | pumice p-core | matrix c-core | pumice p-core | pumice p-core |
| Unit | Kauaeranga Rhyolite | Oteao Ignimbrite | Oteao Ignimbrite | Oteao Ignimbrite | Oteao Ignimbrite | Oteao Ignimbrite | Oteao Ignimbrite | Oteao Ignimbrite | Oteao Ignimbrite | Trig Q Ignimbrite | Trig Q Ignimbrite | Trig Q Ignimbrite |
| | wt% | wt% | wt% | wt% | wt% | wt% | wt% | wt% | wt% | wt% | wt% | wt% |
| SiO2 | 56.68 | 51.71 | 67.33 | 52.27 | 50.54 | 53.14 | 60.68 | 58.37 | 57.80 | 54.08 | 58.50 | 56.58 |
| TiO2 | 0.20 | 0.16 | 0.42 | 0.29 | 0.31 | 0.23 | 0.16 | 0.14 | 0.12 | 0.12 | 0.11 | 0.11 |
| Al2O3 | 25.95 | 30.63 | 16.32 | 29.05 | 30.20 | 28.14 | 24.63 | 25.90 | 24.57 | 27.65 | 26.46 | 26.77 |
| FeO | 0.36 | 0.83 | 2.13 | 0.77 | 0.60 | 0.49 | 0.34 | 0.25 | 0.29 | 0.36 | 0.45 | 0.51 |
| MnO | 0.06 | 0.06 | 0.15 | 0.08 | 0.12 | 0.05 | 0.04 | 0.08 | 0.17 | 0.10 | 0.06 | 0.16 |
| MgO | 0.05 | 0.11 | 0.88 | 0.09 | 0.10 | 0.05 | 0.01 | 0.05 | 0.01 | 0.06 | 0.08 | 0.03 |
| CaO | 8.57 | 14.02 | 3.75 | 11.70 | 13.39 | 11.17 | 6.96 | 7.78 | 6.73 | 9.80 | 9.29 | 9.07 |
| Na2O | 6.33 | 3.48 | 3.81 | 4.67 | 3.78 | 5.22 | 6.75 | 6.99 | 7.25 | 5.62 | 6.34 | 6.30 |
| K2O | 0.36 | 0.16 | 3.39 | 0.22 | 0.17 | 0.17 | 0.34 | 0.39 | 0.35 | 0.24 | 0.36 | 0.28 |
| TOTAL | 98.55 | 101.16 | 98.17 | 99.13 | 99.20 | 98.64 | 99.91 | 99.94 | 97.29 | 98.02 | 101.64 | 99.80 |
| | | | | | | | | | | | | |
| Ab | 56.00 | 30.70 | 47.00 | 41.40 | 33.50 | 45.40 | 62.40 | 60.50 | 64.70 | 50.20 | 54.10 | 54.80 |
| An | 41.90 | 68.40 | 25.60 | 57.30 | 65.50 | 53.70 | 35.50 | 37.30 | 33.20 | 48.40 | 43.80 | 43.60 |
| Or | 2.10 | 0.90 | 27.50 | 1.30 | 1.00 | 1.00 | 2.10 | 2.20 | 2.10 | 1.40 | 2.00 | 1.60 |

Table V.2 Electron microprobe analyses and calculated end member compositions of pyroxene phenocrysts and crystals in Kapowai Caldera Complex volcanic units. p-core = phenocryst core; p-rim = phenocryst rim; c-core = crystal core

| Sample | W99601 | W99601 | W99601 | W99601 | W99601 | W99691 | W99691 | W99601 | W99601 | W99601 | W99601 | W99601 | W99601 |
|---|---|---|---|---|---|---|---|---|---|---|---|---|---|
| Analysis | p-core | p-core | p-core | p-core | p-core | p-core | p-core | p-core | p-core | p-core | p-core | p-core | p-core |
| Unit | Taurahuehue Andesite | Taurahuehue Andesite | Taurahuehue Andesite | Taurahuehue Andesite | Taurahuehue Andesite | Taurahuehue Andesite | Taurahuehue Andesite | Taurahuehue Andesite | Taurahuehue Andesite | Taurahuehue Andesite | Taurahuehue Andesite | Taurahuehue Andesite | Taurahuehue Andesite |
| | wt % | wt % | wt % | wt % | wt % | wt % | wt % | wt. % | wt. % | wt. % | wt. % | wt. % | wt. % |
| SiO2 | 52.25 | 51.48 | 50.12 | 52.73 | 52.54 | 53.43 | 52.02 | 52.13 | 51.92 | 52.35 | 53.88 | 50.88 | 54.35 |
| TiO2 | 0.33 | 0.39 | 0.47 | 0.39 | 0.36 | 0.36 | 0.32 | 0.39 | 0.48 | 0.46 | 0.30 | 0.90 | 0.41 |
| Al2O3 | 2.85 | 3.16 | 3.38 | 2.05 | 1.50 | 1.55 | 0.98 | 2.77 | 4.01 | 2.50 | 2.31 | 3.23 | 2.08 |
| FeO | 6.46 | 6.20 | 5.77 | 18.64 | 19.24 | 17.90 | 23.59 | 6.55 | 6.17 | 19.38 | 17.29 | 11.39 | 18.78 |
| MnO | 0.20 | 0.29 | 0.15 | 0.46 | 0.55 | 0.43 | 0.56 | 0.32 | 0.18 | 0.38 | 0.37 | 0.45 | 0.55 |
| MgO | 18.11 | 17.27 | 17.09 | 26.55 | 25.71 | 26.76 | 23.37 | 16.86 | 15.91 | 23.24 | 25.48 | 14.02 | 24.85 |
| CaO | 21.39 | 21.32 | 21.75 | 1.42 | 1.62 | 1.27 | 1.62 | 20.39 | 21.69 | 2.03 | 1.45 | 19.14 | 1.43 |
| Na2O | 0.26 | 0.28 | 0.28 | 0.05 | 0.10 | 0.00 | 0.17 | 0.25 | 0.20 | 0.08 | 0.04 | 0.36 | 0.05 |
| K2O | 0.08 | 0.04 | 0.06 | 0.04 | 0.02 | 0.05 | 0.06 | 0.02 | 0.03 | 0.05 | 0.01 | 0.02 | 0.01 |
| Cl | 0.03 | 0.05 | 0.06 | 0.03 | 0.08 | 0.06 | 0.05 | 0.10 | 0.05 | 0.05 | 0.08 | 0.00 | 0.05 |
| Cr2O3 | 0.15 | 0.29 | 0.62 | 0.00 | 0.05 | 0.16 | 0.09 | 0.24 | 0.43 | 0.03 | 0.18 | 0.03 | 0.01 |
| NiO | 0.14 | 0.02 | 0.05 | 0.00 | 0.00 | 0.08 | 0.11 | 0.03 | 0.03 | 0.01 | 0.12 | 0.06 | 0.10 |
| TOTAL | 102.25 | 100.77 | 99.79 | 102.36 | 101.75 | 102.05 | 102.94 | 100.05 | 101.11 | 100.56 | 101.50 | 100.48 | 102.66 |
| | | | | | | | | | | | | | |
| Wo | 41.31 | 42.29 | 43.37 | 2.66 | 3.06 | 2.40 | 3.05 | 41.4 | 44.5 | 4.1 | 2.9 | 40.0 | 2.8 |
| En | 48.66 | 47.66 | 47.41 | 68.93 | 67.71 | 70.50 | 61.36 | 47.7 | 45.4 | 64.9 | 69.9 | 40.7 | 67.7 |
| Fs | 10.04 | 10.05 | 9.22 | 28.42 | 29.23 | 27.10 | 35.59 | 10.9 | 10.2 | 31.0 | 27.2 | 19.3 | 29.5 |

Table V.2 continued.

| Sample | W99601 | W99601 | W99601 | W99732 | W99732 | W99732 | W99732 | W99732 | W99732 | W99732 | W99732 | W99816 |
|---|---|---|---|---|---|---|---|---|---|---|---|---|
| Analysis | p-core | p-core | p-core | p-rim | p-core | p-core | p-core | p-rim | p-core | p-core | p-core | p-core |
| Unit | Taurahuehue Andesite | Taurahuehue Andesite | Taurahuehue Andesite | Tauraulkau Andesite | Tauraulkau Andesite | Tauraulkau Andesite | Tauraulkau Andesite | Tauraulkau Andesite | Tauraulkau Andesite | Tauraulkau Andesite | Tauraulkau Andesite | Tauraulkau Andesite |
| | wt. % | wt. % | wt. % | wt. % | wt. % | wt. % | wt. % | wt. % | wt. % | wt. % | wt. % | wt % |
| SiO2 | 54.10 | 53.52 | 53.84 | 53.32 | 53.92 | 53.92 | 54.30 | 53.81 | 53.75 | 53.31 | 52.66 | 51.27 |
| TiO2 | 0.32 | 0.35 | 0.38 | 0.25 | 0.31 | 0.31 | 0.17 | 0.17 | 0.18 | 0.19 | 0.37 | 0.29 |
| Al2O3 | 2.07 | 2.67 | 2.22 | 0.92 | 3.87 | 3.87 | 0.67 | 0.76 | 0.71 | 0.84 | 1.41 | 1.74 |
| FeO | 17.66 | 18.49 | 18.10 | 22.39 | 13.32 | 13.32 | 21.77 | 22.30 | 22.11 | 21.42 | 10.41 | 21.72 |
| MnO | 0.46 | 0.57 | 0.45 | 0.76 | 0.51 | 0.51 | 0.78 | 0.62 | 0.67 | 0.86 | 0.53 | 0.63 |
| MgO | 25.67 | 24.07 | 25.40 | 22.57 | 26.82 | 26.82 | 22.44 | 22.79 | 23.06 | 22.86 | 14.56 | 22.66 |
| CaO | 1.38 | 1.15 | 1.49 | 1.45 | 1.67 | 1.67 | 1.32 | 1.28 | 1.17 | 1.25 | 20.91 | 2.20 |
| Na2O | 0.08 | 0.00 | 0.06 | 0.03 | 0.01 | 0.01 | 0.09 | 0.11 | 0.07 | 0.00 | 0.35 | 0.05 |
| K2O | 0.04 | 0.02 | 0.06 | 0.03 | 0.00 | 0.00 | 0.02 | 0.05 | 0.10 | 0.04 | 0.02 | 0.08 |
| Cl | 0.05 | 0.00 | 0.06 | 0.10 | 0.04 | 0.04 | 0.12 | 0.04 | 0.03 | 0.06 | 0.06 | 0.05 |
| Cr2O3 | 0.15 | 0.00 | 0.13 | 0.16 | 0.08 | 0.08 | 0.17 | 0.04 | 0.15 | 0.07 | 0.02 | 0.14 |
| NiO | 0.10 | 0.12 | 0.08 | 0.15 | 0.05 | 0.05 | 0.09 | 0.01 | 0.02 | 0.22 | 0.15 | 0.07 |
| TOTAL | 102.08 | 100.96 | 102.25 | 102.13 | 100.60 | 100.60 | 101.95 | 101.99 | 102.03 | 101.13 | 101.45 | 100.91 |
| | | | | | | | | | | | | |
| Wo | 2.7 | 2.3 | 2.9 | 2.8 | 3.4 | 3.4 | 2.6 | 2.5 | 2.3 | 2.5 | 42.1 | 4.30 |
| En | 69.7 | 67.6 | 68.9 | 61.7 | 75.0 | 75.0 | 62.3 | 62.3 | 62.9 | 63.0 | 40.8 | 61.60 |
| Fs | 27.6 | 30.1 | 28.2 | 35.5 | 21.7 | 21.7 | 35.1 | 35.2 | 34.8 | 34.5 | 17.2 | 34.10 |

Table V.2 continued.

| Sample | W99816 | W99816 | W99816 | W99732 | W99732 | W99732 | W99732 | W99732 | W99816 | W99816 | W99816 | W99816 | W99816 |
|---|---|---|---|---|---|---|---|---|---|---|---|---|---|
| Analysis | p-core | p-core | p-core | p-core | p-core | p-core | p-core | p-core | p-core | p-core | p-core | p-core | p-core |
| Unit | Tauraulkau Andesite | Tauraulkau Andesite | Tauraulkau Andesite | Tauraulkau Andesite | Tauraulkau Andesite | Tauraulkau Andesite | Tauraulkau Andesite | Tauraulkau Andesite | Tauraulkau Andesite | Tauraulkau Andesite | Tauraulkau Andesite | Tauraulkau Andesite | Tauraulkau Andesite |
| | wt % | wt % | wt % | wt. % | wt. % | wt. % | wt. % | wt. % | wt. % | wt. % | wt. % | wt. % | wt. % |
| SiO2 | 50.61 | 50.53 | 51.89 | 53.14 | 53.60 | 53.55 | 54.15 | 54.00 | 52.65 | 54.42 | 54.54 | 54.47 | 53.24 |
| TiO2 | 0.37 | 0.50 | 0.34 | 0.18 | 0.29 | 0.24 | 0.24 | 0.26 | 0.35 | 0.23 | 0.22 | 0.21 | 0.27 |
| Al2O3 | 1.48 | 1.29 | 0.65 | 1.27 | 0.76 | 0.67 | 0.70 | 0.92 | 1.19 | 0.72 | 0.68 | 0.63 | 1.14 |
| FeO | 9.90 | 10.07 | 21.68 | 22.04 | 21.55 | 21.78 | 22.46 | 22.30 | 10.34 | 21.94 | 21.97 | 21.49 | 9.92 |
| MnO | 0.46 | 0.41 | 0.77 | 0.89 | 0.62 | 0.63 | 0.67 | 0.55 | 0.47 | 0.68 | 0.79 | 0.71 | 0.36 |
| MgO | 15.25 | 15.24 | 23.69 | 22.29 | 22.73 | 22.51 | 22.87 | 22.29 | 14.65 | 22.90 | 22.70 | 23.13 | 14.54 |
| CaO | 21.09 | 21.19 | 1.38 | 1.34 | 1.31 | 1.23 | 1.20 | 1.29 | 21.18 | 1.28 | 1.28 | 1.23 | 22.67 |
| Na2O | 0.28 | 0.27 | 0.03 | 0.12 | 0.00 | 0.09 | 0.07 | 0.00 | 0.24 | 0.04 | 0.07 | 0.04 | 0.33 |
| K2O | 0.09 | 0.06 | 0.07 | 0.02 | 0.00 | 0.00 | 0.05 | 0.04 | 0.02 | 0.04 | 0.02 | 0.03 | 0.04 |
| Cl | 0.10 | 0.06 | 0.07 | 0.02 | 0.05 | 0.00 | 0.07 | 0.00 | 0.05 | 0.00 | 0.03 | 0.01 | 0.01 |
| Cr2O3 | 0.12 | 0.13 | 0.06 | 0.10 | 0.05 | 0.03 | 0.23 | 0.09 | 0.05 | 0.01 | 0.00 | 0.03 | 0.11 |
| NiO | 0.04 | 0.01 | 0.03 | 0.09 | 0.07 | 0.06 | 0.00 | 0.07 | 0.06 | 0.08 | 0.06 | 0.12 | 0.00 |
| TOTAL | 99.77 | 99.77 | 100.67 | 101.48 | 101.04 | 100.80 | 102.72 | 101.81 | 101.26 | 102.35 | 102.38 | 102.11 | 102.63 |
| | | | | | | | | | | | | | |
| Wo | 41.85 | 41.89 | 2.66 | 2.7 | 2.6 | 2.5 | 2.3 | 2.6 | 42.4 | 2.5 | 2.5 | 2.4 | 44.5 |
| En | 42.11 | 41.92 | 63.55 | 61.7 | 62.9 | 62.6 | 62.3 | 61.8 | 40.8 | 62.7 | 62.4 | 63.4 | 39.7 |
| Fs | 16.04 | 16.19 | 33.79 | 35.6 | 34.5 | 35.0 | 35.4 | 35.6 | 16.9 | 34.8 | 35.1 | 34.2 | 15.8 |

Table V.2 continued.

| Sample | W99816 | W99816 | W99816 | W99951 | W99951 | W99951 | W99951 | W99951 | W99951 | W99951 | W99895 | W99895 | W99912 |
|---|---|---|---|---|---|---|---|---|---|---|---|---|---|
| Analysis | p-core | p-core | p-core | p-core | p-core | p-core | p-core | p-core | p-core | p-core | p-core | p-core | p-core |
| Unit | Tauraulkau Andesite | Tauraulkau Andesite | Tauraulkau Andesite | Tapuaetahi Andesite | Tapuaetahi Andesite | Tapuaetahi Andesite | Tapuaetahi Andesite | Tapuaetahi Andesite | Tapuaetahi Andesite | Tapuaetahi Andesite | Kapowai Rhyolite | Kapowai Rhyolite | Precipice Rhyolite |
| | wt. % | wt. % | wt. % | wt % | wt % | wt. % | wt. % | wt. % | wt. % | wt. % | wt % | wt % | wt % |
| SiO2 | 52.76 | 53.35 | 53.59 | 52.54 | 53.97 | 53.56 | 54.04 | 52.40 | 49.67 | 53.37 | 52.49 | 51.77 | 48.41 |
| TiO2 | 0.44 | 0.16 | 0.15 | 0.21 | 0.16 | 0.25 | 0.31 | 0.33 | 1.04 | 0.18 | 0.38 | 0.38 | 0.37 |
| Al2O3 | 1.38 | 1.01 | 0.75 | 1.20 | 1.81 | 1.78 | 1.77 | 2.88 | 5.29 | 1.28 | 1.05 | 1.17 | 1.42 |
| FeO | 10.46 | 22.24 | 20.99 | 22.51 | 10.20 | 5.01 | 5.12 | 5.71 | 8.92 | 21.76 | 22.02 | 20.12 | 25.55 |
| MnO | 0.30 | 0.79 | 0.56 | 0.51 | 0.31 | 0.22 | 0.26 | 0.12 | 0.31 | 0.53 | 0.58 | 0.45 | 1.02 |
| MgO | 14.44 | 22.25 | 22.92 | 24.17 | 32.57 | 17.93 | 18.27 | 16.72 | 15.51 | 22.66 | 23.88 | 25.57 | 21.10 |
| CaO | 20.92 | 1.23 | 1.23 | 1.16 | 1.40 | 21.25 | 20.68 | 21.75 | 19.12 | 1.20 | 1.52 | 1.77 | 1.56 |
| Na2O | 0.28 | 0.10 | 0.11 | 0.09 | 0.05 | 0.26 | 0.24 | 0.27 | 0.26 | 0.07 | 0.07 | 0.01 | 0.16 |
| K2O | 0.07 | 0.00 | 0.04 | 0.09 | 0.03 | 0.05 | 0.04 | 0.05 | 0.00 | 0.02 | 0.11 | 0.08 | 0.01 |
| Cl | 0.07 | 0.04 | 0.15 | 0.04 | 0.02 | 0.03 | 0.01 | 0.06 | 0.13 | 0.00 | 0.10 | 0.09 | 0.07 |
| Cr2O3 | 0.01 | 0.00 | 0.06 | 0.12 | 0.13 | 0.30 | 0.44 | 0.35 | 0.06 | 0.08 | 0.12 | 0.06 | 0.06 |
| NiO | 0.03 | 0.08 | 0.04 | 0.11 | 0.14 | 0.05 | 0.03 | 0.05 | 0.03 | 0.01 | 0.10 | 0.00 | 0.00 |
| TOTAL | 101.15 | 101.25 | 100.59 | 102.72 | 100.79 | 100.69 | 101.22 | 100.68 | 100.33 | 101.16 | 102.40 | 101.47 | 99.71 |
| | | | | | | | | | | | | | |
| Wo | 42.3 | 2.5 | 2.5 | 2.19 | 2.55 | 42.3 | 41.1 | 43.9 | 39.9 | 2.4 | 2.89 | 3.32 | 3.01 |
| En | 40.7 | 61.7 | 63.8 | 63.75 | 82.50 | 49.6 | 50.5 | 46.9 | 45.0 | 62.9 | 63.43 | 66.62 | 56.83 |
| Fs | 17.0 | 35.8 | 33.7 | 34.06 | 14.95 | 8.1 | 8.4 | 9.2 | 15.0 | 34.7 | 33.68 | 30.06 | 40.17 |

Table V.2 continued.

| Sample | W99912 | W99912 | W99912 | W99912 | W99912 | W99912 | W99912 | W99912 | W99912 | W99912 | W99912 | W991002 | W991002 |
|---|---|---|---|---|---|---|---|---|---|---|---|---|---|
| Analysis | p-core | p-core | p-core | p-core | p-core | p-core | p-core | p-core | p-core | p-core | p-core | p-core | p-core |
| Unit | Precipice Rhyolite | Precipice Rhyolite | Precipice Rhyolite | Precipice Rhyolite | Precipice Rhyolite | Precipice Rhyolite | Precipice Rhyolite | Precipice Rhyolite | Precipice Rhyolite | Precipice Rhyolite | Precipice Rhyolite | Kokonga Rhyolite | Kokonga Rhyolite |
| | wt % | wt. % | wt. % | wt. % | wt. % | wt. % | wt. % | wt. % | wt. % | wt. % | wt. % | wt % | wt % |
| SiO2 | 50.18 | 51.92 | 52.40 | 51.94 | 52.44 | 52.56 | 53.98 | 54.28 | 53.95 | 52.93 | 53.16 | 51.11 | 50.17 |
| TiO2 | 0.52 | 0.26 | 0.18 | 0.18 | 0.34 | 0.28 | 0.34 | 0.35 | 0.29 | 0.23 | 0.23 | 0.39 | 0.64 |
| Al2O3 | 1.84 | 1.03 | 0.63 | 0.70 | 1.64 | 0.79 | 1.21 | 1.04 | 1.28 | 0.85 | 1.01 | 1.28 | 1.91 |
| FeO | 10.01 | 12.23 | 26.69 | 25.76 | 21.45 | 24.60 | 20.00 | 19.52 | 20.46 | 11.82 | 22.39 | 22.28 | 9.17 |
| MnO | 0.56 | 0.62 | 1.09 | 1.28 | 1.25 | 1.10 | 0.79 | 0.96 | 0.94 | 0.72 | 1.08 | 1.18 | 0.38 |
| MgO | 15.25 | 13.55 | 17.82 | 18.72 | 22.38 | 20.34 | 24.22 | 23.72 | 23.22 | 13.25 | 22.09 | 22.85 | 15.82 |
| CaO | 20.84 | 20.55 | 1.27 | 1.29 | 1.26 | 1.38 | 1.55 | 1.38 | 1.42 | 20.40 | 1.38 | 1.52 | 21.71 |
| Na2O | 0.31 | 0.31 | 0.06 | 0.11 | 0.10 | 0.07 | 0.11 | 0.01 | 0.08 | 0.25 | 0.07 | 0.10 | 0.34 |
| K2O | 0.07 | 0.03 | 0.13 | 0.01 | 0.01 | 0.07 | 0.08 | 0.02 | 0.02 | 0.04 | 0.03 | 0.07 | 0.13 |
| Cl | 0.25 | 0.07 | 0.03 | 0.05 | 0.10 | 0.04 | 0.02 | 0.06 | 0.11 | 0.02 | 0.00 | 0.17 | 0.06 |
| Cr2O3 | 0.06 | 0.00 | 0.00 | 0.09 | 0.00 | 0.15 | 0.22 | 0.09 | 0.18 | 0.07 | 0.00 | 0.00 | 0.01 |
| NiO | 0.04 | 0.03 | 0.03 | 0.06 | 0.11 | 0.04 | 0.04 | 0.14 | 0.01 | 0.05 | 0.09 | 0.00 | 0.03 |
| TOTAL | 99.93 | 100.60 | 100.33 | 100.20 | 101.08 | 101.43 | 102.55 | 101.55 | 101.96 | 100.62 | 101.54 | 100.96 | 100.37 |
| | | | | | | | | | | | | | |
| Wo | 41.42 | 41.6 | 2.7 | 2.7 | 2.5 | 2.8 | 3.0 | 2.7 | 2.8 | 41.9 | 2.7 | 2.95 | 42.43 |
| En | 42.17 | 38.1 | 51.9 | 53.8 | 62.1 | 56.9 | 65.5 | 65.5 | 64.1 | 37.9 | 60.9 | 61.56 | 43.00 |
| Fs | 16.41 | 20.3 | 45.4 | 43.6 | 35.4 | 40.3 | 31.5 | 31.8 | 33.1 | 20.1 | 36.3 | 35.49 | 14.58 |

Table V.2 continued.

| Sample | W99994 | W99994 | W99994 | W99990 | W99612 | W99612 | W99612 | W99612 | W99612 | W99612 | W99908 | W99908 |
|---|---|---|---|---|---|---|---|---|---|---|---|---|
| Analysis | p-core | p-core | p-core | matrix c-core | matrix c-core | matrix c-core | matrix c-core | scoria p-core | pumice p-core | pumice p-core | matrix c-core | matrix c-core |
| Unit | Camp Rhyolite | Camp Rhyolite | Camp Rhyolite | Trig Q Ignimbrite | Oteao Ignimbrite | Oteao Ignimbrite | Oteao Ignimbrite | Oteao Ignimbrite | Oteao Ignimbrite | Oteao Ignimbrite | Manuka Ignimbrite | Manuka Ignimbrite |
| | wt % | wt % | wt % | wt % | wt % | wt % | wt % | wt % | wt % | wt % | wt. % | wt. % |
| SiO2 | 49.56 | 50.63 | 47.83 | 54.32 | 50.47 | 50.09 | 49.99 | 48.97 | 49.49 | 51.37 | 51.96 | 52.64 |
| TiO2 | 0.26 | 0.30 | 0.19 | 0.32 | 0.73 | 0.73 | 0.66 | 0.23 | 0.29 | 0.30 | 0.16 | 0.21 |
| Al2O3 | 0.47 | 0.46 | 0.71 | 1.16 | 2.40 | 1.92 | 2.17 | 1.31 | 0.40 | 0.64 | 0.52 | 0.71 |
| FeO | 25.78 | 25.58 | 30.81 | 14.36 | 10.11 | 9.84 | 10.52 | 27.43 | 26.71 | 26.64 | 26.51 | 27.29 |
| MnO | 1.57 | 1.67 | 1.78 | 0.39 | 0.61 | 0.25 | 0.40 | 1.46 | 1.47 | 1.58 | 1.84 | 1.65 |
| MgO | 19.45 | 19.51 | 15.32 | 29.65 | 14.60 | 15.90 | 16.06 | 17.87 | 18.70 | 18.78 | 18.43 | 18.56 |
| CaO | 1.36 | 1.40 | 1.43 | 1.69 | 20.74 | 20.07 | 20.15 | 1.36 | 1.34 | 1.58 | 1.16 | 1.37 |
| Na2O | 0.01 | 0.01 | 0.18 | 0.00 | 0.34 | 0.37 | 0.30 | 0.01 | 0.14 | 0.03 | 0.14 | 0.00 |
| K2O | 0.02 | 0.11 | 0.10 | 0.07 | 0.07 | 0.05 | 0.10 | 0.09 | 0.09 | 0.09 | 0.03 | 0.06 |
| Cl | 0.18 | 0.09 | 0.05 | 0.08 | 0.18 | 0.02 | 0.12 | 0.14 | 0.12 | 0.10 | 0.03 | 0.00 |
| Cr2O3 | 0.02 | 0.09 | 0.08 | 0.11 | 0.03 | 0.09 | 0.05 | 0.00 | 0.04 | 0.08 | 0.11 | 0.16 |
| NiO | 0.02 | 0.02 | 0.05 | 0.00 | 0.06 | 0.08 | 0.05 | 0.02 | 0.00 | 0.00 | 0.07 | 0.02 |
| TOTAL | 98.71 | 99.87 | 98.53 | 102.15 | 100.35 | 99.40 | 100.56 | 98.90 | 98.80 | 101.18 | 100.95 | 102.68 |
| | | | | | | | | | | | | |
| Wo | 2.73 | 2.81 | 2.97 | 3.11 | 41.95 | 40.08 | 39.49 | 2.79 | 2.72 | 3.17 | 2.4 | 2.8 |
| En | 54.36 | 54.48 | 44.23 | 75.75 | 41.10 | 44.18 | 43.79 | 50.97 | 52.70 | 52.52 | 52.4 | 51.9 |
| Fs | 42.91 | 42.72 | 52.81 | 21.15 | 16.94 | 15.73 | 16.72 | 46.24 | 44.58 | 44.31 | 45.2 | 45.4 |

Table V.2 continued.

| Sample | W99908 | W99908 |
|---|---|---|
| Analysis | p-core | p-core |
| Unit | Manuka Ignimbrite | Manuka Ignimbrite |
| | wt. % | wt. % |
| SiO2 | 52.52 | 53.92 |
| TiO2 | 0.24 | 0.24 |
| Al2O3 | 0.35 | 0.94 |
| FeO | 26.94 | 20.69 |
| MnO | 1.67 | 0.61 |
| MgO | 18.55 | 23.74 |
| CaO | 1.17 | 1.36 |
| Na2O | 0.01 | 0.09 |
| K2O | 0.03 | 0.00 |
| Cl | 0.09 | 0.05 |
| Cr2O3 | 0.00 | 0.17 |
| NiO | 0.03 | 0.00 |
| TOTAL | 101.61 | 101.79 |
| | | |
| Wo | 2.4 | 2.7 |
| En | 52.3 | 64.7 |
| Fs | 45.3 | 32.6 |

Table V.3 Electron microprobe analyses and calculated Mg# composition of amphibole phenocrysts in Slip Rhyolite lava. p-core = phenocryst core.

| Sample | W99788 | W99788 | W99788 | W99788 | W99788 |
|---|---|---|---|---|---|
| Analysis | p-core | p-core | p-core | p-core | p-core |
| | wt% | wt% | wt% | wt% | wt% |
| SiO2 | 45.6 | 45.64 | 44.89 | 47.35 | 45.35 |
| TiO2 | 1.75 | 1.74 | 1.75 | 1.63 | 1.73 |
| Al2O3 | 6.84 | 6.84 | 7.41 | 6.3 | 6.8 |
| FeO | 16.93 | 17.03 | 18.5 | 13.56 | 18.27 |
| MnO | 0.44 | 0.22 | 0.37 | 0.29 | 0.56 |
| MgO | 13.69 | 13.18 | 12.54 | 15.34 | 12.38 |
| CaO | 11.31 | 11.15 | 10.48 | 10.94 | 10.67 |
| Na2O | 1.45 | 1.46 | 1.53 | 1.45 | 1.63 |
| K2O | 0.41 | 0.47 | 0.55 | 0.48 | 0.44 |
| Cl | 0.26 | 0.24 | 0.18 | 0.13 | 0.22 |
| Cr2O3 | 0.08 | 0.16 | 0.04 | 0.08 | 0.06 |
| NiO | 0.07 | 0.10 | 0.02 | 0.03 | 0.17 |
| TOTAL | 98.84 | 98.23 | 98.24 | 97.55 | 98.28 |
| | | | | | |
| Mg# | 44 | 44 | 40 | 53 | 40 |

Table V.4 Electron microprobe analyses and calculated Mg# composition of biotite phenocrysts in Kapowai Caldera Complex volcanic units. p-core = phenocryst core.

| Sample | W99834 | W99834 | W99834 | W99834 | W991005 | W991005 | W991005 | W99951 | W99951 |
|---|---|---|---|---|---|---|---|---|---|
| Analysis | p-core | p-core | p-core | p-core | p-core | p-core | p-core | p-core | p-core |
| Unit | Welcome Jack Rhyolite | Welcome Jack Rhyolite | Welcome Jack Rhyolite | Welcome Jack Rhyolite | Ruahine Rhyolite | Ruahine Rhyolite | Ruahine Rhyolite | Tapuaetahi Andesite | Tapuaetahi Andesite |
| Oxide | wt% | wt% | wt% | wt% | wt% | wt% | wt% | wt% | wt% |
| SiO2 | 37.33 | 36.54 | 36.32 | 35.86 | 38.29 | 33.02 | 35.16 | 37.23 | 37.46 |
| TiO2 | 4.39 | 4.14 | 3.86 | 4.38 | 2.87 | 5.45 | 4.40 | 4.61 | 4.21 |
| Al2O3 | 13.18 | 13.15 | 13.24 | 13.59 | 22.09 | 14.90 | 14.66 | 15.27 | 15.59 |
| FeO | 18.99 | 20.35 | 20.35 | 19.93 | 16.68 | 22.97 | 17.56 | 14.69 | 11.92 |
| MnO | 0.28 | 0.21 | 0.37 | 0.17 | 0.27 | 0.11 | 0.16 | 0.22 | 0.01 |
| MgO | 12.64 | 12.56 | 12.33 | 12.70 | 7.55 | 8.39 | 13.24 | 17.19 | 19.31 |
| CaO | 0.13 | 0.09 | 0.12 | 0.08 | 0.12 | 0.14 | 0.14 | 0.02 | 0.09 |
| Na2O | 0.68 | 0.64 | 0.77 | 0.70 | 0.33 | 0.12 | 0.36 | 0.69 | 0.73 |
| K2O | 8.30 | 8.28 | 8.26 | 8.73 | 5.26 | 7.54 | 8.42 | 9.35 | 9.27 |
| Cl | 0.37 | 0.50 | 0.45 | 0.37 | 0.19 | 0.21 | 0.23 | 0.32 | 0.37 |
| Cr2O3 | 0.03 | 0.04 | 0.05 | 0.00 | 0.00 | 0.04 | 0.00 | 0.17 | 0.19 |
| NiO | 0.15 | 0.07 | 0.01 | 0.09 | 0.01 | 0.19 | 0.02 | 0.06 | 0.14 |
| TOTAL | 96.48 | 96.55 | 96.14 | 96.60 | 93.65 | 93.08 | 94.36 | 99.83 | 99.28 |
| | | | | | | | | | |
| Mg# | 40 | 38 | 38 | 39 | 25 | 27 | 43 | 54 | 62 |

Table V.5 Electron microprobe analyses of Fe-Ti oxide phenocrysts in Kapowai Caldera Complex volcanic units. p-core = phenocryst core.

| Sample | W99601 | W99951 | W99951 | W99951 | W99951 | W99951 | W99951 | W99691 | W99691 | W99816 | W99816 | W99816 | W99816 |
|---|---|---|---|---|---|---|---|---|---|---|---|---|---|
| Analysis | p-core | p-core | p-core | p-core | p-core | p-core | p-core | p-core | p-core | p-core | p-core | p-core | p-core |
| Unit | Taurahuehue Andesite | Tapuaetahi Andesite | Tapuaetahi Andesite | Tapuaetahi Andesite | Tapuaetahi Andesite | Tapuaetahi Andesite | Tapuaetahi Andesite | Taurahuehue Andesite | Taurahuehue Andesite | Taurauikau Andesite | Taurauikau Andesite | Taurauikau Andesite | Taurauikau Andesite |
| OXIDE | wt% | wt% | wt% | wt% | wt% | wt% | wt% | wt% | wt% | wt% | wt% | wt% | wt% |
| SiO2 | 0.70 | 0.11 | 0.08 | 0.12 | 0.09 | 0.42 | 0.24 | 0.14 | 0.37 | 0.15 | 0.05 | 0.20 | 0.19 |
| TiO2 | 16.25 | 49.37 | 55.86 | 46.24 | 45.43 | 2.38 | 8.12 | 16.80 | 40.87 | 45.38 | 44.73 | 10.27 | 10.51 |
| Al2O3 | 3.79 | 0.36 | 0.48 | 0.26 | 0.19 | 2.13 | 1.45 | 2.06 | 16.56 | 0.19 | 0.25 | 1.20 | 1.20 |
| FeO | 66.70 | 38.25 | 38.84 | 50.17 | 49.93 | 87.50 | 83.55 | 70.85 | 40.53 | 47.94 | 48.49 | 81.12 | 81.63 |
| MnO | 0.37 | 0.38 | 0.13 | 0.41 | 0.54 | 0.42 | 1.67 | 2.98 | 0.22 | 0.65 | 0.72 | 0.48 | 0.54 |
| MgO | 2.33 | 4.56 | 1.39 | 2.54 | 2.01 | 0.34 | 0.33 | 0.76 | 1.07 | 2.25 | 2.11 | 0.99 | 0.92 |
| CaO | 0.09 | 0.16 | 0.10 | 0.10 | 0.06 | 0.13 | 0.12 | 0.09 | 0.10 | 0.11 | 0.09 | 0.09 | 0.12 |
| Na2O | 0.00 | 0.35 | 0.01 | 0.00 | 0.26 | 0.00 | 0.11 | 0.00 | 0.43 | 0.00 | 0.01 | 0.01 | 0.00 |
| K2O | 0.07 | 0.05 | 0.03 | 0.09 | 0.00 | 0.09 | 0.09 | 0.07 | 0.05 | 0.10 | 0.05 | 0.02 | 0.10 |
| Cl | 0.05 | 0.04 | 0.07 | 0.06 | 0.02 | 0.07 | 0.03 | 0.06 | 0.23 | 0.07 | 0.10 | 0.09 | 0.06 |
| Cr2O3 | 0.38 | 0.06 | 0.00 | 0.07 | 0.25 | 0.11 | 0.10 | 0.94 | 0.14 | 0.10 | 0.08 | 0.55 | 0.45 |
| NiO | 0.05 | 0.05 | 0.09 | 0.16 | 0.03 | 0.06 | 0.11 | 0.16 | 0.08 | 0.05 | 0.16 | 0.09 | 0.03 |
| TOTAL | 90.77 | 93.75 | 97.08 | 100.20 | 98.80 | 93.64 | 95.92 | 94.89 | 100.66 | 96.98 | 96.84 | 95.12 | 95.73 |

Table V.5 continued.

| Sample | W99600 | W99600 | W99600 | W99600 | W99600 | W99600 | W99600 | W99905 | W99905 | W99905 | W99912 | W991002 | W991002 |
|---|---|---|---|---|---|---|---|---|---|---|---|---|---|
| Analysis | p-core | p-core | p-core | p-core | p-core | p-core | p-core | p-core | p-core | p-core | p-core | p-core | p-core |
| Unit | Rangihau Rhyolite | Rangihau Rhyolite | Rangihau Rhyolite | Rangihau Rhyolite | Rangihau Rhyolite | Rangihau Rhyolite | Rangihau Rhyolite | Kapowai Rhyolite | Kapowai Rhyolite | Kapowai Rhyolite | Precipice Rhyolite | Kokonga Rhyolite | Kokonga Rhyolite |
| OXIDE | wt% | wt% | wt% | wt% | wt% | wt% | wt% | wt% | wt% | wt% | wt% | wt% | wt% |
| SiO2 | 0.07 | 0.16 | 0.08 | 0.72 | 0.46 | 0.22 | 0.56 | 0.27 | 0.22 | 0.25 | 0.33 | 0.09 | 0.56 |
| TiO2 | 46.85 | 46.81 | 46.68 | 12.69 | 13.31 | 46.79 | 13.54 | 13.73 | 48.13 | 45.19 | 11.87 | 46.41 | 11.96 |
| Al2O3 | 0.37 | 0.21 | 0.16 | 2.26 | 2.19 | 0.21 | 2.15 | 1.48 | 0.14 | 0.23 | 1.64 | 0.19 | 2.20 |
| FeO | 47.13 | 46.77 | 46.53 | 73.14 | 74.04 | 48.61 | 74.38 | 76.73 | 45.90 | 49.72 | 80.51 | 51.27 | 76.48 |
| MnO | 1.32 | 1.62 | 1.39 | 0.99 | 1.06 | 1.24 | 1.05 | 1.00 | 2.68 | 1.21 | 0.75 | 1.46 | 0.94 |
| MgO | 1.48 | 0.87 | 1.24 | 0.80 | 0.93 | 1.11 | 0.71 | 0.54 | 0.75 | 0.55 | 0.64 | 1.24 | 0.72 |
| CaO | 0.11 | 0.15 | 0.08 | 0.14 | 0.13 | 0.10 | 0.19 | 0.21 | 0.11 | 0.21 | 0.14 | 0.09 | 0.10 |
| Na2O | 0.11 | 0.00 | 0.00 | 0.15 | 0.01 | 0.00 | 0.31 | 0.00 | 0.01 | 0.15 | 0.06 | 0.22 | 0.09 |
| K2O | 0.05 | 0.10 | 0.07 | 0.11 | 0.11 | 0.09 | 0.09 | 0.13 | 0.10 | 0.15 | 0.05 | 0.04 | 0.08 |
| Cl | 0.05 | 0.06 | 0.04 | 0.11 | 0.12 | 0.13 | 0.07 | 0.13 | 0.12 | 0.11 | 0.03 | 0.06 | 0.05 |
| Cr2O3 | 0.02 | 0.15 | 0.07 | 0.02 | 0.16 | 0.06 | 0.04 | 0.14 | 0.02 | 0.02 | 0.11 | 0.11 | 0.14 |
| NiO | 0.11 | 0.01 | 0.10 | 0.03 | 0.09 | 0.00 | 0.04 | 0.14 | 0.04 | 0.04 | 0.02 | 0.01 | 0.05 |
| TOTAL | 97.66 | 96.89 | 96.41 | 91.16 | 92.61 | 98.56 | 93.11 | 94.48 | 98.21 | 97.85 | 96.14 | 101.19 | 93.38 |

Table V.5 continued.

| Sample | W991002 | W99865 | W99865 | W99865 | W99834 | W99834 | W99834 | W99834 | W99834 | W991005 | W991005 | W99788 | W99788 |
|---|---|---|---|---|---|---|---|---|---|---|---|---|---|
| Analysis | p-core | p-core | p-core | p-core | p-core | p-core | p-core | p-core | p-core | p-core | p-core | p-core | p-core |
| Unit | Kokonga Rhyolite | Tauranikau Rhyolite | Tauranikau Rhyolite | Tauranikau Rhyolite | Welcome Jack Rhyolite | Welcome Jack Rhyolite | Welcome Jack Rhyolite | Welcome Jack Rhyolite | Welcome Jack Rhyolite | Ruahine Rhyolite | Ruahine Rhyolite | Slip Rhyolite | Slip Rhyolite |
| OXIDE | wt% | wt% | wt% | wt% | wt% | wt% | wt% | wt% | wt% | wt% | wt% | wt% | wt% |
| SiO2 | 0.37 | 0.41 | 0.23 | 0.53 | 0.16 | 0.08 | 0.09 | 0.13 | 1.38 | 0.17 | 0.20 | 0.40 | 0.30 |
| TiO2 | 12.49 | 12.02 | 45.83 | 12.85 | 46.54 | 45.28 | 46.14 | 46.94 | 11.34 | 8.52 | 49.43 | 11.51 | 44.29 |
| Al2O3 | 2.09 | 4.31 | 0.21 | 1.17 | 0.12 | 0.21 | 0.10 | 0.17 | 1.14 | 2.61 | 0.22 | 1.94 | 0.31 |
| FeO | 77.57 | 73.42 | 47.11 | 74.42 | 50.03 | 48.63 | 47.80 | 49.34 | 81.36 | 85.41 | 47.63 | 76.12 | 53.02 |
| MnO | 0.98 | 1.21 | 2.36 | 1.29 | 1.09 | 1.57 | 2.12 | 2.00 | 0.09 | 0.77 | 1.36 | 0.41 | 0.75 |
| MgO | 0.61 | 0.13 | 0.31 | 0.16 | 0.59 | 0.34 | 0.26 | 0.36 | 0.01 | 0.77 | 0.99 | 1.06 | 1.08 |
| CaO | 0.12 | 0.09 | 0.11 | 0.11 | 0.08 | 0.09 | 0.08 | 0.08 | 0.15 | 0.11 | 0.05 | 0.08 | 0.11 |
| Na2O | 0.01 | 0.08 | 0.08 | 0.08 | 0.07 | 0.14 | 0.00 | 0.15 | 0.14 | 0.19 | 0.20 | 0.26 | 0.01 |
| K2O | 0.11 | 0.10 | 0.10 | 0.03 | 0.10 | 0.11 | 0.11 | 0.07 | 0.13 | 0.09 | 0.13 | 0.06 | 0.10 |
| Cl | 0.10 | 0.09 | 0.05 | 0.15 | 0.13 | 0.09 | 0.06 | 0.08 | 0.13 | 0.06 | 0.12 | 0.20 | 0.01 |
| Cr2O3 | 0.00 | 0.09 | 0.08 | 0.00 | 0.00 | 0.12 | 0.01 | 0.06 | 0.14 | 0.09 | 0.02 | 0.17 | 0.10 |
| NiO | 0.12 | 0.07 | 0.08 | 0.24 | 0.03 | 0.11 | 0.00 | 0.04 | 0.15 | 0.12 | 0.02 | 0.01 | 0.09 |
| TOTAL | 94.57 | 92.02 | 96.54 | 91.02 | 98.93 | 96.77 | 96.77 | 99.43 | 96.13 | 98.91 | 100.36 | 92.23 | 100.16 |

Table V.5 continued.

| Sample | W99994 | W99994 | W99994 | W99995 | W99995 | W99995 | W99876 | W99876 | W99612 |
|---|---|---|---|---|---|---|---|---|---|
| Analysis | p-core | p-core | p-core | p-core | p-core | p-core | p-core | p-core | p-core |
| Unit | Camp Rhyolite | Camp Rhyolite | Camp Rhyolite | Pinnacles Rhyolite | Pinnacles Rhyolite | Pinnacles Rhyolite | Kauaeranga Rhyolite | Kauaeranga Rhyolite | Otaio Ignimbrite |
| OXIDE | wt% | wt% | wt% | wt% | wt% | wt% | wt% | wt% | wt% |
| SiO2 | 0.63 | 0.44 | 0.17 | 0.09 | 0.70 | 0.18 | 0.15 | 0.30 | 0.08 |
| TiO2 | 12.26 | 13.13 | 45.41 | 46.88 | 14.41 | 47.27 | 43.26 | 12.22 | 12.40 |
| Al2O3 | 1.95 | 1.42 | 0.30 | 0.10 | 0.90 | 0.17 | 0.31 | 5.29 | 3.44 |
| FeO | 74.63 | 74.84 | 47.20 | 47.40 | 76.42 | 47.41 | 50.85 | 74.64 | 75.28 |
| MnO | 0.94 | 0.97 | 1.40 | 1.52 | 1.10 | 1.53 | 0.91 | 0.98 | 0.49 |
| MgO | 1.19 | 0.92 | 1.50 | 1.07 | 0.42 | 0.96 | 1.66 | 1.53 | 3.43 |
| CaO | 0.18 | 0.02 | 0.32 | 0.09 | 0.18 | 0.13 | 0.10 | 0.15 | 0.07 |
| Na2O | 0.08 | 0.13 | 0.00 | 0.05 | 0.00 | 0.01 | 0.00 | 0.00 | 0.09 |
| K2O | 0.09 | 0.14 | 0.06 | 0.08 | 0.06 | 0.12 | 0.09 | 0.05 | 0.10 |
| Cl | 0.15 | 0.27 | 0.12 | 0.09 | 0.08 | 0.08 | 0.12 | 0.10 | 0.10 |
| Cr2O3 | 0.10 | 0.03 | 0.08 | 0.06 | 0.01 | 0.15 | 0.13 | 0.01 | 0.18 |
| NiO | 0.11 | 0.03 | 0.12 | 0.07 | 0.06 | 0.00 | 0.19 | 0.04 | 0.03 |
| TOTAL | 92.30 | 92.32 | 96.67 | 97.48 | 94.35 | 98.00 | 97.75 | 95.30 | 95.68 |

# Appendix VI

## XRF data

Table VI.1 Whole rock major element (normalised to 100%, volatile free) and trace element XRF analyses of pre-caldera and caldera andesite lavas of the Kapowai Caldera Complex. * original totals; + total Fe as $Fe_2O_3$.

| Sample | W99601 | W99681 | W99691 | W99877 | W99940 | W99706 | W99732 | W99816 | W99797 | W99799 | W99914A |
|---|---|---|---|---|---|---|---|---|---|---|---|
| Unit | Taurahuehue Andesite | Taurahuehue Andesite | Taurahuehue Andesite | Taurahuehue Andesite | Tapuaetahi Andesite | Taurauikau Andesite | Taurauikau Andesite | Taurauikau Andesite | Taurauikau Andesite | Taurauikau Andesite | Taurauikau Andesite |
| wt.% | | | | | | | | | | | |
| SiO2 | 56.14 | 61.23 | 61.49 | 61.83 | 64.45 | 60.08 | 63.83 | 63.33 | 63.98 | 61.74 | 64.62 |
| TiO2 | 1.00 | 0.76 | 0.72 | 0.74 | 0.55 | 0.63 | 0.64 | 0.62 | 0.65 | 0.64 | 0.55 |
| Al2O3 | 18.59 | 17.42 | 16.86 | 16.89 | 16.44 | 16.29 | 16.10 | 16.04 | 17.02 | 16.83 | 15.84 |
| Fe2O3+ | 8.41 | 6.00 | 6.27 | 5.97 | 5.14 | 6.50 | 5.50 | 5.77 | 4.43 | 5.84 | 5.40 |
| MnO | 0.24 | 0.08 | 0.11 | 0.09 | 0.05 | 0.11 | 0.09 | 0.09 | 0.08 | 0.09 | 0.08 |
| MgO | 3.35 | 3.18 | 3.37 | 3.35 | 2.57 | 4.55 | 3.17 | 3.14 | 3.26 | 3.42 | 2.87 |
| CaO | 7.47 | 6.32 | 6.09 | 6.03 | 5.48 | 7.28 | 5.43 | 5.81 | 5.72 | 6.57 | 5.43 |
| Na2O | 3.26 | 3.28 | 3.28 | 3.27 | 3.26 | 2.97 | 3.32 | 3.35 | 3.03 | 3.21 | 3.03 |
| K2O | 1.37 | 1.59 | 1.69 | 1.69 | 1.95 | 1.47 | 1.77 | 1.72 | 1.71 | 1.54 | 2.08 |
| P2O5 | 0.18 | 0.14 | 0.13 | 0.14 | 0.10 | 0.12 | 0.13 | 0.12 | 0.13 | 0.12 | 0.10 |
| LOI* | 0.89 | 0.56 | 0.11 | 0.30 | 0.51 | 0.13 | 0.56 | 0.27 | 1.21 | 0.80 | 1.32 |
| Total* | 100.37 | 100.39 | 100.23 | 100.19 | 100.37 | 100.30 | 100.29 | 100.24 | 100.24 | 100.24 | 100.21 |
| ppm | | | | | | | | | | | |
| Ba | 311 | 373 | 357 | 420 | 428 | 390 | 520 | 440 | 450 | 443 | 474 |
| Rb | 47 | 59 | 65 | 61 | 73 | 48 | 65 | 61 | 57 | 52 | 67 |
| Sr | 324 | 247 | 239 | 238 | 215 | 293 | 214 | 223 | 215 | 252 | 215 |
| Y | 25 | 22 | 24 | 25 | 21 | 21 | 31 | 25 | 29 | 28 | 75 |
| Zr | 136 | 153 | 161 | 161 | 129 | 130 | 171 | 163 | 160 | 145 | 153 |
| Nb | 7 | 6 | 6 | 6 | 5 | 5 | 6 | 6 | 5 | 5 | 3 |
| Th | 5 | 5 | 4 | 3 | 6 | 5 | 5 | 6 | 6 | 5 | 6 |
| Pb | 2 | 1 | 1 | 2 | 1 | 4 | 2 | 1 | 1 | 1 | 1 |
| Ga | 20 | 17 | 17 | 16 | 15 | 16 | 16 | 16 | 17 | 17 | 16 |
| Zn | 77 | 59 | 59 | 64 | 56 | 56 | 55 | 56 | 89 | 51 | 65 |
| Ni | 6 | 24 | 27 | 27 | 25 | 35 | 15 | 17 | 16 | 14 | 17 |
| V | 224 | 167 | 132 | 149 | 127 | 166 | 132 | 120 | 157 | 166 | 115 |
| Cr | 23 | 58 | 58 | 61 | 50 | 112 | 49 | 47 | 70 | 48 | 52 |
| La | 6 | 14 | 10 | 12 | 14 | 14 | 20 | 17 | 28 | 12 | 36 |
| Ce | 30 | 27 | 29 | 33 | 34 | 24 | 50 | 39 | 56 | 23 | 62 |
| Nd | 16 | 15 | 20 | 11 | 24 | 11 | 23 | 10 | 41 | 22 | 56 |
| K/Rb | 241 | 224 | 216 | 230 | 222 | 254 | 227 | 234 | 248 | 246 | 258 |
| Rb/Sr | 0.15 | 0.24 | 0.27 | 0.26 | 0.34 | 0.16 | 0.30 | 0.27 | 0.27 | 0.21 | 0.31 |

Table VI.2 Whole rock major element (normalised to 100%, volatile free) and trace element XRF analyses of Kapowai Caldera Complex rhyolite lavas. * original totals; + total Fe as $Fe_2O_3$.

| Sample | W99618 | W99622 | W99971 | W99946 | W99737 | W99743 | W99745 | W99839 | W99920 | W991002 | W99783 | W99858 | W99865 |
|---|---|---|---|---|---|---|---|---|---|---|---|---|---|
| Unit | Wharepapa | Waiwhatawhata | Waiwhatawhata | Waiwhatawhata | Bulls Run | Bulls Run | Bulls Run | Big Beetle | Kydd | Kokonga | Starvation | Tauranikau | Tauranikau |
| group | I | I | I | I | I | I | I | I | I | I | I | I | I |
| wt.% | | | | | | | | | | | | | |
| SiO2 | 76.47 | 72.65 | 74.18 | 73.90 | 75.72 | 76.06 | 74.60 | 72.04 | 74.67 | 73.89 | 75.75 | 74.30 | 77.47 |
| TiO2 | 0.10 | 0.57 | 0.35 | 0.41 | 0.34 | 0.33 | 0.35 | 0.59 | 0.34 | 0.36 | 0.30 | 0.40 | 0.22 |
| Al2O3 | 13.41 | 16.82 | 13.97 | 14.47 | 13.79 | 12.89 | 14.20 | 15.16 | 13.29 | 14.24 | 13.83 | 15.69 | 12.65 |
| Fe2O3+ | 1.34 | 2.03 | 2.54 | 2.64 | 0.99 | 2.15 | 2.08 | 2.85 | 2.29 | 2.53 | 1.69 | 2.41 | 1.30 |
| MnO | 0.02 | 0.02 | 0.03 | 0.03 | 0.01 | 0.06 | 0.04 | 0.04 | 0.08 | 0.04 | 0.02 | 0.03 | 0.01 |
| MgO | 0.05 | 0.11 | 0.23 | 0.21 | 0.07 | 0.23 | 0.21 | 0.28 | 0.30 | 0.24 | 0.09 | 0.14 | 0.06 |
| CaO | 0.88 | 1.40 | 1.44 | 1.43 | 1.55 | 1.54 | 1.28 | 2.03 | 1.46 | 1.48 | 1.13 | 0.98 | 0.74 |
| Na2O | 3.81 | 3.85 | 4.67 | 4.46 | 4.81 | 4.18 | 4.41 | 4.59 | 4.76 | 4.65 | 4.58 | 3.78 | 4.55 |
| K2O | 3.88 | 2.46 | 2.57 | 2.40 | 2.66 | 2.50 | 2.76 | 2.29 | 2.75 | 2.52 | 2.59 | 2.26 | 2.98 |
| P2O5 | 0.02 | 0.08 | 0.02 | 0.03 | 0.06 | 0.06 | 0.06 | 0.13 | 0.05 | 0.05 | 0.02 | 0.01 | 0.02 |
| LOI* | 0.72 | 2.62 | 0.83 | 1.14 | 0.18 | 0.82 | 1.04 | 1.02 | 2.96 | 0.83 | 0.65 | 2.36 | 0.42 |
| Total* | 100.40 | 100.29 | 100.35 | 100.23 | 100.18 | 100.18 | 100.34 | 100.43 | 100.15 | 100.28 | 100.09 | 100.27 | 100.30 |
| ppm | | | | | | | | | | | | | |
| Ba | 835 | 641 | 673 | 648 | 664 | 640 | 759 | 611 | 665 | 648 | 656 | 724 | 724 |
| Rb | 131 | 74 | 69 | 76 | 69 | 76 | 85 | 68 | 80 | 77 | 77 | 63 | 88 |
| Sr | 77 | 131 | 121 | 121 | 129 | 126 | 128 | 150 | 101 | 124 | 94 | 86 | 57 |
| Y | 26 | 32 | 34 | 34 | 39 | 40 | 30 | 47 | 46 | 41 | 40 | 28 | 44 |
| Zr | 138 | 270 | 259 | 266 | 265 | 237 | 262 | 247 | 270 | 266 | 250 | 289 | 220 |
| Nb | 8 | 9 | 8 | 9 | 9 | 7 | 9 | 8 | 8 | 8 | 9 | 10 | 9 |
| Th | 13 | 8 | 8 | 8 | 10 | 6 | 8 | 6 | 8 | 7 | 8 | 9 | 10 |
| Pb | 19 | 12 | 2 | 1 | 18 | 6 | 2 | 1 | 13 | 4 | 17 | 4 | 17 |
| Ga | 15 | 17 | 15 | 16 | 14 | 14 | 14 | 16 | 15 | 15 | 15 | 16 | 13 |
| Zn | 33 | 60 | 51 | 60 | 27 | 53 | 67 | 61 | 55 | 56 | 67 | 51 | 36 |
| Ni | 3 | 3 | 3 | 3 | 3 | 3 | 3 | 3 | 3 | 3 | 3 | 3 | 3 |
| V | 3 | 21 | 11 | 9 | 7 | 9 | 9 | 20 | 9 | 6 | 8 | 3 | 4 |
| Cr | 5 | 3 | 3 | 3 | 6 | 9 | 4 | 3 | 5 | 4 | 9 | 3 | 3 |
| La | 24 | 25 | 15 | 24 | 17 | 17 | 17 | 27 | 23 | 23 | 21 | 11 | 21 |
| Ce | 53 | 41 | 59 | 38 | 58 | 54 | 44 | 44 | 61 | 57 | 63 | 32 | 56 |
| Nd | 23 | 19 | 31 | 26 | 24 | 30 | 14 | 42 | 34 | 19 | 23 | 15 | 27 |
| K/Rb | 246 | 276 | 309 | 262 | 320 | 273 | 269 | 280 | 285 | 272 | 280 | 297 | 281 |
| Rb/Sr | 1.70 | 0.56 | 0.57 | 0.63 | 0.53 | 0.60 | 0.66 | 0.45 | 0.79 | 0.62 | 0.82 | 0.73 | 1.54 |

Table VI.2 Continued.

| Sample | W99993 | W99993 | W99995 | W99876 | W99894 | W99905 | W99902 | W99912 | W99600 | W99725 | W99807 | W99834 | W99835 | W991005 | W99788 | W99976 |
|---|---|---|---|---|---|---|---|---|---|---|---|---|---|---|---|---|
| Unit | Camp | Camp | Pinnacles | Kauaeranga | Kapowai | Kapowai | Precipice | Precipice | Rangihau | Acadia | Welcome Jack | Welcome Jack | Welcome Jack | Ruahine | Slip | Miller Flat |
| group | I | I | I | I | I | I | I | I | III | III | II | II | II | II | IV | IV |
| wt.% | | | | | | | | | | | | | | | | |
| SiO2 | 74.04 | 73.01 | 74.02 | 72.86 | 75.68 | 72.41 | 71.04 | 71.14 | 75.41 | 74.64 | 78.88 | 78.13 | 77.43 | 75.75 | 72.93 | 75.02 |
| TiO2 | 0.38 | 0.40 | 0.48 | 0.46 | 0.26 | 0.46 | 0.47 | 0.46 | 0.36 | 0.41 | 0.20 | 0.21 | 0.20 | 0.22 | 0.45 | 0.28 |
| Al2O3 | 14.62 | 14.80 | 13.98 | 14.25 | 13.36 | 14.94 | 14.81 | 14.53 | 13.89 | 13.45 | 11.79 | 12.23 | 12.60 | 13.62 | 15.17 | 13.39 |
| Fe2O3+ | 2.66 | 2.44 | 2.99 | 2.86 | 2.00 | 2.15 | 3.17 | 3.77 | 1.31 | 3.11 | 1.20 | 1.90 | 1.73 | 1.91 | 1.79 | 2.31 |
| MnO | 0.06 | 0.08 | 0.03 | 0.05 | 0.03 | 0.03 | 0.08 | 0.05 | 0.02 | 0.03 | 0.01 | 0.01 | 0.02 | 0.02 | 0.02 | 0.02 |
| MgO | 0.18 | 0.37 | 0.11 | 0.30 | 0.19 | 0.42 | 0.72 | 0.51 | 0.06 | 0.37 | 0.15 | 0.17 | 0.16 | 0.11 | 0.23 | 0.12 |
| CaO | 1.08 | 1.64 | 1.35 | 1.89 | 1.18 | 2.25 | 2.65 | 2.42 | 1.42 | 1.29 | 0.83 | 0.70 | 0.81 | 1.38 | 2.49 | 1.35 |
| Na2O | 4.46 | 4.75 | 4.50 | 4.85 | 4.30 | 4.71 | 3.96 | 4.53 | 4.83 | 4.27 | 3.16 | 2.88 | 3.33 | 3.32 | 3.76 | 4.47 |
| K2O | 2.48 | 2.47 | 2.51 | 2.39 | 2.98 | 2.52 | 2.98 | 2.48 | 2.66 | 2.40 | 3.75 | 3.76 | 3.71 | 3.63 | 3.06 | 3.01 |
| P2O5 | 0.04 | 0.05 | 0.04 | 0.09 | 0.03 | 0.10 | 0.10 | 0.11 | 0.04 | 0.02 | 0.03 | 0.02 | 0.02 | 0.03 | 0.09 | 0.03 |
| LOI* | 1.26 | 2.56 | 0.92 | 0.64 | 0.68 | 0.50 | 4.33 | 0.41 | 0.43 | 1.26 | 0.83 | 1.11 | 0.90 | 0.78 | 0.53 | 0.46 |
| Total* | 100.21 | 100.26 | 100.29 | 100.35 | 100.17 | 100.31 | 100.20 | 100.17 | 100.30 | 100.31 | 100.32 | 100.23 | 100.22 | 100.08 | 100.17 | 100.16 |
| ppm | | | | | | | | | | | | | | | | |
| Ba | 630 | 709 | 652 | 630 | 708 | 647 | 641 | 629 | 674 | 680 | 791 | 743 | 774 | 814 | 735 | 722 |
| Rb | 73 | 72 | 70 | 70 | 93 | 79 | 127 | 79 | 77 | 48 | 126 | 128 | 125 | 128 | 102 | 93 |
| Sr | 83 | 121 | 109 | 153 | 90 | 167 | 172 | 170 | 111 | 111 | 60 | 51 | 56 | 100 | 149 | 105 |
| Y | 50 | 51 | 30 | 43 | 45 | 33 | 38 | 36 | 45 | 29 | 30 | 24 | 26 | 12 | 36 | 43 |
| Zr | 289 | 282 | 286 | 254 | 219 | 251 | 231 | 238 | 283 | 246 | 150 | 158 | 154 | 111 | 227 | 228 |
| Nb | 9 | 9 | 9 | 9 | 8 | 9 | 7 | 8 | 9 | 11 | 7 | 8 | 7 | 7 | 7 | 7 |
| Th | 9 | 9 | 8 | 6 | 9 | 7 | 7 | 8 | 8 | 8 | 15 | 15 | 13 | 15 | 10 | 8 |
| Pb | 10 | 12 | 1 | 1 | 15 | 16 | 3 | 1 | 11 | 1 | 15 | 17 | 20 | 14 | 8 | 5 |
| Ga | 15 | 16 | 16 | 16 | 14 | 16 | 14 | 15 | 16 | 17 | 12 | 13 | 12 | 12 | 16 | 14 |
| Zn | 63 | 68 | 58 | 64 | 48 | 47 | 52 | 52 | 33 | 67 | 28 | 25 | 27 | 32 | 58 | 48 |
| Ni | 3 | 3 | 3 | 3 | 3 | 3 | 3 | 3 | 3 | 3 | 3 | 3 | 3 | 3 | 4 | 3 |
| V | 10 | 11 | 13 | 10 | 7 | 19 | 18 | 17 | 10 | 9 | 9 | 10 | 11 | 18 | 54 | 10 |
| Cr | 26 | 3 | 3 | 18 | 3 | 3 | 14 | 11 | 3 | 3 | 8 | 8 | 8 | 3 | 12 | 6 |
| La | 34 | 30 | 19 | 21 | 31 | 24 | 20 | 24 | 21 | 17 | 22 | 20 | 28 | 24 | 24 | 26 |
| Ce | 67 | 62 | 46 | 55 | 66 | 43 | 48 | 48 | 62 | 45 | 53 | 45 | 53 | 36 | 53 | 47 |
| Nd | 32 | 34 | 21 | 30 | 44 | 32 | 29 | 26 | 35 | 27 | 14 | 12 | 29 | 17 | 36 | 28 |
| K/Rb | 282 | 284 | 297 | 283 | 266 | 265 | 195 | 260 | 286 | 415 | 247 | 244 | 246 | 235 | 249 | 269 |
| Rb/Sr | 0.88 | 0.60 | 0.64 | 0.46 | 1.03 | 0.47 | 0.74 | 0.46 | 0.69 | 0.43 | 2.10 | 2.51 | 2.23 | 1.28 | 0.68 | 0.89 |

Table VI.3 Whole rock major element (normalised to 100%, volatile free) and trace element XRF analyses of lava lithic fragments sampled from Kapowai Caldera Complex ignimbrites. * original totals; + total Fe as $Fe_2O_3$.

| Sample | W99615LB | W99694LA | W99772LF | W99780LE | W99849LC | W99859LC | W99874LC | W99950LE | W99972LC | W99975LC |
|---|---|---|---|---|---|---|---|---|---|---|
| Lithology | rhyolite lava | rhyolite lava | rhyolite lava | rhyolite lava | rhyolite lava | rhyolite lava | andesite lava | andesite lava | rhyolite lava | andesite lava |
| wt.% | | | | | | | | | | |
| SiO2 | 75.02 | 75.75 | 77.23 | 73.51 | 70.54 | 74.17 | 64.17 | 61.96 | 75.20 | 61.39 |
| TiO2 | 0.31 | 0.32 | 0.26 | 0.44 | 0.64 | 0.38 | 0.57 | 1.03 | 0.31 | 1.03 |
| Al2O3 | 13.47 | 12.94 | 12.32 | 13.64 | 14.83 | 13.52 | 17.82 | 16.61 | 13.37 | 17.47 |
| Fe2O3+ | 2.00 | 2.03 | 1.81 | 2.78 | 3.51 | 2.33 | 5.36 | 6.80 | 2.05 | 6.61 |
| MnO | 0.04 | 0.05 | 0.03 | 0.06 | 0.06 | 0.09 | 0.06 | 0.13 | 0.04 | 0.11 |
| MgO | 0.24 | 0.25 | 0.12 | 0.46 | 0.57 | 0.36 | 1.74 | 2.24 | 0.28 | 2.01 |
| CaO | 1.52 | 1.78 | 1.29 | 2.59 | 2.75 | 1.56 | 5.38 | 5.59 | 1.56 | 5.88 |
| Na2O | 4.65 | 4.42 | 4.30 | 4.16 | 4.87 | 4.75 | 3.44 | 3.50 | 4.57 | 3.41 |
| K2O | 2.73 | 2.42 | 2.61 | 2.26 | 2.12 | 2.78 | 1.35 | 1.85 | 2.58 | 1.68 |
| P2O5 | 0.03 | 0.06 | 0.04 | 0.10 | 0.11 | 0.06 | 0.12 | 0.29 | 0.04 | 0.41 |
| LOI* | 0.39 | 0.30 | 0.25 | 0.40 | 0.34 | 2.61 | 1.28 | 1.46 | 0.32 | 1.76 |
| Total* | 100.04 | 99.95 | 99.84 | 100.26 | 100.30 | 99.96 | 100.16 | 100.04 | 100.19 | 100.07 |
| ppm | | | | | | | | | | |
| Ba | 917 | 609 | 656 | 537 | 564 | 686 | 379 | 468 | 732 | 595 |
| Rb | 84 | 78 | 81 | 65 | 64 | 83 | 48 | 47 | 80 | 50 |
| Sr | 126 | 131 | 98 | 171 | 187 | 113 | 226 | 257 | 121 | 263 |
| Y | 34 | 38 | 25 | 32 | 32 | 46 | 22 | 31 | 84 | 56 |
| Zr | 246 | 226 | 231 | 198 | 228 | 276 | 100 | 158 | 253 | 156 |
| Nb | 10 | 9 | 9 | 7 | 9 | 10 | 5 | 7 | 7 | 6 |
| Th | 12 | 10 | 13 | 7 | 6 | 12 | 1 | 5 | 7 | 4 |
| Pb | 15 | 13 | 11 | 11 | 11 | 17 | 7 | 12 | 12 | 11 |
| Ga | 14 | 14 | 14 | 13 | 16 | 15 | 16 | 18 | 15 | 19 |
| Zn | 44 | 47 | 44 | 44 | 53 | 65 | 84 | 98 | 44 | 97 |
| Ni | 4 | 3 | 3 | 3 | 3 | 4 | 15 | 3 | 3 | 5 |
| V | 9 | 6 | 7 | 12 | 26 | 8 | 148 | 166 | 10 | 169 |
| Cr | 3 | 3 | 3 | 3 | 3 | 3 | 16 | 4 | 3 | 4 |
| La | 32 | 25 | 20 | 20 | 16 | 31 | 17 | 17 | 46 | 20 |
| Ce | 43 | 53 | 38 | 44 | 36 | 62 | 39 | 37 | 90 | 43 |
| Nd | 33 | 32 | 21 | 23 | 27 | 36 | 29 | 26 | 46 | 43 |
| K/Rb | 270 | 257 | 267 | 289 | 275 | 278 | 234 | 326 | 268 | 279 |
| Rb/Sr | 0.67 | 0.60 | 0.83 | 0.38 | 0.34 | 0.73 | 0.21 | 0.18 | 0.66 | 0.19 |

Table VI. 4 Whole rock and juvenile major element (normalised to 100%, volatile free) and trace element XRF analyses of Kapowai Caldera Complex ignimbrites. * original totals; + total Fe as $Fe_2O_3$. w-rock = whole rock

| Sample | W99886 | W99614 | W99614 | W99922 | W99633 | W99952 | W99850 | W99973 | W99950 | W99988 | W99989 | W99990 | W99986 | W99612 | W99612 | W99612 |
|---|---|---|---|---|---|---|---|---|---|---|---|---|---|---|---|---|
| Unit | WES-1 | WES-1 | WES-1 | WES-4 | WES-4 | WES-4 | WES-1 | WES-1 | WES-1 | Trig Q | Trig Q | Trig Q | CP-2 | Oteao | Oteao | Oteao |
| Analysis | pumice | pumice | pumice | w-rock | w-rock | w-rock | w-rock | w-rock | w-rock | w-rock | w-rock | w-rock | w-rock | scoria | scoria | scoria |
| wt.% | | | | | | | | | | | | | | | | |
| SiO2 | 72.75 | 65.41 | 65.88 | 75.39 | 72.73 | 68.15 | 72.50 | 71.59 | 71.83 | 73.32 | 75.36 | 68.22 | 69.52 | 58.11 | 58.03 | 57.26 |
| TiO2 | 0.38 | 1.01 | 1.02 | 0.34 | 0.55 | 0.63 | 0.53 | 0.49 | 0.47 | 0.64 | 0.63 | 0.76 | 0.82 | 1.04 | 1.03 | 1.11 |
| Al2O3 | 15.05 | 20.21 | 21.67 | 13.98 | 16.45 | 18.02 | 16.26 | 16.46 | 15.14 | 15.77 | 14.36 | 17.22 | 18.98 | 17.97 | 17.62 | 17.88 |
| Fe2O3+ | 2.88 | 6.36 | 6.57 | 2.20 | 3.90 | 4.92 | 3.70 | 3.60 | 3.81 | 3.93 | 3.92 | 4.69 | 5.07 | 7.92 | 8.07 | 8.29 |
| MnO | 0.69 | 0.10 | 0.15 | 0.07 | 0.05 | 0.09 | 0.05 | 0.06 | 0.07 | 0.06 | 0.06 | 0.07 | 0.05 | 0.11 | 0.18 | 0.12 |
| MgO | 0.76 | 0.99 | 0.89 | 0.21 | 0.42 | 1.49 | 0.33 | 0.77 | 0.91 | 0.94 | 0.87 | 0.87 | 0.77 | 3.68 | 3.87 | 3.69 |
| CaO | 1.76 | 2.46 | 1.70 | 1.35 | 1.38 | 2.17 | 1.61 | 1.91 | 2.26 | 1.79 | 1.65 | 2.64 | 1.66 | 7.18 | 7.10 | 7.30 |
| Na2O | 2.88 | 1.85 | 1.12 | 2.92 | 1.87 | 2.21 | 1.96 | 2.62 | 2.62 | 1.94 | 1.94 | 3.20 | 1.83 | 2.75 | 2.82 | 3.10 |
| K2O | 2.80 | 1.48 | 0.90 | 3.50 | 2.61 | 2.24 | 3.02 | 2.46 | 2.81 | 1.58 | 1.18 | 2.27 | 1.27 | 1.03 | 1.08 | 1.00 |
| P2O5 | 0.04 | 0.14 | 0.10 | 0.03 | 0.03 | 0.09 | 0.03 | 0.03 | 0.07 | 0.03 | 0.03 | 0.05 | 0.03 | 0.20 | 0.19 | 0.25 |
| LOI* | 5.21 | 7.75 | 9.48 | 4.78 | 6.75 | 6.28 | 6.21 | 6.51 | 5.77 | 6.02 | 6.09 | 4.27 | 6.89 | 3.46 | 2.61 | 1.77 |
| Total* | 99.88 | 100.25 | 99.83 | 100.08 | 100.09 | 100.22 | 100.23 | 100.32 | 99.97 | 100.43 | 100.13 | 100.32 | 100.02 | 100.41 | 100.26 | 100.38 |
| ppm | | | | | | | | | | | | | | | | |
| Ba | 1426 | 656 | 438 | 688 | 606 | 1830 | 674 | 1186 | 2106 | 1245 | 938 | 843 | 679 | 333 | 314 | 273 |
| Rb | 80 | 91 | 55 | 82 | 89 | 84 | 91 | 71 | 88 | 50 | 39 | 69 | 55 | 49 | 48 | 46 |
| Sr | 140 | 414 | 116 | 96 | 111 | 262 | 227 | 175 | 200 | 147 | 140 | 207 | 141 | 417 | 349 | 349 |
| Y | 94 | 18 | 38 | 45 | 38 | 32 | 48 | 35 | 46 | 22 | 19 | 27 | 18 | 18 | 21 | 20 |
| Zr | 244 | 228 | 171 | 272 | 218 | 186 | 235 | 248 | 225 | 227 | 165 | 229 | 239 | 107 | 111 | 103 |
| Nb | 5 | 4 | 6 | 8 | 7 | 6 | 7 | 8 | 7 | 8 | 7 | 8 | 10 | 5 | 5 | 5 |
| Th | 7 | 4 | 4 | 8 | 6 | 5 | 6 | 7 | 6 | 3 | 2 | 5 | 5 | 3 | 3 | 2 |
| Pb | 1 | 1 | 1 | 13 | 1 | 1 | 1 | 4 | 1 | 1 | 1 | 1 | 11 | 3 | 3 | 4 |
| Ga | 16 | 14 | 19 | 14 | 16 | 16 | 15 | 15 | 15 | 15 | 14 | 17 | 18 | 18 | 18 | 18 |
| Zn | 118 | 61 | 68 | 58 | 58 | 62 | 64 | 59 | 61 | 66 | 59 | 62 | 59 | 76 | 74 | 69 |
| Ni | 6 | 4 | 7 | 3 | 4 | 6 | 4 | 3 | 3 | 3 | 3 | 3 | 3 | 11 | 14 | 10 |
| V | 33 | 25 | 87 | 9 | 35 | 57 | 29 | 23 | 38 | 26 | 33 | 45 | 36 | 174 | 185 | 171 |
| Cr | 3 | 3 | 6 | 3 | 27 | 11 | 8 | 7 | 5 | 3 | 3 | 8 | 5 | 27 | 31 | 46 |
| La | 48 | 9 | 21 | 20 | 20 | 23 | 35 | 18 | 31 | 10 | 8 | 16 | 10 | 7 | 6 | 9 |
| Ce | 99 | 30 | 49 | 57 | 40 | 51 | 74 | 49 | 66 | 24 | 22 | 29 | 26 | 15 | 31 | 19 |
| Nd | 61 | 10 | 24 | 36 | 20 | 11 | 37 | 15 | 29 | 10 | 10 | 11 | 17 | 15 | 14 | 13 |
| K/Rb | 290 | 135 | 135 | 355 | 244 | 221 | 276 | 288 | 265 | 262 | 251 | 273 | 191 | 175 | 186 | 181 |
| Rb/Sr | 0.57 | 0.22 | 0.47 | 0.85 | 0.80 | 0.32 | 0.40 | 0.41 | 0.44 | 0.34 | 0.28 | 0.33 | 0.39 | 0.12 | 0.14 | 0.13 |

Table VI. 4 Continued.

| Sample | W99612 | W99612 | W99612 | W99612 | W99898 | W99693 |
|---|---|---|---|---|---|---|
| Unit | Oteao | Oteao | Oteao | Oteao | Manuka | Webb Creek |
| Analysis | scoria | scoria | mixed | pumice | w-rock | pumice |
| wt.% | | | | | | |
| SiO2 | 59.34 | 57.74 | 63.23 | 69.55 | 71.22 | 71.51 |
| TiO2 | 1.06 | 1.34 | 1.08 | 0.51 | 0.46 | 0.45 |
| Al2O3 | 17.09 | 17.09 | 16.80 | 16.03 | 14.85 | 15.27 |
| Fe2O3+ | 7.70 | 8.93 | 7.21 | 4.37 | 3.30 | 3.69 |
| MnO | 0.14 | 0.13 | 0.10 | 0.14 | 0.12 | 0.08 |
| MgO | 3.44 | 3.44 | 3.01 | 1.55 | 0.87 | 2.07 |
| CaO | 6.60 | 6.89 | 5.18 | 3.10 | 2.88 | 3.49 |
| Na2O | 3.15 | 3.00 | 1.91 | 2.19 | 3.42 | 1.60 |
| K2O | 1.23 | 1.15 | 1.31 | 2.49 | 2.81 | 1.74 |
| P2O5 | 0.25 | 0.29 | 0.16 | 0.08 | 0.07 | 0.09 |
| LOI* | 2.42 | 2.31 | 6.74 | 7.71 | 3.50 | 7.04 |
| Total* | 100.28 | 100.31 | 100.34 | 100.03 | 100.07 | 99.61 |
| | | | | | | |
| ppm | | | | | | |
| Ba | 358 | 348 | 438 | 609 | 894 | 409 |
| Rb | 51 | 52 | 70 | 91 | 96 | 58 |
| Sr | 333 | 395 | 557 | 497 | 254 | 146 |
| Y | 23 | 22 | 21 | 46 | 51 | 33 |
| Zr | 127 | 121 | 136 | 260 | 229 | 174 |
| Nb | 5 | 6 | 8 | 5 | 6 | 6 |
| Th | 4 | 3 | 3 | 9 | 6 | 4 |
| Pb | 6 | 5 | 13 | 1 | 1 | 1 |
| Ga | 17 | 18 | 15 | 14 | 15 | 19 |
| Zn | 77 | 75 | 101 | 41 | 79 | 63 |
| Ni | 10 | 9 | 9 | 10 | 5 | 6 |
| V | 177 | 171 | 135 | 48 | 32 | 108 |
| Cr | 31 | 37 | 15 | 6 | 6 | 8 |
| La | 10 | 10 | 12 | 28 | 24 | 19 |
| Ce | 25 | 25 | 30 | 70 | 55 | 49 |
| Nd | 17 | 13 | 28 | 37 | 38 | 22 |
| | | | | | | |
| K/Rb | 200 | 184 | 156 | 227 | 243 | 249 |
| Rb/Sr | 0.15 | 0.13 | 0.13 | 0.18 | 0.38 | 0.40 |

# Appendix VII

## ICP-MS REE and trace element data

Table VII.1 Whole rock trace element and REE analyses of group I rhyolite lavas of the Kapowai Caldera Complex determined by ICP-MS. values in ppm.* Eu/Eu* calculated using the geometric mean where $Eu/Eu^* = Eu_N/\bullet[(Sm_N).(Gd_N)]$ (Taylor and McLennan, 1985).

| Sample | W99737 | W991002 | W99622 | W99618 | W99783 | W99876 | W99995 | W99994 | W99865 | W99839 | W99905 | W99912 |
|---|---|---|---|---|---|---|---|---|---|---|---|---|
| Unit | Bulls Run | Kokonga | Waiwhatawhata | Wharepapa | Starvation | Kauaeranga | Pinnacles | Camp | Tauraunikau | Big Beetle | Kapowai | Precipice |
| Sc | 10 | 11 | 14 | 4 | 9 | 11 | 11 | 12 | 10 | 14 | 12 | 5 |
| Ti | 2011 | 2342 | 3346 | 786 | 1856 | 2657 | 3041 | 2556 | 1517 | 3277 | 2374 | 1252 |
| V | 4 | 5 | 18 | 2 | 4 | 6 | 12 | 8 | 1 | 16 | 14 | 8 |
| Cr | 1 | 1 | 1 | 3 | 1 | 1 | 1 | 1 | 2 | 1 | 2 | 1 |
| Mn | 77 | 307 | 136 | 109 | 136 | 316 | 190 | 563 | 81 | 298 | 232 | 160 |
| Co | 25 | 11 | 10 | 19 | 6 | 24 | 8 | 11 | 18 | 10 | 15 | 4 |
| Ni | 0 | 1 | 0 | 0 | N/D | 0 | N/D | 0 | N/D | 1 | 1 | 1 |
| Cu | 2 | 2 | 4 | 2 | 2 | 1 | 3 | 3 | 1 | 3 | 4 | 2 |
| Zn | 29 | 65 | 67 | 31 | 70 | 53 | 55 | 64 | 37 | 58 | 52 | 22 |
| Rb | 86 | 91 | 86 | 150 | 88 | 72 | 82 | 88 | 106 | 76 | 90 | 40 |
| Sr | 132 | 124 | 129 | 78 | 77 | 135 | 110 | 126 | 58 | 143 | 167 | 74 |
| Y | 38 | 40 | 31 | 25 | 34 | 36 | 29 | 51 | 42 | 44 | 33 | 15 |
| Zr | 247 | 256 | 263 | 123 | 172 | 217 | 286 | 270 | 178 | 231 | 218 | 82 |
| Nb | 8 | 8 | 8 | 7 | 10 | 9 | 12 | 9 | 8 | 7 | 7 | 4 |
| Mo | 2 | 1 | 1 | 2 | 1 | 1 | 2 | 1 | 5 | 1 | 0 | 1 |
| Sn | 3 | 2 | 3 | 4 | 2 | 3 | 3 | 3 | 3 | 2 | 1 | 1 |
| Ce | 1 | 4 | 1 | 4 | 3 | 2 | 2 | 4 | 3 | 2 | 1 | 1 |
| Ba | 698 | 666 | 663 | 814 | 583 | 606 | 683 | 749 | 747 | 579 | 647 | 269 |
| La | 24 | 26 | 26 | 28 | 23 | 23 | 23 | 30 | 26 | 26 | 23 | 10 |
| Ce | 53 | 53 | 38 | 58 | 51 | 43 | 45 | 61 | 57 | 45 | 45 | 23 |
| Pr | 6 | 7 | 6 | 7 | 6 | 6 | 6 | 9 | 7 | 8 | 6 | 3 |
| Nd | 25 | 28 | 23 | 23 | 24 | 26 | 23 | 34 | 27 | 32 | 22 | 11 |
| Sm | 5 | 6 | 5 | 4 | 5 | 6 | 5 | 8 | 6 | 7 | 5 | 2 |
| Eu | 1 | 1 | 2 | 1 | 1 | 2 | 1 | 2 | 1 | 2 | 1 | 1 |
| Gd | 6 | 6 | 5 | 4 | 5 | 6 | 5 | 8 | 6 | 7 | 5 | 2 |
| Tb | 1 | 1 | 1 | 1 | 1 | 1 | 1 | 1 | 1 | 1 | 1 | 0 |
| Dy | 6 | 6 | 5 | 4 | 5 | 6 | 5 | 8 | 6 | 7 | 5 | 2 |
| Ho | 1 | 1 | 1 | 1 | 1 | 1 | 1 | 2 | 1 | 1 | 1 | 1 |
| Er | 4 | 4 | 3 | 2 | 3 | 3 | 3 | 5 | 4 | 4 | 3 | 1 |
| Tm | 1 | 1 | 0 | 0 | 1 | 1 | 0 | 1 | 1 | 1 | 0 | 0 |
| Yb | 4 | 4 | 3 | 2 | 3 | 3 | 3 | 5 | 4 | 4 | 3 | 1 |
| Lu | 1 | 1 | 0 | 0 | 1 | 1 | 0 | 1 | 1 | 1 | 1 | 0 |
| Hf | 6 | 7 | 7 | 4 | 5 | 6 | 7 | 7 | 6 | 6 | 6 | 2 |
| Ta | 1 | 1 | 1 | 1 | 1 | 1 | 1 | 1 | 1 | 1 | 1 | 0 |
| Pb | 18 | 19 | 17 | 21 | 17 | 14 | 15 | 20 | 16 | 13 | 18 | 7 |
| Th | 7 | 7 | 7 | 12 | 6 | 6 | 7 | 7 | 8 | 6 | 8 | 3 |
| U | 2 | 2 | 2 | 2 | 2 | 1 | 2 | 2 | 2 | 2 | 2 | 1 |
| $La_N/Yb_N$ | 4.26 | 4.46 | 5.52 | 8.24 | 4.70 | 4.42 | 4.96 | 4.16 | 4.27 | 4.08 | 4.81 | 4.81 |
| Eu/Eu* | 0.80 | 0.74 | 0.92 | 0.66 | 0.71 | 0.83 | 0.91 | 0.68 | 0.59 | 0.70 | 0.93 | 0.76 |

Table VII.2 Whole rock trace element and REE analyses of group II-IV rhyolite lavas of the Kapowai Caldera Complex determined by ICP-MS. values in ppm. Eu/Eu* calculated using the geometric mean where $Eu/Eu^* = Eu_N / \bullet[(Sm_N).(Gd_N)]$ (Taylor and McLennan, 1985).

| Sample | W99834 | W991005 | W99725 | W99600 | W99788 |
|---|---|---|---|---|---|
| Unit | Welcome Jack | Ruahine | Acadia | Rangihau | Slip |
| group | II | II | III | III | IV |
| Sc | 4 | 4 | 8 | 11 | 11 |
| Ti | 1434 | 1442 | 1856 | 2369 | 2494 |
| V | 6 | 15 | 5 | 6 | 39 |
| Cr | 4 | 3 | 2 | 2 | 11 |
| Mn | 53 | 117 | 186 | 146 | 148 |
| Co | 10 | 20 | 7 | 32 | 10 |
| Ni | 0 | 1 | 0 | 1 | 2 |
| Cu | 3 | 2 | 3 | 2 | 7 |
| Zn | 23 | 30 | 61 | 39 | 57 |
| Rb | 144 | 150 | 39 | 92 | 120 |
| Sr | 51 | 104 | 84 | 110 | 154 |
| Y | 22 | 10 | 21 | 43 | 34 |
| Zr | 81 | 88 | 158 | 263 | 177 |
| Nb | 6 | 6 | 7 | 8 | 6 |
| Mo | 2 | 1 | 2 | 1 | 2 |
| Sn | 4 | 2 | 3 | 3 | 2 |
| Ce | 5 | 5 | 1 | 1 | 3 |
| Ba | 762 | 835 | 538 | 674 | 776 |
| La | 24 | 24 | 17 | 27 | 28 |
| Ce | 39 | 38 | 28 | 58 | 58 |
| Pr | 6 | 4 | 5 | 7 | 7 |
| Nd | 20 | 14 | 18 | 28 | 27 |
| Sm | 4 | 2 | 4 | 6 | 6 |
| Eu | 1 | 1 | 1 | 2 | 1 |
| Gd | 4 | 2 | 4 | 6 | 6 |
| Tb | 1 | 0 | 1 | 1 | 1 |
| Dy | 3 | 2 | 4 | 6 | 5 |
| Ho | 1 | 0 | 1 | 1 | 1 |
| Er | 2 | 1 | 2 | 4 | 3 |
| Tm | 0 | 0 | 0 | 1 | 0 |
| Yb | 2 | 1 | 2 | 4 | 3 |
| Lu | 0 | 0 | 0 | 1 | 0 |
| Hf | 3 | 3 | 4 | 6 | 5 |
| Ta | 0 | 1 | 0 | 1 | 1 |
| Pb | 17 | 17 | 11 | 16 | 18 |
| Th | 11 | 12 | 5 | 7 | 9 |
| U | 3 | 3 | 1 | 2 | 2 |
| $La_N/Yb_N$ | 6.87 | 15.03 | 5.19 | 4.36 | 6.21 |
| Eu/Eu* | 0.58 | 0.95 | 0.88 | 0.72 | 0.72 |

Table VII.3 Trace element and REE analyses of andesite lavas and ignimbrites of the Kapowai Caldera Complex determined by ICP-MS. values in ppm. Eu/Eu* calculated using the geometric mean where $Eu/Eu^* = Eu_N / \bullet[(Sm_N).(Gd_N)]$ (Taylor and McLennan, 1985).

| Sample | W99951 | W99601 | W99877 | W99706 | W99922 | W99886 | W99612 | W99612 | W99612 |
|---|---|---|---|---|---|---|---|---|---|
| Analysis | whole rock | whole rock | whole rock | whole rock | pumice | pumice | scoria | pumice | mixed scoria |
| Unit | Tapuaetahi Andesite | Taurahuehue Andesite | Taurahuehue Andesite | Taurauikau Andesite | WES-4 Ignimbrite | WES-1 Ignimbrite | Oteao Ignimbrite | Oteao Ignimbrite | Oteao Ignimbrite |
| Sc | 17 | 28 | 20 | 27 | 10 | 14 | 29 | 17 | 22 |
| Ti | 3473 | 6378 | 4484 | 4138 | 2151 | 2393 | 6983 | 3104 | 5995 |
| V | 122 | 232 | 149 | 175 | 5 | 30 | 191 | 42 | 127 |
| Cr | 53 | 29 | 71 | 147 | 1 | 2 | 37 | 5 | 23 |
| Mn | 410 | 1784 | 661 | 831 | 483 | 4960 | 924 | 1005 | 645 |
| Co | 26 | 30 | 27 | 30 | 34 | 33 | 26 | 22 | 46 |
| Ni | 26 | 9 | 30 | 39 | 0 | 4 | 13 | 10 | 10 |
| Cu | 20 | 19 | 27 | 32 | 8 | 7 | 21 | 30 | 30 |
| Zn | 53 | 88 | 63 | 60 | 54 | 110 | 67 | 46 | 88 |
| Rb | 77 | 49 | 61 | 49 | 98 | 94 | 42 | 102 | 79 |
| Sr | 220 | 330 | 240 | 304 | 98 | 141 | 330 | 501 | 562 |
| Y | 22 | 27 | 25 | 22 | 43 | 94 | 20 | 45 | 21 |
| Zr | 94 | 138 | 156 | 132 | 227 | 220 | 94 | 210 | 130 |
| Nb | 7 | 9 | 8 | 6 | 9 | 7 | 6 | 8 | 8 |
| Mo | 1 | 2 | 3 | 3 | 2 | 3 | 1 | 2 | 2 |
| Sn | 2 | 2 | 2 | 2 | 4 | 3 | 7 | 4 | 2 |
| Ce | 3 | 2 | 2 | 2 | 5 | 4 | 2 | 3 | 3 |
| Ba | 442 | 329 | 405 | 393 | 693 | 1416 | 264 | 582 | 435 |
| La | 15 | 15 | 15 | 15 | 24 | 55 | 11 | 31 | 12 |
| Ce | 32 | 35 | 35 | 31 | 54 | 109 | 23 | 64 | 20 |
| Pr | 4 | 4 | 4 | 4 | 7 | 16 | 3 | 9 | 3 |
| Nd | 15 | 18 | 17 | 16 | 26 | 64 | 13 | 38 | 14 |
| Sm | 3 | 4 | 4 | 3 | 6 | 15 | 3 | 8 | 3 |
| Eu | 1 | 1 | 1 | 1 | 1 | 3 | 1 | 2 | 1 |
| Gd | 3 | 4 | 4 | 4 | 6 | 16 | 4 | 8 | 4 |
| Tb | 1 | 1 | 1 | 1 | 1 | 3 | 1 | 1 | 1 |
| Dy | 3 | 4 | 4 | 3 | 6 | 15 | 3 | 7 | 3 |
| Ho | 1 | 1 | 1 | 1 | 1 | 3 | 1 | 2 | 1 |
| Er | 2 | 2 | 2 | 2 | 4 | 8 | 2 | 4 | 2 |
| Tm | 0 | 0 | 0 | 0 | 1 | 1 | 0 | 1 | 0 |
| Yb | 2 | 3 | 2 | 2 | 4 | 8 | 2 | 4 | 2 |
| Lu | 0 | 0 | 0 | 0 | 1 | 1 | 0 | 1 | 0 |
| Hf | 3 | 4 | 4 | 4 | 6 | 6 | 3 | 6 | 4 |
| Ta | 1 | 1 | 1 | 1 | 1 | 1 | 1 | 1 | 1 |
| Pb | 10 | 9 | 11 | 8 | 20 | 21 | 7 | 8 | 17 |
| Th | 6 | 4 | 5 | 5 | 7 | 7 | 2 | 7 | 4 |
| U | 2 | 1 | 1 | 1 | 2 | 2 | 1 | 2 | 1 |
| $La_N/Yb_N$ | 4.96 | 4.04 | 4.47 | 4.98 | 3.88 | 4.59 | 4.21 | 5.17 | 3.75 |
| Eu/Eu* | 0.85 | 0.88 | 0.77 | 0.84 | 0.67 | 0.67 | 1.00 | 0.78 | 0.96 |

# Appendix VIII

## XRD traces

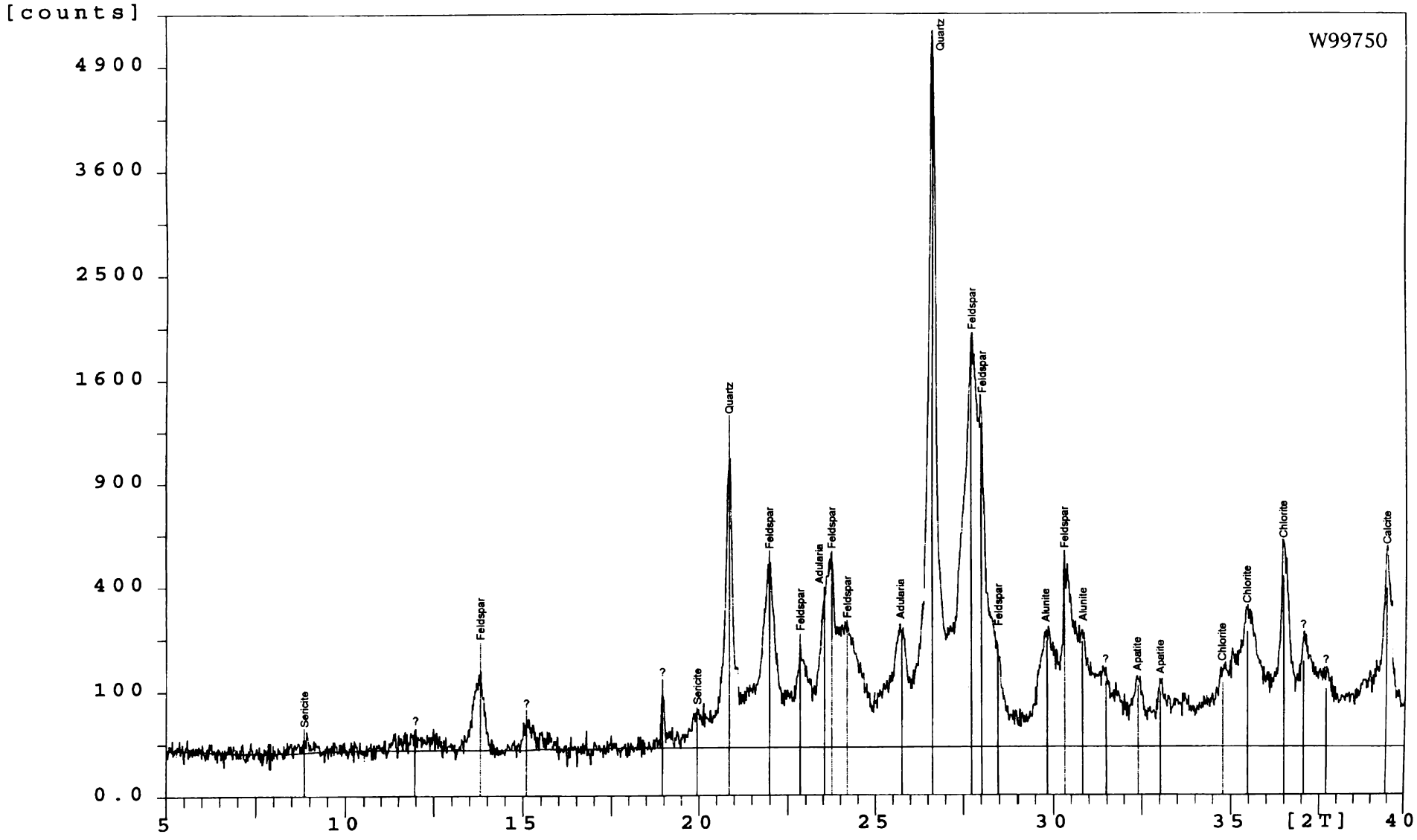
[counts]
4900
3600
2500
1600
900
400
100
0.0
W99750
Quartz
Feldspar
Feldspar
Feldspar
Quartz
Feldspar
Feldspar
Adularia
Feldspar
Feldspar
Adularia
Alunite
Feldspar
Alunite
Apatite
Apatite
Chlorite
Chlorite
Chlorite
Calcite
Sericite
Sericite
?
?
?
?
?
5
10
15
20
25
30
35
[2T]
40

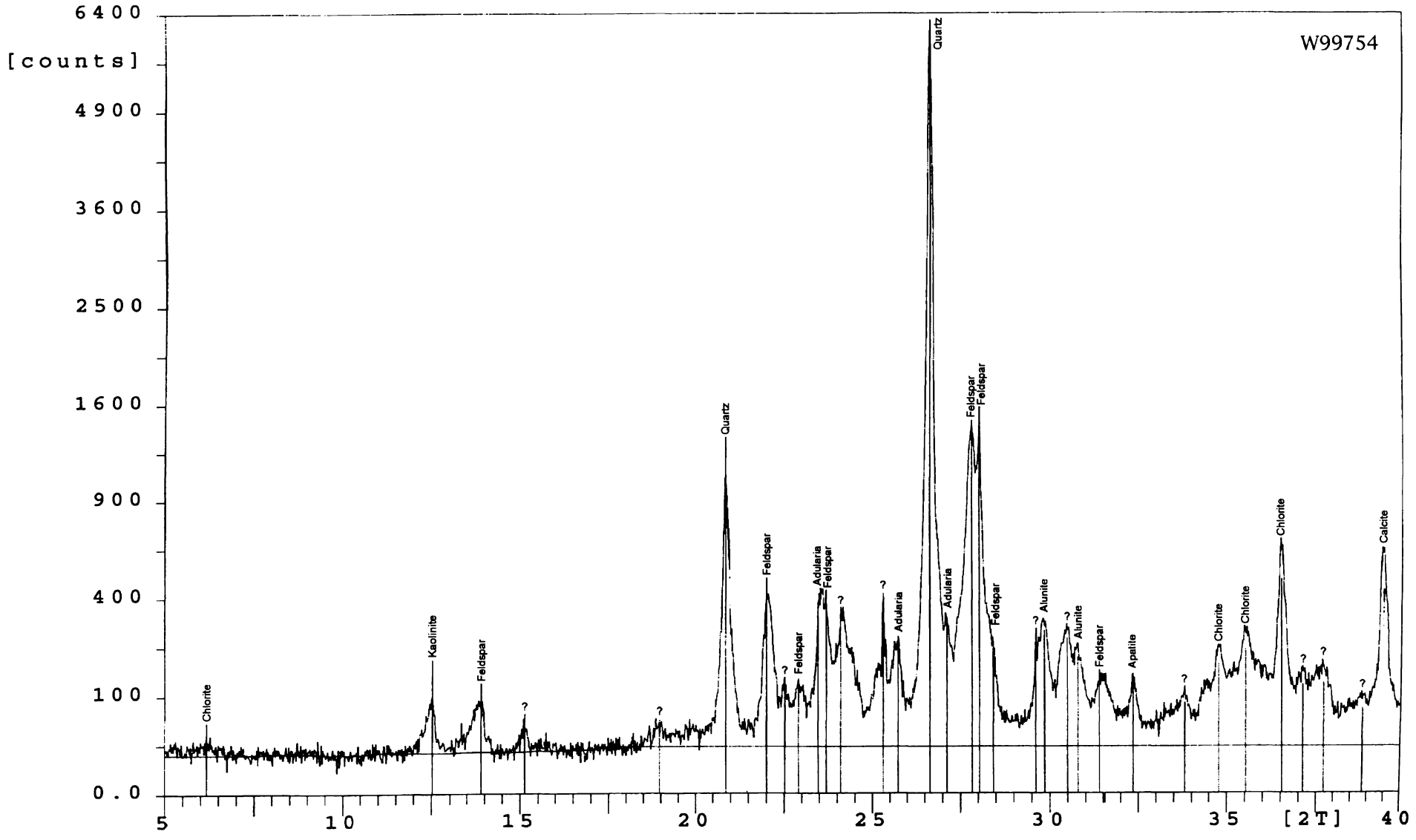
W99754
6400
[counts]
4900
3600
2500
1600
900
400
100
0.0
5
10
15
20
25
30
35
[2T]
40
Chlorite
Kaolinite
Feldspar
Quartz
Feldspar
Adularia
Feldspar
Adularia
Quartz
Adularia
Feldspar
Feldspar
Alunite
Alunite
Feldspar
Apatite
Chlorite
Chlorite
Chlorite
Calcite

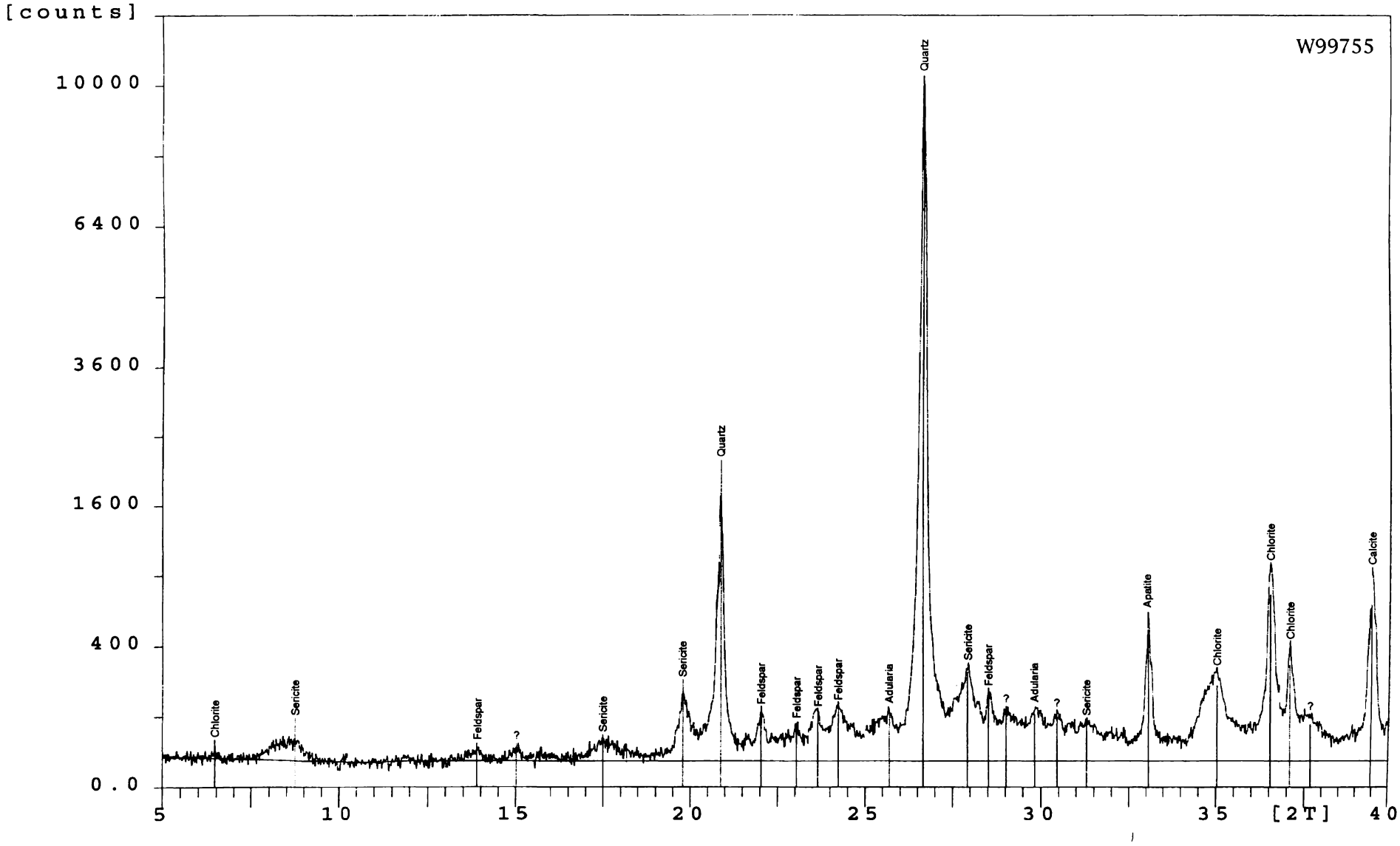
[counts]
W99755
10000
6400
3600
1600
400
0.0
5
10
15
20
25
30
35
[2T]
40
Chlorite
Sericite
Feldspar
?
Sericite
Sericite
Quartz
Feldspar
Feldspar
Feldspar
Feldspar
Adularia
Quartz
Sericite
Feldspar
?
Adularia
?
Sericite
Apatite
Chlorite
Chlorite
Chlorite
?
Calcite

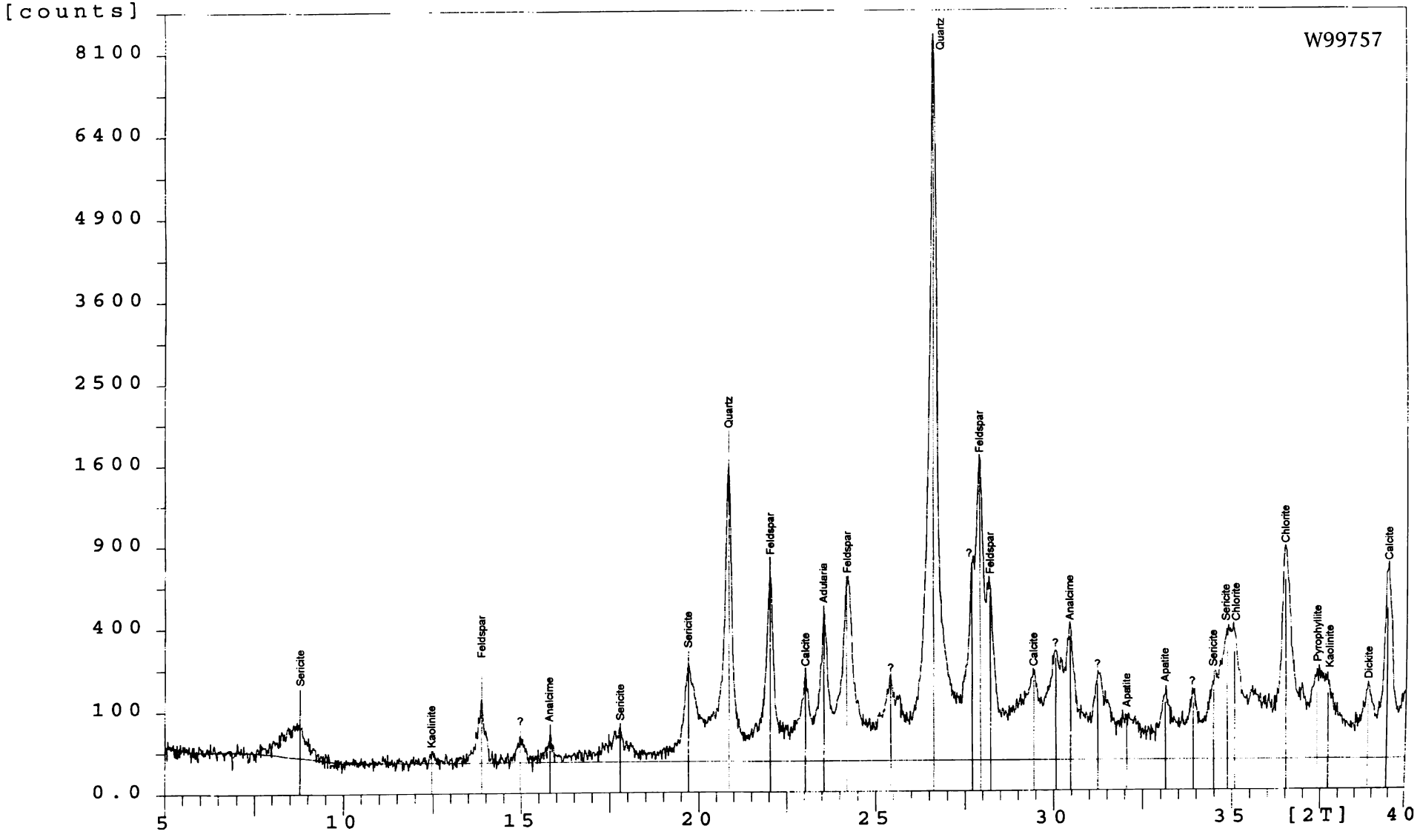
[counts]
8100
6400
4900
3600
2500
1600
900
400
100
0.0
W99757
Quartz
Sericite
Kaolinite
Feldspar
?
Analcime
Sericite
Sericite
Quartz
Feldspar
Calcite
Adularia
Feldspar
?
Quartz
?
Feldspar
Feldspar
Calcite
?
Analcime
?
Apatite
Apatite
?
Sericite
Sericite
Chlorite
Chlorite
Pyrophyllite
Kaolinite
Dickite
Calcite
5
10
15
20
25
30
35
[2T]
40

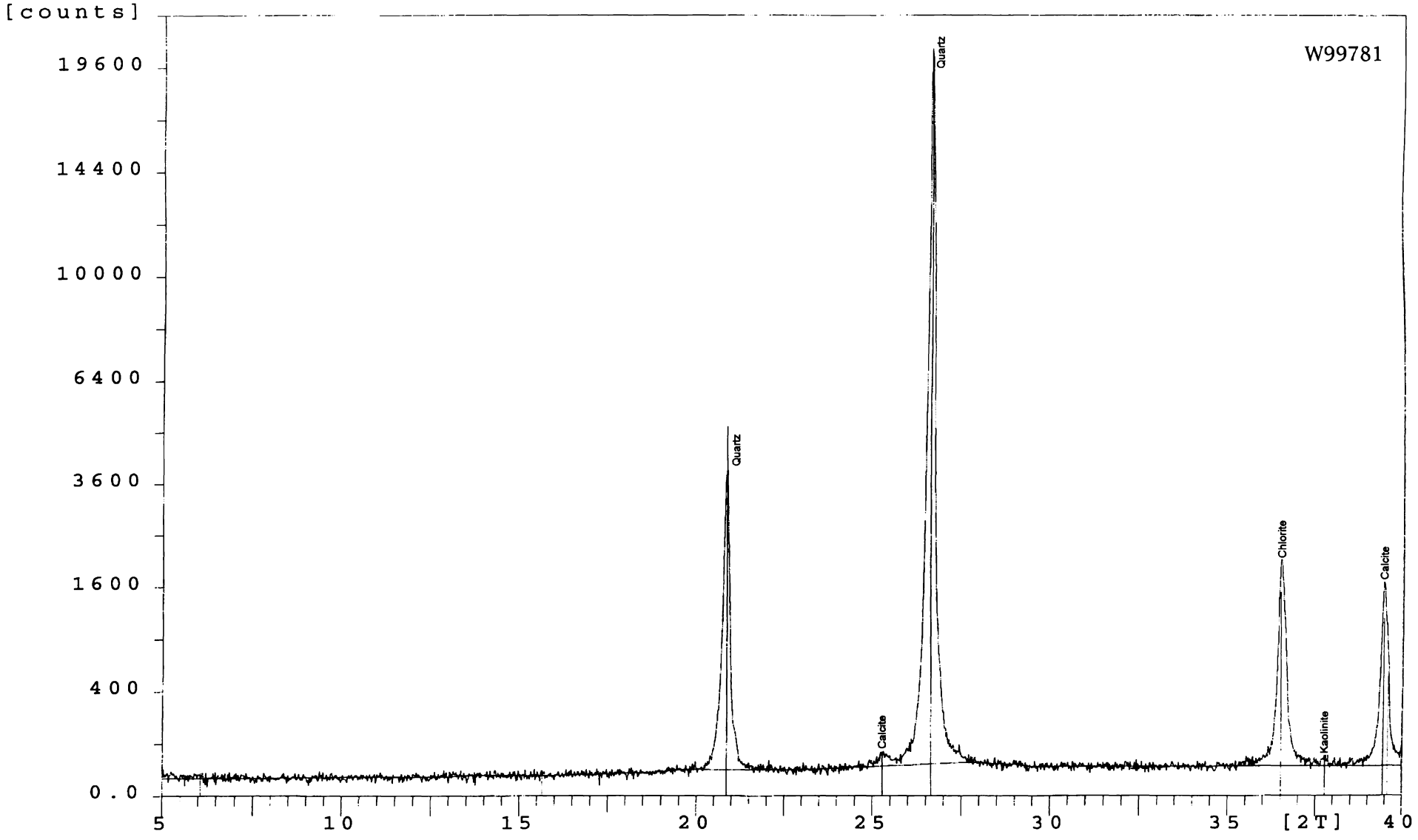
[counts]
19600
14400
10000
6400
3600
1600
400
0.0
W99781
Quartz
Quartz
Calcite
Chlorite
Kaolinite
Calcite
5
10
15
20
25
30
35
[2T]
40

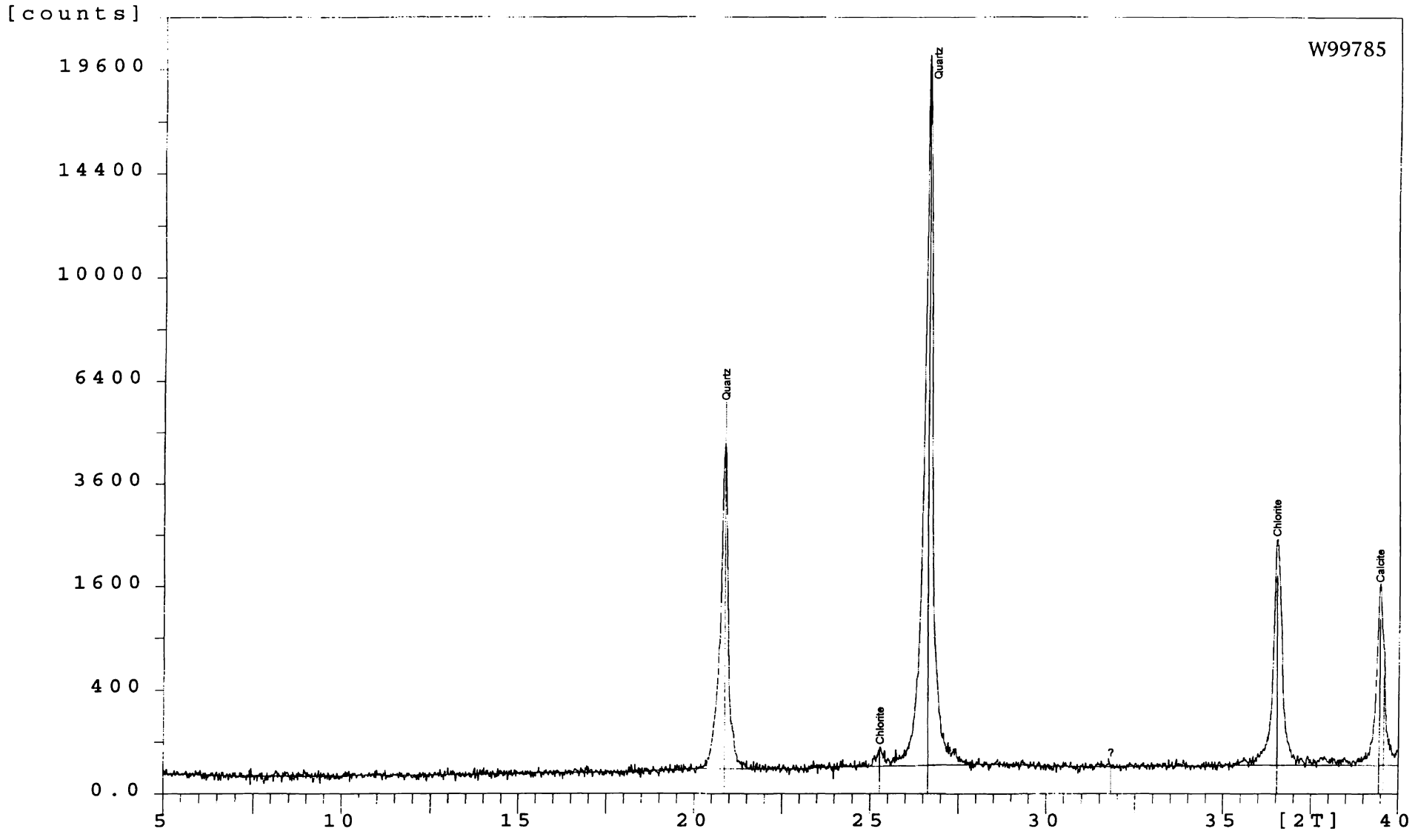
[counts]
19600
14400
10000
6400
3600
1600
400
0.0
W99785
Quartz
Quartz
Chlorite
?
Chlorite
Calcite
5
10
15
20
25
30
35
[2T]
40

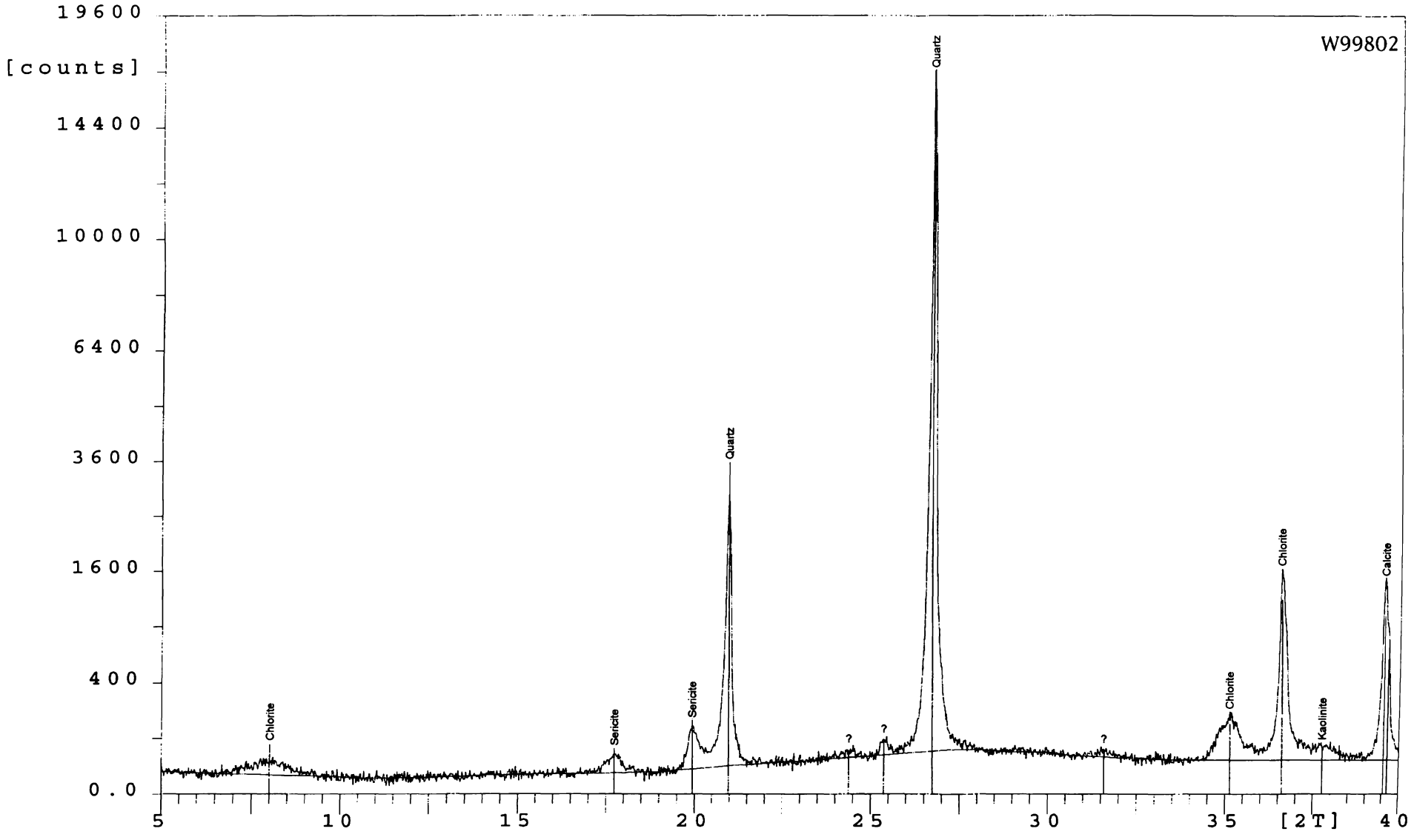
W99802
19600
[counts]
14400
10000
6400
3600
1600
400
0.0
5
10
15
20
25
30
35
[2T]
40
Chlorite
Sericite
Sericite
Quartz
?
?
Quartz
?
Chlorite
Chlorite
Kaolinite
Calcite

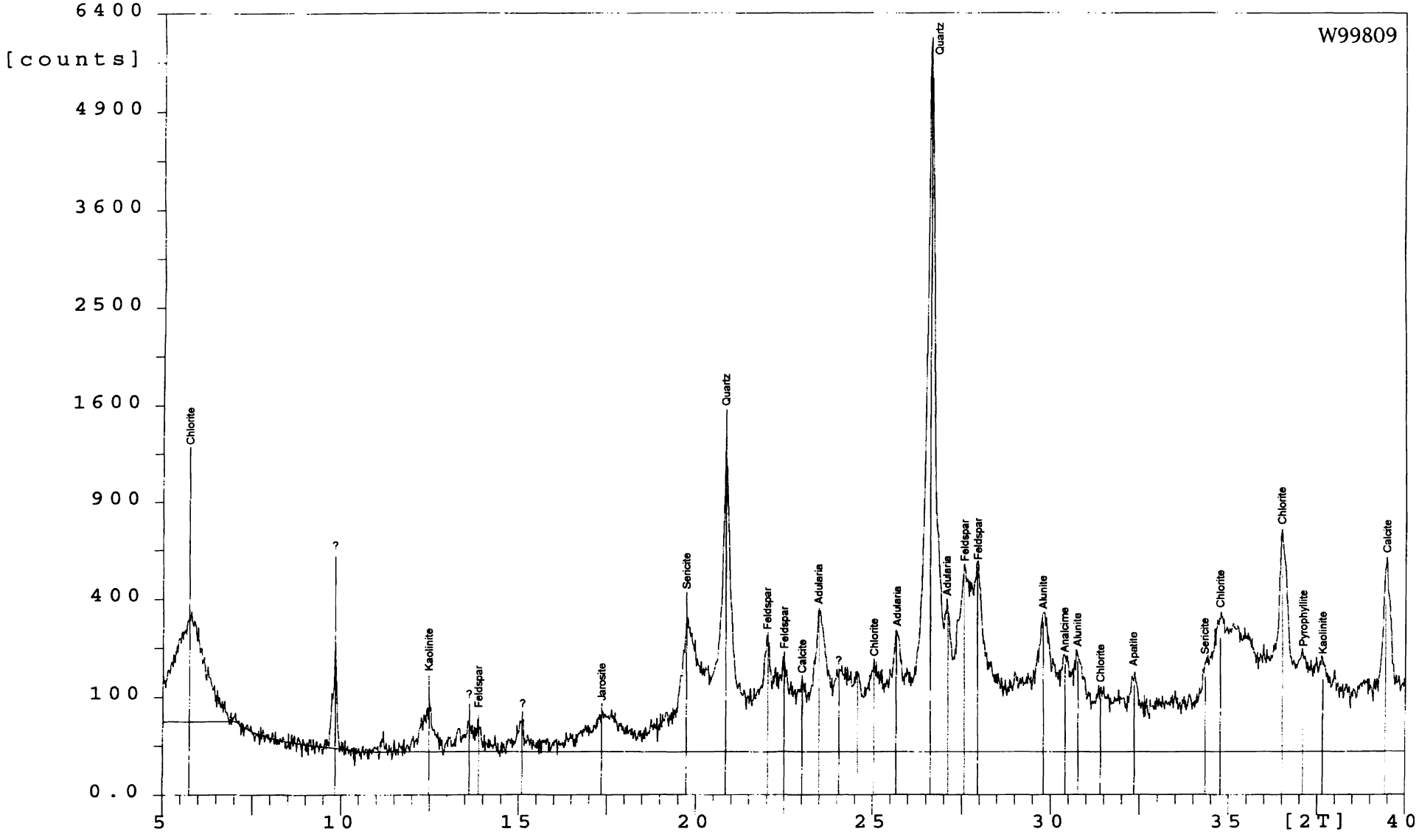
W99809
[counts]
6400
4900
3600
2500
1600
900
400
100
0.0
5
10
15
20
25
30
35
40
[2T]
Chlorite
?
Kaolinite
?
Feldspar
?
Jarosite
Sericite
Quartz
Feldspar
Feldspar
Calcite
Adularia
?
Chlorite
Adularia
Quartz
Adularia
Feldspar
Feldspar
Alunite
Analcime
Alunite
Chlorite
Apatite
Sericite
Chlorite
Chlorite
Pyrophyllite
Kaolinite
Calcite

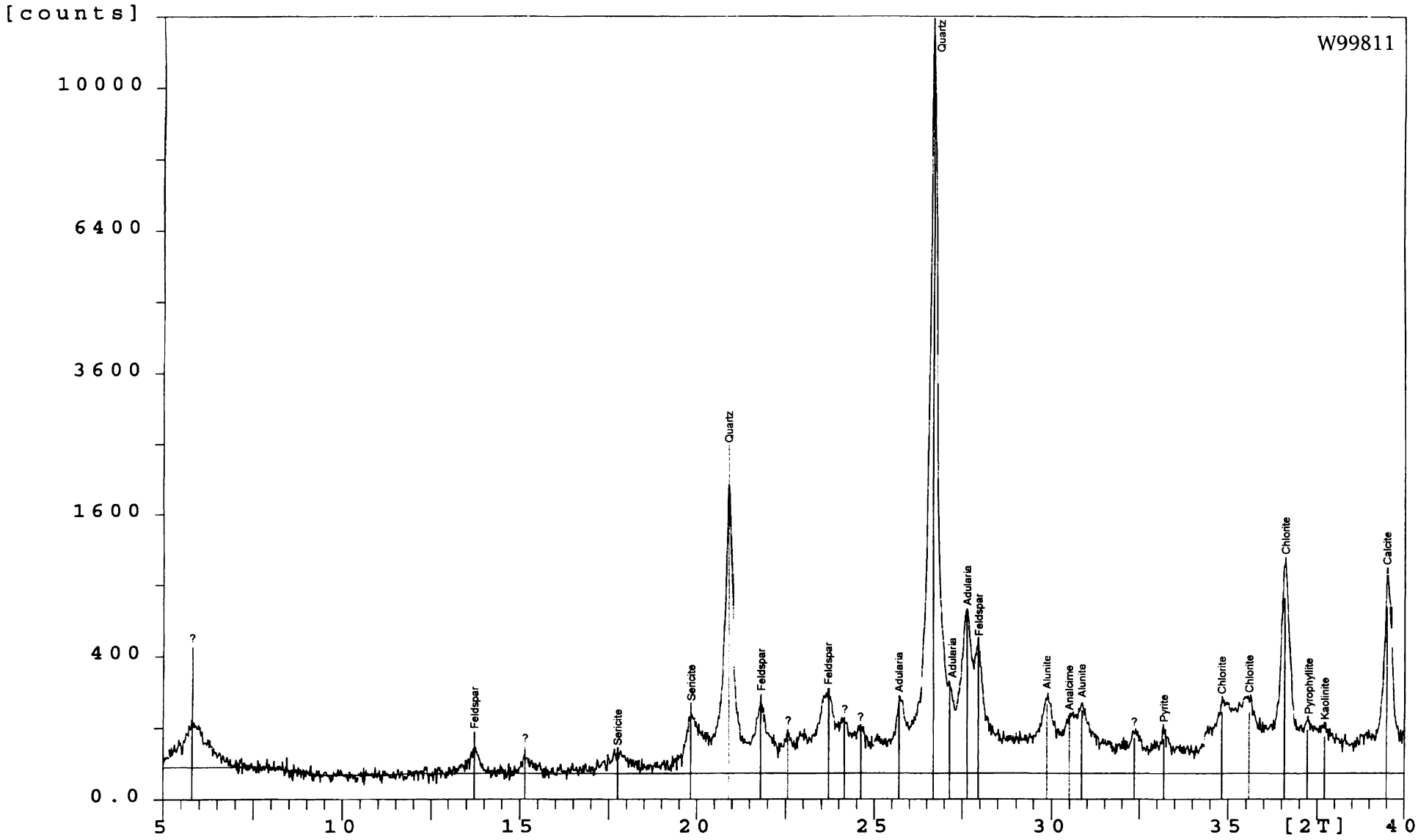
[counts]
10000
6400
3600
1600
400
0.0
W99811
Quartz
Quartz
Sericite
Feldspar
Sericite
Feldspar
Feldspar
Adularia
Adularia
Adularia
Feldspar
Alunite
Analcime
Alunite
Pyrite
Chlorite
Chlorite
Chlorite
Pyrophyllite
Kaolinite
Calcite
?
?
?
?
?
?
5
10
15
20
25
30
35
[2T]
40

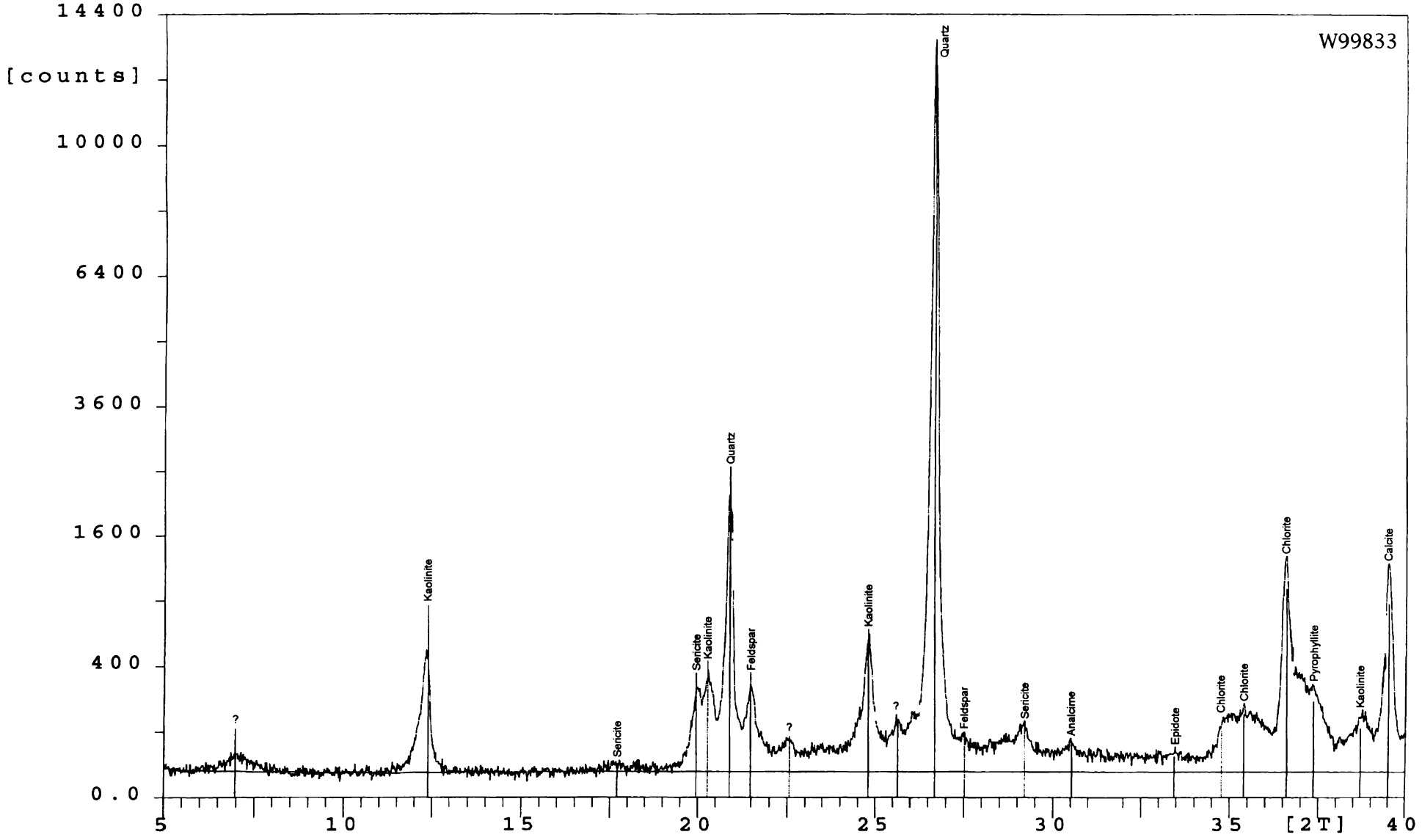
14400
[counts]
10000
6400
3600
1600
400
0.0
W99833
Quartz
Kaolinite
Quartz
Sericite
Kaolinite
Feldspar
Kaolinite
Sericite
Feldspar
Sericite
Analcime
Epidote
Chlorite
Chlorite
Chlorite
Pyrophyllite
Kaolinite
Calcite
?
?
?
5
10
15
20
25
30
35
[2T]
40

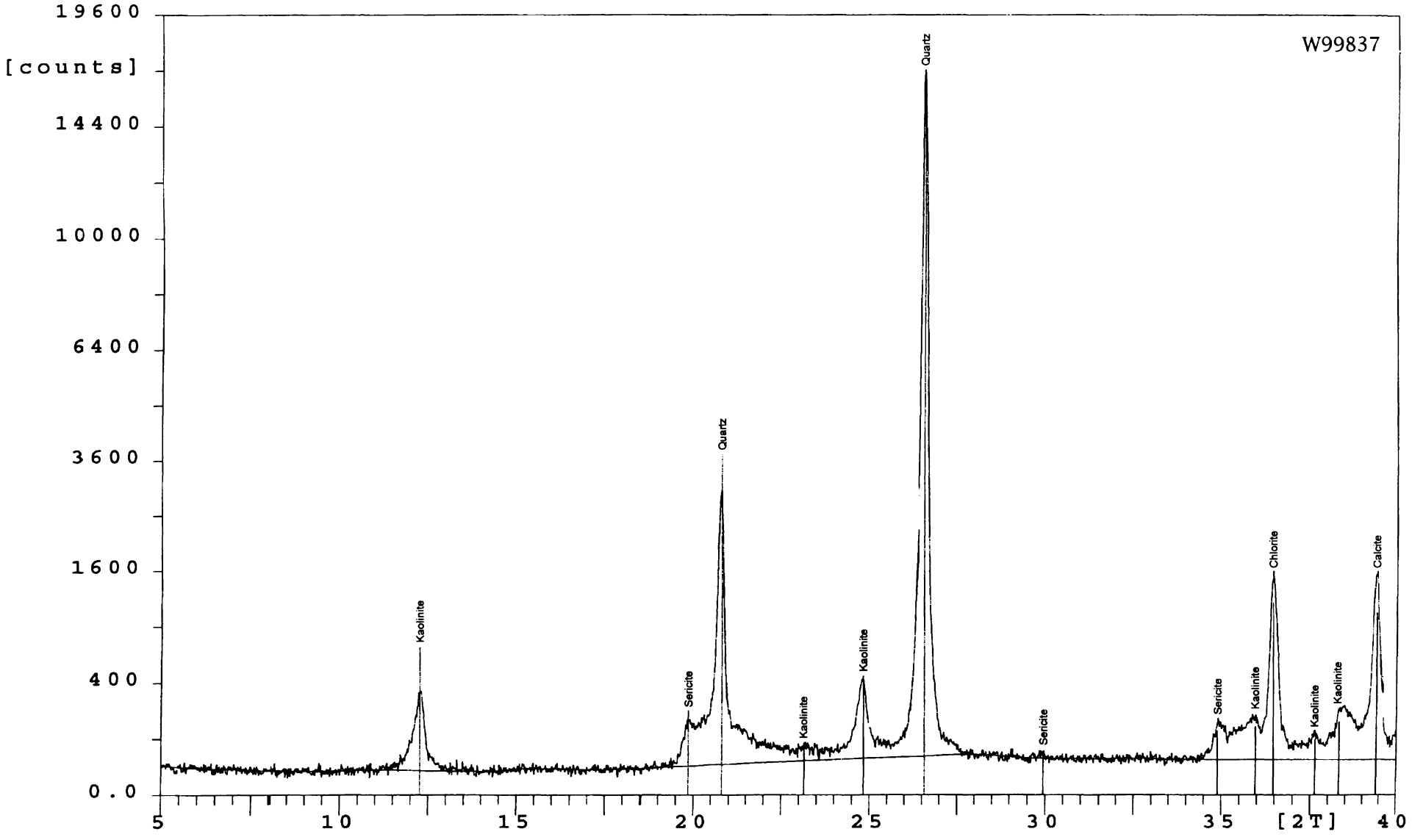
W99837
19600
[counts]
14400
10000
6400
3600
1600
400
0.0
5
10
15
20
25
30
35
[2T]
40
Kaolinite
Sericite
Quartz
Kaolinite
Kaolinite
Quartz
Sericite
Sericite
Kaolinite
Chlorite
Kaolinite
Kaolinite
Calcite

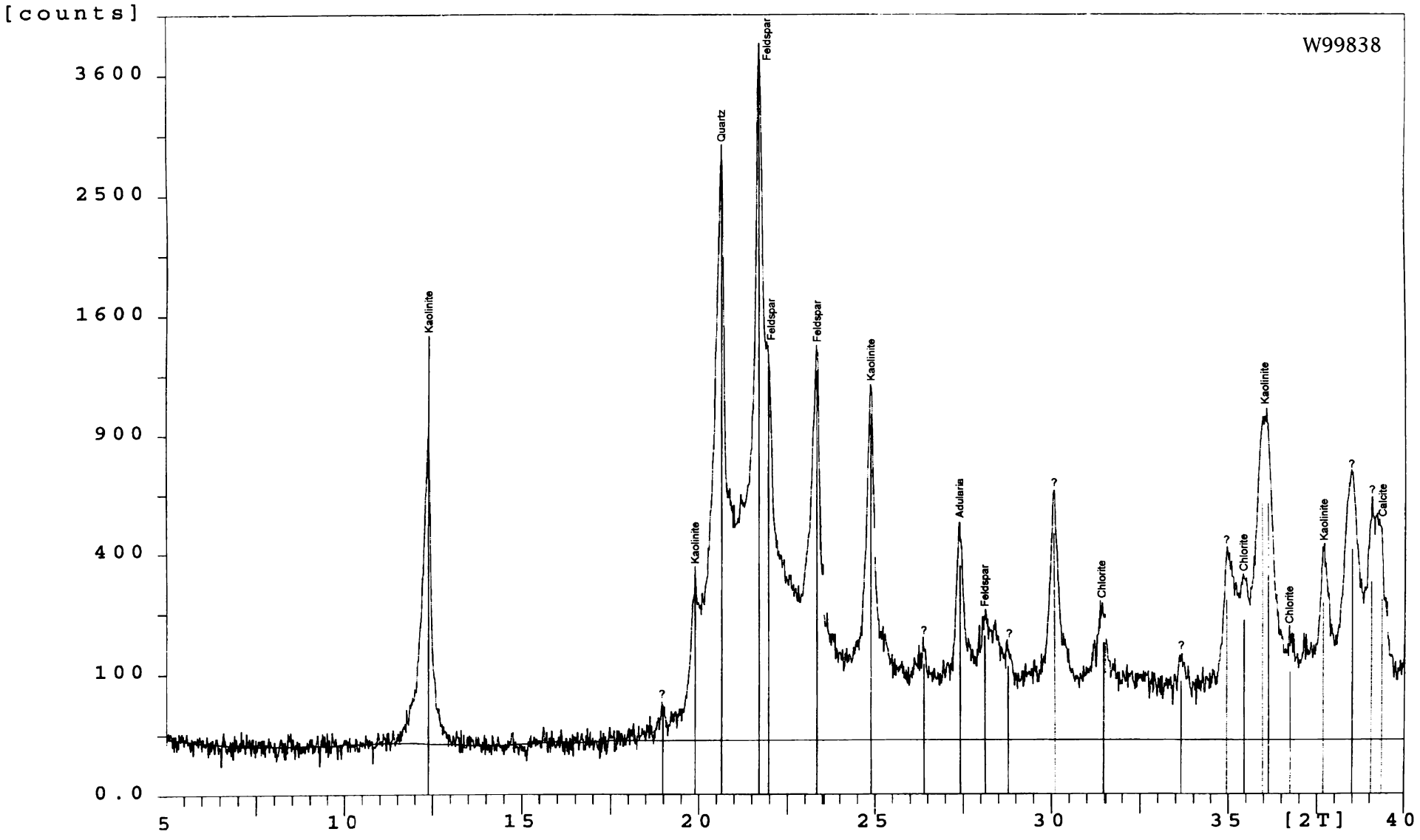
[counts]
3600
2500
1600
900
400
100
0.0
W99838
Kaolinite
Kaolinite
Quartz
Feldspar
Feldspar
Feldspar
Kaolinite
Adularia
Feldspar
Chlorite
Chlorite
Kaolinite
Chlorite
Kaolinite
Calcite
?
5
10
15
20
25
30
35
[2T]
40

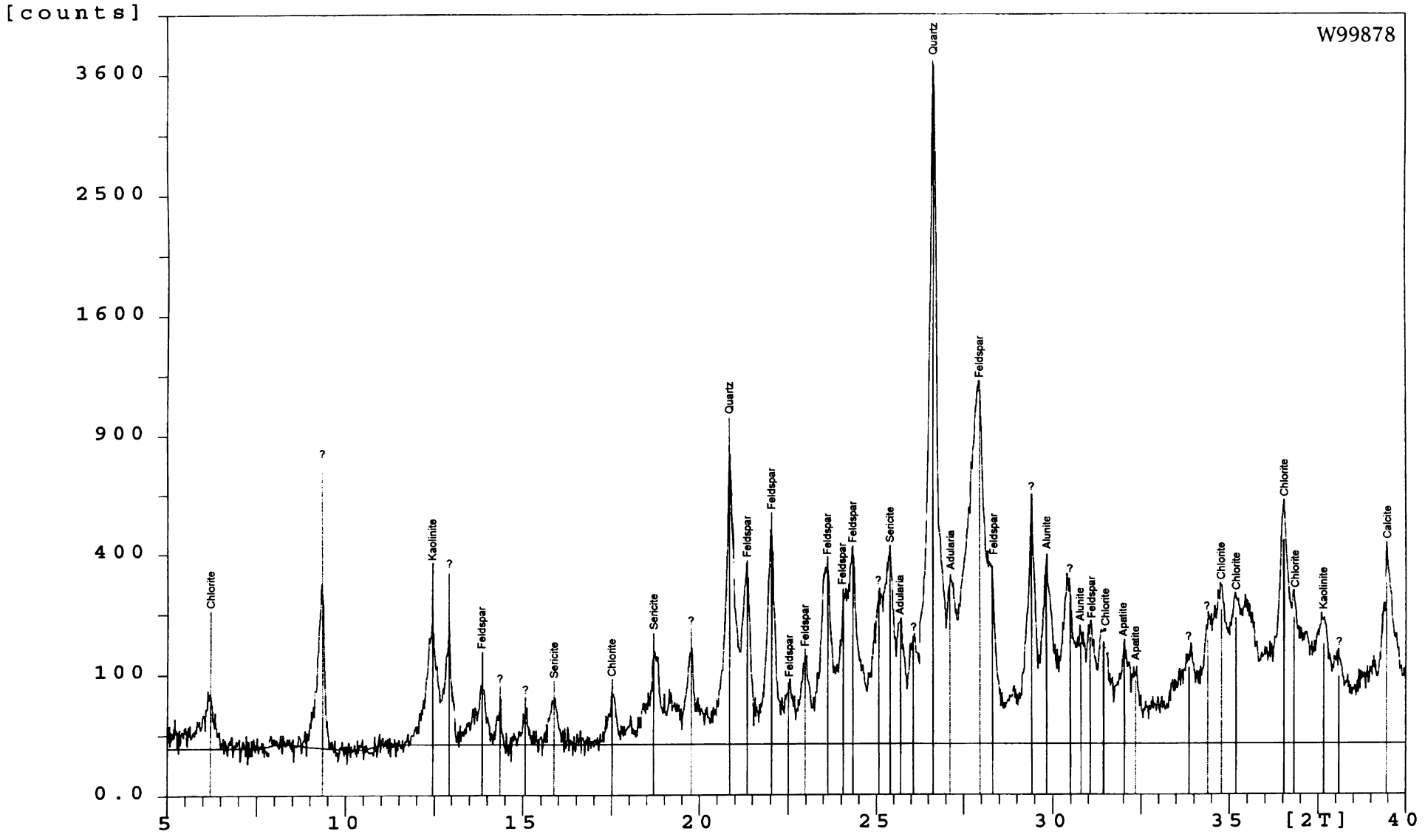
[counts]
W99878
3600
2500
1600
900
400
100
0.0
5
10
15
20
25
30
35
[2T]
40
Chlorite
?
Kaolinite
?
Feldspar
?
?
Sericite
Chlorite
Sericite
?
Quartz
Feldspar
Feldspar
Feldspar
Feldspar
Feldspar
Feldspar
Sericite
Adularia
?
Quartz
Adularia
Feldspar
Feldspar
?
Alunite
?
Alunite
Feldspar
Chlorite
Apatite
Apatite
?
?
Chlorite
Chlorite
Chlorite
Chlorite
Kaolinite
?
Calcite

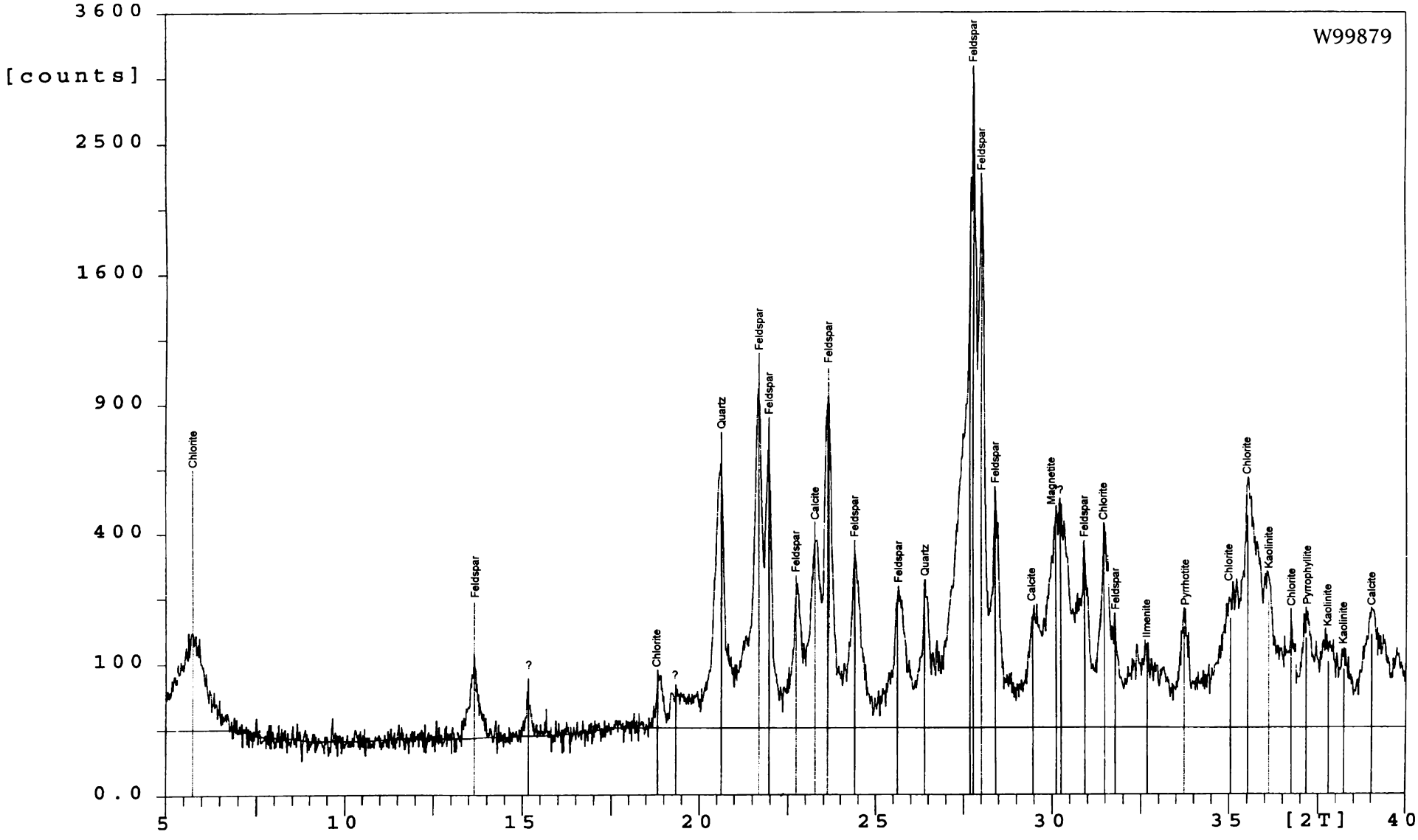
W99879
[counts]
3600
2500
1600
900
400
100
0.0
5
10
15
20
25
30
35
40
[2T]
Chlorite
Feldspar
?
Chlorite
?
Quartz
Feldspar
Feldspar
Feldspar
Calcite
Feldspar
Feldspar
Feldspar
Quartz
Feldspar
Feldspar
Feldspar
Calcite
Magnetite
?
Feldspar
Chlorite
Feldspar
Ilmenite
Pyrrhotite
Chlorite
Chlorite
Kaolinite
Chlorite
Pyrophyllite
Kaolinite
Kaolinite
Calcite

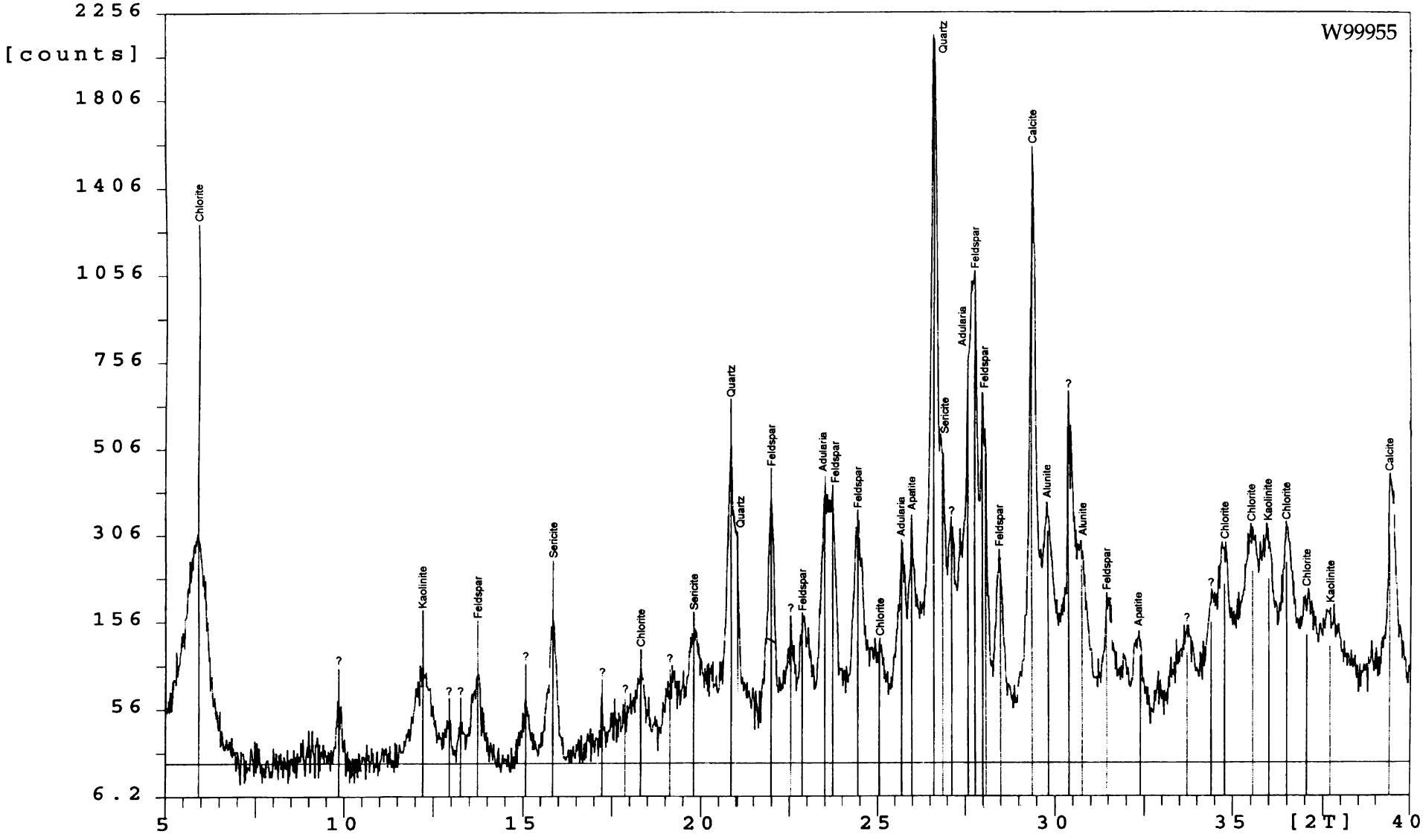
W99955
2256
[counts]
1806
1406
1056
756
506
306
156
56
6.2
5
10
15
20
25
30
35
[2T]
40
Chlorite
Kaolinite
Feldspar
Sericite
Chlorite
Sericite
Quartz
Quartz
Feldspar
Feldspar
Adularia
Feldspar
Feldspar
Chlorite
Adularia
Apatite
Quartz
Sericite
Adularia
Feldspar
Feldspar
Feldspar
Calcite
Alunite
Alunite
Feldspar
Apatite
Chlorite
Chlorite
Kaolinite
Chlorite
Chlorite
Kaolinite
Calcite

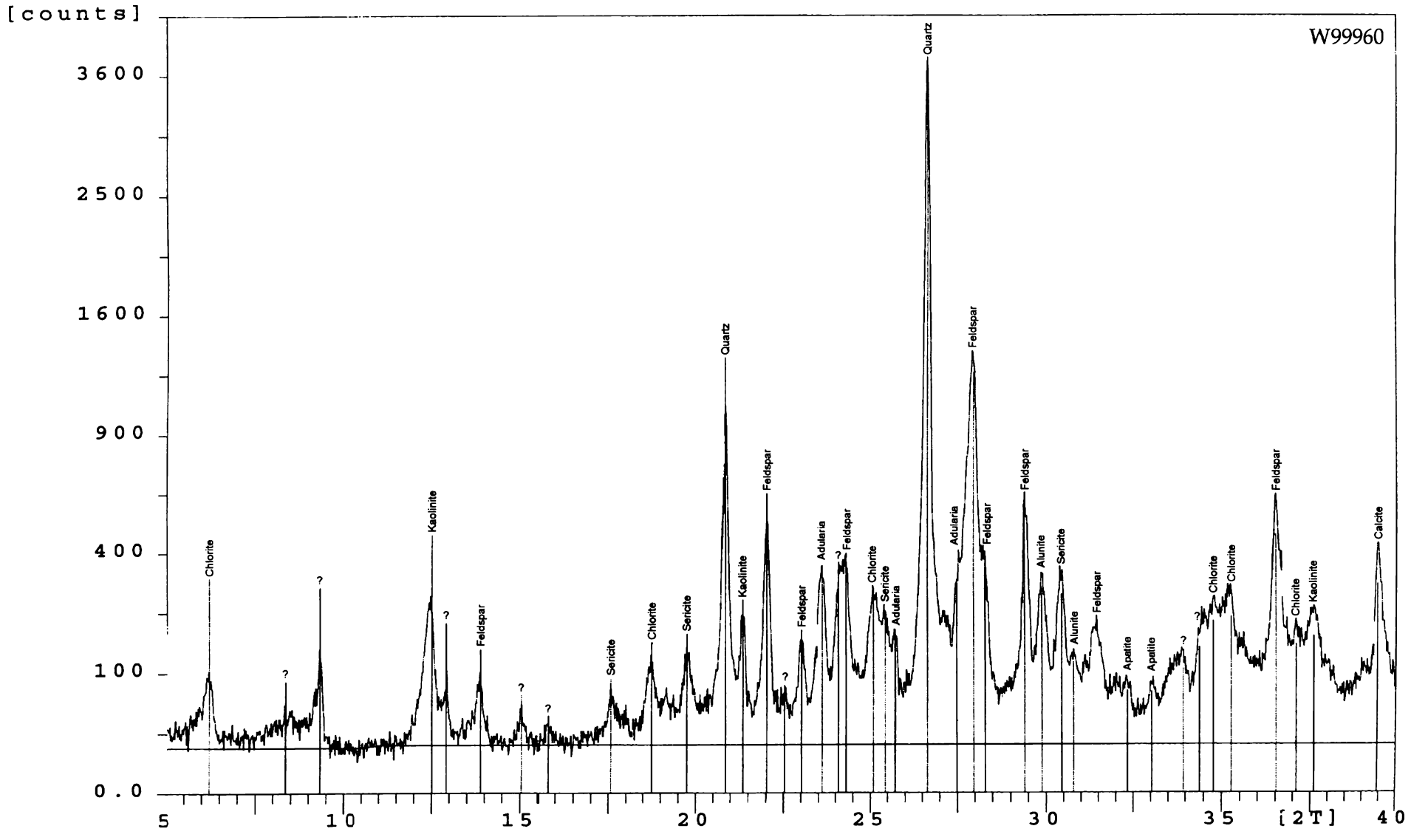
[counts]
3600
2500
1600
900
400
100
0.0
W99960
Chlorite
?
?
Kaolinite
?
Feldspar
?
?
Sericite
Chlorite
Sericite
Quartz
Kaolinite
Feldspar
?
Feldspar
Adularia
?
Feldspar
Chlorite
Sericite
Adularia
Quartz
Adularia
Feldspar
Feldspar
Feldspar
Alunite
Sericite
Alunite
Feldspar
Apatite
Apatite
?
Chlorite
Chlorite
Feldspar
Chlorite
Kaolinite
Calcite
5
10
15
20
25
30
35
[2T]
40

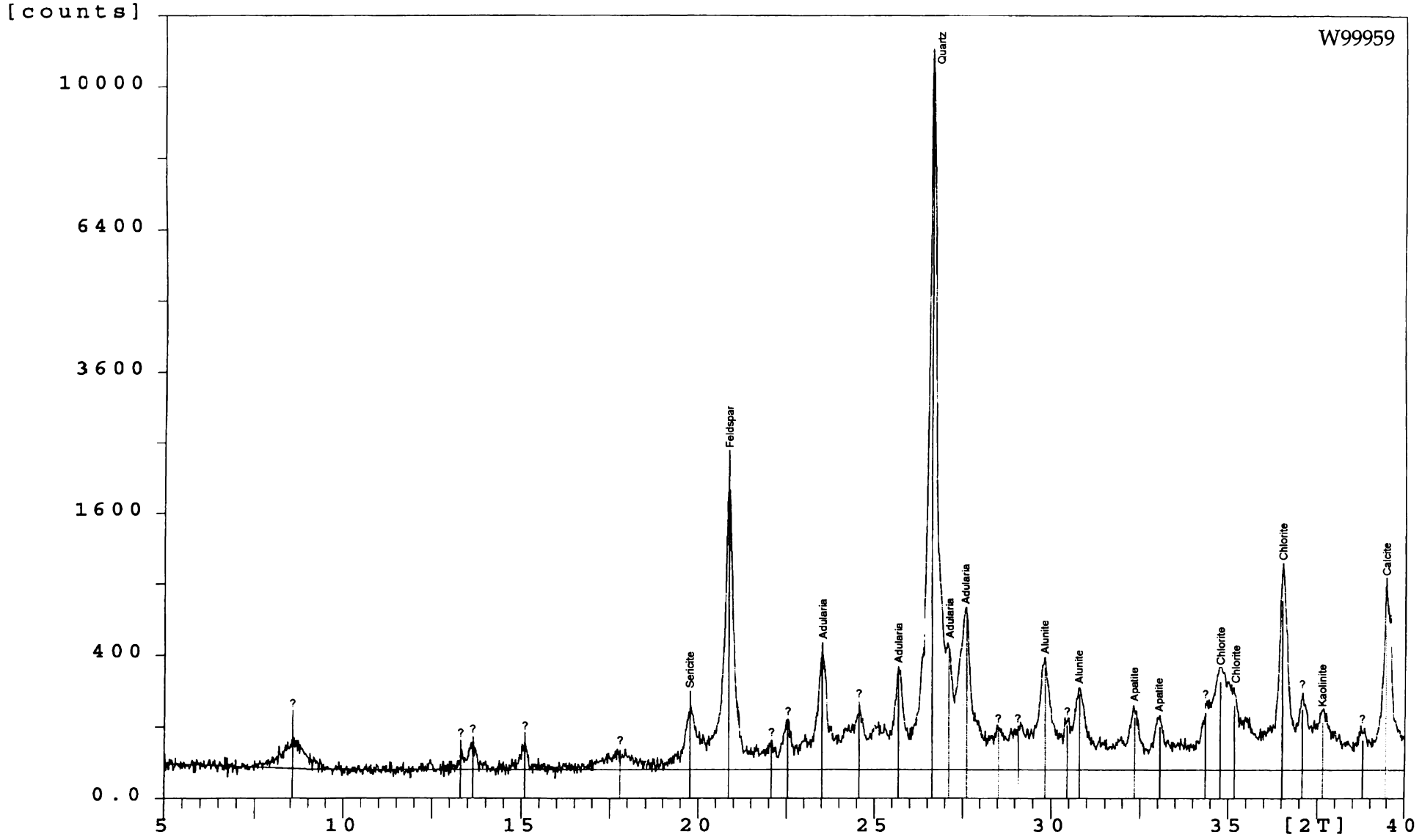
[counts]
W99959
10000
6400
3600
1600
400
0.0
5
10
15
20
25
30
35
[2T]
40
Quartz
Feldspar
Sericite
Adularia
Adularia
Adularia
Adularia
Alunite
Alunite
Apatite
Apatite
Chlorite
Chlorite
Chlorite
Kaolinite
Calcite
?

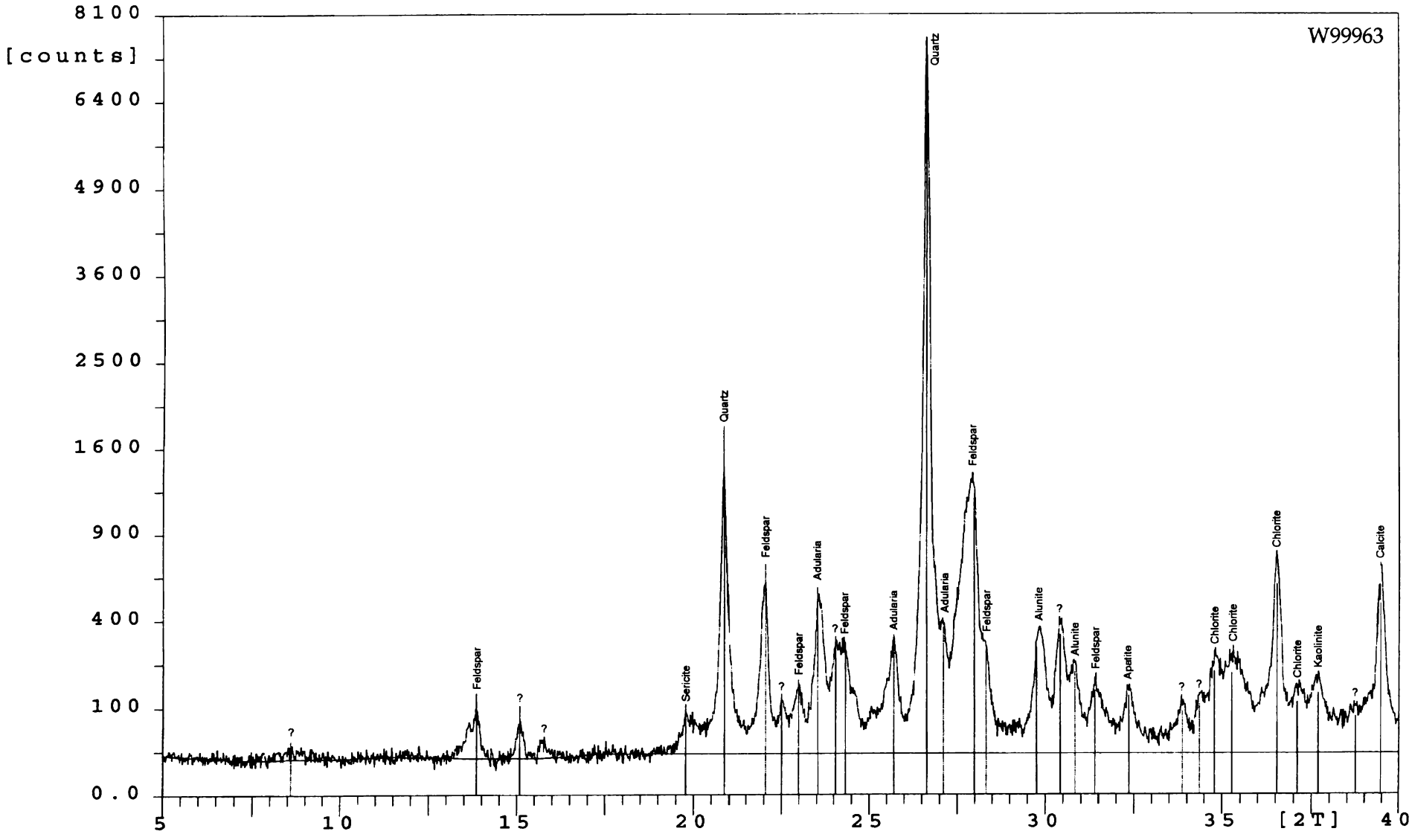
W99963
[counts]
8100
6400
4900
3600
2500
1600
900
400
100
0.0
5
10
15
20
25
30
35
40
[2T]
?
Feldspar
?
?
Sericite
Quartz
Feldspar
?
Feldspar
Adularia
?
Feldspar
Adularia
Quartz
Adularia
Feldspar
Feldspar
Alunite
?
Alunite
Feldspar
Apatite
?
?
Chlorite
Chlorite
Chlorite
Chlorite
Kaolinite
?
Calcite

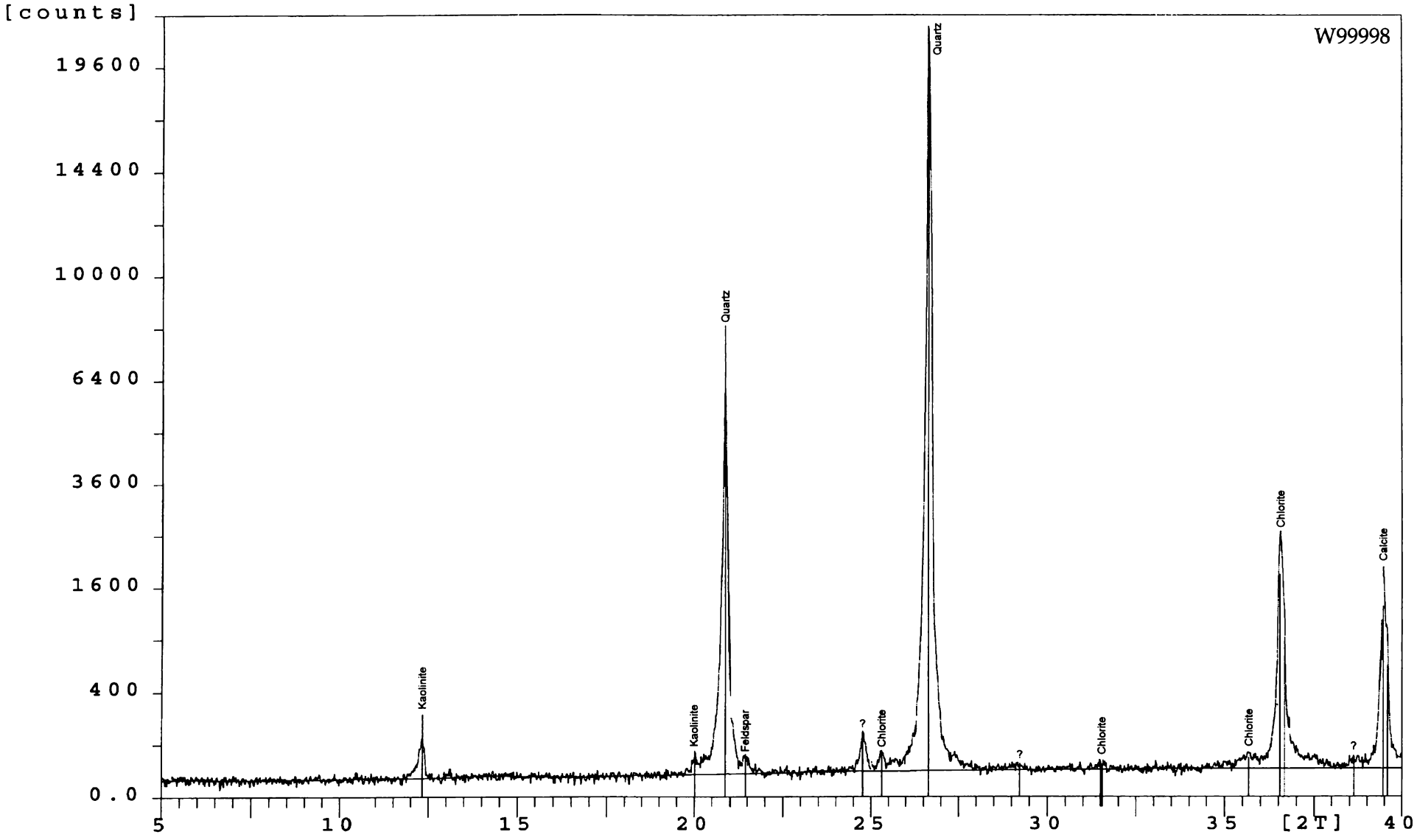
[counts]
19600
14400
10000
6400
3600
1600
400
0.0
W99998
Quartz
Quartz
Kaolinite
Kaolinite
Feldspar
?
Chlorite
?
Chlorite
Chlorite
Chlorite
?
Calcite
5
10
15
20
25
30
35
[2T]
40

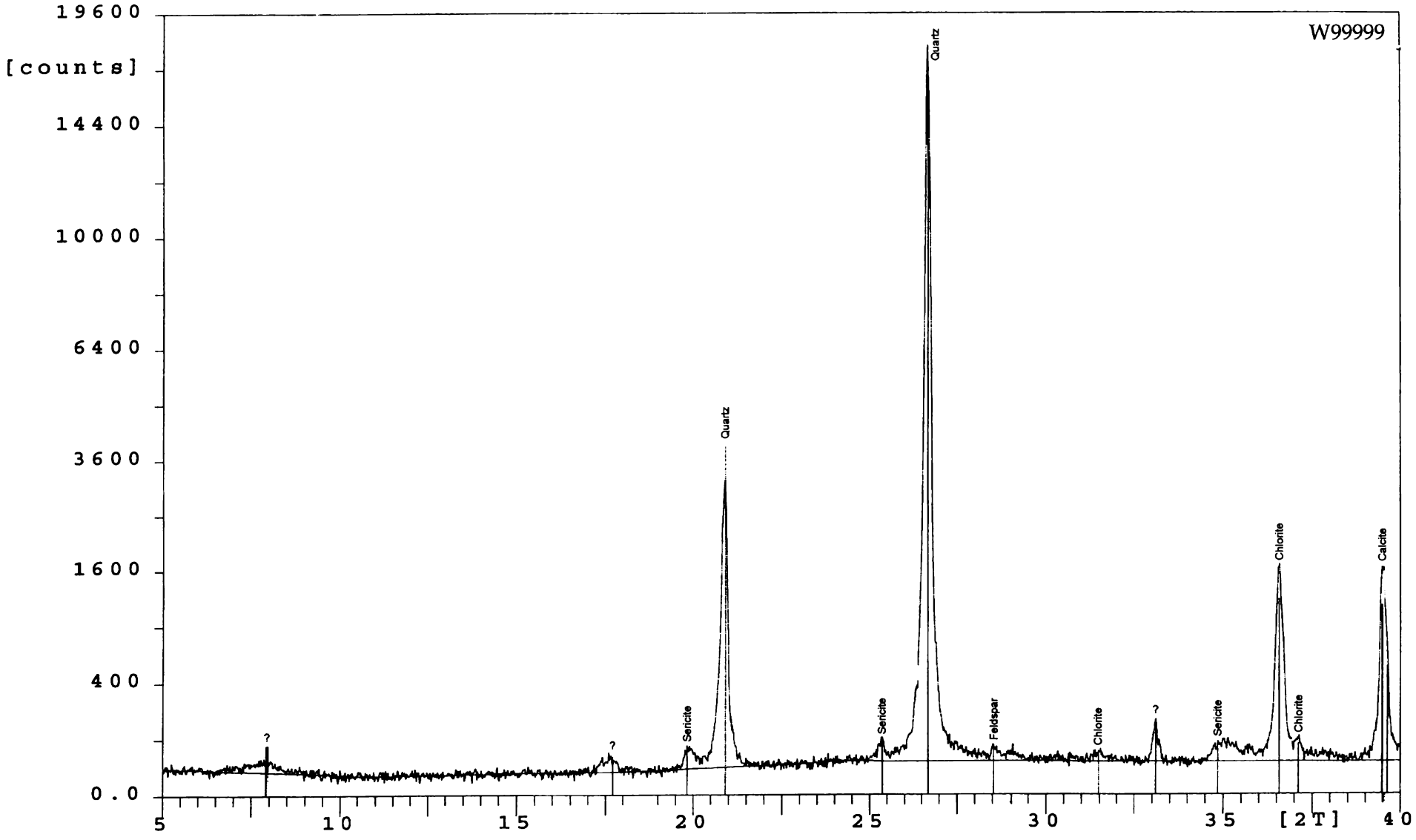
W99999
19600
[counts]
14400
10000
6400
3600
1600
400
0.0
5
10
15
20
25
30
35
[2T]
40
?
?
Sericite
Quartz
Sericite
Quartz
Feldspar
Chlorite
?
Sericite
Chlorite
Chlorite
Calcite